

10th International Fluid Power Conference (10. IFK)

**March 8 – 10, 2016
in Dresden**

Volume 2 – Conference: Wednesday, March 9

Group 1 | 2: Novel System Structures

Group 3 | 5: Pumps

Group 4: Thermal Behaviour

Group 6: Industrial Hydraulics

Publisher:

Dresdner Verein zur Förderung der Fluidtechnik e. V. Dresden
c/o Institut für Fluidtechnik
Technische Universität Dresden
01062 Dresden

Alle Rechte vorbehalten.

Alle hier veröffentlichten Beiträge sind als Manuskript gedruckt.

Die Autoren sind für ihren Beitrag inhaltlich und redaktionell verantwortlich.

Nachdruck – auch auszugsweise – nur mit Zustimmung des Herausgebers und des Verfassers.

All rights reserved.

All papers are published as manuscript.

The authors are responsible as regards content and edition.

No part of this publication – also in extracts – may be produced without prior permission of the publishers.

Online Publication:

Eine elektronische Version der Tagungsbände wird dauerhaft archiviert und öffentlich zur freien Benutzung bereitgestellt.

Sie finden die Dokumente unter der dauerhaften stabilen urn:nbn:de:bsz:14-qucosa-196676

An electronic version of these proceedings will be permanently archived and publicly available for free personal use.

It can be found using the persistent identifier urn:nbn:de:bsz:14-qucosa-196676



<http://nbn-resolving.de/urn:nbn:de:bsz:14-qucosa-196676>

Sehr geehrte Damen und Herren,

wir freuen uns, Ihnen die Tagungsbände zur 10. Auflage des Internationalen Fluidtechnischen Kolloquium präsentieren zu können. Als eine der weltweit wichtigsten Tagungen im Bereich der hydraulischen und pneumatischen Antriebs-, Steuerungs- und Regelungstechnik hat sich das IFK als zentrale Austauschplattform für Experten der Branche in Europa etabliert. Es bietet im internationalen Rahmen Anwendern, Herstellern und Wissenschaftlern die Möglichkeit, Innovationen zu präsentieren und über Entwicklungstrends zu diskutieren

Das Institut für Fluidtechnik (IFD) der Technischen Universität Dresden organisiert und veranstaltet nun zum fünften Mal das IFK, welches sich wachsender Teilnehmer- und Vortragszahlen erfreut. Mitveranstalter ist der Fachverband Fluidtechnik im Verband Deutscher Maschinen- und Anlagenbau e. V. (VDMA). Die Organisation und der Austragungsort wechseln alle zwei Jahre zwischen dem IFD in Dresden und dem Institut für fluidtechnische Antriebe und Steuerungen (IFAS) in Aachen.

Am ersten Tag der Veranstaltung widmet sich das Symposium methoden- und grundlagenfokussierten Beiträgen. Die beiden folgenden Konferenztage bieten einen umfassenden anwendungs- und technologieorientierten Überblick über den neuesten Stand der Fluidtechnik. In dieser Kombination ist das IFK ein einzigartiges Forum zum Austausch zwischen universitärer Grundlagenforschung und industrieller Anwendererfahrung. Eine parallele Fachausstellung bietet die Möglichkeit, sich direkt über Produkte zu informieren und mit Herstellern, Forschern und Anwendern von morgen zu vernetzen.

Das Motto des 10. IFK lautet „Smart Fluid Power“, womit die Tagung einen der großen Trends der Branche in den Fokus stellt: Durch ihr hohes Maß an Flexibilität bieten sich nahezu unbegrenzte Möglichkeiten der Integration fluidmechatronischer Systeme in intelligente Netzwerke. Das IFK lebt von interessanten und hochwertigen wissenschaftlichen Beiträgen.

Für einen ungezwungenen Austausch sorgen wir mit einem umfangreichen Rahmen- und Kulturprogramm, bestehend aus Get-Together, Festabend, Hallenfest und verschiedenen Exkursionen und kulturellen Ausflügen – ein kleiner Einblick in das, was die Stadt Dresden sonst zu bieten hat.

Ich wünsche Ihnen viel Spaß beim Lesen der Tagungsbeiträge.



Prof. Dr.-Ing. Jürgen Weber

Dear Sir or Madam,

we are pleased to present the Proceedings for the 10th edition of the International Fluid Power Conference (IFK). The IFK is one of the world's most significant scientific conferences on fluid power control technology and systems. It offers a common platform for the presentation and discussion of trends and innovations to manufacturers, users and scientists.

The Institute of Fluid Power (IFD) at the TU Dresden is organising and hosting the IFK for the fifth time, which has shown constant growth in number of participants and presentations. Supporting host is the Fluid Power Association of the German Engineering Federation (VDMA). The organization and the conference location alternates every two years between Dresden at the IFD and Aachen at the Institute for Fluid Power Drives and Controls (IFAS).

The symposium on the first day is dedicated to presentations focused on methodology and fundamental research. The two following conference days offer a wide variety of application and technology orientated papers about the latest state of the art in fluid power. It is this combination that makes the IFK a unique and excellent forum for the exchange of academic research and industrial application experience. A simultaneously ongoing exhibition offers the possibility to get product information and to have individual talks with manufacturers. The conference is followed by excursions to regional companies and technical sights.

The theme of the 10th IFK will be "Smart Fluid Power", covering a growing trend in the fluid power industry. Through its great versatility fluid power has nearly limitless possibilities for the integration of fluid-mechatronic systems into intelligent networks.

We will create an atmosphere for casual exchange by offering a vast frame and cultural program. It consists of a get-together, a Gala dinner, laboratory festivities and various excursions as well as cultural trips – a little peek into what this city has to offer.

I hope you enjoy reading the conference proceedings.



Prof. Dr.-Ing. Jürgen Weber

Program Committee

Achten, P.	Dr. ir., INNAS B.V., Breda (NL)
Bauer, F.	Dr.-Ing., HYDAC International GmbH, Sulzbach / Saar
Binz, D.	Dr.-Ing., Bürkert Werke GmbH, Ingelfingen
Boes, C.	Dr.-Ing., Moog GmbH, Böblingen
Fedde, T.	Dr.-Ing., CLAAS Tractor, Paderborn
Fiedler, M.	Dr.-Ing., Norgren GmbH, Fellbach
Fischer, M.	Dr.-Ing., Argo Hytos GmbH, Kraichtal
Hahmann, W.	Dr.-Ing., Hydac International GmbH, Sulzbach/Saar
Hunger, I.	Lic. oec., Hunger DFE GmbH, Würzburg
Huster, G.	Dipl.-Ing., KraussMaffei Technologies GmbH, München
Igelhorst, W.	Dipl.-Ing., SMS-Siemag AG, Hilchenbach
Klug, D.	Dr.-Ing., Schuler Pressen GmbH, Waghäusel
Knobloch, M.	Dipl.-Ing. (FH), HAWE Hydraulik SE, München
Knobloch, J.	Dipl.-Ing., AGCO GmbH, Marktoberdorf
Krallmann, J.	Dr.-Ing., Thomas Magnete GmbH, Herdorf
Krieg, M.	Dr.-Ing., Parker Hannifin Manufacturing Germany GmbH & Co. KG, Chemnitz
Kunze, T.	Dr.-Ing., Liebherr Machines Bulle S.A., Bulle (CH)
Langen, A.	Dr.-Ing., Linde Hydraulics GmbH & Co. KG, Aschaffenburg
Lausch, H.	Dr.-Ing., Bosch Rexroth AG, Lohr am Main
Legner, J.	Dipl.-Ing. (FH), ZF Friedrichshafen AG, Friedrichshafen
Lindemann, L.	Dr., Fuchs Petrolub SE, Mannheim
Lüüs, H.	Dipl.-Ing., Bucher Hydraulics GmbH, Klettgau
Martens, O.	Dr., KOMATSU Mining Germany GmbH, Düsseldorf
Murrenhoff, H.	Prof. Dr.-Ing., RWTH Aachen
Pfab, H.	Dr.-Ing., Liebherr-Werk Bischofshofen GmbH, Bischofshofen (A)
Post, P.	Prof. Dr.-Ing., Festo AG und Co. KG, Esslingen
Rahmfeld, R.	Dr.-Ing., Danfoss Power Solutions GmbH & Co. OHG, Neumünster
Saffe, P.	Dr.-Ing., Aventics GmbH, Laatzen
Schramm, A.	Dipl.-Ing., Sumitomo (SHI) Demag Plastics Machinery GmbH, Schwaig
Schultz, A. W.	Dr.-Ing. (MBA), Magnet Schultz GmbH und Co. Fabrikations- und Vertriebs-KG, Memmingen
Synek, P.	Dipl.-Ing., Fachverband Fluidtechnik im VDMA, Frankfurt am Main
Weber, J.	Prof. Dr.-Ing., TU Dresden
Welschhof, B.	Dr.-Ing., Tadano Faun GmbH, Lauf a.d. Pegnitz
Wittkop, S.	Dr.-Ing., Hauhinco Maschinenfabrik G. Hausherr, Jochums GmbH & Co. KG, Sprockhövel

International Advisory Committee**Professor Eric Bideaux***Fluid Power Center*

INSA de Lyon, France

Professor Kalevi Huhtala*Department for Intelligent Hydraulics and Automation*

Tampere University of Technology, Finland

Professor Monika Ivantysynova*MAHA Fluid Power Systems**Agricultural & Biological Engineering*

Purdue University, USA

Professor Petter Krus*Division of Fluid and Mechatronic Systems*

Lingköping University, Sweden

Professor Takao Nishiumi*Department of Mechanical Systems Engineering*

School of Systems Engineering

National Defense Academy of Japan

Professor Andrew Plummer*Centre for Power Transmission*

University of Bath, United Kingdom

Professor Kazushi Sanada*Division of Systems Research*

Yokohama National University, Japan

Professor Rudolf Scheidl*Institute of Machine Design and Hydraulic Drives*

Johannes Kepler University Linz, Austria

Professor Kim Stelson*Center for Compact and Efficient Fluid Power*

University of Minnesota, USA

Professor Huayong Yang*State Key Laboratory of Fluid Power and Mechatronic Systems*

Zhejiang University, China

Peer Review beim 10. IFK

Auch in diesem Jahr bieten wir allen Autoren die Möglichkeit eines optionalen Peer Reviews für ihr Paper. Dies stellt sicher, dass die begutachteten Paper hohen wissenschaftlichen Anforderungen genügen und für Förderprojekte oder Promotionsarbeiten die entsprechende Anerkennung erhalten. Diese Paper werden im Tagungsband mit dem Hinweis - **peer reviewed** - gekennzeichnet.

Ein vom Autor zum Review ausgewähltes Paper wird durch insgesamt drei wissenschaftliche Spezialisten einer unabhängigen Begutachtung unterzogen. Diese wird von den Mitglieder des Programmausschusses (siehe Seite 5) sowie zusätzlich vom Institut für Fluidtechnik der TU Dresden oder dem Institut für Fluidtechnische Antriebe und Steuerung der RWTH Aachen übernommen. Nach dieser ersten Bewertung haben die Autoren die Möglichkeit, ihr Paper falls erforderlich, mit den geforderten Änderungen zu überarbeiten und erneut einzureichen. Nehmen die Gutachter die Änderungen an, wird der Beitrag als - **peer reviewed** - in den Tagungsband aufgenommen.

Dieser aufwändige Begutachtungsprozess dient der inhaltlichen und formellen Qualitätssicherung und wäre ohne die fachliche Unterstützung des Programmausschusses nicht möglich gewesen. Die Organisatoren des IFK bedanken sich bei allen Gutachtern für ihre Unterstützung.

Peer Review at the 10th IFK

This year we once again give all authors the opportunity of an optional peer review of their papers. This guarantees that the examined papers meet the high scientific requirements, and may receive their respective appreciation for funded projects or doctoral theses. Those papers will be marked – **peer reviewed** –.

A paper that has been chosen by the author to be reviewed will be subjected to an independent examination by a total of 3 specialized experts among the Program Committee (see page 5) as well as the Institute of Fluid Power at the TU Dresden, or the Institute for Fluid Power Drives and Controls at RWTH Aachen University. After this initial evaluation, the authors have the opportunity to revise their paper as needed and re-submit it with the necessary changes. If the reviewers accept the changes, the paper will be included in the conference transcript as – **peer reviewed** –.

This extensive assessment process serves the purpose of quality assurance in terms of content and form, and would not have been possible without the expert support of the Program Committee. The organizers of the IFK want to thank all reviewers for their support.

Group 1 | 2: Novel System Structures

1-0	General Lecture: Novel System Architectures by Individual Drives _____	29
	Jürgen Weber, TU Dresden, IFD, Germany	
1-1	Green Wheel Loader – improving fuel economy through efficient drive and control concepts _____	63
	Markus Schneider, TU Dresden, IFD, Germany	
1-2	Decentralized energy-saving hydraulic concepts for mobile working machines _____	79
	Johann Lodewyks, HSLU, CC Mechanical Systems, Switzerland	
2-1	Electric hydrostatic actuation - modular building blocks for industrial applications _____	93
	Achim Helbig, Moog GmbH, Germany	
2-2	Pressure Impulse Generation with Energy Recovery _____	103
	Siegfried Rotthäuser, IgH GmbH, Germany	
2-3	Increased energy efficiency of hydraulic hybrid drives by means of a multi-chamber accumulator _____	117
	Frank Bauer, HYDAC Technology GmbH, Germany	
2-4	A complete analysis for single rod electro hydrostatic actuators _____	119
	Hakan Çalışkan, Middle East Technical University, Turkey	

Group 3 | 5: Pumps

3-0	General Lecture: Technologies and Innovations for Hydraulic Pumps _____	135
	Monika Ivantysynova, Purdue University, Maha Fluid Power Research Center, USA	
3-1	Swash plate pumps - the key to the future _____	139
	Gordon Mohn, Rexroth (Bosch Group), Germany	
3-2	Customer focused development of a variable bent-axis pump/motor for open circuit hydrostatic transmissions, e.g. in hydraulic hybrid drives _____	151
	Conny Hugosson, Parker Hannifin Manufacturing Sweden AB, Sweden	
3-3	The control of an open-circuit, floating cup variable displacement pump _____	163
	Peter Achten, INNAS, Netherlands	
5-1	Tribolayer Formation on Bronze CuSn12Ni2 in the Tribological Contact between Cylinder and Control Plate in an Axial Piston Pump with Swashplate Design _____	251
	Andreas Paulus, Bosch Rexroth AG, Germany	
5-2	A Flow Control System for a Novel Concept of Variable Delivery External Gear Pump _____	263
	Andrea Vacca, Purdue University, USA	
5-3	Brimming bubbles? On an Innovative Piston Design of Dosing Pumps _____	277
	Axel Müller, Thomas Magnete GmbH, Germany	
5-4	The Impact of Micro-Surface Shaping of the Piston on the Piston/Cylinder Interface of an Axial Piston Machine _____	289
	Ashley Wondergem, Purdue University, USA	
5-5	Bulk Modulus and Traction Effects in Hydraulic Pump and Motors _____	301
	Paul Michael, Milwaukee School of Engineering, USA	
5-6	Energy efficiency improvement by the application of nano-structured coatings on axial piston pump slippers _____	313
	Giuseppe Rizzo, IMAMOTER – C.N.R., Italy	

Group 4: Thermal Behaviour

- 4-0 **General Lecture: Thermo Energetic Design of Machine Tools and Requirements for Smart Fluid Power Systems** _____ 177
Christian Brecher, RWTH Aachen University, Laboratory for Machine Tools and Production Engineering (WZL), Germany
- 4-1 **Thermo-energetic Analysis of the Fluid Systems in Cutting Machine Tools** _____ 195
Juliane Weber, TU Dresden, IFD, Germany
- 4-2 **Comparison of Heat-Properties and its Implications between Standard-Oil and Bio-Oil** _____ 207
Marcel Rückert, RWTH Aachen University, Institute for Fluid Power Drives and Controls (IFAS), Germany
- 4-3 **Prediction of the thermo energetic behaviour of an electrohydraulic compact drive** _____ 219
Sebastian Michel, TU Dresden, IFD, Germany
- 4-4 **A Thermal analysis of Direct Driven Hydraulics** _____ 235
Tatiana Minav, Aalto University, Finland

Group 6: Industrial Hydraulics

- 6-1 **Consistent automation solutions of Electrohydraulic Drives as contribution to Industry 4.0** _____ 331
Albert Köckemann, Bosch Rexroth AG, Germany
- 6-2 **Adaptive process control for stabilizing the production process** _____ 341
Reinhard Schiffers, KrausMaffei Technologies GmbH, Germany
- 6-3 **On the compensation of dynamic reaction forces in stationary machinery** _____ 353
Tobias Radermacher, TU Dresden, IFD, Germany
- 6-4 **Improvement of hydraulic control quality for deep drawing presses through retrofit** _____ 367
Marcus Helmke, TRsystems GmbH, Germany
- 6-5 **Potentials of Speed and Displacement Variable Pumps in Hydraulic Applications** _____ 379
Johannes Willkomm, Bosch Rexroth, Germany
- 6-6 **Condition Monitoring for Hydraulic Power Units - the user-oriented Step into industry 4.0** _____ 393
Martin Laube, Bosch Rexroth AG, Germany

Group 7: Hydraulic Components

- 7-0 **General Lecture: Electrohydraulic servovalves – past, present, and future** _____ 405
Andrew Plummer, University of Bath, Department of Mechanical Engineering, UK
- 7-1 **A new energy saving load adaptive counterbalance valve** ____ 425
Bernd Zähe, Sunhydraulik Deutschland, Germany
- 7-2 **Development of an Electronically Controlled Self-Teaching Lift Valve Family** _____ 437
Eneko Goenechea, Bucher Hydraulics AG, Switzerland
- 7-3 **Development of an innovative diaphragm accumulator design and assembly process** _____ 451
Thorsten Hillesheim, Freudenberg Sealing Technologies GmbH & Co. KG, Germany
- 7-4 **Potential and application fields of lightweight hydraulic components in multi-material design** _____ 463
Andreas Ulbricht, CG Rail GmbH, Germany
- 7-5 **CFD Simulation and Measurement of Flow Forces Acting on a Spool Valve** _____ 473
Patrik Bordovsky, RWTH Aachen University, Institute for Fluid Power Drives and Controls (IFAS), Germany

Abstracts: Group 1 | 2 - Novel System Structures

1-0 General Lecture: Novel System Architectures by Individual Drives

Jürgen Weber, TU Dresden, IFD, Germany

Measures of individualization and integration offer a great potential for further development and optimization in hydraulic drive technology. Advantages are seen especially for energy efficiency and functionality. These potentials motivate current research activities for displacement controlled systems and for valve controlled structures. For the latter, the focus lies on strategies of independent metering. Furthermore, expected challenges for the future are discussed.

1-1 Green Wheel Loader – improving fuel economy through efficient drive and control concepts

Markus Schneider, TU Dresden, IFD, Germany

The drive train components and the machine control system significantly influence the fuel consumption of mobile machinery. The demonstrator vehicle “Green Wheel Loader” developed within the joint research project “TEAM” combines the most promising drive concepts currently available for mobile machines with an innovative operating strategy. The developed drive and control system proved its functionality and performance under realistic operation conditions in a gravel pit. Reference test showed 10 – 15 % fuel savings of the prototype vehicle compared to a state-of-the-art series machine.

1-2 Decentralized energy-saving hydraulic concepts for mobile working machines

Johann Lodewyks, HSLU, CC Mechanical Systems, Switzerland

The high price of batteries in working machines with electric drives offer a potential for investment in energy-saving hydraulic systems. The decentralized power network opens up new approaches for hydraulic- and hybrid circuits. In addition, the regeneration of energy can be used at any point of the machine. For the example of an excavator arm drive with a double cylinder two compact hydraulic circuits are presented, which relieve a central hydraulic system.

2-1 Electric hydrostatic actuation - modular building blocks for industrial applications

Achim Helbig, Moog GmbH, Germany

Electro Hydrostatic Actuators (EHA) are emerging as a viable option for industrial machine builders as the design combines the best of both electro-mechanical and electro-hydraulic technologies. The EHA is a highly integrated, compact alternative to traditional hydraulic solutions. Automation engineers moving toward electro-mechanical actuation in pursuit of energy efficiency and environmental cleanliness, will find an EHA an attractive option for high force density actuators.

This paper will address the factors to consider when assessing an industrial machine's application suitability for this latest innovation in actuation. It describes principal base circuits, a concept for EHA building blocks and a realized pilot application as well as challenges on actuator and components level.

2-2 Pressure Impulse Generation with Energy Recovery

Siegfried Rothhäuser, IgH GmbH, Germany

The Pressure Impulse test-rig uses the principal energetic advantages of displacement-controlled systems versus valve-controlled systems. The use of digital-control technology enables a high dynamic in the pressure curve, according to the requirements of ISO6605. Accumulators, along with inertia, make energy recovery possible, as well as, enabling the compression energy to be re-used. As a result of this, there is a drastic reduction in operating costs. A simulation of the system before starting the project allows the development risks to be calculated and the physically achievable performance limits to be shown.

2-3 Increased energy efficiency of hydraulic hybrid drives by means of a multi-chamber accumulator

Frank Bauer, HYDAC Technology GmbH, Germany

The focus of the present contribution is hydraulic energy recovery by means of hydro-pneumatic multi-chamber accumulators. A simulation study is presented comparing two different multi-chamber accumulator concepts for energy recovery in an exemplary load case involving a forklift mast. The first concept is based on the "Double Piston Accumulator" /1/. It is compared to the so-called "Digital Accumulator" /2/. Both similarities and differences of the two concepts are discussed in the presentation.

2-4 A complete analysis for single rod electro hydrostatic actuators

Hakan Çalışkan, Middle East Technical University, Turkey

In the current study a variable speed pump controlled hydrostatic circuit where an underlapped shuttle valve is utilized to compensate the unequal flow rate of a single rod actuator is analyzed. Parameters of the shuttle valve are included in the system analysis, rather than treating it as an ideal switching element as handled in literature. A linearized model of the system is obtained. An inverse kinematic model, which calculates the required pump drive speed for a desired actuator speed and given pilot pressure input, is formed. A numerical stability analysis program is developed, and the stability of all possible shuttle valve spool positions is determined. The theoretical findings are validated by non-linear simulation model responses.

Abstracts: Group 3 | 5 - Pumps**3-0 General Lecture: Technologies and Innovations for Hydraulic Pumps**

Monika Ivantysynova, Purdue University, Maha Fluid Power Research Center, USA

Positive displacement machines working as hydraulic pumps or hydraulic motors have always been, are and will be an essential part of any hydraulic system. Current trends and future demands on energy efficient systems will not only drastically increase the number of positive displacement machines needed for modern efficient hydraulic circuits but will significantly change the performance requirements of pumps and motors. Throttleless system configurations will change the landscape of hydraulic actuation in aerospace, mobile machines, automotive and many other areas and will definitely open the door for new applications due to its enhanced competitiveness with electric and electro-mechanical systems.

3-1 Swash plate pumps - the key to the future

Gordon Mohn, Rexroth (Bosch Group), Germany

Due to many advantages, swash plate pumps are wide spread in hydraulic systems. The main advantages are the through drive capability, the adjustability and most of all, the high power density. Their application range is limited, historically, to 450bar including medium and higher volume sizes. In higher pressure range, constant pumps such as wobbling disks or radial piston pumps are normally used. This is because the higher stressed parts can be dimensioned much bigger. Pumps with lower power such as constant displacement gear pumps are generally used in low price applications.

In order to enlarge the application range of swash plate pumps, their advantages have to be further improved and strengthened. This paper shows by example how the pressure of the basic series A4VSO was increased up to a nominal pressure of 630bar and the historical pressure mark of 450bar could be exceeded. This increase in pressure level enables for example steel treatment manufacturers to reduce their component sizes without the need of a pressure transducer. Furthermore the power density of the redesigned HA4VSO was increased by 36%, compared to the standard A4VSO, by significantly increasing the self-priming speed.

On the other side of the application range, in lower power mobile applications such as small tractors, forklift and skid steer loader, there is an increasing demand for less exhaust emissions and better fuel economy. The energy saving potential by changing from a hydraulic system with constant hydraulic pumps to variable hydraulic pumps is already proven on high power applications. By developing the variable axial piston pump A1VO to the requirements of lower horse power application, it is now also possible to realize such savings in lower horse power applications.

Furthermore efficiency of the pump itself can be improved. An example of this is shown by way of the new A4 series 33.

3-2 Customer focused development of a variable bent-axis pump/motor for open circuit hydrostatic transmissions, e.g. in hydraulic hybrid drives

Conny Hugosson, Parker Hannifin Manufacturing Sweden AB, Sweden

The paper presents the development methodology of a hydrostatic pump/motor for use in Parker Hannifin's advanced series hydraulic hybrid transmissions for medium and heavy duty commercial vehicles. With Parker's established bent-axis pump/motor technology for heavy duty mobile applications as a basis, it describes the main stages of further development and qualification for demanding automotive main drive transmissions. Parker's APQP based, customer focused product development model was employed for this development which resulted in the variable bent-axis pump/motor C24 for open circuit hydrostatic transmissions.

Positive customer results from a large fleet of in-service refuse collection trucks and parcel delivery vans with Parker advanced hydraulic hybrid drive systems using C24 pumps/motors serve as evidence of Parker's product development model effectiveness. High reliability, good fuel economy, increased productivity and long brake life of the vehicles can directly be traced back to the streamlined, front-loaded and iterative development model.

3-3 The control of an open-circuit, floating cup variable displacement pump

Peter Achten, INNAS, Netherlands

The floating cup principle is a general hydrostatic principle for both constant and variable displacement pumps and motors, as well as for hydraulic transformers. In this paper, the focus will be entirely on the control of the displacement of the variable 28 cc Floating Cup pump (FCVP28). The floating cup principle features two opposed swash plates, for which both angular positions need to be controlled in order to cover the entire range from zero to full displacement. The results of both extended numerical analysis as well as simplified linearized models will be compared to test results on a 28 cc FCVP. Special emphasis will be on the dynamic behaviour of the displacement control.

5-1 Tribolayer Formation on Bronze CuSn12Ni2 in the Tribological Contact between Cylinder and Control Plate in an Axial Piston Pump with Swashplate Design

Andreas Paulus, Bosch Rexroth AG, Germany

The present study investigates the formation of tribolayers on bronze CuSn12Ni2. Two different test rigs are used, of which one is a sliding bearing test rig in order to perform lubricated thrust bearing tests. Bronze CuSn12Ni2 is used for the sliding elements and the counter body is made of C45 steel. In addition to that, an axial piston pump test rig was used to determine the transferability of the results to the axial piston pump. The test conditions are set up in a way that the tribological loads in the contacts are similar to each other.

Changes in the subsurface morphology and the chemical composition of the tribolayer were analysed using electron probe micro analysis (EPMA), transmission electron microscopy (TEM), energy dispersive X-ray spectroscopy (EDS) and X-ray photoelectron spectroscopy (XPS). Focused ion beam (FIB) milling was used to prepare site-specific TEM foils from the wear track. The formation of a nanoscale tribolayer was associated with reduced wear, which leads to low leakage in the axial piston pump. This tribolayer is enriched with oxygen, sulfur and zinc, which is an effect of tribochemical reactions of environment molecules and surface molecules.

5-2 A Flow Control System for a Novel Concept of Variable Delivery External Gear Pump

Andrea Vacca, Purdue University, USA

This paper describes a novel concept for a low cost variable delivery external gear pump (VD-EGP). The proposed VD-EGP is based on the realization of a variable timing for the connections of the internal displacement chambers with the inlet and outlet ports. With respect to a standard EGP, an additional element (slider) is used along with asymmetric gears to realize the variable timing principle. Previously performed tests confirmed the validity of the concept, for a design capable of varying the flow in the 65%-100% range.

Although the VD-EGP concept is suitable for various flow control system typologies (manual, electro-actuated, hydraulically flow- or pressure- compensated), this paper particularly details the design and the test results for a prototype that includes both a manual flow control system and a pressure compensator. Flow vs pressure and volumetric efficiency curves are discussed along with transient (outlet flow fluctuation) features of the VD-EGP.

5-3 Brimming bubbles? On an Innovative Piston Design of Dosing Pumps

Axel Müller, Thomas Magnete GmbH, Germany

For delivery, dosing and pressure control of fluids in mobile and stationary applications electromagnetically operated piston pumps are an established solution. The volume per stroke is exactly defined by the geometry. Nevertheless cavitation, more likely with the new fuel blends containing a high proportion of ethanol [1], deteriorates the dosing precision of the liquid portion.

One important criterion of precise metering is the transport of the liquids through the reciprocating piston pump without transferring bubbles. Especially, pumping in the range of vapour pressure of gasoline fuels implies challenges for precision. The objective of this work is revealing potential sources of reduced cavitation by optimising the design. For doing so, optical investigations have been applied. In addition to this, cavitation can be diminished controlling the piston's travel externally.

The second important item covers pumping of degenerated fluids even without negative effects on the pump's performance. Up to now, wide, inefficient gaps or high force surplus are necessary. A new helix-design [2] has been investigated and built up in order to reduce the described effort. The effects coming with the helix allow a permanent rinsing of the stressed surfaces, leading to lubrication and lower temperature loads. The results are shown in simulation, fundamental tests and is validated in practical pump operation.

5-4 The Impact of Micro-Surface Shaping of the Piston on the Piston/Cylinder Interface of an Axial Piston Machine

Ashley Wondergem, Purdue University, USA

Axial piston machines of the swashplate type are commonly used in various hydraulic systems and with recent developments in displacement control, it is essential to maximize their efficiency further reducing operation costs as well as improving performance and reliability. This paper reports findings of a research study conducted for the piston-cylinder interface utilizing a novel fluid structure thermal interaction model considering solid body deformation due to thermal and pressure effects in order to accurately predict the transient fluid film within the gap. A large reduction in energy dissipation is possible due to reduced clearances allowable due to the surface shaping of the piston resulting in a reduction in leakage. From this study, it is shown that surface shaping of the piston in combination with a reduced clearance is not only beneficial by improving the efficiency of a machine, but also increases the reliability and the performance of the machine as the load support is enhanced.

5-5 Bulk Modulus and Traction Effects in Hydraulic Pump and Motors

Paul Michael, Milwaukee School of Engineering, USA

This paper describes an investigation into the effects of fluid bulk modulus and traction coefficient properties on piston pump flow losses and radial piston motor torque losses through experimentation, modelling and simulation. Synthetic ester, high bulk modulus, multi-grade, and single grade mineral oils were evaluated. The high bulk modulus fluid exhibited 20% lower pump case and compensator flow losses than a conventional mineral oil of the same viscosity grade. Low traction coefficient fluids reduced the low-speed torque losses of the radial piston motor by 50%. Physical models for pump case flow and motor torque losses were derived from the experimental data. Field data was collected from a hydraulically propelled agricultural machine. This data was used to model fluid performance in the machine. The simulation results predict that at an operating temperature of 80°C, optimizing the bulk modulus and traction coefficients of the fluid could reduce flow losses by 18% and torque losses by 5%. These findings demonstrate the potential of combining comprehensive fluid analysis with modeling and simulation to optimize fluids for the efficient transmission of power.

5-6 Energy efficiency improvement by the application of nano-structured coatings on axial piston pump slippers

Giuseppe Rizzo, IMAMOTER – C.N.R, Italy

Axial piston pumps and motors are widely used in heavy-duty applications and play a fundamental role in hydrostatic and power split drives. The mechanical power losses in hydraulic piston pumps come from the friction between parts in relative motion. The improvement, albeit marginal, in overall efficiency of these components may significantly impact the global efficiency of the machine. The friction between slipper and swash plate is a functional key in an axial piston pump, especially when the pump (at low rotational speed or at partial displacement) works in the critical areas where the efficiency is low. The application of special surface treatments have been exploited in pioneering works in the past, trying different surface finishing or adding ceramic or heterogeneous metallic layers. The potential of structured coatings at nanoscale, with superhydrophobic and oleophobic characteristics, has never been exploited. Due to the difficulty to reproduce the real working conditions of axial piston pump slippers, it has been made a hydraulic test bench properly designed in order to compare the performance of nano-coated slippers with respect to standard ones. The nano-coated and standard slippers have been subjected to the following working conditions: a test at variable pressure and constant rotational speed, a test at constant pressure and variable rotational speed. The comparison between standard and nano-coated slippers, for both working conditions, shows clearly that more than 20% of friction reduction can be achieved using the proposed nano-coating methodology.

Abstracts: Group 4 - Thermal Behaviour

4-0 General Lecture: Thermo Energetic Design of Machine Tools and Requirements for Smart Fluid Power Systems

Christian Brecher, RWTH Aachen University, Laboratory for Machine Tools and Production Engineering (WZL), Germany

Modern production systems have to allow high performance cutting processes in a flexible production system environment at a high level of accuracy. The final workpiece accuracy is mainly influenced by the thermo-elastic behavior of the machine tool and can be improved by additional measures, compensation strategies and an optimized machine design. These measures are often implemented as stand-alone solutions. According to the Industry 4.0 all information should be connected in a single model of the actual machine state to increase machining accuracy. It is therefore necessary to integrate upcoming smart fluid power systems into the machine network.

4-1 Thermo-energetic Analysis of the Fluid Systems in Cutting Machine Tools

Juliane Weber, TU Dresden, IFD, Germany

Controlling the thermo-elastic behavior of tooling machines can only be achieved by systematic analysis, characterization and design of their fluidic system. In the first stage of this project, fundamental work was done to develop simulation methods for the calculation of the thermodynamic behavior of a representative example of a milling machine and each of its components. With experimental and numerical data it was proven, that significant improvement can be achieved by a proper design of heat transfer conditions of the fluidic system. To correct and counterbalance thermo-energetic effects, it will be necessary to develop new structures of the tooling machines systems which ensure the temperature-control of local subsystems in dependence of the actual working process. The work which is documented in this paper deals with the thermodynamic behavior of the motor spindle.

4-2 Comparison of Heat-Properties and its Implications between Standard-Oil and Bio-Oil

Marcel Rückert, RWTH Aachen University, Institute for Fluid Power Drives and Controls (IFAS), Germany

An important criteria for optimising hydraulic systems is their size. Especially for tanks and heat exchangers oil parameters as heat capacity and thermal conductivity have a big influence on the size. Additionally, various oils differ in their parameters. Accordingly, the heat capacity and thermal conductivity need to be known. However, little research has been done. Data-sheets usually do not provide any thermal data. In this paper, the thermal conductivity is measured for varying types of hydraulic oils. The thermal conductivity is determined by a newly designed test-rig measuring the radial temperature difference in a tube at a quasi-static state using a constant heat flux. Thus, an overview over the thermal conductivity of different oils is achieved. Based on the results, a comparison between different types of fluid is made.

4-3 Prediction of the thermo energetic behaviour of an electrohydraulic compact drive

Sebastian Michel, TU Dresden, IFD, Germany

Due to good energy-efficiency of electrohydraulic compact drives a cooling aggregate often is not installed. The prevailing operating temperature is governed by the complex interaction between dissipative heat input and passive heat output. This paper highlights the simulation of the thermo-energetic behaviour of an electrohydraulic compact drive by means of a lumped parameter model in order to predict the operating temperature. The developed thermo-hydraulic model is validated against measurements utilising thermoelements and a thermographic camera to capture temperature. It shows that the thermoenergetic behaviour of the demonstrator is predicted sufficiently precise in order to support development, optimisation and examination of possible fields of application of electrohydraulic compact drives.

4-4 A Thermal analysis of Direct Driven Hydraulics

Tatiana Minav, Aalto University, Finland

This paper focuses on thermal analysis of a direct driven hydraulic setup (DDH). DDH combines the benefits of electric with hydraulic technology in compact package with high power density, high performance and good controllability. DDH enables for reduction of parasitic losses for better fuel efficiency and lower operating costs. This one-piece housing design delivers system simplicity and lowers both installation and maintenance costs. Advantages of the presented architecture are the reduced hydraulic tubing and the amount of potential leakage points. The prediction of the thermal behavior and its management represents an open challenge for the system as temperature is a determinant parameter in terms of performance, lifespan and safety. Therefore, the electro-hydraulic model of a DDH involving a variable motor speed, fixed-displacement internal gear pump/motors was developed at system level for thermal analysis. In addition, a generic model was proposed for the electric machine, energy losses dependent on velocity, torque and temperature was validated by measurements under various operative conditions. Results of model investigation predict ricing of temperature during lifting cycle, and flattened during lowering in pimp/motor. Conclusions are drawn concerning the DDH thermal behavior.

Abstracts: Group 6 - Industrial Hydraulics

6-1 Consistent automation solutions of Electrohydraulic Drives as contribution to Industry 4.0

Albert Köckemann, Bosch Rexroth AG, Germany

Electrohydraulic drives are primarily used whenever a low power/weight ratio, a compact build and/or large forces are required for individual applications. These drives are often used together with electric drive technology in machines. However, in terms of automation, unlike electric drives, electrohydraulic drives are still largely connected via analog interfaces and centralized closed control loops today. To compensate for this competitive disadvantage of hydraulic drive technology and, at the same time, significantly enhance its performance and diagnostics capability, a consistent automation solution has been developed that can be configured for both centralized and decentralized solutions. This contribution firstly gives an overview over this complete solution already available and its classification in the automation world. In a second step, the subset of decentralized drive solutions contained therein is presented in more detail and their benefits are explained on the basis of some exemplary applications.

6-2 Adaptive process control for stabilizing the production process

Reinhard Schiffers, KrausMaffei Technologies GmbH, Germany

Plastic injection moulding machines are a positive example of the possibilities in terms of performance and energy efficiency of modern hydraulic drives technology. In addition to the performance and energy efficiency of the machines, the quality of the plastic mouldings and an easy to use machines control is the focus. To ensure a constant plastics part quality the set process parameters of the injection moulding machines are kept constant by appropriate closed loop control strategies today. Assuming a constant quality of the processed plastic raw material, this strategy is effective. If it comes to a qualitative variation in the processed plastics, which often leads to a change in viscosity of the plastics melt, keeping processing parameters constant will not lead to a constant quality of the moulded parts. The deviations in the plastics viscosity have such a great influence on the moulding process that the relevant process parameters have to be adjusted manually in many cases. Often the stroke of the reciprocating screw system has to be adapted to reach a constant filling volume of the cavity and therefore avoid burr formation or short shots. In this paper an approach for adaptive process control is introduced. This control loop is able to correct the set points of specific machines parameters online within the production cycle and therefore is able to avoid changes in the produced parts quality.

6-3 On the compensation of dynamic reaction forces in stationary machinery

Tobias Radermacher, TU Dresden, IFD, Germany

This paper studies a method for active electrohydraulic force compensation in industrial scale high power applications. A valve controlled cylinder drive moves a mass using the force of inertia to compensate for the reaction forces of an industrial scale process. Two strategies for force compensation are developed and investigated in a demonstrator aiming to significantly reduce the excitation of a 160 ton clamping unit of an injection moulding machine. Results of the different strategies are shown and evaluated. Advantages and drawbacks of the developed electrohydraulic force compensation are discussed.

6-4 Improvement of hydraulic control quality for deep drawing presses through retrofit

Marcus Helmke, TRsystems GmbH , Germany

Retrofits of hydraulic and mechanical deep drawing presses often stop with the exchange of the electrical and the hydraulic parts. But that is only half the job. The use of high definition control electronics, faster CPUs and more dynamic hydraulic actuators, offers the opportunity of redesigning the already existing control concepts of the press. In this paper we present how the performance of the press, i.e. the control quality, can be increased for hydraulic ram and cushion axes. The improvement in control quality is achieved through the use of intelligent closed-loop and open-loop-control algorithms. Therefore, creasing and crack formation can be reduced, since enhancements in control quality have direct influence on the quality of the forming process. Results will be shown for hydraulic drawing cushion control, i.e. pressure control, as well as for hydraulic ram control, i.e. position, velocity and parallelism control. We present findings for hydraulic cushion control of a mechanical press type Arisa S-4-1600-470-230-LDE (link-drive press with 10 hydraulic cushions) and for ram- / cushion-control of hydraulic press type Müller-Weingarten ZE2100 (multi-curve press with 8-point cushion).

6-5 Potentials of Speed and Displacement Variable Pumps in Hydraulic Applications

Johannes Willkomm, Bosch Rexroth, Germany

Speed and displacement variable pumps offer a degree of freedom for process control. As a certain operation point can be supplied by different combinations of drive speed and pump displacement intelligent control strategies can address major issues like en-ergy efficiency, process dynamics and noise level in industrial applications. This paper will provide an overview of recent research and development activities to evaluate the named potentials.

6-6 Condition Monitoring for Hydraulic Power Units - the user-oriented Step into industry 4.0

Martin Laube, Bosch Rexroth AG, Germany

One of Bosch Rexroth's newest developments is the ABPAC power unit, which is both modular and configurable. The modular design of the ABPAC is enhanced by a self-contained Condition Monitoring System (CMS), which can also be used to retrofit existing designs. This dissertation shows how Industry 4.0-Technology provides special advantages for the diverse user profiles. Today, Hydraulic Power Units have either scheduled intervals for preventive maintenance or are repaired in case of component failures. Preventive maintenance concepts, until now, did not fully utilize the entire life expectancy of the components, causing higher maintenance costs and prolonged downtimes. Risk of unscheduled downtime forces the customer to stock an array of spare parts leading to higher inventory costs or in the event a spare is not readily available, the customer may encounter long delivery times and extended downtime. Bearing this in mind, we've conceived the idea of a self-contained intelligent Condition Monitoring System including a predictive maintenance concept, which is explained in the following.

Abstracts: Group 7 - Hydraulic Components

7-0 General Lecture: Electrohydraulic servovalves – past, present, and future

Andrew Plummer, University of Bath, Department of Mechanical Engineering, UK

In 2016 it is 70 years since the first patent for a two-stage servovalve was filed, and 60 years since the double nozzle-flapper two-stage valve patent was granted. This paper reviews the many alternative servovalve designs that were investigated at that time, focusing on two-stage valves. The development of single-stage valves – otherwise known as direct drive or proportional valves – for industrial rather than aerospace application is also briefly reviewed. Ongoing research into alternative valve technology is then discussed, particularly focussing on piezoelectric actuation and the opportunities afforded by additive manufacturing.

7-1 A new energy saving load adaptive counterbalance valve

Bernd Zähe, Sunhydraulik Deutschland, Germany

The paper shows standard circuits with load reactive and non load reactive counterbalance valves. A Matlab simulation based on a linear model for the circuit with load reactive counterbalance valves shows what parameters have a significant influence on the stability of the system. The most important parameters of the counterbalance valve that influence the stability are pilot gain and relief gain. The factors describe how pilot pressure and load pressure affect the flow across the counterbalance valve. A new counterbalance valve (patent pending) has the pilot gain and relief gain required for stability only in operating ranges that require the parameters for stability. When the load is not moving or the counterbalance valve is not required for positive (non overrunning) loads, the new valve has a higher pilot ratio, which means that the valve opens further at lower inlet pressures. The new counterbalance valves saves about 30% power compared with a standard counterbalance valve that has the same parameters for stability when it is lowering an overrunning load. The standard counterbalance can be replaced with the new load adaptive valve in the same cavity. The paper shows test results and the design of the valve.

7-2 Development of an Electronically Controlled Self-Teaching Lift Valve Family

Eneko Goenechea, Bucher Hydraulics AG, Switzerland

Other than mobile hydraulics and high voltage switchgears, Bucher Hydraulics is also involved in the less-known area of hydraulic lifts. In fact, Bucher Hydraulics did invent the electronically controlled lift valve in the 1970s. Since then, Bucher Hydraulics developed a wide line of products for hydraulic elevators, such as valves and power units. In 2012, this valve family included various sizes, pressure ranges, systems with constant motor speeds, inverter-driven motors, energy-efficient solutions with hydraulic counterweight, as well as customized solutions. As the common principle, all these solutions apply an electronic closed-loop control that uses a volumetric flow sensor and a proportional actuator. Since 2012, Bucher Hydraulics is substituting this valve family with a new generation, the iValve. Every iValve uses several self-teaching algorithms to adapt to its environment. Their on-board and cabinet electronics control solenoid currents and measure flow, pressure, and temperature. These features enable the iValve to self-monitor, to adapt to operating parameters, and to analyze and log information about itself and the attached system. This report on a highly specialized product is meant to provide inspiring insights.

7-3 Development of an innovative diaphragm accumulator design and assembly process

Thorsten Hillesheim, Freudenberg Sealing Technologies GmbH & Co. KG, Germany

Freudenberg Sealing Technologies has developed a new concept for the manufacture of diaphragm accumulators. Its advantages are a reduced need for components, fewer process steps, shorter assembly times, a higher level of product cleanliness, and an expansion of the product portfolio into additional fields of application. These diaphragm accumulators also weigh significantly less. This is opening up new opportunities for applications in the automotive and industrial fields. The assembly concept is based on a hermetically sealed pressure chamber in which the joining of the two housing halves with the help electromagnetic pulse technology (EMPT) as well as the filling of the gas side with nitrogen takes place in a single operation. In this way, downstream filling to generate the initial gas charge is no longer necessary.

7-4 Potential and application fields of lightweight hydraulic components in multi-material design

Andreas Ulbricht, CG Rail GmbH, Germany

Hydraulic systems are used in many fields of applications for different functions like energy storage in hybrid systems. Generally the mass of hydraulic systems plays a key role especially for mobile hydraulics (construction machines, trucks, cars) and hydraulic aircraft systems. The main product properties like energy efficiency or payload can be improved by reducing the mass. In this connection carbon fiber reinforced plastics (CFRP) with their superior specific strength and stiffness open up new chances to acquire new lightweight potentials compared to metallic components. However, complex quality control and failure identification slow down the substitution of metals by fiber-reinforced plastics (FRP). But the lower manufacturing temperatures of FRP compared to metals allow the integration of sensors within FRP-components. These sensors then can be advantageously used for many functions like quality control during the manufacturing process or structural health monitoring (SHM) for failure detection during their life cycle.

Thus, lightweight hydraulic components made of composite materials as well as sensor integration in composite components are a main fields of research and development at the Institute of Lightweight Engineering and Polymer Technology (ILK) of the TU Dresden as well as at the Leichtbau-Zentrum Sachsen GmbH (LZS).

7-5 CFD Simulation and Measurement of Flow Forces Acting on a Spool Valve

Patrik Bordovsky, RWTH Aachen University, Institute for Fluid Power Drives and Controls (IFAS), Germany

Directional control valves are widely used in hydraulic systems to control the flow direction and the flow rate. In order to design an actuator for such a valve a preliminary analysis of forces acting on the spool is necessary. The dominant axial force is the so called steady flow force, which is analysed within this study. For this purpose a 2/2-way spool valve with a sharp control edge was manufactured and investigated. CFD simulations were carried out to visualize the fluid flow inside the valve. The measured and simulated axial forces and pressure drops across the test valve are compared and show good qualitative correlation. However, the simulated values of axial forces are in average by 32 % lower compared with the measured ones. Therefore, the components of the axial force were scrutinized revealing a dominance of the pressure force acting on ring areas in the spool chamber. Although CFD simulations are preferably used to save resources, the results of this study emphasise the importance of the experiments.

Group 1: Novel System Structures

Novel System Architectures by Individual Drives

Prof. Dr.-Ing. Jürgen Weber

Dipl.-Ing. Benjamin Beck

Dipl.-Ing. Eric Fischer

M. Sc. Roman Ivantysyn

Dipl.-Ing. Giacomo Kolks

Dipl.-Ing. Markus Kunkis

Dr.-Ing. Harald Lohse

Dipl.-Ing. Jan Lübbert

Dipl.-Ing. Sebastian Michel

Dipl.-Ing. Markus Schneider

M. Sc. Linart Shabi

Dipl.-Ing. André Sitte

Dipl.-Ing. Juliane Weber

Institute of Fluid Power (IFD), Technische Universität Dresden, Helmholtzstraße 7a,
01069 Dresden, E-Mail: mailbox@ifd.mw.tu-dresden.de

Dipl.-Ing. Johannes Willkomm

Bosch Rexroth AG, Bgm.-Dr.-Nebel-Straße 2, 97816 Lohr am Main,
E-Mail: johannes.willkomm@boschrexroth.de

Abstract

Measures of individualization and integration offer a great potential for further development and optimization in hydraulic drive technology. Advantages are seen especially for energy efficiency and functionality. These potentials motivate current research activities for displacement controlled systems and for valve controlled structures. For the latter, the focus lies on strategies of independent metering. Furthermore, expected challenges for the future are discussed.

KEYWORDS: individual drives, displacement control, independent metering

1. Introduction

Hydraulic drive technology has major advantages regarding e.g. power density, robustness and flexibility of system design as well as motion control. However, other competing drive technologies like electromechanical linear drives have also undertaken massive further developments during the last decades. Hence, to remain in a winning position compared to electromechanical drives or to achieve even more potentials out of the intelligent combination of both technologies in the future, there is an everlasting need for innovation in fluid power.

Over the last century, electromechanical drive technology has made an enormous step forward from centralized power sources with inflexible belt transmission to application-

specific individual drives, in which power electronics, electric motor und mechanical transmission are highly integrated. In a somewhat provocative point of view, classical valve controlled hydraulic systems with a central power supply unit can be seen as counterpart to those ancient centralized mechanical systems. However, in many applications this kind of system structure is still state of the art in present days. Thus, it becomes obvious that there is still a lot of potential for measures of individualization and integration in practical utilization of fluid power technology. The main advantages would be an improved energy efficiency and an extended functionality. In the author's point of view it is necessary to continue consequently the process of innovation and optimization for individual and decentralized hydrostatic architectures.

Strategies for individualization have already been scientifically investigated for both, displacement controlled and valve controlled systems. This contribute gives an overview over the status quo with the focus on research activities. At the end, some challenges are discussed, which should be topic of research and development in the near future.

2. Individualized displacement control

2.1. Individualization levels of displacement controlled actuators

Indisputably, primary displacement control features many benefits, predominantly good energy efficiency, but also low noise, low cooling effort, etc. For technological reasons it is evident that with primary displacement control only one actuator can be controlled by one pump at a time. Nevertheless, different levels of individualization are in use in practice – dependent on the requirements and constraints of the application.

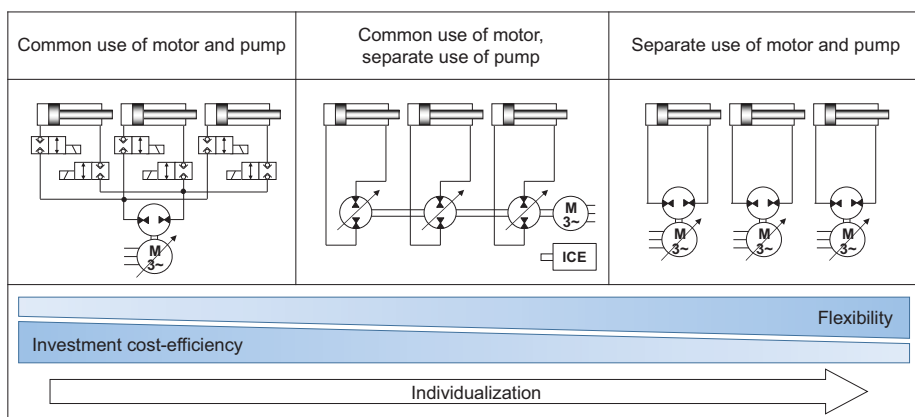


Figure 1: Individualization levels of displacement controlled actuators

The schematics in **Figure 1** give an overview of the levels of individualization of displacement controlled actuators. The known principles are classified with regard to their individual use of pumps and motors. Please note that instead of the depicted speed controlled pumps also variable displacement pumps are feasible.

The lowest level of individualization is the common use of one motor-pump-unit for the actuation of a certain number of actuators. This kind of circuit is restricted to applications, in which actuators perform a strictly sequential working cycle, or in other words, never work together at the same time. In this case, the speed controlled pump can be connected to various actuators by means of switching valves. In particular, in industry some applications exist that show a strictly sequential working process. /1/ for example published a concept for an injection-molding machine, in which all motion tasks (five drives) are managed with only two motor-pump-units. The effort on components decreases significantly. Also in mobile machinery, pump switching control has been investigated in order to reduce the amount of necessary pumps /2/.

The next level of individualizations is the separate assignment of a variable displacement pump to each actuator while maintaining a common motor. Corresponding circuits can be found primarily in mobile machinery, where a central combustion engine is installed and parallel motion tasks are demanded inherently. Extensive research on this subject is conducted by Professor Ivantysynova et al. /3/. This architecture is especially beneficial in combination with other energy efficient drive technologies, such as power split transmissions and hybrid systems. The overall energy saving potential was demonstrated with the prototype vehicle "Green Wheel Loader", which was jointly developed by an industrial consortium and the IFD within the research project TEAM /4/.

The highest level of individualization and grade of flexibility feature the systems that use a separate motor-pump-unit for every single actuator. However, those configurations show also the highest effort on components. They can be found in both, industrial and mobile machinery. In high power applications, even the assignment of two motor-pump-units to one single actuator is common /5/. Research on the characteristics and performance of speed variable pump circuits was carried out intensively, e.g. /6, 7, 8, 9/.

2.2. Electrohydraulic compact drives

In the context of individualization of hydraulic drive structures, a trend to constructive integration of components and decentralization of circuits can be observed, in particular for the systems with a separate use of motor and pump. The highest grade of integration

is present in electrohydraulic compact drives, which are fully self-sufficient and feature mechanical and electrical interfaces only. The basic configuration is shown in **Figure 2**.

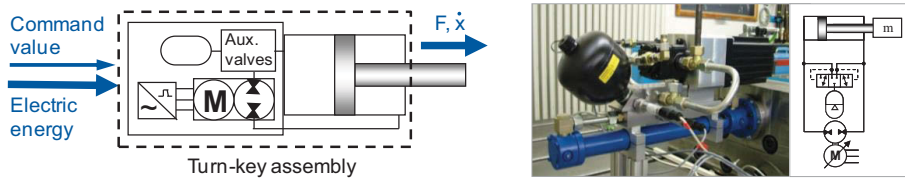


Figure 2: Basic configuration (left) and demonstrator (right) of an electrohydraulic compact drive

Electrohydraulic compact drives combine many of the inherent advantages of hydraulic drive technology, i.e. reliability, robustness, large forces, high transmissions, good overload protection, easy gear change, ease of use, low maintenance effort, compact design and easy 'plug and play' connectivity. Further concept specific key properties are hermetic sealed hydraulic circuit, very small oil volume, lifespan filling of oil and no active cooling aggregate. A demonstrator of an electrohydraulic compact drive, which was investigated in /10/, is exemplarily illustrated in Figure 2.

Historically, electrohydraulic compact drives – also called electric-hydrostatic actuators (EHA) – emerged in aircraft industry in the early 1990s /11, 12/. Those drives were developed for the special requirements of aircrafts and are an inherent part in this branch nowadays – for example in the Airbus A380 /13/. It was to take until the late 2000s, until compact drives were adapted to the requirements of industrial applications, which are mainly cost-efficiency and the use of a single rod cylinder. In recent years, a number of commercial products have been introduced to the market.

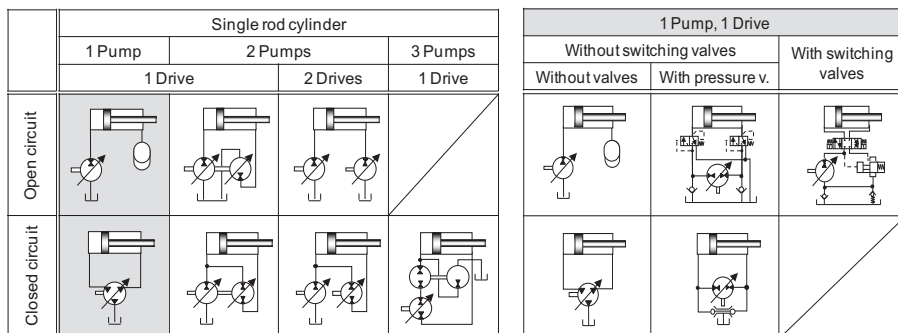


Figure 3: Pump control of a single rod cylinder, general (left) and in particular with one pump (right) /10/

In case of a pump controlled single rod cylinder the balancing volume flow has to be managed. The systematics in **Figure 3** gives an overview of possible solutions with a particular regard to a compact and reasonably priced design /10/. Static and dynamic behavior of favored circuits were investigated by /6, 9, 10, 14, 15, 16, 17, 18, 19/. It could be shown that electrohydraulic compact drives are able to achieve a similarly good energy efficiency as electromechanical drives /10/.

Due to the concept specific conditions, new challenges arise in context with electrohydraulic compact drives. Primarily, the thermo-energetic behavior has to be mentioned. Since these drives are not equipped with an active cooling aggregate, the knowledge and prediction of the thermo-energetic behavior is of high significance – in order to guarantee a temperature stable process or to examine possible fields of application without elaborate experiments. The prediction of the thermo-energetic behavior by means of lumped parameter simulation is targeted by /20, 21/ for aviation related and by /22, 23/ for industrial related applications. Furthermore, investigations on oil aging and wear in electrohydraulic compact drives are carried out at present.

2.3. Benefits of speed and displacement variable pumps

With a demand for energy efficient production, displacement controlled drive systems have established in the last decades. Besides pumps with variable displacement, the use of speed variable pump systems could proof potential energy savings in a wide area of applications /10, 24/. In addition to energy efficiency, process dynamics plays a crucial role in industrial applications. Shorter cycle times directly increase the production volume and therefore contribute to the profitability of a production machine /25/.

Combining a variable displacement pump with a speed variable motor results in a so-called HydroGear system /26/. The two set values pump displacement and pump speed allow a decoupling of volume flow and drive speed. The resulting degree of freedom can be efficiently used for process control /9/.

Recent research demonstrates the potentials of HydroGear systems in terms of energy efficiency and process dynamics /26, 27/. By means of model predictive methods, the control task can be transformed into a mathematical optimization problem. Regarding optimum energy efficiency, the overall system losses will be used as an objective function while any system limits can be considered as additional constraints. The solution will finally provide the optimum set values for drive speed and pump displacement, respectively. **Figure 4** illustrates the proposed concept of model predictive optimization.

Thereby the hydraulic application is abstracted by specifying pressure and volume flow for a given process cycle.

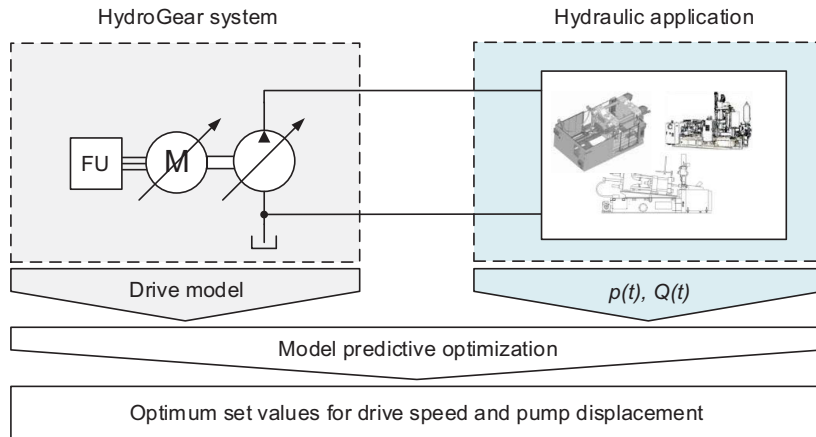


Figure 4: Model predictive optimization of HydroGear systems

In measurements, HydroGear systems reach energy savings of 20 % and more in comparison to pure displacement variable or pure speed variable pumps. Experiments further showed that by considering the mutual influences of motor and pump dynamics the model predictive concept is able to improve the rising time for a set point jump of volume flow while lowering the maximum necessary pump speed at the same time [27], see **Figure 5**.

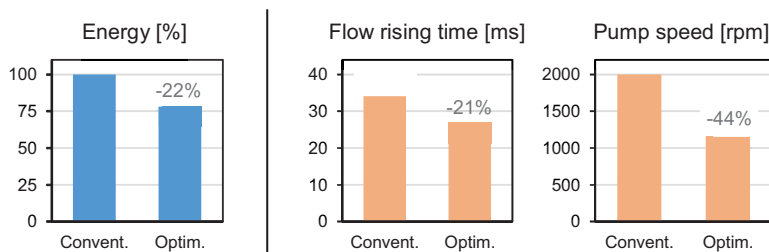


Figure 5: Potentials of HydroGear systems

To match different industrial needs, HydroGear systems are scalable in costs and performance. Besides asynchronous and synchronous motors, various low cost to high-end actuator systems of the pump displacement are available. Regarding different applications like hydraulic power units, presses or injection molding machines the model predictive approach allows to consider individual requirements. For example, the avoidance of critical speed ranges or the surveillance of security-relevant system values

can be efficiently integrated into the optimization problem. Thus, future studies have to focus on user-friendly methods to combine multiple objectives into one single control concept.

2.4. Application examples

2.4.1. Hydraulic deep drawing presses

Hydraulic deep drawing presses are one of the main applications of stationary hydraulics. These machines produce sheet metal parts mainly for cars but also for other purposes, e.g. domestic appliances. Deep drawing presses commonly have two main drives: the slide drive, which is responsible for the forming movement, and the die cushion drive, which controls the material flow during deep drawing, see **Figure 6**.

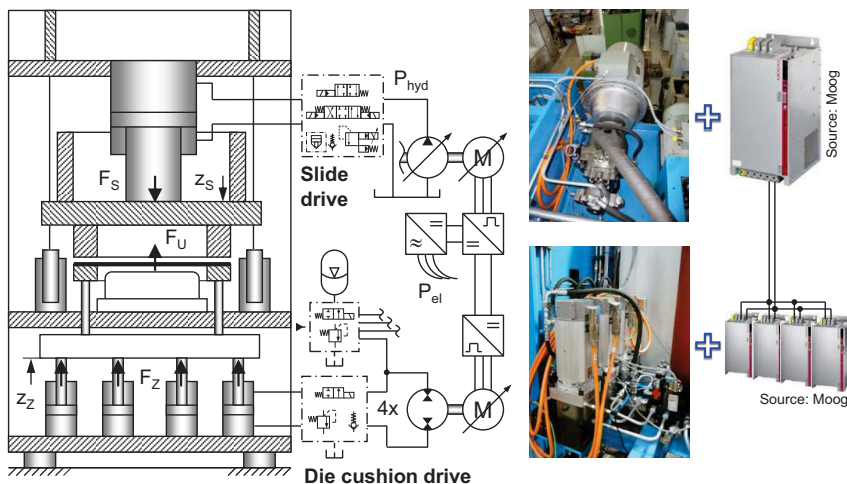


Figure 6: Hydraulic deep drawing press with pump controlled die cushion drive

The slide drive of production presses is mostly a pump controlled system with variable-displacement pumps, which are driven by asynchronous motors running at constant speed. Some additional valves are necessary for safety reasons, for controlling the moving direction of the slide and for the limitation of the system pressure. Due to the growing availability and decreasing costs of high power frequency converters and servomotors, there are also slide drive systems with speed variable motor-pump-units available today [28]. The main advantage is a better energy efficiency, especially in partial load and in idle. Furthermore, the noise emissions can be reduced significantly.

The die cushion drive is normally a valve controlled system, because it has to fulfill highest demands in dynamics and precision of closed-loop pressure or force control. The

main disadvantage of valve controlled die cushion systems is their high energetic loss. The latter can typically reach up to 30 % of the machine's overall energy consumption during the forming process. This loss can be avoided by replacing the valve controlled die cushion drive by a pump controlled system. Because of the expected high energy savings, pump controlled die cushion drives have already been discussed in scientific literature for several times, for example in /29, 30, 31, 32/.

To proof the energy saving potential of those pump controlled systems, a research press was modified at the IFD. Figure 6 illustrates the chosen, new structure. The die cushion drive, which was valve controlled formerly, has now four motor-pump-units, each consisting of a highly dynamic brushless servomotor and a constant volume radial piston pump. Frequency converters control the motor speed. The die cushion drive and the slide drive, which was also equipped with a frequency converter, have a common intermediate circuit. Hence, the electric energy, which is recuperated from the die cushion during deep drawing, is directly transferred into the slide motor. A low-pressure hydraulic accumulator is linked to the piston rod sides of the die cushion cylinders in order to compensate the stroke-dependently changing cylinder volumes. The new pump controlled die cushion drive completely fulfills the demands, regarding the quality of closed-loop force and position control. The dynamic behavior is even comparable to valve controlled systems. In a typical deep drawing process, the measured energy savings for the whole machine reach about 30 % in comparison with the original, unmodified system /33/.

2.4.2. Implement functions of mobile working machines

In contrast to stationary machinery, the implement functions of mobile working machines are characterized by highly variable operating conditions as well as parallel actuation of multiple consumers, which are directly controlled by the machine operator. Therefore, conventional valve controlled drive systems usually feature low energy efficiency due to the inherent throttling losses and the simultaneous actuation of the valves' meter-in and meter-out control edges. Furthermore, mutual interference of the different functions can deteriorate machine's operability and performance.

By using displacement control for each individual function, these disadvantages can be evaded. Each actuator operates at its own load-dependent pressure level. The function's speed is controlled by altering the pump's displacement or rotational speed. **Figure 7** shows the two basic concepts of displacement control. Open circuit solutions need an additional switching valve besides an over-center pump to allow for 4-quadrant operation. In closed circuit architectures, this can be achieved by solely controlling the

pump. However, special measures are necessary to compensate the flow difference between the working ports when actuating a differential cylinder. Both systems offer load-independent control of the actuator velocity as well as the possibility to recirculate energy in case of aiding loads.

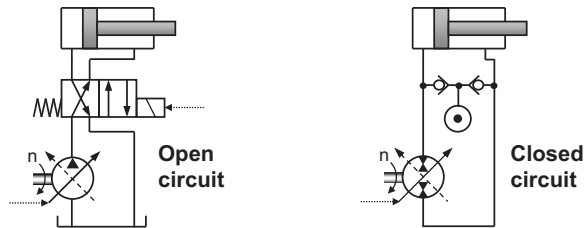


Figure 7: Basic concepts of displacement control

Extensive research has been carried out on displacement controlled systems so far. Rahmfeld and Ivantysynova proposed a closed circuit architecture and successfully applied it to a wheel loader's implement /34, 35/, its steering system /36/ and an excavator /14/. Heybroek investigated open-circuit solutions using a wheel loader /37/.

Recent research activities combine the approach of closed-circuit displacement controlled implement functions with novel energy efficient drive technology and innovative operating strategies in a large-size wheel loader /38, 39/.

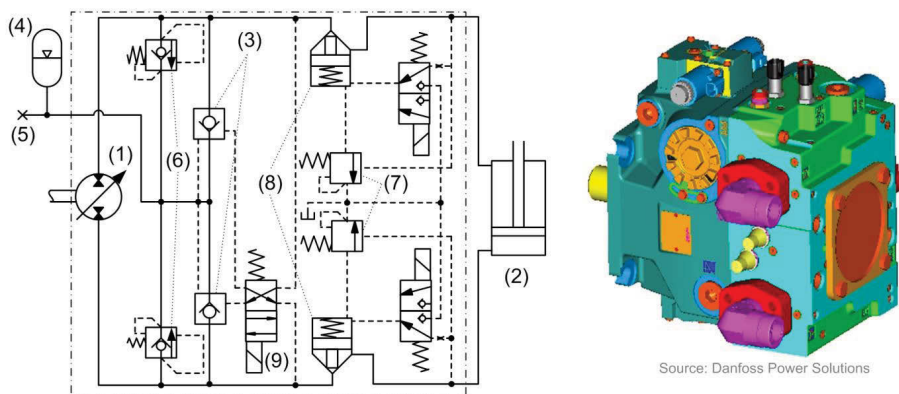


Figure 8: Schematic of a working function of the “Green Wheel Loader”

Figure 8 shows the schematic and packaging of the implemented hydraulic circuit for one implement function. The variable displacement unit's (1) flow directly drives the hydraulic cylinder (2) by varying displacement and rotational speed. The single-rod cylinder's differential volume is compensated by means of pilot-operated check valves (3) and a low-pressure accumulator (4). A low-pressure supply (5) compensates leakage

and delivers flow to the pump's control system. Additional functions, such as pressure limitation, primary (6) and secondary (7) pressure relief, load-holding (8) and float function (9) are also included. The necessary valves are directly integrated into the displacement unit.

Together with an optimized diesel engine, a power-split travel drive and a hydrostatic parallel hybrid the technology was implemented into a 24-t demonstrator machine and tested under realistic operating conditions, see **Figure 9**. The "Green Wheel Loader" showed the functionality and efficiency potential of the developed drive system. In reference tests, the prototype vehicle showed fuel savings of 10...15 % compared to a state-of-the-art series machine /4/.



Figure 9: "Green Wheel Loader" demonstrator vehicle during testing in a gravel pit

Furthermore an open circuit displacement control system was developed for a 290 t mining excavator. The standard open circuit valve controlled system was replaced with an innovative displacement control architecture with dynamic pump sharing. The proposed circuit is shown in **Figure 10** and resulted in simulated fuel savings of up to 40 % over a common digging cycle /40/. Today's machines already use several pumps to drive one actuator, so no additional pump installment was necessary. Due to the open circuit architecture there is no necessity for large accumulators to store the differential volume of the cylinders as would be necessary in a closed loop configuration. Furthermore the open circuit nature allowed for an easy integration of float valves that ensure a rapid lowering of the implement under aiding load and the flow relief to tank using discharge valves. With this set up the operator is manually able to choose between modes of high energy recovery, or lower cycle times.

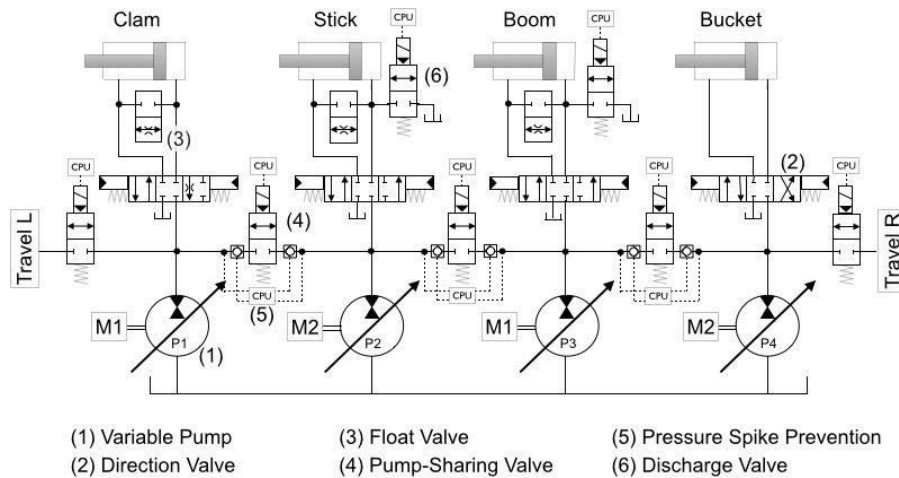


Figure 10: Circuit diagram of a 290 t mining excavator

3. Individualized valve control

3.1. Individualization levels of valve controlled actuators

Manufacturers of mobile as well as industrial machinery find themselves increasingly confronted with rising energy costs and stringent emission regulations. At the same time there is a constant demand for higher productivity and enhanced flexibility. Considering this, decentralized valve controlled systems with independent control edges offer a promising technical approach as an alternative to displacement controlled systems. With reference to the schematics in Figure 1, **Figure 11** gives a brief overview of the levels of individualization of valve controlled actuators. A distinction can be made regarding type and arrangement of the used valve technology.

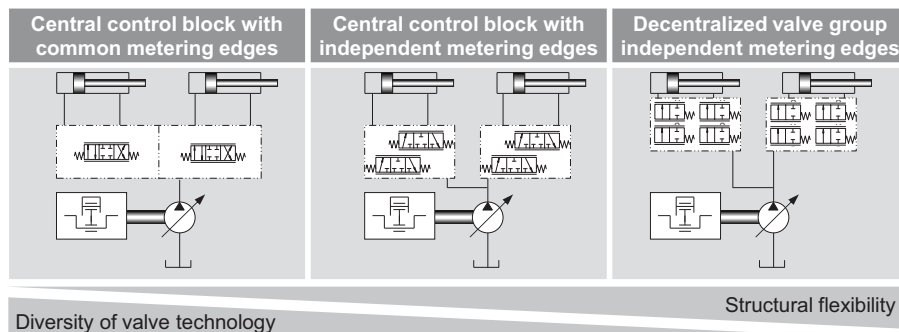


Figure 11: Individualization levels of valve controlled actuators

Individual metering refers to the opportunity of separate control of in- and outflow of the hydraulic working ports. The system topology opens up for differential modes of operation of the hydraulic consumers. These free flow paths are the most significant characteristic of independent metering (IM) systems allowing regeneration in many variants depending on the valve structure.

Beginning with possible valve arrangements, **Figure 12** gives a brief overview over possible structures. Equivalent implementations can be found in literature as well as numerous patents. The systematic decoupling of mechanical and functional constraints results in different hardware layouts. The circuit principles can be classified in those incorporating 3-way valves, 2-way valves mixed versions. In addition a functional decoupling is possible by applying switching valves for directional control in series to proportional valves for the metering function.

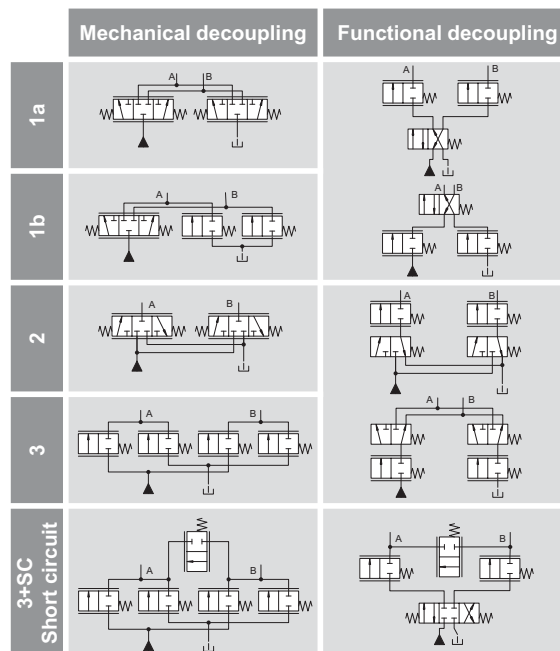


Figure 12: Different variants of valve structures

The decision which circuit principle is most suitable for the considered applications depends on various aspects like preferred valve technology and mounting conditions. The following potentials arise from the use of systems with independent metering edges:

- Independent control of inlet and outlet orifice
- energy-efficient operating modes (without reducing the valve resolution)

- Simplification of valve technology (2-way valve technology)
- Standardization of valve technology
- Functional integration (counterbalancing and metering)
- Flexible system configuration (decentralized arrangement)
- Transfer of functionality from hardware to software
- Advanced control features (oscillation damping, etc.)

To gain the maximum benefit with individual metering, the whole system layout which consists of valve structure, pump control, sensor equipment and overall control strategy, must be taken into account. In particular three different control strategies can be identified, see **Figure 13**. A direct flow control is uncommon since flow sensors are expensive and not robust enough for industrial use. Pressure differential control utilizing pressure compensators or pressure transducers are commonly used in mobile machines. Position or velocity control can be found especially in industrial applications.

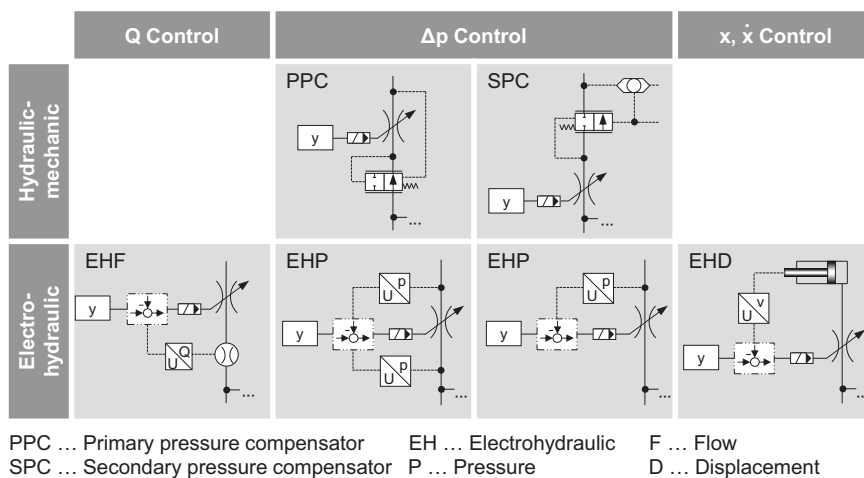



Figure 13: Possible control layouts for flow, pressure, differential pressure and position / velocity control

The resulting diversity of different layouts, structural complexity and expected high control effort still hinder a successful spread into industrial / commercial application.

In mobile applications there are load and movement conditions in several quadrants. Mechanically linked main spools for inlet and outlet side are therefore always a compromise between controllability of pulling loads and energy efficiency. An active load detection by means of sensors and electrohydraulics is only just beginning to be implemented. In industrial applications on the other hand, valve, supply, and control

specifications are often governed by demanding requirements regarding precision and dynamics of the hydraulic actuator. Most applications require closed loop control which demands a high degree of sensor implementation. The acceptance of sensors in hydraulic systems enables engineers to make full use of the benefits that independent metering incorporates through their naturally increased degree of freedom. Through the use of independent metering, diversification of functionality can be transferred to software, by exploiting the additional degrees of freedom. Thus, different control aims in a wide working area can be met using the same valve technology. Separate metering valves offer an opportunity to adapt to low loads despite high supply pressure by making use of regeneration flow paths. Thus, volume flow from the supply can be reduced significantly. The key differences between mobile and industrial applications are illustrated in **Figure 14**.



	Industrial Applications	Mobile Applications
Operation	<ul style="list-style-type: none"> • Specific, defined motion- and working cycles • automated processes 	<ul style="list-style-type: none"> • Wide spectrum of applications and operating conditions • Operator controlled functions
Requirements	<ul style="list-style-type: none"> • High dynamic requirements • High precision • Closed-loop controlled functions (mostly position, force) 	<ul style="list-style-type: none"> • Medium dynamic requirements • Open-loop controlled functions (mostly velocity) • Load compensation
Potentials and aims	<ul style="list-style-type: none"> • Adaption of pressure level • New control concepts • Robust control strategies 	<ul style="list-style-type: none"> • Simplification of control edge design • Simplification of valve- and system architectures • Additional functions (float)
	<ul style="list-style-type: none"> • Improvement of energy efficiency • Utilization of regeneration and recuperation potentials • Flexibility in system setup • Safety related functions 	

Figure 14: Comparison of industrial and mobile boundary conditions

3.2. Control strategies for independent metering structures

Independent metering structures involve increased degrees of freedom, compared with conventional valve drives. These can be turned into benefit by a multitude of different control approaches. Various control strategies have been applied to achieve the desired

motion characteristic and to attain secondary goals, such as energy efficiency. Basically, control approaches can be subdivided into three categories, see **Figure 15**. In the first category, one output variable such as cylinder velocity is controlled by an open loop strategy (*feed-forward control*). Here, the coupling of different control edges occurs through a coupling law, which can also consider system state information, such as load. The second category comprises a coupling law as well, with an outer-layer closed control loop ensuring command variable tracking of the target set variable (*closed-loop SISO control*). In the third category, the degrees of freedom of the system are used to control more than one target variable in closed-loop control (*closed-loop MIMO control*).

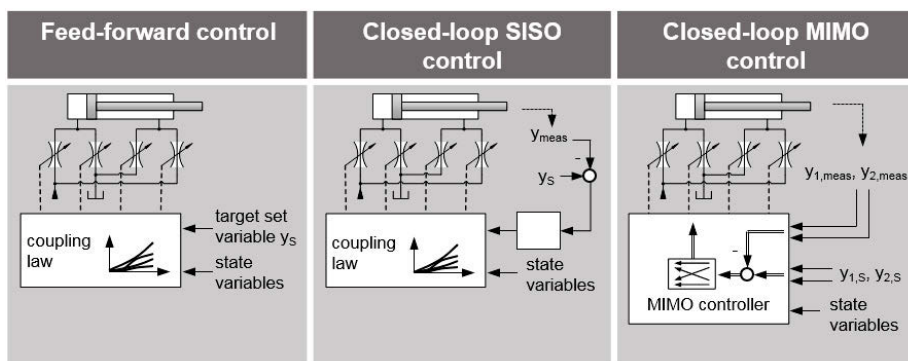


Figure 15: Control architectures of independent metering systems

Feed-forward control approaches have been investigated primarily for mobile applications. Focus has been put on detecting the load and adjusting the balance of meter-in versus meter-out in order to decrease the necessary supply pressure and avoid cavitation at the existence of overrunning loads. In /41/, Sitte and Beck propose the Flow Matching pump control algorithm in combination with meter-in pressure compensators for load compensation. The coupling law is defined by a closed-loop controller which keeps the pressure compensator in a wide open control range. This work, carried out at the IFD, is described in further detail in chapter 3.3.2. Another approach which uses pressure compensator spool positions is taken in /42/. Although the aforementioned approaches control cylinder speeds by means of pressure compensators, no direct speed measurement is carried out, thus being classified as open loop control concepts with regard to their primary target variables.

Closed-loop control concepts with only one controlled target variable are not a commonly adopted approach with separate metering valves. Closed-loop control requires an implementation of sensors and little extra effort in terms of components is needed for a full multiple-input multiple-output (MIMO) closed-loop system. An objective of MIMO

control which many researchers seek is to control both pressure level and motion of a hydraulic cylinder. Mattila and Virvalo /43/ show that supply pressure level can be reduced significantly using an input/output-linearization approach for the control of pressures on both sides of a cylinder, while motion accuracy is maintained. Similar results are shown in /44/ using an adaptive robust controller design. Bindel /45/ makes use of the independent manipulation of pressure level and motion for dynamically connecting various hydraulic consumers to different pumps with a flatness based control strategy.

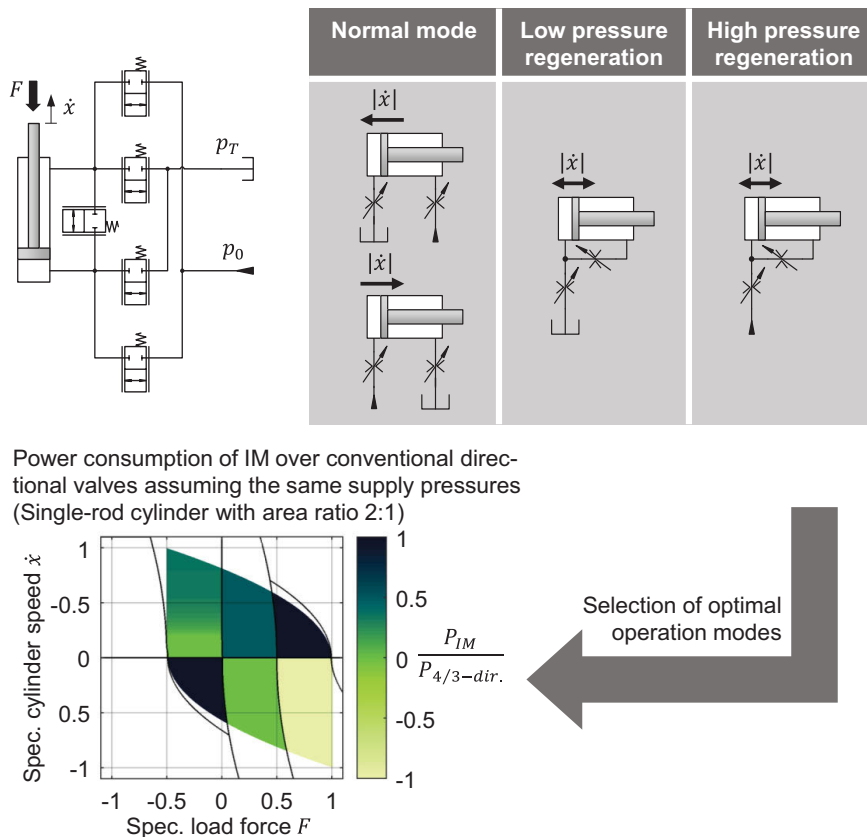


Figure 16: Generalized independent metering system and operation modes

Many independent metering structures allow different operation modes, shown in **Figure 16**. These modes allow a reduction of required pump flow at a given cylinder speed. At the IFD, a methodology to assess the potentials gained through optimal operation modes has been developed /46/. A smooth mode switching algorithm based on a closed-loop MIMO control, that overcomes the discrete mode boundaries, is part of the aforementioned work. Two of five 2/2-directional valves are commanded by an inner

flatness based control loop, while an outer axis controller assigns drive modes and switching strategies, consisting of pressure trajectories and command trajectories for the remaining three valves. Using this pressure based switching method, energy efficiency of the switching strategy can be optimized. With sensor-based load detection and the target trajectory in regard to desired speed and acceleration, a working point specific operation mode is detected and engaged without disturbance of the cylinder motion.

3.3. Examples in stationary and construction area

In the following two examples are discussed, where independent metering strategies are advantageous. These are a cardboard press and the implement functions of a mobile excavator.

3.3.1. Cardboard packaging press

In industrial and high-precision applications, independent metering systems can improve energy efficiency considerably, if large fractions of the involved cycles consist of loads under the nominal load, idle-travel or even overrunning loads. Under such circumstances, pump flow and thus energy consumption can be significantly reduced by means of regeneration modes even under constant pressure systems.

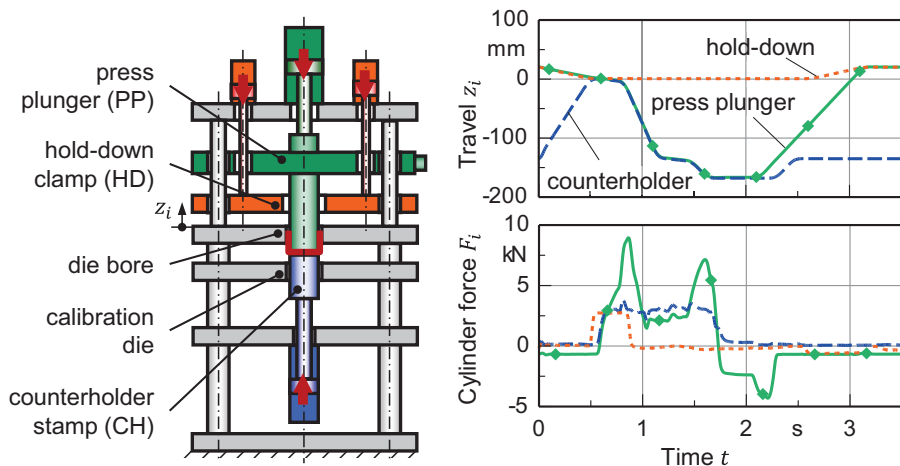


Figure 17: Structure of a cardboard packaging press and exemplary duty cycle

The duty cycle of a cardboard packaging press (CPP) is used here as an example for industrial applications in which potentials of IM can be leveraged, see **Figure 17**. The CPP is a machine used for the production of cup-shaped cardboard packaging containers. Plane cardboard material is fixed on a forming die bore by a hold-down clamp

(HD), applying a defined clamping force. A press plunger (PP) pulls the cardboard through the die bore and a calibration die against a defined counterforce exerted by a counterholder stamp (CH). Afterwards, all axes retreat into their initial positions.

In the examined machine, two parallel hydraulic single-rod cylinders, which are operated by one servo valve, drive the hold-down clamp. One single-rod cylinder and a servo valve each actuate the press plunger and the counterholder stamp. The supply system comprises two constant pressure sources with $p_{0,A} = 300$ bar for the hold-down clamp and the press plunger and $p_{0,B} = 50$ bar for the counterholder stamp.

The energy savings gained by implementing independent metering edges against an approach with conventional 4/3-directional valves are shown in **Figure 18** by comparing the required hydraulic energy exerted by the supply system for conventional valves and IM valves. These results are based on the method proposed by Kolks /46/. In total, 30 % of the supply energy can be saved using optimal operation modes. Most of the savings are due to extension of the PP-cylinder in high-pressure regeneration mode while retracting the CH-cylinder using low-pressure regeneration. Also, during the initial feed motion of the CH-cylinder at the beginning of the process, energy saving occurs due to high-pressure regeneration of this cylinder during extension.

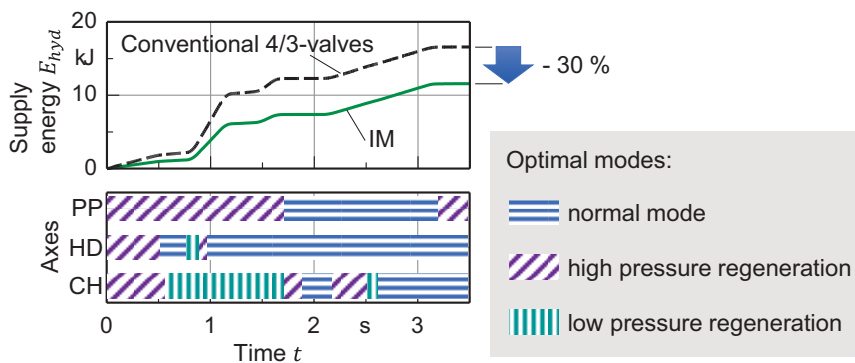


Figure 18: Energy savings of a cardboard press through efficient modes

High-pressure regeneration during extension is only possible under partial load. The shown cardboard pressing machine is over-dimensioned over most of the cycle time in terms of load capacity, enabling energy efficient high-pressure regeneration. However, high supply pressure is required for high precision controls and for covering process force peaks. In this case, the IM system will dynamically switch to normal mode. The great potential of independent metering systems lies in the dynamic load adaption they are capable of.

3.3.2. Mobile excavator

Continuously increasing demands on cost effectiveness, productivity and energy efficiency of mobile working machines constantly push new developments in the fields of hydraulic systems. Especially individual metering of a consumers inlet and outlet flow has moved into focus of research more intensely in the past decade because this approach promises benefits in terms of energy efficiency and flexibility. Industrial acceptance of newly developed systems heavily depends on investment costs, reliability and simplicity. It seems that currently published approaches hardly satisfy these demands yet, since implementations of individual metering hardware in serial production are still rare. Some examples are the Incova system by HUSCO and the Ultronics valve block offered by EATON /47/. Further works on IM systems in mobile machines can be found in /48, 49, 50/.

A new approach developed at the IFD uses only off-the-shelf components and a very simple control algorithm to facilitate the transfer into industry. The concept has been verified at a test rig shown in **Figure 19**.

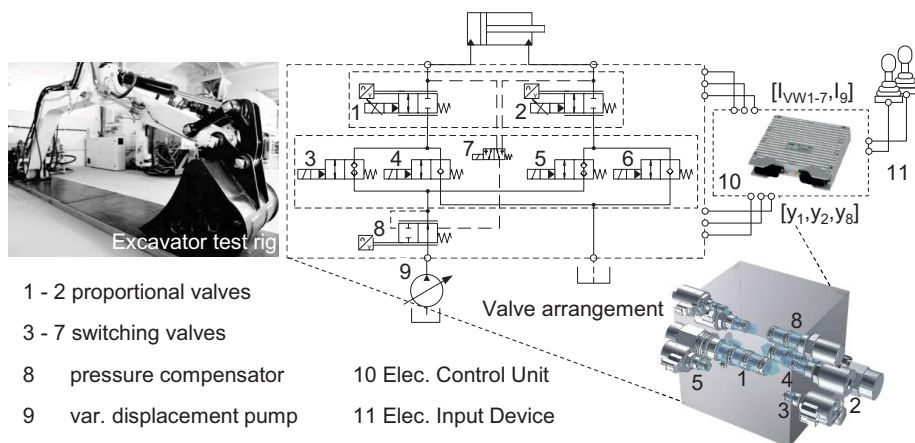


Figure 19: Test rig setup

The depicted valve structure is used to actuate the boom and stick cylinder of an excavator implement. Individual metering systems are multiple-input-multiple-output systems (MIMO). Usually these require complex multi-variable control strategies. An individual pressure compensator (IPC) in the inlet flow path is advantageous to decouple piston load force and velocity. This enables single-variable control approaches /41, 51, 52/. The actuator's velocity is always controlled with the inlet throttling edge in an open loop manner without load feedback. Depending on the load situation, measured by two chamber pressure sensors, the outlet throttling edge opens widely in case of resistive

loads thus preventing unnecessary losses in the outlet path and narrowly when balancing an aiding load. In low-priced mobile machines it is not common to measure the current position of the implement. Thus, the current dynamic properties of the hydraulic actuator are unknown. Under these circumstances model-based approaches are not reasonable. Instead, a simple and easily commissionable non-adaptive linear controller has been chosen.

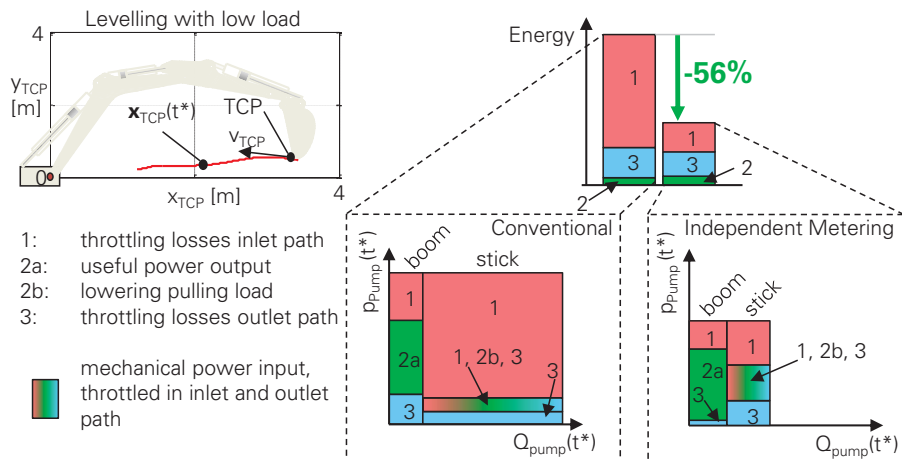


Figure 20: Energetic comparison between coupled and individual metering

Test results, depicted in **Figure 20**, show high energy saving potential when operating under partial load conditions or moving aiding loads by reducing the pump pressure. High-pressure regeneration greatly reduces the pump flow and thus energy consumption when operating several actuators at once. The overall system's handling characteristics are comparable to common coupled metering systems but additionally feature load compensated lowering.

3.4. Safety and reliability of independent metering

Looking on safety as an OEM, it is necessary to use the quantification process included in ISO 13849 to benefit from the presumption of conformity with the European machinery directive in case of an accident. But ISO 13849 only takes predefined categories for executing the safety function into account [53]. These categories fit for the most conventional drive systems. It is easy to associate these structures with the safety category and there is a lot of practical experience with conventional drive systems. Due to the complexity of IM structures considering all failure combinations of the components and the possible operation modes it is not possible to associate these IM systems with the categories of ISO 13849. Alternative analysis methods are needed.

3.4.1. Methodology to quantify safety and availability

Safety and reliability can be quantified through different methods. The overall goal is to calculate the probability of failure of:

- the safety function to quantify safety and
- the working function to quantify reliability.

Fault Tree Analysis (FTA) is one feasible opportunity to analyse and quantify complex structures like IM. The advantages of FTA are a vivid depiction of the systemic connections and an easy quantification by means of Boolean algebra /54/. Therefore FTA is also applicable for quantifying reliability. Based on a constant repair rate this leads to information on the availability of different IM structures. The construction of the fault tree is necessary for a quantitative calculation. A precise definition of the top event, which represents the safety or the working function depending on whether safety or reliability are regarded, is basic prerequisite for the structure of the fault tree. When it comes to IM structures in particular, the structure of the fault tree is furthermore influenced by the operating point and the possible operation modes (e.g. regeneration) as well as the impact of the malfunction of the components on the IM system. Using systematic analysis considering this aspects, a complete safety and reliability evaluation of any IM structure for arbitrary operating points can be made.

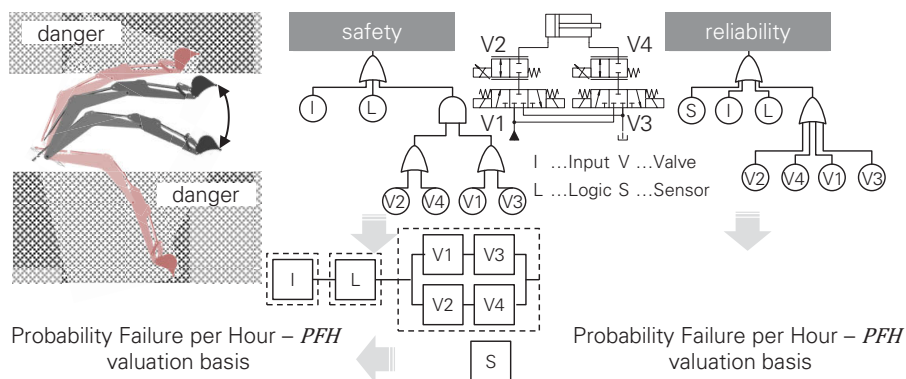


Figure 21: Safety and Reliability analysis of a selected IM structure in favour of four-quadrant movement

Figure 21 illustrates the boom function of an excavator's attachment. The working function is defined as extending and retracting the boom cylinder by avoiding cavitation on the opposite side of the load. A safe stop function is the most common safety function in mobile machines to reduce the risk to a minimum /55/. Looking on the excavator the boom cylinder is thereby not allowed to move unintentional neither due to an active

energy supply by the pump nor due to the external load. In addition, Figure 21 shows the fault trees of a selected IM system in favour of a four-quadrant movement regarding safety and reliability. Furthermore the safety related block diagram derived from the safety fault tree is pictured.

Implementing the probability of failure of each component or subsystem and calculating the *PFH*-value leads to an objective valuation basis. With this methodology IM structures can be filtered out, which are characterised by a high availability and meet the safety requirements from the application making this technology more accessible to the market. The system shown above can be used up to a Performance Level $PL = e$ depending on the fault detection.

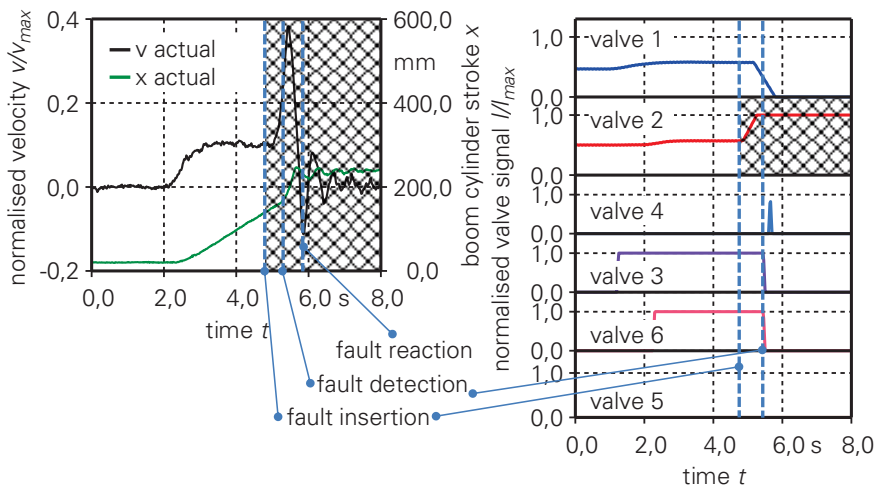


Figure 22: Test of safety function “Stop” - fault detection with pressure sensors

Besides structure design and reliability of the used components fault detection is one way to increase safety. /56/ gives a good overview over possible fault detection methods. Using the functionally necessary sensors in combination with simple fault detection methods to detect deviations from the normal state is the prior goal in cost sensitive applications like mobile machines. From the functional side of view pressure sensors have a good cost-benefit ratio. But their signals also contain information about the load and friction, which is problematic for the fault detection. Nevertheless, the safety function “Stop” was tested on the boom function of the test rig setup shown in Figure 19 using a combined limit and tendency monitoring on the basis of the pressure sensors. **Figure 22** displays the test results in case of a fully opened valve 2 at $t = 4.8 s$ while lowering the attachment. After that the velocity rises until the fault is detected at $t = 5 s$. As a result, the safety function “Stop” becomes active which means that all valves are closed and

the boom stops at $t = 5.8 \text{ s}$, as shown in Figure 22. Testing all safety critical faults leads to a reached Diagnostic Coverage of $DC = 99 \%$. This enables to use the proposed concept up to a required safety of $PL_r = e$.

3.4.2. Example for tractor steering

Due to their functional and safety-related potentials, valve structures with independent metering are proper for various applications and operation purposes such as steering systems in mobile machines. Conventional hydrostatic steering systems are limited in terms of steering comfort and driver assistance. For realisation of appropriate steering functions, electro-hydraulic solutions are necessary. There are high requirements for an electro-hydraulic steering system that should meet demands to enable road approval until a maximum speed of 60 km/h. Therefore, valve structures with independent metering are appropriate. In addition to fully redundant steer-by-wire solutions /57/, superimposed steering systems with independent meter-in and meter-out valves are a promising approach for an on-road usage /58/. Therefore, a parallel valve structure is superposed to the conventional steering unit, see **Figure 23**.

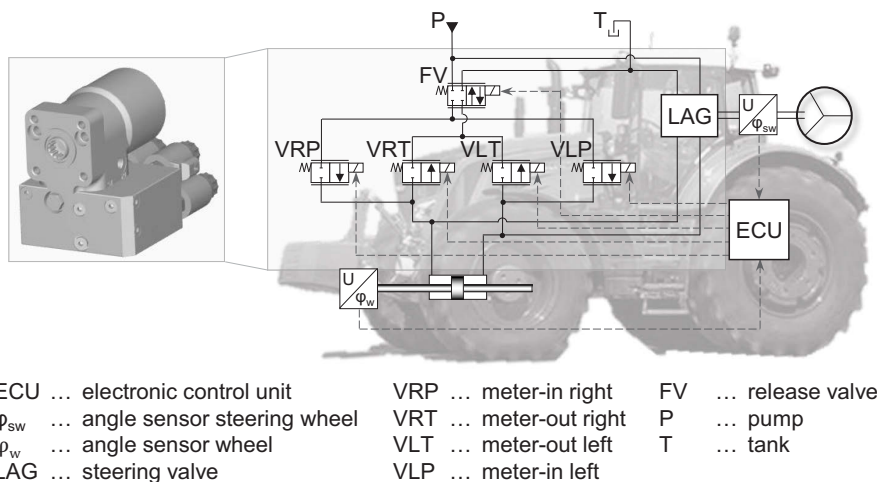


Figure 23: Structure of the electrohydraulic superimposed steering system with independent metering

Through a systematically developed valve control, it is possible to compensate single failures inside the configuration or reduce their adverse effects. Accordingly, there are no safety-critical states. The system reaches a high safety level without using a fully redundant structure. Thus, steering functions are usable for on-road application and increases the ease of operation. The realisation of a variable steering ratio depending

on the driving state enables for example a good directional stability at high velocities and comfortable handling for slow driving. The functionality of assistance functions and the effectiveness of the safety concept can be proven using a test rig and a demonstrator vehicle.

4. Outlook

4.1. Challenges in developing future displacement machines

The two main challenges that pump and motor designers will be facing in the near future are a further increase of power density and the optimization of their machines for enhanced part load operation.

Power density of displacement machines has not significantly increased over the past 20 years /59/. Main reasons for that are the limited accessibility and transparency of the flow phenomena inside these machines. An increase of power density can be achieved by extended operating pressures and volumetric flowrates respectively rotational speeds /60/. The operating pressure is predetermined by the application whereas an increase of the maximum rotational speed and thereby of the delivery flowrate will allow the installation of a smaller pump or motor. Cavitation effects are limiting the machine's rotational speed, since they lead to the partial filling of the displacement volumes with gas causing a flowrate breakdown and may cause damage to their components due to cavitation. A steadily increasing availability of computational power and the fast development of commercial CFD tools allows the visualization and analysis of these effects and the deviation of technologic and constructive countermeasures. Understanding, predicting and preventing cavitation by means of CFD is the key to lift displacement machines' power density to a new level, as it is proven by the latest scientific works on this topic /60, 61, 62, 63, 64/.

Besides an increased power density, enhanced part load capabilities and efficiency will be crucial product features of future displacement machines since increasing economical, ecological and societal requirements to energy efficiency make the application of displacement controlled systems highly attractive /9/. At low operating pressures and rotational speeds, the reduced hydrostatic and hydrodynamic load carrying capacity of the machines' tribological contacts limit their part load operation range. In part load, increased friction causes high power losses, which is the reason for relatively low efficiencies compared to full load operation /65/. Pressure and flow induced movements as well as pressure and temperature induced deformations of the involved components play an important role in this impact chain /66/. Therefore, a detailed

understanding of their sources and interactions is crucial for the development of low-friction tribological contacts. These effects are hard to capture using experimental measures. Therefore, most recent simulation tools and methods such as CFD, fluid structure interaction and conjugate heat transfer need to be utilized in the future.

Another challenge in the development of variable speed and/or displacement machines are high requirements to the units' dynamics. They will have to ensure an immediate response to changes of the requested flowrate in order to be able to compete with highly dynamic resistance controls. Pump and motor manufacturers are currently facing significantly higher failure rates of highly dynamically operated displacement machines compared to those operated in a more stationary manner. The reason is cavitation and cavitation erosion induced by additional accelerations during expansion of the displacement volume respectively swashing for axial piston pumps and during positive gradients of rotational speed. Such effects can be encountered by constructive optimizations based on CFD, as described above, or by advanced control strategies such as the implementation of operation point specific gradients of rotational speed and/or displacement volume onto intelligent pump/motor controllers.

Furthermore, intelligent control strategies show great potential for efficiency optimization in part-load operation. State-of-the-art machines are able to adjust their delivery flowrate either by changing their displacement volume or their rotational speed. For any requested flowrate, an arbitrary number of combinations of speed and displacement is available and there is an energetic optimum of both for each operation point. Latest works on system simulation show the immense amount of energy that could be saved if this potential would be fully and optimally exploited using intelligent machine controllers /27/.

Additional challenges include the reduction of noise and vibration and failure prediction by means of condition monitoring. Noise and vibration are induced by pressure pulsations and friction. The fundamental phenomena can be analyzed using the above-mentioned advanced simulation methods. Potential countermeasures are constructive optimizations, choice of materials and active damping using small-scale quick-acting valves and intelligent controls /67, 68, 69/.

4.2. Challenges for valve technology suppliers

In terms of valve specifications, component manufacturers are facing new challenges. Independent metering technology offers the potential of individualizing the system design in function and load response. For the use in industrial applications, single-edge valves

with a fast spool response and little hysteresis, especially in low relative opening regimes, are needed. These dynamic characteristics are often in conflict with the demand for low manufacturing costs and a low-leakage and precisely overlapped closed position. Furthermore, for most of the system approaches currently under research, bi-directional flow characteristics is mandatory.

A major challenge to be overcome is the high number of high-end valves involved in a system with independent metering edges, clearly increasing the system costs. There are efforts of decreasing the number of proportional actuators by using integrate directional valves. But this affects the degree of freedom, required for instance for smooth mode switching or variable control targets. Implications of valve characteristics and system architecture on the performance and availability of features of independent metering systems have yet to be determined and analyzed in detail.

4.3. Fluidic temperature control systems

Recent scientific studies focused on the topic of efficiency improvements in production technology found that an optimization of auxiliary units and their switching characteristic offers the greatest energy savings potential [70]. In this respect investigations of a machining center within the SFB/TR 96 have shown that the current system structure with a central supply and cooling unit does not meet the different component requirements [71, 72, 73]. Therefore, a holistic adjustment of the cooling systems on the specific component requirements provides further potential improving productivity and energy efficiency. One approach for energy optimization of cooling circuits applicable to machine tools comes from the building technology. In a new concept of the company WILO [74] the usually existing central pump of the heating system is replaced by decentralized miniature pumps. Furthermore, the pumps can replace the proportional valves, which would be alternatively necessary for a demand-oriented supply, see **Figure 24**. This approach is applied to fluid power systems of machine tools in the second project phase of the SFB/TR 96 and described in detail in [73].

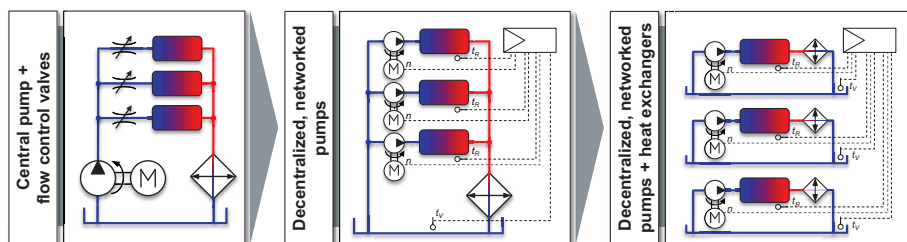


Figure 24: Decentralizing levels of the fluid system structure of machine tools

5. References

- /1/ Helbig, A.: Energieeffizientes elektrisch-hydrostatisches Antriebssystem am Beispiel der Kunststoff-Spritzgießmaschine. Dissertation, TU Dresden, 2007
- /2/ Busquets, E.; Ivantysynova, M.: Priority-Based Supervisory Controller for a Displacement-Controlled Excavator with Pump Switching. ASME/Bath 2015 Symposium on Fluid Power and Motion Control, Chicago (USA), 2015
- /3/ Ivantysynova, M.: Quo Vadis Fluid Power? ASME/BATH 2015 Symposium on Fluid Power and Motion Control, Chicago (USA), 2015
- /4/ Schneider, M.; Koch, O.; Weber, J.: Green Wheel Loader – Improving fuel economy through energy efficient drive and control concepts. 10th International Fluid Power Conference, Dresden, 2016
- /5/ Siemer, E.: Variable-Speed Pump Drive System for a 5000 kN Ring Expander. 8th International Fluid Power Conference, Dresden, 2012, vol. 3 pp. 45-56
- /6/ Rühlicke, I.: Elektrohydraulische Antriebssysteme mit drehzahlveränderbarer Pumpe. Dissertation, TU Dresden, 1997
- /7/ Kazmeier, B.: Energieverbrauchsoptimierte Regelung eines elektrohydraulischen Linearantriebs kleiner Leistung mit drehzahlgeregeltem Elektromotor und Verstellpumpe. Dissertation, TU Hamburg-Harburg, 1998
- /8/ Klug, D.: Hydraulische Antriebe mit drehzahlgeregeltem Elektromotor. Dissertation, TU Chemnitz, 2000
- /9/ Neubert, T. Untersuchung von drehzahlveränderbaren Pumpen. Dissertation, TU Dresden, 2002
- /10/ Michel, S.; Weber, J.: Energy-efficient electrohydraulic compact drives for low power applications. Fluid Power and Motion Control FPMC 2012, Bath (GB), 2012, pp. 93-107
- /11/ Bildstein, M.: Application of electro-hydrostatic actuators for future aircraft primary flight controls. 1. Internationales Fluidtechnisches Kolloquium, Aachen, 1998, vol. 1 pp. 93-105
- /12/ Maré, J.-C.: From Douglas DC3 to Airbus A380 – Seventy years of innovation in aerospace hydraulics. 4th International Fluid Power Conference, Dresden, 2004, vol. 2 pp. 95–108

- /13/ Todeschi, M.: A380 flight control actuation lessons learned on EHAs design. International conference on recent advances in aerospace actuation systems and components, Toulouse (France), 2007, pp. 21-26
- /14/ Williamson, C.: Power Management for Multi-Actor Mobile Machines with Displacement Controlled Actuators. PhD Thesis, Purdue University, West Lafayette (USA), 2010
- /15/ Michel, S.; Weber, J.: Electrohydraulic compact-drives for low power applications considering energy-efficiency and high inertial loads. 7th FPNI PhD Symposium on Fluid Power, Reggio Emilia (Italy), 2012, pp. 869-888
- /16/ Brahmer, B.: CLDP – Hybrid Drive using Servo Pump in Closed Loop. 8th International Fluid Power Conference, Dresden, 2012, vol. 3 pp. 93-104
- /17/ Wang, L.; Book, W. J.: Using Leakage to Stabilize a Hydraulic Circuit for Pump Controlled Actuators. Journal of Dynamic Systems, Measurement, and Control 135 (2013) no. 6, pp. 061007/1-12
- /18/ Minav, T.; Bonato, C.; Sainio, P.; Pietola, M.: Direct Driven Hydraulic Drive. 9th International Fluid Power Conference, Aachen, 2014, vol. 2 pp. 520-529
- /19/ Çaliskan, H.; Balkan, T.; Platin, B. E.: A Complete Analysis and a Novel Solution for Instability in Pump Controlled Asymmetric Actuators. Journal of Dynamic Systems, Measurement, and Control 137 (2015) no. 9, pp. 091008/1-14
- /20/ Chen, W.-Z.; Lin, T.; Hill, B. P.; Brown, J. T.: Thermal Modelling of a Flight-Critical Electrohydrostatic Actuator. Aerospace Atlantic Conference, 1995, SAE Technical Paper 951403
- /21/ Johansson, B.; Andersson, J.; Krus, P.: Thermal Modelling of an electro-hydrostatic actuation system. Recent advances in aerospace actuation systems and components, Toulouse (France), 2001, pp. 49–54
- /22/ Michel, S.; Schulze, T.; Weber, J.: Energy-efficiency and thermo energetic behaviour of electrohydraulic compact drives. 9th International Fluid Power Conference, Aachen, 2014, vol. 1 pp. 162-177
- /23/ Michel, S.; Weber, J.: Energy-efficiency and thermo energetic behaviour of electrohydraulic compact drives. 10th International Fluid Power Conference, Dresden, 2016

- /24/ Helduser, S.: Elektrisch-hydraulische Systemtechnik – Entwicklungsschwerpunkte in der Stationärhydraulik. O+P Ölhydraulik und Pneumatik 1/2006, pp. 16-23
- /25/ Radermacher, T., Mäsing, R., Helduser, S. The Drive Counts. Kunststoffe international 4/2010, pp. 24-28
- /26/ Willkomm, J.; Wahler, M.; Weber, J.: Model Predictive Control of Speed-Variable Variable-Displacement Pumps to Optimize Energy Efficiency. 9th International Fluid Power Conference, Aachen, 2014, vol. 1 pp. 372-385
- /27/ Willkomm, J.; Wahler, M.; Weber, J.: Process-Adapted Control to Maximize Dynamics of Speed- and Displacement-Variable Pumps. ASME/Bath 2014 Symposium on Fluid Power and Motion Control, Bath (GB), 2014
- /28/ Mann, S.; Kuttruf, W.: PSH Press Drive Servo Hybrid – Servo Pump Drive System for Hydraulic Presses. 7th International Fluid Power Conference, Aachen, 2010, vol. 4 pp. 189-200
- /29/ Richter, M.: Moderne Antriebskonzepte im Pressenbau. O+P Ölhydraulik und Pneumatik 40 (1996) no. 10, pp. 688-695
- /30/ Neugebauer, R.; Sterzing, A.: Ressourceneffiziente Umformtechnik. 5. Chemnitzer Karosseriekolloquium CBC 2008, Chemnitz, 2008, pp. 81-95
- /31/ Rüger, H.: Energieeffiziente Hydraulikpressen durch Servodirektantrieb. 19. Sächsische Fachtagung Umformtechnik SFU 2012, Chemnitz, 2012, pp. 365-378
- /32/ Papaioanu, A.; Liewald, M.: Servotechnologie im Pressenbau. wt Werkstattstechnik online 103 (2013) no. 10, pp. 776-782
- /33/ Lohse, H.; Weber, J.; Neumann, S.; Händle, W.; Klug, D.: Investigation and Improvement of the Energy Efficiency of Hydraulic Deep Drawing Presses. The Fourteenth Scandinavian International Conference on Fluid Power, Tampere (Finland), 2015
- /34/ Rahmfeld, R.: Development and Control of Energy Saving Hydraulic Servo Drives for Mobile Systems. Dissertation, TU Hamburg-Harburg, 2002

- /35/ Rahmfeld, R.; Ivantysynova, M.; Weber, J.: Displacement Controlled Wheel Loader – a simple and clever solution. 4th International Fluid Power Conference, Dresden, 2004
- /36/ Daher, N.; Ivantysynova, M.: Pump Controlled Steer-by-Wire System. SAE 2013 Commercial Vehicle Engineering Congress, Rosemont (USA), 2013, SAE Technical Paper 2013-01-2349
- /37/ Heybroek, K.: Saving energy in construction machinery using displacement control hydraulics: concept realization and validation. PhD Thesis, Linköping University (Sweden), 2008
- /38/ Schneider, M.; Koch, O.; Weber, J.; Bach, M.; Jacobs, G.: Green Wheel Loader – Development of an energy efficient drive and control system. 9th International Fluid Power Conference, Aachen, 2014, vol. 2 pp. 262-278
- /39/ Schneider, M.; Koch, O.; Weber, J.: Green Wheel Loader – Operating Strategy of an Energy Efficient Hybrid Drive Train. SAE 2014 Commercial Vehicle Engineering Congress, Rosemont (USA), 2014, SAE Technical Paper 2014-01-2400
- /40/ Ivantysyn, R.; Weber, J.: Novel Open Circuit Displacement Control Architecture in Heavy Machinery. The 8th FPNI PhD Symposium on Fluid Power, Lappeenranta (Finland), 2014
- /41/ Sitte, A.; Beck, B.; Weber, J.: Design of independent metering control systems. 9th International Fluid Power Conference, Aachen, 2014, vol. 3 pp. 428-440
- /42/ Eriksson, B.: Control Strategy for Energy Efficient Fluid Power Actuators: Utilizing Individual Metering. Licentiate Thesis, Linköping University (Sweden), 2007
- /43/ Mattila, J.; Virvalo, T.: Energy-efficient motion control of a hydraulic manipulator. 2000 IEEE International Conference on Robotics and Automation, San Francisco (USA), 2000, pp. 3000-3006
- /44/ Liu, S.; Yao, B.: Coordinate Control of Energy Saving Programmable Valves. IEEE Transactions on Control Systems Technology 16 (2008) no. 1, pp. 34-45

- /45/ Bindel, R.: Antriebssysteme zur Reduzierung der Energieverluste bei rechnergesteuerten Großmanipulatoren mit Gelenkarmkinematik. Dissertation, University of Stuttgart, 1999
- /46/ Kolks, G.; Weber, J.: Modiciency – Efficient industrial hydraulic drives through independent metering using optimal operating modes. 10th International Fluid Power Conference, Dresden, 2016
- /47/ N.N.: Eaton Ultronics™ Management System: Electro-hydraulic CAN Bus Control System. Eden Prairie (USA), 2005
- /48/ N.N.: Hybrid-Hydraulikbagger CAT 336E H – Kompromisslose Leistung bei niedrigem Verbrauch. URL: http://www.cat.com/de_DE/news/machine-press-releases/cat-336e-h-hydraulichybridexcavatordelivers-nocompromisefuelsavin.html, access: 07.12.2015
- /49/ N.N.: Das neue Hyundai Hydrauliksystem “HI-POSS” auf der Bauma 2013. URL: <http://constructionequipment.hyundai.eu/de/press/detail/das-neue-hyundai-hydrauliksystem-quot-hi-poss-quot-auf-der-bauma-2013>, access: 07.12.2015
- /50/ Vukovic, M.; Sgro, S.; Murrenhoff, H.: STEAM – a holistic approach to designing excavator systems. 9th International Fluid Power Conference, Aachen, vol. 2 pp. 250-260
- /51/ Sitte, A.; Weber, J.: Structural design of independent metering control systems. The 13th Scandinavian International Conference on Fluid Power SICFP 2013, Linköping (Sweden), 2013
- /52/ Lübbert, J.; Sitte, A.; Weber, J.: Pressure compensator control of novel independent metering control system. 10th International Fluid Power Conference, Dresden, 2016
- /53/ Standard ISO 13849-1:2006. Safety of machinery – Safety-related parts of control systems – Part 1: General principles for design
- /54/ Standard IEC 60300-3-1:2003. Dependability management – Part 3-1: Application guide – Analysis techniques for dependability – Guide on methodology

- /55/ Standard ISO/TS 15998-2:2012. Earth-moving machinery – Machine control systems (MCS) using electronic components – Part 2: Use and application of ISO 15998
- /56/ Isermann, R.: Überwachung und Fehlerdiagnose – Moderne Methoden und ihre Anwendungen bei technischen Systemen. VDI-Verlag, Düsseldorf, 1994
- /57/ Schmitz, D.: Entwurf eines fehlertoleranten Lenkventils für Steer-by-Wire Anwendungen bei Traktoren. Dissertation, Karlsruhe Institute of Technology, 2014
- /58/ Fischer, E.; Sitte, A.; Weber, J.; Bergmann, E.; de la Motte, M.: Safety Related Development of an Electro-Hydraulic Active Steering System. 18th ITI Symposium, Dresden, 2015, pp. 263-270
- /59/ Achten, P.: Innovation in the Fluid Power Industry. 9th International Fluid Power Conference, Aachen, 2014
- /60/ Mohn, G.; Nafz, T.: Swash Plate Pumps – the Key to the Future. 10th International Fluid Power Conference, Dresden, 2016
- /61/ Bügener, N.; Klecker, J.; Weber, J.: Analysis and Improvement of the Suction Performance of Axial Piston Pumps in Swash Plate Design. International Journal of Fluid Power 10/2014
- /62/ Bügener, N.: Analyse und Verbesserung des Ansaugverhaltens von Axialkolbenpumpen in Schrägscheibenbauweise. Dissertation, TU Dresden, 2014
- /63/ Wustmann, W.: Experimentelle und numerische Untersuchung der Strömungsvorgänge in hydrostatischen Verdrängereinheiten am Beispiel von Außenzahnrad- und Axialkolbenpumpe. Dissertation, TU Dresden, 2009
- /64/ Schlehs, C.; Viennet, E.; Deeken, M.; Ding, H.; Xia, Y.; Lowry, S.; Murrenhoff, H.: 3D-CFD Simulation of an Axial Piston Displacement Unit. 9th International Fluid Power Conference, Aachen, 2014, vol. 3 pp. 332-343
- /65/ Wegner, S.; Gels, S.; Murrenhoff, H.: Simulation of the Tribological Contact Cylinder Block / Valve Plate and Influence of Geometry and Operating Points on the Friction Torque in Axial Piston Machines. 9th International Fluid Power Conference, Aachen, 2014, vol. 1 pp. 26-38

- /66/ Zecchi, M.: A Novel Fluid Structure Interaction and Thermal Model to Predict the Cylinder Block / Valve Plate Interface Performance in Swash Plate Type Axial Piston Machines. PhD Thesis, Purdue University, West Lafayette (USA), 2013
- /67/ Klecker, J.: Saugleitungsmodellierung einer Axialkolbenpumpe unter Berücksichtigung der Fluid-Struktur-Interaktion. Final report, TU Dresden, 2014
- /68/ Jensen, S.: Pump control on a piston-by-piston basis. URL: <http://www.oemoffhighway.com/article/10898642/pump-control-on-a-piston-by-piston-basis>, access: 01.12.2015
- /69/ Nafz, T.: Aktive Ventilumsteuerung von Axialkolbenpumpen zur Geräuschreduktion hydraulischer Anlagen. Dissertation, RWTH Aachen, 2011
- /70/ Neugebauer, R.: Energieeffiziente Produkt- und Prozessinnovationen in der Produktionstechnik. Ergebnisse des sächsischen Spitzentechnologieclusters, TU Chemnitz, 2014
- /71/ Weber, J.; Weber, J.: Thermo-energetic modelling of fluid power systems. Thermo-energetic Design of Machine Tools. Springer Berlin Heidelberg, Heidelberg, 2014, pp. 49-60.
- /72/ Weber, J.; Weber, J.: Thermo-energetic analysis of the fluidic cooling systems in tooling machines. 9th International Fluid Power Conference, Aachen, 2014, vol. 2 pp. 292-303
- /73/ Weber, J.; Lohse, H.; Weber, J.: Thermo-energetic Analysis of the Fluid Systems in Cutting Machine Tools. 10th International Fluid Power Conference, Dresden, 2016
- /74/ Sinnesbichler, H.; Schade, A.; Eberl, M.: Vergleichende messtechnische Untersuchung zwischen einer Heizungsanlage mit dezentralen Heizungs-pumpen (WILO Geniux) und einer konventionellen Heizungsanlage. Abstract IBP-Abschlussbericht ESB-003/2010 H5KI, Valley, 2010

6. Nomenclature

DC	Diagnostic Coverage	%
E	Energy	J
F	Force	N
I	Current	A
m	Mass	kg
n	Rotational speed	1/s
P	Power	W
p	Pressure	bar
PFH	Probability of Failure per Hour	1/h
PL	Performance Level	-
Q	Volume flow	dm ³ /min
t	Time	s
U	Voltage	V
v	Velocity	m/s
x, y, z	Position	m
y	Set value	V
φ	Angle	°

Green Wheel Loader – improving fuel economy through energy efficient drive and control concepts

Dipl.-Ing. Markus Schneider, Dipl.-Ing. Oliver Koch, Prof. Dr.-Ing. Jürgen Weber

Institut für Fluidtechnik (IFD), Technische Universität Dresden, Helmholtzstrasse 7a,
01069 Dresden, E-mail: mailbox@ifd.mw.tu-dresden.de

Abstract

The drive train components and the machine control system significantly influence the fuel consumption of mobile machinery. The demonstrator vehicle “Green Wheel Loader” developed within the joint research project “TEAM” combines the most promising drive concepts currently available for mobile machines with an innovative operating strategy. The developed drive and control system proved its functionality and performance under realistic operation conditions in a gravel pit. Reference test showed 10 – 15 % fuel savings of the prototype vehicle compared to a state-of-the-art series machine.

KEYWORDS: mobile machines, energy efficient drive trains, operating strategy

1. Introduction

Mobile equipment manufacturers are currently focusing their engineering activities on the increase of productivity, operator comfort and energy efficiency as well as the compliance to exhaust emission regulations (TIER 4 final, EU stage 4). Against this background, the use of new, energy efficient drive technologies is becoming more and more attractive. Agricultural machinery and construction equipment still offer significant fuel saving potential, which can be exploited through efficient drive train components and optimised control of their interaction. In recent years, new innovative solutions have been developed besides the continuous improvement of conventional drive technology. Concepts like power split travel drives /1 - 3/, displacement controlled implement drives /4 -6/ and hybrid solutions /7 - 9/ already showed their potential in practical applications. Previous research activities focused on the substitution of individual subsystems of the machines. A consequent implementation of new drive technology and the holistic operating strategies has not been done so far.

Within the joint research initiative “TEAM – Development of technologies for energy-saving drives of mobile machines”, the most promising technologies currently available are combined for the first time in a wheel loader with an operating weight of 24 t and

200 kW installed engine power. Besides efficiency advantages compared to conventional solutions, the subsystems regenerative capabilities and the possibility to improve the machine systems adjustment are expected to result in fuel savings.

2. Drive train and control system

2.1. Drive train

Figure 1 shows the “Green Wheel Loader’s” drive train layout /10/. A turbo-charged diesel engine optimized for low speed and high torque operation serves as primary energy source. It was also developed within the “TEAM” research project /11/, offers an output power of 200 kW at 7,8 l displacement and fulfils the emission standards of US TIER 4 final and EU stage 4. The travel drive’s power split transmission is driven via the pump transfer gear and a cardan shaft. It features three drive ranges, of which the first is purely hydrostatic and the second and third are of input coupled power split structure.

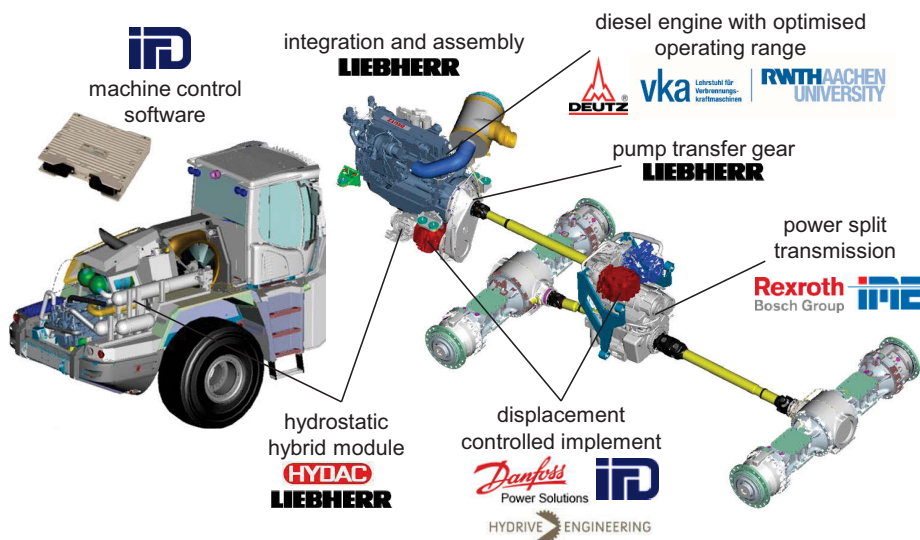


Figure 1: Drive train layout of the “Green Wheel Loader”

The implement’s lift and tilt function are operated displacement-controlled by separate closed hydrostatic circuits. In order to use identical displacement units despite the functions’ different flow demands, the pumps run at different speeds. Both, travel and implement drive enable energy recirculation in case of aiding loads or deceleration of the vehicle. This energy can be either directly reused by other subsystems or stored in a hydrostatic parallel hybrid. This consists of a closed-circuit 4-quadrant displacement unit for torque metering and a double piston accumulator /12/ to store the energy.

The displayed drive train is integrated into the chassis of a 24 t Liebherr L576 loader. Safety relevant systems such as brake or steering circuit are adopted with minor changes from the series machine. The central machine controller manages the complex interaction of the different subsystems and forms the link to the operator.

2.2. Control system architecture

The “Green Wheel Loaders” drive system consists of various complex subsystems, which are engineered by multiple partners. To ensure time and resource-efficient development of the control strategies and software, machine functionality is modularized and distributed among the drive train subsystems. **Figure 2** shows the structure of the control system.

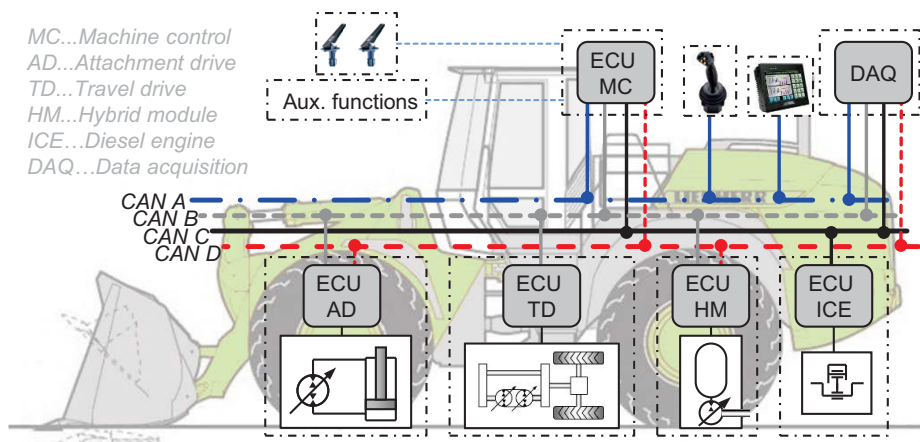


Figure 2: Control system architecture of the “Green Wheel Loader”

A central machine controller (ECU MC) interprets the operator inputs and generates the subsystems’ set values according to the implemented operating strategy. Additionally, functions such as control of peripheral systems, monitoring and calibration routines are handled. Each subsystem comprises a separate controller for realising the machine controller’s demands by controlling the subsystem’s integrated actors. Furthermore, subsystem-specific data acquisition and monitoring functions are implemented. Data is only exchanged between the subsystems and the machine controller, a mutual control interference between subsystems is not permitted. Thus, the individual self-contained subsystems can be developed independently. The CAN-Bus “CAN A” forms the link between the machine controller and the HMI devices such as joysticks and display. CAN Buses “B and C” are used exclusively for the data exchange between subsystems and machine controller. This offered the possibility to specify the communications interfaces

during an early stage of the development process but also to modify them in later phases. For acquisition of not control-relevant data, a separate CAN-Bus “CAN D” is used. Thus, the busload on CAN buses necessary for machine operation is reduced and disturbance of the machine functions by incorrect communication can be avoided.

3. Operating strategy and machine control software

3.1. Operating strategy

The „Green Wheel Loader’s” drive and control architecture enables new approaches for the subsystems’ interaction. **Figure 3** shows the operating strategy’s basic structure.

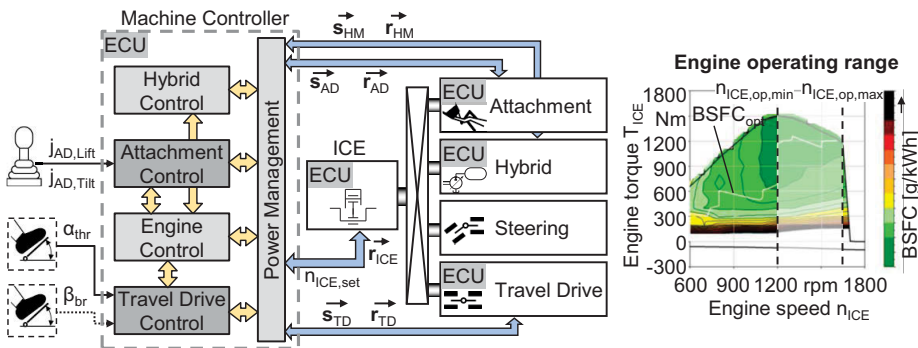


Figure 3: Basic structure of the “Green Wheel Loader’s” operating strategy

In contrast to conventional vehicle control systems, the operator does not directly influence the diesel engine speed using the throttle pedal. Instead, the machine controller interprets the input signals from joystick and pedal as speed demands for implement functions and travel drive. Based on that, the software determines the minimum engine speed necessary to fulfil these demands. By comparison and prioritization of the different engine speed demands, the set value $n_{ICE,set}$ is calculated so that all operator demands can be satisfied. Thus, the machine can operate at the minimum engine speed technically possible. Besides lower drag losses in the driveline, this leads to higher torque and thus higher efficiency of the diesel engine. For reasons of engine dynamics and load response characteristics, the permissible engine speed range is limited. During loading operation, the engine operates in a set speed range of 1200 to 1600 rpm. Depending on the machine’s actual operating conditions, the superordinated power management meters the hybrid module’s torque to support the engine dynamically. Furthermore, it protects the engine from stalling or over speed conditions by influencing the subsystems’ set values.

The machine controller determines the subsystems' set values based on the operator inputs and the nominal engine speed $n_{ICE,set}$ instead of using the actual value $n_{ICE,act}$. Thus, closed-loop control structures prone to oscillation can be avoided to a large extent. Due to the engine lugging under load, this also leads to a certain load sensitivity of the drive train, which serves as feedback for the machine operator. A detailed description of the individual subsystems' control algorithms is given in /13/.

3.2. Machine control software development

The functionality and effectiveness of the developed operating strategy and the subsystems' control algorithms were tested using detailed simulation models. However, these algorithms only represent a fraction of the functionality necessary to control the demonstrator machine. Additionally, functions such as control of peripheral systems, error detection and handling as well as monitoring and calibration routines have to be provided. For reasons of robustness, a commercially available electronic control unit (ECU) suitable for mobile applications is used as implementation target. This increases the software's complexity significantly. To ensure an efficient software development process and to detect coding errors as early as possible, a Hardware-in-the-Loop (HiL) test bench is used, see **figure 4**.

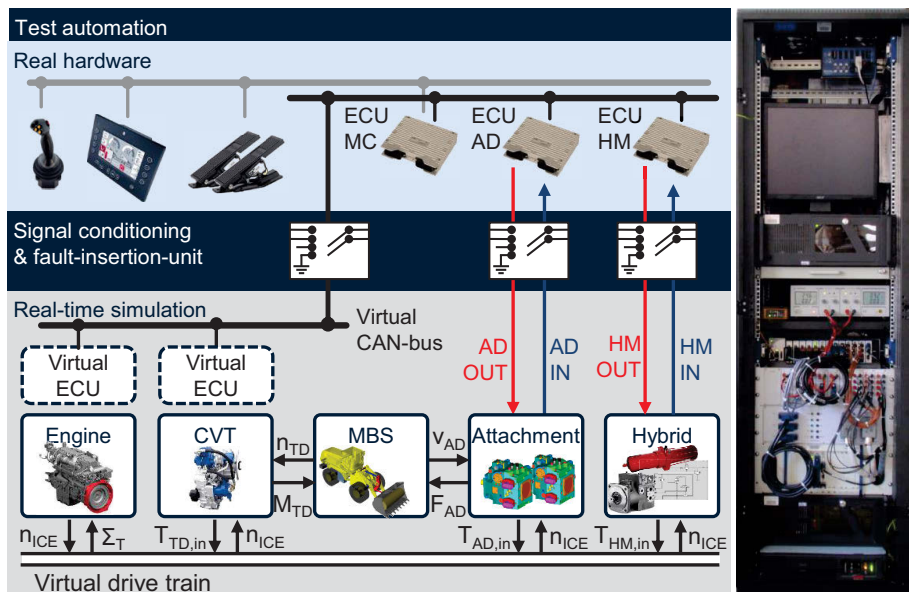


Figure 4: Basic structure of the used Hardware-in-the-Loop (HiL) test bench

Simulation models used before for algorithm development are modified to calculate in real-time [14]. They emulate the machine behaviour while signal condition modules integrate real hardware components such as ECUs, HMI and peripheral devices into the simulation. Thus, the developed machine control software can be easily tested on the real controller independently of the actual prototype machine.

By using test automation software the HiL test bench's benefit can be further increased. Once the test cases and the respective expected machine reactions are defined, new versions of the machine control software can be tested automatically for errors and changes in machine behaviour. Thus, a high level of maturity is ensured during the whole software development process and the effort for error detection and correction during commissioning of the prototype is reduced significantly.

4. Commissioning and testing

The aforementioned subsystems and the developed operating strategy were integrated into a demonstrator vehicle. After commissioning of the individual subsystems and first functional tests the machine was transferred to a gravel pit for testing and adjustment under realistic conditions, **figure 5**.



Figure 5: Integration, commissioning and testing of the „Green Wheel Loader“

The proof of the operating strategy's functionality and its parameterisation under realistic operating conditions are the basis for a sound evaluation of the developed drive and control system. Therefore, professional machine operators regularly evaluated the machines' behaviour and controllability in order to ensure a practice-orientated machine development. The adjustment activities focused on:

- Tuning of acceleration, deceleration and reversing characteristics
- Tuning of traction force metering characteristics at low speeds
- Tuning of the drive train's behaviour during static and dynamic loading situations

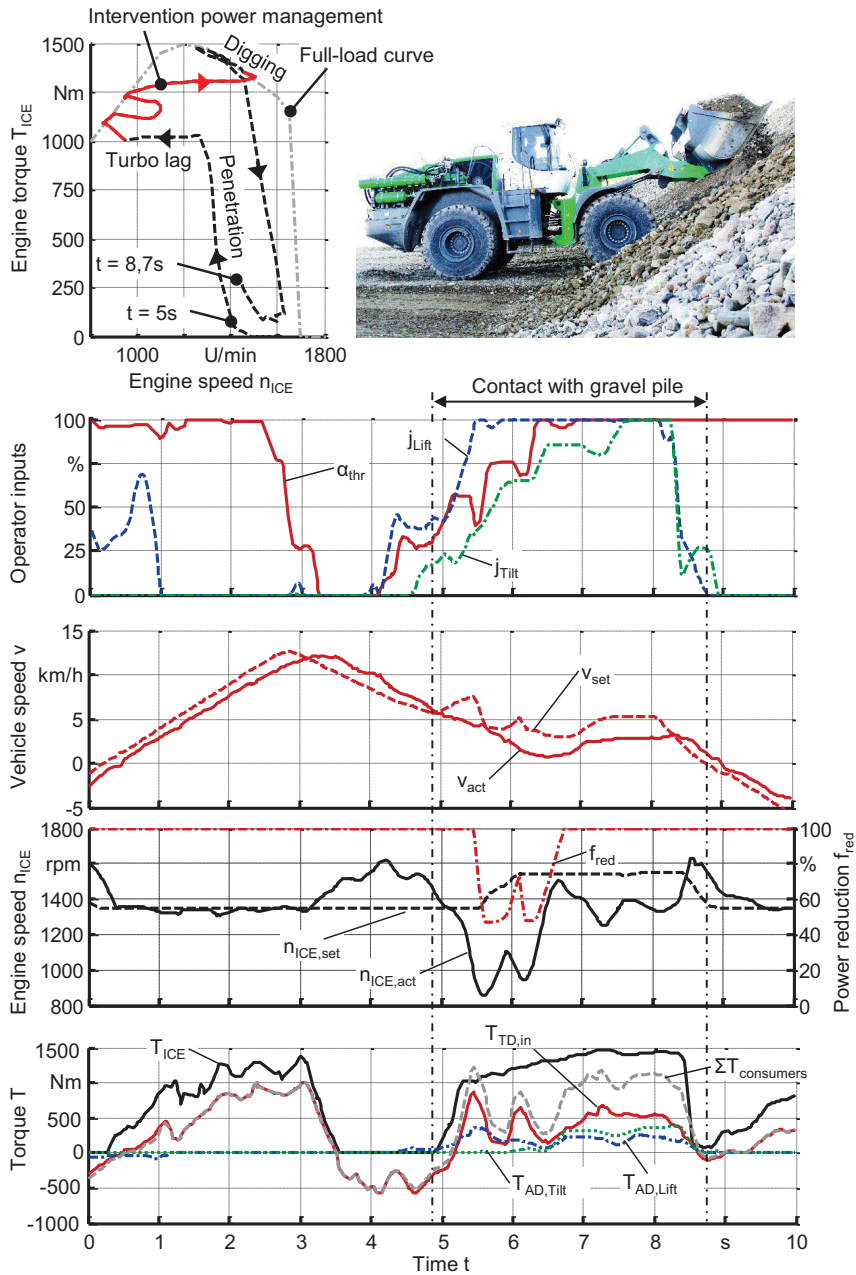


Figure 6: Measured load scenario "pile penetration"

Tuning the machine's acceleration and reversing characteristics as well as the system's behaviour during dynamic load situations posed the biggest challenges. **Figure 6** shows an exemplary measurement of a "pile penetration" load scenario. The operator accelerates the wheel loader with full throttle at maximum acceleration towards the gravel pile. Just before arriving at the obstacle's base, he decelerates the machine before penetrating the pile at a vehicle speed of 6 km/h. While filling the bucket, the operator actuates all input devices to 100 %, despite the fact that the machine is already working at its power limit. This happens subconsciously as the operator instinctively demands for more power than there is available. The machine's power management protects the diesel engine from stalling, despite the operator input signals. This is especially crucial at the moment of pile penetration. During the approach's last phase the vehicle decelerates, so the transmission capable of 4-quadrant operation recirculates energy. As no other consumers have significant power demands at that point this excess energy is dissipated by drag operation of the engine. The motor's speed regulator reacts by reducing the amount of fuel injected, which leads to lower exhaust output rate and therefore lower charge-air pressure generated by the turbocharger. When hitting the pile, the engine load increases instantaneously due to simultaneous actuation of all main consumers. As charge-air pressure is low, the engine can only provide a fraction of its nominal torque. The result is a drastic reduction of the engine speed. The power management counteracts by reducing the subsystems set values by means of the signal f_{red} . The resulting load relief leads to a recovery of the engine speed, until the motor is capable of bearing the whole load torque. During the filling process of the bucket, no intervention of the power management is necessary; the engine operates at maximum torque. Thus, reliable and speedy loading operation of the wheel loader can be ensured. During testing operation, the challenge was to tune the power management for effective engine stall protection in case of dynamic load situations. On the other hand, smaller load peaks during non-critical situations should must not negatively influence the vehicle's operating behaviour.

5. Energetic analysis

5.1. Reference testing

To evaluate the energy saving potential of the developed drive and control system, reference testing was done against a state-of-the-art machine (year of manufacture 2014) which already has an elaborate control strategy. Like the "Green Wheel Loader", the machine with an operating weight of 24 tons features a 220 kW engine that fulfils the exhaust emission regulations of EU Stage 4 and US TIER 4 final. The travel drive

consists of a hydrodynamic torque converter with lock-up clutch and a 4-speed power shift transmission. By using the operating brakes for reversing instead of the torque converter its fuel consumption is already reduced compared to other machines. For implement actuation, two load-sensing pumps are used of which one also feeds the steering circuit via a common priority valve.

For reference testing, both machines performed a short loading cycle under comparable operating conditions, driven by experienced operators. **Figure 7** shows the reference test's setup. Both machines transfer material from a pile of loose, homogenous material to a location in a distance of 20 m. For each test, the cycle is repeated 30 times. The ground is flat and consists of compacted raw gravel, which leads to relatively high driving resistances and therefore high power demand of the travel drive.



Figure 7: Setup for reference testing

Figure 8 shows the subsystems' power demand and the vehicle speed and traction force for two exemplary consecutive working cycles. The hybrid module was deactivated during this test. Vehicle speed and traction force are calculated based on transmission output speed and transmission-internal sensor signals, as direct measurement of these values is not possible. The subsystems' power demand is also calculated based on subsystem-internal measurands and loss maps used before for system simulation, as it was not possible to use torque measurement equipment.

Both operating cycles last for about 35 s, the average duration of all 30 cycles was 34,6 s. This is comparable to conventional machines. The plot of the engine power P_{ICE} shows that the machine operates at its power limit very frequently. During penetration of the pile (phase 2), power consumption of travel and attachment drive is about equally high. The power management manipulates the subsystems' set values so the engine is kept operating at maximum output power. Also during the machine's acceleration (phase 1, 3, 4 and 5) the engine load rises to its maximum. Transmission-internal protection mechanisms and the superordinated power management intervene to protect the drive

train from overloading. This is especially crucial during phase 4, when the machine accelerates to the unloading site and the implement with fully loaded bucket is lifted simultaneously.

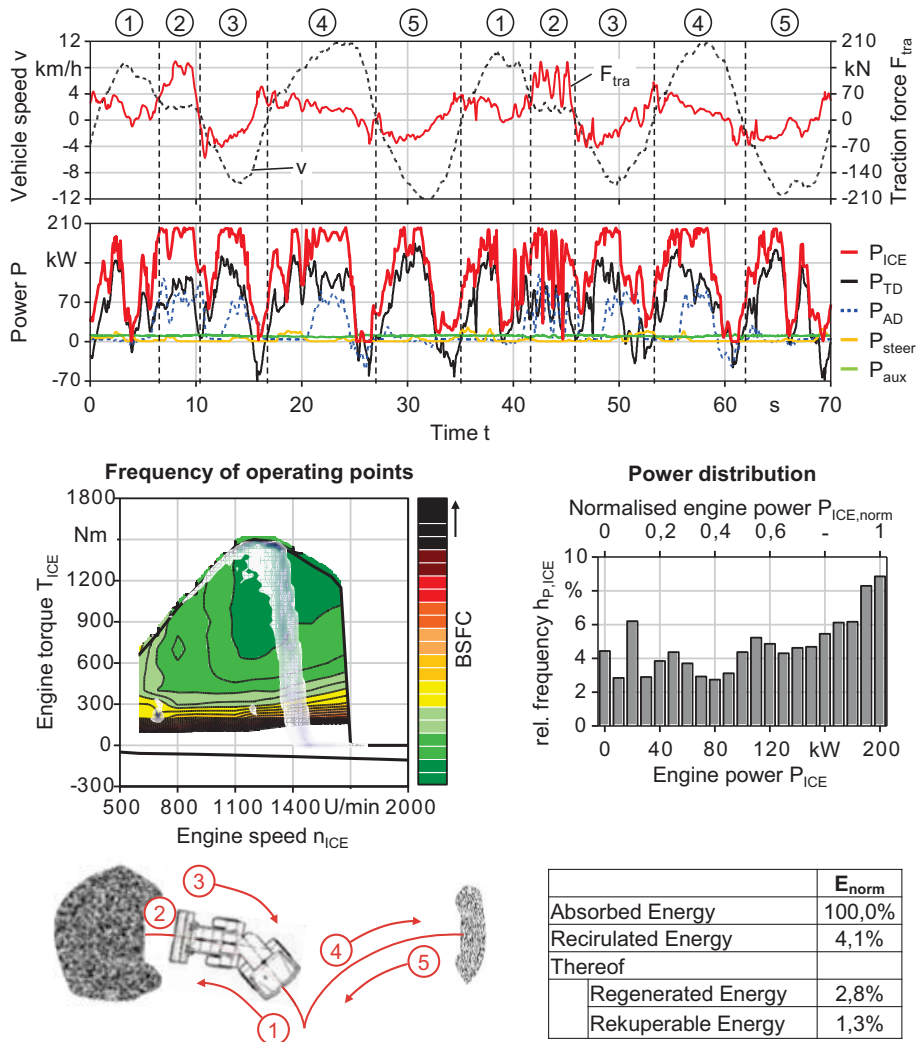


Figure 8: Measurement results of the reference testing

The distribution of the engine's output power shows an accumulation between 160 and 200 kW, which emphasizes the high loading of the diesel engine. The time average over all 30 load cycles is 120 kW or 60 % of maximum output power. The engine's main operating range is between 1000 to 1450 rpm at high torque, so energy is converted in the range of motor's highest efficiency.

Both travel and implement drive feed power back to the drive train. During deceleration of the vehicle, the negative power input of the travel drive rises up to 60 kW. However, this phase only lasts for 1 – 2 s, so the transferred amount of energy is low. The implement drive mainly recirculates power during unloading of the bucket. Over all 30 load cycles, 4 % of the engine's output energy are recirculated to the drive shaft. The majority is directly reused to power other subsystems, thus relieving the engine and reducing fuel consumption. Only 1 % cannot be used otherwise and is available for recuperation in the hybrid module. This operating condition only occurs during emptying of the bucket over the unloading site, when travel and implement drive both recirculate power and only auxiliary consumers absorb the excess torque. The engine is relieved completely and the surplus power dissipates in drag losses.

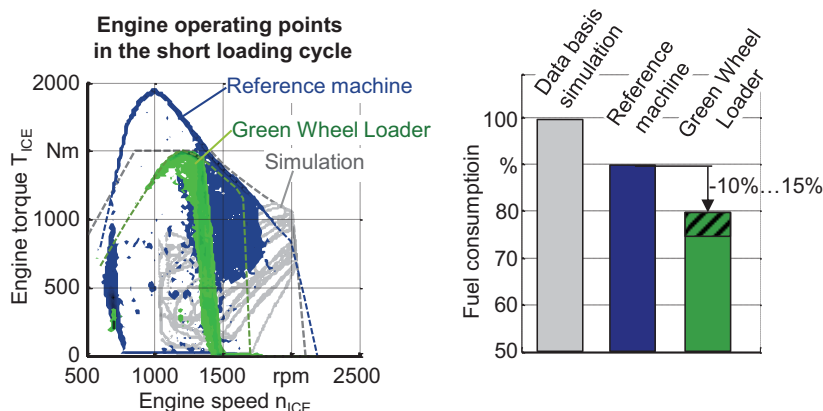


Figure 9: Comparison of engine operating points

The fuel consumption of both wheel loaders, reference and demonstrator vehicle, was measured by weighting of external fuel reservoirs. In repeated measurements, the “Green Wheel Loader” consumed 10 – 15 % less fuel than the reference machine with regard to the moved mass of gravel. **Figure 9** shows the engine operating points of both machines as well as simulation results obtained in an early stage of the research project [10], [13]. Compared to the simulations the measurement results show deviations, which are mainly due to the data basis used for system simulation. The reference machine is considerably advanced compared to the configuration modelled in simulation. Especially the different diesel engine with lower idle speed and higher torque as well as the optimised torque converter configuration lead to an already significantly increased fuel efficiency. Under consideration of these effects, the simulation results supplement the experiments. The simulations show engine operations points at high engine speeds

and medium to high torques. The reference machine converts the majority of energy at significantly lower engine speeds, which already reduces fuel consumption significantly. The "Green Wheel Loader's" engine speed range is even lower. Together with the recirculated energy used to relieve the engine this results in the measured fuel savings.

5.2. Impact of the hybrid system

Due to the wheel loader's operating characteristics and the used efficient subsystems capable of energy recirculation, the majority of the recirculated energy in the "Green Wheel Loader's" drive train is regenerated and directly absorbed by other consumers. Only a small fraction of the engine output energy is available for recuperation in the hybrid module. Due to the small amount of energy and the lossy conversion processes, practically no energy is stored in the hybrid accumulator. Therefore, no additional power is available to support the engine during phases of high loads. In order to provide boost functionality increased machine performance, the necessary energy has to be supplied by the diesel engine by actively loading the hybrid's accumulator. Measurements showed an increased machine performance due to the additional torque available. Especially during phases of dynamic power demand, engine speed undershoots could be reduced and more power was available for digging operation. The influence on the loading cycles' duration is low, as acceleration and deceleration characteristics mainly depend on the machine control's tuning and transmission-internal boundaries. Therefore, a significant increase of machine productivity is not to be expected. The increased machine performance leads to a surplus in fuel consumption of 7 % compared to measurements with deactivated hybrid, as besides the additionally necessary energy for filling the hybrid's accumulator significant losses occur during the multiple conversion processes. Furthermore, the hybrid's displacement unit causes drag and leakage losses, which additionally strain the "Green Wheel Loader's" drive train.

By opening the engine's operating speed range to lower values, further fuel consumption reduction is possible despite the hybrid's additional losses. Lower engine speeds allow for decreased fuel consumption, but dynamic load capacity and available torques also deteriorate significantly. The hybrid module can compensate these functional deficits by dynamically supporting the engine. Thus, the machine's functionality and performance are maintained while lowering fuel consumption. This approach was not part of the current research project and has to be addressed in future activities.

6. Conclusion and outlook

The joint research project “TEAM Green Wheel Loader” combines for the first time the most promising drive concepts currently available for mobile machinery in an innovative and energy efficient drive system. The drive system’s main consumers offer additional degrees of freedom in control compared to conventional solutions and the capability of energy recirculation. The developed operating strategy decouples the machine operator from directly governing the engine and rather controls it based on the individual subsystems’ demands.

Extensive testing of the demonstrator vehicle under realistic operating conditions in a gravel pit proved the developed drive and control system’s functionality. Professional machine operators regularly evaluated machines’ behaviour and controllability in order to ensure a practice-orientated machine development. Compared to a state-of-the-art series machine the “Green Wheel Loader” showed fuel savings of 10 – 15 % at the first attempt in a short loading cycle. Due to the low amounts of recuperable energy available in the load cycle, the parallel hybrid system could not contribute to the fuel savings.

With the “Green Wheel Loader, a functioning test vehicle is available for the evaluation of innovative drive and control concepts for mobile machinery. The testing under realistic operating conditions revealed continuative optimisation potential. Regarding the subsystems’ hardware configuration, potential lies in the improvement of load stiffness and dynamic behaviour. The operating strategy can be further enhances regarding engine speed control and machine operability. By further improving the machine control structure, the engine speed can be lowered while improving the load response characteristic at the same time, thus enabling additional fuel savings.

The research and development project “TEAM – Development of Technologies for Energy-saving Drives of Mobile Machinery” is funded by the German Federal Ministry of Education and Research (BMBF) within the Framework Concept “Research for Tomorrow’s Production” and managed by the Project Management Agency Forschungszentrum Karlsruhe, Production and Manufacturing Technologies Division (PTKA-PFT).

GEFÖRDERT VOM



**Bundesministerium
für Bildung
und Forschung**

BETREUT VOM



PTKA
Projektträger Karlsruhe
Karlsruher Institut für Technologie

7. References

- /1/ N. N.: "ZF cPOWER – continuously variable transmissions for wheel loaders", press release ZF FRIEDRICHSHAFEN AG, Germany, 2010.
- /2/ Mutschler, S.; Müller, M.; Möller, D.; Panizzolo, F.: „HVT – The power-split transmissions for wheel loaders“ Antriebstechnisches Kolloquium 2013, ATK 2013, Aachen, Germany, 2013.
- /3/ Jähne, H.: „Struktursystematik und Effizienzpotential hydraulischer Fahr-antriebe unter Berücksichtigung der Applikation“ PhD Thesis, Technische Universität Dresden, Dresden, Germany, 2013.
- /4/ Rahmfeld, R.: "Development and Control of Energy Saving Hydraulic Servo Drives for Mobile Systems" PhD Thesis, Technische Universität Hamburg-Harburg, Hamburg, Germany, 2002.
- /5/ Williamson, C.: "Power Management for Multi-Actor Mobile Machines with Displacement Controlled Actuators" PhD Thesis, Purdue University, West Lafayette, USA, 2010.
- /6/ Heybroek, K.: "Saving energy in construction machinery using displacement control hydraulics: concept realization and validation" PhD Thesis, Linköping University, Linköping, Schweden, 2008.
- /7/ Thiebes, P.: "Hybridantriebe für mobile Arbeitsmaschinen" PhD Thesis, Karlsruher Institut für Technologie, Karlsruhe, Germany, 2011.
- /8/ Hui, S.; Jing J.: "Research on the System Configuration and Energy Control Strategy for Parallel Hydraulic Hybrid Loader" In: Automation in Construction 19 (2), 2009.
- /9/ Ponticel, P.: "Caterpillar Hybridizes the Excavator Using Hydraulics Technology." SAE Article, 28.12.2012, <http://articles.sae.org/11692/>.
- /10/ Schneider, M.; Koch, O.; Weber, J.; Bach, M.; Jacobs, G.: "Green Wheel Loader - Development of an energy efficient drive and control system" 9th International Fluid Power Conference (IFK), Aachen, Germany, 24. – 26.03.2014.
- /11/ Schönfeld, S.; Günther, M.: „Verbundprojekt TEAM - Mehr Motor mit weniger Diesel?“ In: Mobile Maschinen, 3/2014.

- /12/ Bauer, F.; Feld, D.; Grün, S.: „Double piston accumulator – innovative hydraulic accumulator for mobile working machines” 3rd conference on hybrid drives for mobile working machines (3. Fachtagung Hybridantriebe für mobile Arbeitsmaschinen), Karlsruhe, Germany, 17.02.2011.
- /13/ Schneider, M.; Koch, O.; Weber, J.: “Green Wheel Loader – Operating Strategy of an Energy Efficient Hybrid Drive Train” SAE Technical Paper 2014-01-2400, presented at SAE Commercial Vehicle Engineering Congress (ComVec), Rosemont (IL), USA, 7. – 9.10.2014.
- /14/ Koch, O.; Richter, S.; Weber, J.; Eichler, A.: “Process-Efficient Real-Time Simulation to test the functionality of Drive and Control Systems” 17th ITI Symposium, Dresden, Germany, 4. – 5.11.2014.

8. Nomenclature

Variables

$BSFC$	Brake specific fuel consumption	g/kWh
E	Energy	kJ
j	Joystick signal	-
n	Rotational speed	rpm
P	Power	kW
\vec{r}	Return values from subsystem controller	-
\vec{s}	Set values for subsystem controller	-
T	Torque	Nm
α_{thr}	Throttle / drive pedal signal	-
β_{br}	Brake pedal signal	-

Indices

act	Actual value
AD	Attachment drive
HM	Hybrid module
ICE	Diesel engine (internal combustion engine)
$Lift$	Attachment lift function
set	Set value
TD	Travel drive
$Tilt$	Attachment tilt function

Decentralized energy-saving hydraulic concepts for mobile working machines

Professor Dr.-Ing. Johann Lodewyks

Competence Center Mechanische Systeme (CCMS), Hochschule Luzern, Technikumstr. 21,
CH-6048 Horw, Schweiz, E-mail: johann.lodewyks@hslu.ch

Dipl.-Ing. Pascal Zurbrügg

SUNCAR HK AG, Inspire c/o ETH Technoparkstr. 1, PFA H13, CH-8005 Zürich, Schweiz,
E-Mail: zurbruegg.pascal@bluewin.ch

Abstract

The high price of batteries in working machines with electric drives offer a potential for investment in energy-saving hydraulic systems. The decentralized power network opens up new approaches for hydraulic- and hybrid circuits. In addition, the regeneration of energy can be used at any point of the machine. For the example of an excavator arm drive with a double cylinder two compact hydraulic circuits are presented, which relieve a central hydraulic system.

KEYWORDS: e-drive excavator, hybrid hydraulic system, energy regeneration, three areas cylinder drive, accumulator system

1. Introduction

The undeniable and physically justified advantages of hydraulic drives are the unmatched power density, reliability and easy generation of linear movements. This contrasts with still the disadvantage of poor system efficiency. The causes of this are significant throttling losses that inevitably occur in a nearly incompressible medium at any kind of flow resistance. The advantage of a simple hydraulic drive structure is always connected to the disadvantage of large energy losses. Constant displacement pumps for the construction of a constant pressure grid and throttle controls for sensitive control and regulation of the drives are the main cause for the poor energy balance. This technology has enormous, systemic losses and is not capable of regenerating energy. The efficiency of hydraulic displacement units is, in many areas of the efficiency diagram as well as that of e-drives. There are therefore many years' efforts to develop hydraulic controls without throttle losses. Hydrostatic transmissions have proven themselves in practice for a long time in stationary applications with large

driving power. However, once the linear drives are to be used in the form of differential cylinders, it becomes difficult to connect the asymmetric flow rates of the consumer with the balanced volume flow of the pump /2/, /4/.

1.1. State of the art

Compensation options with the help of hydro transformers or storage systems have been found, but most of them are very expensive /6/, /8/. Other variants imply by shifting pressure and hence flow pulses which are noticeable in the driving behavior /3/, /5/. In stationary installations, the space advantage over a synchronous cylinder is large enough to employ such solutions only with a stroke of several meters.

The path of digital hydraulics is an alternative for smaller drives, because the switching dynamic even for bigger valves is increasing. Similar to a PWM signal in electrical engineering, an analog signal of individual pulses is composed of variable width /7/, /5/. Due to the complete opening of the valve most of the throttling losses are reduced. However, it is to be expected with considerable noise, which is at higher power range becoming a problem.

1.2. Mobile Hydraulic

An important field of hydraulics is mobile work machine industry, for example the in large numbers produced construction machines. The demands in the part of the drive technology are very high. The drives must not only be compact and powerful, but also very robust and insensitive to contamination and shock loads. In lifting equipment of all kinds high security requirements are valid. An accidental move of the load, for example an uncontrolled lowering of the lifting device must be prevented in any case. This is today ensured by load control valves or pipe rupture valves, but they cause additional throttle losses in the power flow.

The classic drive concept of a construction machine consists of a central energy source, the diesel engine and a central pressure supply unit, which may well consist of several pumps of different type. All hydraulic consumer units are supplied with energy by a constant-pressure system, and there are various ways of adapting the pressure level to the needs of the highest loaded consumer (LS, NFC) /5/. Recent studies have shown that it is energetically worthwhile to build a multi pressure network with graduated pressure levels /1/, /9/. These systems can also be combined with accumulator solutions.

2. Battery electrical excavator

A completely new situation arises when the diesel drive is replaced with a battery-powered drive. Then a high-voltage electric power is available in the entire operating device, which is even able to absorb large amounts of energy quickly in the case of regeneration. Now every consumer can optionally be operated electrically, hydraulically or as a hybrid. Each kind of drive solution can make sense based on the local requirements in the machine. Today, these are still special solutions that are not competitive in the breadth of applications. However, if energy prices increase again in the future and if emission regulations become more restrictive, then the market conditions will change in favor of these solutions. It is therefore today at the development of technically robust and practicable solutions, to be ready for the demands of the future.

One such example is a 16 t - excavator from the Japanese Takeuchi Company, which has been rebuilt at the ETH Zurich under the guidance of the company SUNCAR HK AG from a diesel drive to a battery-powered drive. The valuable construction space is used optimally, because the diesel tank, the exhaust gas treatment, the exhaust system and the diesel engine itself are not any longer necessary. Instead of these components, a compact frequency-controlled electric motor is used. The hydraulic system could be adopted without any change.

In the case of the excavator, the great weight of the batteries is not a disadvantage, because they simply replace the classic counterweight. The advantages of such a device are the "zero emissions" at the workplace, the low noise and a good and dynamic controllability of all working movements. The first experiences show, that the response of the electric motor is significantly faster and more sensitive. A pleasant, quiet, zero emission and vibration-free working is possible now. The high battery price today is the reason for substantially higher investment costs, that's why the market penetration is still limited. Cost advantages for the E-excavator expect first assessments after about seven or eight years, because of lower energy and maintenance costs.

The efficiency of the frequency controlled permanent magnet axial flow motor is located in many areas of the engine map by over 90% (**Figure 1**). Significant energy savings result therefore in comparison to the diesel engine which has an efficiency of about 35% in maximum. At the same time the rectangular form of the characteristic field fits much better to a hydraulic drive, because now the corner power can be exploited. In addition, both components are able to regenerate energy.

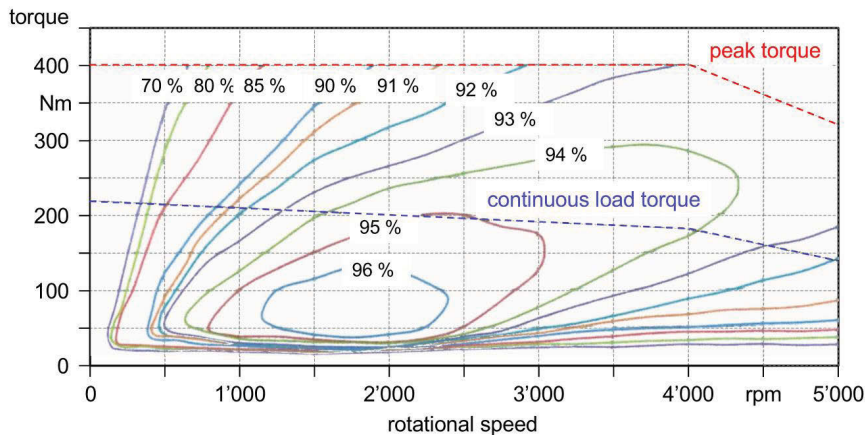


Figure 1: Characteristic curves of the axial flow motor

With this drive concept, a continuous operation time of six hours is possible. Even without optimizing the hydraulic system. For a comprehensive eco balance also the way of power generation is to be regarded. But as well the power generation cost of oil is rising (deep water drilling, oil sand, fracking) and so a simple answer to this question is not possible.

2.1. Energy management solutions

The energy management system can now be reconsidered and it begs the question: What role can the hydraulic system play in such a device? The high battery costs (>100'000 CHF) justify a higher investment budget for energy-saving drive solutions.

The following scenarios are conceivable:

1. E - actuators replace the hydraulic drive
2. Hydraulic Stand-Alone Drives are used
3. Hydrostatic Drives are used
4. Hydro Transformers for linear actuators are used
5. Digital Hydraulic Drives for auxiliary equipment
6. Secondary controlled motors at constant pressure network

The use of an electro-mechanical linear drive in the excavator is severely limited. Their low power density and the sensitivity to dirt and vibration are problematic. Stand-Alone Drives have the advantage that the power supply can be optimized for the individual exposure of the consumer. A pressure reduce from a constant-pressure network is not necessary and prevents losses. The individual pressure generation caused a greater expenditure of components and is therefore a disadvantage.

Hydrostatic Drives are useful for heavy-duty rotary actuators, such as the swivel drive of the superstructure, and correspond to the state of the art. However, linear drives require complex circuitry compensations and therefore often require too much construction space. The Hydraulic Transformer is a very smart way to adapt asymmetrical consumers at a constant pressure network. So far, however, there are no such components that have prevailed in the market.

The Digital Hydraulics is limited by the performance of switching valves. An increase in the volume flow is possible by parallel connection of several valves. In fact thereby the expenses for each drive increase significantly. The secondary control is an energetically interesting solution for rotary actuators at a constant pressure network. The separation of the motor part and pressure supply part, allows optimizing the pump drive regardless of the demands of the consumer's /1/. However, linear actuators cannot work without additional components at a constant pressure network.

2.2. Regeneration

An important contribution to the efficiency improvement is the consistent use of energy regeneration. Lifting devices offer potential energy and all braking processes kinetic energy that can be used. Therefore compact and powerful energy storage devices are required. A comparison of electrical, mechanical and hydraulic energy storage devices shows that the classical hydraulic accumulator has very good results and works with high efficiency (**Figure 2**).

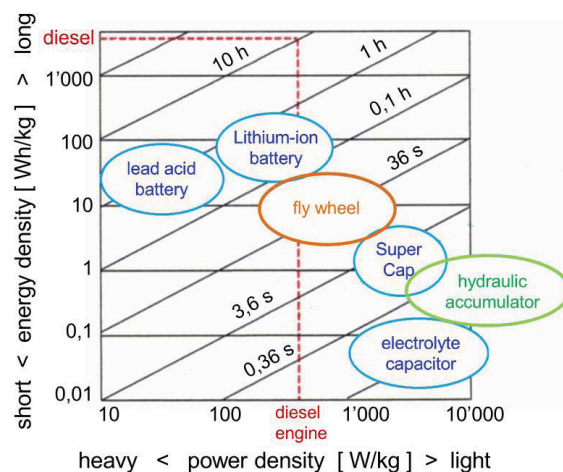


Figure 2: Comparison of energy storage devices

The braking energy of rotational movements of the superstructure, for example, can be regenerated with a hydrostatic transmission to the e-power grid. It can however be recovered only half of the power, even if all components (hydraulic motor-hydraulic pump -E-motor) have an individual efficiency of 90 %, because the energy flows thru the whole chain of components in both directions. Nevertheless, the change makes sense, since the central hydraulic system is relieved and also the efficiency is significantly better than a throttle control.

The movement cycle of heavy excavator arm is a source of potential energy that should be noted. Based on the information about the maximum load of the excavator an overview of the load pressures can be calculated in the workspace (**Figure 3 left side**). There are work points at which the maximum load pressure of 227bar is not achieved, because the risk of tipping consists. The efficiency of a hydraulic throttle control is proportional to the ratio of load pressure and the supply pressure of the system. In an optimum control of the supply pump arises in looking at work space of the excavator, an average efficiency of hydraulic control of 54% at full load. This also is the maximum value achievable. The mean, mechanical drive power of the boom cylinder is 30kW. The magnitude of renewable energy can be estimated by considering the load pressures in the boom cylinder with a movement of the empty bucket (Figure 3 right side). The mean efficiency of the throttle control is lowered in this case to 23%. If a lowering operation carried out with an empty bucket and maximum working speed, which happens very often, so this corresponds to an average power of 12.7kW.

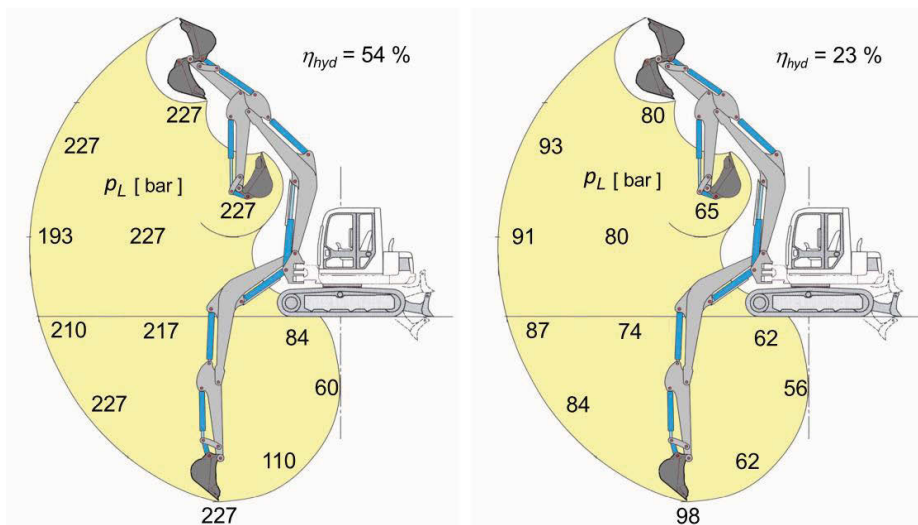


Figure 3: Maximum and Minimum load pressure in the boom cylinder

The benefits of the change from a diesel engine to an e-drive show the energy flow diagrams and the numerical example of the average power of the boom cylinder (**Figure 4**). The need for power is reduced from 200kW diesel fuel to 77kW of electrical power. At the same time it becomes clear that the throttling losses and the inability of regeneration are the greatest potential for further savings.

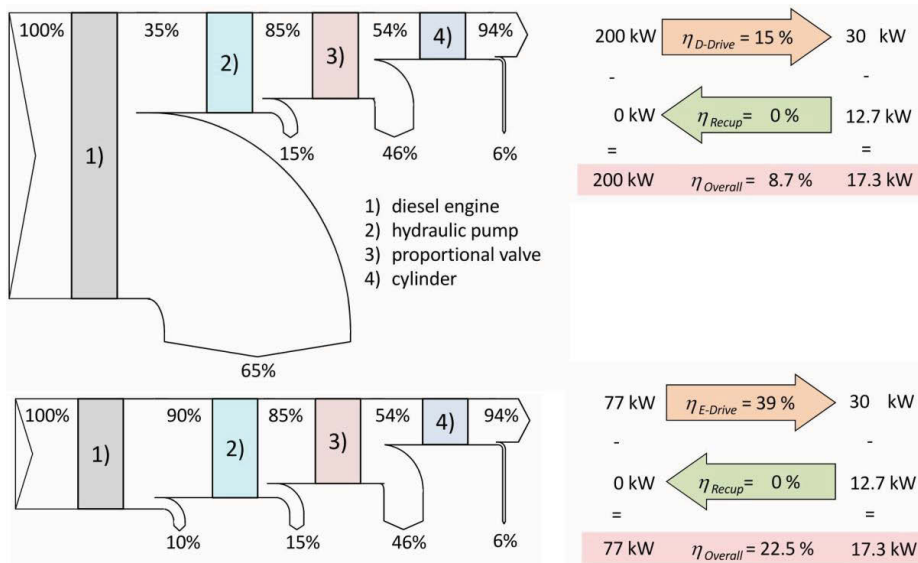


Figure 4: Efficiency comparison without a possibility of power regeneration

3. Three areas hybrid circuit

A three areas hybrid circuit for tandem linear actuators with an area ratio of 0.5 and with a large, static pressure load share (F_L) has been developed (**Figure 6**). This version combines many advantages of the already known solutions. The annular spaces of the tandem cylinders will be connected and thus act as an area with one pressure (p_B). The servo fixed displacement pump (HP) is connected to these annular chambers and a piston chamber and thus provides symmetrical area ratios. The third piston area with pressure (p_{A1}) can be connected to the pressure of the central hydraulic source (p_o), additionally (or exclusively) with an accumulator (SP) /10/. A feed pressure (p_{min}) supply compensates the pump leakage and prevents cavitation. The leak-free load holding at a standstill is achieved by switching valves. A separate pressure relief valve is not necessary if the drive torque of the servo constant pump (HP) is limited.

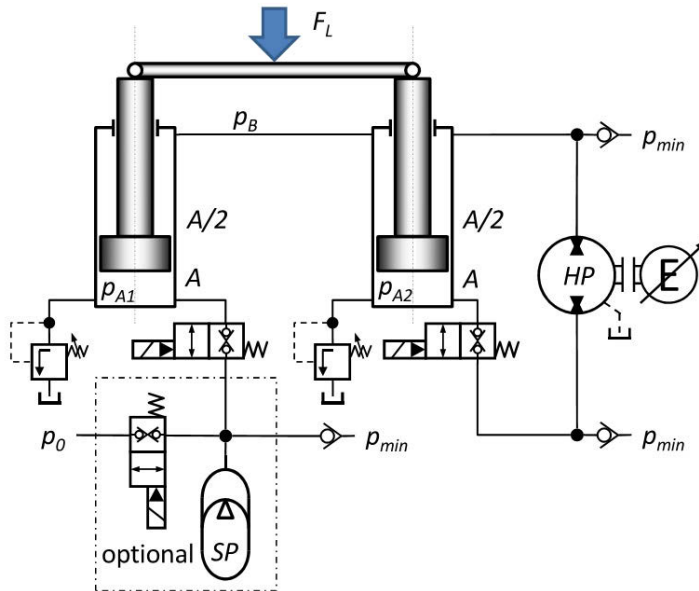


Figure 6: Three areas hybrid circuit for tandem cylinder drives

E-motor and fixed displacement pump can also be overloaded in the short term, so that the drive can also build train loads of approximately 20% of the pressure load and thus a four-quadrant operation is possible. The servo constant pump (HP) is speed controlled substantially. Load changes or variations in pressure (p_0) in the main circuit lead to positional errors in the field of oil elasticity, which is in the range of millimeters. The different pressure forces of the two cylinders are balanced by the massive mechanics of the boom arms again. An uncontrolled lowering of the load is reliably prevented by the redundancy of the drives, the blocking valves and the fact that the storage volume of accumulator is limited.

The energy flow diagrams (**Figure 7**) show the efficiency improvement in the drive part and in the regenerating part and the example of the power results in an efficiency increase to over 50%. This efficiency may optionally increase with the use of a 20 l - accumulator. Even if the storage volume takes over only 30% of the volume exchange, the effect with an increase in efficiency to 60% is significant.

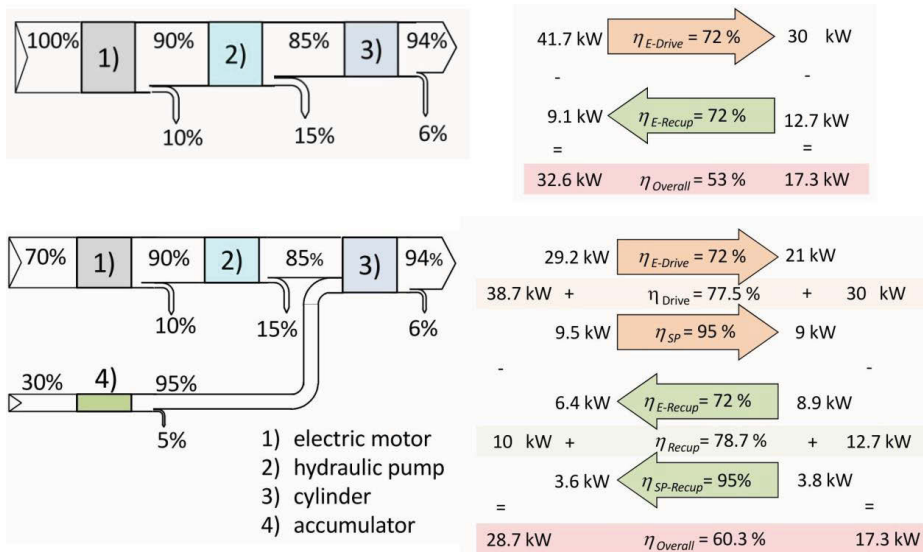


Figure 7: Efficiency comparison with the possibility of power regeneration

For this circuit configuration, the following advantages, which are particularly important for the lifting cylinder in an excavator, arise.

1. Compact cylinder with one piston rod
2. Flexible arrangement of the components
3. High safety level by redundant drives
4. All variants of hydrostatic drives are possible
5. Only one hydraulic motor unit without compensating elements
6. Only marketable hydraulic components are needed
7. Power regeneration in the electrical grid and/or with an accumulator
8. Least number of switching operations
9. Load distribution on hybrid drives
10. four-quadrant operation possibility

More advantages base on the connection to the Central hydraulics.

1. Flexible load distribution
2. Small, compact hydrostatic drive
3. Low installation space requirement near the cylinder
4. Easy and safe load holding at a standstill
5. Combination with multi pressure level systems is possible
6. Use of Load - Sensing possible
9. No throttling losses between central hydraulic and the cylinder control

Another variant can be used as a substitute for the arm cylinder (**Figure 8**), or even as a tandem unit, with balanced pressure conditions /11/, /12/, /13/, /14/. Disadvantage is the higher cost of such a special cylinder. In the case of E-excavator a hydrostatic drive with frequency controlled electric motor is particularly interesting. In return, high pressure hydraulic motors have the largest possible maximum speed, such as a bent axis motor with up to 10'000 rev/min. The high speed reduces the required displacement and thus the torque load on the electric motor. The entire unit is thereby very compact and can easily be integrated near the cylinder.

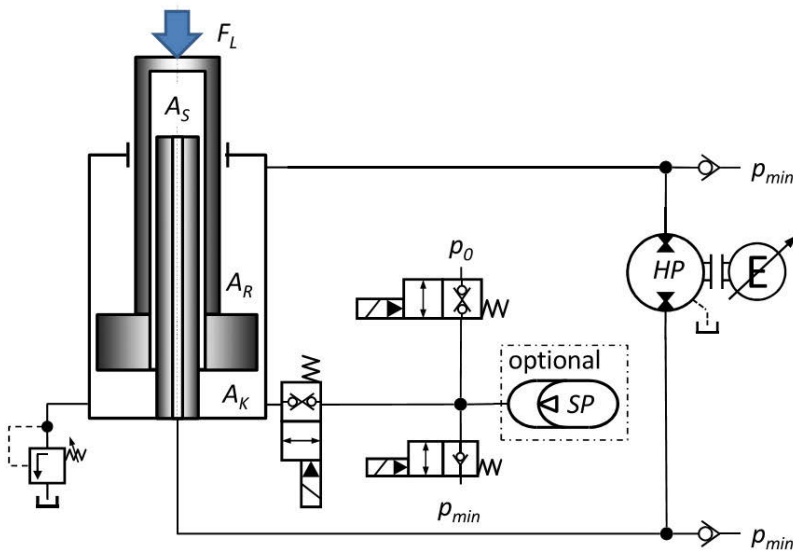


Figure 8: Three areas hybrid circuit for single or tandem cylinder

An initial cost-benefit analysis has shown that only an optimized boom cylinder can reduce the investment costs already at least 4.5% (5% with accumulator). The three area hybrid circuit is saving money from first day. In the further course of the project, such a drive is first constructed separately and examined on a test bench. In addition to the interaction of the hydraulic and electrical components an optimal drive and control concept has to be developed.

4. Summary

Disclosed is a three areas hybrid circuit, which has been specially optimized for lifting tasks in a work machine. It combines the advantages of a symmetrical hydrostatic drive with the advantages of a differential cylinder. The third piston area enables load sharing between direct drive and a central hydraulic system.

The direct drive may be a variable displacement pump, but also a fixed displacement pump with a frequency controlled electric motor. This combination makes sense, if the fixed displacement pump can run although the same high speed, the torque load of the electric motor decreases and the drive is smaller and more compact. The corner power can be exploited by two drive units and they are able to regenerate energy.

For the construction of the three areas hybrid circuit only marketable drive components are required and the drive can be flexibly integrated in different drive concepts. Both classical load sensing, as well as more recent approaches of a multi-level pressure network are conceivable. The redundancy of drives leads to a very high, systemic safety and reduces problems when starting up or when using numerous switching valves in the power section.

This compact drive concept is suitable for many lifting drives, also in the stationary area and the differential cylinder thus becomes a symmetrical consumer. The combination with a constant pressure network, which compensated the static loads, simplifies the control and allows optimizing the efficiency and the central drive.

5. References

- /1/ Sgro & Sebastian & Vukovic, Milos & Murrenhoff, Hubertus. 2012. Energieeffiziente Ansteuerung durch Volumenstromkopplung bei Einzelantrieb und digitale Druckkopplung bei mehreren Verbrauchern, 5. Fachtagung Baumaschinentechnik, Karlsruhe, Germany
- /2/ Becker, Robert 2012. Energieeffizienter Hydraulikantrieb mit Differentialzylinder, Elektrifizierung der mobilen Arbeitsmaschine, IHA
- /3/ Shen, Wie & Jiang, Jihai & Su, Xiaoyu & Karimi, Hamid Reza 2013. Energy Saving Analysis of Hydraulic Hybrid Excavator Based on Common Pressure Rail, Hindawi
- /4/ Quan, Zhongyi & Quan, Long & Zhang, Jinman 2014. Review of energy efficient direct pump controlled cylinder electro hydraulic technology, Renewable and Sustainable Energy Reviews, Elsevier
- /5/ Scherer, Martin 2015. Beitrag zur Effizienzsteigerung mobiler Arbeitsmaschinen, Karsruher Schriftenreihe Fahrzeugtechnik Band 32, KIT, Karlsruhe, Germany

- /6/ Peitsmeyer, Dierk 2012. Elektrifizierung der Arbeitsausrüstung mit Zylinderantrieben, Karsruher Schriftenreihe Fahrzeugtechnik Band 14, KIT, Karlsruhe, Germany
- /7/ Digitalhydraulik 2012. 5. Workshop on digital fluid power, Tampere, Finland
- /8/ Vael, Georges E.M. & Achten, Peter A. J. & Fu, Zhao 2000. The Innas Hydraulic Transformer, Society of Automotive Engineers, Innas
- /9/ Geimer, Markus & Dengler, Peter & Schuster, Gerhard & Baum, Heiko & Dombrowski, René & Wessing, Christoph & Paul, Werner 2012. Effizienzsteigerung eines Konstantdrucksystems durch eine Zwischendruckleitung – KonZwi, Schlussbericht zum Forschungsprojekt, BMBF, Germany
- /10/ Landmann, Thomas & Holländer, Claus & Späth, Ralf 2013. Energieübertragungs- und Speicherlösungen für Hydraulikbagger, Karsruher Schriftenreihe Fahrzeugtechnik Band 15, KIT, Karlsruhe, Germany
- /11/ Baron, George 1974. Power shovel and crowd system therefor, Patent US4046270
- /12/ Kubik, Philip 1985. Power shovel and crowd system therefor, Patent US4738101
- /13/ Aarestad, Robert 2003. Cylinder with internal pushrod, Patent US2005066655
- /14/ Fröhlich, Udo & Krug, Sebastian & Dörtoluk, Ibrahim 2012. Hydraulische Stelleinrichtung, Patent DE102012012142

6. Nomenclature

η	efficiency	
p	pressure	bar
A	area	mm ²
F	force	N

Group 2: Novel System Structures

Electric Hydrostatic Actuation - modular building blocks for industrial applications

Dr.-Ing. Achim Helbig

Moog GmbH, Hanns-Klemm-Str. 28, D-71034 Böblingen, Germany, Innovation Projects Manager, E-Mail: ahelbig@moog.com

Dr.-Ing. Christoph Boes

Moog GmbH, Hanns-Klemm-Str. 28, D-71034 Böblingen, Germany, Director Engineering Innovation Projects, E-Mail: cboes@moog.com

Abstract

Electro Hydrostatic Actuators (EHA) are emerging as a viable option for industrial machine builders as the design combines the best of both electro-mechanical and electro-hydraulic technologies. The EHA is a highly integrated, compact alternative to traditional hydraulic solutions. Automation engineers moving toward electro-mechanical actuation in pursuit of energy efficiency and environmental cleanliness, will find an EHA an attractive option for high force density actuators.

This paper will address the factors to consider when assessing an industrial machine's application suitability for this latest innovation in actuation. It describes principal base circuits, a concept for EHA building blocks and a realized pilot application as well as challenges on actuator and components level.

KEYWORDS: Modern fluid power, Energy consumption, Power by wire, Hydraulic systems, Pumps, Hydrostatic gearbox, Industrial Hydraulics, Industrial Automation, Autonomous Systems

1. Introduction

An electro hydrostatic actuator (EHA) is a self-contained hydraulic actuation system that integrates a cylinder, auxiliary valves, feedback unit, variable speed pump, servo motor, electric drive and control electronics, into a compact unit requiring only an electrical connection. The integration of separate components for classic hydraulic actuation solutions along with the elimination of hoses and couplings are the readily apparent differences from a traditional hydraulic solution. The pump, servo motor, and servo drive are Moog building block products available in different variations and sizes

which are combined with manifolds and a cylinder to create an integrated EHA that can be customized in terms of speed, force, space requirements and functionality.

Electro-Hydrostatic Actuation (EHA)

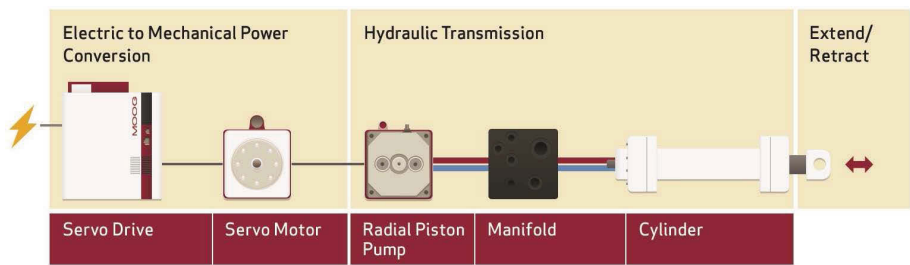


Figure 1: General layout of an EHA actuator

The EHA, as shown in Figure 1, converts energy from electric via hydraulic to mechanical energy. An electric servo motor drives a bidirectional, variable speed pump which is connected to the two chambers of a hydraulic cylinder. Depending on the direction of the flow, the axis is extending or retracting. In contrast to the classic hydraulic system, the power control is done by the motor/ pump unit. Varying the speed of the pump means varying the flow and thus the velocity of a cylinder. The pressures in the chambers are load-dependent. This enables the electro-hydrostatic actuator to use energy most efficiently and deliver power on demand (see **Figure 1**, **Table 1**).

	EM	EH	EHA
Energy Efficiency	✓	✗	✓
Environmental Cleanliness	✓	✗	✓
Low Noise Emission	✓	✗	✓
High Forces	✗	✓	✓
No Backlash	✗	✓	✓

Table 1: Benefits of actuation technologies

Due to the energy efficiency of the system, the hydraulic oil absorbs little heat. Heating is typically in the range of only 40°C to 60°C in a n environment of 25°C. Convection cooling of the hydrostatic gearbox is usually sufficient for an electro-hydrostatic actuator. This allows designers to build compact, modular units with a self contained hydraulic system. The oil of such an actuator ages very little and does not usually need to be changed during the entire lifetime of the system. The design of an EHA axis is

highly flexible, various layouts are possible and it can be adjusted to carry out fail-safe options. Serial movements of several axes supplied from a single pump are also feasible.

Machine builders, who are seeking a transition to an all electric machine actuation solution, should evaluate the EHA for a number of compelling reasons. For those motion control axes that require higher forces or large gearbox ratios the EHA concept offers significant benefits. Furthermore, machine builders will benefit from the all-electric interface.

2. Base functionality

Hydrostatic actuators are currently used in mobile and aircraft applications. The motivation to use the technology is similar to the benefits mentioned in Table 1. Additional arguments like compactness and light weight are crucial in these applications. Generally, there are four characteristic base circuits for EHA's. Application and customer specific solutions can be simplified to these circuits, see **Figure 2**.

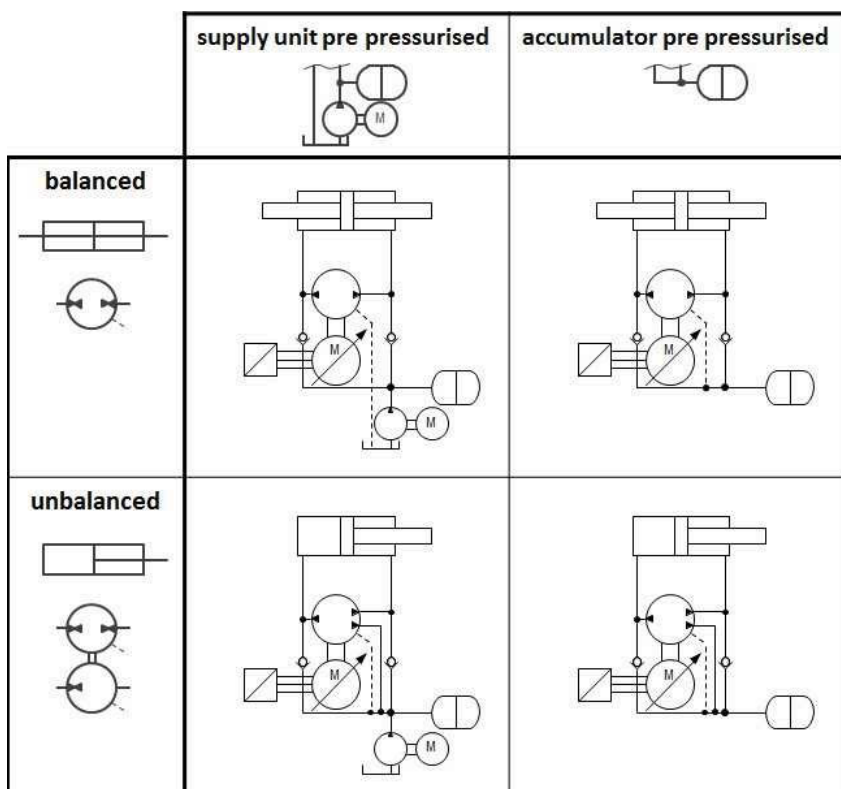


Figure 2: Characteristic base circuits for EHA's

The simplest system layout for an electro hydrostatic actuator can be done for a balanced cylinder. For unbalanced cylinders the unequal flows of the two cylinder chambers have to be compensated. A typical solution for the compensation of the non equal flows Q_A and Q_B , is the use of two pumps as shown in Figure 2. This compensation circuit is well known from the literature and established as a standard solution in many applications. The use of a customized 3-port pump is a smart solution, which allows a reduction of components and therefore a reduction of system costs. Such a pump design is currently in development.

In all hydrostatic transmissions the internal and external leakages of the components, especially the pump and the cylinder can be compensated by two different approaches. Either via a small auxiliary supply unit or via a pump housing connection to the pre pressure path. In both cases a low pressure accumulator is used to pre pressurize the hydrostatic gearbox. A supply unit in combination with an open tank allows a complete decompression of the system for maintenance, service operations, fail-safe or during emergency stop. Furthermore the supply unit can be used to realize a centralized filtering and cooling. Usually this approach is used in applications where more than two EHA axes are used and the distance between the axes slightly small.

On the other hand an accumulator with a pre charged reservoir changes the actuator into a completely closed system. Such a totally closed system with an accumulator as a reservoir allows the use of the actuator in clean room applications. In parallel these systems define a line replaceable unit, which could be easily and quickly changed in the field. Service or maintenance tasks, which require an opening and decompression of the system, imply a bleeding and pre charging of the system.

3. Concept of building blocks

Leveraging a combination of engineering skills in hydraulics, electric servo drives and brushless servo motor design Moog formulated an EHA that is suitable for the industrial automation market requirements relative to costs, environmental certification, and connectivity. The continual price decline in power electronics and servo motors has played a role in enabling the Moog engineering group to develop an EHA that is ideally suited for many industrial applications. EHAs are now at a price point where they are a competitive alternative to traditional (valve controlled) hydraulic solutions. Factoring in the elimination of hydraulic plumbing, auxiliary pumps, servo valves, and the ongoing maintenance of filters and valves the EHA provides a significant value proposition. The self contained systems approach translates into much higher reliability as failure and

maintenance associated with individual components of a traditional electro-hydraulic solutions are mitigated, if not eliminated altogether.

To make the EHA system accessible to more applications, Moog is adopting a modular approach combining standard building blocks such as servo drives and a servo motor/pump combination in typical sizes with a manifold and cylinder that will be customized to the exact needs of the application. This will improve the time to market and reduce the engineering and sizing efforts for machine builders to incorporate this technology in new generation machines, see **Figure 3**.

This concept allows a customer and application specific scope of supply. It ensures a high flexibility in terms of functionality, pressure/flow or force/velocity needs, mechanical interface and envelope requirements. The customer interface can be freely selected; existing infrastructure equipment can be used further.


Available Building Blocks		Customized Building Blocks based on Customer Requirements		Customer Project
 Servo Drive		 Servo Motor Pump Unit		
				
Size	Current [A]	V_{max} [cm ³]	Q_{max} [l/min]	p_{max} [bar]
BG5	45	19	85	350
BG5	60	32	118	350
BG5	72	45	148	280
BG6	90	63	189	350
BG6	110	80	216	350
BG6	143	100	250	280
BG6A	210	140	322	280
BG7	250	250	450	350
		+		
		 Manifold		 Cylinder
				
		Customized in terms of:		Customized in terms of:
		a) Pressure/Flow Needs b) Envelope Requirements c) Functionality		a) Force/Velocity Needs b) Envelope Requirements c) Mechanical Interface
		→		

Figure 3: Moog range of “EHA ready” standard and customized building blocks

The standard building blocks components (Figure 3, left) are evaluated and field proven for many years. These components are adapted to the specific requirements in an EHA. For example, the pump housing, the pump interface and the motor direct connection has been adapted. Base pump technology is a radial piston engine. In addition to high efficiency and low noise behavior, this engine allows the 4 quadrant operation. These are features of prime importance. On the other hand a two gears hydrostatic transmission can be realized via the “Dual Displacement” pump adjustment very easy.

4. Applications and Challenges

4.1. Deep Drawing Press

Moog worked with the Fluid Power Institute of Dresden University to incorporate the EHA technology on a Die Cushion Press so it could be objectively compared to a traditional servo control system using servo valves. The objective of this project was an improved energy efficiency of the system with the same dynamic performance as known from the original, classic system architecture.

The conventional system was a hydraulic press machine and the architecture for the die cushion actuation was four separate cylinders, each controlled via servo valves. All of these four axes were supplied by a variable displacement pump. Next an EHA system was installed for each cylinder in the die cushion including a servo electric motor connected with a radial piston pump. All of the four axes were connected with an accumulator to support the low pressure level. During the deep drawing process the servo motor/pump unit was acting in generator mode. Via the servo drive, it was possible to provide the recovered energy from the die cushion to the ram actuator, see **Figure 4**.

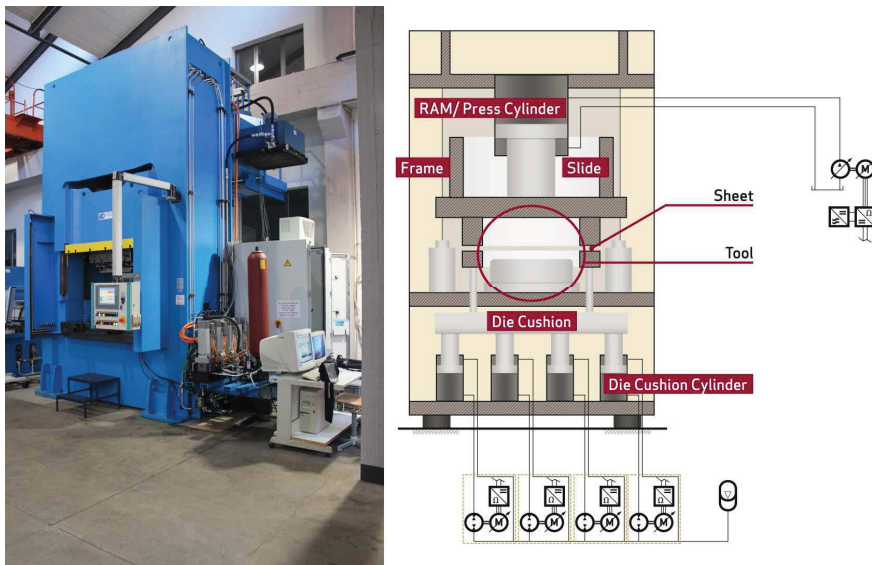


Figure 4: Deep drawing press layout using EHA for die cushion /2/

Energy savings during a complete machine cycle of approximately 30% could be achieved during tests while maintaining comparable dynamics and pressure control functionality. An improved energy efficiency of 30% provided by the EHA solution is a

significant improvement especially considering the large amount of energy consumed by this type of machine in a single year. An additional advantage is the substantial reduction or even substitution of oil cooling due to elimination of throttle losses.

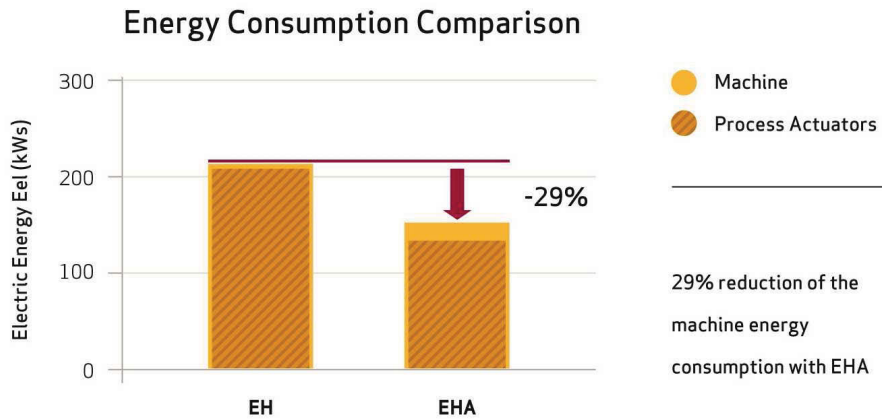


Figure 5: Energy efficiency of the test machine equipped with EHA /2/

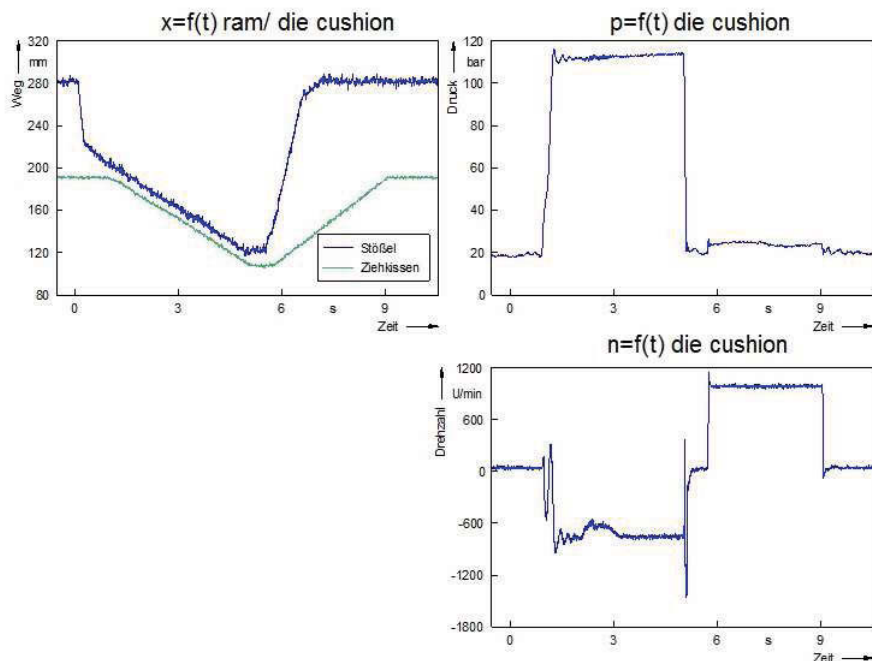


Figure 6: Plot of die cushion cycle /2/

This test suggests EHA technology is a viable alternative motion control system from a performance standpoint with the advantage of impressive energy efficiency; see **Figure 5** and **Figure 6**.

To evaluate whether an EHA is suitable for a machine control application requires both an economic and performance assessment. As mentioned earlier, from a black box perspective an EHA functions equivalently to an EM solution. Thus, from the automation controller (PLC in most cases) perspective the interfaces are all identical where motion profiles are all planned through digital interfaces. With that in mind, there are two scenarios that characterize the ideal application for an EHA.

1. Electro-mechanical machine conversions that need the force capability or power density of hydraulics for a small number of axes e.g. injection molding machines.
2. All hydraulic machines e.g. presses, rolling mills or steam turbines.

Machines that require a relatively small number of hydraulic axes are generally excellent candidates for EHA.

4.2. Challenges on actuator level

The unsymmetrical flow in and out of the two chambers of an unbalanced cylinder, as shown in Figure 2, effects a significant increase of the pressure in the low pressure reservoir by retracting the axis. The displaced volume out of the piston chamber of the actuator must be covered by an appropriately sized accumulator. This leads to an unintentional sizing of the low pressure accumulator in case of extremely unbalanced area ratios of the actuator.

A system layout with pre pressurized accumulators, as shown in the right column of Figure 2, ensures that the system is pressurized at all times. This characteristic requires additional efforts in the design and the maintenance of the system. Additional safety valves should be added in the flow paths between actuator and pump to avoid an unintentional movement of the axis.

A field service in the hydraulic system requires a decompression of the hydraulic lines. After the service the system must be pre charged and bled. Therefore a special, field suitable filling and bleeding unit is necessary.

Filtration and cooling of the fluid could be easily implemented in a system architecture according to the left column of Figure 2. The design with an open tank allows easy implementation of additional filtration and cooling unit.

4.3. Requirements at component level

There are additional requirements for components, which are used in hydrostatic transmissions actuators:

- The transmission pump must be designed for a 4 quadrant operation, which means, two directions to turn the pump and torque and speed in the same and in the opposite direction. This requirement is an obstacle for certain design concepts of the pump. Here a radial piston pump has been selected. This pump principle allows an easy implementation of bidirectional flow and torque – in other words: this pump is able to operate in pump and motor mode.
- Parallel pressure hold phases in the duty cycle of the machine represent a challenge for the pump or in general for the design concept of the pump. In pressure hold mode, the torque is high and the flow low or close to zero. Only the internal (pump) and external (cylinder) leakages have to be compensated. Piston pumps are more suited for this load cycles due to the option of using an additional leakage port. This allows heat dissipation out of the power harness.
- In comparison to valve controlled actuators, pump controlled actuators are characterized by an unsteady flow, especially in the range of small or very small flows ($< 5\%$ of the rated flow). This flow pulsation is based on the respective design concept of the pump. The high bandwidth of the speed loop of the servo motor allows a compensation of this unintentional unsteady flow characteristic.
- The pressure gain of the pump is determined by the geometric design parameters, especially the control joint. In this application the pump shows high pressure gain like it is known from zero lapped servo valves. Here the accuracy of the position control of the hydrostatic axis is similar to valve controlled hydraulic actuation systems.

5. Summary and Conclusion

This paper shows that Electro Hydrostatic Actuators represent a class of actuators which combine the advantages of classical electro hydraulic actuators and electro mechanical actuators to provide easy and cost efficient implementation, energy efficiency, and control performance. Of particular note is that the required high dynamic performance can be implemented with a significant reduction of energy consumption. To make the EHA system accessible to more applications, a modular approach combining standard building blocks and customized manifolds and cylinders was developed to meet the exact needs of the applications. Several critical and limiting topics have been discussed and solutions have been demonstrated.

6. References

- /1/ Boes, C. & Helbig, A. Electro Hydrostatic Actuators for Industrial Applications, 9th International Fluid Power Conference, Aachen, 2014

- /2/ Klug, D. Czeppel, T. Händle, W. Neumann, S. Weber, J. Lohse, H. Verbesserung der Energieeffizienz hydraulischer Tiefziehpressen (ENEHYT), Schlussbericht, Dresden, 2014

- /3/ Lohse, H. Modellierung hydraulischer Tiefziehpressen für Prozesskopplung, Reglerauslegung und energetische Bilanzierung; Dissertation, TU Dresden, 2014

Pressure Pulse Generation with Energy Recovery

Dr.-Ing. Siegfried Rotthäuser

Ingenieurgemeinschaft IgH GmbH, Heinz-Bäcker-Str. 34, D-45356 Essen,
E-mail: rt@igh.de

Dr.-Ing. Wilhelm Hagemeister

Ingenieurgemeinschaft IgH GmbH, Heinz-Bäcker-Str. 34, D-45356 Essen,
E-mail: hm@igh.de

Dr.-Ing. Harald Pott

Voss Fluid GmbH, Lüdenscheider Str. 52-54, D-51688 Wipperfürth,
E-Mail: harald.pott@voss.net

Abstract

The Pressure Impulse test-rig uses the principal energetic advantages of displacement-controlled systems versus valve-controlled systems. The use of digital-control technology enables a high dynamic in the pressure curve, according to the requirements of ISO6605. Accumulators, along with inertia, make energy recovery possible, as well as, enabling the compression energy to be re-used. As a result of this, there is a drastic reduction in operating costs. A simulation of the system before starting the project allows the development risks to be calculated and the physically achievable performance limits to be shown.

KEYWORDS: pressure pulse generation, pressure amplifier, variable displacement, energy recovery, flywheel energy storage, ISO6605

1. Mission

Fittings for hydraulic systems must be subjected to extensive testing before introducing them onto the market. In order to ensure the fatigue strength of the fittings, the Pressure Impulse test rig can be used, which is modelled using DIN EN ISO 19879, along with the pressure profile of ISO 6605. The test specimens will undergo 1×10^6 load cycles and be subjected to a test pressure of 1,33, yield pressure, which, without interference, lasts 12 days. Due to the large variety of fittings that exists, the test-rig would be in continuous operation. A reduction of power by one kW reduces the operating costs (based 2015) annually by approximately 2.500 EUR.

The task is to find a concept and implement this concept into the testing of the fittings while consuming the least amount of energy possible. The demands on the dynamics of the pressure profile are very high. The pressure curve, see **Figure 1**, must not exceed A and must approach into a tight tolerance zone at B.

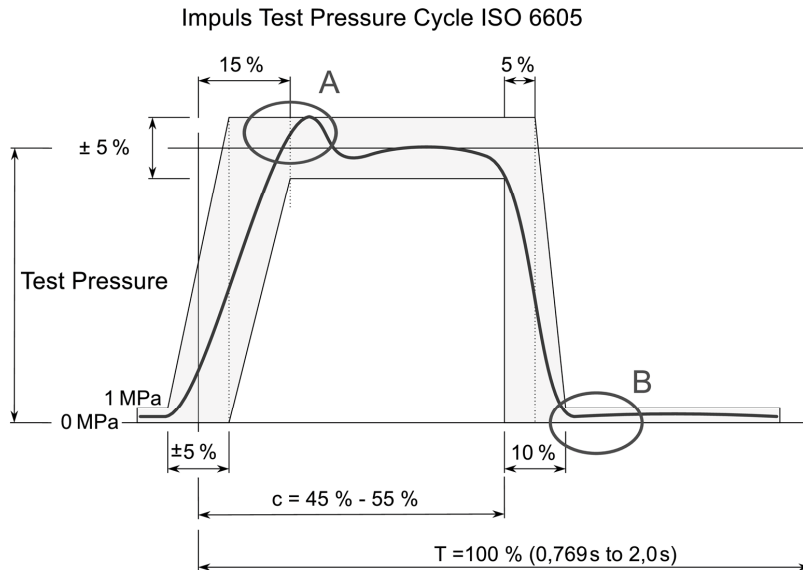


Figure 1: Test Zyklus nach ISO 6605

2. Concept

The energy required for compression to a desired pressure level is derived from the rigidity of the fluid medium and the elasticity of the pressure chamber. The increase of volume due to the expansion of the test specimen is proportional to the intake of compressed oil within a single digit percentage range. The proportion can be altered, if other variations of test specimen are used, as provided in the standard.

Taking into account the pressure-dependent compressibility results, **Figure 2** shows the pressure and the compression energy. The compression energy is determined using corresponding equation 1.

$$E_c = - \int_{V_0}^{V_0 - V_c} p(V) dV \quad (1)$$

For example, if a test pressure of 100 MPa is required, and a per-liter test volume of approximately $E_c = 2,5$ kJ of compression energy applied, this correlates to a volume of $V_c = 0,057$ liters.

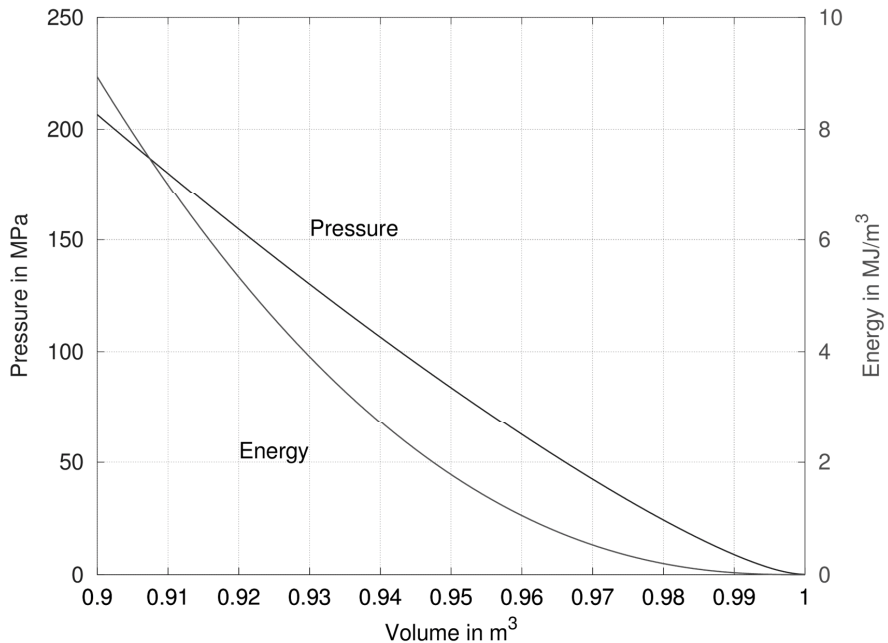


Figure 2: Pressure and Compression Energy

The compression energy in the test medium will be delivered by way of a pressure intensifier. The pressure intensifier consists of a high-pressure surface, a driving part (Working Cylinder) with two identical surfaces, each being twice as large as the high-pressure surface (A), and a counter-pressure part with triple the surface area, see **Figure 3**.

This incrementation of the surfaces allows the operation to work in such a way that when half of the test pressure is applied, the drive part must not exert a pressure difference when the back pressure is set to $1/6$ the test pressure. In the end position the drive member requires a pressure difference, which is only one quarter of the test pressure.

Comparing the control of such a pressure intensifier equipped with a $4/3$ -way valve (pilot valve), which is driven by a quick variable-displacement pump, the following picture emerges.

In the control valve concept, a constant supply pressure of $3/2$ the maximum load pressure is required in order to reach the required dynamic behavior. The supply amount withdrawn equates to two strokes per cycle.

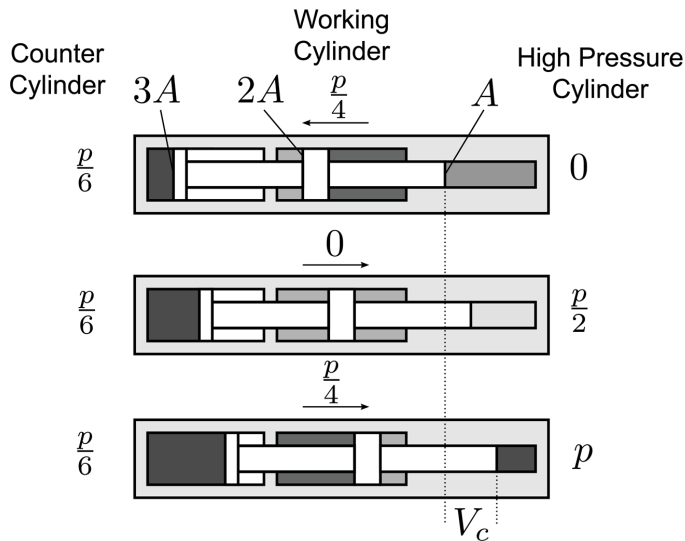


Figure 3: Area and Pressure Concept

In the example where test pressure $p = 100$ MPa and the compression volume, results $V_c = 0,057$ l in an energy E_v from

$$E_v = 1,5 \cdot \frac{p}{4} \cdot 2 \cdot 2V_c = 8,55 \text{ kJ} \quad (2)$$

per cycle. Now, imagine the theoretical efficiency as a ratio of the quantity of energy removed per cycle to the amount of compression energy, which produces a result of less than 30. Without the counter cylinder, twice the amount of energy is to be expended and the efficiency is less than 15%. Assuming a linear increasing of the pressure versus the stroke the efficiency is exactly $1/3$ or $1/6$.

Respectively, when the controlled-displacement system is the only driving power, which is actually necessary, there are no control-related throttling losses. The use of a pump in a closed circuit offers the advantage that a symmetrical operation is possible [1]. The counter cylinder, with its energy saving abilities, takes over nearly 75% of the energy expenditure is transferred, see **Figure 4**.

With the same rotational direction and the same pivot angle of the transition from the pumps, the motor operates automatically as soon as the pressure difference on the working cylinder changes sign.

In the differential pressure vs. flow-rate chart the axial piston unit works in 4-quadrant operation, while the speed-torque diagram works in 2-quadrant operation.

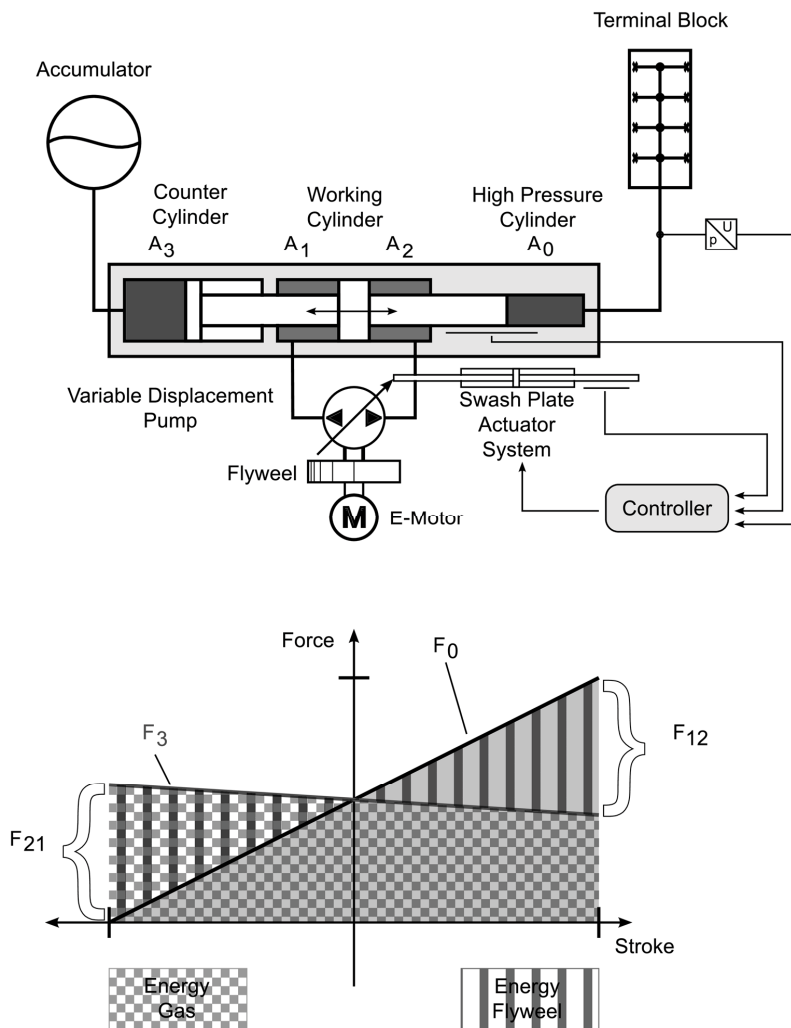


Figure 4: Concept with Energy Recovery

Losses in this set-up emerge from the valve controlled displacement system, the efficiency of the pump and the resulting, necessary, purging of the closed circuit, which

in the case of the test rig, accounts for approximately 250J per cycle on the actuating system, thus, approximately 10% of the compression energy.

Therefore, the energy can be used from the compression volume later, however, it must be stored for a short time. For this purpose, the mass moment of inertia of the axial piston unit is increased by a flywheel. Due to the rotational energy increasing quadratically with the rotational speed, a rotational pump speed of approximately 3000U/min is suggested. The high base speed translates to only a small change in speed during intake or release of the compression energy. The mass moment of inertia, 2kgm^2 , is selected in order to keep the change in speed at approximately 2%.

The test medium will not be replaced, because the compression and decompression takes place virtually without loss. A flushing of the closed drive circuit is necessary in order to purge the power losses of the axial piston and the pressure intensifier. The purge will be completed depending on the temperature, via a control valve, which operates parallel to the adjustment unit.

3. Validation

It is necessary to examine whether the developed concept is feasible with the components currently available. To this end, some questions must be answered, which was carried out through the use of simulation tools.

- Using this concept, are the required dynamics in the pressure profile of the ISO6605 achievable when standard market components are used?
- What requirements must the control system of the axial piston meet?
- What control strategy is required for this task and is this technology available?
- What losses are to be expected and should the flushing system be implemented?
- What are the physical limitations?

Answers to these questions have delivered an extensive and thorough simulation of the hydraulic system, see **Figure 5**. The software MATLAB/Simulink® was used for the simulation. The components could be well parameterized, because the necessary details about their internal construction is provided by the manufacturers. A reference cycle was initially used for the simulation (100MPa, 1 Liter test volume, 1Hz), in order to determine the appropriate components. It could then be explained, if, with these components, other test pressures, frequencies and volumes can be realized.

Arrangements using different volumetric displacements and pressure intensifiers with different stroke-area ratios have been investigated. The size of the adjustments were

determined in such a way that the pivoting angle in the reference cycle assumes a value of up to 50%. Smaller values result in poor efficiency and higher values offer too little reserve capacity with the use of larger test volumes. Use finds an A4VSG40 (swash plate with 40cm³) axial piston with servo-hydraulic adjustment, as described in secondary-controlled drives, is used. The control system is highly dynamic (30ms 0-100%) and designed for continuous operation.

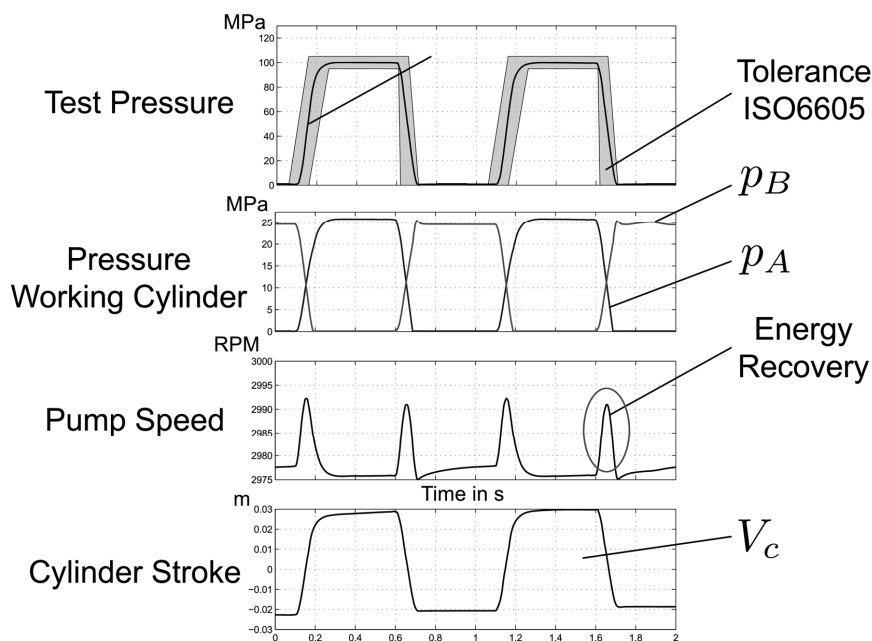


Figure 5: Results of Simulation

The design of the pressure intensifier is simple. The idea is to make the stroke as large as necessary and as small as possible. A very short stroke results due to the lack of lubrication and rapid seal wear. Also, an unnecessarily long stroke increases the piston speed, which is disadvantageous for the pressure intensifier and also creates unnecessary stress on the seals. By choosing a diameter of 40mm and 70mm and a stroke of 100mm a compromise was made, which resulted in a piston speed of less than 1m/s.

After the simulation of the hydraulic system, different control strategies were investigated and later modelled. It quickly became apparent that a subordinate swivel angle controller is required and that a direct connection of reference signals makes sense. The required control performance could be reached in the simulation. Another refinement was carried out on the test-rig itself as part of the start-up procedure.

To design of the purge system, it was important to estimate the hydraulic losses. For this purpose, power losses have been calculated in the model, resulting from the leakage and friction of the components.

The sum of these losses must be compensated by the power of the drive motor and must be discharged by the purging system. It turned out that the results of the performance calculation are very sensitive to the parameterization. This is understandable because, in a system with no basic losses, a small change in leakage values can greatly affect the heat balance. For safety reasons, and considering that a large electric motor at partial load still has good efficiency, it is the driving power and thus, the cooling capacity, has been dimensioned generously.

Once the concept was validated through the simulation and the availability of the necessary components was assured, the actual construction could begin.

4. Design

The starting point of the design was the flywheel, which stores energy. It was designed with a rotational inertia of 2 kgm^2 and rotates at 3000U/min. The flywheel is designed with a fit tolerance and is assembled by way of a flange on a shaft, see **Figure 6**. The shaft is mounted in a standard spindle ball bearing assembly, as would be found in the machine tool industry. The bearing is greatly oversized and in normal operation has a virtually unlimited service life. In case of accidental movement of the entire test rig (i.e. with a forklift) the bearings can hereby absorb the resulting rotational moments.

The connection between the pump-shaft and flywheel is exposed to a permanent torsional stress. The internal teeth of the flywheel have been manufactured with tighter tolerances, as provided by DIN5980, and forms an essentially backlash-free connection.

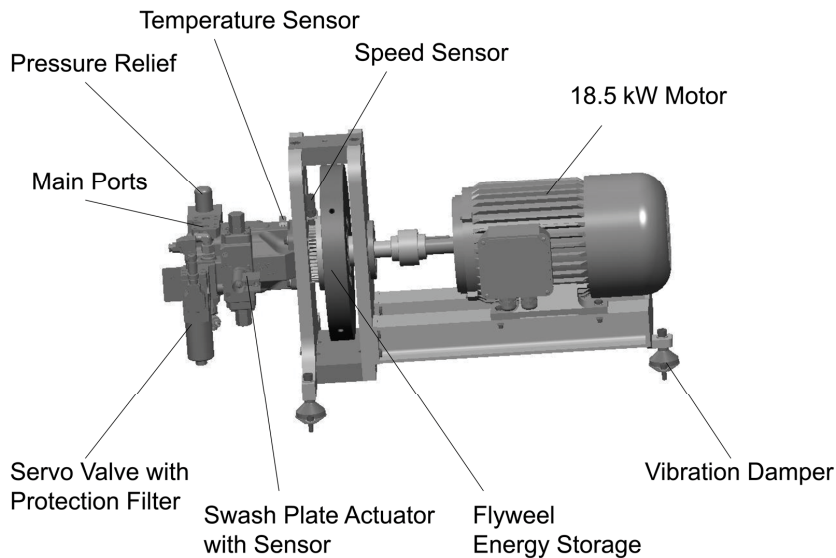


Figure 6: Pump with Flywheel and Motor

The pressure intensifier relies on proven principles. The piston rod of the high-pressure part, the rod of the driving part and the drive piston are firmly joined together and work as a single unit. As a result, a high accuracy is achieved, which demonstrates that the radial forces in the bearing points is reduced, which is necessary for continuous operation.

5. Control System

The controlled variable of the system is the amount of pressure in the test volume, which is detected through two independent sensors. One sensor is used to regulate the system and the second sensor is used for measuring the system. The target pressure curve has been generated from the cycle in Figure 1 accordingly and in **Figure 7** the optimization strategy is shown. Through the use of the tolerance field it is possible to shape the transition of the pressure curve in such a way that the theoretically required accelerations of the control system are limited. This skillful preparation contributes by preventing high-frequency stimulation, which results in very quiet and smooth machine operation.

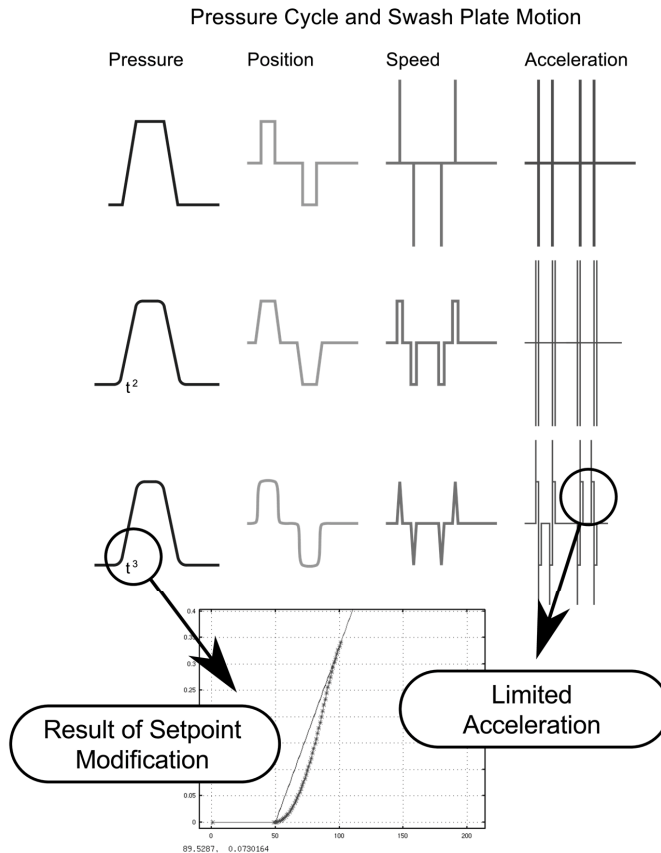


Figure 7: Reference Variable Preparation

The reference variable is transmitted to the controller with a delay, making it possible to give a dynamic reference variable intrusion on the controller directly over the pump positioning system. This leads to notably better tracking behavior in regard to fast changes.

The output of the pressure regulator is scaled with the measured stiffness. The stiffness depends greatly on the test volume. The stiffness is recalculated after each cycle using the average quotient of the derivations of the path and pressure with respect to time. This yields a stable process regardless of the pressure level and the working position of pressure intensifier.

A leakage compensation is provided to avoid increasing of the integrator output during the holding phases of the cycle.

The scaled output of the pressure regulator, together with the leakage compensation and the reference variable implementation (dynamic intrusion), is used as a set-point for the position-control-system.

Since the displacement system has integration properties /3/, the underlying system will now be controlled by using a simple P-controller. It makes the system behavior to a first order lag element /2/.

In order to prevent striking of the adjusting piston in the end positions, the actuating signal is limited to the servo valve on either side when it nears the end position.

The realized control structure, see **Figure 8**, in this test-rig can be robustly parameterized and show, during operation, a very good and stable behavior independent of the connected test volume.

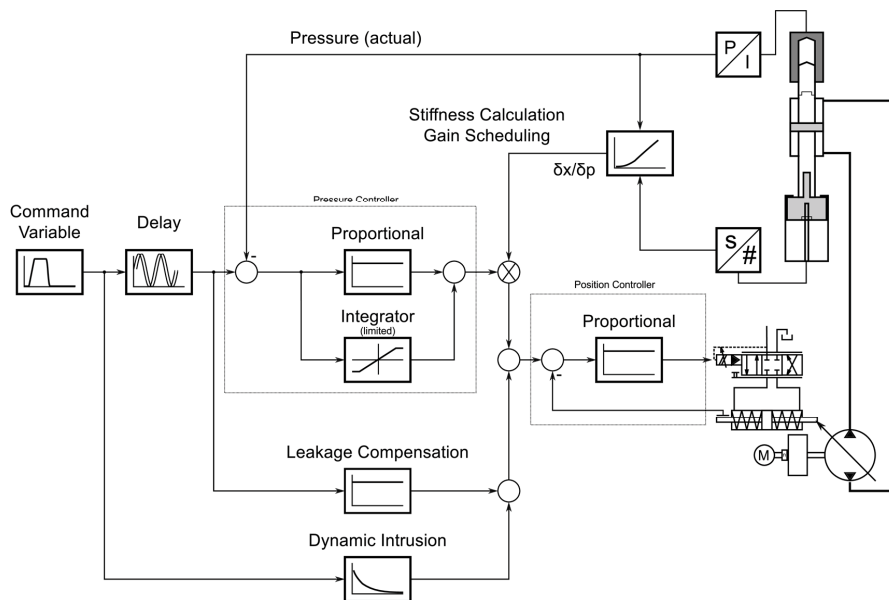


Figure 8: Controller Structure of the Test-Rig

6. Results

The realized test-rig concepts show that a considerable saving potential can be tapped by using a combination of hydraulic displacement systems and digital control technology. Wherever valve controls are in use, it is worth analyzing whether an alternative hydraulic control system is possible. With the ever increasing cost of energy, it is worth taking into consideration, a one-time investment in order to decrease operating costs in the future.

In conclusion, it can be said that the absence of a valve control system will not result in the impairment of the test-rig control, see **Figure 9**. The automatic adaptation of the adjustment control system to the current testing condition can significantly increased the operating experience. The complete test-rig is shown in **Figure 10**.

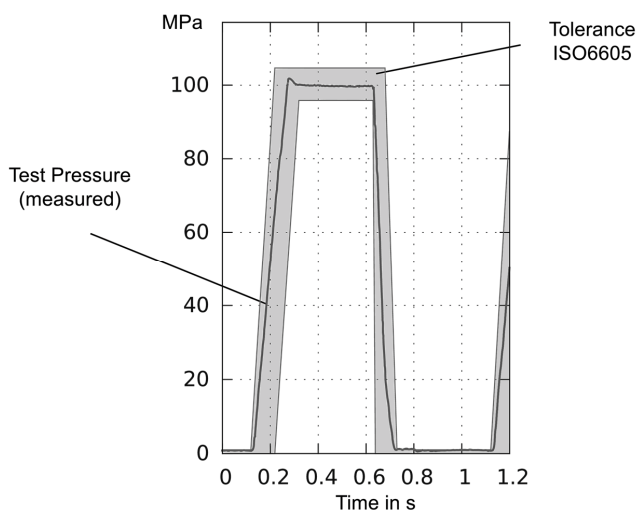


Figure 9: Measurement at the Test-Rig

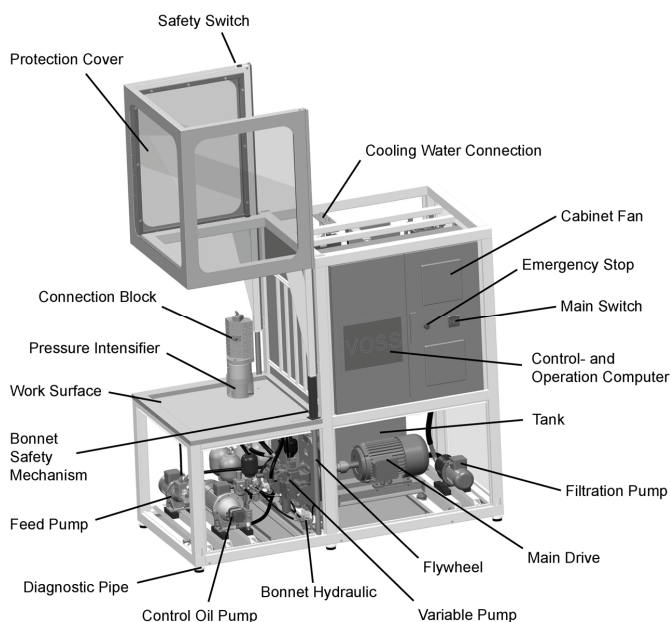


Figure 10: Test-Rig Overview

7. References

- /1/ Jürgen Berbuer. Neuartige Servoantriebe mit primärer Verdrängersteuerung. PhD thesis, RWTH Aachen, 1988.
- /2/ Otto Föllinger, Ulrich Konigorski, Boris Lohmann, Günter Roppenecker, and Ansgar Trächtler. Regelungstechnik: Einführung in die Methoden und ihre Anwendung. VDE VERLAG GmbH, 11. edition, 2013.
- /3/ Hans-Jürgen Haas. Sekundärgeregelte hydrostatische Antriebe im Drehzahl- und Drehwinkelregelkreis. PhD thesis, RWTH Aachen, 1989.

Increased energy efficiency of hydraulic hybrid drives by means of a multi-chamber accumulator

Dr.-Ing. Frank Bauer, Daniel Feld

HYDAC International GmbH, Industriestraße, D-66280 Sulzbach/Saar, Deutschland, E-mail:
frank.bauer@hydac.com, daniel.feld@hydac.com

Christian Stauch

ZeMA - Zentrum für Mechatronik und Automatisierungstechnik gemeinnützige GmbH,
Eschbergerweg 46, D-66121 Saarbrücken, E-Mail: christian.stauch@zema.de

Abstract

The focus of the present contribution is hydraulic energy recovery by means of hydro-pneumatic multi-chamber accumulators. A simulation study is presented comparing two different multi-chamber accumulator concepts for energy recovery in an exemplary load case involving a forklift mast. The first concept is based on the “Double Piston Accumulator” /1/. It is compared to the so-called “Digital Accumulator” /2/. Both similarities and differences of the two concepts are discussed in the presentation.

KEYWORDS: energy efficiency, hydraulic hybrid, multi-chamber accumulator

Information

Due to corporate reasons at this position the abstract is printed only. The complete contribution will follow in the online publication of the proceedings.

References

- /1/ F. Bauer and D. Feld, Hydraulic Double Piston Accumulator - Innovative hydraulic accumulator for hydraulic hybrid drives, Energy Efficient Hydraulics and Pneumatics Conference, Chicago, USA, November 17-19, 2011.
- /2/ C. Stauch and J. Rudolph, Energy Saving Using a Multi-Chamber Accumulator: Experimental Results and Proof of Concept, in: Proc. 14th Scandinavian International Conference on Fluid Power, SICFP15, Tampere, Finland, May 19-22, 2015.

A Complete Analysis for Pump Controlled Single Rod Actuators

Dr. Hakan Çalışkan

Mechanical Eng. Dept., Middle East Technical University (METU), G135, 06800 Ankara, Turkey,
E-mail: chakan@metu.edu.tr

Professor Dr. Tuna Balkan

Mechanical Eng. Dept., Middle East Technical University (METU), E307, 06800 Ankara, Turkey,
E-mail: balkan@metu.edu.tr

Professor Dr. Bülent E. Platin

Mechanical Eng. Dept., Middle East Technical University (METU), G305, 06800 Ankara, Turkey,
E-mail: platin@metu.edu.tr

Abstract

In the current study a variable speed pump controlled hydrostatic circuit where an underlapped shuttle valve is utilized to compensate the unequal flow rate of a single rod actuator is analyzed. Parameters of the shuttle valve are included in the system analysis, rather than treating it as an ideal switching element as handled in literature. A linearized model of the system is obtained. An inverse kinematic model, which calculates the required pump drive speed for a desired actuator speed and given pilot pressure input, is formed. A numerical stability analysis program is developed, and the stability of all possible shuttle valve spool positions is determined. The theoretical findings are validated by non-linear simulation model responses.

KEYWORDS: EHA, shuttle valve, single rod, hydrostatic, stability

1. Introduction

The electro hydrostatic actuator (EHA) refers to an integrated electric and hydraulic system, where an electric motor driven bi-directional pump is directly connected to the two chambers of a hydraulic cylinder. EHA systems are first developed by aerospace industry with regard to “the more electric aircraft” concept, which aims to eliminate the central hydraulic supply system limitation, proposes a localized control and power transmission by electric cable instead of hydraulic hoses. The EHA combines the advantages of electro-hydraulic and electro-mechanical systems. The compact and direct driven EHA provides high forces without mechanical gearing, enables flexible motion control and is energy efficient since it delivers power on demand. Recent years

new products are introduced in the market, and EHA seems to move into machine industry, especially for low power applications.

The single-rod actuator is a challenge for the hydrostatic systems due to its asymmetric structure. There exist unequal flow rates at the two ports of the actuator, as shown in **Figure 1**. Therefore, either a deficient or excess flow rate is always formed in the closed circuit, corresponding to the difference between the swept fluid volumes by piston areas of the cap and rod sides. The unequal flow rate is named as “differential flow” and is formulated as follows.

$$\Delta q = (1 - \alpha)Av_A \quad (1)$$

where, $\alpha \in (0,1)$ is the ratio of piston areas of the rod side and the cap side of the actuator, and A is the piston area of the cap side.

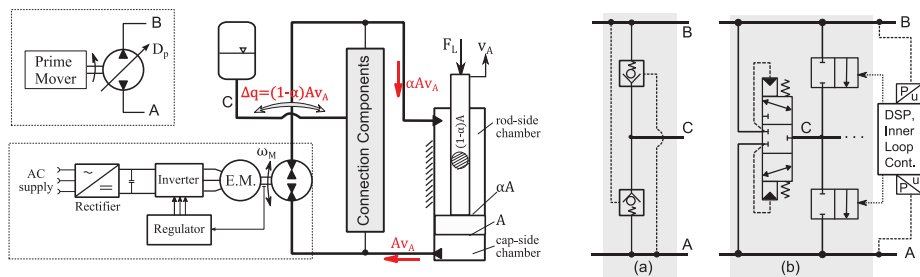


Figure 1 Differential Flow Rate Compensation, (a) pilot operated check valves, (b) closed center shuttle valve

There exists several solutions for the differential flow compensation problem: use of secondary pump [1], [2], use of hydraulic transformer [3], use of 3-port (asymmetric pump) [4], [5]. On the other hand the circuit solutions that utilize a single (conventional two-port) pump are limited. The conceptual solution with single used pump is shown in the right side of Figure 1. A hydraulic accumulator, treated as a source/sink, compensates the differential flow rate, Δq , over some connection components. In literature mainly two different connection components are proposed: (i) pilot operated check valves, (ii) shuttle valves. Rahmfeld and Ivantsysnova proposed the usage of two pilot operated check valves, as shown Figure 1 (a), and is theoretically investigated and implemented [6], [7]. A 3/2 shuttle valve is proposed by Hewet in a patent application [8]. This principle is further exploited by Wang et. al. and Michel et. al. with the use of 3/3 internal pilot operated closed center shuttle valve, as shown Figure 1 (b) [9], [10]. The two valve solutions suffer from undesired and uncontrolled pressure and velocity oscillations, which are named as pump mode switching [11], or system internal

instability [9]. In order to eliminate the instability, Wang et. al. proposed to include two additional 2/2 flow control valves, whose switching's are determined by an inner loop controller according to the chamber pressure feedback, Figure 1 (b) [9]. In the current literature, the studies related with the pump stability, commonly neglect the valve dynamics and treat the shuttle valve as an “ideal switching element”. Consequently, the pump controlled system is modeled as a combination of two stable linear systems switching according to a critical load value, [11], [12], [13].

In our previous study, the stability problem is investigated by considering the shuttle valve parameters, in which both theoretically and experimentally it is shown that the underlapped valve provides a stable operation region up to certain retraction speeds [14]. In the scope of this paper, the stability analysis made in [14], is further extended by considering the circular orifice geometry on the shuttle valve sleeve and by considering the shuttle valve dynamics rather than defining a static relation between chamber pressures and spool position. Furthermore, the transformer ratio in between the actuator and pump drive speed is obtained by a kinematic model. An inverse kinematic model, which calculates the required pump drive speed for a desired actuator speed and given pilot pressure input, is formed. By using the linearize system model and inverse kinematic model, a numerical stability analysis program is developed, and the stability of all possible shuttle valve spool positons is determined.

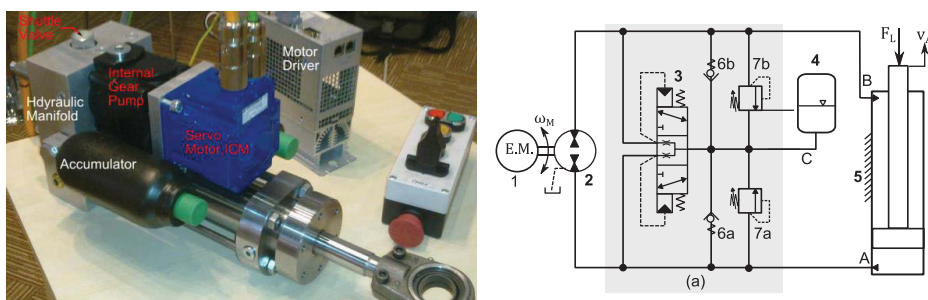


Figure 2 The Developed Single Rod Electro Hydrostatic Actuator (EHA)

2. The Single Rod Electro Hydrostatic Actuator

The single rod electro-hydrostatic actuator (EHA), together with its hydraulic circuit is shown in **Figure 2**. An internal coupling (ICM) servo motor (1) regulates the drive speed of a fixed displacement internal gear pump (2). The two ports of the pump are directly connected to the single rod actuator (5), over the hydraulic manifold. The hydraulic accumulator (4) compensates the differential flow rate over the internal pilot operated 3-way, 3-position, underlapped shuttle valve (3). The shuttle valve has 3-ports

where, the ports A and B are connected to the cap and rod side of the actuator, respectively, and the remaining port C is connected to the accumulator. Furthermore, two back to back connected check valves (6) and pressure relief valves (7) are utilized to prevent cavitation and limit operating pressure, respectively. All the hydraulic valve components are of cartridge type and are implemented inside the hydraulic manifold.

3. Shuttle Valve Model

The cartridge type internal pilot operated shuttle valve is shown in the bottom-right of **Figure 3**. It consists of a spool, centering spring, sleeve and a valve heading. The valve spool dynamics is modelled by an equivalent time constant, T_s , as follows.

$$T_s \dot{y}_s + y_s = \frac{A_s}{k_s} \cdot f_s(\Delta P_{ab}) \quad (2)$$

where, y_s is the spool positions, A_s is the pilot pressure sensitive area of the spool, k_s is the stiffness of the centering spring. The function $f_s(\Delta P_{ab})$ represents the net pressure acting on the valve spool, and ΔP_{ab} represents the effective pilot pressure on the two sides of the spool, $\Delta P_{ab} = P_a - P_b$, which is determined by the cap and rod side chamber pressures, P_a and P_b , respectively. The spool starts to move when, the pilot pressure is greater than the valve cracking pressure, $|\Delta P_{ab}| \geq P_{sc}$. Therefore, the net pressure function is defined as $f_s(\cdot) = 0$ if $|\Delta P_{ab}| \leq P_{sc}$, and is $f_s(\cdot) = \Delta P_{ab} - P_{sc} \cdot \text{sgn}(\Delta P_{ab})$ if $|\Delta P_{ab}| > P_{sc}$. According to the positive directions definitions given in Figure 3, the orifice openings, u_{va} and u_{vb} are related with the spool position y_s as follows.

$$u_{va} = u_{v0} - y_s \quad (3)$$

$$u_{vb} = u_{v0} + y_s \quad (4)$$

where, u_{v0} is the orifice pre-opening and the spool position, y_s is physically limited with $y_{sMax,Min} = \pm(u_{vMax} - u_{v0})$. The shuttle valve flow rate is defined as follows.

$$Q_v = G_v(u_v) \sqrt{|\Delta P|} \text{sgn}(\Delta P) \quad (5)$$

where, G_v is the hydraulic conductance, ΔP is the relative chamber pressure w.r.t the hydraulic accumulator pressure, P_c , i.e. $\Delta P_a = P_a - P_c$. The hydraulic conductance is function of orifice opening u_{va} or u_{vb} , and is defined as follows.

$$G_v(u_v) = C_d \sqrt{\frac{2}{\rho}} \cdot n_h \frac{1}{2} r_h^2 [2\theta_v(u_v) - \sin(2\theta_v(u_v))] \quad (6)$$

where, C_d is the discharge coefficient, ρ is the fluid density, r_h is the hole radius, n_h is the number of holes on the valve sleeve and θ_v is the angle as shown in Figure 3, and defined as follows.

$$\theta_v(u_v) = \text{atan2}\left(\sqrt{r_h^2 - |r_h - u_v|^2}, (r_h - u_v)\right) \quad (7)$$

By using the parameters given in **Table 1**, the position of the shuttle valve spool y_s , together with the orifice openings u_{va}, u_{vb} , are plotted w.r.t. pilot pressure ΔP_{ab} as shown in **Figure 4** (b). It is seen that the orifice openings, therefore, hydraulic conductance's are constant, $G_v(u_{vMax}) = G_{vMax}$ and $G_v(u_{v0}) = G_{v0}$, for the saturated and centered spool positions, corresponding the pressure intervals $|\Delta P_{ab}| \geq P_{uMax}$, where, $P_{uMax} = P_{sc} + (u_{vMax} - u_{v0})k_s/A_s$, and $|\Delta P_{ab}| \leq P_{sc}$, the respectively.

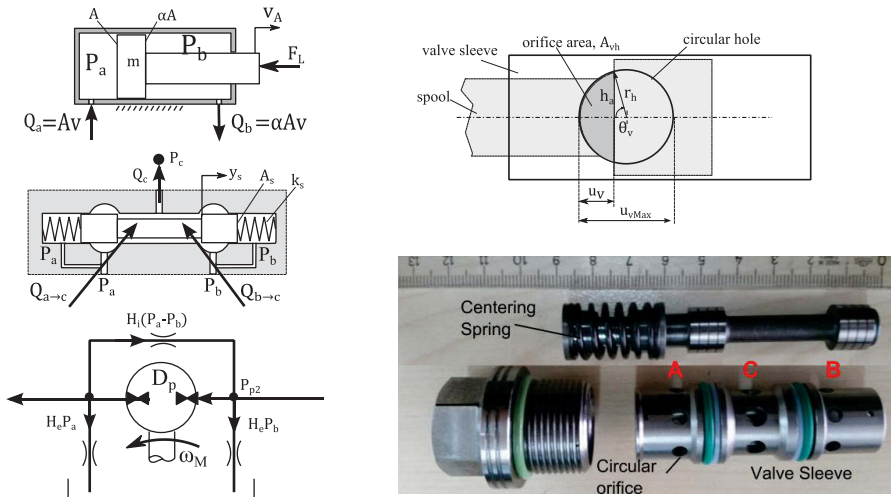


Figure 3 Free body of the EHA model (left), orifice area model and shuttle valve components (right)

4. Load Pressure State and Critical Region

The shuttle valve position is determined by the external load, F_L , acting on the actuator, which is proportional to load pressure state, $F_L \approx AP_L$, as defined follows.

$$P_L = P_a - \alpha P_b \quad (8)$$

In **Figure 4** (a), the three possible circuit configurations based on the shuttle valve positions are shown; namely, the accumulator is connected to (i) cap-side (ii) both cap and rod side (iii) rod-side chamber. The intermediate region corresponds to either centered or partially opened spool positions, and is defined as critical region. Its

location is determined by the accumulator pressure as $P_{Lcr} = P_a - \alpha P_b = (1 - \alpha)P_c$. The size of this region is mainly determined by shuttle valve cracking pressure. Considering the condition $P_a > P_b + P_{u0}$, where $P_{u0} = P_{sc} + u_{v0} \cdot k_s/A_s$, which is required by the 3rd circuit configuration, and assuming $P_b \approx P_c$ and inserting into (8), the upper limit of the critical region is roughly determined as $P_{L1} \approx P_{Lcr} + P_{u0}$. Following a similar procedure, the lower limit is roughly defined by $P_{L1} \approx P_{Lcr} - \alpha P_{u0}$.

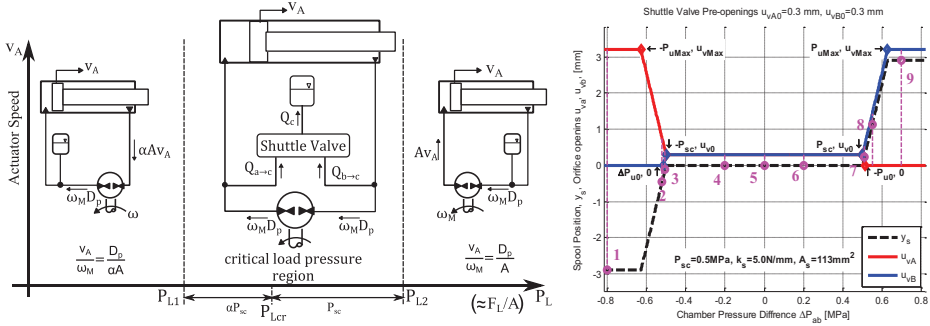


Figure 4 (a) Possible Hydraulic Circuit Configurations, (b) Orifice Openings

5. Linearized Mathematical Model

In the linearized mathematical model of the system, the pump is treated as an ideal flow rate source. Furthermore, pressure dynamics of the hydraulic accumulator, $\delta P_c = 0$ and the transmission line losses are neglected. The transmission line volumes together with the dead volumes are lumped into the actuator chambers, and the mass of the circulating fluid is lumped into the moving mass of the actuator. The equation of motion of the actuator, in terms of state variations, is written as follows.

$$m\delta\dot{v}_A + b\delta v_A + F_L = A(P_a - \alpha P_b) \quad (9)$$

where, m is the combined moving mass of the hydraulic actuator, b is the viscous friction coefficient. The pressure dynamics of the cap and rod side chambers are defined by the flow continuity equations, in terms of state variations, as follows.

$$C_a\delta\dot{P}_a = D_p\delta\omega_M - A\delta v_A - H_e\delta P_a - H_i(P_a - P_b) - \delta Q_{a \rightarrow c} \quad (10)$$

$$C_b\delta\dot{P}_b = \alpha A\delta v_A - D_p\delta\omega_M - H_e\delta P_b + H_i(P_a - P_b) - \delta Q_{b \rightarrow c} \quad (11)$$

where D_p is the pump displacement, H_e and H_i are external and internal leakage coefficients of the pump, and ω_M is the pump drive speed, C_a and C_b are the hydraulic capacitance of the cap and rod side chambers, respectively. Lastly, the $\delta Q_{a \rightarrow c}$ and $\delta Q_{b \rightarrow c}$ terms represent the variation of shuttle valve flow rates, over the AC and BC

ports, respectively. The shuttle valve flow rate defined in (5) is linearized at an operating point, P_{aeq} , P_{beq} , defined by the cap and rod side actuator chamber pressures, as follows.

$$\delta Q_v = G_v(u_{veq}) \frac{1}{2\sqrt{|\Delta P_{eq}|}} \delta(\Delta P) + \sqrt{|\Delta P_{eq}|} \operatorname{sgn}(\Delta P_{eq}) \delta G_v(u_v) \quad (12)$$

where, δQ_v is the variation of shuttle valve flow rate and ΔP is the relative chamber pressure. The variation of hydraulic conductance $\delta G_v(u_v)$, is re-written in terms of orifice opening δu_v as follows.

$$\delta G_v = C_d \sqrt{\frac{2}{\rho}} \cdot n_h h_{aeq} (\Delta P_{abeq}) \cdot \delta u_v \cdot \operatorname{Cond}_h \quad (13)$$

where, h_{aeq} is the chord length of the orifice hole formed by the spool edge as shown in Figure 3. Using the geometric relation, it is defined as $h_{aeq} = 2 |r_h \sin(\theta_{aeq})|$, and can be calculated by (7), for the given operating point $\Delta P_{abeq} = P_{aeq} - P_{beq}$. The condition operator, Cond_h is utilized to indicate the hydraulic conductance is constant, $\delta G_v = 0$, if the shuttle valve spool is stationary, i.e., if $\Delta P_{ab} \leq |P_{sc}|$, $\operatorname{Cond}_h = 0$, else $\operatorname{Cond}_h = 1$.

Considering the positive direction definitions and writing the orifice opening variation, δu_v , in terms of spool position, $\delta u_{va} = -\delta y_s$ and $\delta u_{vb} = \delta y_s$, the shuttle valve flow rates are linearized as follows.

$$\delta Q_{a \rightarrow c} = K_{aP} \delta P_a + K_{aY} (-\delta y_s) \quad (14)$$

$$\delta Q_{b \rightarrow c} = K_{bP} \delta P_b + K_{bY} (\delta y_s) \quad (15)$$

where, the pressure gains, K_{aP} and K_{bP} are,

$$K_{aP} = G_v(u_{vaeq}) \frac{1}{2\sqrt{|\Delta P_{aeq}|}} \quad K_{bP} = G_v(u_{vbeq}) \frac{1}{2\sqrt{|\Delta P_{beq}|}} \quad (16)$$

and the spool position gains, K_{aY} and K_{bY} are defined as follows.

$$K_{aY} = \quad K_{bY} = \quad (17)$$

$$C_d \sqrt{\frac{2}{\rho}} n_h 2 |r_h \sin(\theta_{aeq})| \sqrt{|\Delta P_{aeq}|} \operatorname{sgn}(\Delta P_{aeq}) \operatorname{Cond}_h \quad C_d \sqrt{\frac{2}{\rho}} n_h 2 |r_h \sin(\theta_{aeq})| \sqrt{|\Delta P_{beq}|} \operatorname{sgn}(\Delta P_{beq}) \operatorname{Cond}_h$$

Inserting the linearized shuttle valve flow rates, (14) and (15), into the flow continuity equations, (10) and (11), using the equation of motion of the hydraulic actuator, (9), and the spool (2), the state space representation of the EHA is derived as follows.

$$\begin{bmatrix} \delta \dot{v}_A \\ \delta \dot{P}_a \\ \delta \dot{P}_b \\ \delta \dot{y}_s \end{bmatrix} = \begin{bmatrix} \frac{-b}{m} & \frac{A}{m} & \frac{-\alpha A}{m} & 0 \\ -A & -K_{aP} - H_e - H_i & \frac{H_i}{C_a} & \frac{K_{aY}}{C_a} \\ \frac{C_a}{\alpha A} & \frac{H_i}{C_b} & \frac{-K_{bP} - H_e - H_i}{C_b} & \frac{-K_{bY}}{C_b} \\ \frac{C_b}{0} & \frac{A_s}{k_s T_s} & \frac{-A_s}{k_s T_s} & \frac{-1}{T_s} \end{bmatrix} \begin{bmatrix} \delta v_A \\ \delta P_a \\ \delta P_b \\ \delta y_s \end{bmatrix} + \begin{bmatrix} \frac{-1}{m} & 0 \\ \frac{D_p}{C_b} & 0 \\ 0 & \frac{-D_p}{C_b} \\ 0 & 0 \end{bmatrix} \begin{bmatrix} \delta F_L \\ \delta \omega_M \end{bmatrix} \quad (18)$$

6. Steady State Relations and Inverse Kinematic Model

Considering the equilibrium, $\delta \dot{x} = 0$, and neglecting the pump leakage losses $H_e = H_i = 0$, the actuator and pump speeds are derived as follows.

$$-(1 - \alpha)A \cdot v_A = Q_{a \rightarrow c} + Q_{b \rightarrow c} \quad (19)$$

$$-(1 - \alpha)D_p \cdot \omega_M = \alpha Q_{a \rightarrow c} + Q_{b \rightarrow c} \quad (20)$$

Consequently a kinematic relation is defined by the transformer ratio (TR) as follows.

$$\text{TR} = \frac{v_A}{\omega_M} = \frac{D_p}{A} \cdot \frac{Q_{a \rightarrow c} + Q_{b \rightarrow c}}{\alpha Q_{a \rightarrow c} + Q_{b \rightarrow c}} \quad (21)$$

The TR is constant if only one orifice is open, i.e. either $Q_{a \rightarrow c}$ or $Q_{b \rightarrow c}$ is zero. Therefore, in the hydraulic circuit configurations given in Figure 4 (a), the transformer ratio is $\text{TR} = D_p/A$ if $\Delta P_{ab} \geq P_{u0}$ and is $\text{TR} = D_p/\alpha A$ if $\Delta P_{ab} \leq -P_{u0}$. However, if the two orifices are opened at the same time then the TR depends on the chamber pressure values and is possible to vary in between zero and infinity since it is possible to have $Q_{a \rightarrow c} + Q_{b \rightarrow c} = 0$, for some actuator chamber pressure, P_a , P_b , values.

The inverse the kinematic model is utilized in order to find the transformer ratio. The inputs are the desired actuator speed, v_A , and the pilot pressure ΔP_{ab} , which can be considered as the spool position since $y_s = \Delta P_{ab} \cdot A_s/k_s$. The outputs of the model are the required pump speed ω_M and the load pressure P_L , which can be considered as the external load $F_L \approx AP_L$. The actuator speed defined in (19) is re-written as follows.

$$-(1 - \alpha)Av_A = G_{va}(u_{va})\sqrt{|\Delta P_a|}\text{sgn}(\Delta P_a) + G_{vb}(u_{vb})\sqrt{|\Delta P_b|}\text{sgn}(\Delta P_b) \quad (22)$$

The first term corresponds to $Q_{a \rightarrow c}$ flow rate and the second term corresponds to $Q_{b \rightarrow c}$ flow rate. For a given pilot pressure ΔP_{ab} input a single and unique hydraulic conductance, G_v , is calculated as given in section 3. Considering each flow term separately, the function between ΔP_b (or ΔP_a) and v_A is bijective, i.e. every single ΔP_b defines a unique v_A , and every single v_A corresponds a unique ΔP_b . Therefore,

inserting, $\Delta P_a = \Delta P_{ab} + \Delta P_b$, equation (22) can be solved for ΔP_b for the given v_A and ΔP_{ab} input as follows.

$$\Delta P_b = \text{Cond}_B \left(\frac{-b - \sqrt{b^2 - 4ac}}{2a} \right)^2 \quad (23)$$

where,

$$\left. \begin{aligned} a &= K_{v2}^2 - K_{v1}^2 \cdot \text{Cond}_A \cdot \text{Cond}_B \\ b &= 2(v_A)K_{v2} \cdot \text{Cond}_A \\ c &= (v_A)^2 - K_{v1}^2 \Delta P_{ab} \cdot \text{Cond}_A \end{aligned} \right\} \begin{aligned} \text{Cond}_B &= \begin{cases} \text{sgn}(-v_A) & \text{for } v_A \notin (v_{c1}, v_{c2}) \\ -\text{sgn}(\Delta P_{ab}) & \text{for } v_A \in (v_{c1}, v_{c2}) \end{cases} \\ \text{Cond}_A &= \begin{cases} \text{sgn}(-v_A) & \text{for } v_A \notin (v_{c1}, v_{c2}) \\ \text{sgn}(\Delta P_{ab}) & \text{for } v_A \in (v_{c1}, v_{c2}) \end{cases} \end{aligned} \quad (24)$$

and the gains $K_{v1} = \frac{G_{va}(u_{va})}{(1-\alpha)A}$ and $K_{v2} = \frac{G_{vb}(u_{vb})}{(1-\alpha)A}$. Solving Eq.(23), load pressure and pump speed can be calculated by (8) and (20), respectively.

7. Numerical Stability Analysis Program

A numerical stability analysis program is constructed in order to investigate the stability of the system for each possible shuttle valve spool position. The inputs are an array of pilot pressures, $\Delta P_{ab} \in [-\Delta P_{Max}, \Delta P_{Max}]$ and an array of desired actuator velocities $v_A \in [v_{Min}, v_{Max}]$. The structure of the stability analysis program is as follows; (i) for each pilot pressure input ΔP_{ab} , the hydraulic conductance G_{va} and G_{vb} are calculated as given in section 3, (ii) the chamber pressures, P_a and P_b are find for each actuator velocity input, v_A as given in section 6, (iii) the linearized flow gains are calculated for the operating relative chamber pressures, $\Delta P_a = P_a - P_c$ and $\Delta P_b = P_b - P_c$, (iv) the state matrix is formed and the stability of the system for the corresponding $(\Delta P_{ab}, v_A)$ point is determined by checking the eigen value locations.

An underlapped shuttle valve with $P_{sc} = 0.5 \text{ MPa}$, cracking pressure is utilized, the orifice pre-opening is $u_{v0} = 0.3 \text{ mm}$, while maximum opening is $u_{vMax} = 4 \text{ mm}$. The remaining shuttle valve parameters are given in Table 1. The input velocity array, v_A , is formed in between $[-500, 500] \text{ mm/s}$, with 20 mm/s , intervals. Furthermore pilot pressure array is formed in between $[-0.94, 0.94] \text{ MPa}$, with $18.8 \cdot 10^{-3} \text{ MPa}$ intervals. The input points forms a rectangular region on $\Delta P_{ab} - v_A$ plane and is shown in **Figure 5 (a)**. By using a right sided secondary y-axis, the spool position and the orifice openings are also shown on the same figure. It is seen that the selected ΔP_{ab} input array covers all possible openings.

In Figure 5 (a) the stability of each point on $\Delta P_{ab} - v_A$ plane is checked through the above mentioned procedure. It is seen that the equilibrium points which corresponds to the centered and fully opened spool positions are stable, cyan colored dot markers. Unstable equilibrium points, red colored star markers, correspond to partially opened spool positions. The instability region depends on the actuator velocity, as well as orifice openings. For the extension of the actuator $v_A > 0$, the equilibrium points are unstable for a limited opening at the AC port. However, for the retraction case $v_A < 0$, the equilibrium points are unstable for all partially opened spool positions.

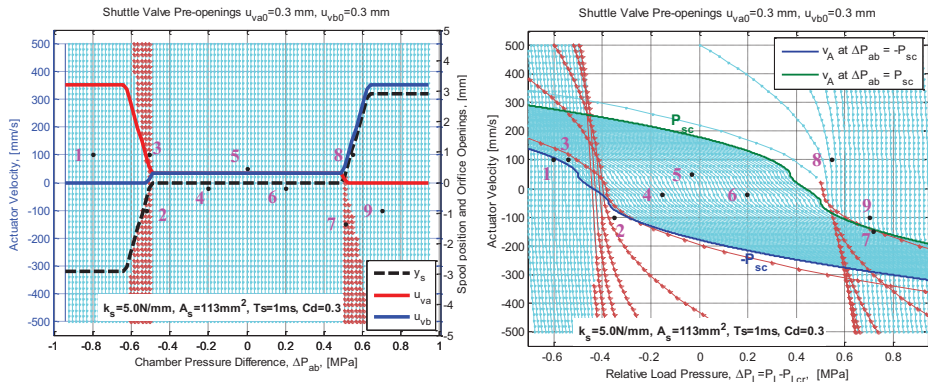


Figure 5 Stability of the EHA System (a) $\Delta P_{ab} - v_A$ plane, (b) $\Delta P_L - v_A$ plane

In **Figure 5** (b) the input $\Delta P_{ab}, v_A$ points are mapped onto the load pressure versus actuator speed, $\Delta P_L - v_A$, plane. It is seen that the mapping is not one to one, and overlapped regions occurs. The overlapping of the input $\Delta P_{ab}, v_A$ points to a single $\Delta P_L, v_A$ point, means that an equilibrium velocity (v_{Aeq}) and under a defined external load (P_{Leq}) can be satisfied by different spool positions, i.e. ΔP_{ab} values. This figure reveals that although the function in between chamber pressure state (ΔP_a or ΔP_b) and actuator velocity v_A is bijective, the same is not true for their difference, i.e. pilot pressure ΔP_{ab} . There may exists several ΔP_{ab} (spool position, y_s) that correspond to a single v_A . Lastly, on $\Delta P_L - v_A$ plane it is seen that the equilibrium points corresponding to centered spool positions (in between $\Delta P_{ab} = \pm P_{sc}$ curves) are stable, however, if the retraction speed is increased (below, $\Delta P_{ab} = -P_{sc}$ blue-curve), the increased differential flow rate cannot be compensated by the centered valve, therefore, the spool opens partially, but the spool cannot remain in this position, since the resulting point is unstable. The theoretical findings are illustrated by the numerical simulation model.

8. Non-Linear Simulation Model

The non-linear simulation model is developed in MATLAB®/SimHydraulics® environment and is shown in **Figure 6**. The model consists of hydraulic pump unit, shuttle and check valves, hydraulic accumulator, and hydraulic actuator together with the mass and frictional elements. The input of the simulation model is the pump drive speed, ω_M , and external force acting on the actuator, F_L .

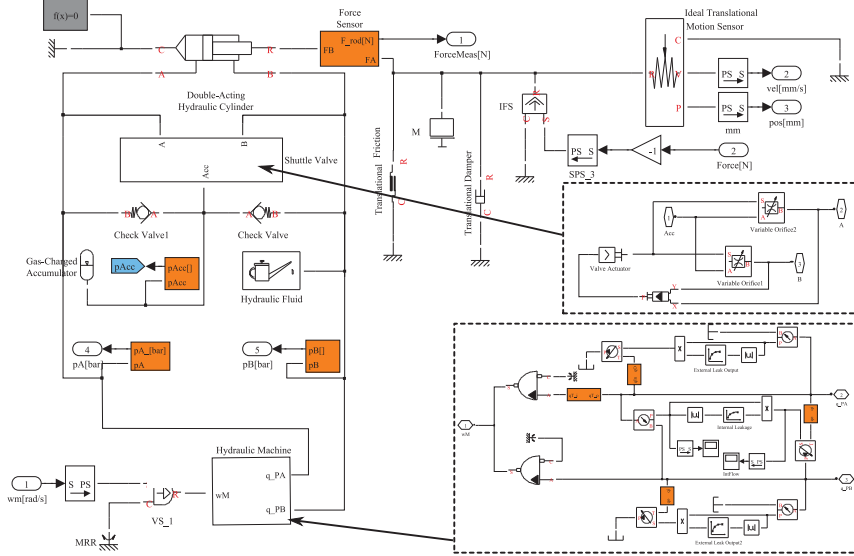


Figure 6 MATLAB®/SimHydraulics®, Non-linear Simulation Model of the EHA

The sub-system model of the shuttle valve is given at the mid right of Figure 6. The flow characteristics of the variable orifices are defined by orifice area vs. opening table. The pre-compression force of the centering spring and the stroke limits of the spool are implemented in the double acting valve actuator block, which is based on static force equilibrium. The shuttle valve spool dynamics is modelled by the valve actuator block, which is simply a linear transfer function with a time constant of $T_s = 1ms$. The pump sub-system model is shown at the mid right of Figure 6. Two hydro mechanical converters are used to generate flow rate by the input pump speed and the leakage flow losses are modelled by look up tables whose data is taken from the manufacturer.

9. Numerical Simulations

In the numerical simulations, nine different test points, which are the desired pilot pressure and actuator speed, $\Delta P_{ab}, v_A$, are utilized. The test points are given in Table 1 (b). Furthermore, the test points are also shown on the y_s vs. ΔP_{ab} plane in Figure 4 (b), where it is clearly seen that the selected, ΔP_{ab} test points cover all possible spool positions. The inverse kinematic model which is introduced in section 6

is implemented into the non-linear simulation model. The inverse kinematic model can be considered as an open loop controller, which determines the required pump drive speed ω_M for the desired actuator speed v_A . Furthermore, the inverse model calculates the load pressure i.e. the external load that will be applied on the actuator to achieve the desired pilot pressure ΔP_{ab} i.e. the spool position, y_s .

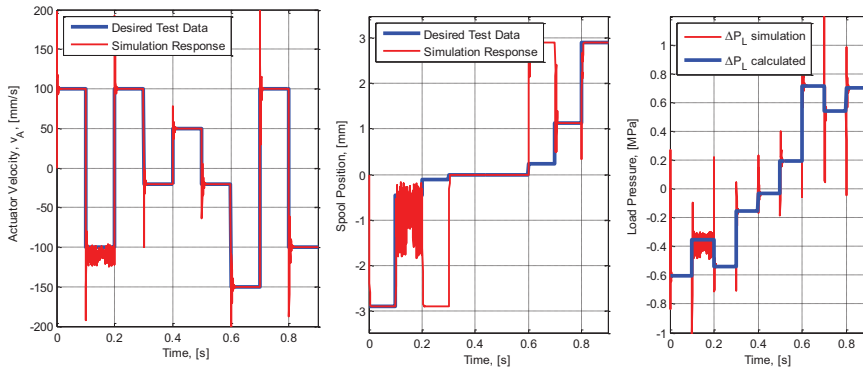


Figure 7 Actuator Velocity, Spool Position, Load Pressure Response of the Model

The actuator velocity and the spool position responses together with the load pressure response are given in **Figure 7**. It is seen that the at the test points that corresponds to centered (4th, 5th, 6th test points) or partially opened spool positions (1st, 9th test points), the actuator speed and spool position responses are the same with the desired ones. In Figure 5, it is also seen that these points are stable, and no overlapping occurs between $\Delta P_{ab} - v_A$ and $\Delta P_L - v_A$ planes. The overlapping occurs at the 3rd and 7th test points. Note that, in Figure 5(a), it is clear that these two points are unstable and corresponds to a partially opened spool position. In Figure 5(b) it is seen that desired speed of the 3rd and 7th test points can be achieved by and another pilot pressure ΔP_{ab} value which corresponds to a stable spool position. This conclusion is validated in Figure 7, it is seen that the desired speeds of the 3rd and 7th test points are satisfied by a fully opened spool position. Note that, the partially opened spool position is not always unstable. In Figure 5(a) it is seen that the 8th test point corresponds to a partially opened spool at orifice BC and is stable, and is verified by the simulation response given in Figure 7. The 2nd test point is unstable and corresponds to a partially opened spool position, different from the 3rd and 7th points, in Figure 5(b), it is seen that the desired actuator speed cannot be achieved by a different spool opening. The simulation results are compatible with Figure 5. In Figure 7 it is seen that the 2nd test point is not stable, the spool makes continuous oscillations around the partially opened position.

10. Conclusion

In the scope of this study, the stability of a single rod electro-hydrostatic actuator is investigated. The analysis given here is not limited to the speed controlled systems, but can be extended to the displacement controlled actuators. An internal pilot operated 3-way / 3-position shuttle valve is utilized to compensate the differential flow rate, which is formed by the asymmetric piston areas of the actuator. The shuttle valve dynamics is modelled, as a low pass filter with an equivalent time constant. On the other hand, all the non-linearity's, such as spring pre-loading, circular orifice geometry, are considered in the mathematical model. The linearized shuttle valve flow gains are derived and a state space of the system is obtained. An inverse kinematic model, which calculates the required pump drive speed for a desired actuator speed and given pilot pressure, is formed. A numerical stability analysis program is developed by using the inverse kinematic model and the state matrix of the linearized system. By using this program the stability of all possible shuttle valve spool positions are determined. It is shown that, the equilibrium points corresponding to centered and fully opened valve positions are stable. On the other hand, unstable equilibrium points exist for the partially opened spool positions. It is shown, in some regions on $\Delta P_L - v_A$ plane, the function between the actuator velocity and the pilot pressure ΔP_{ab} is not-bijective, which means that the desired actuator speed can be satisfied by different spool positions. The theoretical findings are validated by numerical simulations.

Shuttle Valve Parameters				Test Inputs		
u_{v0}	Orifice pre-opening,	0.3	mm	N o	ΔP_{ab}	v_A
u_{vMax}	Orifice maximum opening	4	mm		MPa	mm/s
P_{sc}	Cracking pressure	0.5	MPa	1	-0.8	100
k_s	Spring stiffness is	5	N/mm	2	-0.52	-100
A_s	Pilot area on spool surface	100	mm ²	3	-0.505	100
n_h	Number of holes on valve sleeve	8		4	-0.2	-20
r_h	Hole radius	1.6	mm	5	0	50
C_d	Flow coefficient	0.325		6	0.2	-20
ρ	Hydraulic fluid density	850	kg/m ³	7	0.51	-150
Actuator and Pump Parameters				8	0.55	100
α	Area ratio	0.75		9	0.7	-100
D_p	Hydraulic pump displacement	8	cm ³ /rev			
A	Cap-side piston area	2827.4	mm ²			

Table 1: (a) Simulation Model Parameters, (b) Numerical Simulation Model Test Inputs

11. References

- /1/ S. Helduser, "Electric-hydrostatic drive—an innovative energy-saving power and motion control system," *Proc. Inst. Mech. Eng. Part I J. Syst. Control Eng.*, vol. 213, no. 5, pp. 427–437, Jan. 1999.
- /2/ K. G. Cleasby and A. R. Plummer, "A novel high efficiency electro-hydrostatic flight simulator motion system," in *Fluid Power and Motion Control (FPMC 2008)*, 2008, pp. 437–449.
- /3/ G. Vael, P. Achten, and J. Potma, "Cylinder Control with Floating Cup Hydraulic Transformer," in *The 8th Scandinavian International Conference on Fluid Power, SICFP'03*, 2003.
- /4/ R. L. Kenyon, D. Scanderbeg, M. E. Nolan, and W. D. Wilkerson, "Electro-hydraulic actuator," EP 0 395 420 B1, 1990.
- /5/ J. Huang, H. Zhao, L. Quan, and X. Zhang, "Development of an asymmetric axial piston pump for displacement-controlled system," *Proc. Inst. Mech. Eng. Part C J. Mech. Eng. Sci.*, vol. 228, no. 8, pp. 1418–1430, 2013.
- /6/ R. Rahmfeld and M. Ivantysynova, "Development and Control of Energy Saving Hydraulic Servo Drives," *Proc. 1st FPNI-PhD Symp.*, pp. 167–180, 2000.
- /7/ R. Rahmfeld, "Development and Control of Energy Saving Hydraulic Servo Drives for Mobile Systems," *Technischen Universität Hamburg-Harburg*, 2002.
- /8/ A. J. Hewett, "Hydraulic circuit flow control," A1 2,112,929, 1994.
- /9/ L. Wang, W. J. Book, and J. D. Huggins, "A Hydraulic Circuit for Single Rod Cylinders," *J. Dyn. Syst. Meas. Control*, vol. 134, no. 1, p. 011019, 2012.
- /10/ S. Michel and J. Weber, "Energy-efficient electrohydraulic compact drives for low power applications," in *Fluid Power and Motion Control (FPMC 2012)*, 2012, pp. 93–107.
- /11/ C. Williamson and M. Ivantysynova, "Pump Mode Prediction for Four-Quadrant Velocity Control of Valveless Hydraulic Actuators," *Proc. JFPS Int. Symp. Fluid Power*, vol. 2008, no. 7–2, pp. 323–328, 2008.
- /12/ S. Michel and J. Weber, "Electrohydraulic Compact-Drives For Low Power Applications Considering Energy-Efficiency And High Inertial Loads," in *7th FPNI PhD Symposium on Fluid Power*, 2012.
- /13/ L. Wang and W. J. Book, "Using Leakage to Stabilize a Hydraulic Circuit for Pump Controlled Actuators," *J. Dyn. Syst. Meas. Control*, vol. 135, no. 6, p. 061007, 2013.
- /14/ H. Çaliskan, T. Balkan, and B. E. Platin, "A Complete Analysis and A Novel Solution for Instability in Pump Controlled Asymmetric Actuators," *J. Dyn. Syst. Meas. Control*, vol. 137, no. September, 2015.

Group 3: Pumps

Technologies and Innovations for Hydraulic Pumps

Dr. Monika Ivantysynova, Maha Professor Fluid Power Systems

Director Maha Fluid Power Research Center, Purdue University, 1500 Kepner Drive, Lafayette, IN, 47905, USA. E-mail: mivantys@purdue.edu

Abstract

Positive displacement machines working as hydraulic pumps or hydraulic motors have always been, are and will be an essential part of any hydraulic system. Current trends and future demands on energy efficient systems will not only drastically increase the number of positive displacement machines needed for modern efficient hydraulic circuits but will significantly change the performance requirements of pumps and motors. Throttleless system configurations will change the landscape of hydraulic actuation in aerospace, mobile machines, automotive and many other areas and will definitely open the door for new applications due to its enhanced competitiveness with electric and electro-mechanical systems.

History of Hydraulic Pump Design

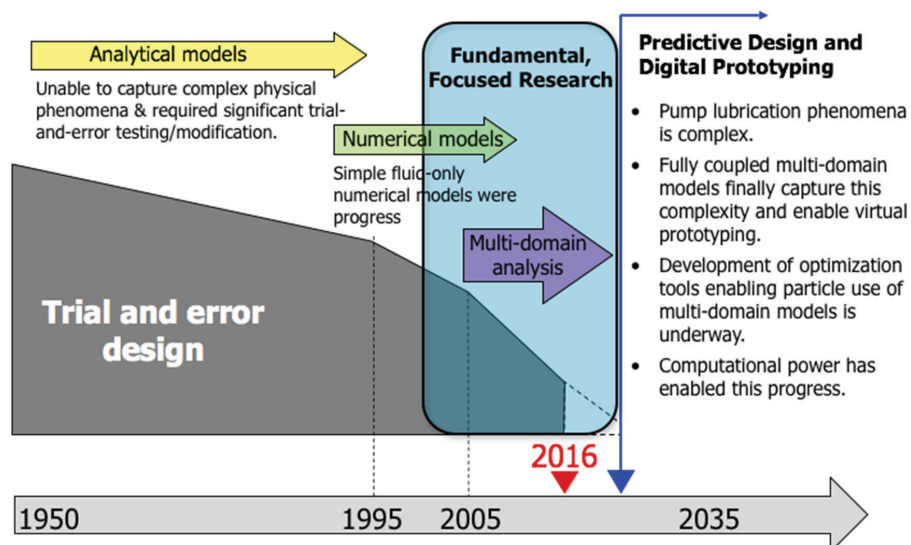


Figure 1: New directions in pump design

A few examples for novel energy efficient system concepts will be provided and used to derive future demands on pump design and pump performance. The main part of the lecture will focus on detailing the author's view of the importance of revolutionizing the design process of positive displacement machines through replacement of trial and error by powerful tools and new technologies, see **Figure 1**. First, the importance of fully understanding the various and complex physical phenomena, influencing the fluid flow and fluid-structure interaction inside the positive displacement machine, will be explained. Examples of breakthroughs in understanding and successful modeling these will be given. Among others it will be explained how important the consideration and the choice of material properties like heat capacity, heat conductivity and the shape of pump parts is in order to minimize or utilize thermal elastic deformation of pump parts for a pump design allowing efficient and reliable operation. Another very innovative technology is surface shaping. Examples of recent results of the author's research group will be given, such as the waved valve plate as exemplarily shown in **Figure 2**.

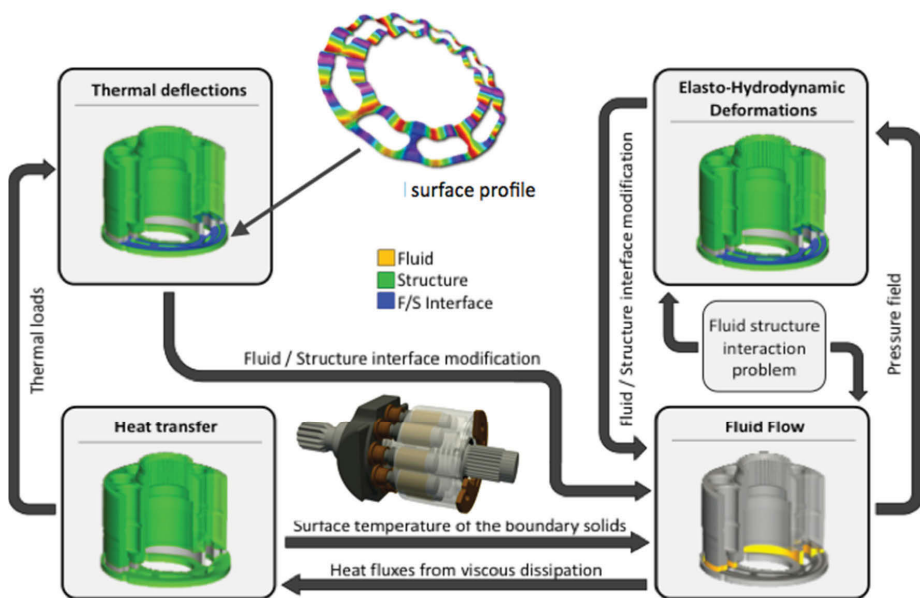


Figure 2: Computational pump design and virtual prototyping

High efficiency, compactness, high power density, simple design, highest reliability and long service life are only a subset of requirements for future pump design. Low noise level is another remaining challenge. The importance of further improvements of our understanding and modelling of noise generation and transmission in positive displacement machines will be discussed briefly.

The last part of the lecture will discuss the opportunities for innovations in design of smart pumps. The majority of currently manufactured pumps and motors have been designed for use in human or hydraulically controlled systems with rather low requirements on dynamic response and system bandwidth. Pump control systems requiring low power and achieving high bandwidth will be required in order to make throttleless actuation the technology of choice for many application. The integration of sensors, controls and embedded software is another challenge for future pump design but also a huge opportunity for fluid power technology.

Swash plate pumps – the key to the future

Dipl.-Ing. Gordon Mohn

Bosch Rexroth AG, An den Kelterwiesen 14, D-72160 Horb am Neckar,
E-Mail: gordon.mohn@boschrexroth.de

Dr.-Ing. Timo Nafz

Bosch Rexroth AG, An den Kelterwiesen 14, D-72160 Horb am Neckar,
E-Mail: timo.nafz@boschrexroth.de

Abstract

Due to many advantages, swash plate pumps are wide spread in hydraulic systems. The main advantages are the through drive capability, the adjustability and most of all, the high power density. Their application range is limited, historically, to 450bar including medium and higher volume sizes. In higher pressure range, constant pumps such as wobbling disks or radial piston pumps are normally used. This is because the higher stressed parts can be dimensioned much bigger. Pumps with lower power such as constant displacement gear pumps are generally used in low price applications.

In order to enlarge the application range of swash plate pumps, their advantages have to be further improved and strengthened. This paper shows by example how the pressure of the basic series A4VSO was increased up to a nominal pressure of 630bar and the historical pressure mark of 450bar could be exceeded. This increase in pressure level enables for example steel treatment manufacturers to reduce their component sizes without the need of a pressure transducer. Furthermore the power density of the redesigned HA4VSO was increased by 36%, compared to the standard A4VSO, by significantly increasing the self-priming speed.

On the other side of the application range, in lower power mobile applications such as small tractors, forklift and skid steer loader, there is an increasing demand for less exhaust emissions and better fuel economy. The energy saving potential by changing from a hydraulic system with constant hydraulic pumps to variable hydraulic pumps is already proven on high power applications. By developing the variable axial piston pump A1VO to the requirements of lower horse power application, it is now also possible to realize such savings in lower horse power applications.

Furthermore efficiency of the pump itself can be improved. An example of this is shown by way of the new A4 series 33.

KEYWORDS: swash plate pump, power density, efficiency, speed, pressure

2. Strengthening the strength of swash plate pumps: power density

The performance criteria concerning the rotary group can be summarized to power density. This is also the main strength of swash plate pumps and therefore the key to the future. In order to increase this strength of swash plate pumps even more, power density needs to be increased even more:

$$\Phi = \frac{P_{\text{eff}}}{m} = \frac{\Delta p \cdot V_G \cdot n \cdot \eta}{m} \quad (1)$$

Equation (1) shows the guideline for the further development of swash plate pumps. Therefore we see four directions to develop. Operating pressure needs to be increased, as well as speed increased, efficiency optimized and the packaging (V_G/m) improved. Furthermore, this performance has to be produced within a reasonable cost range to provide an optimal Total Cost of Ownership to the customer.

In the following it is shown, how recent developments at Bosch Rexroth meet these requirements in increasing the strength of swash plate pumps and build the key to the future.

2.1. Rising the pressure level

Especially in steel plants high pressures are demanded in order to keep the sizes of the cylinders and the framework as small as possible. In order to do so, expensive pressure intensifiers are needed to increase the pressure up to a typical level of well above 600bar. In order to reduce the installation equipment, a high pressure pump is required, that directly provides such a high pressure level.

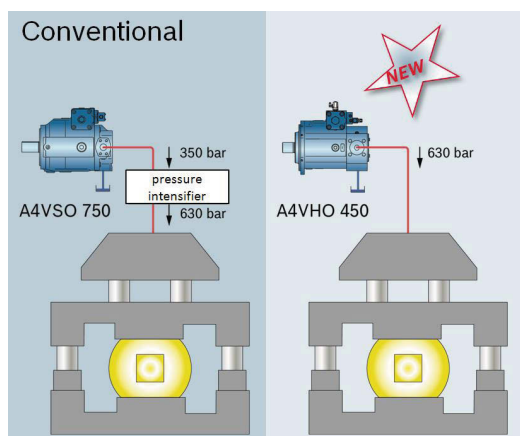


Figure 2: Reduced installation equipment in steel plants with A4VHO450

To fulfil this requirement the development of the new A4VHO was started. The intention is to provide a pump that can handle a nominal pressure of 630bar and a maximum pressure of 700bar. This development is based upon the A4VS family which can already handle a nominal pressure level of 450bar in the A4VBO version.

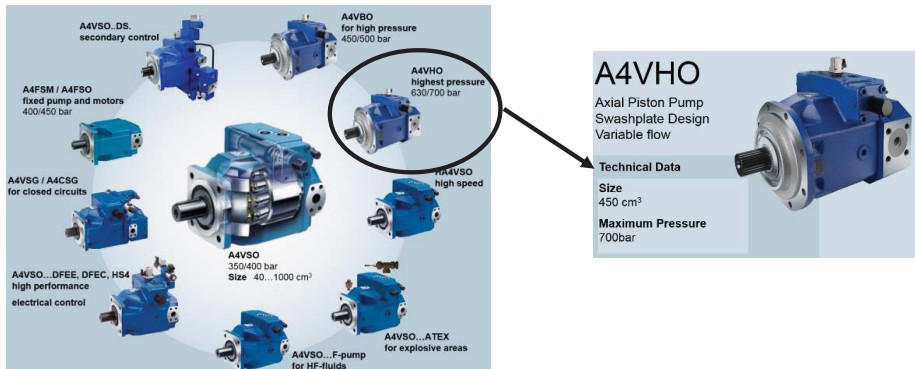


Figure 3: A4VHO450 as new member of the A4VS family

This new pressure level leads to very high contact pressures inside the rotary group and therefore many improvements have been carried out. For example, a specially formed contour in the slipper pads was introduced in order to reduce the stress and handle higher loads. With this new design, stress was reduced significantly, making the slipper pad suitable for pressure peaks up to 700bar.

Another very important task is the balancing of the cylinder barrel, which was not designed for 700bar initially. Logically the optimal design for the feed-through in the cylinder barrel are circular holes. Furthermore the hydraulic balancing varies with the alternating piston forces, due to the odd number of pistons. This gets even more important, when coming to higher pressures. In order to have a very well balanced and stable running cylinder barrel, the balancing was designed in a totally new way.

With this new design, hydraulic balancing is adapted to the alternating piston forces and therefore no longer varies significantly. This enables the cylinder barrel to run very smoothly.

In order to qualify the pump for a maximum pressure of 700bar a special test was set up. Both pumps were set up as a tandem unit with one driveshaft, one unit operating as pump and the other unit operating as motor. The high pressure side was fed directly from the pump into the motor via a steel pipe. In this way standard testing equipment could be used and the secondary unit is already tested in motor mode.

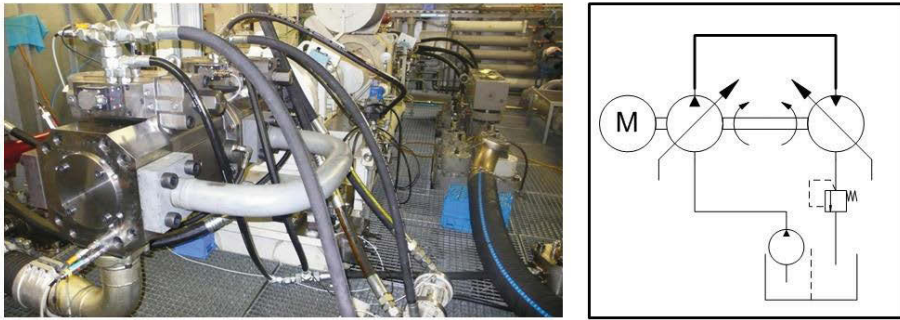


Figure 4: Testing the A4VHO for peak pressure 700bar

With this features and testing technique, the first commercially available swash plate pump A4VHO for peak pressures up to 700bar was developed.

2.2. Increasing speed

Increasing the speed of swash plate pumps gives the customer the opportunity to downsize installed electrical engines and therefore reduce their installation costs significantly. Especially if the pump can operate at ambient pressure and no boost of the suction is required.

The development of the new HA4VSO was therefore started. The intention is to provide a pump that operates at ambient pressure of 1barA and can provide 250l/min at a speed of 3.600rpm. This development is based upon the A4VSO family.

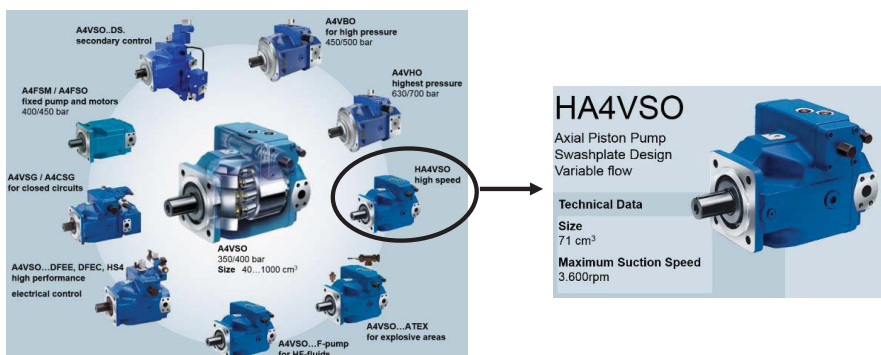


Figure 5: HA4VSO as member of the A4VS family

This increase of speed of 36% compared to the standard version demands a very good suction performance of the rotary group and of the entire suction line. This development only became possible due to new design methods such as CFD-simulation. A very important part in this optimization are the oil flow conditions from the suction line into the

cylinder barrel. This task was optimized using Computational Fluid Dynamics technology (CFD). In this way, suction conditions were improved significantly.

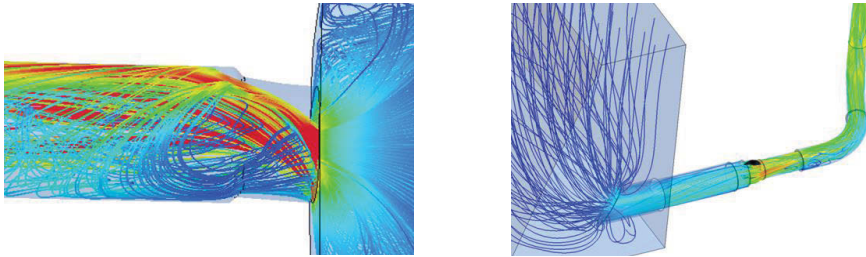


Figure 6: CFD simulation of cylinder barrel and suction line

Considering the complete suction installation of the customer's application is just as important. The entire pressure loss from tank to cylinder barrel was considered in the CFD-Analyses. This and more optimizations lead to the first pump size 71 that can operate at 3.600rpm at full stroke and ambient pressure. This results in a significant increase of power density of 36% compared to the standard version, which gives a huge advantage to the customer and his applications.

2.3. Increasing Efficiency

Thinking ecologically and economically it is important for hydraulic systems to have high efficiency. In this paper two examples are shown, how the swash plate pump can firstly, improve the efficiency of the system and secondly, how its own efficiency can further be improved.

2.3.1. System Efficiency

Every hydraulic system has to be set up according to the maximum required horse power. This includes the hydraulic pumps which have to be selected to fulfil the maximum flow and pressure demand.

The open-center hydraulic system is still used in low power mobile machinery because of the low installation costs. As long as the system is running at the maximum flow and maximum pressure the efficiency is good. Looking at the load cycle of many applications, most of the time full flow and full pressure is not needed. During these periods constant pumps are still generating full flow at maximum pressure, which leads to a high loss of energy.

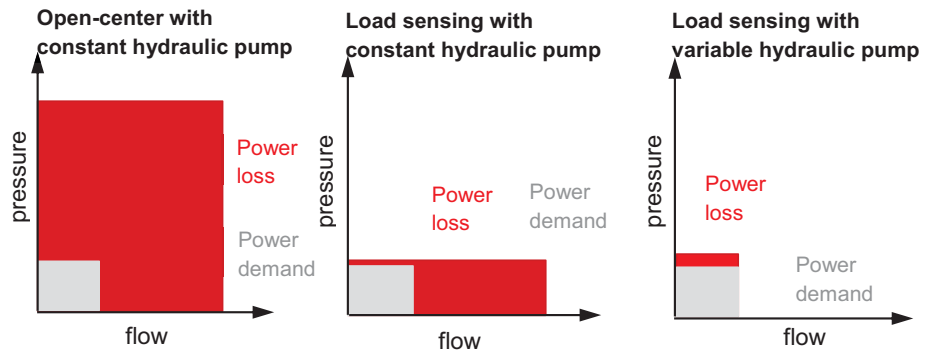


Figure 7: Hydraulic systems with constant and variable hydraulic pump

One step towards a better efficiency is a load sensing hydraulic system, with constant hydraulic pumps. As opposed to the open-center, the hydraulic system is sensing the pressure demand and is lowering the pressure level according to the required level. Nevertheless the generated flow cannot be adjusted, which leads to energy losses during these working conditions.

Only by using a variable displacement pump, is it possible to adjust the pressure and flow in all working conditions to the real demand of the hydraulics system.

In high power applications open-center systems with variable hydraulic pumps are state of the art and have already proven the huge potential of energy saving. Actual analyses of low power application load cycles show that there is a big energy saving potential, too. The following figure shows a typical load cycle of a 90 hp tractor.

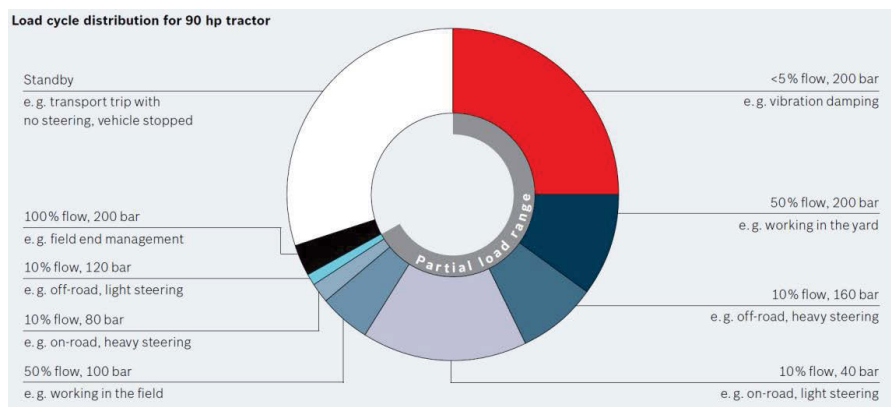


Figure 8: Load cycle distribution

Variable axial piston units open up significant saving potentials in the partial load range. This includes all work which does not demand full hydraulic power, such as vibration damping of the attachment, the chassis and the cabin while traveling on field and road. Also steering movements or various other activities in the yard and the field. Accounting for more than two thirds of the time, such operations considerably outweigh the times under full load or in standby mode when the possible savings are nearly zero due to system considerations. The engine characteristics of the diesel can be used to calculate the actual fuel consumption per cycle, enabling a comparison between a variable displacement pump and a constant displacement pump. The maximum savings result – as shown in the table – when the diesel motor only provides as much power as actually needed.

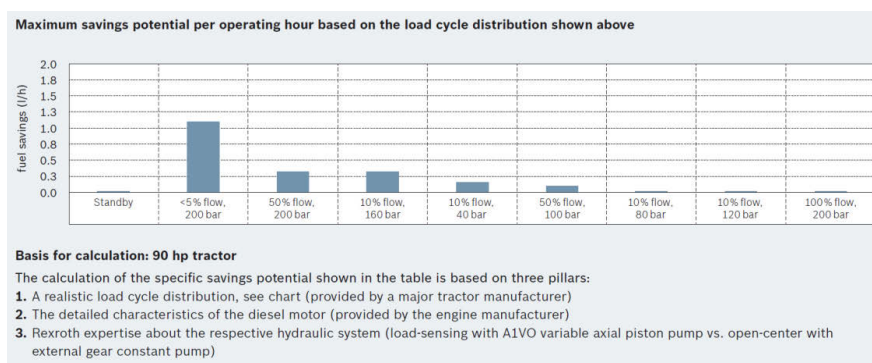


Figure 9: Maximum savings potential per operating hour

Based on this typical tractor load cycle fuel savings between 10 and 15 % per operating hour in mixed use is realistic. Assuming a life time of 6,000 hours for the tractor, this translates into fuel savings of up to 10,000 liters.

Similar calculations have been made for a typical forklift application. Based on the Transport & Opslag-cycle, a de-facto standard load profile for forklift trucks, the expected fuel savings amount to 0.7 liters per hour. This translates into approximately 7,000 liters of fuel savings during the 10,000 hours of typical machine life of a forklift truck.

When comparing a variable hydraulic pump fan drive with a conventional belt drive, the savings potential becomes evident. Based on the typical fan drive duty cycle in a combine harvester, as provided by a major manufacturer, the calculations show a fuel saving of 3.9 liters per hour which results in over 29,000 liters during the average life time of 7,500 hours.

Depending on the respective load cycles, similarly great fuel savings can be achieved in many other application areas – and all without sacrificing performance.

2.3.2. Pump Efficiency

If the system is already optimized for high efficiency, energy consumption can be further improved by increasing the efficiency of the swash plate pump. Therefore, the new A4VSO / VSG / CSG series 33 is specially optimized for efficiency.

The first step for this improvement is to know, where the losses occur. **Figure 11** shows the distribution of the power loss in a swash plate type piston pump.

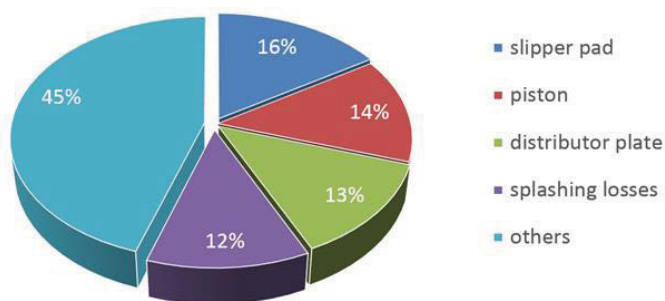


Figure 10: Distribution of power losses in a swash plate type compact pump

The importance of the piston contact is described in /7/. Furthermore, splashing losses show a huge potential to further improve the efficiency as also shown in /8/ and /9/.

Regardless, a totally empty housing is not preferred since the bearings and shaft seals need to be lubricated and cooled. A detailed analysis of the splashing losses was therefore performed and validated with measurements.

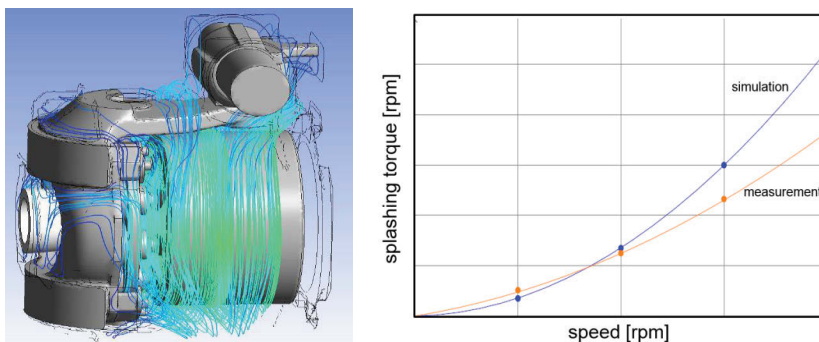


Figure 11: CFD simulation of the splashing losses in a swash plate piston pump

In this detailed simulation the location of the main splashing losses was identified and solutions were found to improve the splashing losses significantly without needing an empty housing. This and more features are implemented in the new A4VSO/VSG/CSG series 33 and lead to a significant improvement in total pump efficiency.

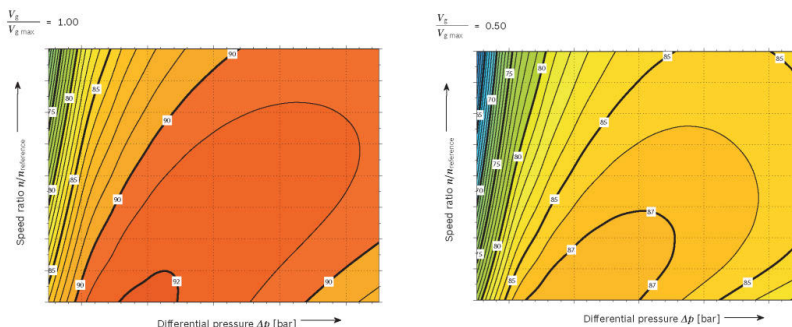


Figure 12: Efficiency diagramm A1VO

The A1VO proves that closing the price gap to a constant pump does not mean making any compromises on performance or efficiency. The internal hydrodynamic bearings such as cylinder / piston, cylinder / distributor plate, piston shoe / swashplate are optimized to realize a maximum overall efficiency well above 90% and a high efficiency level in a wide range of operation.

2.4. Total cost of ownership and pump pricing

To perform transition of lower power mobile machinery to an energy efficient load sensing system with variable displacement pumps, the key to success is to close the price gap to open-center systems and load sensing with constant pumps. The A1VO enables such an attractive price/performance ratio by significantly reducing the number of different variants, moving all ports to one part, reducing the amount of internal parts. Also the optimized design allows for an efficient high quantity production and assembly.

Technical data

Size:	35 cm ³
Nominal pressure:	250 bar
Maximum pressure:	280 bar
Speed:	3,000 min ⁻¹
Through drives:	Universal through drive makes it simple to change the through drive type without changing the part number
Hydraulic ports:	Available with inch threads
Mounting flange:	SAE-B
Shafts:	1" 15T



Figure 13: Variable displacement pump A1VO

3. Conclusion

The measures shown in this paper make the swash plate pumps the key to the future. The main advantages are through drive capability, adjustability and most of all the high power density. It is shown how the already high power density can be increased even further by increasing pressure, speed and efficiency.

The paper shows by example how the pressure of the A4VSO basic series was increased up to a nominal pressure of 630bar which is a pressure increase of 40% compared to the A4VBO. Furthermore the suction speed at ambient pressure of the new HA4VSO is increased by 36% compared to the standard A4VSO. Additionally, the new A4VSO series 33 gives significantly higher efficiency than its predecessor series 30.

The energy saving potential by changing from a hydraulic system with constant hydraulic pumps to variable hydraulic pumps is already state of the art. By optimizing the variable axial piston pump A1VO to the requirements of lower horse power application, it is now possible to realize such savings in lower horse power applications, as well.

The A1VO proves that closing the price gap to a constant pump does not mean making any compromises on performance or efficiency.

All these measures make the swash plate pump the key to the future.

4. References

- /1/ Patentschrift, DE000000455513A, 1928
- /2/ Forster, F., Welschhof, B., Den Schrägscheiben gehört schon immer die Zukunft, O+P Zeitschrift für Fluidtechnik 48, Nr. 8, 2004
- /3/ Matthies, H. J., Renius, K. T., Einführung in die Ölhydraulik, Vieweg+Teubner Verlag, 7. Auflage, 2011
- /4/ Ivantysyn, J. u. M., Hydrostatische Pumpen und Motoren, Konstruktion und Berechnung, Vogel Buchverlag, 1993
- /5/ Grabow, G., Optimalbereiche von Fluidenergiemaschinen - Pumpen und Verdichter, Forschung im Ingenieurwesen 67, Springer-Verlag, 2002
- /6/ Nafz, T., Aktive Ventilumsteuerung von Axialkolbenpumpen zur Geräuschreduktion hydraulischer Anlagen, Dissertation, RWTH Aachen University, IFAS, Germany, 2011

- /7/ Gels S., Einsatz konturierter und beschichteter Kolben-Buchse-Paare in Axialkolbenmaschinen in Schrägscheibenbauweise, Dissertation, RWTH Aachen University, IFAS, Germany, 2011
- /8/ Jang D. S., Verlustanalyse an Axialkolbeneinheiten, Dissertation, RWTH Aachen University, IFAS, Germany, 1997
- /9/ Enekes K., Ausgewählte Maßnahmen zur Effizienzsteigerung von Axialkolbenmaschinen, Dissertation, RWTH Aachen University, IFAS, Germany, 2012

5. Nomenclature

m	<i>mass</i>
n	<i>drive speed</i>
P_{eff}	<i>effective output power</i>
Δp	<i>pressure difference</i>
V_g	<i>geometrical stroke volume</i>
Φ	<i>power density</i>
η	<i>efficiency</i>

Customer focused development of a variable bent-axis pump/motor for open circuit hydrostatic transmissions, e.g. in hydraulic hybrid drives

M.Sc. Conny Hugosson

Parker Hannifin Manufacturing Sweden AB, SE-46182 Trollhättan, Sweden, email: conny.hugosson@parker.com

M.Sc. Omer Kayani

Parker Hannifin Manufacturing Sweden AB, SE-46182 Trollhättan, Sweden, email: omer.kayani@parker.com

Dr.-Ing. Mark Krieg

Parker Hannifin Manufacturing Germany GmbH & Co. KG, Neefestrasse 96, 09116 Chemnitz, Germany, email: mark.krieg@parker.com

Abstract

The paper presents the development methodology of a hydrostatic pump/motor for use in Parker Hannifin's advanced series hydraulic hybrid transmissions for medium and heavy duty commercial vehicles. With Parker's established bent-axis pump/motor technology for heavy duty mobile applications as a basis, it describes the main stages of further development and qualification for demanding automotive main drive transmissions. Parker's APQP based, customer focused product development model was employed for this development which resulted in the variable bent-axis pump/motor C24 for open circuit hydrostatic transmissions.

Positive customer results from a large fleet of in-service refuse collection trucks and parcel delivery vans with Parker advanced hydraulic hybrid drive systems using C24 pumps/motors serve as evidence of Parker's product development model effectiveness. High reliability, good fuel economy, increased productivity and long brake life of the vehicles can directly be traced back to the streamlined, front-loaded and iterative development model.

KEYWORDS: Customer focused development, Duty cycle analysis, Test methods, APQP, Pump/motor, Bent axis, Open circuit, Hydraulic Hybrid

1. Introduction

Runwise is an advanced series hydraulic hybrid drive developed by Parker Hannifin for refuse collection truck applications /1/ /2/ /3/. Prior to its launch for serial production, simulations, verification testing in lab and vehicles as well as field demonstrations all had shown encouraging results in terms of significant reduction in fuel consumption, exhaust gas emissions and brake wear. Good driving performance and high reliability were also demonstrated during the tests.

Another Parker Hannifin advanced series hydraulic hybrid drive is a *power split IVT* developed for urban delivery trucks /4/. A field demonstration program with 48 delivery vehicles equipped with power split IVTs has verified high reliability, good fuel economy and long brake life as expected.

2. System architectures

System layout selection, control strategy determination, sizing of system and sub-system level components for the aforementioned Parker hydraulic hybrid systems were based on results from simulation models with vehicle-level input data, measured on a conventional – baseline – vehicle.

The resulting systems combine mechanical and hydrostatic portions in order to enable transition from mainly hydrostatic power transmission at low vehicle speed to mainly mechanical power transmission at high vehicle speed, hence maximizing efficiency for the complete speed range.

Through the system level simulations, optimal type of hydrostatic sub system was found to be an open circuit with secondary controlled over-center variable bent-axis piston pumps/motors, a hydro-pneumatic accumulator and a pressurized oil reservoir. The Parker pump/motor specifically developed for this system design is named C24, currently available with a maximum displacement of 195 cc/rev.

2.1. Runwise

The hydrostatic portion of *Runwise* is combined with a three step mechanical transmission, the Power Drive Unit (PDU). The PDU connects one C24 pump/motor, the primary unit, to the engine at the input shaft of the transmission. PDU in the first and the second gears connects the two C24 pumps/motors, the secondary units, to the output shaft with two different gear ratios.

For each of the two gears the system provides infinitely variable power transmission in four quadrants (acceleration/deceleration, forward/reverse) up to approximately 70 km/h

with a gear shift point at approximately 30 km/h. The third gear provides maximum possible efficiency at vehicle speeds above 70 km/h through direct drive to the output shaft from the engine at the input shaft. The secondary units are disconnected from the output shaft during this driving mode.

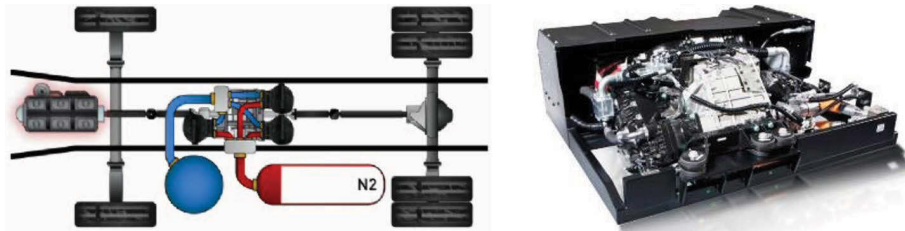


Figure 1: Parker Runwise: System architecture (left) and picture (right)

2.2. Power split IVT

Like Runwise, the power split IVT consists of an open circuit hydrostatic transmission with pumps/motors C24 and an accumulator combined with a mechanical transmission, which, however, is of planetary type.

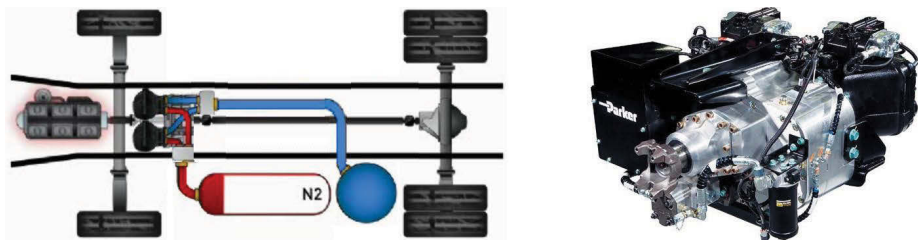


Figure 2: Parker power split IVT: System architecture (left) and picture (right)

This provides a continuously variable transition from mainly hydrostatic power transmission at low vehicle speed to mainly mechanical power transmission at high vehicle speed. The controls of Parker power split IVT also include an engine-off feature for driving modes where the vehicle is decelerating, standing still or accelerated by recycled energy.

3. Structured product development model

The product development model behind the pump/motor, other hydraulic hybrid components and the systems themselves basically applies guidelines of *Automotive Industry Action Group (AIAG) reference manual Advanced Product Quality Planning (APQP)* and Control Plan /5/.

At the core of the development model lies the design and verification of the product and its production processes, driven by requirement specifications which are determined by the customer application, **Figure 3**. The model covers the product development on application (system) level as well as on sub-system, component and part levels.

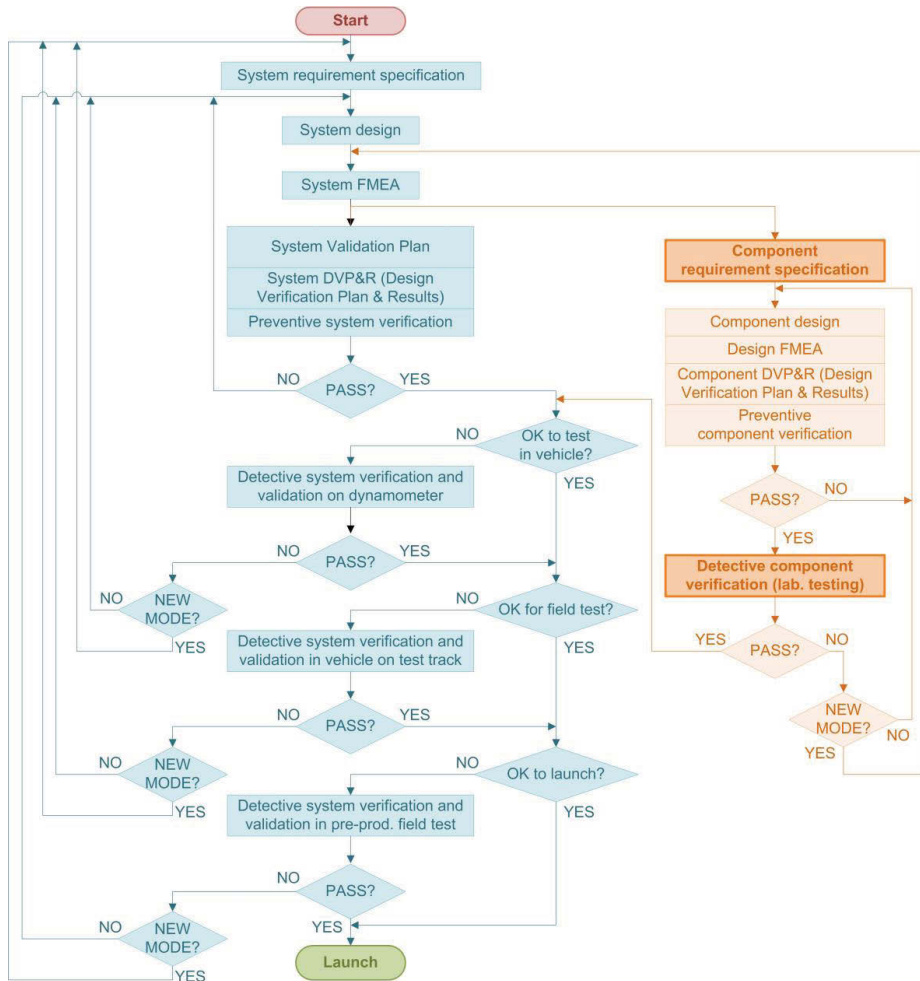


Figure 3: Product design development model

Risks of failure to meet the requirement specifications are listed and assessed using the structured tool *Failure Mode and Effects Analysis* (FMEA), for system design (SFMEA) as well as for component design (DFMEA) and production processes (PFMEA).

Here, it is worth mentioning that the fact that this paper focuses on product design development does not mean that development of the production processes for the product is less important.

4. Requirement specifications

For a complex *new to the world* product like a hydraulic hybrid drive system, it is a challenging task to formulate relevant requirement specifications – for the whole product, its sub systems, components and individual parts. Identifying all the key requirements and parameters is a significant challenge at the initial stages of development.

Specialist knowledge within the new technology does not automatically bring enough knowledge of targeted applications to enable identification of all required key parameters at an initial stage. Input from targeted customers, their customers and end users is of high value at this stage. However due to possible unfamiliarity of the new technology's characteristics and capabilities as compared to the conventional products, potential knowledge gaps still exist. An obvious example for a hydraulic hybrid drive system with brake energy recovery is the characteristic *energy storage capacity*, which is not at all relevant for a conventional transmission. These initial knowledge gaps can be filled by developing the initial requirement specification on real-world measurements using simulation models, hence resulting in a more streamlined development process. An approach with less focus on developing comprehensive initial requirement specifications requires more design iterations in order to incorporate requirements as they are detected during the development.

As earlier mentioned, the initial requirement specifications – characteristic operating parameters for the product as used by the customer – for Parker hydraulic hybrid drive systems and components were based on simulations and other calculations with measured vehicle speed profiles and other vehicle related data of baseline vehicles as input. Thanks to the proactive and iterative nature of the product development model, results fed back from detective verification of system and components enabled requirements, which were not identified initially, to be gradually added during the product development.

4.1. Pump/motor requirement specification determination

Pump/motor operation can basically be described as time dependent variations in rotation speed, pressure, displacement and temperature, **Figure 4**.

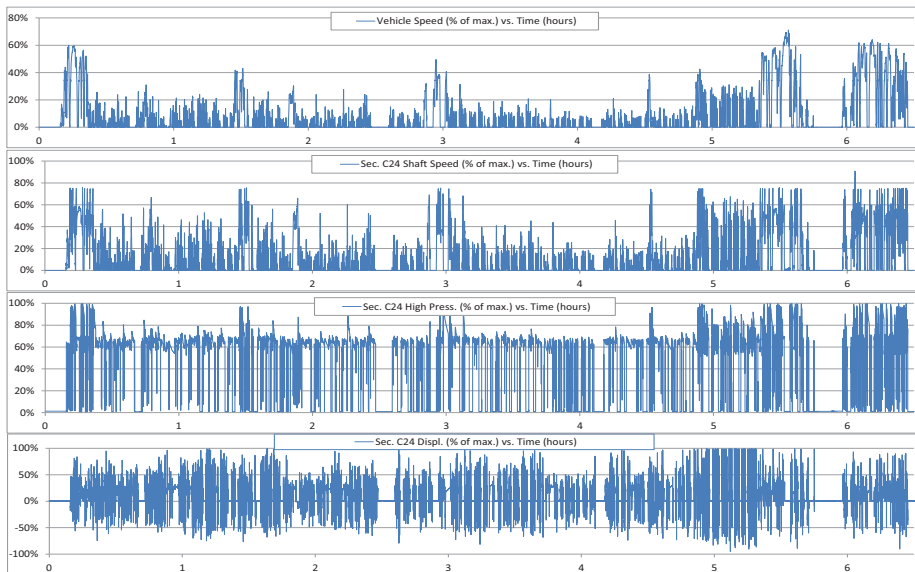


Figure 4: Example of operating parameter patterns of a refuse collection truck

System level simulation results show complex patterns of variation for these parameters. Detailed knowledge of the variations is an important input to determine requirements on each of the functions of which the pump/motor consists. At the same time, methods for breaking such complex operating profiles down into a few simplified typical modes of operation had to be applied in order to customize easily feasible test methods for the pump/motor; each test method focusing on a few or several of the pump/motor functions.

4.2. Pump/motor basic functions

A variable displacement bent-axis pump/motor is a complex component and can be defined as a sub system. It consists of several mechanisms with various functional purposes.

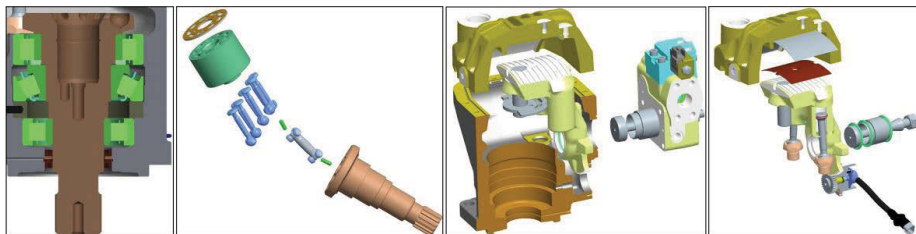


Figure 5: Four basic pump/motor functions: shaft bearings, rotating pressure-loaded parts, pressure-loaded body parts and displacement control parts (left to right)

Profound insights into operating conditions and requirements on performance, reliability and durability of each one of the functions are necessary for development of a successful product. As an example, **Figure 5** shows four important basic C24 functions.

The following examples focus on durability requirements and detective methods for verification of chosen design solutions.

4.2.1. Shaft bearings

From the extracted pump/motor pressure, displacement, shaft speed and temperature profiles; bearing loads, oil viscosity and cleanliness level were determined. Expected life of the cylindrical and tapered roller bearings under these conditions were calculated using established standards /6/ /7/.

4.2.2. Pressure-loaded rotating parts

Variations of speed and pressure at the rotating group can be described in terms of load amplitudes and the number of cycles for each load amplitude. Through knowledge of fatigue behaviour of used materials, required fatigue life could be defined in form of a Load-Life Diagram, **Figure 6**.

4.2.3. Pressure-loaded body parts

Similar to the pressure-loaded rotating parts, a Load-Life Diagram can be used to define required fatigue life for pressure-loaded body parts. Here, however, the irregular nature of system pressure variations makes it challenging to identify relevant fatigue load cycles and subsequently load amplitudes and the number of load cycles. To generate requirement Load-Life Diagrams for C24 pump/motor this difficulty was overcome through application of rainflow analysis /8/ to the spectrum of system pressure.

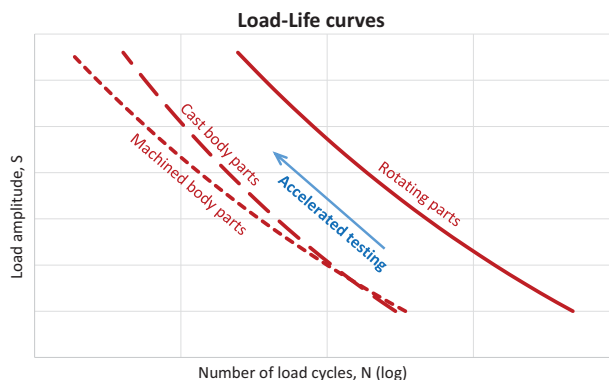


Figure 6: Fatigue life requirements expressed through Load-Life (Wöhler) curves

4.2.4. Displacement control parts

In principle, requirements on parts with the purpose of displacement actuation and feedback are defined by three parameters: displacement travel, force/pressure and fluid viscosity. For polymer materials also relationships between temperature and durability are considered.

5. Design verification methods: Pump/motor laboratory tests

After the product development process stages where the design solutions – targeted to meet the requirement specifications – are defined and verified through failure *preventive* methods like calculations/simulations and design reviews, it is important to get design verification feedback from failure *detective* methods as soon as possible. Trial assembly is an example of an elementary type of detective verification method while laboratory testing includes a variety of more complex and time consuming methods.

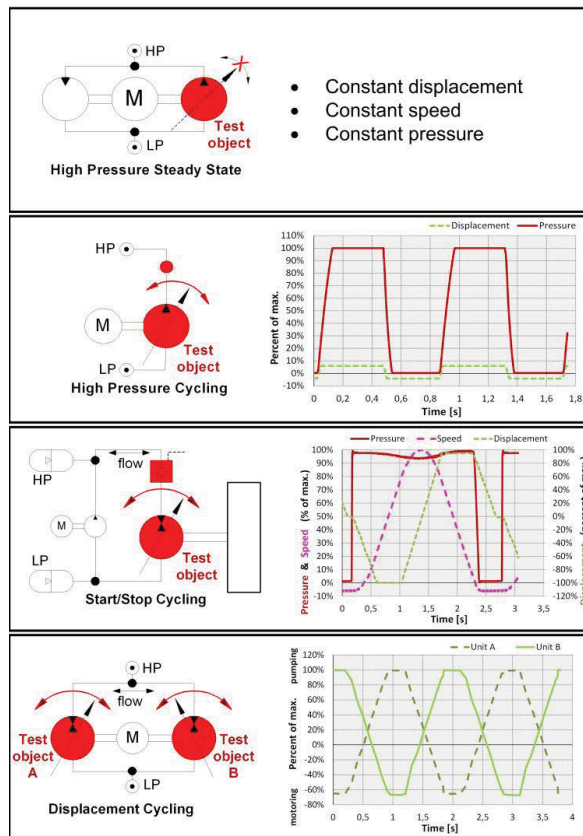


Figure 7: A selection of pump/motor lab test methods focusing on durability

For verification of all critical functions of C24 pump/motor a large number of test methods were applied. Several internal standard methods, since long established for testing of pumps/motors for mobile and industrial applications in general, could often be directly applied. In addition, customized test methods had to be developed in order to cover C24 specific functions and operating conditions. Here, a selection of laboratory test methods used for durability and reliability verification of C24 pump/motor are briefly described in terms of high level hydraulic schematics and time traces of characteristic test parameters, **Figure 7**.

Design of durability test methods include considering several characteristics such as:

- Possibility to realize with existing/easily achievable laboratory facilities
- Number of parts/functions tested by the method
- Definition of loading (load level and number of load cycles) for each tested function
- Load acceleration factor for each function tested by the test method

Load acceleration factor is defined as the relationship between the required product life under real world conditions and the testing time required to verify that the tested function fulfils the durability requirement.

Each of the four test methods shown above were basically designed to test one or a limited number of pump/motor functions in the shortest time. Still, they provide a significant degree of overlap, which reduces the required number of test samples for each method.

Test method	Pressure-loaded rotating parts		Pressure-loaded body parts	
	Shaft bearings		Displacement control parts	
High Pressure Steady State	84	6223	n/a	n/a
High Pressure Cycling	17	883	566	7,4
Start/Stop Cycling	3,8	67	45	34
Displacement Cycling	16	61	n/a	97

Figure 8: Load acceleration factors for basic pump/motor functions for selected lab test methods

Good knowledge of load acceleration factors, **Figure 8**, enables effective utilization of testing resources. It also enables risk assessment from occurred testing failures, which can be translated to expected life in the customer application. Once validated through testing of the system in which the component is included, this knowledge also helps reducing cost and time consumption for verification of future design improvements. With reference to the process flow diagram shown in Figure 3, the knowledge can make

component test results reliable enough to bypass dynamometer and/or vehicle testing on test track and instead proceed directly to field testing with a limited test fleet over a limited test period.

6. Customer experience

A summary of customer feedback about the Runwise and power split IVT on-field performance is presented below.

Prior to production launch of Parker Runwise hydraulic hybrid drive system for refuse collection trucks, system simulations as well as vehicle testing on test track and field demonstrations had shown a potential reduction of fuel consumption in the range of 35-60 % compared to baseline vehicles. Variations were mainly influenced by operated route and vehicle load.

In the middle of 2015 there were more than 160 refuse collection trucks with Runwise hydraulic hybrid drive system in regular service at over 20 locations across North America. In average, customers report 43 % fuel saving compared with their conventional trucks. Foundation brakes wear significantly less; change of brakes once during the life of the truck is foreseen instead of several times per year. Productivity has increased by 5-15 % thanks to good acceleration and deceleration performance with smooth transitions. As far as reliability is concerned, the American fleet of Runwise trucks has shown an average uptime of 97 %.

The pre-production fleet of 48 parcel delivery trucks with Parker power split IVT system shows an average of 30 % reduction of fuel consumption, despite a lower start/stop frequency than refuse collection trucks and a less favourable relationship between kinetic energy and running resistance. There has been no need for neither foundation brake service nor engine starter replacement on these trucks.

High reliability and performance of the systems can be traced back to the streamlined, front-loaded and iterative pump/motor product development model, **Figure 9**.

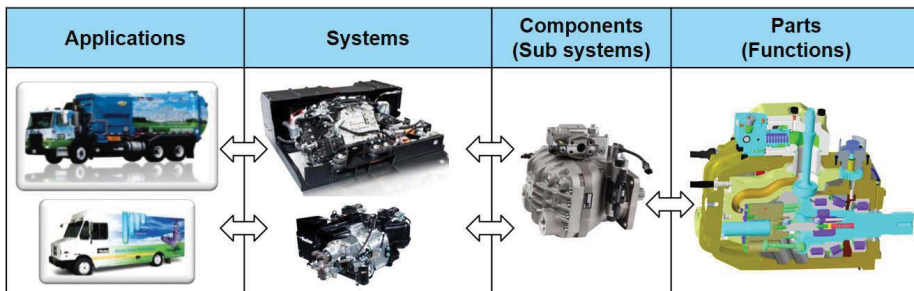


Figure 9: Reversible relationships between applications and individual parts

7. Conclusions

C24 variable bent-axis pump/motor for open circuit hydrostatic transmissions was developed according to an APQP based product development model with focus on customer requirements.

A large fleet of customer owned hydraulic hybrid vehicles with Parker advanced hydraulic hybrid drive systems and their C24 pumps/motors developed according to the described model are in regular field operation. The customers report positive results in terms of fuel economy, reliability and productivity – results which serve as evidence of the employed product development model effectiveness.

8. References

- /1/ "Hybrid Drive Systems Division" Hydraulic Hybrid Transmissions. 2012. Accessed September 15, 2015. <http://parkerhybrid.parker.com/>.
- /2/ "Parker Runwise: Advance Series Hybrid - Brochure." 2013. Accessed September 30, 2015. [http://www.parker.com/Literature/Hybrid Drive Systems Division/PH_RunWiseBroch-Final-2013.pdf](http://www.parker.com/Literature/Hybrid%20Drive%20Systems%20Division/PH_RunWiseBroch-Final-2013.pdf).
- /3/ Johansson, A. and Ossyra, J.-C. 2010. Hydraulic Hybrid Transmission Design Considerations for Optimal Customer Satisfaction. Proceedings of the 7th International Fluid Power Conference, March 22-24, 2010, Aachen, Germany.
- /4/ Hartter, L., Birkett A., Casciani T., Pomerlau M. and Subramaniam M. 2010. Series Hydraulic System for Urban Vehicles. Proceedings of the 7th International Fluid Power Conference, March 22-24, 2010, Aachen, Germany.
- /5/ Advanced Product Quality Planning (APQP) and Control Plan, Second edition, July 2008.

- /6/ Rolling bearings – Dynamic load ratings and rating life. International Standard ISO 281:2007(E).
- /7/ Rolling bearings – Dynamic load ratings and rating life, AMENDMENT 2: Life modification factor a_{XYZ} . International Standard ISO 281:1990/Amd.2:2000(E).
- /8/ Downing, S.D., Socie, D.F. (1982). Simple rainflow counting algorithms. International Journal of Fatigue, Volume 4, Issue 1, January, 31-40.

The control of an open-circuit, floating cup variable displacement pump

Dr.-Ing. Peter Achten, Dipl.-Ing. Sjoerd Eggenkamp

INNAS, Nikkelstr. 15, Breda, The Netherlands E-mail: pachten@innas.com

Abstract

The floating cup principle is a general hydrostatic principle for both constant and variable displacement pumps and motors, as well as for hydraulic transformers. In this paper, the focus will be entirely on the control of the displacement of the variable 28 cc Floating Cup pump (FCVP28). The floating cup principle features two opposed swash plates, for which both angular positions need to be controlled in order to cover the entire range from zero to full displacement. The results of both extended numerical analysis as well as simplified linearized models will be compared to test results on a 28 cc FCVP. Special emphasis will be on the dynamic behaviour of the displacement control.

KEYWORDS: Floating cup, variable displacement, control

1. Introduction

The Floating Cup (FC) principle is a relatively new axial piston principle /1...5/. Unlike in bent axis and slipper type machines, the pistons are locked onto the main rotor i.e. drive shaft. Furthermore, the cylinders are detached and separated from the barrel: each piston has its own, cuplike cylinder, which is 'floating' on and supported by a rotating barrel plate. Piston rings are not needed; the piston crown has a cavity, which will make the piston expand to a same degree as the cylinder annex cup, thereby closing the gap between the piston and its paired cylinder under all circumstances.

The FC-principle is essentially a multi-piston principle. The number of pistons is typically somewhere between 24 and 30 pistons, which is three to four times as much as in current axial piston principles. The pistons are arranged in two rings, one on each side of the central rotor. The swash angle of the barrels is limited to about 8°.

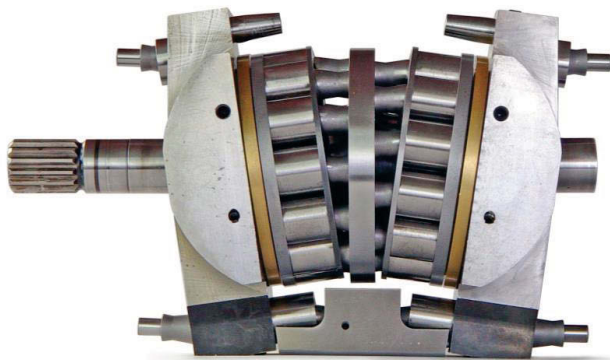


Fig. 1: Inner parts of the FCVP28, excluding bias springs, bearings and shaft seal

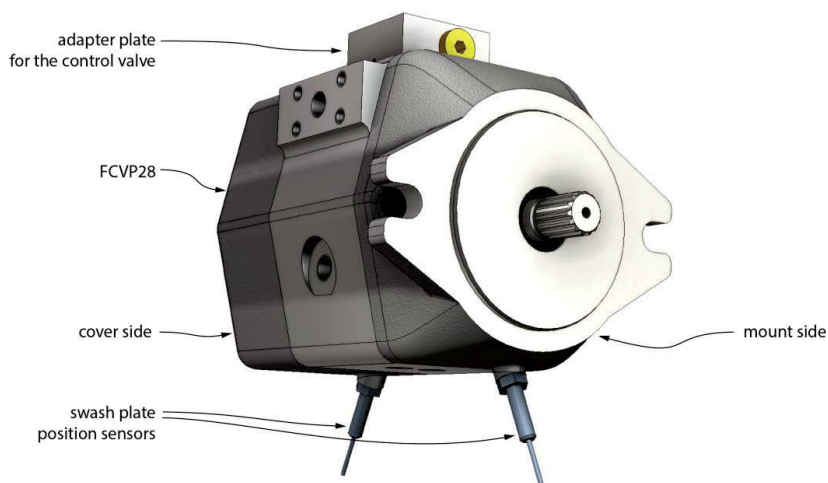


Fig. 2: The FCVP-prototype excluding the control valve

In 2005, a variable displacement floating cup pump (FCVP28) was presented by INNAS /6/. The FCVP28 is an open circuit pump with a maximum displacement of 28 cc. The pump is designed for operating pressures up to 350 bar and has the same control options as conventional open circuit pumps, including a position feedback of the swash plates for power control.

This paper is about the control itself. Section 3 describes the general principle of the swash plate control. A special hydraulic control circuit is applied in the FCVP, which is described in section 4. Two simulation models have been developed: a straightforward linear model and a detailed sophisticated non-linear model. Section 5 describes the test results and compares these with the results from the simulation models.

2. The variable displacement FC-pump

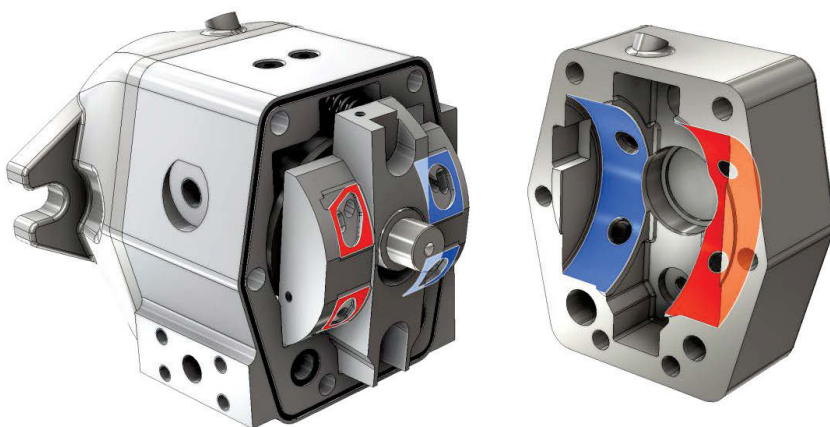


Fig. 3: Swash plate bearings (high pressure side in red and low pressure side marked blue)

There are several challenges to the design of the variable displacement floating cup pump. The first and biggest challenge is the supply of oil to and from the barrels via the swash plates. The barrels run on port plates, which are located on top of the swash plates. The lubricated interface between the rotating barrel and the stationary port plate is one of the most delicate design details of axial piston machines, acting both as a face seal and a thrust bearing. On each side of the pump, oil needs to be supplied to the low-pressure side, via the swash plate and the port plate to the barrel. During the pump stroke, the oil is forced to the high pressure side, through the swash plate to the channels and ducts in the housing.

Another bearing and sealing interface is on the backside of the swash plate, where the oil is passing from the housing to the swash plate and vice versa. Both sealing and bearing interfaces require a minimum deformation of the components, despite the high hydrostatic loads and possible temperature effects.

One of the advantages of the floating cup principle is the small maximum tilt angle of the swash plate: for the open circuit floating cup pump considered here, the swash plate position only needs to be varied between 0 and 8° . The relatively small angular variation facilitates the contact between the moving ports of the swash plate and the stationary ports of the housing.

In the FCVP28, both swash plate positions are varied and controlled. The control does not need to be simultaneous, but could also be sequential, having one swash plate rotating before the other. However, also if both swash plates are controlled in the same way, then the control angles do not need to be exactly equal at all times. In the end, the average angular position of both swash plates will determine the total displacement of the FCVP28. This average swash angle can simply be determined by a small and simple mechanism as shown in Figure 4. The mechanism causes the central pin to move up and down. The pin is connected to the optional control valve, and sets the position of the inner spool valve, thereby limiting the power output of the pump. This option is not further discussed in this paper.

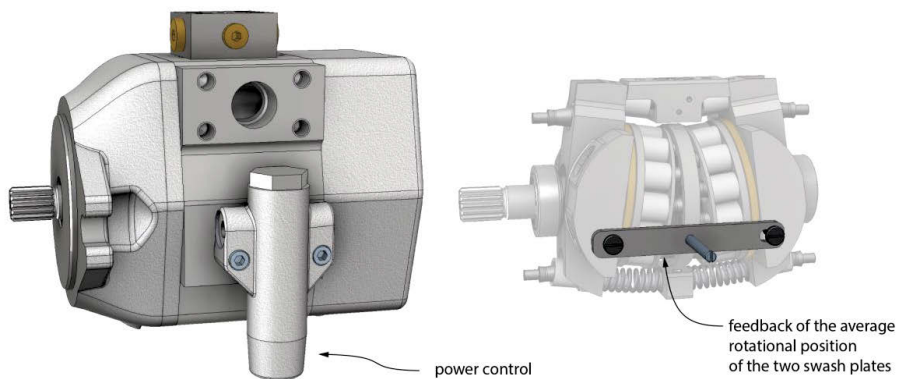


Fig. 4: Power control option with a feedback of the average swash plate position

3. Swash plate actuation and position control

In the FCVP28, the bias springs and the bias pistons push the swash plates initially to the maximum swash angle. The torque of these pistons and springs is counteracted by the control pistons and cylinders annex cups (see Figure 5). Each swash plate has one bias piston and two control pistons and cups, which are essentially the same as the pistons and cups of the rotating group.

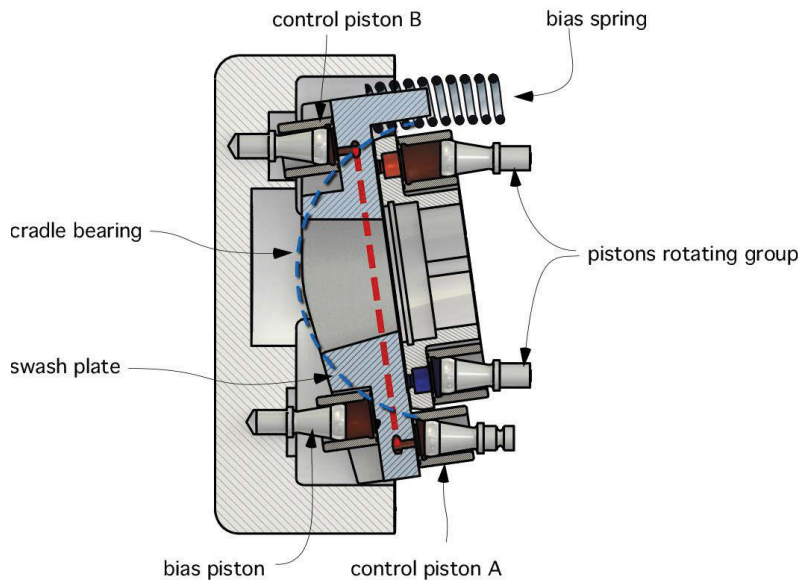


Fig. 5: One of the swash plates piston including the control pistons, the bias piston and the bias spring

The load on the swash plate bearing needs to be reduced to the minimum:

- Impact wear and brinelling are known issues for the bearing races of the swash plate. The wear can only be reduced by means of reducing the load;
- Bearing loads are rather unpredictable reaction forces, which make it much more difficult to minimize the structural deformation of the swash plates;
- Bearing loads create friction and stick-slip effects, which are difficult to handle in control systems. They limit the dynamic performance of the pump control.

In order to fulfil this requirement, several measures have been taken:

- Each barrel has an even number of cups and pistons: the FCVP28 has 24 pistons, 12 on each side, of which 6 pistons are always creating an axial load on the swash plate. This results in an almost constant axial barrel force, which can be balanced by the size and position of the bearing ports at the back of the swash plate;

- Each swash plate has two actuators, which are positioned in opposite directions. As a result, the actuators create a pure torque and there is no net axial force from the actuators acting on the swash plate;
- Hard end stops, to limit the minimum and maximum swash plate positions, are avoided. Instead, a hydraulic valve system is build to limit the swash plate system (see /7/ and /8/ for further details).

4. Damping the swash plate oscillations

The most important load on the swash plates comes from the rotating group of cups. But also the centrifugal forces and the potential friction forces create a torque load, which tends to tip the swash plate /9/. The torque is not constant but varies strongly as a result of the rotating movement of the barrels and the continuous variation between high and low pressure levels. This torque load is counteracted by the actuator or control pistons.

The variation of the torque load results in an oscillation of the angular position of the swash plate. This also occurs in conventional axial piston pumps /10/, but the oscillation behaviour will be somewhat different in the FCVP /7, 8/ due to the larger number of pistons, the even number of pistons instead of odd number of pistons and the much lower friction between the swash plate and its bearing.

In conventional pumps, the actuators act as dampers or shock breakers, thereby using the resistances in control valve to build up pressure in the control cylinders. Aside from the oscillation damping, the resistances used in the valve also define the dynamic behaviour of the pump control. Figure 6 shows the extended and simplified representation of the pump control. The control can be regarded as a series of a variable and a constant resistance. The circuit acts as a pressure divider, which is needed for the variation of the control pressure. But it also uses the resistances to damp the swash plate oscillation. The combined functionality sets limits to both the control and the damping function.

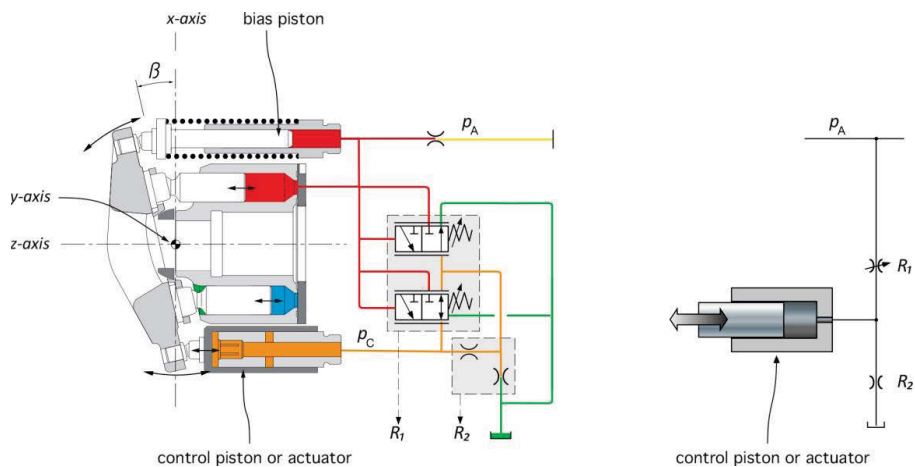


Fig. 6: Hydraulic circuit (left) and simplified diagram (right) of a conventional pump control

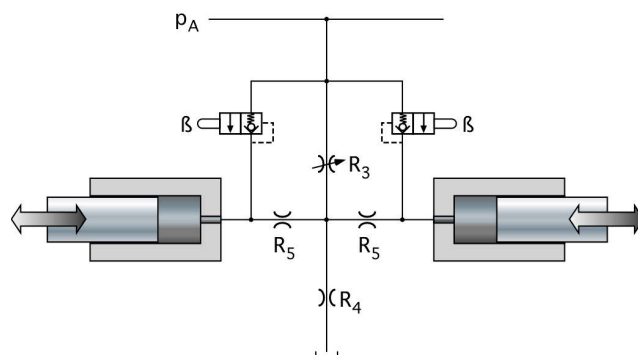


Fig. 7: Simplified hydraulic circuit for the floating cup pump. The valves indicated with β are applied to limit the maximum swash angle

In the FCVP, the double, mirrored construction is used to split these two functions. Figure 7 shows the simplified hydraulic circuit. The pair of actuators of each swash plate is represented in this figure by just a single piston, one for the left swash plate, and for the right. The oscillation of the left swash plate is out of phase with the oscillation of the right swash plate (Figure 8). Oil is therefore transferred from the left actuator to the right, and vice versa, thereby passing the resistances R_5 . The construction offers much better opportunities for optimisation than the conventional control valve.

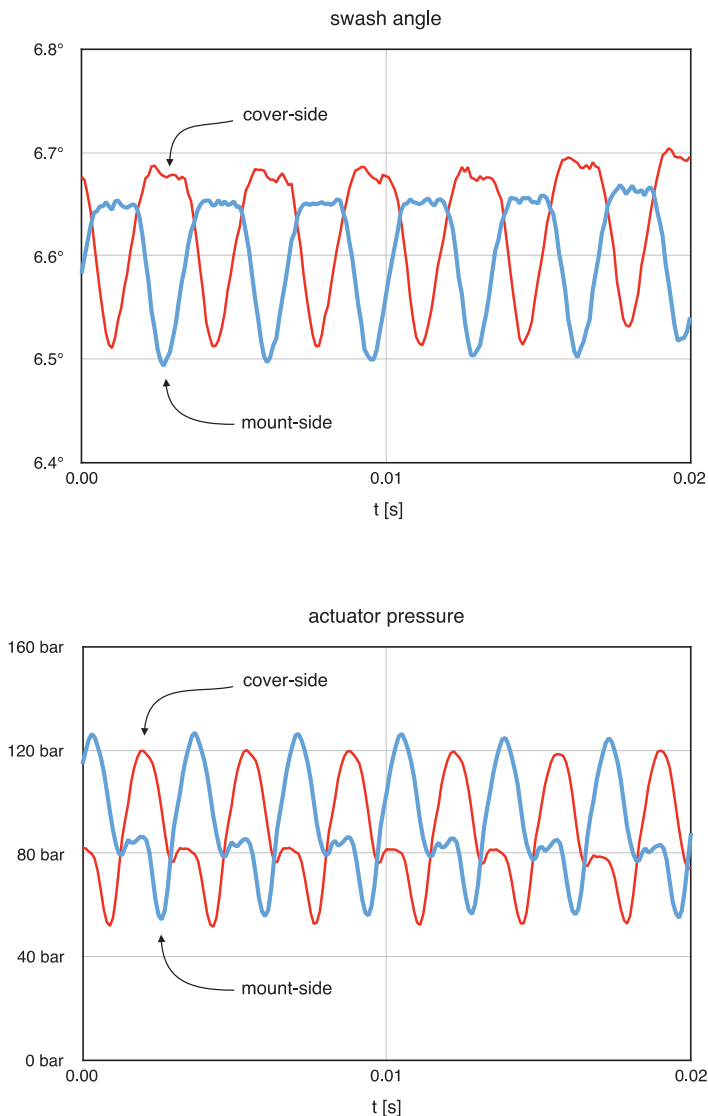


Fig. 8: Swash plate oscillation and actuator pressure for the two swash plates of the FCVP, measured at 200 bar and 1500 rpm (see Figure 2 for the definitions of mount and cover side)

5. Swash plate control

The FCVP28-prototype is equipped with a standard DFR-valve of a Bosch Rexroth A10VSO-pump. The valve is integrated in the hydraulic circuit shown in Figure 7, in which resistances R_3 and R_4 represent the resistances of the DFR-valve. The

resistances indicated with R_5 are optimized for damping the swash plate oscillations. These resistances can be found again in the diagram of the test circuit (Figure 9.). In this figure, the floating cup pump is depicted as a combination of two variable displacement pumps, the left side being the mount side, and the right side the cover side.

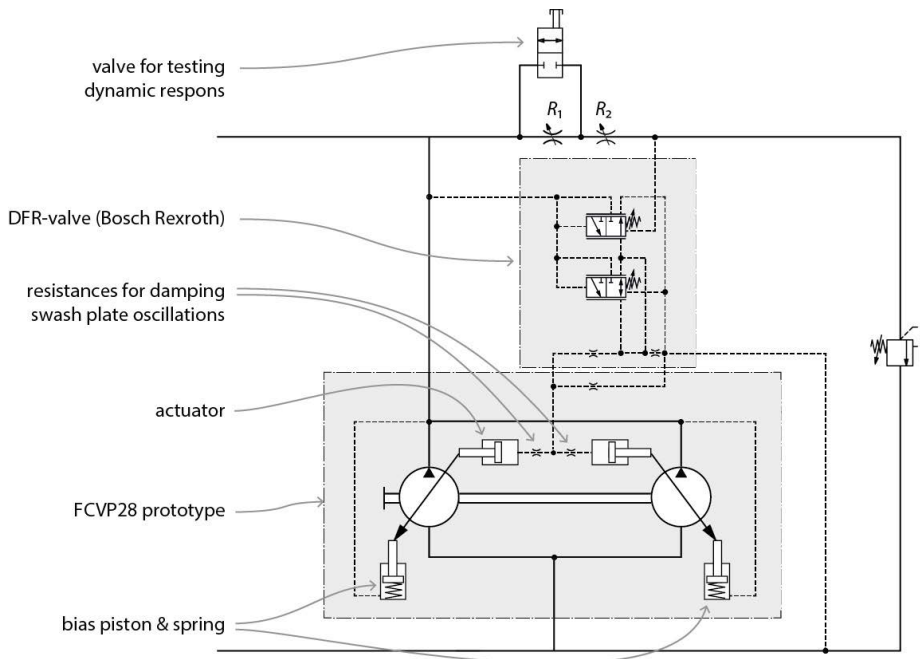


Fig. 9: Test circuit. The FCVP28 is illustrated as a combination of two variable displacement pumps, having a common shaft and housing.

The flow control part of the DFR-valve is set at a Δp of 20 bar. The pump flow is delivered to two variable resistances R_1 and R_2 in series, followed by a pressure relief valve. A 2/2-valve is included parallel to R_1 . When this valve is opened, the pump flow bypasses this resistance. By doing this, the test mimics a sudden change in the flow demand. The flow-control part of the DFR-valve responds to the change, and increases or reduces the average pressure in the actuators. This results in a change of the swash plate positions and, consequently, in a change of the flow through the metering resistance R_2 or the combined resistance of R_1 plus R_2 . The bypass valve is opened manually. The opening time is estimated to be 0,1 seconds.

Figure 10 shows two test results at a pump pressure of 200 bar and a rotational speed of 1500 rpm. Both the pump discharge pressure and the rotational positions of the

swash plates are shown. The measurements show that both swash plates respond almost synchronously: the swash angle variation on the mount side is almost identical to the swash angle variation of the cover side. The swash plates are only linked together via the hydraulic circuit as shown in Figure 9.

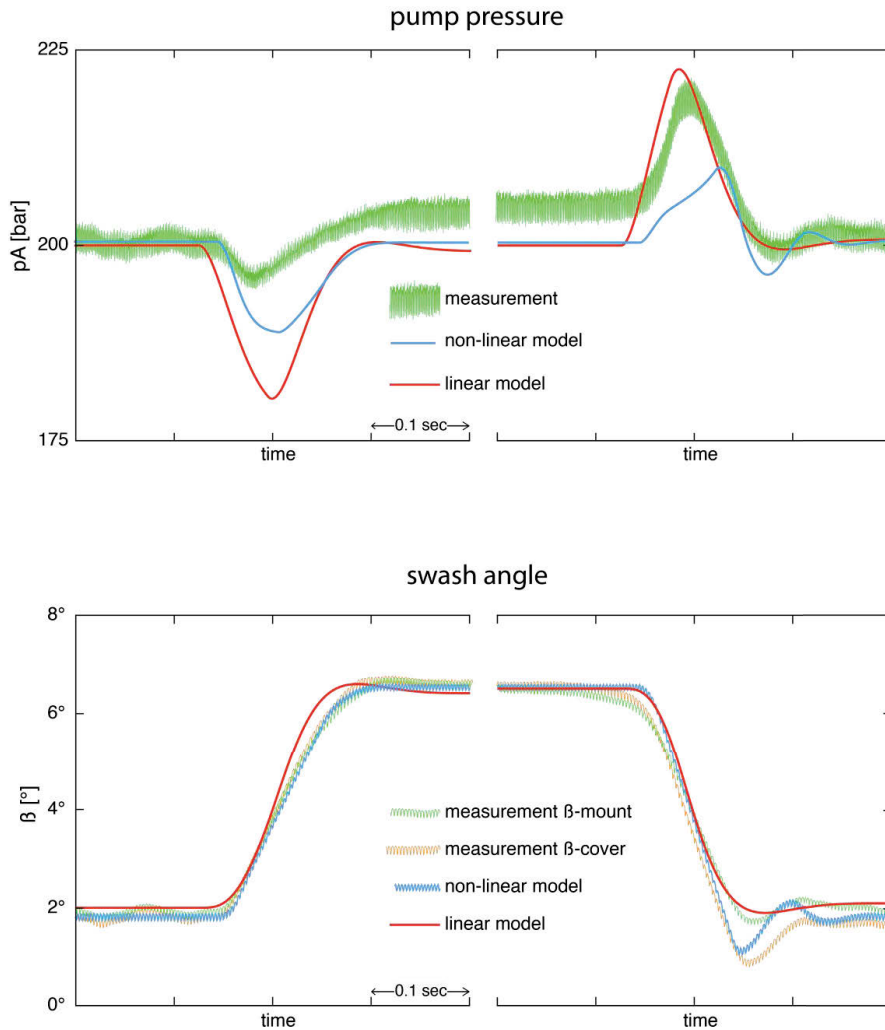


Fig. 10: Measured and simulated pump pressure and swash angle at 200 bar and 1500 rpm.
The time scale on the horizontal axis is 0,1 second per division.

Both a linear and a detailed non-linear model have been developed. The linear model is a straightforward model of the FCVP28, based on similar algorithms as have been applied for conventional slipper type pumps. In order to account for the swash plate

oscillations and other more detailed phenomena, an extended non-linear model has been conceived. The basic outlines of this model are described in earlier literature [11].

As can be seen in Figure 10, both models are adequate to predict the general dynamic behaviour of the pump. The most important differences relate to the variation of the discharge pressure as a response to the switching of the bypass valve of resistance R_1 .

6. Conclusion and future work

Tests and analysis of a prototype of a 28 cc variable displacement floating cup pump (FCVP28) have proven that it is possible to control both swash plates with a single pump control. The swash plates respond almost identical to the signals of the control valve. A new configuration has been applied in which the damping function of the control valve can be isolated of the control function itself. The response time of the FCVP28 is about 0,1 seconds. In this measurement we have taken the DFR-valve from Bosch Rexroth as it is.

In a next phase of the development, the simulation models will be used to modify and optimize the design of the control valve and its parameters.

7. References

- /1/ Achten, P.A.J., 'Designing the impossible pump. Paper for Hydraulikdagarna, Linköping University, 2003
- /2/ G. Vael, T. van den Brink, T. Paardenkooper, Achten, P., 'Some design aspects of the floating cup hydraulic transformer. Paper for PTMC 2003, 10-12 September, 2003, University of Bath
- /3/ Achten, P.A.J., 'Power density of the floating cup axial piston principle', ASME, Proceedings of IMECE 2004, California, USA
- /4/ Achten, P.A.J., Schellekens, M.P.A., Murrenhoff, H., Deeken, M., 'Efficiency and low speed behavior of the floating cup pump', SAE paper 2004-01-2653
- /5/ Achten, P.A.J., 'Volumetric Losses of a Multi Piston Floating Cup Pump', paper for NFPA / IFPE 2005, Las Vegas, March 16-18, 2005
- /6/ Achten, P.A.J., Brink, T.van den, Schellekens, M., 'Design of a Variable Displacement Floating Cup Pump', paper for SICFP'05 - Linköping, Sweden, 2005

- /7/ Achten, P., Eggenkamp, S., Potma, H.W., Swash plate oscillation in a variable displacement floating cup pump, Proc. SICFP2013, June 3-5, 2013, Linköping, Sweden
- /8/ Achten, P., Dynamic high-frequency behaviour of the swash plate in a variable displacement axial piston pump, Proc. IMechE, Part I: Journal of Systems and Control Engineering 2013, vol. 227 no. 6 pp. 529-540
- /9/ Manring, N., 'Tipping the Cylinder Block of an axial-piston swash-plate type hydrostatic machine', Transactions of the ASME, Vol. 122, MARCH 2000, p.216-221
- /10/ Ericson, L., 'Swash plate oscillations due to piston forces in variable in-line pumps', The 9th International Fluid Power Conference, 9. IFK, March 24-26, 2014, Aachen, Germany
- /11/ Ebben, P.P., Flow control of the Floating Cup Variable Pump (FCVP), Thesis 2014, Eindhoven University of Technology

Group 4: Thermal Behaviour

Thermo Energetic Design of Machine Tools and Requirements for Smart Fluid Power Systems

Professor Dr.-Ing. Christian Brecher

Laboratory for Machine Tools and Production Engineering (WZL, RWTH Aachen),
Steinbachstraße 19, 52074 Aachen, E-mail: C.Brecher@wzl.rwth-aachen.de

Dipl.-Ing. David Jasper

Laboratory for Machine Tools and Production Engineering (WZL, RWTH Aachen),
Steinbachstraße 19, 52074 Aachen, E-mail: D.Jasper@wzl.rwth-aachen.de

Dipl.-Ing. Dipl.-Wirt. Ing. Matthias Wennemer

Laboratory for Machine Tools and Production Engineering (WZL, RWTH Aachen),
Steinbachstraße 19, 52074 Aachen, E-mail: M.Wennemer@wzl.rwth-aachen.de

Dipl.-Ing. Michel Klatte M.Sc.

Fraunhofer Institute for Production Technology IPT, Steinbachstraße 17, 52074 Aachen,
E-mail: Michel.Klatte@ipt.fraunhofer.de

Abstract

Modern production systems have to allow high performance cutting processes in a flexible production system environment at a high level of accuracy. The final workpiece accuracy is mainly influenced by the thermo-elastic behavior of the machine tool and can be improved by additional measures, compensation strategies and an optimized machine design. These measures are often implemented as stand-alone solutions. According to the Industry 4.0 all information should be connected in a single model of the actual machine state to increase machining accuracy. It is therefore necessary to integrate upcoming smart fluid power systems into the machine network.

KEYWORDS: Thermo Energetic Design, Machine Tools, Smart Fluid Power Systems

1. Introduction

In today's markets, the need for machine tools with an increasing productivity and accuracy is apparent /1/. High productivity (high quantity output) results in a high energy consumption of the drive systems, spindle and auxiliary units of the machine tool. Especially heat losses of the main drives are dissipated into the machine structure, which decreases machining accuracy. Therefore, the increase in productivity is limited by thermo-elastic deviations under a certain tolerance limit (**Figure 1**).

Accuracy requirements are continuously increasing /1/. In consequence, the influence of thermo-elastic deviations will most likely increase in the future /2,1/. Current investigations state an amount of thermo-elastic deviations on the overall workpiece error of up to 75 % /3,4/. Thus the thermo-energetic design of machine tools is a key competence for upcoming production systems.

This conflict between power efficiency, accuracy and productivity is the main focus within the CRC/TR 96 financed by the German Research Foundation DFG. Different solutions to enable a high accuracy manufacturing without an additional demand for energy under unstable thermal conditions are investigated. In addition to these measures, smart fluid power systems can contribute to enable both a resource and a cost efficient high accuracy manufacturing technology.

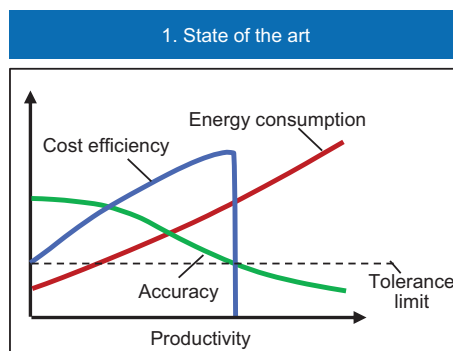


Figure 1: Conflict between power efficiency, accuracy and productivity. In style of /5/

2. Thermo Energetic Design of Machine Tools

The thermal machine characteristics, e.g. the temperature distribution and as a result the deformations of the machine structure (**Figure 2**), are influenced by different design and thermal factors. They can be divided into the categories environmental (external) and machine (internal) influences.

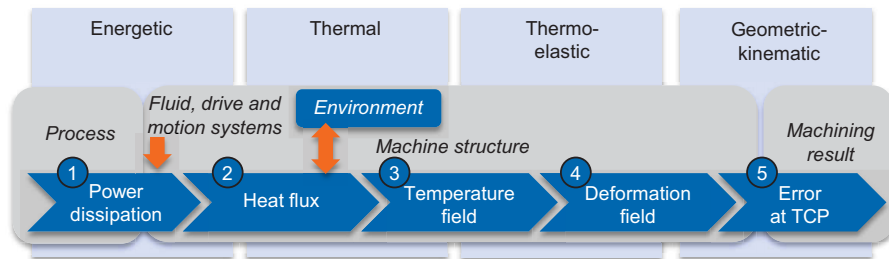


Figure 2: Causes for thermo-elastic deviations. In style of /5/

The ambient temperature of the shop floor is affected by meteorological (e.g. daily fluctuation of the ambient temperature) as well as machine shop specific (e.g. machine waste heat, air conditioning and heating) influences. The main machine internal heat sources and sinks are the drives of the motion systems, especially the main spindle, as well as the process heat and coolant.

These heat sources and sinks (1) lead to a heat transfer in the machine structure (2) which results in an unbalanced and unsteady temperature distribution within the machine structure (3). This distribution is dependent on thermal material properties like heat capacity, heat conductivity and mass distribution as well as on the distance or position to the heat sources and sinks. The temperature field leads to a thermal deformation of the machine structure (4) and finally to deviations and inclinations of the tool center point (TCP) (5). The deformation field is influenced by the effective strain lengths, the expansion coefficients, the components structure (ribbing, thickness), the position of the components to each other and the kind and setup of the position measuring systems.

A reduction of these thermo-elastic deviations of the TCP is done by

- additional measures,
- avoidance of emerge or reduction due to an optimized design,
- control-internal compensation methods or
- a reduced base load.

Additional measures (e.g. cooling, wait for thermal steady state and air conditioning) can reduce the resulting error of the TCP to meet the tolerances under a high productivity and thus a high thermal load of the machine tool (**Figure 3, 2**). These measures results in an increased energy consumption, which affects the cost efficiency negatively. Compensation algorithms can reduce this energy consumption as additional measures can be neglected (**Figure 3, 3**). In this regard, thermo-elastic deviations can be reduced by control-internal compensation models (indirect compensation) or by directly measuring the TCP offset (direct compensation). In case 4 the deviations will not occur due to a change of the machine design and reduction measures without additional energy input (e.g. optimized design, base load reduction, active thermal management).

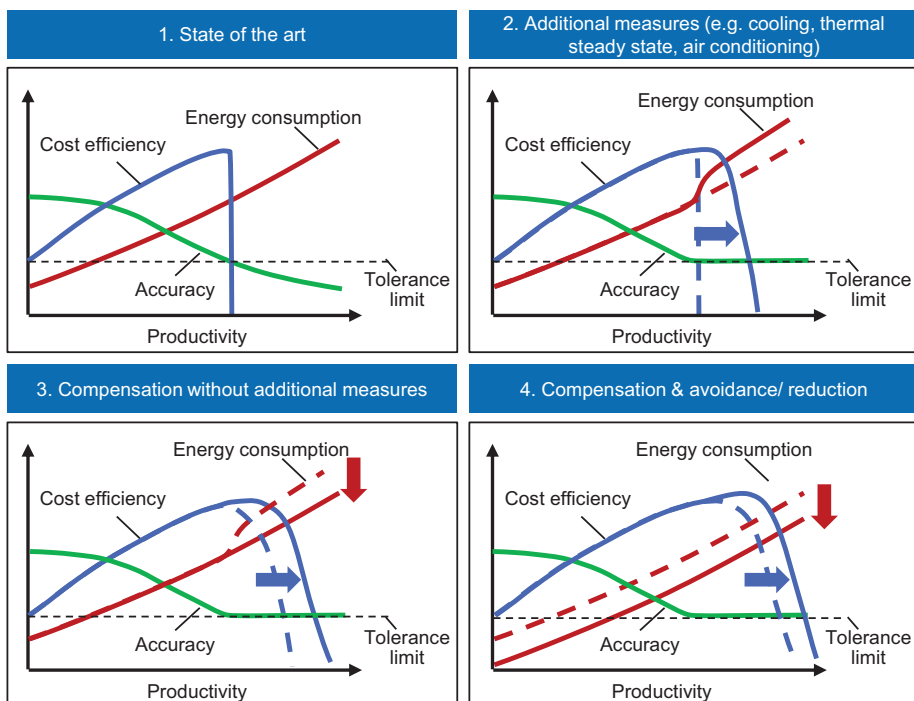


Figure 3: Conflict between power efficiency, accuracy and productivity. In style of /5/

An optimized thermo-elastic design of machine tools requires a deep understanding of the thermo-elastic behavior of the different machine components (**Figure 4**). Therefore, a detailed analysis and simulation of the machine components under typical thermal stresses is part of current research activities (CRC TR/ 96, DFG SPP 1480, EXC 128). An example of a modelling approach to optimize the design of the cooling circuit of a main spindle is given in /6/.

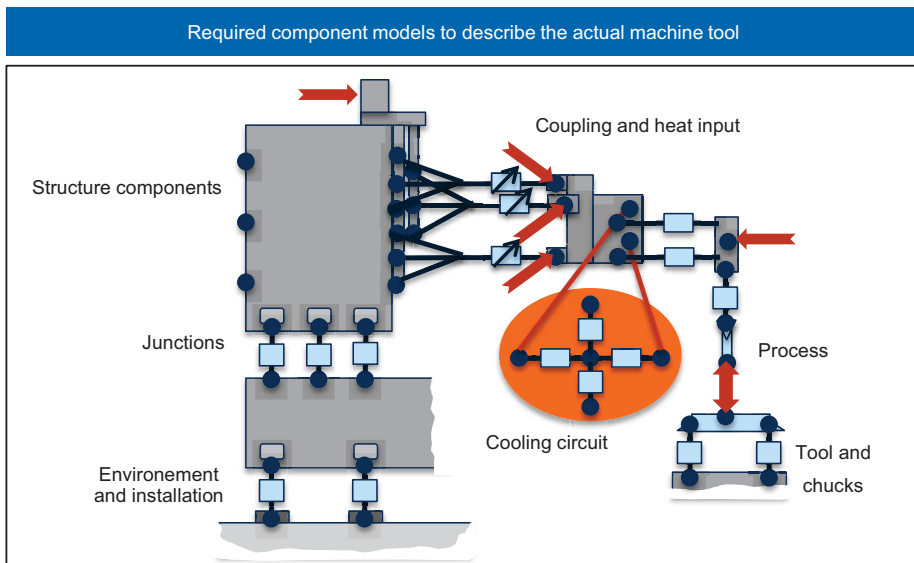


Figure 4: Required components models to describe the actual thermo-elastic behavior of a machine tool

As the machine design is optimized, further improvements of the remaining thermo-elastic deviations can be achieved by compensation. Research activities mainly focus compensation models based on

- control-internal data like power and speed of the drives (Figure 2, 1),
- the temperature field within the machine structure (Figure 2, 3),
- the deformation field (Figure 2, 4) and
- the direct measurement of TCP deviations (Figure 2, 5).

Common industrial thermo-elastic compensation methods are based on temperature measurements. The machine structure components are monitored by approximately 10 - 20 temperature sensors. The ideal position of these sensors can be calculated [7]. The final deviation of the TCP is often calculated by a linear assumption between temperature and resulting cartesian deviation of the TCP. These models are parameterized by deviation measurements under representative thermal loads of the machine structure. The method achieves good compensation results of position-independent deviations typical for a thermal load of the main spindle.

As thermo-elastic deviations often include position dependent deviations (especially due to thermal loads of the linear axes as well as the environment) a volumetric measurement and compensation method is necessary [9,8]. This is subject to current

research topics. A volumetric measuring method based on laser distance measurements is employed to measure the whole machine volume in a short time period /8/. The system consists of an interferometer mounted on two rotational axes able to follow the position of an optical target reflector (**Figure 5, left**). The target reflector is mounted at the TCP, while the interferometer is mounted on the machine table. The TCP with the mounted reflector moves to previously defined positions during measurement, while the interferometer records the relative distance changes between interferometer and reflector position. The position of the interferometer has to be alternated during measurement to at least four different positions. A multilateration technique combined with a rigid body model is used to calculate the deviations of each degree of freedom for each machine tool axis. **Figure 5 (right)** presents a partial result of these calculations. The position dependent yawing motion error of the x-axis of a machine tool over time is shown. An air-cut of the x-axis of 30 m/min over 6 h is applied as a thermal load followed by a cool-down phase of approximately 18 h.

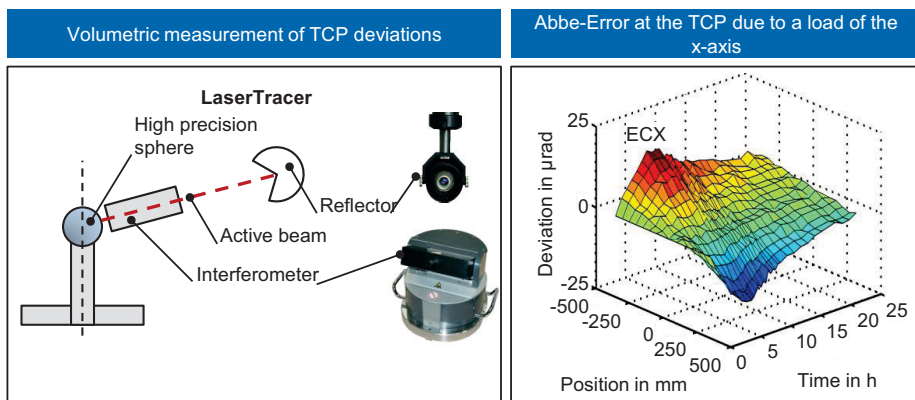


Figure 5: Volumetric TCP deviations of a milling machine due to load of a linear axis.

In style of /8/

The measurement results will be used to develop a volumetric compensation approach based on control-internal data /9/ (**Figure 6**): Control-internal data of the different motion systems like power of the axes are already captured by the Numeric Control (NC). These data streams are averaged (1) to calculate model parameters from a predefined characteristic diagram (2). The characteristic diagram is captured beforehand by volumetric thermo-elastic deviation experiments for representative thermal loads. As a result, the deviation of all three degrees of freedom of single axes under different thermal loads is known. Each of these measured errors is approximated by first-order time delay elements to span the characteristic diagram. The interpolated

model parameters (3) are used to calculate the deviation of each degree of freedom of the single axes in time and in space domain (4). Finally, the computed volumetric deviations over time are stored in the NC for further processing (5). These are used by the NC to calculate the current cartesian offset vector of the TCP to apply its inverse value to the feed drive control.

The presented compensation algorithm based on control-internal data can significantly reduce the resulting error of the TCP due to machine internal influences to values under $5\text{ }\mu\text{m}$ /9,8/. Changes of the environmental temperature and variations of the actual process (coolant) would require a combination of additional compensation approaches, using other sensors.

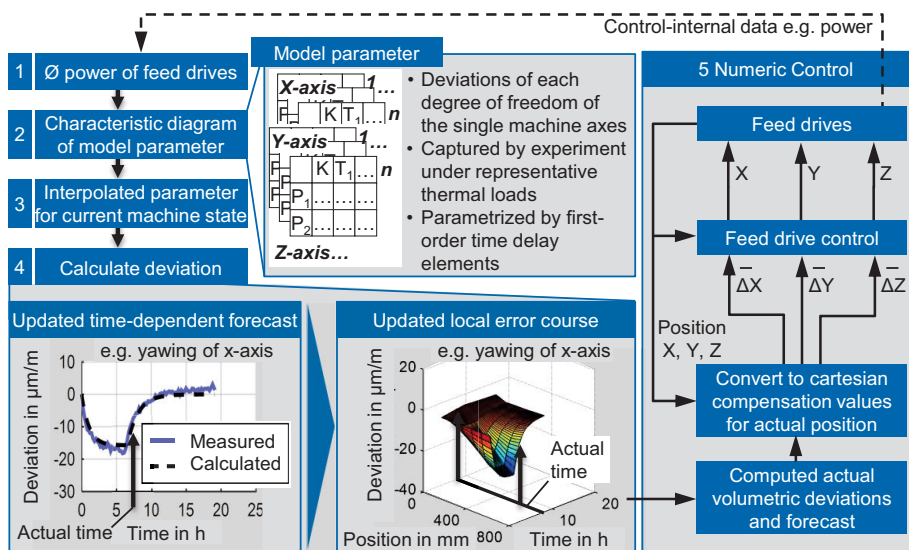


Figure 6: Control-internal volumetric compensation

An additional compensation approach is illustrated in **Figure 7**. Here, the local thermo-elastic relative deformations of relevant structure components are measured by linear strain sensors. The sensors are based on integrated carbon fiber rods in the machine structure, which act as a dimensional reference. With a displacement sensor, the relative mean strain of the respective structure can be measured with high accuracy. When the system is integrated into a machine tool, multiple sensors (usually three) are integrated in a structural component. By this approach, elongation and bending can be distinguished and quantified.

A test machine has been equipped with a system of 24 sensors (three located in the headstock). The headstock is an important component in the kinematic chain and prone to thermal deformation since it is directly exposed to the main spindle and the linear motors. Validation experiments, in which the headstock has been heated by motion of the Z-axis, result in a bending of the component and therefore a deviation of the TCP in Y-direction of up to 80 μm .

With the direct measurement of the deformation and a geometric-kinematic transmission model, the resulting deviation of the TCP can be calculated with good accordance. The experiments show a potential reduction of the resulting deviation of 86 %. The inverse of the calculated deviation is added to the nominal position value in order to correct the deviation via a feed motion of the machine axes /10/.

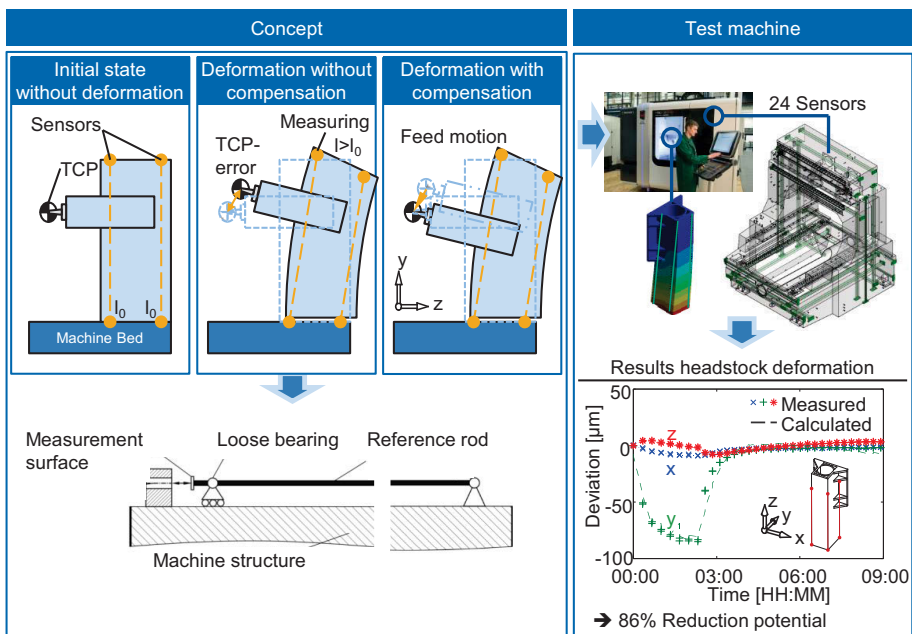


Figure 7: Indirect correction of thermo-elastic deviations by measuring the structural deformations of the machine components. In style of /10/

A direct measurement of the TCP deviation can be used to compensate thermo-elastic deviations. Here, as a rule, the TCP deviation is measured as the cartesian offset vector at one or several specific machine positions. A measurement of the full volumetric geometric state of the machine tool is an exceptional case as the cost and time effort is too great.

Each of the presented possibilities to improve the thermo-elastic machine tool behavior enhances the system understanding of single machine components to build up an understanding of the complete machine. Today, these methods are often used as stand-alone solutions. In the context of Industry 4.0 all available information, e.g. sensor data, control-internal data of the drive and motion systems as well as the auxiliary units and the machining code should be combined in a single model and lead to a profound system understanding. Any information can improve the predictive accuracy of the current thermo-elastic machine state for compensation, base-load reduction and an active thermo-management. In this context, the actual state of the auxiliary systems e.g. spindle cooling and fluid power systems have to be known and controllable by an integrated machine network to enable an active thermo-management.

3. Requirements for Smart Fluid Power Systems

As shown in Figure 3, No. 4, the cost efficiency can be further increased by reducing the energy consumption. Having a closer look at the energy consumption of machine tools during operation, **Figure 8** shows for an exemplary machine tool (Heller H2000) and a test workpiece, that fluid systems (auxiliary components) are the main consumers. The fluid systems “Cutting fluid supply”, “Cooling System” and “Hydraulic” have a share of 66 % of the energy consumption for the exemplary break down of the test workpiece machined on the machine tool. /11/

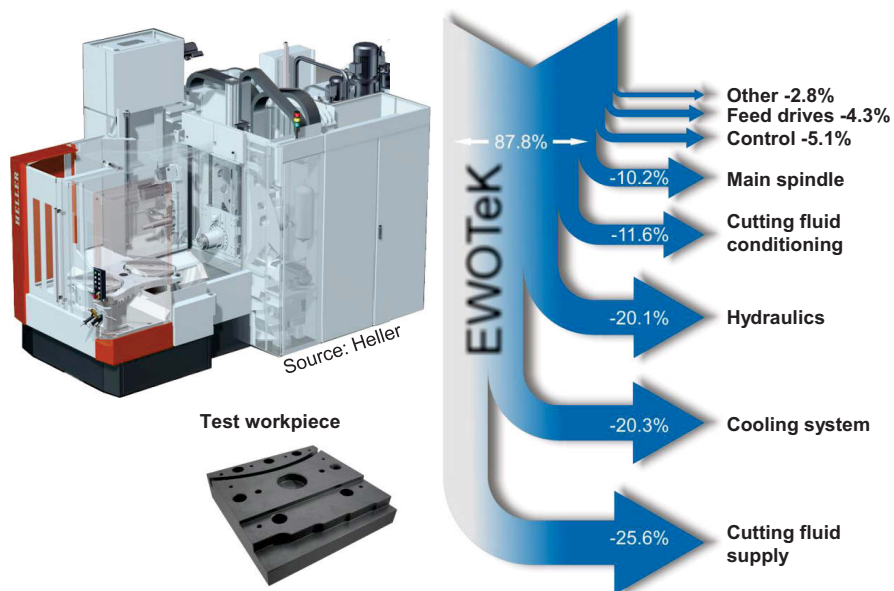


Figure 8: Exemplary break down of the energy consumption of a machine tool /11/

3.1. Approaches to improve the energy efficiency

The following section describes technical approaches to improve the energy efficiency of the fluid systems (auxiliary components). In addition to the state of the art the optimization with the achieved energy savings is shown. The approaches mainly aim a demand-based operation of the fluid systems.

3.1.1. Coolant fluid systems

For cooling and lubrication of the tools from inside, a high pressure pump is used. The high pressure coolant pump represents the highest active power consumer of the coolant system. The coolant is fed to the machining point through channels in the tool. Depending on the tool size, various pressure levels and flow rates for optimal machining are required. Thus, the high pressure coolant pump has a large variety of operating points. But today most of the high pressure coolant pump units are designed to the maximum required coolant volume flow. If a lower coolant volume flow is needed, the excess flows unused over the pressure reducing valve back to the tank (see **Figure 9, top left**). The energy consumption of the coolant fluid system is independent of the operating condition of the machine tool and the pumps are oversized for most applications. Thus, the efficiency under partial conditions is low and head is added unnecessarily to the coolant. /12/

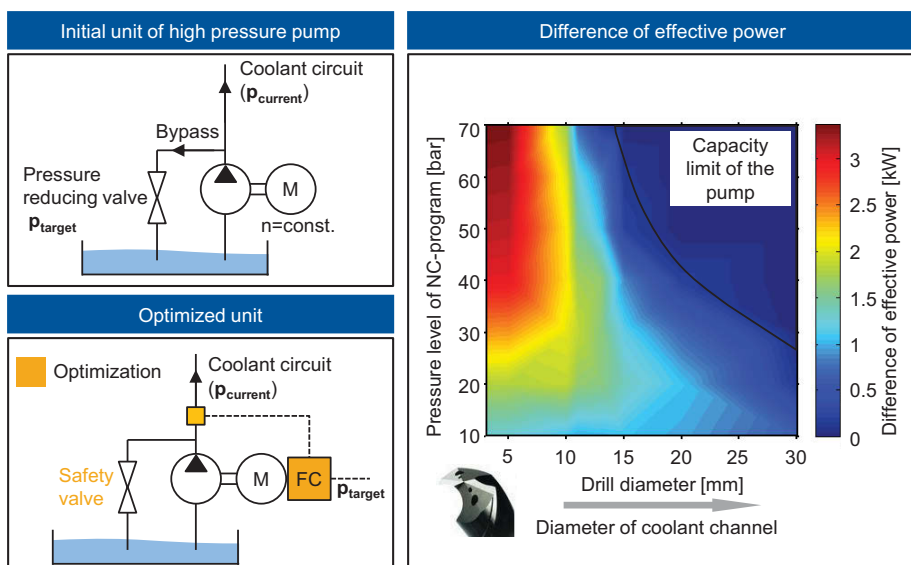


Figure 9: high pressure coolant pump units and difference of effective power /11/

The optimized high pressure coolant pump unit is equipped with a frequency converter and a pressure sensor. The exact flow rate and pressure level for each tool size is provided by the unit (see **Figure 9, bottom left**). The maximum possible power saving is 3.5 kW or 55 % at a pressure level of 70 bar and a tool size of 4 mm diameter (see Figure 9, right). The flow rate is reduced by 22 l/min. This corresponds to a hydraulic power loss in the bypass of 2.6 kW.

3.1.2. Cooling system

Cooling units in machine tools can be operated with water or oil. They serve to cool e.g. the spindle, drives, ball screws, the hydraulic unit, the coolant, the machine bed or the control cabinet. Cooling units are necessary to prevent certain components from overheating and to assure a certain accuracy of the machine tool. For the exemplary machine tool in the initial state, a hot gas bypass cooling unit is used. In general different approaches to energy efficient cooling systems exist.

- Clocked compressor
- Frequency-controlled compressor
- Digital-Scroll compressor

The **clocked compressor** is switched off when it is not used. It is a simple and effective solution to save energy, yet it can only be used for longer on/off intervals otherwise the durability is affected negatively /13/. For that reason the **hot gas bypass** method is the state of the art unit for high-precision machining. The cooling power of a hot gas bypass system can be controlled within the range of 10 – 100 % /14,13/ but as energy is burned off in the bypass, the active power consumption is fairly constant and mostly independent from the actual machine condition. The energy efficiency in the part-load case is low. A **digital-scroll compressor** does not reflect state of the art technology of cooling units of machine tools. First results on the power consumption of a prototypic cooling unit with digital-scroll compressor together with a description of the functionality can be found in /15/. The cooling power of a digital-scroll compressor can be varied between 10 – 100 % with constant speed. Due to the digital control of the compressor power, the active power of the cooling unit can be adapted to the demand.

For the exemplary machine tool the power consumption of the cooling unit with a hot gas bypass ranges from 2.4 kW to 3.3 kW for the three different operating conditions (see Figure 10) /16/. For the exemplary break down of the test workpiece machined on a machine tool (see Figure 8) the cooling system have a share of 20 % of the energy consumption /11/. To optimize the cooling unit, the hot gas bypass was removed and a

digital scroll compressor is used. In addition, the pump and fan motor was equipped with a frequency converter (see **Figure 10**). The power consumption of the cooling unit with digital scroll compressor now ranges from 0,89 kW to 2,7 kW for the three different machine conditions (see Figure 10). Due to the demand-based compressor power, the active power at operating condition “main switch on” (no production) can be reduced over 62 %. /16/

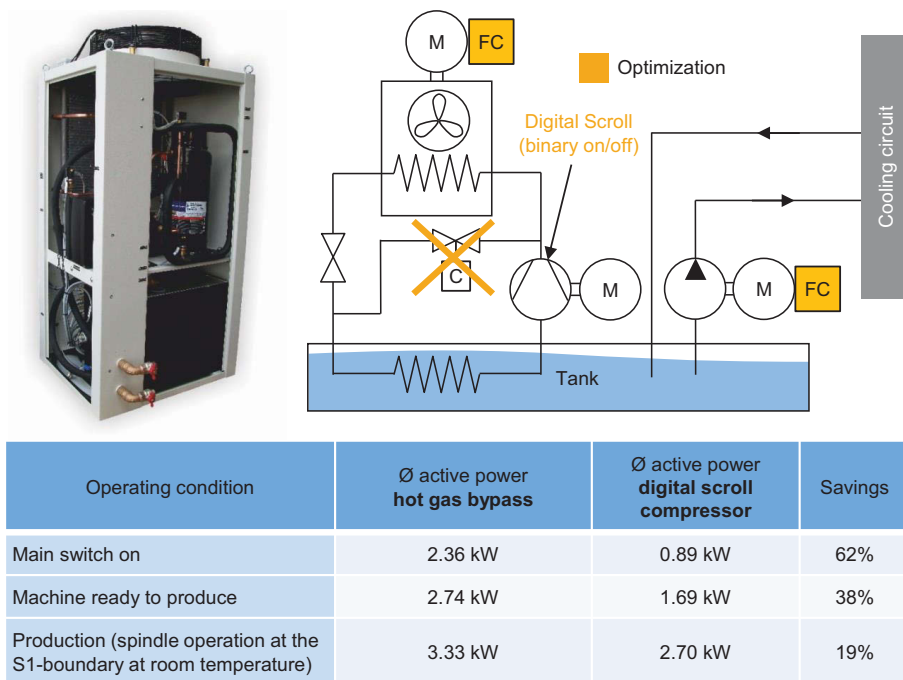


Figure 10: machine cooling Circuit

3.1.3. Hydraulic unit

Hydraulic units of machine tools are one of the main consumers of energy. Hydraulic functionalities of machine tools are for example the tool change, the work piece clamping, the palette change, the weight compensation of vertical axes or the supply of hydrostatic guidings. For the test workpiece machined on the machine tool Heller H2000 (see Figure 8) the hydraulic system has a share of 20 % of the energy consumption /11/. This machine tool has two hydraulic cycles with different hydraulic functions; a high pressure cycle (200 bar) and a low pressure cycle (60 bar). The state-of-the-art hydraulic unit therefore has a low and a high pressure pump on the same shaft and a constant drive. /17/ analyzes the energy efficiency of the state-of-the-art

and two optimized hydraulic units (see **Figure 11**). The description of the functionality of each hydraulic unit and a detailed analysis of the energy consumption for different machining conditions can also be found in /17/. Since there is no hydraulic function during most of the processing time, the behavior of the hydraulic units during base load condition is discussed in the following. For the hydraulic unit of optimization “one” (see Figure 11) the high pressure pump is replaced with a booster. Thus, the power consumption of the hydraulic unit can be reduced by 61 % (from 2,3 kW to 0,9 kW) during base load condition. Furthermore the oil warming could be reduced so that a cooling of the hydraulic unit is no longer needed.

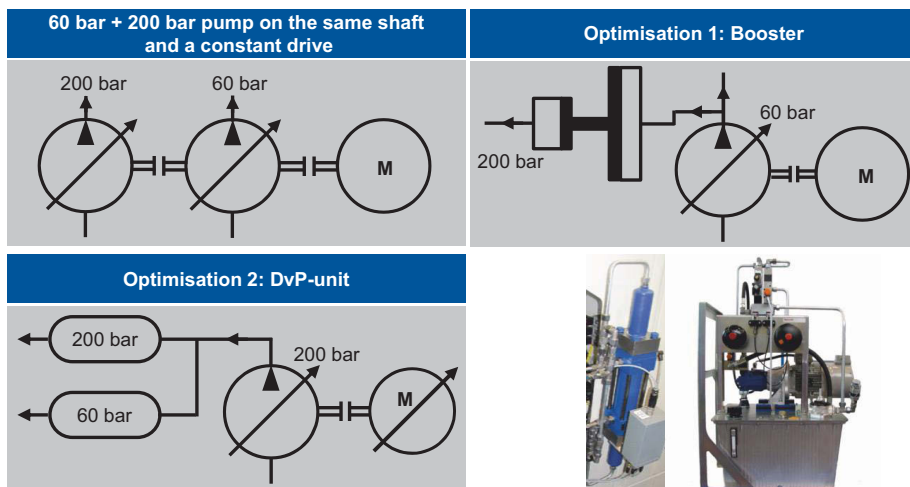


Figure 11: Scheme of the different hydraulic units /17/

The hydraulic unit of optimization “two” (see Figure 11) only has one variable-displacement axial piston pump. The motor is equipped with a pressure controlled frequency converter. The high-pressure pump loads two accumulators one low-pressure accumulator with 60 bar and one high-pressure accumulator with 200 bar. During times where no hydraulic function is fulfilled, the hydraulic drive is reduced to 4 Hz. Thus, the power consumption of the hydraulic unit can be reduced to 0,2 kW which represents a saving to the state-of-the-art unit of 91 %. Further advantages are the noise reduction of the DvP-unit through a very low turning speed and the reduction of thermal losses. /17/

3.2. First Steps to Smart Fluid Power Systems

The results of the described studies show that the base load of the fluid systems can be significantly reduced through demand based supply. Therefore the energy efficiency

can be increased and the heat energy introduced unnecessarily into the machine tool can be reduced. With the DvP-unit (see Figure 11) the hydraulic oil temperature could be reduced from 45°C to near ambient temperature. By the optimizing measures the cooling of the hydraulic oil can be completely avoided. For further optimizations new approaches are needed. A possible one is the use of smart fluid power systems. Following an approach is described which is being investigated in the research project "MinEnerWe – The mineral oil-free, energy-efficient machine tool". A first step towards a "smart fluid power system" has been made by using a combined hydraulic and cooling unit (see **Figure 12**). The combining of the hydraulic and cooling unit is possible due to the optimized DvP-unit described above.

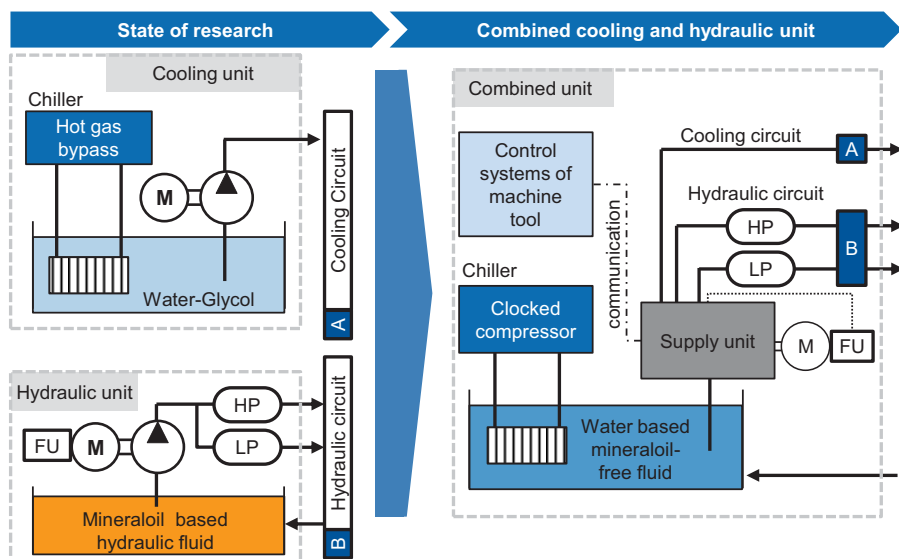


Figure 12: Combined Cooling and hydraulic unit

By combining the cooling and the hydraulic unit, both circuits can be powered from one power supply unit. By merging subfunctions of both units, synergy effects can be utilized. In addition, only one tank is needed and the required space can be reduced. The pressure accumulators in the high- (HP) and low-pressure circuits (LP) allow a shutdown of the hydraulic pump during times where there is no hydraulic function required. Due to the combination of the units the tank volume of the cooling unit is increased. As a result a clocked compressor can be used by holding the accuracy requirements, which previously could not be used (see. chapter 3.1.2). This compressor is both more energy-efficient and more cost-effective, than hot gas bypass units. In order to increase resource efficiency a water-based, mineral oil-free fluid is used that fulfills both the requirement of the hydraulic and the cooling circuit. The age-

related change of the new mineral oil-free fluid /18/ as well as the impact of the new fluid to the sealing materials /19/ are tested according to known procedures.

The common supply unit will be linked to the numeric control (NC) of the machine tool and will predictively analyze the current NC code. Thus, the hydraulic pump can be switched on shortly before a hydraulic function is needed. The cooling unit may in advance increase the flow rate to the spindle for high spindle loads (e. g. roughing).

4. Smart Fluid Power Systems in the context of Industry 4.0

With the measures described above, a first step towards Industry 4.0 in the field of the hydraulic and cooling fluid systems has been done. The future fluid systems will be intelligent and deeper linked with the machine tool (see **Figure 13**). The machine tool could be able to identify the workpiece automatically and load the appropriate NC code with associated thermo-elastic compensation models. The operating state of the machine tool including auxiliary units could be monitored by means of different sensors. Thus, the state of the hydraulic oil and the number of switching cycles of the valves could be analyzed. The coolant unit will show the upcoming maintenance work, for example when the fluid needs to be refilled or replaced. By integrating the sensor data and operating conditions into the machine tool control, the temperature distribution of the machine components, the power losses, the volume flows and active power input are known. These data allow the use of an intelligent thermal management and compensation system to reduce the thermo-elastic deviations of the TCP, which enables a high accuracy and energy efficiency by low demands on the ambient conditions.

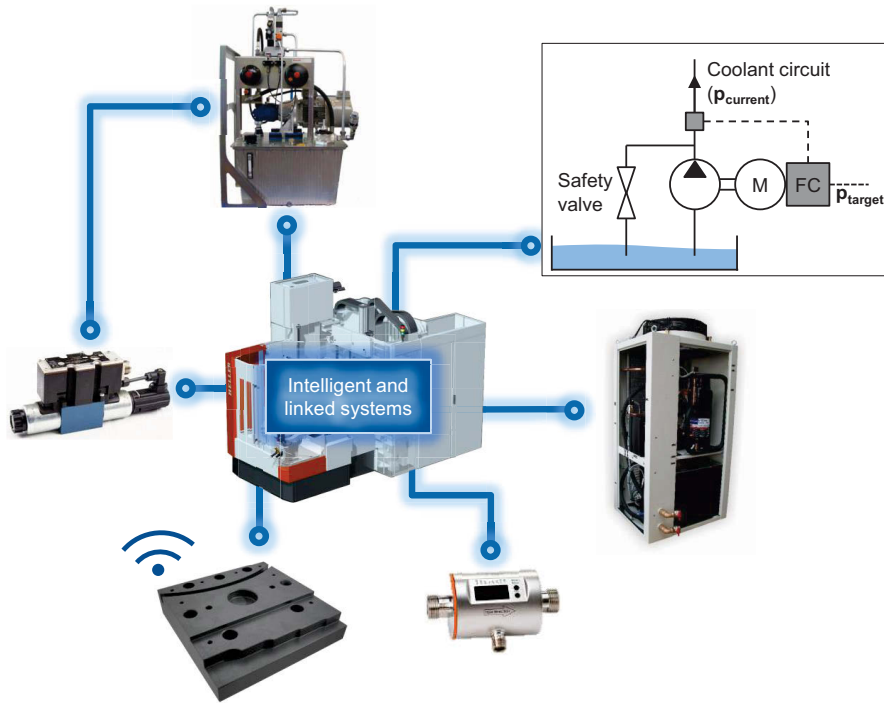


Figure 13: linked systems for an intelligent thermal management

5. Acknowledgments

The authors want to thank the DFG (German Research Foundation) for financial support. The represented findings in chapter 2 result from the subproject B06 “Property model based compensation” and subproject C03 “Structurally Integrated Sensors” of the special research field SFB/Transregio 96 “Thermo-energetic design of machine tools”.

The shown work in chapter 3 was done during the research project “MinEnerWe – The mineral oil-free, energy-efficient machine tool” (DBU-Az. 31555/01-24/0). The authors would like to thank the Deutsche Bundesstiftung Umwelt DBU (German Federal Environmental Foundation) for founding the research project.

6. References

- /1/ Kinkel, S., Lay, G., 2006. Technologietrends in der Produktion: Praxis der Anlagenmodernisierung in der deutschen Metall- und Elektroindustrie. Mitteilungen aus der Produktionsinnovationserhebung 39.

- /2/ Kinkel, S., 2005. Anforderungen an die Fertigungstechnik von morgen: Wie verändern sich Variantenzahlen, Losgrößen, Materialeinsatz, Genauigkeitsanforderungen und Produktlebenszyklen tatsächlich? Mitteilungen aus der Produktionsinnovationserhebung 37.
- /3/ Bryan, J., 39. International Status of Thermal Error Research (1990). CIRP Annals - Manufacturing Technology 1990 (2), pp. 645–656.
- /4/ Mayr, J., Jedrzejewskic, J., Uhlmann, E., Donmez, M.A., Knapp, W., Härtig, F., Wendt, K., Moriwaki, T., Shore, P., Schmitt, R., Brecher, C., Würz, T., Wegener, K., 2012. Thermal Issues in Machine Tools. CIRP Annals - Manufacturing Technology 61 (2), pp. 771–791.
- /5/ Grossmann, K. (Ed.), 2014. Thermo-energetic Design of Machine Tools: A Systemic Approach to Solve the Conflict Between Power Efficiency, Accuracy and Productivity Demonstrated at the Example of Machining Production. Springer, Cham.
- /6/ Weber, J., Weber, J., 2013. Thermo-energetic analysis and simulation of the fluidic cooling system of motorized high-speed spindles, in: 13th Scandinavian International Conference on Fluid Power, June 3-5, 2013, Linköping, Sweden. 2013-06-03. Linköping University Electronic Press, pp. 131–140.
- /7/ Herzog, R., Riedel, I., 2015. Sequentially optimal sensor placement in thermoelastic models for real time applications. Optimization and Engineering 16 (4), pp. 737–766.
- /8/ Brecher, C., Fey, M., Wennemer, M., 2015. Volumetric thermo-elastic machine tool behavior. Prod. Eng. Res. Devel. 9 (1), pp. 119–124.
- /9/ Brecher, C., Fey, M., Wennemer, M., 2015. Control-Internal Compensation Algorithm for thermally induced volumetric Tool-Center-Point Deviations, in: Blunt, L. (Ed.), Laser metrology and machine performance XI. euspen, Bedfordshire, pp. 351–361.
- /10/ Brecher, C., Klatte, M., Wenzel, C., 2015. Application of Machine Integrated Deformation Sensors, in: Blunt, L. (Ed.), Laser metrology and machine performance XI. euspen, Bedfordshire, pp. 8–17.
- /11/ Bäuml, S., Bode, H., Brecher, C., Breitbach, T., Hansch, S., Hennes, N., Prust, D., Tannert, M., Thoma, C., Wagner, P., Witt, S., Würz, T., 2011.

- Ressourceneffizienz im Werkzeugmaschinenbau, in: Brecher, C., Klocke, F., Schmitt, R., Schuh, G. (Eds.), Wettbewerbsfaktor Produktionstechnik. Aachener Perspektiven. Tagungsband Aachener Werkzeugmaschinenkolloquium (AWK).
- /12/ Brecher, C., Triebs, J., Heyers, C., Jasper, D., 2012. Effizienzsteigerung von Werkzeugmaschinen durch Optimierung der Technologien zum Komponentenbetrieb – EWOTeK, 1st ed. Apprimus, Aachen.
- /13/ Rothenbücher, S., Kuhrke, B., 2010. Energiebündel auf dem Prüfstand: Trendbericht: Energiekosten bei spanenden Werkzeugmaschinen. WB Werkstatt und Betrieb (9), pp. 130–137.
- /14/ Rittal GmbH & Co. KG, 2010. Frequenz geregelter Wärmetauscher mit 70 Prozent weniger Energieverbrauch. MAV Maschinen Anlagen Verfahren (9), p. 122.
- /15/ Brecher, C., Bäuml, S., Jasper, D., Triebs, J., 2012. Energy Efficient Cooling Systems for Machine Tools, in: Dornfeld, D., Linke, B. (Eds.), Leveraging Technology for a Sustainable World, CIRP 19th Conference on Lifecycle Engineering, Berkeley, pp. 239–244.
- /16/ Brecher, C., Triebs, J., Dornfeld, D., 2012. Energy Efficient Machine Tools: Comparison of Different Cooling Systems, in: Seliger, G., Kiliç, S.E. (Eds.), 10th global conference on sustainable manufacturing. Towards implementing sustainable manufacturing. CIRP, Istanbul, pp. 650–655.
- /17/ Brecher, C., Triebs, J., Jasper, D., 2013. Energy Efficient Solutions for Hydraulic Units of Machine Tools, in: Nee, A. Y. C., Song, B., Ong, S.-K. (Eds.), Re-engineering manufacturing for sustainability. Proceedings of the 20th CIRP International Conference on Life Cycle Engineering, Singapore 17-19 April, 2013. Springer, Singapore, pp. 191–196.
- /18/ Bressing, J., Dott, W., Murrenhoff, H., Schumacher, J., 2009. Toxikologische Bewertung der alterungsbedingten Veränderung biogener Schmieröle. Tribologie + Schmierungstechnik 56 (4), pp. 5–9.
- /19/ Jan Schumacher, Marko Küppers, Lasse Greiner, Hubertus Murrenhoff, Marcel Liauw, 2009. Dichtungswerkstoffe und biogene Ester. O+P (7), pp. 2–7.

Thermo-energetic Analysis of the Fluid Systems in Cutting Machine Tools

Dipl.-Ing. Juliane Weber

Institut für Fluidtechnik (IFD), Technische Universität Dresden, Helmholtzstrasse 7a,
01069 Dresden, E-mail: juweber@ifd.mw.tu-dresden.de

Dr.-Ing. Harald Lohse

Institut für Fluidtechnik (IFD), Technische Universität Dresden, Helmholtzstrasse 7a,
01069 Dresden, E-mail: lohse@ifd.mw.tu-dresden.de

Professor Dr.-Ing. Jürgen Weber

Institut für Fluidtechnik (IFD), Technische Universität Dresden, Helmholtzstrasse 7a,
01069 Dresden, E-mail: mailbox@ifd.mw.tu-dresden.de

Abstract

Controlling the thermo-elastic behavior of tooling machines can only be achieved by systematic analysis, characterization and design of their fluidic system. In the first stage of this project, fundamental work was done to develop simulation methods for the calculation of the thermodynamic behavior of a representative example of a milling machine and each of its components. With experimental and numerical data it was proven, that significant improvement can be achieved by a proper design of heat transfer conditions of the fluidic system. To correct and counterbalance thermo-energetic effects, it will be necessary to develop new structures of the tooling machines systems which ensure the temperature-control of local subsystems in dependence of the actual working process. The work which is documented in this paper deals with the thermodynamic behavior of the motor spindle

KEYWORDS: Tooling Machine, Heat Transfer, Cooling Circuit, Energy Efficiency, Experimental Investigations, Simulation

1. Introduction

In metal-cutting production still demands are placed with regard to greater accuracy and higher productivity /1/. Therefore, an adequate control of the static design of machine structures and advanced servo technology of feed axes are already contributing to high precision. However, growing quantity outputs require larger amounts of main and feed drive power. In case of the main drives this power is mainly dissipated in heat flows at

the tool center point (TCP) of the cutting process. And in case of the feed drives also higher heat flows are produced indirectly due to increased friction losses of mechanical drives and guide elements or increased power losses of the drives themselves. Both is leading to increased thermo-elastic deformations. Conventional measures concerning the reduction of thermo-elastic errors such as air-conditioning of entire production areas, continuous operation of thermal stabilizing hydraulic circuits even in idle process windows as well as tempering of structural areas of machine tools are already successfully practiced. However, these practices consistently increase the energy consumption and thus, reduce the efficiency. As part of the Collaborative Research Center CRC/TR 96 an approach is pursued focusing on measures to comply with manufacturing accuracy under thermally unstable conditions, without the demand for additional energy [2]. Especially concerning the fluid systems it is necessary to critically review this additional energy demand from an economic and ecological point of view.

2. Overview of the 1st project stage

2.1. The approach and methodology

Regarding a uniform temperature distribution in machine tools, the analysis of thermo-energetic properties and the support in the design of fluid power systems are the main concerns of this project. Due to the increased complexity of fluid power systems its optimization provides a comprehensive working area. Especially with the focus on an optimal thermal performance with a minimal power supply, existing simulation models are not adequate for a scientifically based design. For this purpose the research activities are aimed at the development of principles and simulation models with a holistic approach.

Therefore, the approach was divided into four subdomains. In the first two steps extensive experimental investigations were carried out at the overall tooling machine and selected components. These studies formed the basis for receiving information on characteristic variables and parameters for modeling. Subsequently, extensive numerical simulations (CFD) were performed in the third step. These simulations help making the thermo-energetic exchange processes visible in a high temporal and spatial resolution. Beside experimental data they represent an additional basis for comparison and significantly support the modelling process by deriving structures and parameters, as well. In the last step abstract network-based component models (1D) were developed. In contrast to numerical 3D models they allow a faster computation at the same or even lower capacity. For this reason, 1D network-based models are well suited for the description of complex systems, e. g. the fluid cooling system.

2.2. Selected results of the 1st project stage

2.2.1. Machine analysis of a milling center

In **Figure 1** the investigated main fluid systems of the demonstrator DBF 630 with its key components are depicted. All in all, four systems were analyzed in detail: The cooling circuit, the cooling lubricant system, the lubrication circuit and the hydraulic system. The cooling circuit has a fixed displacement pump (20) and a heat exchanger (22) that cools the heated fluid down to a set temperature. The main components needed to be cooled are the electrical cabinet (6), the rotary table (4) and the main drive (7). The cooling of the electrical cabinet is realized by an air-water heat exchanger (21) and that of the rotary table (4) and the main drive (7) directly by a water/Antifrogen® N mixture that flows through implemented cooling channels. For detailed information on the other fluid power systems refer to /3,4/.

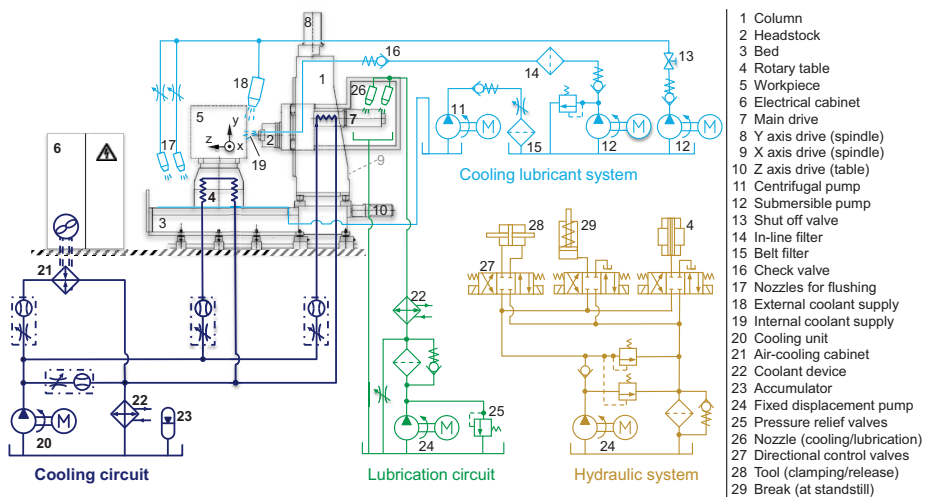


Figure 1: Main fluid systems of the demonstrator DBF 630, adapted from /3,4/.

Figure 2 shows the measured energy demand in the no-load test cycle. The largest amount with approximately 45 % is required to drive the axes. In total, the fluid power systems require 44 %. It remains a residue of 11 %. This energy demand is needed for the auxiliary equipment, such as lighting, CNC control and control circuit or pneumatic subsystems. With a closer look on the fluid systems it becomes obvious that the cooling lubricant system has the highest energy demand of about 16 %. The energy demand within the lubrication system as well as the cooling system is nearly at the same level with approximately 12 % and the smallest share of about 4 % is needed for the hydraulic system.

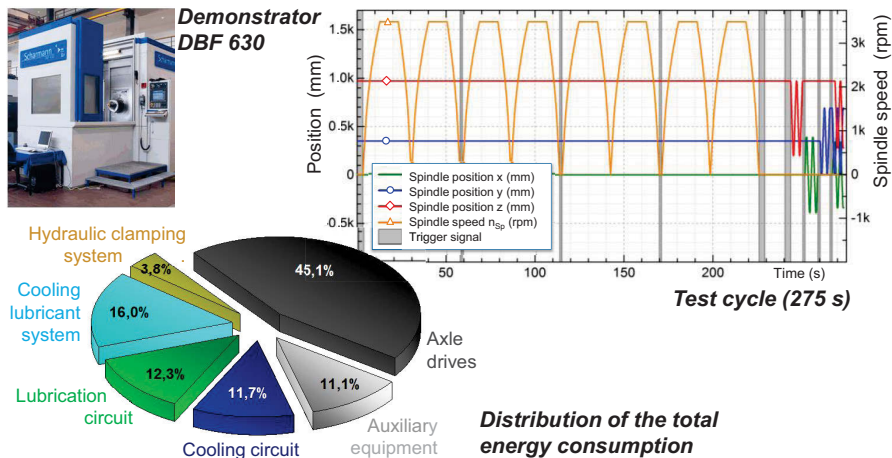


Figure 2: Power consumption of the demonstrator in no-load test cycle

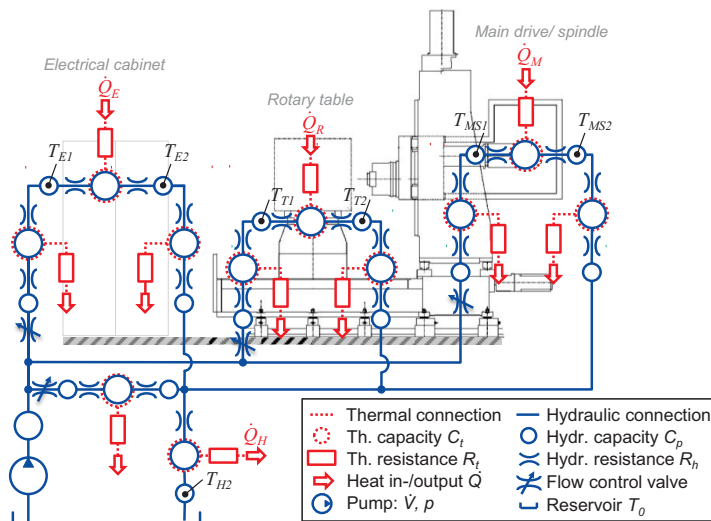


Figure 3: Network-based simulation model of the cooling circuit, adapted from [5].

Furthermore the applicability of existing modelling tools (like SimulationX) was examined for the description of the cooling circuit system, as can be seen from **Figure 3**. The model structure is basically set up in alternating arrangement, because of the correlation between the input and output variables of nodes and elements. The potentials required for the computation are transported by thermal or hydraulic connections between the individual blocks. For a detailed mathematical description of the utilized elements refer to [5,6,7]. **Figure 4** shows exemplarily a comparison between the measured and simulated values of the inlet and outlet temperatures as well as the heat flows at the key components. It is seen that the real system behavior can be predicted with slight

deviations. The reasons for the slight deviations concerning the heat flows need to be clarified by further measurements and a larger data base.

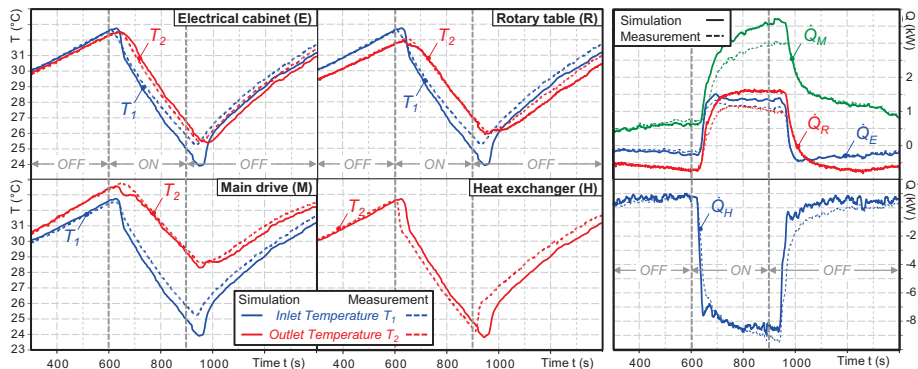


Figure 4: Comparison of measured and simulated temperatures and heat fluxes at the key components of the cooling circuit, adapted from /5/.

2.2.2. Component analysis regarding the spindles cooling system

Especially in the sector of high-speed machining the spindle is directly driven by a built-in motor that is actively cooled via the stator cooling sleeve. The sleeve itself is made of a highly thermally conductive material (e.g. brass), and comprise rib structures at the outer radius improving the heat transfer into the fluid. In order to examine the thermo-energetic characteristics and to validate the network-based and numerical CFD simulation models a test stand was developed, depicted in **Figure 5** and explained in detail in /4,6,7/. The modular design of the test stand permits a simple replacement of the cooling sleeve to examine different flow geometries in detail.

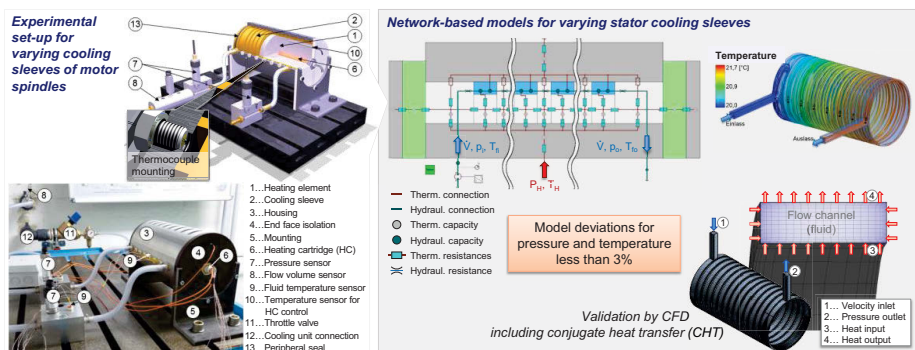


Figure 5: Experimental and simulative component analysis of the motor spindles cooling sleeve.

3. Outlook and planned work in the 2nd project phase

3.1. The approach

The shown works are an important prerequisite for the second phase of the project (see **Figure 6**). Concerning a comprehensive thermo-energetic analysis of fluidic tempering systems in machine tools the methods of network-based simulation are extended and optimized regarding manageability and robustness with respect to parameter variations. For this purpose detailed studies on various complex integration objects are carried out. This allows the analysis of the interaction of different methodological approaches on a more complex level. The aim is to provide design recommendations for thermo-energetic efficient components and an advantageous system structure.

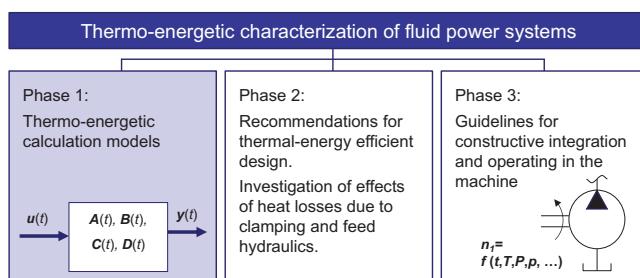


Figure 6: Approach of subproject A04 in the 2nd project phase

Regarding functional and design aspects fluid power systems interact with a variety of tooling machine components. Therefore, they are an important control element for the thermo-energetic behavior within the complex machine structure. To ensure a thermo-energetic efficient system operation the 3rd stage aims at the formulation of guidelines for an intelligent, demand-oriented control logic of the new systems as well as the structural integration into the overall machine. Here, the inclusion of technological and accuracy-related requirements plays an essential role. The work contents of the 2nd phase are an important milestone in this direction. Based on the integration object “motor spindle” the interaction of the developed fluidic model descriptions with the approaches of other projects regarding structural or controlling aspects is analyzed. Compared to the previously used test rig “stator cooling sleeve” the increased complexity of the integration object “motor spindle” supports the validation of the universality of the developed network models.

3.2. Methodology and work contents

The methodology is based on an experimental analysis of fluid power components and systems within selected integration objects and demonstrator machines. On this basis,

the developed computational models for the simplified experimental setup of the 1st project phase will be developed further with a higher degree of complexity for real components. In order to optimize the components and systems regarding their structure and mode of operation first, important parameters must be identified by means of sensitivity analyses. The numerical CFD and network-based models serve as a basis for an automated sensitivity analysis and optimization. Especially for complex system structures the network-based models provide benefits. They allow comprehensive parametric studies without extensive measurements.

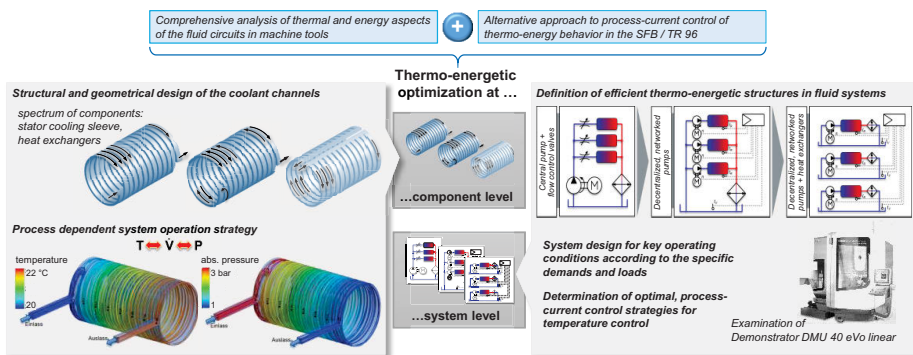


Figure 7: The approach of the subproject A04 „Thermal fluid engineering” in the second stage of the project

3.2.1. Derivation of simulation and experimental strategies

Both at system and component level extensive experimental work provide the basis for modeling. For the parameterization and further development of simulation models important geometrical and thermal (e.g. material) parameters are derived from data sheets and design documentation. The investigation range comprises spindle and motor cooling (integration object “motor spindle”) and further important systems resulting from the investigation of the demonstrator machine (DMG DMU 40 eVo linear). Furthermore, typical operating cycles, major thermal and fluid power measurands as well as the required model scope have to be specified in coordination with other subprojects of the CRC/TR 96.

3.2.2. Experimental analysis of component and system structures

Experimental investigations are performed on selected fluid power components and systems. In contrast to the simplified test rig design of stage 1 the behavior can hereby be analyzed under real operating conditions. Thus, additional influences such as e. g. the heat input resulting from friction in the bearing are included in the considerations, even with fluctuating operating conditions. The evaluation provides statements on the

thermal properties (e. g. temperature level, heat conduction, convective heat transfer wall/fluid). Moreover, information on the fluidic potential and flow variables can be extracted. These enable the identification of flow resistances and losses that are responsible for the heat generation within the fluid power systems. Since in tempering systems drive powers are usually completely converted into heat they are recorded additionally. Finally, the parameters that are necessary for the depiction of the actual components and systems behavior within the simulation model, will be extracted from these measurements. They form the basis for the subsequent sensitivity analysis and optimization.

3.2.3. Simulation-based component analysis and optimization

With the help of the previously determined thermal and fluidic parameters of the design and measured data the cooling circuits of complex, real components are simulated by numerical and network-based models. Therefore, the model structures developed in the 1st project phase serve as a basis. The cross-checking with the experiments at the integration object and the demonstrator machine supports the verification of the developed model descriptions. Subsequently, the components are optimized concerning their structure, design and operational parameters. For this purpose, a sensitivity analysis is carried out with the help of the developed numerical and network models. This step is useful for the identification of relevant design parameters for the subsequent optimization process. Its aim is an improved thermo-energetic behavior, matched to the component-specific demand for temperature control. Here, potentials exist concerning the channel geometry and structure (e. g. channel cross section, pitch, number of helices in cooling sleeves) as well as the adjustment of the operating parameters (e. g. load-dependent flow control).

3.2.4. Simulation-based system analysis and optimization

The focus of this work package is the analysis and further development of entire fluid power system structures. Like previous investigations showed, sufficient cooling capacity is available in machine tools. However, the cooling is insufficiently adjusted to the process and component dependent heat input into the machine that varies in time and place. Thus, the thermo-elastic deformation of the machine can only be reduced insufficiently. To overcome these deficits, two different strategies are examined and evaluated on the basis of the cooling system of a machine tool: On the one hand a decentralization towards autonomous systems (see **Figure 8**) allows a demand-oriented, component specific supply and temperature control. Accordingly, the adjustment of the operating parameters and their control strategy with respect to the

components requirements are included in the considerations. On the other hand the centralization of supply units (e. g. the usage of the hydraulic unit for a parallel pressure build-up in the coolant-lubricant system) promises potential for minimizing the energy consumption and consequently reducing the introduced heat losses into the machine structure.

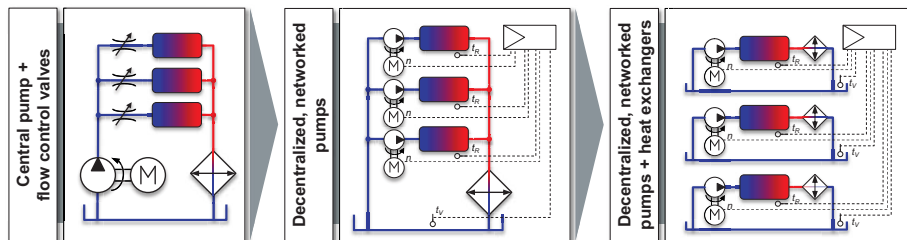


Figure 8: Decentralizing levels of the system structure

3.2.5. Model preparation and data transfer for correction methods

For the analysis of the interaction with the calculation models of other subprojects the fluidic ones are integrated into the overall models of the integration objects. First, this requires a transfer of the simulation models into software independent calculation equations. Furthermore, in this way the models suitability for precise thermo-energetic prediction based on a real system can be validated, which is essential for the use of correction methods.

4. Summary

The aim of the paper is to give a short presentation of the done and planned investigations in the Collaborative Research Centre CRC/TR 96, especially in the sub-project A04 "Thermal fluid engineering". During the 1st phase of the project

- the thermo-energetic balance of selected tooling machines was investigated experimentally and
- particularly relevant subsystems have been identified, for example the cooling circuit and the motor spindle.

Concerning the description of the components

- with the help of numerical CFD simulations and
- experimental studies of individual components
- network-based models have been developed that can predict their thermo-energetic behavior with deviations less than 3 %.

In the subsequent phase of the project, these models are used to optimize the heat transfer and fluid system structures as well as to develop process and demand-oriented control strategies. On the one hand a precise prediction of the thermo-energetic behavior of fluid power components and systems is crucial for the correction of thermo-elastic deformations of the tooling machine. And on the other hand temperature distribution within the tooling machine can be homogenized by means of optimized structures and control strategies. Therefore, thermo-elastic deformations can be compensated in advance.

5. References

- /1/ Kinkel, S.; Lay, G.: Technologietrends in der Produktion. Praxis der Anlagenmodernisierung in der deutschen Metall- und Elektroindustrie. Mitteilungen aus der Produktionsinnovationserhebung 39, 2006.
- /2/ Großmann, K.; Gritt, O.: Introduction. Thermo-energetic Design of Machine Tools. Heidelberg: Springer Berlin Heidelberg, 2014, S. 1-11.
- /3/ Weber, J.; Weber, J.: Thermo-Energetic Analysis of the Fluidic Cooling Systems in Tooling Machines. 9th International Fluid Power Conference, Aachen, 2014.
- /4/ Weber, J.; Weber, J.: Thermo-energetic Modelling of Fluid Power Systems. Thermo-energetic Design of Machine Tools. Heidelberg: Springer Berlin Heidelberg, 2014, S. 49-60.
- /5/ Pursian S. Thermo-energetische Modellierung der Fluidsysteme eines Bearbeitungszentrums. Diploma thesis, TU Dresden; 2015.
- /6/ Weber, J.; Weber, J.: Thermo-energetic analysis and simulation of the fluidic cooling system of motorized high-speed spindles. The 13th Scandinavian International Conference on Fluid Power SICFP'13, Linköping Schweden, 2013.
- /7/ Weber, J.; Weber, J.: Analyse und Simulation der fluidischen Kühlung einer einfach gewendelten Motorspindelkühlhülse. O+P Journal 3/2013, S. 4-15.

6. Nomenclature

n_{Sp}	Spindle speed	rpm
\dot{Q}	Heat flow	k
T	Temperature	°C

t	Time	s
x, y, z	Position	mm

7. Acknowledgements

The presented research activities are part of the Collaborative Research Centre CRC/TR 96 sub-project A04 “Thermo-energetic description of fluid systems”. The authors would like to thank the German Research Foundation DFG for their financial support.

Supported by:



Comparison of Heat-Properties and its Implications between Standard-Oil and Bio-Oil

Marcel Rückert

RWTH Aachen University, Institute for Fluid Power Drives and Controls (IFAS), Aachen, Germany, E-mail: marcel.rueckert@ifas.rwth-aachen.de

Dr.-Ing. Katharina Schmitz

Walter Hunger International GmbH, Alfred-Nobel-Str. 26, 97080 Würzburg, Germany, E-mail: K.Schmitz@hunger-international.de

Professor Dr.-Ing. Hubertus Murrenhoff

RWTH Aachen University, Institute for Fluid Power Drives and Controls (IFAS), Aachen, Germany, E-mail: post@ifas.rwth-aachen.de

Abstract

An important criteria for optimising hydraulic systems is their size. Especially for tanks and heat exchangers oil parameters as heat capacity and thermal conductivity have a big influence on the size. Additionally, various oils differ in their parameters. Accordingly, the heat capacity and thermal conductivity need to be known. However, little research has been done. Data-sheets usually do not provide any thermal data.

In this paper, the thermal conductivity is measured for varying types of hydraulic oils. The thermal conductivity is determined by a newly designed test-rig measuring the radial temperature difference in a tube at a quasi-static state using a constant heat flux. Thus, an overview over the thermal conductivity of different oils is achieved. Based on the results, a comparison between different types of fluid is made.

KEYWORDS: Bio-Oil, Thermal Conductivity, Mineral-Oil, Thermal Properties

1. Introduction

Thermodynamic measuring is strongly dependent on the data available. Witt proposed a model in order to describe thermal effects on viscosity and density of different oils using model equations, /1/. Additionally, he derived a model to describe the hydraulic efficiency using thermodynamic measurements. One of the properties which hasn't been subject of research is the thermal conductivity.

An investigation of the efficiency of an external gear pump as a function of the temperature has been discussed by Lana et al. in [2]. Within this study, a thermodynamic model has been derived and assessed under the experimental and simulative point of view. Additionally, the pump structure has been artificially worn and the influence of the wear on efficiency has been investigated. In the proposed model by, the thermal conductivity is necessary in order to calculate the hydraulic efficiency.

Assuming an incompressible flow, the first law of thermodynamics for a pump can be written as in (1), where ΔT is the difference between the up- and downstream temperature. On the right hand side, β is the coefficient of thermal expansion and v is the specific volume of the fluid. Finally, P and \dot{Q} describe the input shaft power and the heat flux through the pump housing respectively. The latter is given in (2), which is the heat transfer through the surfaces of the pump housing to the surrounding. In order to compute such heat flux, (2) utilises the difference between the average fluid temperature \bar{T} and the surrounding temperature T_s , the heat transfer coefficient h_s and the net exchange surface A_s .

$$\Delta T = \frac{\dot{Q} - P}{\rho Q \bar{c}_p} - \frac{(1 - \beta \bar{T}) \bar{v} \Delta p}{\bar{c}_p} \quad (1)$$

$$\dot{Q} = \bar{h}_e A_s (\bar{T} - T_u) \quad (2)$$

Both equations (1) and (2) are defined for a steady state of the system. For this reason, a homogeneous and isotropic temperature is assumed in. **Figure 1** shows the comparison between the theoretical results and the experimental ones for an external gear pump at a rotational speed of 1750 1/min.

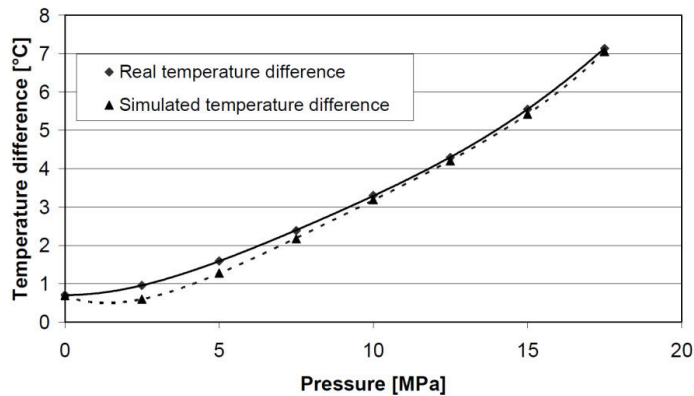


Figure 1: Measured and simulated temperature difference of the in- and outlet of an external gear pump [2]

Next to practical applications, multi-dimensional system simulations also require accurate data, especially when considering CFD simulations. The modelling of the fluid requires detailed information on the thermal properties in order to make precise predictions. Unfortunately, modelling the thermal properties of the fluid is a difficult task, because of lack of data. Especially the thermal conductivity is a parameter that can influence simulation results.

2. Introduction into Thermal Conductivity

In order to calculate the heat flux in (2), it is necessary to possess data regarding the thermal conductivity of the oil used.

The heat flux describes the transport of thermal energy by atomic and molecular interactions. Assuming a body to be homogeneous and isotropic, a temperature difference within the body leads to a heat flux which is independent from other effects. By normalising the heat flux in respect to the cross section area the heat flux density can be defined. According to Fourier there is a proportional relationship between heat flux density and temperature gradient, see (3) and /3/.

$$q'' = -\lambda \cdot \text{grad } T \quad (3)$$

The factor for the proportional relationship between the heat flux density and the temperature gradient is called thermal conductivity λ . The thermal conductivity of oils at 20 °C is shown in **Table 1**.

Oil	HLP46	HETG
λ	0.14	0.17

Table 1: Literature Data for HLP and HETG at 20 °C /4/

For a one-dimensional case the heat flux depends on the distance between two points, the temperature difference across it and the thermal conductivity of the material in between. In **Figure 2** The area normalised heat flux or heat flux density \dot{q}'' enters at the first test point and exits at the second test point in a distance δ . This leads to a temperature difference between the first test point temperature T_i and the second test point temperature T_a . By using equation (4), the heat flux density, the temperature difference and the distance define the thermal conductivity. This one-dimensional case is valid for two large but thin plates touching each other. When heating one of them, the other gets warmer too. Additionally, the effects on the edges of the plates are negligible.



Figure 2: Thermal Conductivity in 1D

$$\dot{q}'' = \lambda \cdot \frac{T_i - T_a}{\delta} \quad (4)$$

An example for a two-dimensional case is a long but thin pipe with a centric heat source. Here the distance between two measurement points is in radial direction. Due to the changing cross section for the heat flux with changing radius, the temperature profile is not linear any more. Instead it has a logarithmic shape, according to (5) and deduced in /5/. A sketch for a two-dimensional case is shown in **Figure 3**. The two-dimensional approach assumes that effects at the end of the pipe can be neglected.

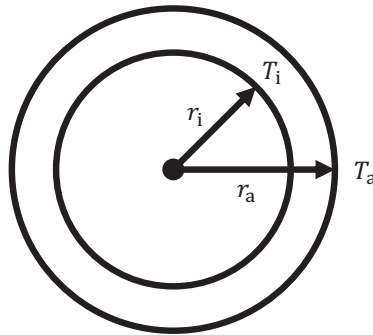


Figure 3: Thermal Conductivity in 2D

$$\dot{q}'' = \lambda \cdot \frac{T_i - T_a}{\ln\left(\frac{r_a}{r_i}\right)} \quad (5)$$

When considering the heat transfer within fluids two effects occur. First the thermal conductivity as explained above leads to a heat transfer. However, due to the motion of the fluid convection might lead to further heat transfer. The separation of both effects is difficult in measurement. Thus the Rayleigh number Ra is used to estimate the extent of the convection. It is defined by Grashof number Gr and Prandtl number Pr , see (6), and describes the relationship between lifting forces and viscosity forces for a temperature difference applied. In case of the Rayleigh number $Ra \ll 1000$ the convection can be neglected. This is valid for the test rig explained later for temperatures below 500 K, compare with /5/.

$$Ra = Gr \cdot Pr \quad (6)$$

Another heat transport mechanism is thermal radiation. Because of the low thermal conductivity of oil and the resulting low temperature differences, radiation can be neglected for the planned test rig.

3. Thermal Conductivity Test Rig

The principal idea of the thermal conductivity test rig is to create a closed volume that can be compressed in order to adjust the pressure to a desired level. Additionally, a defined heat flow can be introduced and the radial temperature difference can be measured at various positions. The measurement principle can be seen in **Figure 4**. Temperature sensors are located at varying radial distances around a centric heat source. Through a heat wire a heat flux \dot{Q} is introduced. With the electric resistance R of the heat wire and the current I , the heat flux can be calculated using (7).

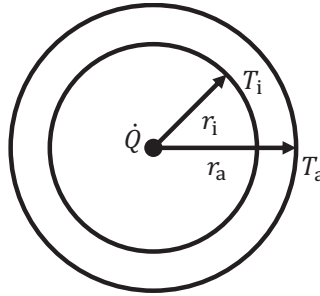


Figure 4: Radial Heat Flow

In order to derive the thermal conductivity, (8) can be expanded by the length of the wire L . After solving for λ , (9) shows the final equation to calculate the thermal conductivity for the test rig.

$$\dot{Q} = U \cdot I = R \cdot I^2 \quad (7)$$

$$\dot{Q} = \lambda L \cdot \frac{\Delta T}{\ln\left(\frac{r_a}{r_i}\right)} \quad (8)$$

$$\lambda = \frac{\dot{Q}}{L} \cdot \frac{\ln\left(\frac{r_a}{r_i}\right)}{\Delta T} = \frac{R \cdot I^2}{L} \cdot \frac{\ln\left(\frac{r_a}{r_i}\right)}{\Delta T} \quad (9)$$

Figure 5 shows a sectional view of the conceptual design of the test rig. The housing consists of a steel pipe and an end cap. The end cap (left) can be moved to adjust the volume. By torquing tie rods the volume and thus various pressures can be applied.

Four sensors are used. The first one is the pressure sensor, the other three are temperature sensors. Their measuring heads are positioned in different distances to the sensors landing, while the sensors are mounted in a row parallel to the test rig's axis.

Through a thread opposite to the end cap the heating wire is integrated. When applying an electric voltage to the wire current flows heating it. Various voltages and thus powers can be provided by the power-supply unit used. The alignment of the wire is ensured by tightening it with a hook integrated in the end cap. The hook is mounted on a spring providing a tightening force despite different end cap positions. Thus a centric and straight position is achieved for all operation points.

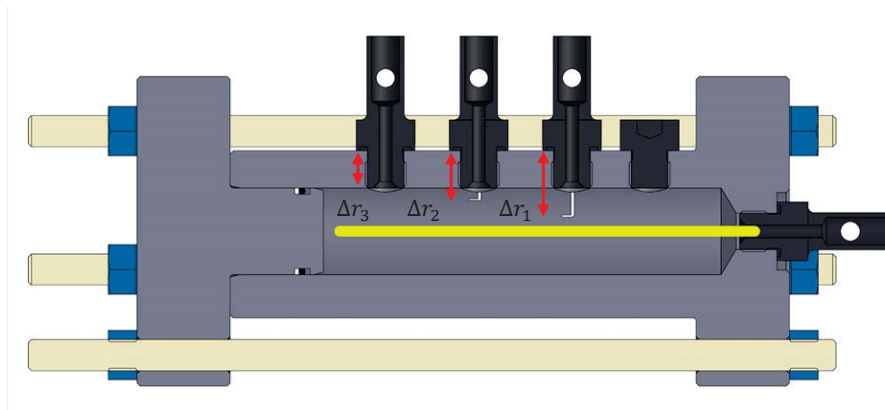


Figure 5: Conceptual Design of the Test Rig

For measurement the wire is heated with the power-supply unit. A defined power is provided. This electric power is converted into heat leading to a heat flow and thus a radial temperature gradient in the oil. Due to the different radial positions of the temperature sensors, this temperature gradient can be measured, see **Figure 6** showing the schematics of the test rig.

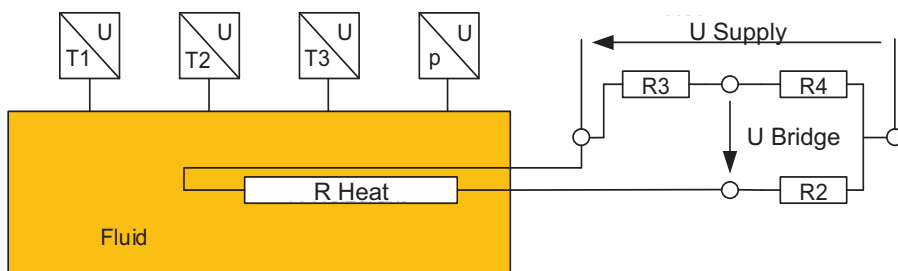


Figure 6: Schematic of the Wheatstone bridge used

The electric power provided to the oil can be calculated from the current and the heating wire resistance. While the current is known from the power-supply unit, the heating wire resistance is unknown and might even change with temperature. However, by using the Wheatstone bridge circuit the heating wire resistance can be deduced with help of three defined and temperature independent resistances. Two resistances in series are placed in parallel to a second set of resistances in series. One of these four resistances is the unknown one. By applying a voltage to the circuit a bridge voltage results from between the serial resistances of one set to the other. Now the unknown resistances can be calculated with (10) and (11). For this the resistances R_1 to R_3 need to be known. Additionally, these reference resistances need to be temperature independent. Otherwise the accuracy of the resistance calculation would be limited. **Figure 7** shows the final test rig setup.

$$U_{Bridge} = U_{Supply} \left(\frac{R_{Heat}}{R_{Heat} + R_2} - \frac{R_3}{R_3 + R_4} \right) \quad (10)$$

$$R_{Heat} = R_2 \frac{\left(\frac{U_{Bridge}}{U_{Supply}} + \frac{R_3}{R_3 + R_4} \right)}{1 - \left(\frac{U_{Bridge}}{U_{Supply}} + \frac{R_3}{R_3 + R_4} \right)} \quad (11)$$

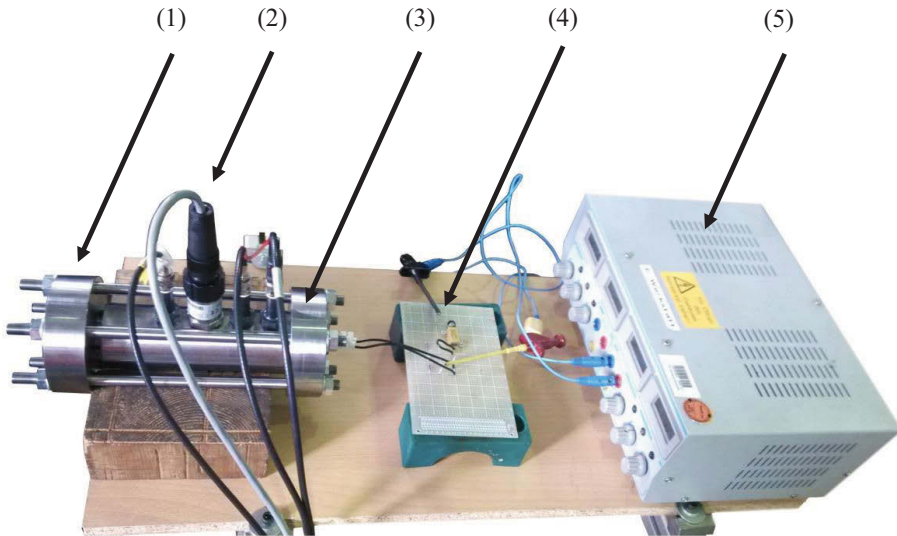


Figure 7: Test rig setup: (1) Lid with spring hook, (2) Sensors, (3) Measuring tube, (4) Wheatstone bridge with heat wire attached, (5) Power supply

4. Calibration of Temperature Sensors

The temperature measurements are conducted using pt1000 sensors. In order to calibrate the sensor, several cooling cycles were run and the electrical resistance was measured with $1/16 \, \Omega$ accuracy. The cycles were run using a oil reservoir on a laboratory hotplate with integrated stirrer to induce a homogenous temperature distribution in the fluid. Additionally the temperature was measured using a calibration thermometer. The results over all the cycles were evaluated and put into a table which translates the resistance into a temperature. Based on the acquired data, this allows to translate a difference of electrical resistance into a temperature difference.

5. Results

To disregard convectional influences, the Rayleigh number is calculated using literature data for HLP46 at $20 \, ^\circ\text{C}$. The result shows a Rayleigh number of 214.65, due to $Gr = 1362.03$ and $Pr = 0.1576$. Therefore, the convectional influences on the measurements can be neglected. Additionally, all the measurements were performed at a pressure level of 1 bar.

In order to measure the thermal conductivity of different oils, a calibration measurement was conducted. The calibration fluid was pure water with an electrical conductivity of less than $1 \, \mu\text{S}/\text{cm}$. The measurements were conducted at 20°C . **Table 2** shows the results compared with literature values. The different λ_i -values show the different combinations of temperature sensors used. The maximum deviation is 21.1 %. However, the deviation is in a tight band.

Fluid	H_2O lit.	H_2O	Deviation [%]
λ_1	0.597	0.493	17.42
λ_2	0.597	0.500	16.24
λ_3	0.597	0.471	21.1

Table 2: Calibration Measurement for H_2O

Figure 8 shows the difference between every combination of sensors regarding their electrical resistance over time. $\Delta R_{i,j}$ represents the difference between sensor i and j . The graph shows that an almost constant state is reached during the measurement. This state stays almost constant over 400 s. Therefore a quasi-static state is achieved with constant temperature differences over each sensor.

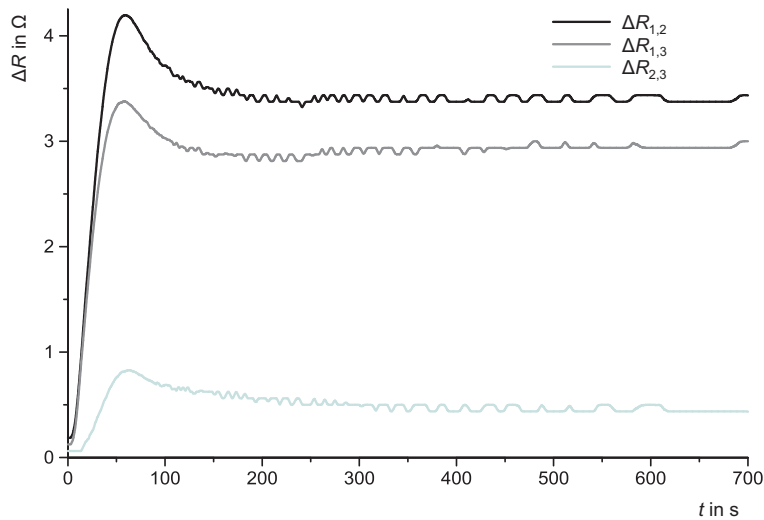


Figure 8: Difference of Resistances in a quasi-static state for HLP46

Table 3 shows the measurement results for three different oils. The focus lies on the measurement of oils with the same viscosity index. Therefore, a viscosity index of 46 was chosen, because it represents a common class for many hydraulic applications. The measurements show, that HLP46 and HEES46 have very similar values for the first two temperature differences. Unfortunately, λ_3 produces an offset for HLP and HETG oil. A possible explanation for this occurrence is that λ_3 is calculated from the data of the two sensors closer to the wall. An influence of the wall on the sensors might cause this effect. Further investigations need to be done in order to determine the reason behind this phenomenon.

Oil	HLP46	HEES46	HETG40
λ_1	0.147	0.156	0.179
λ_2	0.161	0.157	0.183
λ_3	0.065	0.165	0.236

Table 3: Measurement Results for different oils

6. Conclusion and Outlook

In this paper, a short introduction into thermodynamic measurements is given. On basis of the first law of thermodynamics, an equation for the heat flux through a fluid is derived. One integral part of this equation is the thermal conductivity of the fluid. Little research has been done in order to determine those values for hydraulic oils. In order to generate a first understanding of the dimensions of the thermal conductivity of oils, a test rig was

designed to measure the thermal conductivity. The calibration of the temperature sensors was done by measuring the electrical resistance of the pt1000 elements used during several cooling processes. This way, the behavior of the sensors between each other was derived and can be used to measure temperature differences. Next, a calibration measurement with pure water was conducted. The maximum deviation was 21%. Additionally, three oils of a similar viscosity index were investigated.

The results show the tendency, that bio oil in general has a higher thermal conductivity than mineral oil. This impacts hydraulic applications as well as system simulations. The knowledge can be used to design smaller hydraulic tanks. If the thermal conductivity of the oil is higher, heat can be transferred out of the fluid faster. This reduces the idle time in a tank and therefore might reduce its size. The same is valid for heat exchangers.

System simulations always depend on accurate data in order to produce reliable results. If a simulation is used in order to design a whole hydraulic system, a good oil model is needed. Thermal properties play a vital role since isothermal conditions are a simplification of the system. Therefore, measuring the thermal conductivity of oil is a step towards a more holistic simulation approach.

In the future, more work has to be done in order to increase the accuracy of the measurements. Especially regarding the heating wire, power supply and temperature sensors. Additionally, investigations on high pressure states can be obtained by compressing the test tube and therefore generating a working pressure up to 400 bars. This can be done for a variety of oils and a database can be gathered.

7. References

- /1/ Witt, K., 1947. "Die Berechnung physikalischer und thermodynamischer Kennwerte von Druckflüssigkeiten, sowie die Bestimmung des Gesamtwirkungsgrades an Pumpen unter Berücksichtigung der Thermodynamik für die Druckflüssigkeit", Dissertation, University of Eindhoven
- /2/ Dalla Lana, E., De Negri, V.J., 2006. "A New Evaluation Method for Hydraulic Gear Pump Efficiency through Temperature Measurements", SAE Commercial Vehicle Journal, Paper Number 06CV-149
- /3/ Grigull, U., Sandner, H., 1990. "Wärmeleitung", 2nd edition, Springer Berlin Heidelberg, Berlin, Heidelberg
- /4/ Murrenhoff, H., 2014. „Fundamentals of Fluid power – Part 1: Hydraulics“, 7th Edition, Shaker, Aachen

/5/ Kneer, R., 2013. "Vorlesungsskript Wärme und Stoffübertragung I/II", Edition WS13/14, RWTH University Aachen

8. Nomenclature

A_s	Heat transfer area	m^2
\bar{c}	Average heat capacity	$\text{kJ}/(\text{kg K})$
Gr	Grashof number	
\bar{h}_e	Average external heat transfer coefficient	$\text{W}/(\text{m}^2 \text{K})$
I	Electric current	A
L	Length	m
P	Power	W
Pr	Prandtl number	
p	Pressure	bar
p_F	Surface pressure	N/mm^2
Q	Volume flow	l/min
\dot{Q}	Heat flow	W
q''	Heat flow density	W/m^2
R	Electric resistance	Ω
Ra	Rayleigh number	
$r_{i/a}$	Radius, i: inner, a: outer	m
\bar{T}	Average temperature	K
T	Temperature	K
U	Electric voltage	V
\bar{v}	Average velocity	m/s

$\bar{\beta}$	Average coefficient of thermal expansion	1/K
δ	Distance	m
Δp	Pressure difference	bar
ΔT	Temperature difference between two points	K
η	Efficiency	
λ	Thermal conductivity	W/(m ² K)

Prediction of the thermo-energetic behaviour of an electrohydraulic compact drive

Dipl.-Ing. Sebastian Michel

Institute of Fluid Power (IFD), Technische Universität Dresden, Helmholtzstrasse 7a,
01069 Dresden, E-mail: michel@ifd.mw.tu-dresden.de

Professor Dr.-Ing. Jürgen Weber

Institute of Fluid Power (IFD), Technische Universität Dresden, Helmholtzstrasse 7a,
01069 Dresden, E-mail: mailbox@ifd.mw.tu-dresden.de

Abstract

Due to good energy-efficiency of electrohydraulic compact drives a cooling aggregate often is not installed. The operating temperature is governed by the complex interaction between dissipative heat input and passive heat output. This paper targets the simulation of the thermo-energetic behaviour of an electrohydraulic compact drive by means of a lumped parameter model in order to predict the operating temperature. The developed thermo-hydraulic model is validated against measurements utilising thermocouples and a thermographic camera to capture temperatures. The results show, that the presented methodology enables a satisfying accurate prediction of the thermo-energetic behaviour of electrohydraulic compact drives. A further analysis of simulation results is given, highlighting the power losses and heat rejection capabilities of different components. Finally, measures for the improvement of the heat rejection capabilities are studied.

KEYWORDS: Electrohydraulic compact drive, EHA, thermo-energetic simulation, heat transfer processes

1. Introduction

Electrohydraulic compact drives are an interesting alternative to conventional hydraulic or electromechanical drives. Owing to the good efficiency a key property of electrohydraulic compact drives is the possibility to design the actuator without a cooling aggregate. The dissipated energy is discharged via passive heat output of heat conduction, natural convection and radiation – so called calm cooling. Correspondingly, the prevailing operating temperature is governed by the complex interaction between operation dependent power losses and passive heat output, as illustrated in **Figure 1**. In order to guarantee a temperature stable process of electrohydraulic compact drives – or vice

versa to know about the possible fields of application – the knowledge of the thermo-energetic properties is essential.

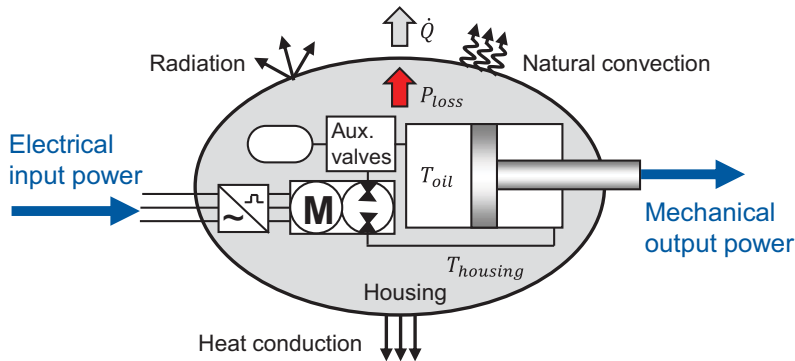


Figure 1: Thermal behaviour of electrohydraulic compact drives /1/

In avoidance of elaborate experiments a lumped parameter simulation is suitable to evaluate the thermo-energetic behaviour of electrohydraulic compact drives. Dynamic and thermo-energetic behaviour with interdependencies as well as dependencies on the operating point can be predicted with reasonable computational effort. The question that has to be answered is, which accuracy in temperature prediction can be achieved and, moreover, is the achieved accuracy satisfying in technical terms. In /1/ an approach was published, how to set up and parameterise a thermo-hydraulic model of an electrohydraulic compact drive demonstrator. First validation results were presented, whereby the accuracy did not match the technical needs yet.

This paper focuses on the prediction of the thermo-energetic behaviour of an electrohydraulic compact drive demonstrator with a thermo-hydraulic model, which was further developed and enables the prediction of operating temperature with sufficient accuracy. Implemented measures to enhance the thermo-hydraulic model are introduced. Additionally, investigation on heat transfer processes on a model shape geometry is presented, which underpins the choice of parameterisation method regarding natural convection. The model is validated against measurements and characteristic results are presented. Apart from thermocouples inside the hydraulic circuit a high-quality thermographic camera is used to provide a detailed capture of outer surface temperatures. Subsequently a further analysis of simulation results is given, highlighting the power losses and heat rejection capabilities of different components. Finally, approaches for the improvement of heat rejection capabilities of the drive are proposed.

2. Electrohydraulic compact drive demonstrator

Before the methodology of thermo-energetic simulation is focused, the electrohydraulic compact drive demonstrator is introduced. A hydraulic scheme and the mechanical design is given in **Figure 2**. Drive's cylinder (1) is controlled by the pump (5), which is driven by a BLDC-motor (6). The differing volume flows of the single rod cylinder are balanced by a hot oil shuttle valve (3), which is connected to a membrane accumulator (4). Adapter- and mounting plates (7, 8) are used to assemble components. The drive is mounted on the cylinder's head side to the test rig (9). More details on the fundamental behaviour of the presented hydraulic circuit can be found in /2/, /3/ and /4/.

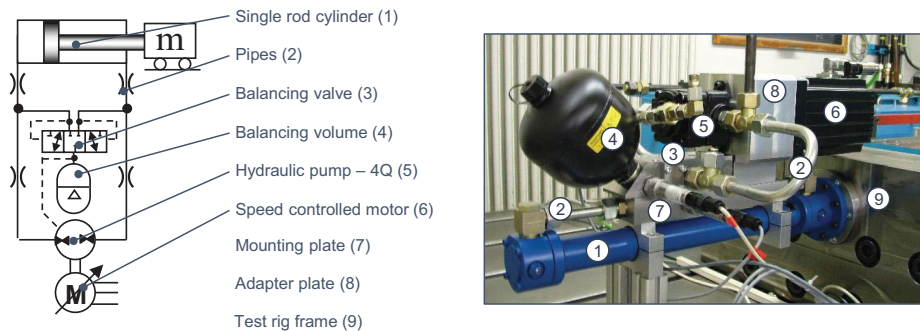


Figure 2: Set-up and design of the electrohydraulic compact drive demonstrator /1/

3. Thermo-energetic modelling of the demonstrator

Thermo-energetic systems simulation with lumped parameters is used in different engineering domains, i.e. in electrical engineering /5/, machine tool engineering /6, 7/ as well as in hydraulic domain /8, 9, 10/. The methodology, which is basically applied, consists of the thermo-energetic analysis and the thermo-energetic modelling and simulation of the system.

The thermo-energetic analysis includes analysis of power losses, which can be regarded as system's heat sources, analysis of heat flows, which represent the paths to the heat sinks and the analysis of thermal resistances located on the way.

Gathered information from thermo-energetic analysis is used to set up and parameterise an energetic and a thermal model that are connected to a dynamic drive model. The resulting thermo-hydraulic model enables the simulation of complex dynamic and thermal processes. In this work, ITI SimulationX®, a commercial multi domain system simulation software, is used as simulation tool.

A detailed description of the thermo-energetic analysis and thermo-energetic modelling of the demonstrator can be found in [1]. In this paper the focus is set on the measures that are taken to further develop the existing thermo-hydraulic model. These are in particular:

- Detailed investigation and implementation of pump efficiency in dependency of operating temperature.
- Basic research on heat transfer at a model shape geometry (cube) regarding natural convection; consequent use of 3D-method to calculate heat transfer number in case of natural convection.
- Refinement of the thermal resistance network.

3.1. Temperature dependent pump efficiency

Main losses in electrohydraulic compact drives are induced by the electric motor and the pump. Subsidiary, friction and flow losses in the cylinder, flow losses in hydraulic piping (including auxiliary valves), accumulator losses as well as frequency converter losses are present. Losses of both motor and pump are dependent on the operating parameters speed and load. Furthermore, in particular pump losses may vary with the operating temperature due to changing fluid viscosity and gap widths [1]. Since temperature dependency was not included in the pump loss model yet, measurements were carried out to quantify temperature influence on efficiency of the used pump. **Figure 3** illustrates the measured pump efficiency in dependency of speed and load at different temperature levels. The results show that with rising temperature the efficiency of the pump decreases especially under high loads, but also increases slightly at higher speeds and small loads.

The complex power loss characteristic of the pump is implemented in form of a 3-dimensional efficiency map $\eta_{Pump} = f(\Delta p, n, \vartheta)$ in simulation – parameterised with the data from measurement. It showed that the implementation of temperature dependent pump efficiency contributes significantly to the enhancement of the accuracy of the thermo-hydraulic model.

Similarly, power losses of the electric motor and friction losses of the cylinder are implemented as 2D-efficiency maps with measured data: $\eta_{Motor} = f(M, n)$, $\eta_{Cylinder} = f(\Delta p, \dot{x})$ respectively. Flow losses are computed by throttle and valve elements.

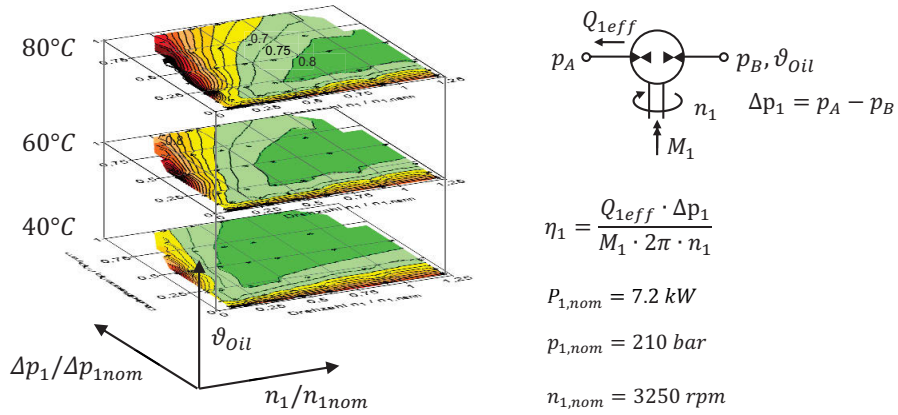


Figure 3: Pump efficiency in dependency of operating temperature

3.2. Calculation of natural convection heat transfer number

The relevant mechanisms on heat transfer on electrohydraulic compact drives are: Enforced convection (inside hydraulic circuit), heat conduction and carriage inside and between solids as well as natural convection and radiation at the free outer surfaces. In case of natural convection the determination of heat transfer numbers is associated with a number of uncertainties. First, the ambient conditions have to be mentioned, which often are not well known. Indoor air flows may influence the heat transfer number in the range of more than 30 % /6/. Second, in literature different approaches exist to calculate natural convection heat transfer problems. Basically the convective heat transfer \dot{Q}_{con} is described by

$$\dot{Q}_{con} = \alpha_{con} \cdot A \cdot \Delta T, \quad (1)$$

with the related area A , the forcing temperature difference ΔT and the heat transfer number

$$\alpha_{con} = Nu \cdot \lambda_{fluid} / L. \quad (2)$$

Here, λ_{fluid} is the heat conductivity of the fluid and L the characteristic length. The Nusselt number Nu , a function of Grashof number Gr and Prandtl number Pr (equation(3)), is calculated for different convection problems by using approaches from relevant tables.

$$Gr = g \cdot L^3 \cdot \beta_{fluid} \cdot \Delta T / \nu^2, Pr = \eta \cdot c_{p,fluid} / \lambda_{fluid} \quad (3)$$

The approaches for calculating Nusselt number either refer to 2D-geometry (horizontal plate, vertical plate), which can be composed to a body, or 3D-geometry as a whole (cube, cylinder and sphere). Both approaches can be found in literature for modelling technical objects, i.e. /6, 7, 9, 10/.

Considering a cube oriented parallel to the ground as simple example, according to /13/ the corresponding approaches for the calculation of Nusselt number are:

$$\begin{array}{ll}
 Nu = 0.766 \cdot [Gr \cdot Pr \cdot f_2(Pr)]^{0.2} & \text{Upper horizontal plate} \\
 Nu = \{0.825 + 0.387 \cdot [Gr \cdot Pr \cdot f_1(Pr)]^{1/6}\}^2 & \text{Vertical plate} \\
 Nu = 0.6 \cdot [Gr \cdot Pr \cdot f_1(Pr)]^{0.2} & \text{Bottom horizontal plate}
 \end{array} \left. \vphantom{\begin{array}{l} \\ \\ \end{array}} \right\} \text{2D} \quad (4)$$

$$\begin{array}{ll}
 Nu = 5,748 + 0,752 \cdot (Gr \cdot Pr / f_4(Pr))^{0,252} & \text{Cube}
 \end{array} \left. \vphantom{\begin{array}{l} \\ \end{array}} \right\} \text{3D} \quad (5)$$

$$f_1(Pr) = [1 + (0.492/Pr)^{9/16}]^{-16/9}, \quad f_2(Pr) = [1 + (0.322/Pr)^{11/20}]^{-20/11}$$

$$f_4(Pr) = [1 + (0.492/Pr)^{9/16}]^{16/9}$$

If one applies the two approaches on a given cube geometry, divergences between the calculated convective heat transfers become apparent. In case of entities, which have a homogeneous temperature distribution, it is reasonable to suppose that a 3D-approach matches the convective behaviour better, since the influence of edges and the geometry as a whole is respected. In order to prove this assumption and to test the applicability of the given approaches, a detailed investigation on a cube model shape geometry was carried out.

The used test set-up is illustrated in **Figure 4**. The model geometry is an aluminium cube, which is mounted freely hanging in a self-contained, windowless room. It can be assumed that except self-induced air flows no other air flows are present in this room. The surface of the cube is covered with chalk spray in order to achieve a defined emissivity ε . As heat source a heating cartridge is installed in the centre of the cube, whose heating power is captured by measuring the electric input power. In steady-state the input heating power equals the rejected heat flow. The surface temperature is captured by a thermographic camera.

The diagram in Figure 4 shows the measured temperature of the cube against the convective heat flow. The convective heat flow \dot{Q}_{con} is determined by subtracting the calculated radiative heat flow \dot{Q}_{rad} from the measured input heating power P_{heat} :

$$\dot{Q}_{con} = P_{heat} - \dot{Q}_{rad} = P_{heat} - \varepsilon \cdot \sigma_S \cdot (T_{surf,meas}^4 - T_{amb,meas}^4) \quad (6)$$

Further the calculated theoretical values according to equation (1) to (5) are depicted as dashed lines. In comparison 3D-method fits better the measured values as 2D-method. The average deviation in terms of heat rejection capability is 3.8 %, in contrast to 12.6 % for the 2D-method. Thus, 3D-approach is used consequently for the calculation and parameterisation of natural convection heat transfer processes in the simulation. If the proportion of dimensions is far from one, a decomposition of geometry is done.

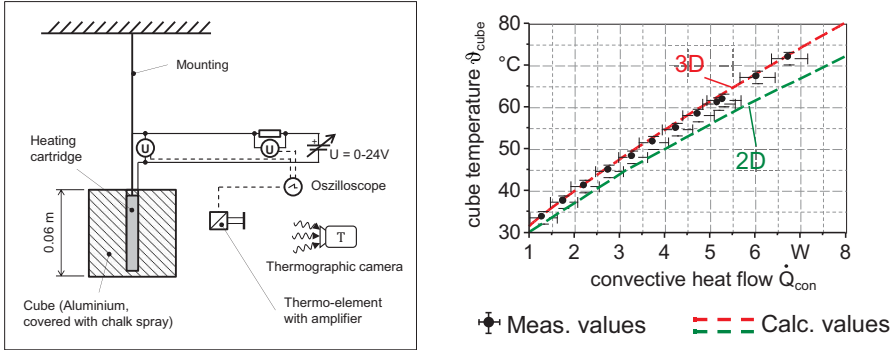


Figure 4: Investigation of natural convection heat transfer processes on a cube

Furthermore, the cube can be used as a reference object to determine ambient conditions, since the heat rejection is well known for ideal, uninfluenced conditions through the investigation. Placing the heated cube next to the compact drive during validation measurements, the test set-up provides information on the influence of occurring indoor airflows and, consequently, strengthens the validation of the model.

3.3. Thermal resistance network

Figure 5 depicts the scheme of the demonstrator's thermal resistance network. With respect to the inclusion of secondary matter components in addition to the main components as well as the consequent use of 3D-method for natural convection processes it is discretised in seven fluidic control volumes A to G and eighteen solid control volumes 1 to 18. The latter represent the housing of the components and the solid construction elements. The heat capacities, which are assigned to each control volume, are connected via thermal resistances to one another, the ambience and the test rig. The thermal resistances R_{th} are determined by the heat transfer number α and the corresponding area A corresponding to the relation

$$R_{th} = 1/(\alpha \cdot A). \quad (7)$$

They consist of enforced convection at the boundaries of the hydraulic system, heat conduction and carriage in the housing and between the demonstrator and the test rig as well as free convection and radiation on the free outer surfaces. The calculation of the heat transfer numbers is done by means of approaches from relevant tables and publications [6, 12, 13]. The losses of the components are inscribed at the control volumes, where they are transferred into the system. Not illustrated in the scheme are the flow losses of the piping.

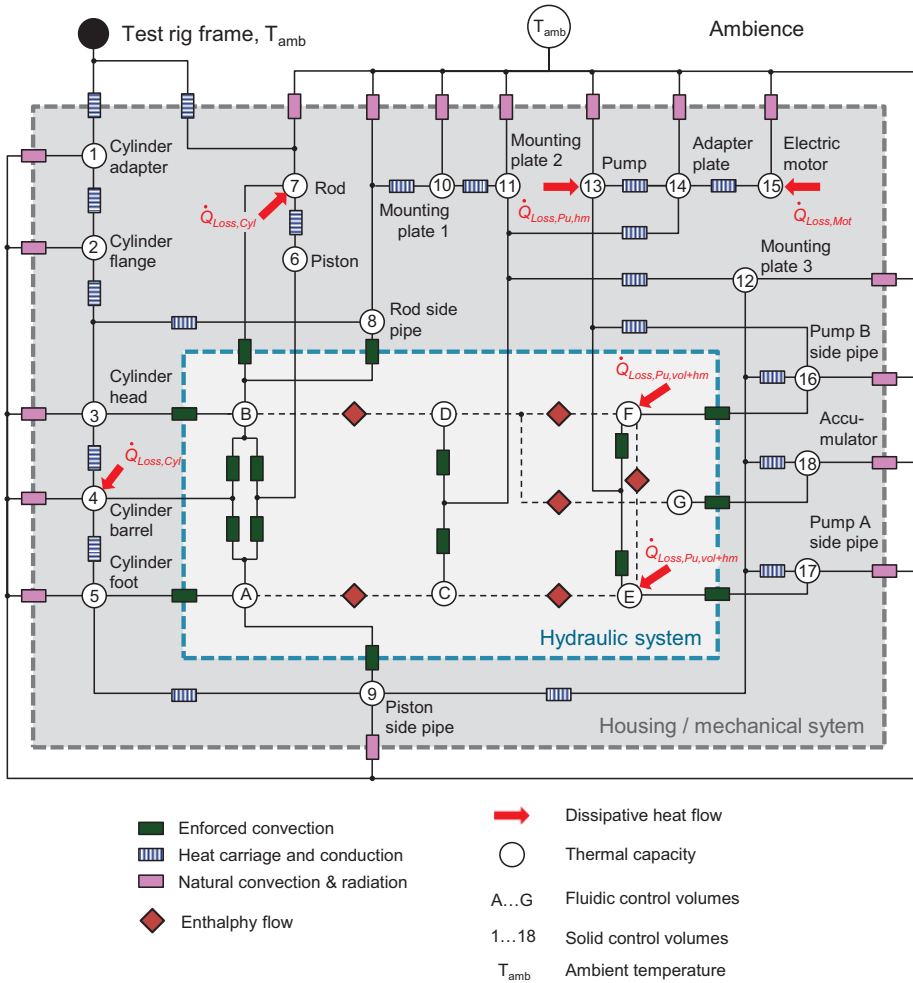


Figure 5: Thermal resistance network of the demonstrator

Basis for the calculation of system's temperatures is the first law of thermodynamics

$$\frac{dE}{dt} = \sum_i \dot{Q}_i(t) + \sum_j P_j(t) + \sum_k \dot{m}_k \left[h + \frac{c^2}{2} + gz \right]_k, \quad (8)$$

which has to be satisfied for each control volume, whereby kinetic and potential energy can be neglected.

4. Test rig and duty cycle

For the validation of the thermo-hydraulic model of the demonstrator the test rig set-up according to **Figure 6** was used. The demonstrator is connected to a moveable mass, on which a desired load force can be applied by means of an electrohydraulic load simulator. Apart from power related quantities the temperature at relevant locations in the system is measured. The oil and the ambient temperature is captured by thermocouples, the outer surface temperatures by a high quality thermographic camera. The thermographic camera provides a detailed capture of outer surface temperatures and enables a validation of surface temperatures in a greater depth.

Additionally, the in chapter 3.2 investigated cube is placed next to the demonstrator. The surface temperature of the heated cube is captured by the thermographic camera as well. The deviation to the thermal behaviour under ideal conditions is a measure for the indoor airflows occurring during the experiment. On the basis of the measured data an averaged correction factor for the convective heat flow is derived, which has the value of 1.16 between the prevailing and the uninfluenced convective heat flow. The correction factor is implemented in simulation and strengthens the validation of the model.

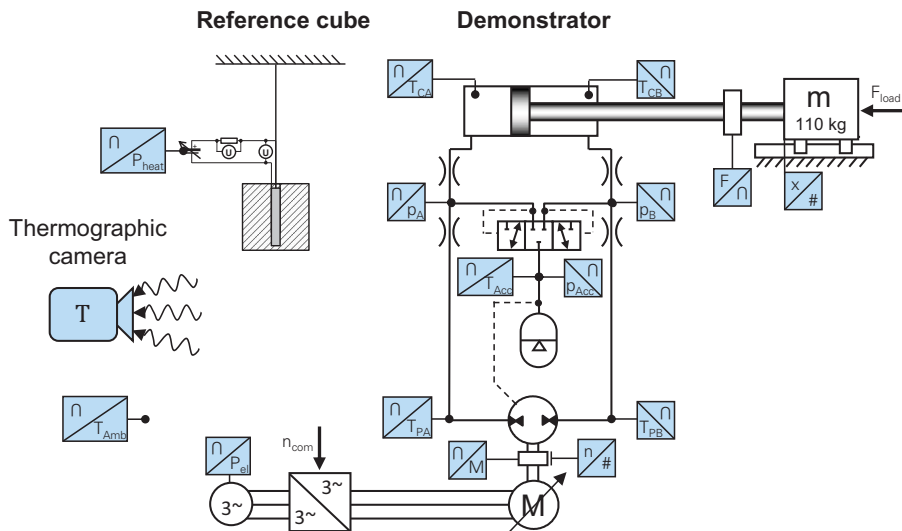


Figure 6: Test rig set-up

As duty cycle, the drive executed a harmonic oscillation of position x with a frequency of $f = 0.4 \text{ Hz}$ and an amplitude of $\hat{x} = 120 \text{ mm}$. The applied load force was set constantly to $F_{load} = 5 \text{ kN}$.

5. Results

5.1. Model validation

Looking at the balance of power a good congruence between simulation and measurement can be stated. The amount of electric energy consumed by the drive executing the prescribed duty cycle differs only to a small extent (about one percent). The simulated and measured oil and surface steady-state temperatures are illustrated in **Figure 7**. It shows that simulated temperatures match measured ones closely with a slight overestimation of oil temperatures. The maximum oil temperature in the system differs 4.4 % between measurement and simulation. Particularly noticeable is the overestimation of oil temperature on the rod side of the cylinder, where the deviation is 15 %. The solid material at the same place (cylinder head) shows the opposite behaviour. This suggests that in the experiment a larger amount of heat is transferred into this component and subsequently to the ambience.

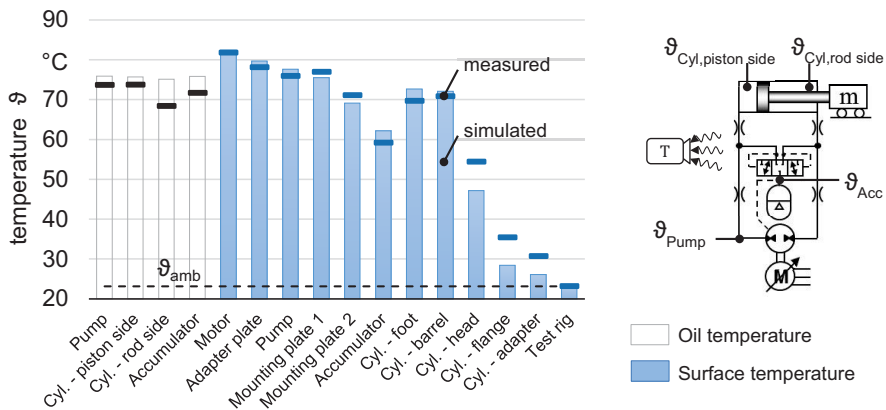


Figure 7: Simulated and measured steady-state temperatures

Even though the thermo-hydraulic model was further developed, various uncertainties in describing thermal and loss behaviour remain. Uncertainties in the parameters, which are necessary to describe the heat carriage between connected surfaces or the reduction to simple model geometries are mentioned exemplarily. Moreover dynamic losses are not taken into account, since steady-state efficiency maps are used to model the loss behaviour of motor, pump and cylinder. In terms of validation the measurement accuracy

of temperature capture has to be mentioned, which is given with ± 1.5 K for the thermographic camera and ± 0.5 K for the thermocouples.

Nevertheless, even though the simulated temperatures do not perfectly match the measured ones, simulation predicts the thermo-energetic behaviour with satisfying precision in order to support development, optimisation and examination of possible fields of application of electrohydraulic compact drives.

Furthermore, the thermo-hydraulic model can be used to analyse drive's thermal behaviour in depth. The left diagram in **Figure 8** shows the power losses and heat rejection distribution among the components. Clearly, pump and motor are the main heat sources, while the most heat rejecting components are the cylinder and the motor. The right handed diagram illustrates the dominant heat transfer mechanisms. With a total heat rejection of approximately $\dot{Q} = 500$ W most heat is transferred by natural convection, followed by radiation and conduction.

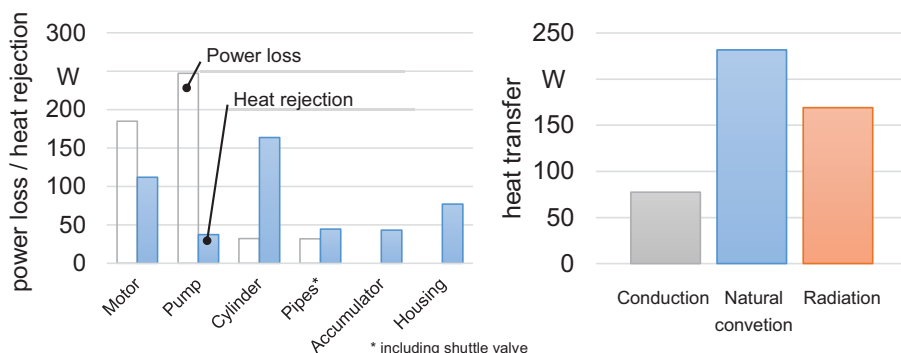


Figure 8: Simulated distribution of steady-state power losses and heat rejection

5.2. Heat rejection improvement studies

Moreover, the validated thermo-hydraulic model enables studies on the heat rejection improvement. Approaches for the improvement of heat rejection are covering blank metallic surfaces with high emissive coatings ($\epsilon_{metal} = 0.05 \dots 0.24$, $\epsilon_{varnish} = 0.92 \dots 0.97$) or provide ribbed surfaces to increase radiative and convective heat transfer respectively. The calculation of heat transfer numbers of ribbed surfaces can be found in /6/.

Figure 9 shows the simulated temperatures of the demonstrator with improved heat rejection behaviour. All metallic surfaces are varnished ($\epsilon_{varnish} = 0.92$) and the motor as well as the mounting plates are equipped with ribbed surfaces. With these measures the maximum oil temperature can be reduced by 22 % from 76 to 64°C.

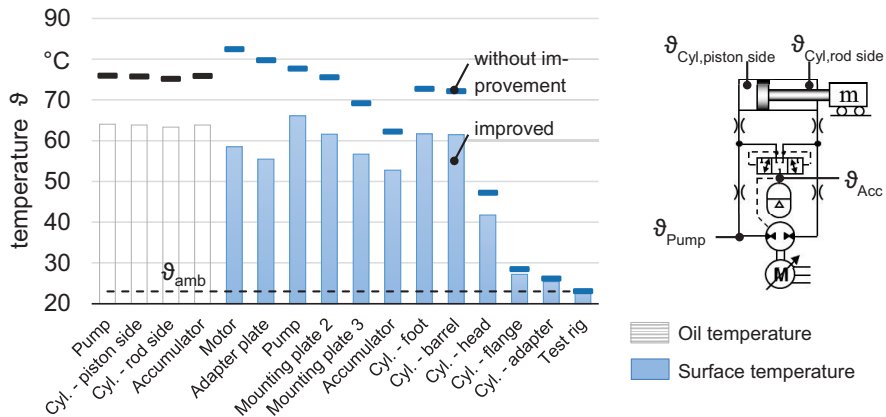


Figure 9: Simulated steady-state temperatures of conventional and improved demonstrator

6. Conclusion

Electrohydraulic compact drives represent an interesting alternative to conventional hydraulic or electromechanical drives. Due to the calm cooling (passive heat output) the prediction of thermo-energetic behaviour is essential in order to guarantee a thermally stable process without elaborate experiments. System simulations with lumped parameters are suitable to predict thermo-energetic behaviour with reasonable computational effort. In this paper, a lumped parameter thermo-hydraulic model of an electrohydraulic compact drive demonstrator is introduced, which combines a dynamic system model with a thermal resistance network. The thermal resistances are parameterised analytically by means of approaches from literature. Further, in particular the temperature dependent losses of the pump and the natural convection heat transfer of a model shape geometry (cube) are focused. Profound studies of the latter enables the identification of ambient conditions during experiments using the cube as a reference object. The validation against measurements shows that the model achieves an accuracy of 4.4 % in the prediction of the system's maximum steady-state oil temperature. This accuracy can be considered as satisfying in technical terms in order to support development, optimisation and examination of possible fields of application of electrohydraulic compact drives. Finally, an analysis of power losses and heat rejection capabilities among the components and a simulation study on the improvement of the heat rejection capability is presented. It is shown that with the use of ribbed surfaces and varnish the system's maximum oil temperature can be reduced by 22 %. Future works will target sensitivity analysis of the thermo-hydraulic model and thermo-energetic behaviour as well as aspects of wear and oil aging in electrohydraulic compact drives.

7. Acknowledgement

The research presented in this paper is based on the project “Thermischer Haushalt und Verschleiß elektrohydraulischer Kompaktantriebe” (Ref.-No. AiF 18051 BR), which is financed and supervised by the Research Association Mechanical Engineering (FKM). In the scope of the Programme to promote Industrial Collective Research it is funded by the German Federation of Industrial Research Associations (AiF) with means of the Federal Ministry of Economic Affairs and Energy (BMWi) on the basis of a decision by the German Bundestag.

Supported by:



on the basis of a decision
by the German Bundestag

8. References

- /1/ Michel, S., Schulze, T., Weber, J.: Energy-efficiency and thermo energetic behaviour of electrohydraulic compact drives. 9th International Fluid Power Conference, Aachen, Germany, Vol. 1, pg. 162–177, 2014
- /2/ Williamson, C.: Power Management for Multi-Actuator Mobile Machines with Displacement Controlled Hydraulic Actuators. Dissertation, Purdue University, 2010
- /3/ Michel, S., Weber, J.: Electrohydraulic Compact Drives for Low Power Applications considering Energy-efficiency and High Inertial Loads. Seventh FPNI-PhD-Symposium, Reggio Emilia, Italy, pg. 869-888, 2012
- /4/ Michel, S.; Weber, J.: Energy-efficient electrohydraulic compact drives for low power applications. In: Johnston, D. N. (ed.): Fluid Power and Motion Control (FPMC 2012). Bath, 2012, pg. 93-107
- /5/ Nerg, J., Rilla, M., Pyrhönen, J.: Thermal Analysis of Radial-Flux Electrical Machines with a High Power Density. IEEE Transactions on industrial electronics, Vol. 55, No. 10, 2008
- /6/ Jungnickel, G., Simulation des thermischen Verhaltens von Werkzeugmaschinen – Modellierung und Parametrierung. Technische Universität Dresden, 2010
- /7/ Buchman, K.; Jungnickel, G.: Wärmeübertragung an Be- und Verarbeitungsmaschinen. Wrocław : Wydawnictwo politechniki wrocławskiej, 1978
- /8/ Sidders, J. A.; Tilley, D. G.; Chapple, P. J.: Thermal-hydraulic performance prediction in fluid power systems. Journal of Systems and Control Engineering, Volume 210 (1996), Nr. 49, pg. 231–242, 1996

- /9/ Rahmfeld, R.: Development and Control of Energy Saving Hydraulic Servo Drives for Mobile Systems, Dissertation, TU Hamburg-Harburg, 2002
- /10/ Busquets, E.; Ivantysynova, M.: Temperature Prediction of Displacement Controlled Multi-Acutator Machines. International Journal of Fluid Power, Vol. 14, No. 1, pg. 25-36, 2013
- /11/ Ivantysyn, J.; Ivantysynova, M.: Hydrostatische Pumpen und Motoren : Konstruktion und Berechnung. Würzburg : Vogel, 1993
- /12/ Yovanovich, M. M.; Thermal contact correlations. In: AIAA 16th Thermophysics Conference, Palo Alto, June 23-25, 1981. New York : AIAA, 1981, pg. 83-95
- /13/ Verein deutscher Ingenieure - VDI-Gesellschaft Verfahrenstechnik und Chemieingenieurwesen (GVC) (Publ.): VDI-Wärmeatlas, Springer, 2013.

9. Nomenclature

A	Area	m^2	Q	Volume flow	l/min
c	Flow velocity	m/s	\dot{Q}	Heat flow	W
c_p	Specific heat capacity	J/(kg*K)	p	Pressure	N/m ²
E	Energy	J	P	Power	W
f	Frequency	Hz	Pr	Prandtl number	-
F	Force	N	R_{th}	Thermal resistance	K/W
g	Gravity	m/s ²	t	Time	s
h	Specific enthalpy	J/kg	T	Temperature	K
Gr	Grashof number	-	U	Voltage	V
L	Characteristic length	m	x	Position	m
\dot{m}	Mass flow	kg/s	z	Height	m
M	Torque	Nm	α	Heat transfer number	W/(m ² *K)
n	Speed	rev/min	β	Expansion coefficient	1/K
Nu	Nusselt number	-	ε	Emissivity	-

η	Efficiency, Dynamic viscosity	-, kg/(m*s)
λ	Heat conductivity	W/(m*K)
ν	Kinematic viscosity	m ² /s
σ_s	Boltzmann constant	J/K
ϑ	Temperature	°C

A Thermal Analysis of Direct Driven Hydraulics

Dr.-Ing. Tatiana Minav

Department of Mechanical Engineering, Aalto University, P.O. Box 14400, 00076, Aalto, Finland, E-mail: tatiana.minav@aalto.fi

Ing. Luca Papini

Power Electronics, Machines and Control Group (PEMC), University of Nottingham, Nottingham, UK, E-mail: luca.papini@nottingham.ac.uk

Professor Dr.-Ing. Matti Pietola

Department of Mechanical Engineering, Aalto University, 00076, Aalto Finland, E-mail: matti.pietola@aalto.fi

Abstract

This paper focuses on thermal analysis of a direct driven hydraulic setup (DDH). DDH combines the benefits of electric with hydraulic technology in compact package with high power density, high performance and good controllability. DDH enables for reduction of parasitic losses for better fuel efficiency and lower operating costs. This one-piece housing design delivers system simplicity and lowers both installation and maintenance costs. Advantages of the presented architecture are the reduced hydraulic tubing and the amount of potential leakage points. The prediction of the thermal behavior and its management represents an open challenge for the system as temperature is a determinant parameter in terms of performance, lifespan and safety. Therefore, the electro-hydraulic model of a DDH involving a variable motor speed, fixed-displacement internal gear pump/motors was developed at system level for thermal analysis. In addition, a generic model was proposed for the electric machine, energy losses dependent on velocity, torque and temperature was validated by measurements under various operative conditions. Results of model investigation predict ricing of temperature during lifting cycle, and flattened during lowering in pimp/motor. Conclusions are drawn concerning the DDH thermal behavior.

KEYWORDS: thermal modelling, direct driven hydraulics, non-road mobile machinery, electro-hydraulic actuator

1. Introduction

The next exhaust limits for engine manufacturers will be implemented in 2019/2020 /1/. This Tier V limit imposes a sharp tightening of exhaust limits, especially in terms of particles. This coming four-year window should be exploited for preparing engines for the upcoming regulations by developing innovative solutions. In order to reach the target environmental requirements, electric and hybrid topologies have seen as suitable solutions. Whereas, a huge potential application area is the Non-road Mobile Machinery (NRMM) industry, which are used in mining, goods manufacturing, forest harvesting, and construction works.

In recent years, an industrial trend can be observed in increased use of compact electro-hydraulic actuators. These actuators are able to deliver powerful, linear movement with valve-controlled or pump-controlled systems. The concept of electrohydraulic actuators have been introduced as zonal hydraulics in NRMM and aircraft applications. For instance in /2/, an electrohydraulic actuator was applied to the power steering of heavy vehicles. In /3, 4/, the new design of electro-hydraulic actuators was developed for aircraft applications, where reliability requirements are very high. Most of the research studies related to electrohydraulic actuators have been conducted to adjust the state of the servo valve /5, 6/, where the set of valves is utilized to balance the flow and to ensure the direction of the electrohydraulic actuator motion. In /7, 8/, the Direct Driven Hydraulics (DDH) unit without conventional directional valves was introduced as an electro-hydraulic actuator. The DDH drive combines the best properties of electric and hydraulic drive technologies in one: Direct control of flow, velocity and position of the actuator; Disconnection of pump units from the internal combustion engine; Possibility of power on demand.

In this research, Direct Driven Hydraulics (DDH) is seen as a tool to convert existing NRMMs to hybrids and/or increase degree of hybridization. In terms of continuous operation, research all around the world is facing the challenge of establishing and maintaining industrial activities in extreme environments. Normally, the heat generated from the equipment operation keeps the fluid warm and enables it to circulate properly. The problems occur at start-up, when everything has cooled down to low temperatures. Equipment failure is unacceptable in remote locations in extreme environments such as the Arctic areas. At the moment, research on the extreme operation of NRMM is limited mostly to the cold-start characteristics of engines /9/ and to the development of new components and hydraulic oils specifically for arctic conditions /10-13/. Heat generation and transfer in oil-hydraulic systems is discussed and researched from an overheating

point of view only /14/ or predicting accurate temperature /15-17/. For instance in /18, 19/, the thermo-dynamical behavior of electro-hydraulic systems were studied in typical working temperatures (above 0 ° C). In /19-22/, a compact drive and its components were investigated from the thermal point of view. New configurations in NRMM with a DDH conversion as hybrid tool are possible without the traditional source of heat and constantly operating engine. Would the DDH unit be self-sufficient from thermal point? Therefore to find answer to this question, this paper investigates directly driven hydraulic setup (DDH) for non-road mobile machinery (NRMM) application from thermal point of view.

The remainder of this paper is organized as follows. The DDH test setup is introduced in Section 2, while Section 3 presents a detail description of the thermal model. The measurement results and their analysis are described in Section 4, thereafter; Section 5 contains discussion and concluding remarks.

2. Test setup

The experimental test setup is illustrated in **Figure 1**. The control of the DDH system is implemented directly with a servo motor drive without conventional hydraulic control valves. Therefore, velocity of the double-acting cylinder is determined by in-coming oil flow from the pump, out-coming flow to the hydraulic motor and angular speed of the electric motor. The electromechanical drive (frequency converter controlled electric motor) is adopted to control the fluid flow, the position of the payload and the direction of the motion. A program for the electric drive is set up to control both the electrical and hydraulic sides of the system, thus allowing good controlled lifting-lowering movement at different speeds and payloads. Test setup consists of two XV-2M internal gear pump/motor by Vivoil with displacement of 14.4 and 22.8 cm³/rev P_2 and P_1 , respectively /23/. The size of the pumps (and thus manufacturer) were chosen to match to the unsymmetrical cylinder chambers (MIRO C-10-60/30x400). Unidrive SP1406 drive converts the AC power supply from the line and allows to set the speed of the permanent magnet brushless servo motor Unimotor 115U2C manufactured by Emerson Control Techniques, taking advantage of the information obtained by the feedback device fitted, to ensure the rotor speed is exactly as demanded /24/. Speed and torque of the motor shaft is monitored by Unidrive SP1406 drive software/25/. **Figure 1a** illustrates simplified schematics of test setup with the locations of pressure and height sensors. The pressures of the lines, pump inlet and outlet, are measured by means of Gems 3100R0400S pressure transducers /26/. The actual velocity and height of the cylinder's

piston rod were measured by means of a wire-actuated encoder SIKO SGI (IV58M-0039) /27/.

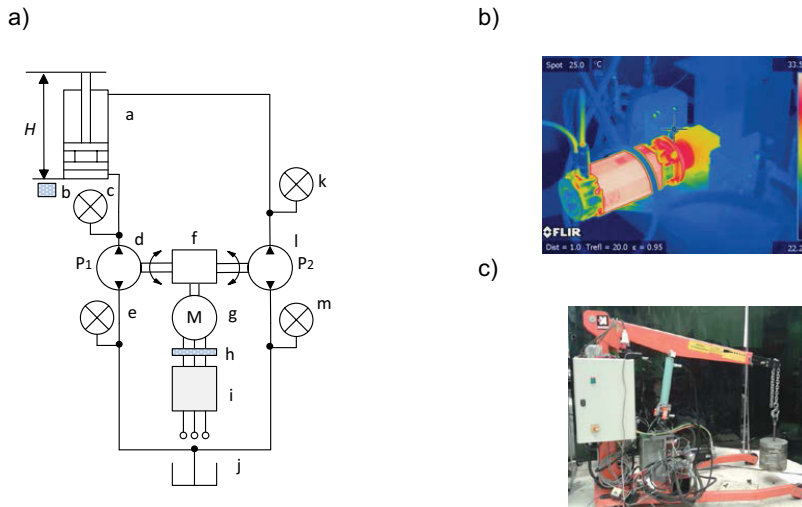


Figure 1: a) schematic of DDH setup, b) thermal image of setup in 10 °C ambient temperature, c) overview of DDH setup

Thermal images across the pump and electrical machine demonstrate of the components different heat loss distribution. Change in fluid temperature (ΔT) across the pump indicates of hydro-mechanical losses within the pump and demonstrates its behavior. Thermal images with larger temperature differential show reduced system efficiency as heat generation results in energy consumption and heat load within the system.

3. Modelling

Modelling of the DDH system is divided to two parts. Thermal modelling of hydraulics is demonstrated in Section 3.1. A thermal generic model is proposed for the electric machine in Section 3.2, where energy losses dependent on velocity, torque and temperature. Thus, simulation results are shown in Section 4. Proposed model was validated by measurements in Section 5.

3.1. Thermal-hydraulic model

Mainly the heat generation of the DDH system appear due to power losses in hydraulic components. Hydraulic oil transfer the heat among hydraulic components. Whereas, exchange between external environment is also happening via convection. According to /28/, direction or circulation of oil is important for the heat transferred among hydraulic components. The thermal model hydraulics. **Figure 2a** depicts the thermal-hydraulic

model, which was built from hydraulic components in SimulationX - commercial multi domain simulation tool.

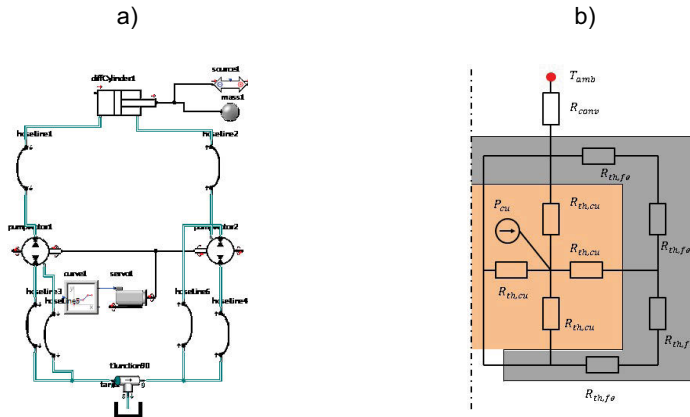


Figure 2: a) Thermal - hydraulic model, b) Lumped parameter model

The DDH system was described as fluidic and solid control volumes, which represents housing of hydraulic components and its solid construction elements. All hydraulic main components are considered in the model. It is assumed that DDH setup has an unlimited heat capacity and remains at ambient temperature equals to 23 ° C.

3.2. Electric machine thermal model

The electrical drive system consisting of the power electronics linked with electrical machine is designed to achieve a full control of the delivered torque. The characterization of the performances results critical to assess the efficiency of the system. The behavior of the machine is modelled according to analytical equations /29-/30/ to determine the torque-current characteristic of the device. The different speed-current conditions in which the drive will be operated are expected having an impact in the thermal behavior of the electrical machine, therefore on the overall drive itself. The load capabilities are expected to be fully exploited during the operation of the DDH which reflects in different set point for current injected in the electrical machine at different operative rotor speed. The parameters that characterize the electromagnetic behavior have an impact in the losses that take place in the electrical machine. The current that is injected in the electrical machine will become a source of Joule losses. The rotor speed at which the machine is operated will have a minimum impact on the windage losses (usually considered as <1% of the total losses /31/), but will have an impact on the iron losses in the stator core due to the time variable magnetic flux provided by the rotor structure. The eddy current losses in the rotor core and permanent magnets are

neglected. The thermal model proposed is designed to evaluate the temperature distribution within the electrical machine structure according to the heat sources that are here considered and dependent on the operative condition of the DDH. The temperature prediction in electrical machine has been a topic highly investigated by many industrial and academic research centers and different techniques has been proposed. Finite Element Methods results as the most accurate technique with the drawbacks of high computational time and time consuming for setting it up; first-second-third order equivalent circuit methods are considered when fast computation is required and are still capable of high accuracy prediction /32/-/33/. Hybrid-mid-complex techniques have been developed to compromise the computational effort and the accuracy of the prediction /34/. The equivalent resistance network /33/ has been selected as the modelling tool which better fit the needs of the thermal estimation for the DDH. The proposed model is based on the assumption of symmetrical supply for the electrical machine and the exploitation of the geometrical symmetries of the structure allows reducing the model to a single stator slot. The Fourier equation has been considered discretized for each macro-part in which the computational domain is divided and equivalent thermal resistance and capacitance are defined according to the material thermal properties. The overall result is a linear thermal network which can be solved by means numerical techniques to evaluate the temperature distribution in the nodes. The inputs of the model are the heat losses as previously described: joule losses in the copper winding, heat losses correspondent to the stator iron losses. Boundary conditions have been defined according to the external condition. The cooling media considered in air and natural convection is considered between the stator housing and the environment. The convection coefficient has been defined according to /31/-/32/ and the ambient temperature has been changed to replicate the test condition in the controlled thermal chamber. **Figure 2b** illustrates lumped parameter model. The permanent magnet brushless servo-motor 115U2C is characterized by $K_t = 1.6 \text{ Nm/A}$ and $K_v = 9.8 \cdot 10^{-2} \text{ V/rpm}$, with a rated torque of $T_r = 8.1 \text{ Nm}$ with an operative maximum speed of $\omega_m = 3000 \text{ rpm}$. The control system is designed to fulfill the dynamics requirements of the DDH. The current injected is controlled up to $I_{MAX} = 23.5 \text{ A}$. Steady state and transitory operative conditions are considered to validate the thermal model of the machine. The rated current considered defines the value of the heat source in the part of the lumped parameters that models the copper region. The variation of the resistivity with respect the temperature is taken into account according to (1)

$$\rho(T) = \rho_{20^\circ\text{C}}(1 + \alpha_{cu} [T - 20]), \quad [S/m] \quad (1)$$

where $\rho_{20^\circ C}$ is the resistivity of the copper at $T = 20^\circ C$, α_{cu} is the thermal coefficient of the copper and T is the operative temperature of the material. The joule losses are defined by means (2)

$$P_{cu} = \kappa_{end} N_{ph} N_{turn} \frac{\rho(T)L}{s} I^2, [W] \quad (2)$$

where κ_{end} is the end region correction factor, N_{ph} is the number of phases, N_{turn} is the number of turn/phase, L is the axial length of the machine, s the cross section of the conductors. The iron losses are estimated according to the Steinmetz equation (3)

$$P_{fe} = \kappa_h f^\alpha B^\beta + \kappa_e (f B)^2, [W/kg] \quad (3)$$

where f is the frequency of the magnetic flux density, B is the peak of the magnetic flux density and α, β, κ_h and κ_e are constant coefficient listed in Table 1. The thermal resistances are defined as (4) and connect the macro-sections in which the computational domain is divided.

Parameter	Value
κ_h	0.039
κ_e	0
α	1
β	1.6886

Table 1: Iron Losses coefficients

$$R_{th} = \frac{C_t s}{L}, \quad (4)$$

$$R_{conv} = h s L, \quad (5)$$

where C_t is the conduction coefficient of the material, h is the convection coefficient, s is the surface of heat exchange and L is the axial length /35/. The thermal convective equivalent resistance between the electrical machine and the environment is defined as (5) where the definition of the thermal convection coefficient can be found in /31/. The number of nodes has been chose as a compromise between the accuracy of the prediction and the computational effort required. The thermal capacity of the iron and copper region has been modelled to account for the thermal transitory behavior of the machine.

4. Simulations Results

The thermal model has been tested in ambient operative conditions. The operative behavior of the DDH is considered to be oscillatory. The rotational speed of the electrical machine is controlled in order to achieve a periodic change in pressure required as an output. The amplitude of the current supplied to the machine is defined by means the

speed loop, featuring peaks when change in directions occurs while only small quantities are required when the speed is kept constant. The torque generated results directly proportional with respect to the q-axis current which is approximated with its first harmonic with respect to the period of the hydraulic oscillation considered and expressed in (6). The joule losses are generated by means the square of the current resulting in I_{heat}

$$I_q(t) = I_M \cos(\Omega_h t + \theta_h) \Rightarrow I_q^2(t) = I_M^2 \cos^2(\Omega_h t + \theta_h) \Rightarrow I_{heat} = \frac{I_M^2}{2}, \quad (6)$$

where I_M is the maximum rms value achieved by the current, Ω_h is the angular speed of the hydraulic oscillation and θ_h its phase angle. The constant equivalent rms current is supplied and the thermal model predicts transitory 1 °C/cycle of increase in the housing and 4 °C/cycle in the hot spot of the winding structure. Results of electric machine thermal modeling is shown in **Figure 3**. The transitory rise of the temperature in the surface where the heat is exchanged, the housing of the electrical machine, is presented in **Figure 3a**. In **Figure 3b**, the temperature in the winding structure, the hot spot of the electrical machine is reported and the maximum temperature achieved in the motor housing is highlighted with the dashed line. The model developed is capable of accounting also for the transitory heat transmission between the region where the heat sources are located and the surface dedicated to the heat exchange.

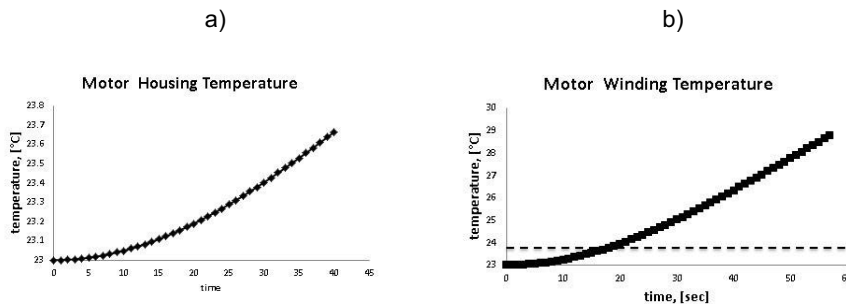


Figure 3: Result of electric machine thermal model: a) Motor housing temperature, b) Motor winding temperature.

Figure 4 shows simulated oil temperature at different locations: pump/motors and tank. As input signal measured data from **Figure 5** was used. Simulation results predict ricing of temperature during lifting cycle, and flattened during lowering in pimp/motor.

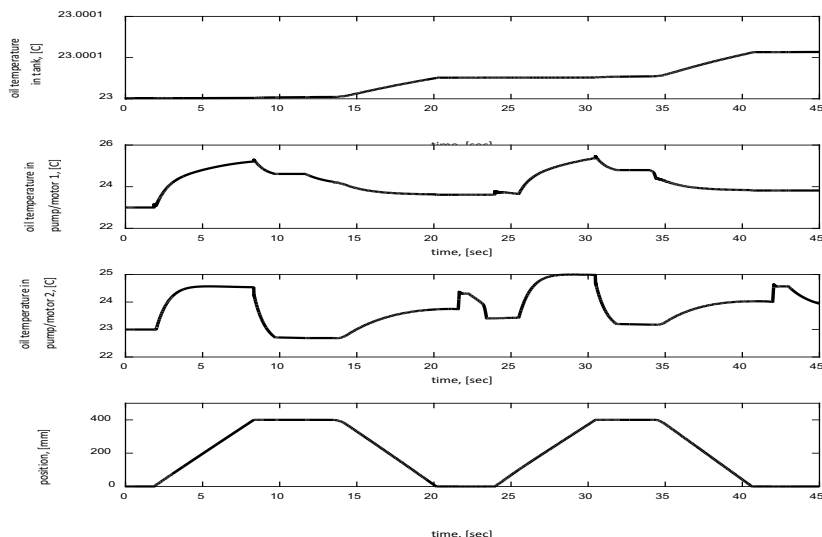


Figure 4: Results of thermal-hydraulic model: position, pump/motors and tank oil temperatures

5. Experimental investigation

The proposed models of DDH is validated by measurements in this Section. The experimental tests are performed in a temperature controlled environment. Essential parameters like pressure, torque, speed, cylinder position and velocity, electric motor voltage, current and ambient temperature are either directly obtained from the setup with sensors or calculated. For experiments a DDH setup was installed according to **Figure 1a**. **Figure 1a** shows the experimental setup with the locations of pressure, height, temperature, current and voltage sensors.

The DDH experimental setup was tested with a payloads of 140 kg at different speeds. The tare weight of the moving boom system is 9.5 kg. **Figure 5** depicts the measurement results for the chosen maximum payload. The payload was lifted to a height of 0.4 m at an average velocity of 0.2 m/s and then lowered to the ground with the same speed. The rotation speed of the PMSM, which corresponds to the pump/motor speed, was 500 rpm. According to **Figure 5**, the torque needed for lifting the payload is equal to 16 Nm, acting pressure reach up to 100 bar. Pressure peak during lifting phase in the system corresponds to unequal pump displacement to cylinder area.

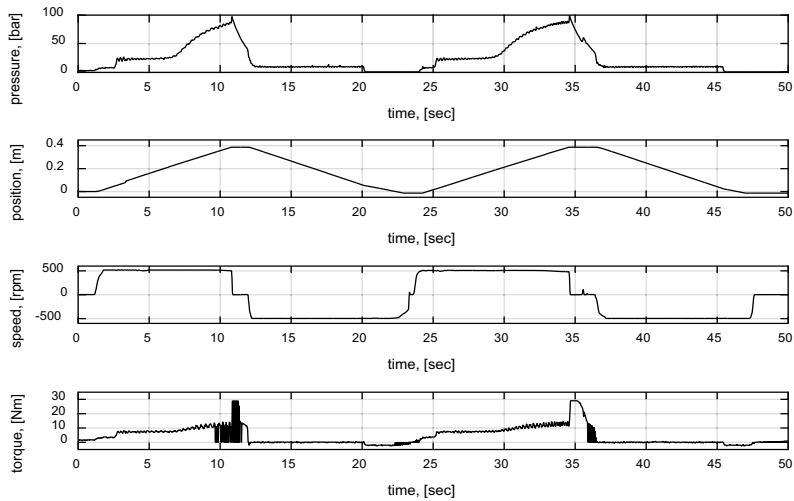


Figure 5: Results of experimental investigation: pressure, height, speed, flowrate and estimated torque.

Figure 6 illustrates temperature changes during lifting lowering cycle.

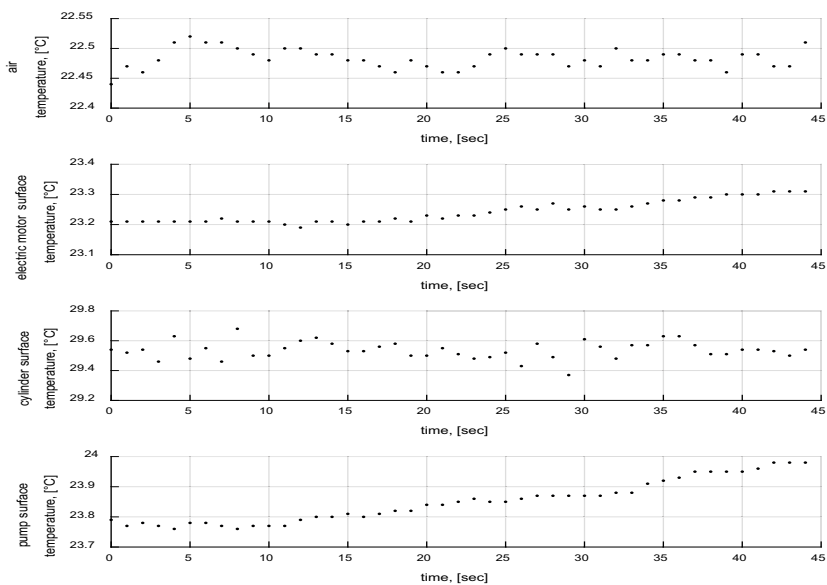


Figure 6: Temperature results of experimental investigation during lifting-lowering cycle.

The comparison of the simulation results with measurements for lifting/lowering cycle with a payload 149.5 kg showed that surface temperature is higher than simulated oil temperature. Influence of pressure peaks in DDH system can be observed in rising temperature in simulation results. Finally, according to simulation during lifting-lowering cycle, the electric motor is the warmest component.

6. Conclusion

There is a rising trend for compact electro-hydraulic actuators in industry. In this study the direct driven hydraulic test setup without control valves was described and investigated from thermal point of view. The comparison between the simulation results and the experimental test data validate the modelling developed for both the electrical machine and the hydraulic system. The experimental tests confirmed rising of temperature during lifting cycle, and flattened during lowering.

7. Acknowledgments

This research was enabled by the financial support of Academy of Finland (project ArcticWell) and internal funding at the Department of Mechanical Engineering at Aalto University. The cooperation of Dr.-Ing Jani Heikkinen is highly appreciated.

8. References

- /1/ Tier 4 Emission Standards for Nonroad Diesel Engines, online, <https://www.dieselnet.com/standards/us/nonroad.php#tier4>
- /2/ Daher, N., Ivantysynova, M., Electro-hydraulic energy-saving power steering systems of the future. 2012. Proceedings of the 7th FPNI PhD Symposium on Fluid Power, June 27-30, 2012, Reggio Emilia, Italy.
- /3/ Youzhe Ji, Song Peng, Li Geng, Zhanlin Wang, Lihua Qiu, Pressure Loop Control of Pump and Valve Combined EHA Based on FFIM. 2009. The Ninth International Conference on Electronic Measurement & Instruments, 2009.
- /4/ Qian Zhang, Bingqiang Li, Feedback Linearization PID Control for Electro-hydrostatic Actuators, 2011.
- /5/ Liang, B., Li, Y., Zhang, Z., Research on Simulation of Aircraft Electro-Hydrostatic Actuator Anti-Skid Braking System. 2011. Third International Conference on Measuring Technology and Mechatronics Automation (ICMTMA), 6-7 Jan. 2011, pp. 78 – 82
- /6/ Altare, G., Vacca, A., Richter, C., A Novel Pump Design for an Efficient and Compact Electro-Hydraulic Actuator, IEEE Aerospace Conference, 2014 IEEE, 2014, pp. 1-12.
- /7/ Minav, T.A., Bonato, C., Sainio, P., Pietola, M., Direct driven hydraulic drive, at IFK, March 2014, Aachen, Germany.

- /8/ Minav, T.A., Bonato, C., Sainio, P., Pietola, M., Efficiency of Direct Driven Hydraulic Drive for Non-road Mobile Working Machines, at ICEM, September 2014, Berlin, Germany.
- /9/ Hydraulic_Fluids, http://www.statoil-ellas.lv/files/Hydraulic_Fluids.pdf
- /10/ Arctic Low Pour Hydraulic Oil, <http://www.phillips66lubricants.com/documents/>
- /11/ Qinghui Zhou, et.al, Development of Control Strategy for SI Engine Cold Start, IEEE International Conference on Information and Automation June 20 - 23, Harbin, China
- /12/ Waleed Nessim, Fujun Zhang, Powertrain Warm-up Improvement using Thermal Management Systems, International Journal of Scientific & Technology Research Volume 1, Issue 4, MAY 2012
- /13/ Kauranen P., et.al. Temperature optimisation of a diesel engine using exhaust gas heat recovery and thermal energy storage, http://www.vtt.fi/inf/julkaisut/muut/2010/PCMAkku_ATE2009_Submitted.pdf
- /14/ Busquets E., Ivantysynova M., Temperature Prediction of Displacement controlled multi-actuator machines, Int. J. of Fluid Power, Jan., 2014;
- /15/ Busquets E., An investigation of the cooling power requirements for displacement-controlled multi-actuator machines, 2013
- /16/ Michel S., et.al. Energy-efficiency and thermo energetic behavior of electrohydraulic compact drives, 9th IFK conf. 2014
- /17/ Minav,T., P. Sainio, M. Pietola, Efficiency of Direct driven hydraulic setup in arctic conditions, SICFP 2015, May 2015, Tampere, Finland.
- /18/ Soudunsaari R.,Hydrauliöljy ja Hydraulipumppu arktissa olosuhteissa , Espoo : VTT, 1985
- /19/ Rovellini, et.al. Induction motors for use in arctic environments, PCIC Europe 2010 Conf. proceedings.
- /20/ Li Y., et.al. Thermal-hydraulic modeling and simulation of high power hydro-motor, 2008, Asia simulation conference proceedings.
- /21/ Tomioka K., et.al., A Method predicting temperature rise of oil-hydraulic system considering heat balance between oil-passage and housing, Int. Conference on Integrated Modelling and analysis in applied control and automation, 2012
- /22/ Tomioka ,K.,et.al., Precise and Practical 1D Analysis Method of Temperature in an oil-hydraulic cylinder chamber considering 3D internal flow, Transaction of the japan fluid power system society, Vol.43, N2,2012
- /23/ Vivoil motor, Data Sheet: reversible motor - series XV, [Online]. Available: http://www.vivoil.com/files/xm_en/xm201.pdf, visited on September 8, 2013
- /24/ Emerson Control Techniques Unimotor 115U 2C, http://www.emersonindustrial.com/en/en/documentcenter/ControlTechniques/Brochures/unimotor_fm_product_data.pdf, visited on September, 2013.

- /25/ Emerson Control Techniques Unidrive SP1406 drive, <http://www.emersonindustrial.com>, visited on September 8, 2013.
- /26/ Gemssensors 3100R0400S pressure transducers, <http://www.gemssensors.com/Products/Pressure/Pressure-Tranducers> , visited on September, 2013.
- /27/ SIKO SGI (IV58M-0039), <http://www.siko-global.com/en-de> , visited on October, 2013.
- /28/ Kai Li, Zhong Lv, Kun Lu, Ping Yu, Thermal-hydraulic modeling and simulation of the hydraulic su=system based on the electro-hydraulic actuator, *procedia Engineering* 80 (2014) 272-281
- /29/ Bolognesi, P., A mid-complexity analysis of long-drum-type electric machines suitable for circuital modeling, *ICEM* 2008, pp.1-5, 6-9 Sept. 2008 doi: 10.1109/ICELMACH.2008.4799879
- /30/ Rodríguez, A.L.; Gómez, D.J.; Villar, I.; López-de-Heredia, A.; Etxeberria-Otadui, I., Improved analytical multiphysical modeling of a surface PMSM, 2014 International Conference on Electrical Machines (ICEM), pp.1224-1230, 2-5 Sept. 2014, doi: 10.1109/ICELMACH.2014.6960338
- /31/ Howey, D.A.; Childs, P.R.N.; Holmes, A.S., Air-Gap Convection in Rotating Electrical Machines, *IEEE Transactions on Industrial Electronics*, vol.59, no.3, pp.1367-1375, March 2012, doi: 10.1109/TIE.2010.2100337
- /32/ Zhe Huang; Marquez-Fernandez, F.J.; Loayza, Y.; Reinap, A.; Alakula, M., Dynamic thermal modeling and application of electrical machine in hybrid drives, 2014 International Conference on Electrical Machines (ICEM), pp.2158-2164, 2-5 Sept. 2014, doi: 10.1109/ICELMACH.2014.6960483
- /33/ Bracikowski, N.; Hecquet, M.; Brochet, P.; Shirinskii, S.V., Multiphysics Modeling of a Permanent Magnet Synchronous Machine by Using Lumped Models, *IEEE Transactions on Industrial Electronics*, vol.59, no.6, pp.2426-2437, June 2012, doi: 10.1109/TIE.2011.2169640
- /34/ Papini, L.; Gerada, C., Thermal-electromagnetic analysis of solid rotor induction machine, 7th IET International Conference on in Power Electronics, Machines and Drives (PEMD 2014), April 2014, doi: 10.1049/cp.2014.0462
- /35/ Boglietti, A.; Carpaneto, E.; Cossale, M.; Lucco Borlera, A., Stator thermal model for short-time thermal transients, 2014 International Conference on in Electrical Machines (ICEM), 2-5 Sept. 2014, doi: 10.1109/ICELMACH.2014.6960367

9. Nomenclature

- B peak of the magnetic flux density
- C_t conduction coefficient of the material
- f frequency of the magnetic flux density

I_{MAX}	maximum current	A
K_t	torque constant	Nm/A
K_v	voltage constant	V/rpm
κ_{end}	end region correction factor	
L	axial length of the electric machine	m
N_{turn}	number of turn/phase	
N_{ph}	number of phases	
h	convection coefficient	
P_{cu}	joule losses	
P_{fe}	iron losses	
T_r	rated torque	Nm
s	cross section of the conductors	
α_{cu}	thermal coefficient of the copper	
$\rho_{20^\circ C}$	resistivity of the copper at $T = 20^\circ C$	
θ_h	phase angle	
Ω_h	angular speed	Rad/sec
ω_m	maximum speed	rpm

Group 5:
Pumps

Tribolayer Formation on Bronze CuSn12Ni2 in the Tribological Contact between Cylinder and Control Plate in an Axial Piston Pump with Swashplate Design

peer reviewed

Dipl.-Ing. Andreas Paulus

Bosch Rexroth AG, Maria-Theresien-Str. 23, 97816 Lohr am Main,
E-Mail: Andreas.Paulus@boschrexroth.de

Univ.-Prof. Dr.-Ing. Georg Jacobs

Institute for Machine Elements and Machine Design (IME), RWTH Aachen University,
Schinkelstraße 10, 52062 Aachen, E-Mail: Jacobs@ime.rwth-aachen.de

Abstract

The present study investigates the formation of tribolayers on bronze CuSn12Ni2. Two different test rigs are used, of which one is a sliding bearing test rig in order to perform lubricated thrust bearing tests. Bronze CuSn12Ni2 is used for the sliding elements and the counter body is made of C45 steel. In addition to that, an axial piston pump test rig was used to determine the transferability of the results to the axial piston pump. The test conditions are set up in a way that the tribological loads in the contacts are similar to each other.

Changes in the subsurface morphology and the chemical composition of the tribolayer were analysed using electron probe micro analysis (EPMA), transmission electron microscopy (TEM), energy dispersive X-ray spectroscopy (EDS) and X-ray photoelectron spectroscopy (XPS). Focused ion beam (FIB) milling was used to prepare site-specific TEM foils from the wear track. The formation of a nanoscale tribolayer was associated with reduced wear, which leads to low leakage in the axial piston pump. This tribolayer is enriched with oxygen, sulfur and zinc, which is an effect of tribochemical reactions of environment molecules and surface molecules.

KEYWORDS: Tribolayer, Bronze, Axial Piston Pump, Wear, Chemical Reactions

1. Introduction

Nowadays, hydrostatic drive systems are widely used in mobile applications such as wheel loaders or excavators because of their superior power density. The requirements in these mobile applications are exceptionally demanding in terms of limited space, contamination of oil and highly variable load spectra. Additionally, the environmental

compatibility of mobile machinery is subject to increasing regulation. For example, the European Union defines limitations for the utilisation of heavy metal containing alloys (/1/).

Amongst other things, this affects axial piston pumps, which are a substantial part of hydrostatic drive systems. In some versions lead-containing copper alloys are used in the tribological contact between cylinder and control plate of axial piston pumps. In these applications the lead content contributes considerably to the positive tribological properties of the copper alloy. It is assumed that the lead dissolves out of the material surface and forms a lead-rich layer on the surface that prevents direct contact between the base material and the counter body. This reduces the friction and wear in the mixed friction regime considerably.

A major goal of manufacturers of those axial piston pumps is to replace the lead-containing alloys by lead-free alloys and thus to meet the rules of the European Union. This has to be achieved without cutbacks in performance or lifetime. To reach this goal, one approach is to utilise chemical surface modifications that result from tribochemical reactions due to tribological stresses in the contact area under the influence of additivated lubricants. Those surface modifications are called tribolayers, which can separate the two bodies in contact in a similar way as the lead-rich layer on lead-containing alloys.

Tribolayers are known to reduce friction and wear for example in roller bearings or gears. In this area, NAVEIRA-SUAREZ and ANDERSSON investigated the effect of tribolayers in model tests and simulated the formation of tribolayers on steel material (/2/, /3/). WOLF examined the influence of the lubricant on the formation of tribolayers (/4/), and HENTSCHE as well as BURGHARDT gave evidence for a significant reduction of wear in roller bearings due to the effect of a tribolayer (/5/, /6/).

The goal of this study is to show that those tribolayers also form on copper alloys under the very different tribological conditions of conformal contacts. They have a positive influence on friction and wear in roller bearings and thus can potentially substitute lead-containing copper alloys in axial piston pumps.

2. Experimental

To prove the formation of tribolayers on lead-free copper alloys one specific alloy, the bronze CuSn12Ni2, is used. This casting alloy shows promising results in wear tests and is used for bearing applications with very high loads (/7/). The mechanical strength properties are measured at 20 °C prior to the tests (see **table 1**).

As lubricant the mineral oil Bantleon Avia Fluid RSL 32 of the viscosity class ISO VG 32 is used. It is additivated for the requirements of hydraulic applications and thus contains a high concentration of sulphur, zinc and phosphorus. In an unused state, its kinematic viscosity at 40 °C is $\nu = 29,35 \frac{\text{mm}^2}{\text{s}}$, and its viscosity index is 100. All the included additives in unused state are listed in **table 2**. The measurement was performed by OELCHECK GmbH.

Hardness HB	118,6
Yield strength $R_{p0,2}$ [MPa]	240,4
Tensile strength R_m [MPa]	432,4
Compression yield strength $\sigma_{d0,2}$ [MPa]	236,8

Table 1: Mechanical strength properties of CuSn12Ni2 at 20 °C

Additives	Concentration (mg/kg)
Calcium	45
Magnesium	7
Zinc	253
Phosphorus	230
Sulphur	1732

Table 2: Additives contained in the test lubricant Avia Fluid RSL 32

2.1. Thrust Bearing Test Rig

The thrust bearing test rig is based on the FE8 test rig introduced by HENTSCHE (/5/). Specific design extensions allow a variable load application, speed control of the shaft, temperature control of the bearing housing and measuring of friction torque.

The inner parts of the bearing housing are specially designed as segmented sliding bearings for the investigation of tribolayers on lead-free copper alloys. The segments are circular and made from bronze CuSn12Ni2. A steel ring is shrunk on the shaft and functions as the counter body. A temperature sensor provides the temperature inside one of the bearing elements about 1 mm below the bearing surface.

To ensure similar lubrication conditions as in the contact between cylinder and control plate of an axial piston pump a state of mixed friction has to prevail. The design of the bearing segments is done according to the work of DETERS (/8/).

The running-in phase is characterised by relatively mild tribological conditions. It is followed by a stepwise increase of the load while all other parameters are held constant. All operating conditions are listed in **table 3**.

After each load level the specimens are disassembled, and their weight was measured to capture the weight loss in the previous load level. Furthermore, the torque measuring shaft provides continuous data for the friction torque.

Phase	Surface pressure [MPa]	Rotational speed [1/min]	Temperature [°C]	Duration [h]
Running-in	2.5	500	50	1
Load level 1	5	250	40	5
Load level 2	7.5	250	40	5
Load level 3	10	250	40	5

Table 3: Operating conditions in the thrust bearing tests

2.2. Axial Piston Pump Test Rig

The second test rig used in this work is the axial piston pump test rig. It is an application-oriented test rig which uses an axial piston pump to drive an axial piston motor. This setup enables the generation of lubricant pressure inside the axial piston pump as it is the case in the application. Thus, most of the relevant effects on the contact between cylinder and control plate can be taken into account by using this test rig. Among those are one-sided hydrostatic compensation of axial forces and cavitation.

The lubricant used is the same as in the thrust bearing tests, Bantleon Avia Fluid RSL 32. The cylinder of the axial piston pump is coated with a layer of CuSn12Ni2 at a thickness of 1 mm. The control plate is made of steel 8CrMo16.

The test procedure of the axial piston pump tests is based on stepwise increase of the tribological loads in the tribological contacts. This is achieved by a stepwise increase of the rotational speed and the hydraulic pressure. The three load levels used in the tests are shown in **table 4**. Load level 3 is identified with the maximum performance of the axial piston pump. In this operating point a maximum local surface pressure of up to 150 MPa is possible in the contact between cylinder and control plate.

Phase	Rotational speed [1/min]	Swivel angle [%]	Hydraulic pressure [bar]	Duration [h]
Load level 1	2000	100	200	0,5
Load level 2	3200	100	400	0,5
Load level 3	3300	100	500	50

Table 4: Operating conditions in the axial piston pump tests

After each load level, the axial piston pump is disassembled, photographed, and examined by an experienced engineer. Since this test is application-oriented, it is not possible to measure friction torque or wear. The wear is rated visually by an experienced engineer. Besides increased leakage, indications for a failure are unusual cavitation damage, unusual discoloration of the surface and crack formation.

3. Results

3.1. Friction and Wear

The friction and wear measurements from the thrust bearing tests are visualized in **figure 1**. This diagram is put together from the single measurements of each load level. Each vertical line represents the end of a load level and the beginning of the next one. The friction torque is measured continuously and is thus represented by the colored lines in figure 1 for each load level. The wear is measured after each load level. The bars in figure 1 represent the total wear in the respective load level. Both friction torque and wear have been normalised.

The wear is less than 10 *mg* in all load levels. The wear level is so low, that wear cannot be measured as erosion of the surface. Consequently, the differences in wear between the load levels have to be relativised especially when considering the measurement inaccuracy of the precision scale of ± 1 *mg*.

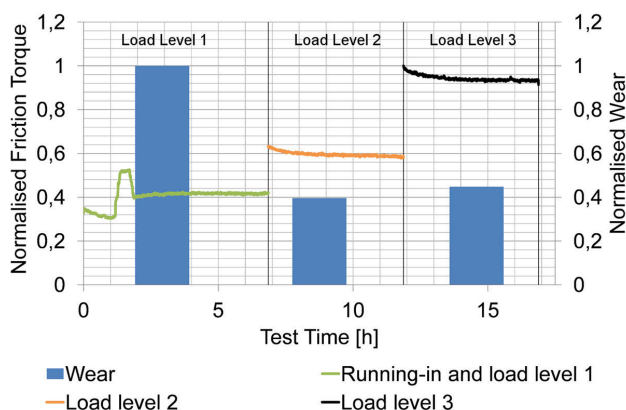


Figure 1: Normalised friction torque and wear of CuSn12Ni2 in thrust bearing tests

Compared to other materials tested on the same test rig the friction torque of CuSn12Ni2 is low in all load levels. It is increasing from a normalised friction torque of approximately 0.45 at the end of load level 1 to approximately 0.59 in load level 2 and 0.95 in load level 3. The temporal course of the friction torque is stable in all load

levels. A slight drop of the friction torque occurs in the first 1.5 hours of load levels 2 and 3. This is due to running-in effects after the disassembly of the bearing segments. The unsteady course of the friction torque at the beginning of the test is caused by changes in surface pressure and rotational speed before and after the running-in phase.

The low wear level in the thrust bearing tests makes CuSn12Ni2 a strong candidate for the substitution of the leaded bronze in axial piston pumps. To verify the applicability, axial piston pump tests were performed. **Figure 2** shows the cylinder surface after each load level.

After load level 1 the surface in contact with the control plate is clearly identifiable. It is delimited by two circular lines, which are dark discolored areas of CuSn12Ni2. The discoloration is due to tribochemical reactions on the material surface, which occur at the most severely stressed areas of the contact. This effect is described in more detail in ensuing chapter 3.2. Between those dark lines the material is clean without discolorations or contaminations. This indicates slight wear within the usual range without strong tribochemical reactions between material and lubricant. No cavitation-induced wear and no cracks are identified. After load level 2 the surface of the cylinder looks similar to the state after load level 1. The dark lines are now slightly thicker but the surface in contact still looks clean and without unusual wear.

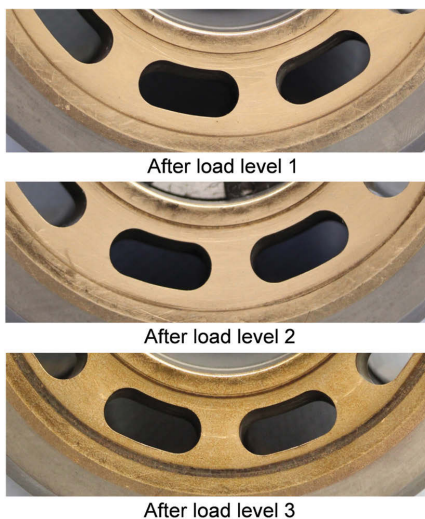


Figure 2: Cylinder surfaces after axial piston pump tests

After load level 3 the width of the outer dark line increased by a factor of 3. The overall wear level is still acceptable in comparison to serial parts, and no unusual leakage occurred. The whole surface appears darker than after the other load levels. The cause for this may be stronger tribochemical reactions due to higher tribological stresses. Between the bores slight cavitation wear is visible. This is not unusual in those areas. Thus, the cylinder with the new lead-free bronze CuSn12Ni2 passed a total of 51 h testing, including 50 h at maximum performance, without damage. The wear is slightly higher than in standard axial piston pumps.

It was noticed that on the control plate very small radial cracks developed. This leads to a classification of the entire test as failed. Considering the fact that this was the first test with a new lead-free material without any optimisation regarding design or manufacturing it is nevertheless a very promising result.

3.2. Tribolayer characterisation

EPMA, FIB/TEM and XPS analyses were conducted to investigate the formation of a tribolayer on CuSn12Ni2. FIB milling was used to prepare site-specific TEM foils from the wear tracks of the specimens.

EPMA-linescans of thrust bearing test specimens started near the center of the bearing segment and progressed in radial direction in the area of most prominent discoloration. Figure 3 depicts the partial mass density of relevant elements in the top layer of the material surface over the measured distance. The top diagram refers to the state after the running-in phase and shows that, besides the alloy elements, O, S and Zn are the dominant elements in the surface of the specimen. Their partial mass densities are mainly in the range of $0.2 - 1.5 \frac{\mu g}{cm^2}$.

After the load level 3 (**figure 3**, bottom diagram), O is the dominant element in the specimen's surface with a partial mass density of $1 - 2.5 \frac{\mu g}{cm^2}$. Zn is the second dominant element with a partial mass density of $0.4 - 0.7 \frac{\mu g}{cm^2}$. S has a partial mass density of $0.1 - 0.2 \frac{\mu g}{cm^2}$.

The EPMA-linescan of the cylinder surface after load level 1 in the axial piston pump test is depicted in **figure 4**. It was measured in radial direction crossing the outer discolored line.

The diagram shows that on both sides of the dark line O is the single dominant element with a partial mass density of $1.5 - 3.5 \frac{\mu g}{cm^2}$. In the area of the dark line the partial mass

densities of S and Zn rise up to $11 - 13 \frac{\mu g}{cm^2}$. O also has a higher partial mass density of $6 - 8 \frac{\mu g}{cm^2}$ in this area.

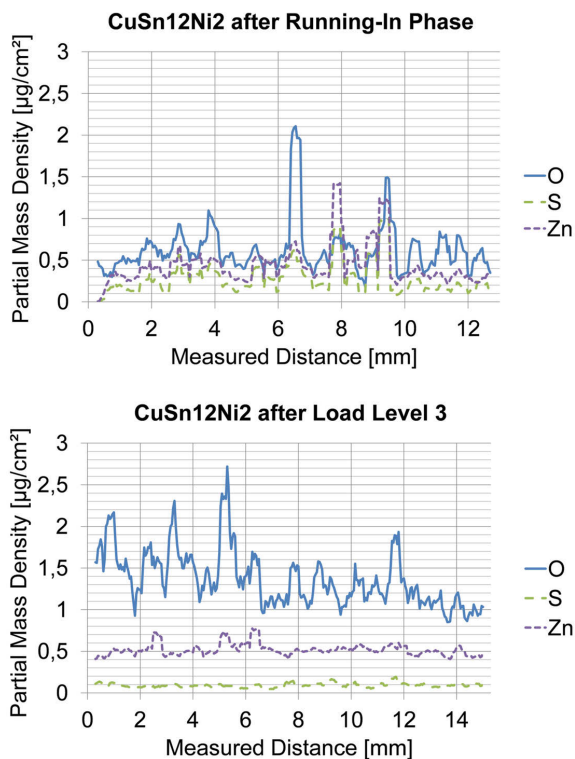


Figure 3: EPMA measurements of CuSn12Ni2 after thrust bearing tests

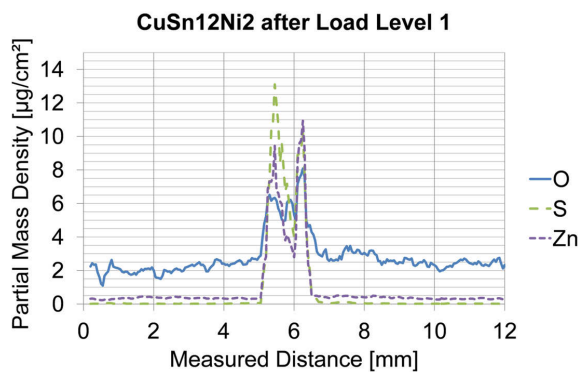


Figure 4: EPMA measurements of CuSn12Ni2 after axial piston pump tests

FIB/TEM analyses were performed on thrust bearing specimens. **Figure 5** shows the TEM image of a FIB foil, which is polished to a thickness of a few nanometers and the EDX spectrum at measuring point EDX03.

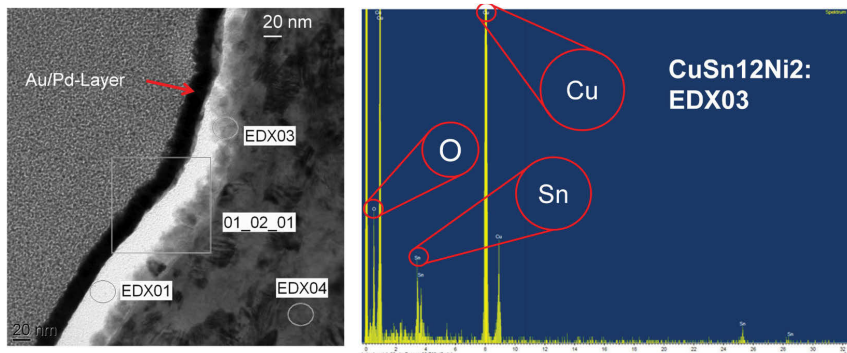


Figure 5: TEM and EDX measurements of CuSn12Ni2 after thrust bearing tests

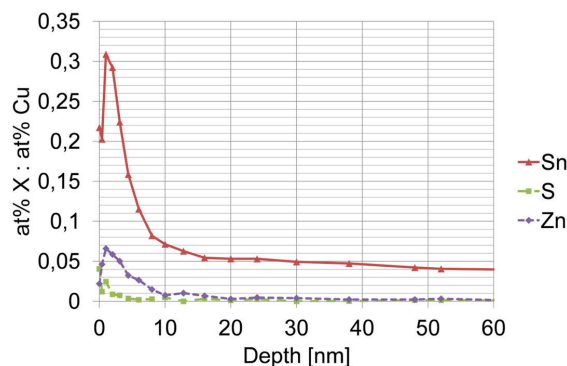


Figure 6: XPS measurements of CuSn12Ni2 after thrust bearing tests

The TEM image shows an Au/Pd-layer which is applied artificially upon the surface during the characterisation process. Underneath that layer the tribolayer is visible. It is divided in a bright oxygen-rich layer (measuring point EDX01) and a grey layer which contains Sn apart from Cu and O (measuring point EDX03). The tribolayer is about 30 – 50 nm thick. Underneath it the ground material begins where no elements from the environment are present (measuring point EDX04).

XPS analyses also detected Zn and S in the top 5 – 10 nm of the surface. Furthermore, an enrichment of Sn is detected in the top 20 nm (see **figure 6**).

4. Discussion

From the test conducted in this study, we conclude that CuSn12Si2 functions very well as bearing material in highly stressed conformal sliding bearing contacts. Most research in this area focuses on the influence of hardness, elastic modulus and solid-state contact pressure. Undoubtedly, those have great influence on friction and wear, however, another important factor should not be left aside: the formation and effect of tribolayers. Other materials with higher hardness and elastic modulus than CuSn12Ni2 show much higher friction and wear in the introduced thrust bearing tests, but they differed strongly in tribolayer composition.

Similar results are observed in axial piston pumps. Most lead-free materials which were tested to substitute the leaded bronze never reached load level 3 in the axial piston pump tests. They failed because of exceeding wear that lead to unacceptable leakage. Although other materials seem to be more promising in terms of mechanical strength properties CuSn12Ni2 reaches load level 3 without unacceptable wear and leakage.

To characterise the tribolayers on CuSn12Ni2 that lead to those positive results in both tests performed EPMA, FIB/TEM and XPS analyses were performed. EPMA analyses show a stable oxide-rich layer on CuSn12Ni2 that contains zinc and/or sulfur in highly stressed areas. Especially on the cylinder in the axial piston pump tests the dark lines which mark the areas of highest contact pressure contain high amounts of zinc and sulfur. This is due to the fact, that the anti-wear (AW) additive ZnDDTP functions best in areas of high temperature and high pressure. The effect mechanism of ZnDDTP is controversial and is out of the scope of this study. It is known that in some way the ZnDDTP molecules get split up, and the individual parts of the molecule can have an effect on the sliding surfaces (/9/).

In the tribological contacts investigated in this study, mainly zinc and sulphur react with the raw material and ensure low wear. Zinc is more common in the thrust bearing specimens, and sulphur is more common in the cylinder of the axial piston pump. Consequently, sulphur has its greatest effect at high surface pressures while zinc is more active in mild mixed friction.

XPS- and TEM-analyses confirm these findings. The thickness of the tribolayer can be determined to 30 – 50 nm. Furthermore, XPS measurements suggest that tin also plays a role in tribolayer formation probably as binding partner for oxide, zinc or sulfur.

5. Conclusion

In this study, the lead-free material CuSn12Ni2 was tested in two test rigs to investigate its usability in the contact between cylinder and control plate in an axial piston pump with swashplate design. Special focus was set on the influence of tribolayers that form on the surface of CuSn12Ni2 due to chemical reactions initiated by the tribological stresses. The main findings are listed as follows:

- The lead-free bronze CuSn12Ni2 shows good wear results both in the thrust bearing tests and in the axial piston pump tests.
- Those good results cannot be explained by mechanical properties alone.
- Tribolayers on CuSn12Ni2 consist of oxygen, zinc and sulphur in different compounds with copper and tin.
- Tribolayers on CuSn12Ni2 ensure additional wear resistance.
- The thickness of the tribolayer varies between 30 – 50 nm and can be subdivided into an oxide-rich top layer and a Sn-rich bottom layer in some areas.

The individual influence and composition of the separate tribolayer molecules is not yet fully understood. More research has to be conducted in this area. Nevertheless, it is now obvious that the influence of tribolayers should be taken into account when searching alternative materials in highly stressed tribological contacts.

6. Acknowledgement

The author gratefully acknowledges financial support by the European Union and the federal state North Rhine-Westphalia through the project "Nanotechnisch optimierte Gleitlager" (w1001nm006a). Furthermore, I would like to thank Univ.-Prof. G. Jacobs and the Institute for Machine Elements and Machine Design at the RWTH Aachen University for the support during my work.

7. References

- /1/ *Richtlinie 2000/53/EG des Europäischen Parlaments und des Rates über Altfahrzeuge*, European Parliament and European Council 2000/53/EG, 2011.
- /2/ J. Andersson, "Modelling of wear and tribofilm growth," PhD Doctoral Thesis, Department of Engineering Sciences and Mathematics, Lulea University of Technology, Lulea, 2012.

- /3/ A. Naveira Suarez, "The behaviour of antiwear additives in lubricated rolling-sliding contacts," Phd Doctoral Thesis, Division of Machine Elements, Lulea University of Technology, Lulea, 2011.
- /4/ T. Wolf, "Schmierstoffabhängiges Verschleißverhalten als Basis für ein Lebensdauermodell von axial belasteten Wälzlager bei Grenzreibung," PhD Doctoral Thesis, Faculty of Mechanical Engineering, RWTH Aachen University, 2008.
- /5/ C. Hentschke, „Prognose des Verschleißverhaltens langsam laufender Wälzlager unter Berücksichtigung der Reaktionsschichtbildung“, PhD Doctoral Thesis, Faculty of Mechanical Engineering, RWTH Aachen University, 2012.
- /6/ G. Burghardt, G. Jacobs, and C. Hentschke, "Einfluss von Einlaufprozessen auf die Ausbildung von Verschleiß schützender Triboschichten im Wälzlager," in *Reibung, Schmierung und Verschleiß: Forschung und praktische Anwendungen; 54. Tribologie-Fachtagung*, Göttingen, 2013, pp. 57-68.
- /7/ W. Weißbach, *Werkstoffkunde* vol. 16. Wiesbaden: Friedr. Vieweg & Sohn Verlag, 2007.
- /8/ L. Deters, "Calculation of high speed axial bearings with circular slippers," *KONSTRUKTION*, vol. 39, pp. 169-178, 1987.
- /9/ J. Schulz and W. Holweger, *Wechselwirkung von Additiven mit Metalloberflächen*. Renningen: expert verlag, 2010.

8. Nomenclature

$R_{p0,2}$	Yield strength	MPa
R_m	Tensile strength	MPa
$\sigma_{d0,2}$	Compression yield strength	MPa
ν	Kinematic viscosity	mm ² /s

A Flow Control System for a Novel Concept of Variable Delivery External Gear Pump

Prof. Andrea Vacca, PhD

Maha Fluid Power Research Center, Purdue University, Lafayette, IN, 47905, USA

E-mail: avacca@purdue.edu

Ram Sudarsan Devendran, PhD

Maha Fluid Power Research Center, Purdue University, Lafayette, IN, 47905, USA

Abstract

This paper describes a novel concept for a low cost variable delivery external gear pump (VD-EGP). The proposed VD-EGP is based on the realization of a variable timing for the connections of the internal displacement chambers with the inlet and outlet ports. With respect to a standard EGP, an additional element (slider) is used along with asymmetric gears to realize the variable timing principle. Previously performed tests confirmed the validity of the concept, for a design capable of varying the flow in the 65%-100% range.

Although the VD-EGP concept is suitable for various flow control system typologies (manual, electro-actuated, hydraulically flow- or pressure- compensated), this paper particularly details the design and the test results for a prototype that includes both a manual flow control system and a pressure compensator. Flow vs pressure and volumetric efficiency curves are discussed along with transient (outlet flow fluctuation) features of the VD-EGP.

KEYWORDS: Variable Displacement Pump, Variable Flow Pump, External Gear Pump

1. Introduction

External gear pumps (EGPs) are widely used in several fluid power applications due to their reliability, low cost, high compactness, good efficiency, good tolerance to contaminants and cavitation. However, the classic EGP design (Fig. 1) is inherently fixed displacement, consequently generation of flow “on demand” cannot be achieved unless controlling the shaft speed. This has limited the diffusion of inexpensive EGPs to modern and high energy efficient hydraulic machines, which are based on architectures layouts that requires variable displacement hydrostatic units. This limitation has driven the effort of many researchers from both academia and industry for formulating variable displacement solutions based on the external gear design. The several different solutions

that have been proposed can be broadly categorized in two sets. The first set is given by the solutions that change the meshing length of the gears (through relative axial motion between the gears), like those described in /1,2,3,4/. The second set of ideas is based on variation of the interaxis of operation of the gears, as described for example in /5,6/. However, none of these solutions has encountered successful commercialization for high pressure applications due to the major issues related to the implementation of movable gears in an EGP design: sealing of the displacement chamber, achieving proper power transmission between the gears, obtaining a good balance of the internal parts for all operating conditions. For these reasons, these solutions can be implemented with reasonable cost and performance only for low pressure applications, such as the automotive application documented in /7/.

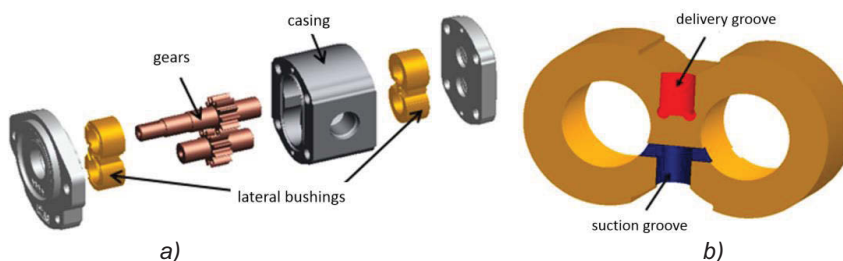


Figure 1: Pressure compensated EGP: exploded view (a), lateral bushings (b)

The authors' have proposed a different concept for variable delivery (VD) EGP that preserves all advantages of traditional EGPs. The novel concept, which will be described in §2, is based on the realization of a variable timing for the connections of the tooth space volumes (TSVs) with both the inlet and the outlet. The solution does not require axial or radial motion of the gears, and for this reason is suitable for high pressure applications. The basic idea was first presented in /8/: in this work a proper design of the gears was presented to permit a flow variation range in the 68-100% interval. Simulation results and proof of concept tests were also discussed to show the potentials of the solution. In /9/, the authors showed that a higher range of flow variation could be achieved by varying the design of the gears.

In this work, a working prototype of the VD-EGP that utilizes the same gears introduced in /8/ is described. The architecture chosen for the flow control system, described in §3, implements in a single device both the manual control of the flow and the pressure limiter, which reduces the displacement only if a certain set pressure is reached at the pump outlet. The last §4 is dedicated to the discussion of the experimental results obtained by the prototype, as concerns steady-state performance and outlet pressure fluctuations.

2. Description of the VD-EGP

The VD-EGP realizes a variation of the timing of the connections of the TSVs with the inlet/outlet lateral grooves machined in the lateral bushings. This timing variation is achieved with the introduction of a single-axis movable element, the *slider* in Fig. 2.

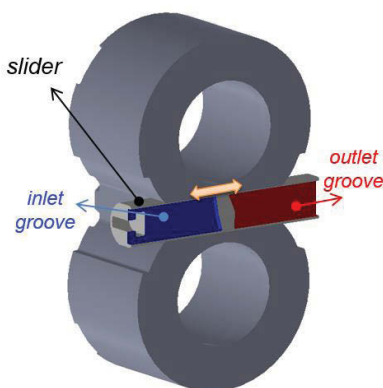


Figure 2: Slider in the bearing block

The position of the slider, which could be also placed in the pump casing for a non-pressure compensated EGM, determines the amount of flow displaced by the unit per revolution of the shaft. In order to understand the mechanism of operation of the VD-EGP, the displacing action for an EGP is shown in Fig. 3. In Fig. 3a, a reference TSV is highlighted; in Fig. 3b, the TSV volume is plotted as a function of the shaft angle.

The displacement of the fluid in the EGP occurs in the angular interval θ , which defines the meshing region. Within this angular interval, there is a sub-interval in which the TSV is trapped between points of contact. The limits of this subinterval are indicated with D and S, which normally (if the contact occurs in the involute part of the tooth) lies on the line of action. In the region D-S, the displacing action is permitted by the inlet/outlet grooves machined in the bearing block (the trace of the grooves is represented in Fig. 3a). In a standard EGP, the commutation of each TSV from the outlet to the inlet is realized when the volume is minimum (point M in Fig. 3a), so that the max volumetric capacity of the pump is utilized. Nevertheless, a small degree of cross-porting will be necessary to obtain an optimal performance in terms of minimizing internal pressure peaks, cavitation and fluid borne noise emissions /10,11/.

In the proposed VD-EGP, the slider (Fig. 2) is capable of a single degree of motion as represented by the arrow; hence, it can vary the position of these grooves affecting the

angular position at which the commutation between the connections of each TSV with the inlet/outlet ports occur. If the slider is positioned at a different location, the inlet/outlet commutation of each TSV occurs at a location different than M, thus a different net flow is displaced by the unit. It is important to notice that this concept is valid only if the commutation point is established by the slider in the angular region D-S; outside this range the slider would realize a direct bypass connection between the inlet and outlet port through the gear depth, being the volume not trapped between contact points.

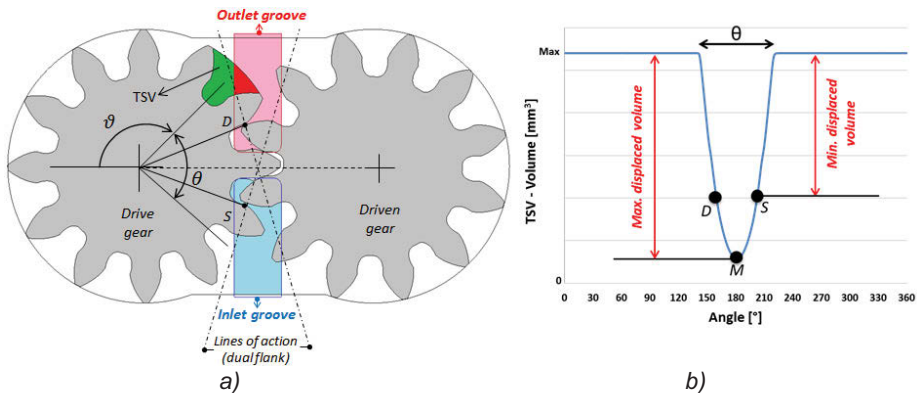


Figure 3 – a) Displacing action for a dual flank EGP; b) TSV volume variation

More details on this concept are described in /8/. In particular, in this work it is detailed the difficulty of achieving a high flow variation range with conventional gear profiles, due to the proximity of the location of points D and S with point M (Fig. 3). For this reason, an unconventional asymmetric tooth profile was chosen, and a numerical optimization procedure based on the software HYGESim (HYdraulic GEAr machines Simulator, /12/) was used to define the optimal tooth profile along with the shape of the grooves to be machined in the slider. In /8/, the authors also presented experimental results obtained from a prototype EGP that used the new gears and two alternative shapes for the grooves machined in the lateral bushings (Fig. 1): one for the maximum flow (100%) and one for the minimum flow (68%). These results permitted not only the validation of the numerical approach, but also showed the potentials of the approach for efficiently the flow of an EGP; in fact a torque reduction in the same order of the flow reduction was observed from all the performed tests. These promising results motivated the following research step aimed at designing an actual prototype that includes a flow actuation system.

3. VD-EGP Prototype

The gears and the slider grooves shape optimized in /8/ were used in this work to implement a fully operational prototype of the VD-EGP. The rationale behind the chosen design for the prototype can be summarized by following points:

- Opportunity of adding the flow regulation system to an existing commercial unit. In this way it can be shown that the VD-EGP could potentially be considered as an add-on feature for commercial pump. This also permitted to reduce the manufacturing cost of the prototype, since the case, the covers and the bearings are those of the existing commercial unit. The commercial unit chosen was an $11.2 \text{ cm}^3/\text{rev}$ CASAPPA PL 20.
- Need of testing the pump operation for well-defined fixed positions for the slider (manual control of flow rate).
- Demonstrate the easiness of implementing hydraulically compensated strategies for the flow regulation system. The case of a pressure compensator (or pressure limiter) was chosen.

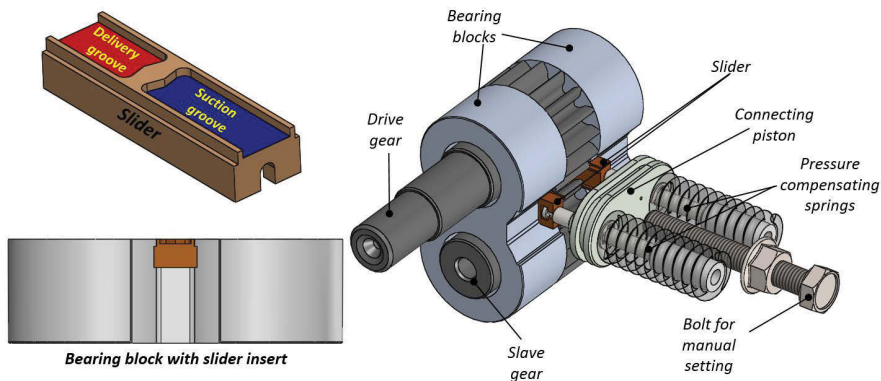


Figure 4 – Slider and its placement on the bearing block (left), complete flow control system (right)

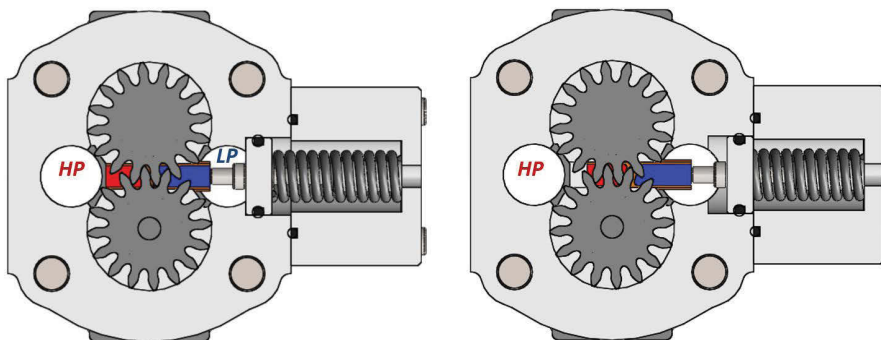


Figure 5 – Operation as pressure compensator: max flow (left) min flow (right)

The Figs. 4 and 5 show the implementation of the flow regulation system on the existing pump: in particular, Fig. 4 shows the different elements used to accomplish both the function of manual adjustment of the flow as well as functioning as pressure compensator. An adjustable bolt is used to force the slider at specific locations (manual setting). In case the bolt is removed or placed far away from the connecting piston (Fig. 4), the operation as pressure compensator is achieved. This operating mode is illustrated in Fig. 5: the delivery pressure acts at one side of the slider, against the spring force. The setting for the spring force used for the VD-EGP in this work was 100 bar.

End stops can be used to limit the position of the slider within the max and min flow range. However, the min flow range end stop can be removed to enable the functioning as pressure relief. In fact, if the slider is moved beyond the min flow position, a bypass flow is established between the outlet and inlet port. For the proposed VD-EGP prototype, the overall slider displacement, to achieve the full flow variation range, is about 6 mm. This displacement range is sufficient for achieving good sensitivity for both the actuation systems considered in this work.

The actual implementation is shown in the picture of Fig. 6.

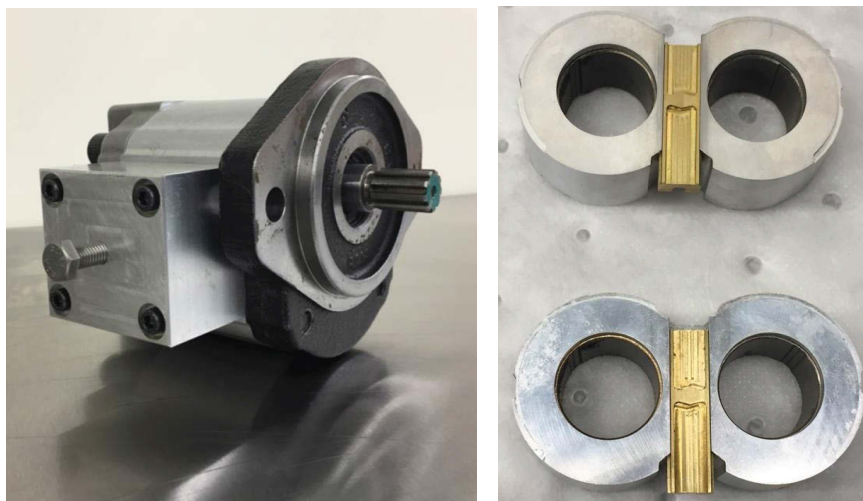


Figure 6 – Picture of the VD-EGP prototype. Details on the lateral bushings

4. Test Results

The VD-EGP of Fig. 6 was tested at the Maha Fluid Power Research Center in accordance with ISO 4409, with the circuit of Fig. 7. An ISO VG46 oil was used for the tests, at a controlled temperature of 50°C. Before performing the tests, the pump case was broken-in by using the commercial gears. This slightly penalizes the optimal radial (at tooth tip) sealing of the VD-EGP, however prototype gears couldn't be used because they were not properly heat treated.

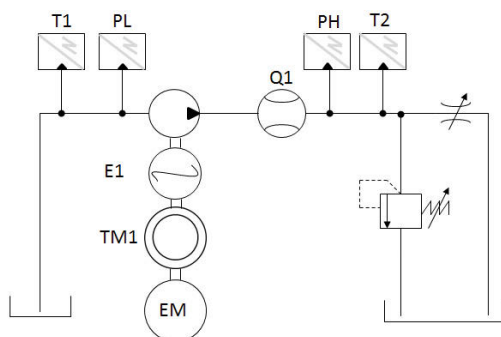


Figure 7 – Hydraulic circuit used for the pump characterization

4.1. Performance of VD-EGP with Manual Setting

By setting the adjustable bolt of Fig. 4 in several positions, it was possible to test the VD-EGP prototype in different positions. Three different settings were chosen for plotting the experimental results in Figs. 8 and 9: 100%, 84% and 68% of maximum flow.

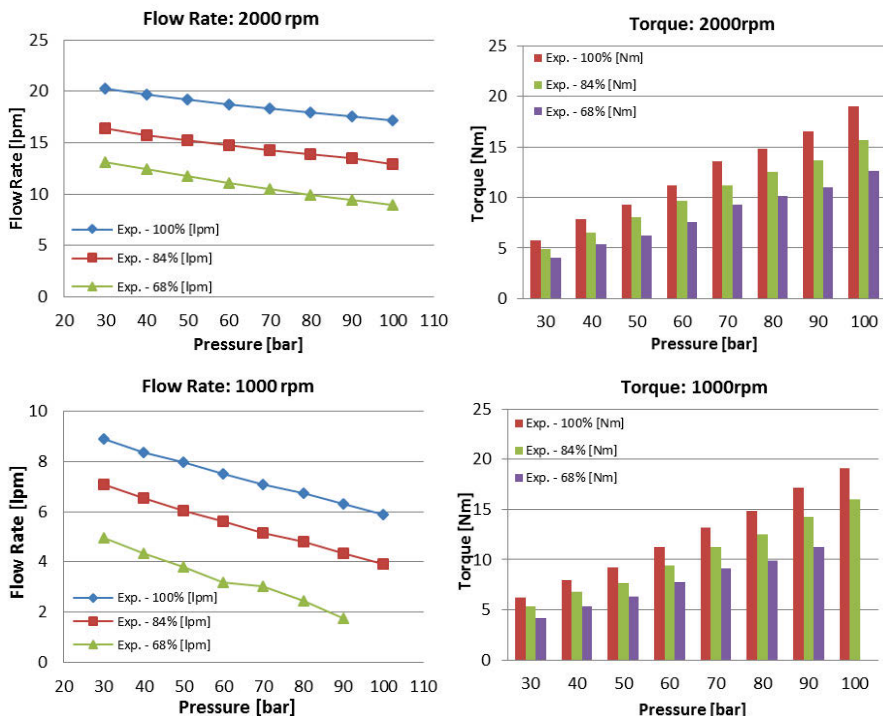


Figure 8 – Operation as pressure compensator: max flow (left) min flow (right)

Figure 8 shows the flow rate vs. pressure and the shaft torque vs. pressure for 1000 rpm and 2000 rpm. The maximum pressure during the test was limited to 100 bar due to the absence of final hardening process on the gears, which would bring the VD-EGP to operate up to 250 bar as the commercial unit taken as reference. The torque plots demonstrate that the shaft torque reduces with the displacement. This is in accordance to the VD-EGP variable timing operating principle, which keeps the TSV pressurized for a longer time during the meshing process, thus decreasing the torque request [8/].

The flow rate plots of Fig. 8 point out a significant decrease in flow rate at a given setting for the slider due to volumetric losses. In terms of volumetric efficiency, this effect can be shown in Fig. 9.

Due to the fact that radial leakages (at the tip of teeth) as well as axial leakages (at the lateral side of gears) ideally do not vary with the slider position, it is expected

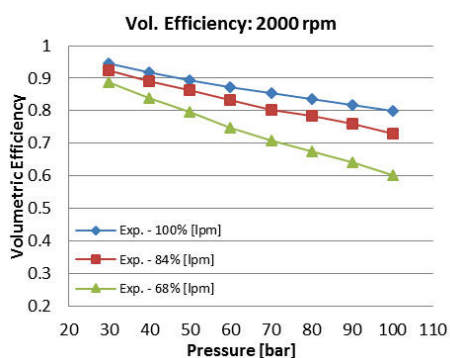


Figure 8 – Volumetric efficiency of

a reduction of volumetric efficiency at reduced flow setting.

the VD-EGP prototype

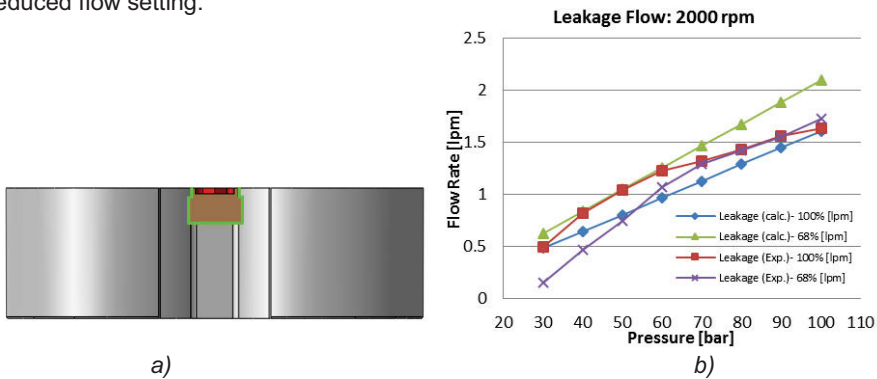


Figure 9 – Additional leakages introduced by the slider

Reasons for efficiency levels lower than a conventional EGP are the imperfection of the gears (realized with a wire electric discharge machining process) and the break-in process used for the VD-EGP prototype described above. However, this do not explain the rapid decrease of volumetric efficiency with pressure which was not observed in the proof of concept tests described in /8/, which utilized the same gears and similar pump case described but in absence of the slider and flow regulation system. In order to better understand source of additional volumetric losses in the VD-EGP prototype, the results of Fig. 8 and the similar one from the proof of concept tests of /8/ were used to derive the additional leakages introduced by the apparatus of Figs. 4 and 5. These results are reported in Fig. 9b, as “exp.” curves; “calc.” curves indicates the results of the Poiseuille’s eq. for the leakages at the slider surfaces (in green in Fig. 9a):

$$Q_{leak} = \frac{h^3}{12 \cdot \mu} \cdot \frac{\Delta p}{L} \cdot b \quad (1)$$

Where, h is the gap height, L is the gap length (which depends on the slider position), b is the gap width and Δp is the difference in pressure across the gap. The comparison between the two trends of Fig. 9 shows how the additional reduction of volumetric efficiency – respect to what expected for a standard EGP, is essentially due the green leakage path of Fig. 9a. Two important considerations can be derived from the result of Fig. 9b:

- The flow control system of Fig. 4, and in particular the slider, didn’t compromise the axial or radial balance of the gears, since additional leakages are only due to the bypass path created by the slider
- The leakages for the VD-EGP could be significantly reduced in case of: a) a lower clearance between the slider and its seat on the bushing were used (the value

obtained for the prototype was higher than a typical clearance of a spool valve); b) a simplified different of the VD-EGP that uses only one slider were used. In fact, only for long gears it would be necessary to use a dual-slider design as the one shown in Fig. 4; c) a seal were introduced between the slider and its seat on the bushings. All these three options are taken into account for the creation of a future VD-EGP high efficient prototype.

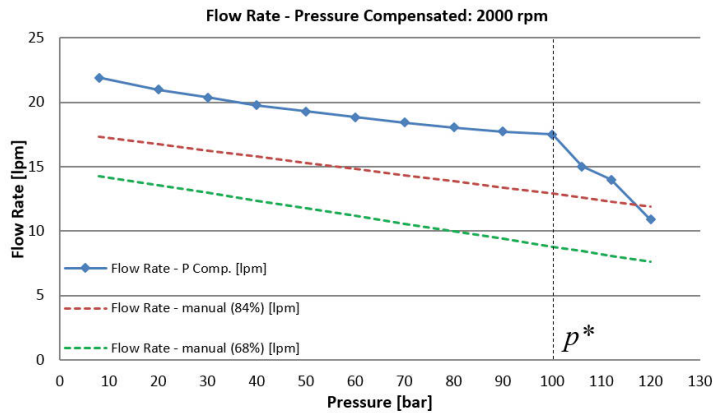


Figure 10 – Tests on VD-EGP (pressure compensator): flow rate vs. pressure

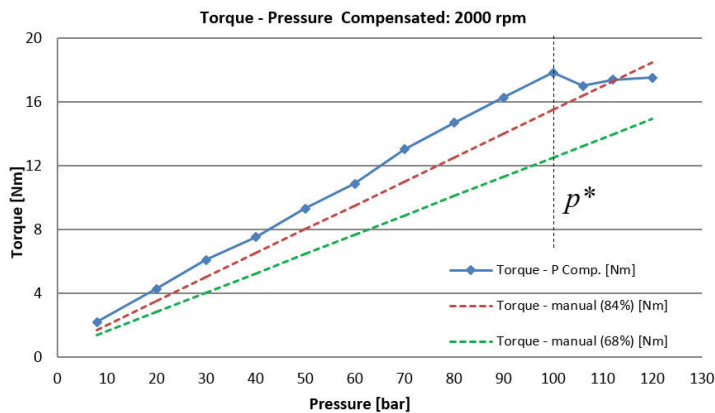


Figure 11 – Tests on VD-EGP (pressure compensator): torque vs. pressure

4.2. Performance of VD-EGP with Pressure Compensator

The operation of the VD-EGP with the pressure compensator was tested using the same test circuit of Fig. 7. Measured flow rate vs. pressure characteristic is shown in Fig. 10 (blue curve). The characteristic resembles the 100% flow curve of Fig. 7 until the pressure reaches the setting p^* . For higher pressure, the flow reduces without requesting

for additional torque, as shown in Fig. 11. The dotted lines in both Figs. 10 and 11 show the characteristics achieved by the measurements of §4.1.

5. Conclusions

This paper presented a working concept for Variable Delivery External Gear Pump (VD-EGP), particularly focusing on the implementation of a prototype that includes the flow variation system. Two different actuation systems were considered: (1) a manual actuation system in which the user can set the level of output flow; (2) a pressure compensator that adjust the outlet flow when a specific pressure setting is reached.

The results focused on the measured steady-state features (flow rate and torque vs. pressure; volumetric efficiency) of the VD-EGP prototype, and demonstrate the validity of the concept for efficiently varying the flow displaced by an external gear machine without compromising the key features of low cost and limited number of parts. Essentially, the VD-EGP design is based on the introduction of a slider at the lateral side of the gears of a traditional EGP, and this can be successfully implemented for both high pressure and low pressure applications. The VD-EGP prototype discussed in this work show the case of a high pressure design (up to 250 bar), although during the experiments the max pressure was limited to 120 bar due to the absence of proper treatment on the gears. The results highlight the design challenge related to the additional leakages introduced by the slider, and possible solutions that will be considered in future VD-EGP development are discussed.

The future work will also focus on more aggressive modification of the gears profile, to achieve a higher range of efficient flow variation.

6. References

- /1/ Winmill, L.F., 2001, Adjustable-Displacement Gear Pump, Patent Application Publication, US2001024618.
- /2/ Bussi, E., 1992, Variable Delivery Gear Pump, European Patent Application, EP0478514.
- /3/ Hoji, T., Nagao, S., Shinozaki, K., 2008, Gear Pump, Patent Application Publication, US2008044308.
- /4/ Clarke, J.M., 2002, Hydraulic Transformer using a Pair of Variable Displacement Gear Pumps, Patent Application Publication, US2002104313.

- /5/ Yang, D., Zhong, D., 1987, Radial-Movable Variable Displacement Gear Pump (Motor), CN85109203.
- /6/ Reiners, W., Wiggermann, W., 1960, Variable Delivery Gear Pumps, The Patent Office London, GB968998.
- /7/ Voigt D., 2011, Variable Flow Spur Gear Oil Pump for Utility Vehicles Engines, MTZ Worldwide eMagazine, Vol. 72, issue 4, pp.24-29.
- /8/ Devendran, R., Vacca, A., 2014, A novel design concept for variable delivery flow external gear pumps and motors, International Journal of Fluid Power, 15:3, 121-137.
- /9/ Devendran, R.S., Vacca, A., 2015, A Novel Concept for a Variable Delivery External Gear Machine, 14th Scandinavian International Conference on Fluid Power, May 20-22, 2015, Tampere, Finland.
- /10/ Borghi M., Milani M., Zardin B., Paltrinieri F., 2006, The Influence of Cavitation and Aeration on Gear Pump and Motors Meshing Volume Pressures, IMECE2006, ASME Int. Mechanical Engineering Congress and Exposition, November 5-10, Chicago, IL, USA.
- /11/ Casoli, P., Vacca, A., Franzoni, G., Guidetti, M., 2008, Effects of Some Relevant Design Parameters on External Gear Pumps Operating: Numerical Predictions and Experimental Investigations, 6IFK Internationales Fluidtechnisches Kolloquium, 31 March – 2 April 2008, Dresden, Germany.
- /12/ Vacca, A., Guidetti, M., 2011, Modelling and Experimental Validation of External Spur Gear Machines for Fluid Power Applications, Elsevier Simulation Modelling Practice and Theory, 19 (2011) 2007–2031.
- /10/ Borghi M., Milani M., Zardin B., Paltrinieri F., 2006, The Influence of Cavitation and Aeration on Gear Pump and Motors Meshing Volume Pressures, IMECE2006, ASME Int. Mechanical Engineering Congress and Exposition, November 5-10, Chicago, IL, USA.

7. Acknowledgment

This research was supported by the Center for Compact and Efficient Fluid Power (CCEFP), a National Science Foundation (NSF) Engineering Research Center (Project 1F.1) funded under cooperative agreement number EEC-0540834. The authors also would like to thank Casappa SpA for providing some of the components used in the VD-EGP prototype.

8. Nomenclature

L	Gap length	mm
Q_{leak}	Leakage Flow	L/min
b	Gap width	mm
h	Gap height	mm
p^*	Spring set pressure	bar
μ	Fluid viscosity	Pa s

Abbreviations

EGP	External Gear Pump
TSV	Tooth Space Volume
VD	Variable Delivery

Brimming bubbles?

On an Innovative Piston Design of Dosing Pumps

Dr.-Ing. Axel Müller, Dipl.-Ing. Mike Heck, Dr.-Ing. Olaf Ohligschläger

Thomas Magnete GmbH, San Fernando 35, 57562 Herdorf, E-mail: info@thomas-magnete.com

Professor Dr.-Ing. Jürgen Weber, Dipl.-Ing. Martin Petzold

Institut für Fluidtechnik (IFD), Technische Universität Dresden, Helmholtzstraße 7a,
01069 Dresden, E-mail: mailbox@ifd.mw.tu-dresden.de

Abstract

For delivery, dosing and pressure control of fluids in mobile and stationary applications electromagnetically operated piston pumps are an established solution. The volume per stroke is exactly defined by the geometry. Nevertheless cavitation, more likely with the new fuel blends containing a high proportion of ethanol /1/, deteriorates the dosing precision of the liquid portion.

One important criterion of precise metering is the transport of the liquids through the reciprocating piston pump without transferring bubbles. Especially, pumping in the range of vapour pressure of gasoline fuels implies challenges for precision. The objective of this work is revealing potential sources of reduced cavitation by optimising the design. For doing so, optical investigations have been applied. In addition to this, cavitation can be diminished controlling the piston's travel externally.

The second important item covers pumping of degenerated fluids even without negative effects on the pump's performance. Up to now, wide, inefficient gaps or high force surplus are necessary. A new helix-design /2/ has been investigated and built up in order to reduce the described effort. The effects coming with the helix allow a permanent rinsing of the stressed surfaces, leading to lubrication and lower temperature loads. The results are shown in simulation, fundamental tests and is validated in practical pump operation.

KEYWORDS: metering, dosing pump, fuel, cavitation, automotive

1. Dosing pumps in automotive applications

Automotive dosing pumps have been available on the market for nearly 40 years now. Initially used for fuel fired heaters in mobile systems - trucks, passenger cars, e. g. -, this

type of a reasonable compact dosing unit nowadays is applied in many fields of applications. Based on the experience of delivering fuels of any kind, the dosing pump was further developed to deliver and dispense more or less any kind of liquid media /3/.

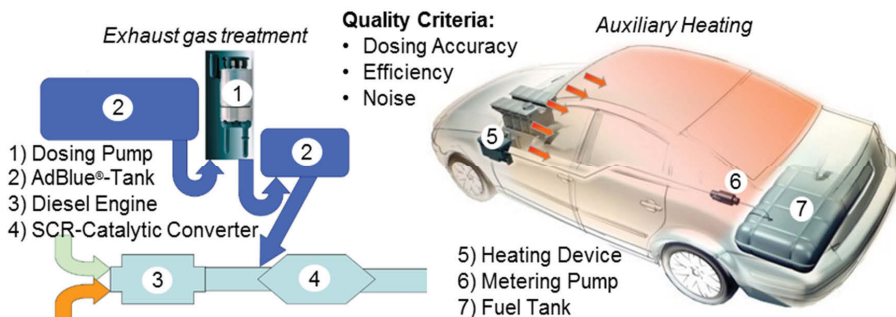


Figure 1: Auxiliary systems with metering pumps in automotive applications

Figure 1 shows the two most common fields of application as there are exhaust treatment systems, like SCR systems reducing NO_x, and the regeneration of diesel soot filters and several auxiliary heating systems.

Dosing units have to deliver the exact amount of liquid throughout their entire life in service. Hence, all pump designs were tested in long-term durability tests with different kinds of fuel, even worst-case bio-fuels containing aggressive substances, salt water or ethanol-blends. The global usage of metering units requires a robust design and robust material surfaces as they are in direct contact to the fluids. Therefore, these pumps have to be able to deliver all kind of fuels that are commercially purchasable as they have been tested with worse. Investigations are also performed to fulfil special demands for biomass fuels that potentially may degenerate. As they are designed as electromagnetically actuated piston pumps, the total flow rate is determined by the frequency of the piston's movement only, which is the basis for easy control to achieve the precise metering ability. Based on relevant test results, the interaction of dosing unit and the individual future fuels is taken into account /3/.

The rising percentage of bio-fuels cause previously unknown interactions with the materials of construction. Rubbers, metals and surfaces, which had been sufficient in the past, have to be replaced by more resistive materials with lower interactions to the fuels, a surrogate for zinc coatings may be stainless steel. Although refined chemical additives and more comprehensive tests on the fuel side should improve fuel quality, more resistant components are necessary. Especially higher temperatures in fuel systems and

more and more legal requirements make robust components of exhaust systems and even auxiliary systems essential.

Beside the chemical interactions between fluid and component, especially the two phase fluid flow is an important issue for fuel pumps. Bubbles of fluid vapour and air occur if the pressure is falling below the tank pressure. So it is indispensable to build up pumps which are able to handle and meter high- and low-volatility fluids.

1.1. Generation of gas bubbles

Gas bubbles are generated in areas where pressure drops or temperature rises. In **figure 2** the appearance of air bubbles is illustrated, when the pressure falls below the saturation pressure or the vapour pressure of the specific fluid.

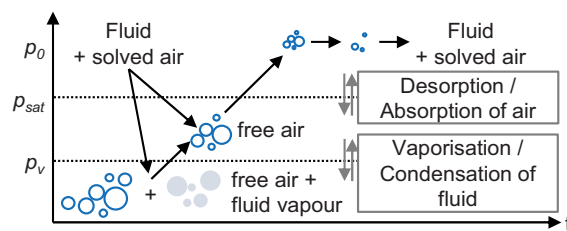


Figure 2: Generation of gas bubbles in fluids

Whereas the vapour pressure p_v depends on fluid and temperature, see **figure 3**, the saturation pressure p_{sat} depends on the history of the fluid – i. e. atmosphere, pressure

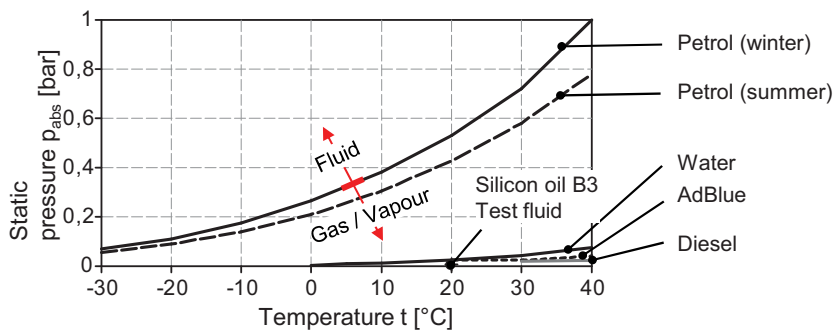


Figure 3: Vapour pressures of fluids at different temperatures

and temperature in the tank for the past time. For example, the saturation volume of air at 1 bar and 20 °C is in diesel: 11 Vol.-% /4/, in gasoline: 21 Vol.-% /4/ and in water: 1.87 Vol.-% /5/. Thus, gasoline is the most critical fluid in vapor pressure and air

saturation and there is a significant difference in winter and summer quality. The quantity of gas is a sum of vaporized fuel and air.

1.2. Pump design – one valve pump

There are mainly two different pump designs. The most popular is the “one valve one slot”-principle, see **figure 4**. The fluid flows into the pump where it has to stream around the armature to enter the pump chamber by passing the outer surface of the pump’s cylinder, i. e. the bearing of the piston and the metering bore. After that, the fluid fills the exactly defined delivery volume t_1 . When the piston overruns the metering bore, the fluid

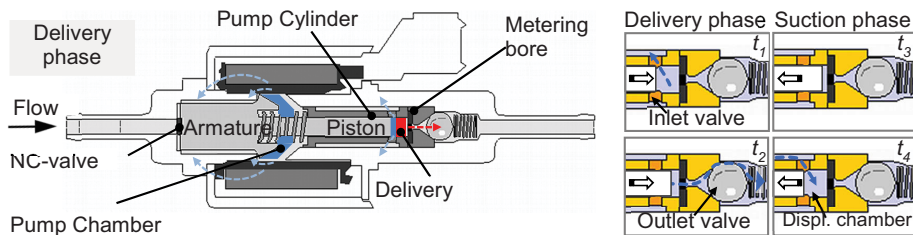


Figure 4: One valve pump

is pushed through the outlet valve t_2 . The armature is actuated by energizing the coil by applying a short voltage pulse. The piston travels actuated with 10 to 20 Hz, e. g. during the suction phase t_3 , the pressure in the delivery volume decreases to the level of vacuum pressure and bubbles release. The low pressure in the volume remains until new fluid enters the metering bores t_4 .

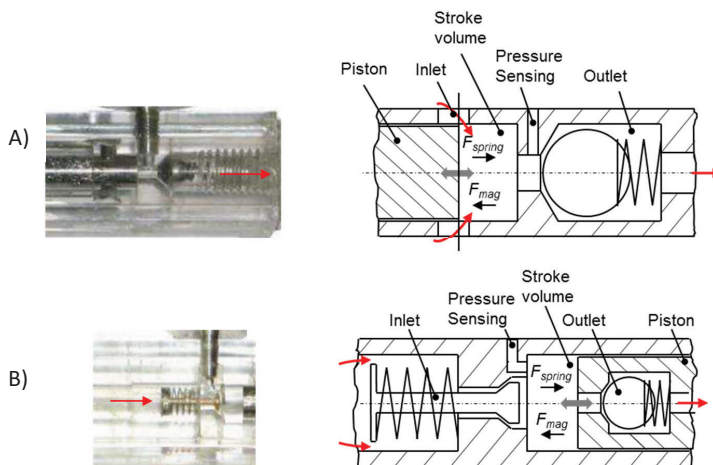


Figure 5: Transparent model of the one valve pump (A) and the two valve pump (B)

To make the effect of bubble release visible, the pump chamber for demonstration with metering bore and outlet valve is built in transparent plastic. The piston is actuated by a separate pump solenoid, see **figure 5**. A pressure sensor measures the pressure inside the displacement volume.

To examine the operation in detail the test bench, see **figure 6**, was build up. A high power LED emits short, triggered pulses of light through a PMMA Model of the displacement chamber and the light is captured by a light-sensitive high speed camera. The one valve design with metering bore shows a lot of air bubbles inside of the delivery chamber at the end of the suction phase.

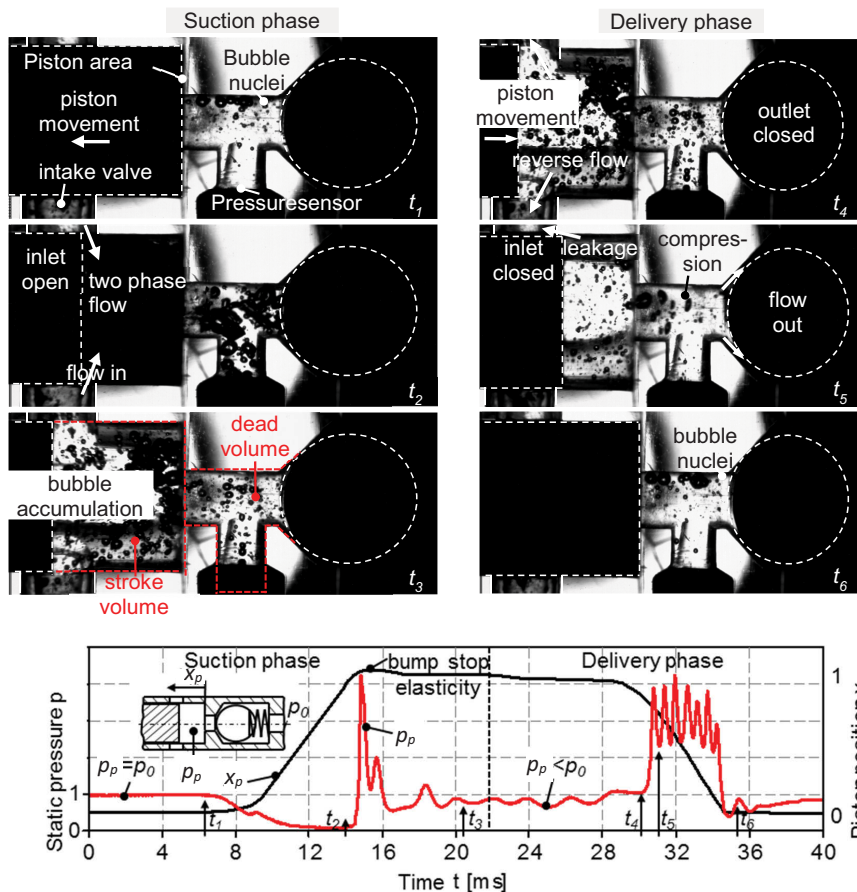


Figure 6: Work Cycle of the one valve pump

In figure 6, the corresponding position and pressure cycle are shown. Between the eleventh and fifteenth micro second, the pressure p_p reaches nearly vacuum ($p_p < p_v$, see figure 2) which explains the high volume of gas inside the delivery volume. This

originates not only from free air or air bubbles escaping from the fluid that contained inherent dissolved air, but also from evaporating fuel, see figure 2.

1.3. Pump design – two valve pump

Also the two valve piston pump was investigated with a transparent model, see figure 5. The inlet valve and the piston are original pump parts. The different phases of delivery are shown **figure 7**. Meanwhile the suction phase t_1 - t_3 , the intake valve opens with low difference pressure and the fluid – here test fluid – can flow in nearly free of bubbles. Even if little bubbles occur at the valve sleeve, see photo bottom left in figure 7, while the flow velocity is at its maximum, no bubble accumulation arises in the stroke volume.

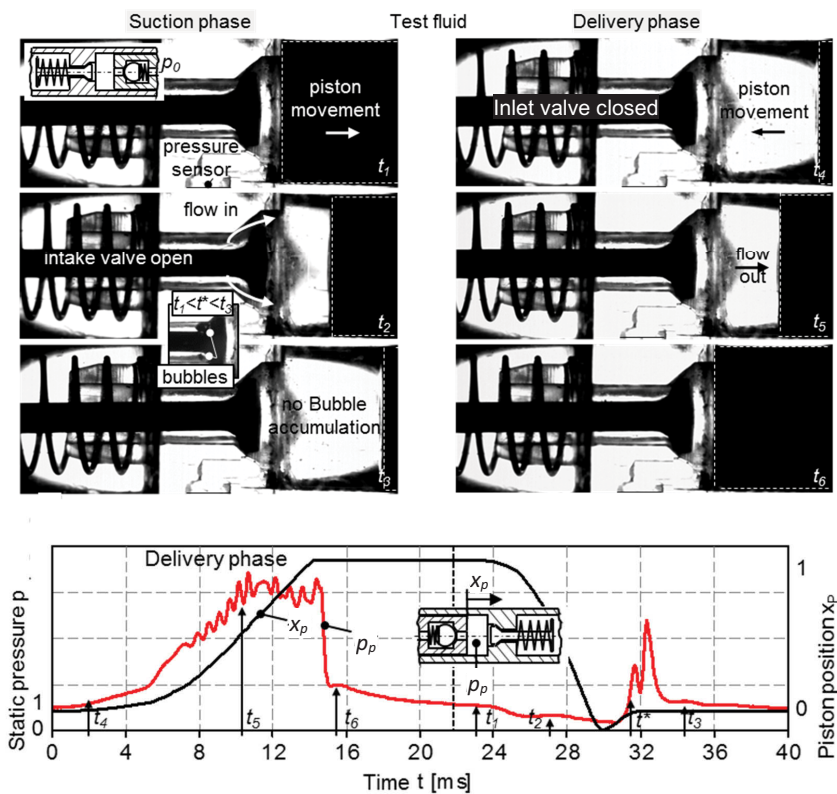


Figure 7: No bubbles in the fluid of the two valve pump during whole work cycle

During the delivery phase t_4 - t_6 , the pressure in the stroke volume is very high and the fluid is delivered through the piston into the fluid volume around the armature of the pump. In this phase, the volume around the armature and the pressure inside of that volume is almost constant.

1.4. Effect of bubbles for delivery

Low pressures, lower than tank pressure, create the evaporation of the fuel and lead to dissolving of air. Also, stationary air bubbles in the intake and the pump chamber cause a partial filling of the pump chamber. This reduces the efficiency of the delivery and may cause disturbances in the following advices.

To reduce unwanted effects of bubbles, an adequate pump design has to be found, avoiding low pressures in the suction area. That means that low flow resistances, a smooth piston movement and a low pressure input valve generate improvements. Otherwise, using a control bore in combination with a high pressure difference at low pressure level is disadvantageous, especially low boiling fluids have to be metered precisely. This characteristic of the pump and pump control has an increasing effect depending on the physical properties of the fluid. This is shown by a flow rate test with bubble detection, see **figure 8**.

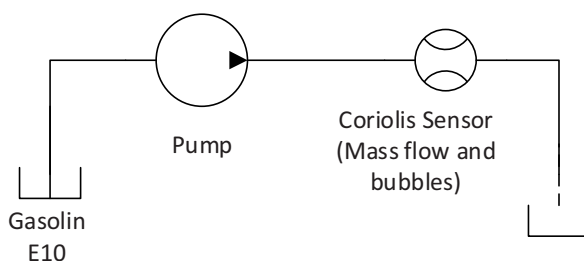


Figure 8: Test rig for pump delivery of mass flow and bubbles

The test rig was built up and operated in a climate chamber with a temperature of 30 °C and gasoline with 22 % Ethanol (E22). The pump has been connected with a short suction line and a 1 m pressure line of 2 mm diameter in effect comparable with automotive applications. The Coriolis sensor measures the volume flow and the fluid density.

Bubbles lead to high frequencies of high amplitudes of the Coriolis signal value shown in **figure 9**. Here also a significant effect of the pump control, voltage e. g., can be observed.

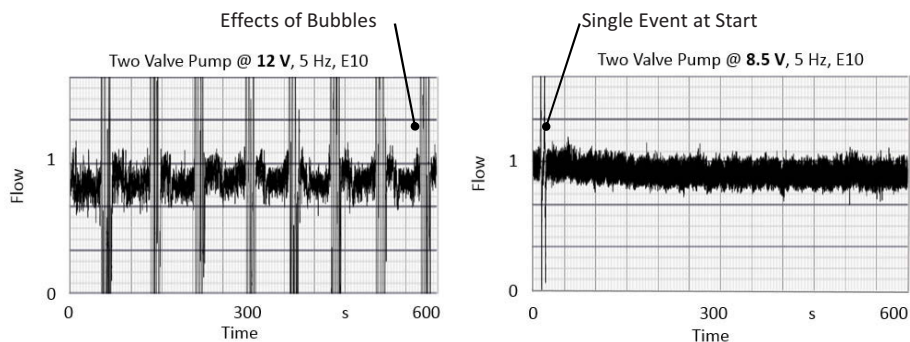


Figure 9: Result with different operating voltages (12 V and 8.5 V)

If the control voltage is unnecessarily high, shown in figure 9 left graph, a lot of bubbles are released and delivered in periodically intervals. The reduction of the voltage to 8.5 V avoids the generation of bubbles. A negligible reduction of the delivery rate is observed.

1.5. Pump design – two valve pump robust against critical fuels

As shown in the chapters before, pumps having two seat valves are to be preferred with respects to the precise delivery of liquids characterized by having low boiling pressures. Hence, the focus in this chapter is set on the pump types with two seat valves as inlet and outlet valve. Modern fuels are typically blends with a certain bio content. Either ethanol for gasoline fuels or biodiesel. Components that are in contact with these fuels have to meet specific requirements. As shown in literature /6/, degenerated biofuels generate deposits or attack surfaces, see also /7/. Thus, more robust pumps have to be designed and brought to market. In addition, ingredients of such bio fuels improperly blended with additives tend to degenerate. For which, an innovative design of the piston is investigated which is characterised by a helix groove in the surface. The intention is to avoid the setting up of deposits respectively layers of them. Inside state-of-the-art pumps liquids are delivered passing dedicated areas besides the gap between piston and cylinder. In **figure 10**, the change of the path of the liquid is illustrated. That gap normally is not wetted by design. With the improved design proposed, this especially dedicated area for the liquids flowing through the pump is just laid in the gap between the piston and the cylinder. This means that the main flow of fuel is passing this helix channel or these helix channels. By doing so, several advantages are won: A flooded gap means that the surfaces are not in direct contact, but are cooled by the liquid. Which then reduces the tribological stress of the surfaces. In case of degenerated fuels, the risk of generating deposits is significantly reduced, as these degenerated fuel contents are pumped through the pump in very little portions and do not settle down to surfaces.

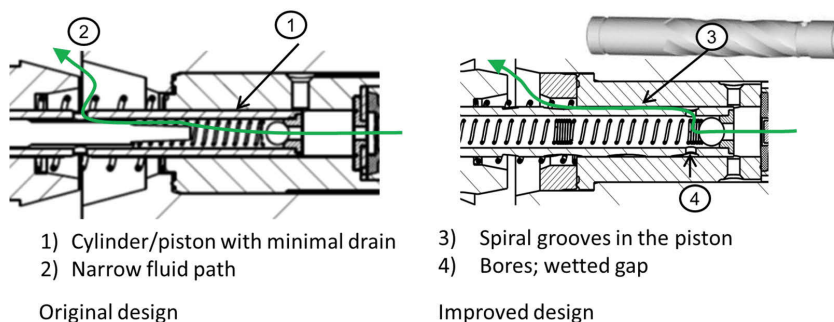


Figure 10: Two-valve pump type with helix grooves (right) at the surface of the piston

Because of the narrow gap ① and the small stroke a cleaning of that gap of a state-of-the-art-pump is not possible, for that reason, the risk of a motionless pump is implied if it is used with not specified fuels. This may be the case if deposits or degenerated fuel trespass the gap and accumulate and built up an adhesive joint between surfaces – ideal to withstand shear loads that are applied when the pump is actuated for further pumping. The improved helix-design leads the fluid from the bores ④ through the grooves of the piston ③. The aim is to rinse residues of fuel and contaminations from the critical areas – especially between piston and bearing. Alternatively, such defined fluid path respectively grooves could be made inside the inner surface of the cylinder. Doing so, no negative effects on the pump's performance even with degenerated fuels were observed. Of course, also these optimized pumps are not designed for pumping honey-like liquids of low viscosity. But this design widens the limits significantly.

As an example of such deposits, in **figure 11** main filters of two test benches positioned centrally are shown that act for a quantity of pumps showing different visual appearances. Both filters have been used in a durability test bench for several months of use. Meanwhile the filter used with proper diesel with a bio content of 20 % looks like new, the filter used with improper bio content is degenerated showing dark deposits.



Figure 11: Example of deposits originating from degenerated biodiesel B20

1.6. Hydraulic effects of the new design

Investigating the new helix design, the main intention is to ensure the performance under relevant conditions compared to the basic design. Therefore, the main functions: tightness, suction and leakage have been tested. All pumps, conventional and innovative helix design, are found to be comparable regarding their basic function. No leakage was observed at all, that's a safety function of course, the flow rate is situated within the specified range and even better with a deviation of approximately 4 %. Also the suction ability was immaculate. Hence, the innovative helix-design of the piston is a superb option for further exploration.

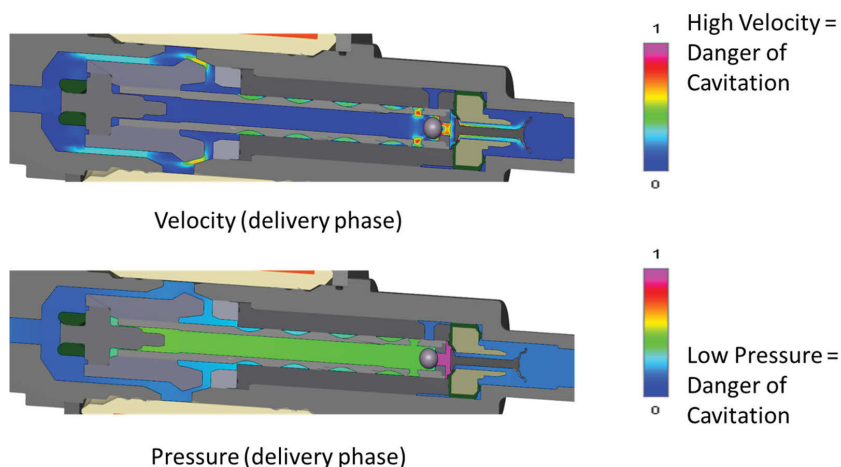


Figure 12: Two-valve principle with helix grooves at the piston

As described, the design has an optimal rinsing around the piston with relative high flow velocity inside of the grooves. The fastest flow occurs in the area of the pump chamber and the outlet valve in an area of high pressure. Here the pump is not able to create bubbles, as can be seen in **figure 12**. A second area of higher flow rates is the cone of the armature, see figure 10 detail ②, where the closing gap between armature and pole in combination with the high volume flow circulating around the armature might be a reason for cavitation. This effect depends on the magnetic force as a consequence of the operating voltage of the pump and refers to the delivery phase.

1.7. Durability test results with critical bio-fuels

As shown, the proposed design is improving the functionality of metering and delivering even bad qualities of bio fuel blends. The question is whether durability of these pumps is affected anyhow. Former studies have shown that properly designed fuel pumps

generally are able to pump bio fuels for a long time in service, see /8, 9/. But it is not proven that the benefits of the new helix design, avoiding deposits, e. g., lead to improvements in real systems. In order to investigate into the endurance behaviour of pumps with the new helix design of the piston, a durability test with challenging fuel qualities, both gasoline and diesel, was performed. The improved design showed no failure during an endurance test over lifetime with E22, diesel B20 and B30. Aggressive B20 showed polymerizing of the degenerated fuel. The pumps with the new helix-design worked properly for the full lifetime – even with this challenging fuel, i. e. 70 % longer compared to pumps having original piston design.

While observing deposits inside the gap between piston and cylinder, parts having pumped gasoline blends like E22 showed the most significant result: In **figure 13** pistons are presented after full durability test. At the original pistons without grooves a formation of deposits is visible whereas at the grooved pistons the running surface is absolutely bare and clean. The endurance test with B30 showed no characteristics at any test pump but it shows that pumps with suitable design for challenging biofuels withstand even unrealistically bad fuel qualities.



Figure 13: Effect of helix grooves at the piston (right) after durability test

2. Summary and outlook

By intensive experimental investigations it could be shown that an elaborate pump design with two valves – intake and outlet valve – has essential advantages compared to simpler systems and reduce cavitation effects like the occurrence of gas bubbles.

Considering the questions of metal-fluid interactions a new helix piston design has been proposed and tested successfully which even allows to rinse gaps between piston and cylinder of piston pumps dosing challenging fuel qualities. Even if these effects occur

only with age sensitive bio fuels it is an additional safety issue for the robustness of the pumps used for automotive auxiliary heater and exhaust systems, e.g.

3. Acknowledgements

The presented research is mainly part of the project KF245260RU3/KF3167601RU3 "Entwicklung einer neuartigen Apparatur zur Dosierung von Biokraftstoffen", which is funded by the Federal Ministry for Economic Affairs and Energy, Germany within the ZIM programme.

Supported by:



Federal Ministry
for Economic Affairs
and Energy

on the basis of a decision
by the German Bundestag

4. References

- /1/ Petzold, M.; Weber, J.; Dautry, E. et al: Analysis of the Flow Conditions in a Dosing Pump with Regard to New Fuels. 8th International Fluid Power Conference, Dresden, March 26-28, 2012, Dresden, Germany, pp. 385–398.
- /2/ Feckler, M.; Heck, M.; et al.: Hubkolbenpumpe mit durchströmtem Gleitlager, Patent DE 10 2012 006 780 A1, Thomas Magnete GmbH, Herdorf, 2012.
- /3/ Rolland, T.; Kappler, H.; Müller, A.: An experimental approach to the capability of metering units for future fuels. European Fuel Cell Forum 2011, June 28 – July 1, 2011, Lucerne Switzerland, Chapter 19 B 13-10/71.
- /4/ Landolt, H., Börnstein, R., Eucken, A.: Zahlenwerte und Funktionen aus Physik, Chemie, Astronomie, Geophysik und Technik. In: Anonymous . Springer, Berlin, 1962.
- /5/ Bollrich, G.: Technische Hydromechanik 1 : Grundlagen, 7. Auflage, Beuth, Berlin, 2013.
- /6/ N.N.; Abschlussbericht des Verbundprojektes: GoBio - Gezielte Optimierung von kraftstoffführenden Komponenten für biogene Kraftstoffe in mobilen Systemen, 2011.
- /7/ SAE J 1681: Gasoline, Alcohol, and Diesel Fuel Surrogates for Materials Testing: 2000-01-10.
- /8/ Müller, A.; Rolland, T.; Fjellgren, C.: Dosing units suitable to future fuels, in: Chahine, R.; Peppley, B.: Hydrogen + Fuel Cells 2011, Canada, 2011.
- /9/ Müller, A., Müller, M. , Rolland, T., Fjellgren, C.: Investigations into the capability of dosing units for future fuels, EFCF Lucern, Switzerland, 2011.

The Impact of Micro-Surface Shaping of the Piston on the Piston/Cylinder Interface of an Axial Piston Machine

Ashley Wondergem and Professor Dr.-Ing. Monika Iwantysynova

Maha Fluid Power Research Center, Purdue University, 225 South University Street West
Lafayette, IN 47907-2093, USA, E-mail: awonderg@purdue.edu, mivantys@purdue.edu

Abstract

Axial piston machines of the swashplate type are commonly used in various hydraulic systems and with recent developments in displacement control, it is essential to maximize their efficiency further reducing operation costs as well as improving performance and reliability. This paper reports findings of a research study conducted for the piston-cylinder interface utilizing a novel fluid structure thermal interaction model considering solid body deformation due to thermal and pressure effects in order to accurately predict the transient fluid film within the gap. A large reduction in energy dissipation is possible due to reduced clearances allowable due to the surface shaping of the piston resulting in a reduction in leakage. From this study, it is shown that surface shaping of the piston in combination with a reduced clearance is not only beneficial by improving the efficiency of a machine, but also increases the reliability and the performance of the machine as the load support is enhanced.

KEYWORDS: Axial piston machine, surface shaping, piston-cylinder interface

1. Introduction

Axial piston machines of the swashplate type are widely used in industrial applications due to the ability to operate at high pressures and variable displacements while maintaining favorable efficiencies and reasonable operating costs. Effective and efficient operation of the unit strongly depends on the three main lubrication interfaces as shown in **Figure 1**. More specifically, the piston-cylinder interface is a key design element of such operation. By adding a micro-surface shape on the piston surface allowing for a decrease in the clearance between the piston and cylinder, the leakages can be greatly reduced while manipulating the fluid film to build up sufficient load support. In other words, the addition of a surface profile could impact the interface in such a way that the energy dissipation is reduced while maintaining or even improving the overall machine operation.

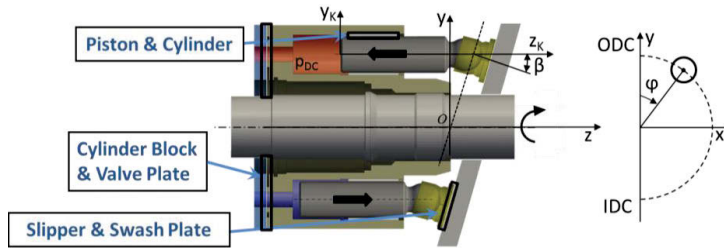


Figure 1: Axial piston machine of the swashplate type

1.1. Piston-Cylinder Interface

In order to better understand the design challenges that arise when designing the piston-cylinder interface to provide an adequate bearing function, minimizing areas of minimum fluid film thickness resulting in either contact or increased viscous friction, while also a sufficient sealing function, minimizing leakages, the forces interacting with the interface, as shown in **Figure 2**, must be accurately defined under normal machine operation. One of the major forces being the pressure force, F_{DK} , acting on the bottom area of the piston due to the displacement chamber pressure, p_{DC} . Also acting in the axial direction is the inertial force, F_{aK} , due to the acceleration of the piston and the viscous friction forces, F_{TK} , due to the viscosity of the fluid. The sum of the axial forces are reciprocated by a reaction force from the swashplate, F_{SK} .

The reaction force from the swashplate results in a remaining side force, F_{SKy} . Further aiding in the side loading of the piston includes the centrifugal force, $F_{\omega K}$, due to the rotation of the mass of the piston-slipper body and the viscous friction force from the slipper-swashplate interface, F_{TG} . This side load must be balanced by a hydrodynamic load generated through the fluid pressure of the lubricating gap in order to prevent contact resulting in wear or failure. Sufficient fluid support is generated through a squeeze effect from the motion of the piston, the deformations of the solid bodies due to thermal and pressure loading, and the self-adjustment of the location of the piston within the cylinder bore. This phenomena is strongly dependent on the dynamically changing fluid film geometry as defined in [1/].

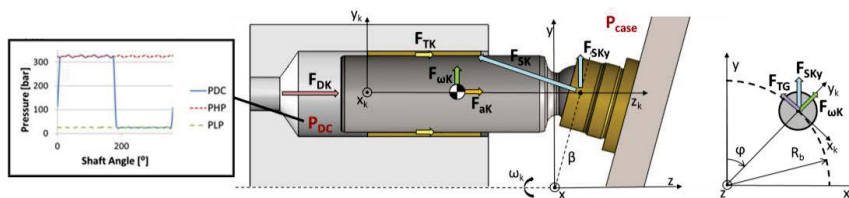


Figure 2: Force acting on the piston-cylinder interface

2. State of the Art

Previous research has been conducted in regards to surface shaping on the piston-cylinder interface. Through various experimental and analytical studies, it was realized that by altering the shape of the piston, the efficiency of the machine could be improved as well as the overall performance. In 1976, Yamaguchi /2/ proposed a tapered piston followed by Ivantysynova /3/ in 1983 in which a barrel like piston was proposed. Further analytical analysis and experimental research was performed by Lasaar and Ivantysynova /4/ on a barrel like piston resulting in a 20% energy dissipation reduction and a 50% reduction in leakages. To further support this study, measurements of such a piston were performed on a specialized test rig /5/ confirming the reduced friction forces. More recently in 2010, Gels and Murrenhoff /6/ studied a contoured piston in combination with a varying gap width and guide length using a simplified modeling approach also demonstrating a considerable reduction in losses.

3. Fluid Structure Thermal Interaction Model

Figure 3 details the fluid structure thermal interaction model utilized for the following research study as proposed by Pelosi /7/. This model solves for the motion of the piston within the cylinder bore based on a balance of external and fluid forces considering the thermal and elastohydrodynamic effects.

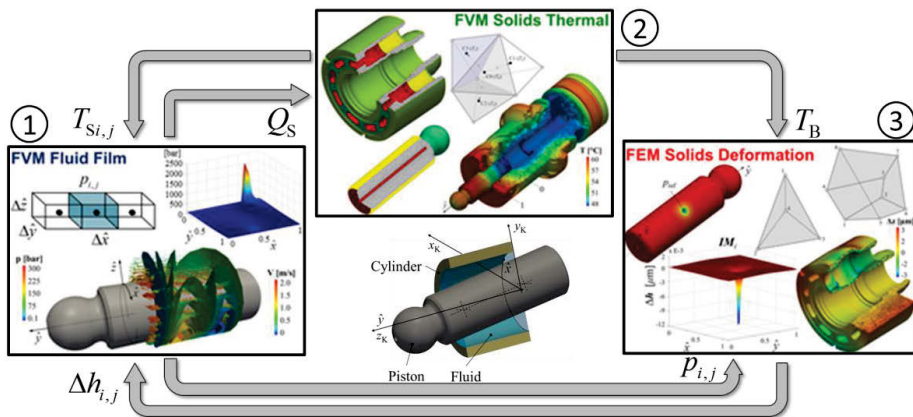


Figure 3: Piston-cylinder fluid structure thermal interaction model

The physical behavior of the piston-cylinder interface is captured through a non-isothermal fluid film flow governed by the Reynolds and energy equations that are simultaneously solved through a finite volume method in module 1. From the energy equation, the energy dissipated in the lubricating gap can be calculated. This energy dissipation is then used to predict the fluid temperature which can be used to determine the fluid viscosity as well as the heat flux on the bounding solid parts. The heat transfer

problem is solved utilizing a finite volume method as shown in module 2. Module 3 then solves for the elastic deformations due to pressure and thermal loading via a finite element method. Since these three modules are co-dependent, several iterations are required to reach a converged predicted fluid film thickness.

4. Novel Piston Designs

Various novel piston micro-surface shapes were investigated using the innovative fluid structure thermal interaction model. In order to quantify the improvements of such designs on the piston-cylinder interface a baseline simulation was conducted for comparison. The baseline unit is a nine piston, 75 cc stock swashplate type axial piston machine in which measured wear profiles were taken into account on both the piston, PW_N , normalized to the piston radius, R_K , as $PW_N = \frac{\max wear [\mu m]}{R_K [mm]} = 0.1$ and the cylinder bore, BW_N , normalized to the cylinder radius, R_Z , as $BW_N = \frac{\max wear [\mu m]}{R_Z [mm]} = 1.21$.

With a standard minimum relative clearance corresponding to the gap height between the piston and the cylinder, h , of $MRC = \frac{h [\mu m]}{R_K [mm]} = 1.64\%$.

As a first alternative design a micro sinusoidal wave on the axial length of the piston was studied; the design presented in **Figure 4A**. The normalized design parameters of the geometry of the sinusoidal wave, the amplitude A and the wave length λ along the length of the piston $L_{piston\ length}$, in which the results are presented in this investigation are defined as:

$$A_N = \frac{A [\mu m]}{R_K [mm]} = 0.29 \quad (1)$$

$$\lambda_N = \frac{\lambda [mm]}{L_{piston\ length} [mm]} = 0.4 \quad (2)$$

A flat sinusoidal wave along the length of the piston was studied as a second alternative design as presented in **Figure 4B**. This design was proposed as a flat, cylindrical piston with a slight sinusoidal wave peak introduced on both ends of the piston; the concept being to represent a pre-manufactured wear profile. The amplitude studied remained the same as the sinusoidal wave profile, (1).

As a third design a barrel surface profile along the length of the piston was also studied, **Figure 4C**. The geometry of the barrel defined in this research study is based on the radii at the ends, R_1 on the DC end and R_3 on the case end, and the apex, R_2 , as well as the location of the apex, L_{Apex} , along the length of the piston:

$$\frac{R_1}{R_2} = 0.9996 \quad \text{and} \quad \frac{R_3}{R_2} = 0.9992 \quad (3)$$

$$\frac{L_{Apex}}{L_{piston\ length}} = 0.4167 \quad (4)$$

As a fourth design a direct combination of the sinusoidal wave and the barrel, a sinusoidal waved barrel micro-surface profile along the axial length of the piston as shown in **Figure 4D** has been analyzed. The design parameters designated in this study include the amplitude, (1), and the wave length of the sinusoidal wave, (2), and a fixed apex location, (4). Due to the sinusoidal wave overlaid on the barrel surface profile with a fixed apex location, the radius of the apex slightly increases:

$$\frac{R_1}{R_2} = 0.9993 \quad \text{and} \quad \frac{R_3}{R_2} = 0.9989 \quad (5)$$

Lastly, a sinusoidal wave around the circumference of a cylindrical piston was investigated as demonstrated in **Figure 4E**. Although the amplitude of this design remained the same to that of the axial design, (1), the number of waves changed in reference to the circumference of the piston, C_K :

$$\lambda_N = \frac{\lambda [mm]}{C_K [mm]} = 0.167 \quad (6)$$

The geometry specifications considered in this investigation were chosen based on a comprehensive design parameter study.

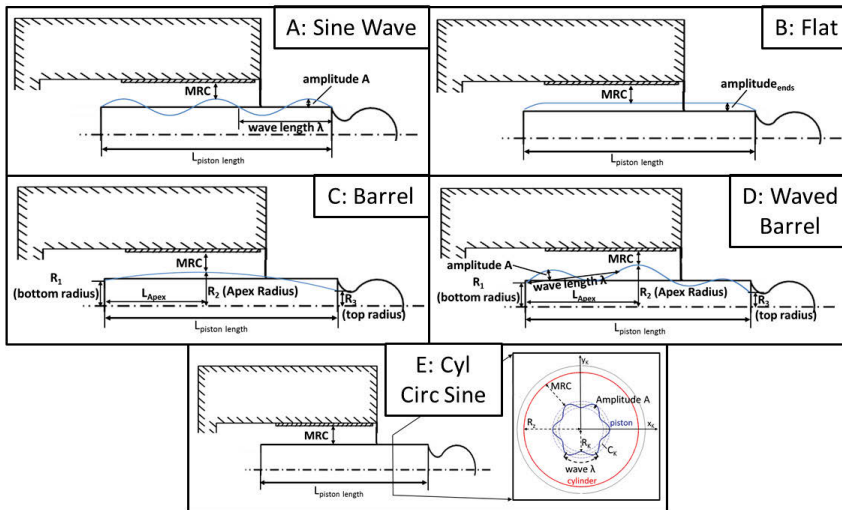


Figure 4: Micro-surface shaped piston designs

5. Piston Micro-Surface Shaping and Clearance Study

An investigation of the impact of various piston micro-surface shapes in combination with different clearances between the piston and the cylinder bore was conducted over a range of critical operating points. The reduced clearance between the piston and cylinder bore was possible due to the surface shaping of the piston in which a balance between the sealing and bearing function of the interface must be maintained. This was observed over a range of clearances reduced from the baseline of 1.64‰ to 1.45‰, 1.21‰, 0.96‰, 0.72‰ and 0.48‰.

5.1. Operating Conditions

This study is performed over the corner operating conditions of a baseline, 75 cc stock unit. The 16 corner operating conditions consist of a low differential pressure of 50 bar and high differential pressure of 450 bar at a low speed of 500 rpm and high speed of 3600 rpm for partial displacement (β) 20% and full displacement in both pumping and motoring mode. For all operating conditions studied, the inlet temperature remained constant at 52°C reflecting an oil viscosity of 20 cSt. Steady state measurements were not available for these conditions of the unit studied and therefore an internal thermal model developed by Shang and Ivantysynova /8/ was used to predict the outlet and case temperatures that were applied as boundary condition inputs for the model.

The authors have published results of similar investigations of various surface profiles utilizing the fluid structure interaction model in which a range of various other, more common operating conditions have been studied and compared to steady state measurements /9/ and /10/.

6. Results

The resulting losses of all nine piston-cylinder interfaces are presented in the following plots as a consequent of piston micro-surface shaping in combination with decreased clearance in which the machine was simulated at the corner operating conditions. For the indicated plots, the operating condition is denoted by a symbol: ● - 500rpm 50bar, ■ - 500rpm 450bar ♦ - 3600rpm 50bar, ▲ - 3600rpm 450bar. The various surface profiles are denoted by a line/color: sine wave - medium grey dotted line, flat – dark grey solid line, barrel – medium grey solid line, waved barrel – light grey dotted line, cylindrical circumferential sine – light grey solid line, baseline – black single symbol.

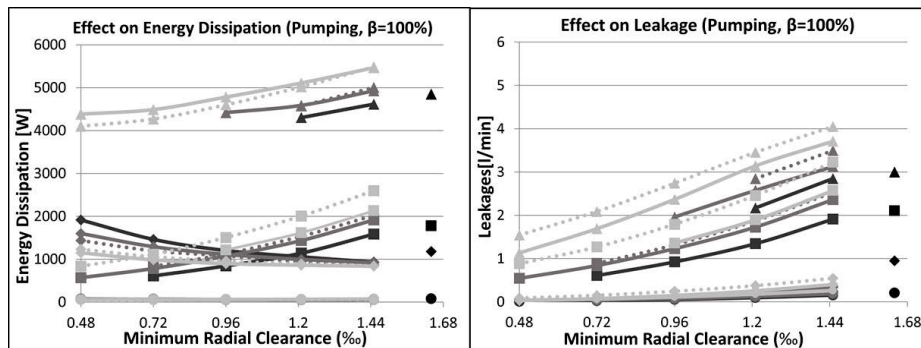


Figure 5: Legend for loss plots

6.1. Pumping Mode Results

The losses due to the addition of a surface shape on the piston as well as reducing the clearance are shown in **Figure 6** and **Figure 9** at the corner operating conditions in pumping mode. Note that for partial displacements, a low speed of 1500 rpm at a high pressure of 350 bar was rather investigated due to convergence issues.

6.1.1. Full Displacement

Figure 6: Losses for pumping, $\beta=100\%$; Energy dissipation (left), Leakages (right)

With the addition of a surface profile leading to the possibility of further reduced clearances, the energy dissipation and leakages can be greatly decreased from the baseline (black symbols); especially so for the higher pressure operating conditions. At higher pressures (curves marked with ■ and ▲), the smaller the clearance the better the improvement as the leakages are greatly decreased without largely increasing the torque losses. This trend holds until the fluid film can no longer support the load. However, at the lower pressure operating conditions (curves marked with ● and ◆), the energy dissipation tends to slightly decrease at the larger clearances studied in which the various surface profiles no longer have an effect. In comparison to the various surface profiles, the waved barrel surface profile (light grey dotted line) does best at the further reduced clearances (0.48‰) in which it is able to generate the required load support for the operating conditions shown while further reducing the leakages in comparison to other surface profiles, such as the barrel (medium grey solid line), at intermediate clearances (0.96‰). The flat surface profile (dark grey solid line) and the sinusoidal wave

profile (medium grey dotted line) are shown to fail at the further reduced clearances at the higher pressure operating conditions in which these designs are not feasible.

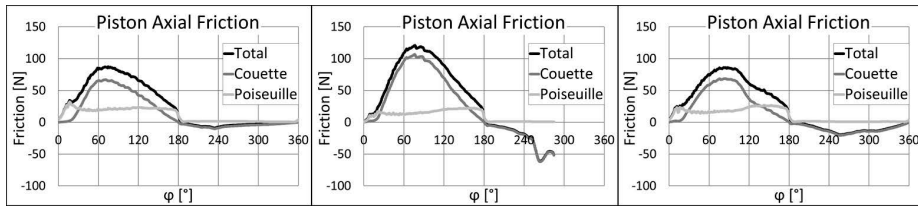


Figure 7: Piston axial friction forces for 3600rpm, 450bar, 100%, pumping mode; Baseline, 1.64‰ (left), Barrel, 0.72‰ (middle), Waved Barrel, 0.72‰ (right)

A comparison between the piston axial friction forces over one revolution at a high pressure (450 bar), and a lower clearance (0.72‰) is made between the baseline, the barrel surface profile, and the waved barrel surface profile in **Figure 7**. It can be seen that the barrel profile fails under these conditions since the friction forces are greatly increased leading to failure in the low pressure stroke. As for the waved barrel, the piston axial friction forces are similar to that of the baseline although the clearance is greatly reduced; the addition of such a wear profile results in manipulation of the fluid film in which the required fluid support is generated.

Multi-plots are shown to better understand the phenomena occurring within the fluid film resulting in the trends shown. Each plot show the film thickness (white contour lines) with the overlaid resulting fluid film pressure (filled contour) for an unwrapped gap between the piston and the cylinder; the x-axis (\hat{y}) representing the gap length and the y-axis (\hat{x}) the gap circumference as the cylinder block rotates. The plots are shown for two different rotational angles, ϕ , measured from outer dead center (ODC).

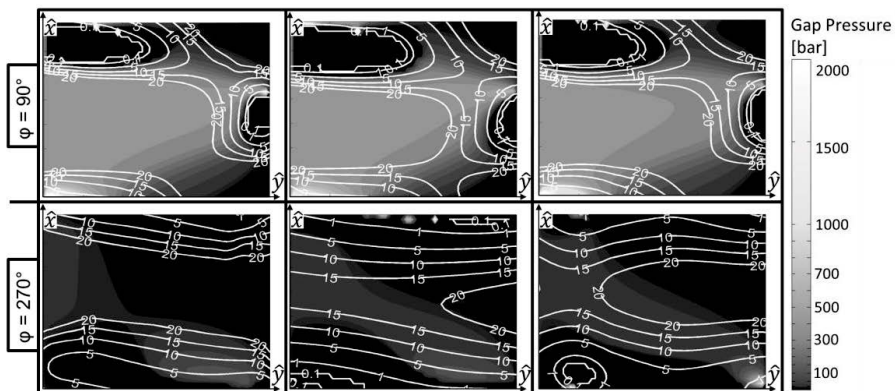


Figure 8: Multi-plots for 3600rpm, 450bar, 100%, pumping mode; Baseline, 1.64‰ (left), Barrel, 0.72‰ (middle), Waved Barrel, 0.72‰ (right)

The multi-plots are respectively shown for the higher pressure operating condition (450 bar) for the baseline in comparison to the barrel and the waved barrel at a reduced clearance (0.72‰) in **Figure 8**. The top row shows the fluid film and pressure build-up during the high pressure stroke (at $\varphi=90^\circ$). The increased friction forces for the barrel profile is a consequence of the larger areas of minimum fluid film thickness on both ends of the gap. As for the waved barrel design, since the friction forces are simply shifted in comparison to the baseline, as shown in Figure 7, the friction forces are larger at this particular rotating angle ($\varphi=90^\circ$) in which larger areas of minimum fluid film are observed. During the low pressure stroke (at $\varphi=270^\circ$) on the bottom row, the barrel surface profile slides across the cylinder bore due to insufficient load support leading to the increased friction forces and eventually failure. The waved barrel tends to tilt under these conditions resulting in some areas of minimum fluid film thickness on each end of the gap producing the slightly larger friction forces shown in the low pressure stroke, but operation is still possible.

6.1.2. Partial Displacement

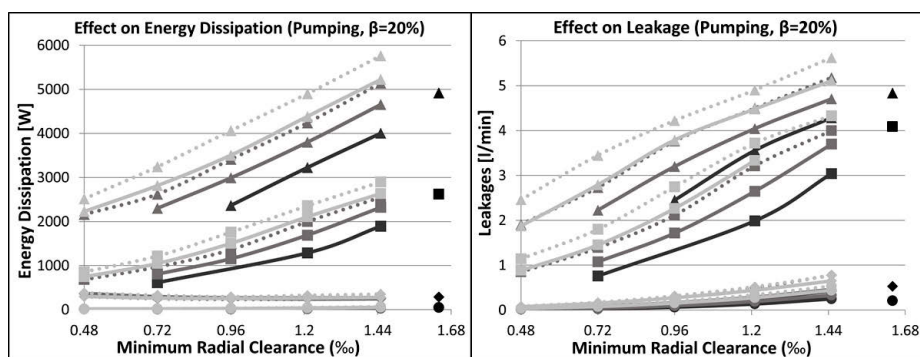


Figure 9: Losses for pumping, $\beta=20\%$; Energy dissipation (left), Leakages (right)

The investigation at partial displacement in pumping mode, revealed that since the side load acting on the piston is greatly reduced the resulting torque losses are minor in which the overall energy dissipation strongly relies on the decreased leakages. Also, this means that since the piston does not tilt as much within the bore, the load is able to be supported in compromise to less of a sealing function contributing to slightly increased leakages. Thus, by reducing the clearance at higher pressures (curves marked with ■ and ▲), the leakages can be greatly decreased in turn reducing the overall energy dissipation; the smaller side loads in combination with the smaller forces at lower pressures (curves marked with ● and ◆) has a negligible impact on the energy dissipation.

6.2. Motoring Mode Results

As a result of surface shaping in combination with decreased clearances at the corner operating conditions in motoring mode the losses are shown in **Figure 10** and **Figure 11**. Note that in motoring mode a differential high pressure of 400 bar was considered in order to not exceed the constraints of the maximum continuous oil temperature specified.

6.2.1. Full Displacement

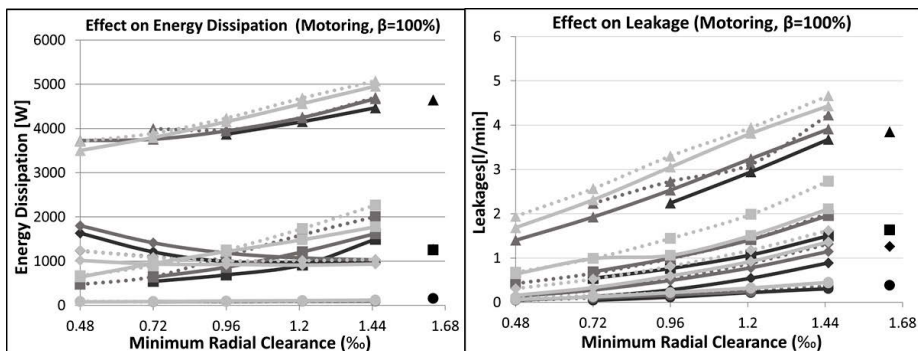


Figure 10: Losses for motoring, $\beta=100\%$; Energy dissipation (left), Leakages (right)

In comparison to pumping mode, the trends of the varying clearance among the various surface profiles studied are similar. It is likewise the tendency that the leakages are greatly decreased at the reduced clearances, especially so at higher pressures (curves marked with ■ and ▲) in which the torque loss are not largely increased resulting in decreased energy dissipation overall in the case that the fluid film is able to support the load. The slight variations in motoring mode is based on the slightly different operating condition as well as the opposite motion of the piston relative to the high and low pressure in the displacement chamber leading to different forces in comparison to pumping mode.

6.2.2. Partial Displacement

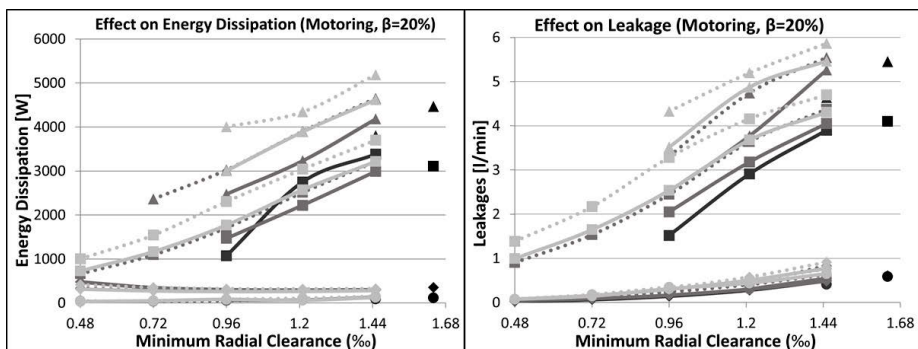


Figure 11: Losses for motoring, $\beta=20\%$; Energy dissipation (left), Leakages (right)

Although the trends are again very similar to that as shown in pumping mode for partial displacement operation the surface profiles are more likely to fail with smaller clearances at higher pressures (curves marked with ■ and ▲).

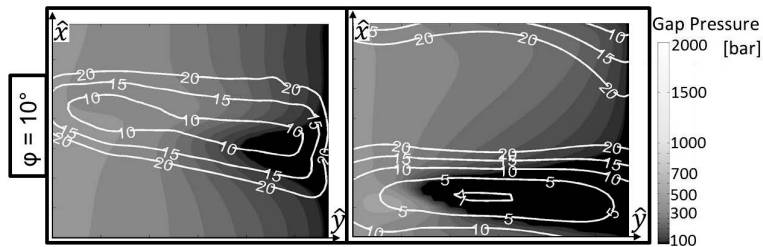


Figure 12: Multi-plots 3600rpm, 400bar, 20%, motoring mode; Baseline, 1.64‰ (left), Waved Barrel, 0.72‰ (right)

In **Figure 12** it can be seen that right away in the simulation in the high pressure stroke ($\varphi=10^\circ$) that the piston with a surface profile does not build up the fluid support required in which the piston then drags and bounces along the cylinder bore leading to failure.

6.3. Conclusion

A comprehensive simulation investigation has been performed for the various novel piston designs presented in combination with decreased clearances at the corner operating conditions in both pumping and motoring mode. It was shown that the addition of a surface profile allowed for a reduction in clearance due to improved load carrying abilities of the interface leading to reduced leakages and an overall reduction in energy dissipation. In general, the reduced clearances are best, especially at higher pressure operating conditions, as long as the load can be supported. More specifically, this study concludes that the waved barrel does best at the further reduced clearances in pumping mode, but since this combination fails at partial displacements in motoring mode, the barrel surface profile at 0.96‰ is the best overall combination for the complete corner operating conditions investigated and presented in this study.

7. References

- /1/ Wieczorek, U. 2003. Ein Simulationsmodell zur Beschreibung der Spaltströmung in Axialkolbenmaschinen der Schrägscheibenbauart. VDI Fortschritt-Berichte. Reihe 7 No. 443. Düsseldorf
- /2/ Yamaguchi, A. 1976. Motion of Pistons in Piston-Type Hydraulic Machines. Bulletin of JSME, Vol. 19, No. 130, pp. 402-419.

- /3/ Ivantysynova, M. (at that time Berge, M.) 1983. An investigation of viscous flow in lubricating gaps. (In Slovak). Dissertation SVST Bratislava, Czechoslovakia.
- /4/ Ivantysynova, M. and Lasaar, R. 2004. An investigation into Micro- and macro geometric design of piston/cylinder assembly of swash plate machines. *International Journal of Fluid Power*, Vol. 5 (2004), No.1 , pp. 23-36.
- /5/ Lasaar, R. 2003. Eine Untersuchung zur mikro-und makrogeometrischen Gestaltung der Kolben/ Zylinderbaugruppe von Schrägscheibenmaschinen.VDI Fortschrittsberichte Reihe 1 No. 364, VDI Verlag Düsseldorf, Germany.
- /6/ Gels, S. and Murrenhoff, H. 2010.Simulation of the Lubrication Film between Contoured Piston and Cylinder. *Internation Journal of Fluid Power*, 11:2, 15-24.
- /7/ Pelosi, M. 2012. An Investigation on the Fluid-Structure Interaction of Piston/Cylinder Interface. PhD thesis, Purdue University.
- /8/ Shang, L. and Ivantysynova, M. 2015. Port and case flow temperature prediction for axial piston machines. *International Journal of Fluid Power*, Vol. 16, Issue 1, pp.35-51.
- /9/ Wondergem, A. and Ivantysynova, M. 2014. The Impact of the Surface Shape of the Piston on Power Losses. *Precedings of the 8th FPNI PhD Symposium*, Lappeenranta, Finland.
- /10/ Wondergem, A. and Ivantysynova, M. 2015. The Imapct of Micro-Surface Shaping on te Piston/Cylinder Interface of Swash Pate Type Machines. *Preceedings of the ASME/Bath 2015 Symposium*, Chicago, IL, USA.

Bulk Modulus and Traction Effects in an Axial Piston Pump and a Radial Piston Motor

Paul W. Michael and Shreya Mettakadapa

Fluid Power Institute, Milwaukee School of Engineering, 1025 N Broadway, Milwaukee, Wisconsin, USA E-mail: michael@msoe.edu

Abstract

This paper describes an investigation into the effects of fluid bulk modulus and traction coefficient properties on piston pump flow losses and radial piston motor torque losses through experimentation, modelling and simulation. Synthetic ester, high bulk modulus, multi-grade, and single grade mineral oils were evaluated. The high bulk modulus fluid exhibited 20% lower pump case and compensator flow losses than a conventional mineral oil of the same viscosity grade. Low traction coefficient fluids reduced the low-speed torque losses of the radial piston motor by 50%. Physical models for pump case flow and motor torque losses were derived from the experimental data. Field data was collected from a hydraulically propelled agricultural machine. This data was used to model fluid performance in the machine. The simulation results predict that at an operating temperature of 80°C, optimizing the bulk modulus and traction coefficients of the fluid could reduce flow losses by 18% and torque losses by 5%. These findings demonstrate the potential of combining comprehensive fluid analysis with modeling and simulation to optimize fluids for the efficient transmission of power.

KEYWORDS: Hydraulic fluids, Bulk modulus, Pump losses, Motor losses

1. Introduction

The flow produced by positive displacement pumps drives hydraulic motors and actuates cylinders in fluid power systems. Pump flow also supports control and feedback functions in pressure compensators and pilot operated valves. The efficiency of fluid power transmission is affected by flow losses. Flow losses generate heat and can reduce the amount of energy available to do work. Propulsion in mobile fluid power applications is frequently supplied by hydraulic motors. The frictional losses that occur in motors generate heat and reduce the torque available to move the payload. Highly sophisticated and accurate modeling and simulation tools have been developed by various researchers to investigate mechanical design factors that affect pump and motor

efficiency. In those studies, conventional mineral oil based hydraulic fluids were employed to limit the number of experimental variables. In this paper, conventional and synthetic hydraulic fluid formulations were examined through experimentation, modeling and simulation.

Previously reported steady-state models for case drain leakage flow and hydraulic motor torque losses were employed in this study. The pump case drain and compensator leakage flow model was an adaptation of Joeng's flow loss model /1/ as described in /2/. The model incorporated viscosity (μ), density (ρ), and bulk modulus (K) as well as rotational frequency (ω), differential pressure (ΔP) and derived displacement (V_E) as shown in Eqn. 1. The coefficients (C_P , C_T , C_K , C_V , C_O) were derived from experimental data via linear regression.

$$Q_L = C_P(\Delta P / \mu) + C_T \sqrt{\Delta P / \rho} + C_K(\omega \Delta P / K) + C_V V_E + C_O \quad (1)$$

The torque efficiency model was an adaptation of the Michaelis-Menten surface adsorption theory as described in /3/. The model incorporated rotational frequency, fluid viscosity, and motor differential pressure as shown in Eqn. 2. The boundary lubrication coefficient (C_{BL}), viscous drag coefficient (C_{SH}) and torque to rotate constants (C_{TTR}) were derived via non-linear regression.

$$\eta_{HM} = \frac{\left(\frac{\mu \omega}{\Delta P} \right)}{\left[C_{BL} + \left(\frac{\mu \omega}{\Delta P} \right) \right]} - C_{SH} \left(\frac{\mu \omega}{\Delta P} \right) - C_{TTR} \quad (2)$$

Hydraulic motor torque losses (T_L) were estimated from the mechanical efficiency model and the theoretical torque of the motor (T_o) using Eqn. 3.

$$T_L = T_o (1 - \eta_{HM}) \quad (3)$$

The duty cycle of an agricultural machine that was propelled by four radial piston motors was obtained for the purpose of mapping the above models to an actual hydraulic application. Histograms of the operating pressures, speeds and displacements of the machine were created using a procedure similar to the one described in /4/. The resulting histograms were used to create a time-weighted simulations for the flow and torque losses of the test fluids. The simulations were used to assess the potential benefit of optimizing fluid bulk modulus and traction coefficient properties for an agricultural specific duty cycle where the machine primarily operates under constant speed conditions.

2. Methods and Materials

2.1. Hydraulic Dynamometer

Pump case drain flow and radial piston motor torque losses were evaluated in the hydraulic circuit shown in **Figure 1**. The circuit incorporated a Danfoss Series 45 open-loop variable-displacement axial piston pump. The pump inlet temperature was controlled to 50 or 80°C ($\pm 1^\circ$). The pump angular velocity was adjusted to 800, 1200 or 1800 rpm. Pump displacement was controlled by a Parker Denison 4VP01 proportional electrohydraulic valve that adjusted the swash plate angle to maintain a desired pump outlet pressure of 7, 10, 14, 17, 21, 24 or 27.5 MPa. The pump supplied power to a Poclain MS02 radial piston motor to yield rotational frequencies ranging from 1 to 200 rpm /5/. Pump data was collected using a modified ISO 4409 procedure /6/. The combined pump case drain and pressure compensator outlet flow rates were measured using a Max Machine G105 Series Gear Flow Meter. Motor data was collected using a modified ISO 4392-1 procedure /7/. Motor torque was measured using an HBM T30 transducer. The resulting data was used to derive coefficients for equations 1 and 2.

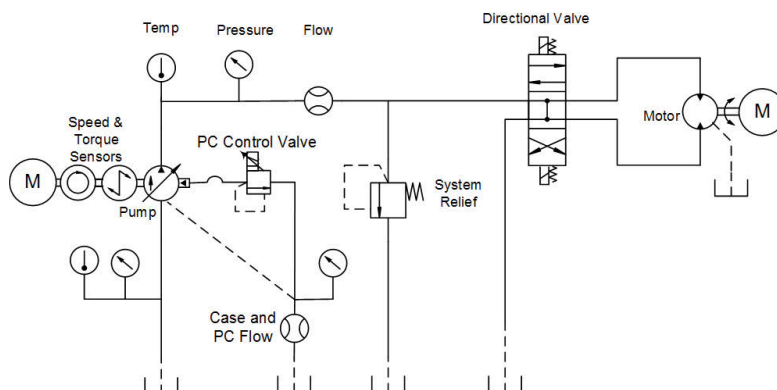


Figure 1: Simplified Circuit Schematic

2.2. Test Fluids

The five ISO 46 viscosity grade hydraulic fluids listed in Table 1 were evaluated in this investigation. HM46 was a straight-grade Group I mineral oil based hydraulic fluid formulated with a commercial ashless antiwear additive package. HV46 was a multi-grade Group III mineral oil based hydraulic fluid that contained a commercial ashless antiwear additive package and a shear-stable polymethacrylate viscosity index improver. HEES46 was a Group V synthetic ester based hydraulic fluid formulated with a commercial ashless antiwear additive package. HBMO46 was a Group V phenyl ester based High Bulk Modulus Oil. HBMO46+FM was the Group V phenyl ester plus a friction

modifier. The HBMO fluid exhibits a high bulk modulus because phenyl groups pack densely and have a low free volume /8/. In addition, ring structures increase the rotational energy barrier between carbon bonds within the molecule. A higher rotational energy results in a stiffer molecule. Molecular rigidity also affects the shear force transferred across a fluid film. This shear force is known as traction, which is the ratio of traction force to normal load. Base stocks that have a high bulk modulus tend to have a high traction coefficient /9/. Low traction is preferable in fluid power applications /3,10/. The HBMO fluid evaluated in this investigation is formulated with a polycyclic compound that incorporates ester function groups for reduced traction /11/.

2.3. Viscosity Stability

The kinematic viscosity was determined at 40° and 100°C before and after the ASTM D5621 40-minute sonic shear test. This method was found to correlate with pump case drain flow and motor torque losses in earlier investigations /2,3/. All of the fluids exhibited a high-degree of shear stability with a viscosity loss of less than 6%.

Fluid	HM46	HV46	HEES46	HBMO46	HBMO46+FM
Base stock	mineral oil, solvent ref	mineral oil, hydrocracked	polyol ester	phenyl ester	phenyl ester
Viscosity index	104	197	192	122	Same
KV 40°C, cSt new D445	46.5	50.5	51.1	45.2	Same
KV 100°C, cSt new D445	6.90	10.24	10.12	7.27	Same
KV 40°C, cSt sheared D5621	46.1	48.1	49.0	42.1	Same
KV 100°C, cSt sheared D5621	6.83	9.64	9.67	6.94	Same
Density g/cc @ 15C	0.8772	0.8524	0.9192	1.140	Same
Coefficient of thermal expansion, /°C	0.000687	0.000728	0.0007307	0.000754	Same
Traction coeff. @ 50N, 20mm/s, 50°C	0.0721	0.0616	0.0482	0.0606	0.0478
Bulk modulus at 80C and 250 bar, /GPa	1.386	1.336	1.457	1.917	Same

Table 1: Test fluid properties

2.4. Traction Measurements

Traction curves were generated using a PCS Instruments Mini-Traction Machine (MTM). The MTM is a ball-on-disc tribometer. In the MTM, the ball is loaded against the face of the disc and the ball and disc are driven independently to create a mixed rolling/sliding contact. In this series of tests the applied load was 50N, the slide-to-roll ratio was 20%,

and tests were conducted at 50, 80 and 125°C. As shown in **Figure 2**, the HEES46 and HBMO+FM formulations exhibit low traction coefficients at low entrainment velocities.

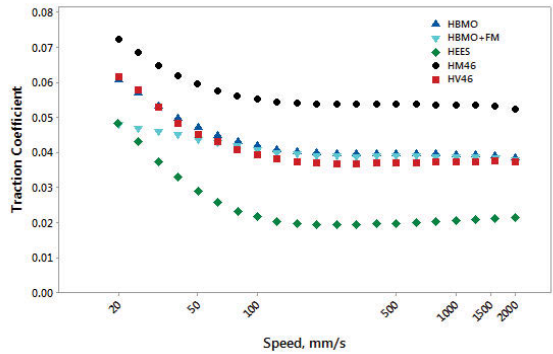


Figure 2: MTM Traction coefficients of test fluids at 50°C

2.5. Bulk Modulus

The pressure-dependence of volume was determined at 20, 50 and 80°C at pressures up to 300 MPa from the change in length of a metal bellows housed within a pressure vessel as described in /12/. Relative volume calibrations were performed using the NIST certified density for water. These measurements were used to determine pressure and temperature rate of change parameters for use in the Tait equation in order to determine the bulk modulus of the fluid at operating conditions /2/. As shown in **Figure 3**, the bulk modulus of the HBMO fluid at 25 MPa was approximately 25% higher than that of the other fluids.

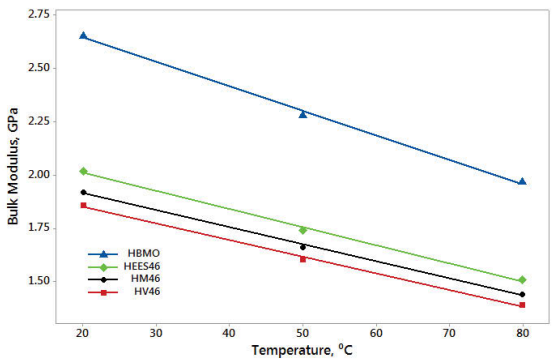


Figure 3: Bulk modulus of test fluids at 25 Mpa

3. Results and Discussion

3.1. Pump Case Flow

Steady state performance tests were conducted as described above to yield approximately 400 data points per fluid. The combined pump case drain and remote pressure compensator flow rates were measured and 95% confidence intervals for the mean flow rates were determined. The HM46 oil served as a reference fluid for this study and was evaluated at the start, middle and end of the test sequence. As shown in **Figure 4**, the mean case flow rates for the HBMO and HBMO46+FM fluids were approximately 20% less than those of the HM46 baseline. The mean case flow rates for both of the HBMO blends were also less than that of the HEES46 and HV46 fluids. These findings were somewhat surprising since the HBMO fluids had a lower viscosity than the HEES46 and HV46 as shown in Table 1. Step-wise linear regression of Eqn. 1 was used to investigate the correlation between fluid properties and leakage flow [2]. As shown in Table 2, when a single parameter was considered, bulk modulus yielded a higher correlation (R^2) and lower standard error than viscosity or density.

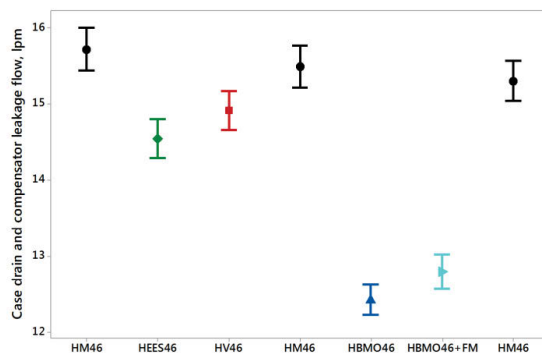


Figure 4: Mean axial piston pump case drain and compensator flow rates

Parameters	μ	ρ	K	R^2	Std. Error l/min
Viscosity	✓			61.9	2.72
Density		✓		65.2	2.60
Bulk modulus			✓	74.4	2.23
Viscosity and bulk modulus	✓		✓	85.9	1.66
Viscosity, density, and bulk modulus	✓	✓	✓	87.1	1.58

Table 2: Correlation of fluid properties with pump case and compensator flow rates

3.2. Motor Torque Loss

Steady state efficiency tests were conducted on the radial piston motor at rotational frequencies ranging from 1 to 200 rpm. Two temperatures, three pump speeds, seven motor differential pressures, and ten motor speeds were evaluated to yield approximately 400 data points per fluid. Torque losses were determined by subtracting the measured torque output of the motor from the theoretical torque value. Torque losses in motors are affected by variations in friction that occur as operating conditions transition through boundary, mixed-film and hydrodynamic regimes. At low speeds, boundary and mixed-film friction affect torque losses because the entrainment velocities are insufficient to support full-film lubrication. At high speeds, the formation of a hydrodynamic lubricating film prevents surface contact, however viscous drag and pumping losses have a parasitic effect. As shown in **Figure 5**, there were significant differences in the torque losses of the fluids at low speeds. At high speeds the differences in the torque losses were less pronounced. At 1 RPM, the torque losses of the HEES46 and HBMO46+FM fluids were 50% less than those of the HM46. HEES46 and HBMO46+FM also had a low traction coefficient in the MTM test as shown in figure 2.

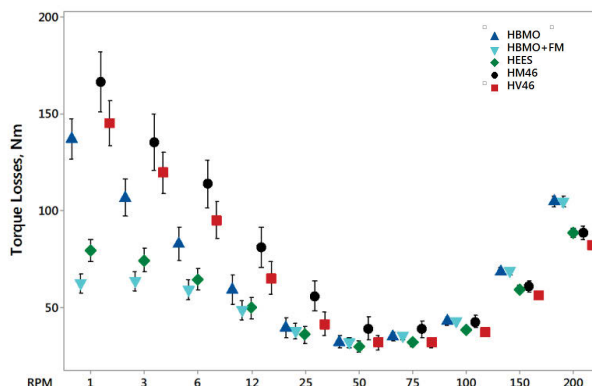


Figure 5: Mean radial piston motor torque losses at 50 and 80°C

Fluids that exhibit low traction coefficients enable hydraulic motors to transition from boundary into the hydrodynamic lubrication regime at lower speeds, thereby reducing low speed torque losses [3]. Non-linear regression was used to determine the coefficients for Eqn. 2 listed in Table 3. These values were used to estimate motor torque losses in the machine simulation.

Fluid	$C_{BL}(10^{-11})$	C_{SH}	C_{TTR}	MSE
HM46	1.35	267000	0.024	0.00291
HV46	1.40	238000	0.024	0.00219
HEES46	0.75	221000	0.024	0.00112
HBMO	1.39	257000	0.024	0.00246
HBMO+FM	0.60	261000	0.024	0.00107

Table 3: Coefficients for radial piston motor mechanical efficeincy model

3.3. Machine Simulation

The operating conditions within a hydraulic machine (pressure, temperature, and the rotational frequency of pumps and motors) can significantly affect the viscosity of hydraulic fluids. Typically, viscosity increases with pressure, decreases with temperature and decreases with shear rate. Therefore, there is a complex interrelationship between the effect of component operating conditions on viscosity and the effect of viscosity on component performance. In order to investigate this relationship, speed, pressure and load data from a hydraulically propelled agricultural machine was collected as it repeatedly traversed the length of a field. Histograms of the operating conditions were constructed from 508 different combinations of speed, temperature and motor displacement. As shown in **Figure 6**, the machine operated much of the time at 60 and 140 RPM and an operating pressure of 10 to 15 MPa.

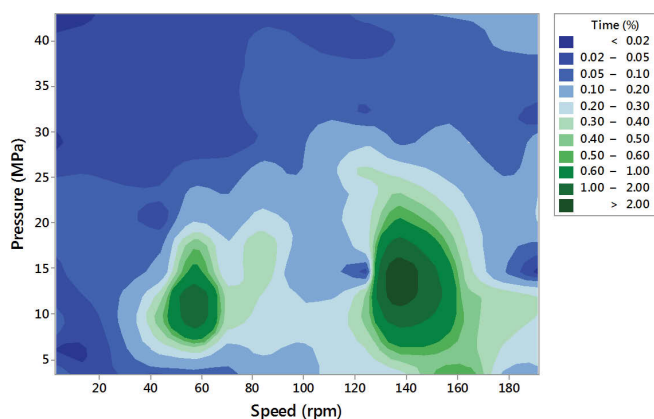


Figure 6: Contour plot of motor speed and system pressure in an agricultural machine

A MATLAB program was developed to simulate pump case flow and motor torque losses for the 508 combinations of hydraulic motor speed, pressure and displacement from the machine field study. The program outputs the case flow and torque losses for each

combination of pump pressure and motor speed based upon inputs of the fluid properties and equations 1, 2 and 3. In addition to calculating the losses at specific conditions, the results are time-weighted based upon the duty cycle data. Comparisons of the simulated pump case flow and motor torque losses are shown in Tables 4 and 5. These simulation indicate that at an operating temperature of 80°C, optimizing the bulk modulus properties of the fluid could reduce pump case flow losses by 18%.

Temp (°C)	HM46	HV46	HEES46	HBMO46	HBMO+FM
50	-1.3	0	-5.8	-17.3	-17.3
80	0	-2.5	-9.1	-18.0	-18.0
100	0	-5.8	-12.7	-19.4	-19.4

Table 4: Simulated pump case flow losses for agricultural duty cycle

At an operating temperature of 80°C, optimizing the traction coefficient properties of the fluid could reduce motor torque losses by less than 5%. This is because an agricultural machine traversing a field operates at relatively high speed most of the time and only slows down when it turns to reverse direction.

Temp (°C)	HM46	HV46	HEES46	HBMO46	HBMO+FM
50	-2.3	-2.8	-4.7	0.0	-1.3
80	0	-0.6	-4.6	-0.3	-4.8
100	0	-2.4	-8.7	-2.3	-9.2

Table 5: Simulated motor torque losses for agricultural duty cycle

4. Conclusions

This study presents an investigation of the effects of fluid properties on axial piston pump case drain and radial piston motor torque losses through experimentation, modelling and simulation. Hydraulic fluids that utilized synthetic and conventional base stocks were evaluated. The subject fluids were all ISO VG 46 but varied in viscosity index, density, and bulk modulus. A prototype high bulk modulus fluid exhibited 20% lower pump case flow losses than a conventional mineral oil. Prototype fluids with low traction coefficients exhibited 50% lower motor torque losses at low speeds. Models derived from test data were used to simulate fluid performance in a hydraulically propelled agricultural machine. The simulation predicts that at an operating temperature of 80°C, fluid optimization could reduce flow losses by 18% and torque losses by less than 5%. These findings demonstrate the potential of combining comprehensive fluid analysis with modelling and simulation to optimize fluids for the efficient transmission of power.

5. Acknowledgements and Funding

The authors are grateful for the generous support provided by Danfoss Fluid Power, Evonik Oil Additives, Idemitsu Lubricants, Lubrizol, and Poclain Hydraulics. Special thanks to Dr. Scott Bair of the Georgia Institute of Technology for providing bulk modulus measurements and assisting with the modelling effort. This research was supported by the Center for Compact and Efficient Fluid Power, a National Science Foundation Engineering Research Center funded under cooperative agreement number EEC-0540834.

6. References

- /1/ Jeong, H-S., 2007. "A Novel Performance Model Given by the Physical Dimensions of Hydraulic Axial Piston Motors: Model Derivation," *Journal of Mechanical Science and Technology*, Vol. 21, No. 1, pp. 83-97
- /2/ Mettakadapa, S. Bair, S. Aoki, S. Kobessho, M. Carter, L. Kamimura, H. and Michael, P., 2015. "A Fluid Property Model for Piston Pump Case Drain and Pressure Compensator Flow Losses," *Proceedings of the AMSE/BATH 2015 Symposium on Fluid Power and Motion Control*, Paper FPMC2015-9515, Chicago, IL
- /3/ Michael, P. Mettakadapa, S. and Shahahmadi, S., 2015. "An Adsorption Model for Hydraulic Motor Lubrication," *J Tribol*, 137:4
- /4/ Garcia, JM. Johnson, J. and Michael P., 2015. "Toward the Development of a Pump Energy Rating System based upon Performance Indexes," *Proceedings of the Fluid Power Innovation Research Conference*, Chicago, IL
- /5/ Miller, MK. Khalid, H. Michael, P. Guevremont, JM. Garelick, KJ. Pollard, GW. Whitworth, AJ. and Devlin, MT., 2014. "An Investigation of Hydraulic Motor Efficiency and Tribological Surface Properties," *Tribology Transactions*, 57: 622-630
- /6/ International Organization for Standardization, 2007. "ISO 4409:2007(E) Hydraulic Fluid Power – Positive Displacement Pumps, Motors and Integral Transmissions – Methods of Testing and Presenting Basic Steady State Performance." Geneva

- /7/ International Organization for Standardization, 2002. "ISO 4293-1:2002(E) Hydraulic fluid power — Determination of characteristics of motors — Part 1: At constant low speed and constant pressure." Geneva
- /8/ Ohno, N., Ziaur Rahman, M.D., and Kakuda, K., 2005. "Bulk Modulus of Lubricating Oils as Predominant Factor Affecting Tractional Behavior in High-Pressure Elastohydrodynamic Contacts," *Tribology Transactions*, Vol. 48, pp. 165-170
- /9/ Hata, H., and Tsubouchi, T., 1998. "Molecular Structures of Traction Fluids in relation to Traction Properties," *Tribology Letters*, Vol. 5, pp. 69–74, DOI: 10.1023/A: 1019108800961
- /10/ Michael, P. Burgess, K. Radle, E. Wanke, T. Devlin, M. and Hux, K. 2010. "An Investigation of Hydraulic Fluid Properties and Low-Speed Motor Efficiency," *Proceedings of the 7th International Fluid Power Conference*, Aachen, Germany, Vol. 3, pp. 341-353
- /11/ Tsubouchi, T., and Shinoda, J., 2010. "Oily High Bulk Modulus Fluid of New Concept," *Proceedings of the 7th International Fluid Power Conference*, Aachen, Germany, Vol. 3, pp. 367-378,
- /12/ Bair, S., *High Pressure Rheology for Quantitative Elastohydrodynamics*, Elsevier Science, Amsterdam, 2007

7. Nomenclature

C_{xx}	Regression coefficient	dimensionless
FM	Friction Modifier	
HBMO	Hydraulic fluid, synthetic high bulk modulus	
HEES	Hydraulic fluid, synthetic ester base, environmentally acceptable type	
HM	Hydraulic fluid, mineral oil base, rust and oxidation inhibited with improved antiwear performance	
HV	Hydraulic fluid, mineral oil base, antiwear type with improved viscosity/temperature properties	
K	Bulk modulus	GPa

MSE	Mean square error	dimensionless
η_{hm}	Mechanical efficiency	dimensionless
Q_L	Flow loss	litres per minute
T_0	Torque theoretical	Nm
T_L	Torque loss	Nm
V_E	Pump displacement (effective)	cc/revolution
ΔP	Differential pressure	Pascal
μ	Viscosity	Pascal seconds
ρ	Density	g/cm ³
ω	Rotational frequency	radians per second

Energy efficiency improvement by the application of nano-structured coatings on axial piston pump slippers

peer reviewed

Dr. Giuseppe Rizzo

Institute for Agricultural and Earthmoving Machines – IMAMOTER – C.N.R., via Canal Bianco 28, 44124 Ferrara, Italy, email: g.rizzo@imamoter.cnr.it

Dr. Antonino Bonanno, Dr. Giorgio Paolo Massarotti, Dr. Luca Pastorello, *Dr. Mariarosa Raimondo, *Dr. Federico Veronesi, *Dr. Magda Blosi

*Institute of Science and Technology for Ceramics – ISTEC – C.N.R., via Granarolo 64, 48018 Faenza (RA), Italy

Abstract

Axial piston pumps and motors are widely used in heavy-duty applications and play a fundamental role in hydrostatic and power split drives. The mechanical power losses in hydraulic piston pumps come from the friction between parts in relative motion. The improvement, albeit marginal, in overall efficiency of these components may significantly impact the global efficiency of the machine. The friction between slipper and swash plate is a functional key in an axial piston pump, especially when the pump (at low rotational speed or at partial displacement) works in the critical areas where the efficiency is low.

The application of special surface treatments have been exploited in pioneering works in the past, trying different surface finishing or adding ceramic or heterogeneous metallic layers. The potential of structured coatings at nanoscale, with superhydrophobic and oleophobic characteristics, has never been exploited.

Due to the difficulty to reproduce the real working conditions of axial piston pump slippers, it has been made a hydraulic test bench properly designed in order to compare the performance of nano-coated slippers with respect to standard ones.

The nano-coated and standard slippers have been subjected to the following working conditions: a test at variable pressure and constant rotational speed, a test at constant pressure and variable rotational speed. The comparison between standard and nano-coated slippers, for both working conditions, shows clearly that more than 20% of friction reduction can be achieved using the proposed nano-coating methodology.

KEYWORDS: oleophobic, nano-coating, slipper, friction coefficient

1 Introduction

There are several challenging issues associated with the pump, such as conflicts between lubrication and wear, and between sealing and leakage. Particularly, in an axial piston pump, slipper and swash plate can form a key friction pair, where the above conflicts exist and may result in significant influences on the pump performance.

Figure 1 shows a general scheme of an axial piston pump.

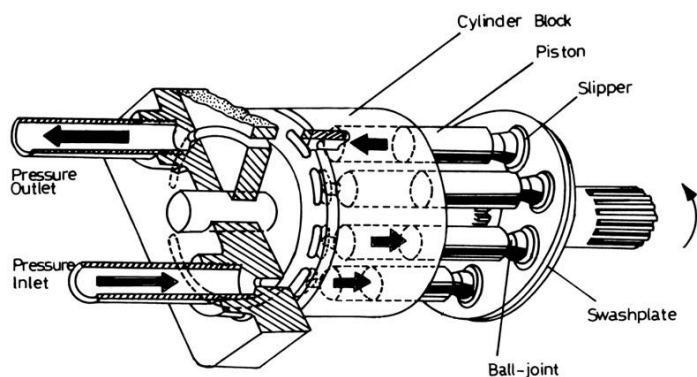


Figure 1: General scheme of an axial piston pump

Hydrostatic slipper bearing is an effective way to maintain a fluid film between slipper and swash plate that slide reciprocally, and thereby mitigating surface-to-surface direct contact.

The working principle of the slipper designed according to the hydrostatic bearing theory is shown in **figure 2**. High-pressure oil flows into the oil chamber under the slipper through damper orifice and generate hydraulic separating force, then the oil leaks from oil chamber to the pump case.

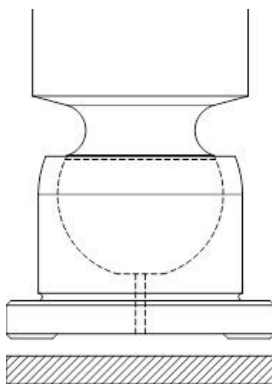


Figure 2: Hydrostatic slipper bearing with an annular orifice damper

Proper design is aimed to keep balance between the hydraulic separating force and pressing force that act on the slipper, and forms an oil film. When the axial piston pump works, the pressing force that acts on it constantly changes but, due to damping effect made by the orifice, it ensures an oil film thickness under the slipper, maintaining stability despite the variation of load. So that reliable fluid lubrication is provided, and direct contact between the slipper and the swash plate is avoided.

In this context it is useful to introduce the concept of wettability [1] which is one of the important properties of solid surfaces from both fundamental and practical aspects. The main wettability influencing factors are the surface energy and the surface roughness. Lowering the surface energy is possible to enhance the hydrophobic behavior of the surface.

Adamson, Israelachvili, Bhushan [2] [3] [4] defined that hydrophobicity and oleophobicity properties of a surface (wettability) are characterized by the static contact angle, or simply contact angle, made between a water or oil droplet and a surface. If the contact angle is less than 90° , a surface can be considered as hydrophilic whereas the hydrophobic behavior is fully developed if the contact angle is greater than 90° (**Figure 3**). Surfaces with the contact angle greater than 150° and 120° are called superhydrophobic and oleophobic respectively. The contact angle depends on several factors, such as surface energy, roughness, the manner of surface preparation, and surface cleanliness.

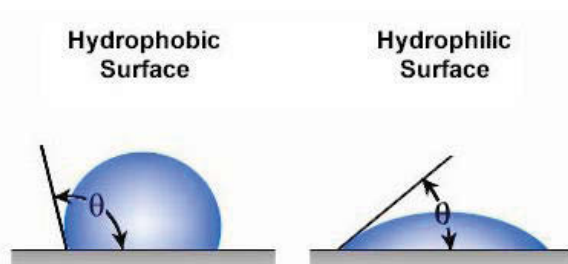


Figure 3: Hydrophobic and hydrophilic surface

The lubrication and wettability properties are the key factors to understand the friction and wear phenomena that occur between the slippers and the swash plate in hydraulic pumps. A better wettability between the two surfaces leads to a greater oil thickness and therefore a friction coefficient reduction. The friction coefficient reduction between surfaces, mutually in contact to each other, brings about an improvement of the mechanical efficiency and therefore the overall efficiency of the machine increases.

Many studies on hydrostatic thrust bearing in hydraulic axial piston equipment have been carried out considering multiple impact factors such as operating conditions, geometric parameters, and matching materials.

Kazama and Yamaguchi [5] [6] focused on reasonable design criteria for optimum sizes of the bearing and the seal parts of the hydraulic equipment, under the conditions of concentric loads and steady state.

Pang et al. [7] studied the lubrication condition between the slipper and the oblique plate of a high pressure pump that affects its operating life. They investigated oil film pressure distribution and load characteristics considering (a) the pressure–viscosity effect of the lubricant, (b) the pressure–elasticity effect of the lubricating surface, and (c) the properties of dynamic stiffness in the oil film.

Koc and Hooke et al. [8] [9] carried out an experimental and theoretical investigation of the effects of deformation in slipper pad, clamping ratio and orifice size on the load-carrying capacity of hydrostatic thrust bearing under a low-speed condition in axial piston pumps and motors.

Li KY and Hooke [10] measured the friction of water-based slippers. The results were consistent with the clearances predicted using the model developed for oil-based slippers, although the clearances are now typically below 1 μm .

In the last years, using metals, alloys or polymers as substrates, many different strategies have been developed to design functional materials with enhanced repellence to polar or non-polar fluids. However, the application of surface functionalization in the field of fluid power design is a completely new area of application. The engineering of textured surfaces that repel a range of polar and non-polar liquid through appropriate combination of local surface features and alteration is still a hard task. No reference exists in literature, in practice or in patent databases directly addressing the potential benefits to hydraulic pumps and motors of the approach proposed.

Considering the “state of the art” exposed and based on the results obtained in the previous study by the same authors [11], a new set of experimental tests, using the same hydraulic test bench, has been performed in order to compare the performances, in terms of friction coefficient, of nano-coated slippers with respect to standard ones at different working conditions.

2 The tested samples

The piston is located in the cylinder block and oil is fed to the slipper pocket via orifices in the ball-joint and slipper. The slipper pocket is a recess surrounded by the inner land and sometimes an outer land for extra stability. This design is based on the assumption that pocket pressure is equal to piston pressure at zero clearance, and this creates lift in the pocket area which lifts the slipper allowing oil to flow across the lands until the load generated under the slipper matches the load on the piston. The slipper is pivoted

on the ball at the end of the piston to allow it to adjust to the swash plate angle and to rotate relative to the piston. High pressure fluid from above the piston is connected via the control orifices in the piston and slipper to the central slipper pool allowing most of the piston load to be carried hydrostatically. **Figure 4** shows a typical standard slipper.



Figure 4: Standard sample (STD)

The design and synthesis of hybrid organic-inorganic coatings - with a tailored nanostructure and a controlled chemistry - able to significantly reduce the wettability of metals and alloys against fluids have been developed and patented by ISTE-C.N.R [12] [13] [14]. The coating composition is fully compatible from the chemical point of view with the component to be functionalized. The functionalized sample is depicted in **figure 5**. For further details please refer to the above mentioned patents [12] [13].

In this context, precursors of the organic-inorganic coatings have been obtained in form of stable nanosuspensions in water by a sol-gel approach [15] [16], getting a high control degree on phases, particle size (average particle dimensions of about 40 nm) and composition.



Figure 5: Functionalized sample (FNZ)

Each sample has been characterized both with water and with oil (ISO VG 46) and the standard deviation has been calculated. In particular, 2 pairs of standard (STD) slippers and 2 pairs of nano-coated (FNZ) slippers have been tested. The laboratory results are shown in **table 1**.

Laboratory characterization						
Sample	WCA (°)	St. dev.	CAH (°)	St. dev.	OCA (°)	St. dev.
Standard 1	95.6	7.8	22.6	3.2	26.0	5.0
Standard 2	100.8	5.0	25.6	1.4	37.9	6.4
Standard 3	100.0	3.6	26.1	1.7	32.5	3.4
Standard 4	98.1	4.6	27.8	1.0	26.0	2.9
Standard mean	98.6	5.6	25.5	2.7	30.6	6.7
Nano-coated 1	153.9	26.1	9.3	5.4	123.0	15.8
Nano-coated 2	164.9	27.6	9.0	7.8	134.3	22.7
Nano-coated 3	167.4	23.0	4.8	6.3	135.8	24.2
Nano-coated 4	155.6	27.0	10.7	10.2	120.1	18.4
Nano-coated mean	160.4	25.4	9.0	7.3	128.3	20.8

Table 1: Water contact angle (WCA), contact angle hysteresis (CAH), oil contact angle (OCA) for STD and FNZ samples

3 The experimental tests

The activity has focused on the characterization, by means of experimental analysis, of nano-coated (FNZ) slippers with respect to standard (STD) ones.

It is not easy to analyze the real working conditions directly using an axial piston pump. For this purpose an experimental test bench has been designed at IMAMOTER-C.N.R. with the aim to assess the performance of the slipper surface.

The working principle of the test bench is exactly inverse to a real pump (**figure 6**). The slippers are fixed, while the swash plate rotates around axis with a defined rotational speed. The swash plate rotational speed is controlled by a hydraulic motor.

The slippers power supply system (**figure 7**) is controlled by a proportional valve, adapting an existing setup at IMAMOTER-CNR institute. The resistant torque between the slippers and the swash plate is acquired by means of a force sensor (load cell) and a dedicated acquisition set. For further details please refer to the paper [11].

The oil flow rate at the output of the slipper orifice is included between 0.7 and 2.3 l/min depending on the operating conditions.

The superhydrophobic and oleophobic functionalized components, obtained by deposition of inorganic and hybrid organic-inorganic systems, have been mounted on the hydraulic test bench and subjected to the following experimental tests:

- functional test at variable pressure and constant rotational speed
- functional test at constant pressure and variable rotational speed

it is important to underline that the functional tests have been performed with an inclination angle between slippers and swash plate equal to 0° . Therefore the tests simulate a hydraulic pump to zero displacement.

The complete test bench and the hydraulic diagram are depicted in figure 6 and 7.

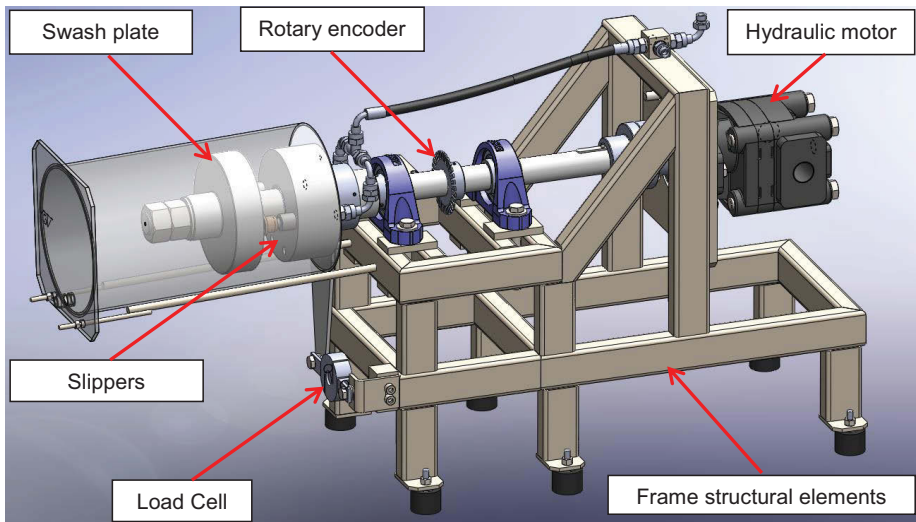


Figure 6: Inverse kinematic test bench

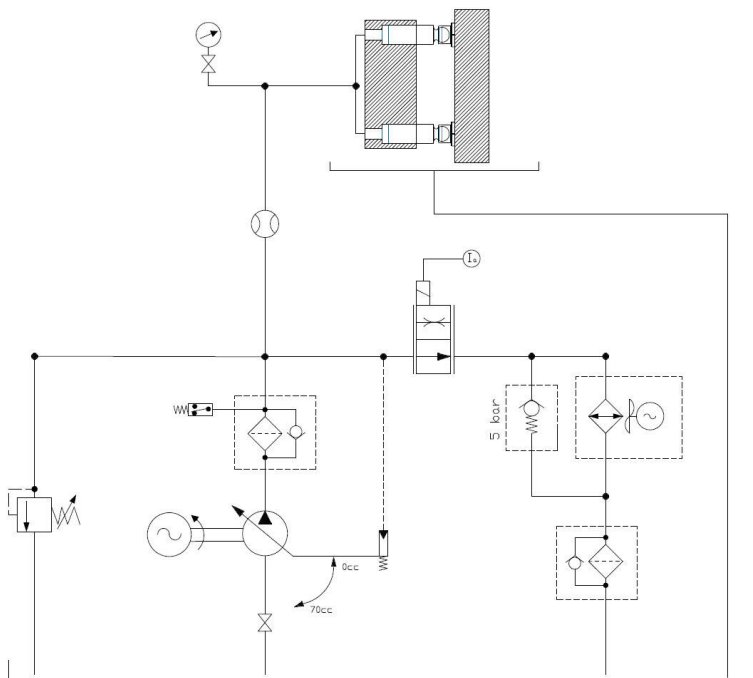


Figure 7: Hydraulic scheme of the slippers power supply system

Before defining the tests performed and the results obtained, let us focus on analytical aspect of the problem.

Known the slipper surface and the supply pressure, the force (load capacity) that the slipper exercise on the swash plate has been calculated as:

$$W = (p_s - p_a) \cdot \frac{\pi}{2} \frac{R_2^2 - R_1^2}{\log\left(\frac{R_2}{R_1}\right)} \quad [\text{N}]$$

Known the axial force acting on swash plate and the load of the cell, the resistant torque has been calculated using the following equation:

$$T_r = (L_c \cdot g) \cdot b_r \quad [\text{Nm}]$$

Known the resistant torque, the friction force has been calculated as:

$$F_f = \frac{T_r}{b_f} \quad [\text{N}]$$

Known the friction force, the friction coefficient has been calculated by means of the following equation:

$$C_f = \frac{F_f}{W}$$

The input data, related to the operating conditions, are defined below:

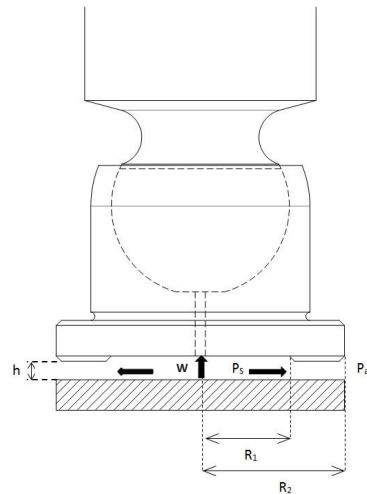


Figure 8: Slipper geometric configuration

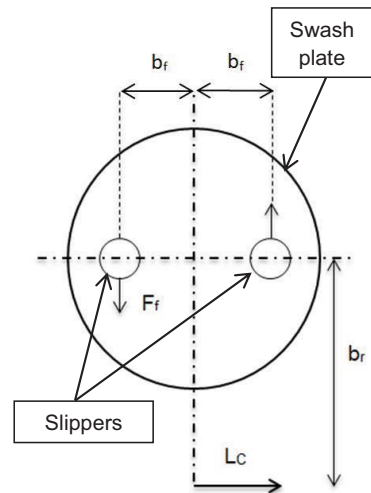


Figure 9: Test bench operating conditions

Test bench Data		
Parameters	Magnitude	Unit
Dynamic load bearing	81	kN
Reaction arm (b_r)	0.23	m
Frictional arm (b_f)	0.15	m
slipper surface	404.5	mm ²

Table 2: Input data

4 Results

As mentioned above, standard (STD) and nano-coated (FNZ) slippers have been tested in order to assess the behavior and the performance from a mechanical point of view. In particular 2 pairs of standard (STD) slippers and 2 pairs of nano-coated (FNZ) slippers have been compared and subjected to the following tests:

- functional test at variable pressure and constant rotational speed (Standard samples 1-2, functionalized samples 1 - 2)
- functional test at constant pressure and variable rotational speed (Standard samples 3-4, functionalized samples 3 - 4)

4.1 Functional test at variable pressure and constant velocity

The tests have been carried out at rotational speed of 1000 rpm and at variable pressure from 10 to 100 bar. Three test have been performed for both standard (1-2) and nano-coated (1-2) slippers under the same working conditions.

The results for standard (**table 3**) and nano-coated (**table 4**) slippers are listed below:

STD slippers				
Pressure [bar]	Test 1	Test 2	Test 3	Mean value
10	1.92E-02 ± 8.86%	2.29E-02 ± 3.71%	1.85E-02 ± 6.81%	2.02E-02 ± 11.70%
20	1.03E-02 ± 7.77%	1.21E-02 ± 5.68%	1.00E-02 ± 4.56%	1.08E-02 ± 10.62%
30	7.31E-03 ± 8.25%	8.66E-03 ± 3.55%	7.05E-03 ± 6.78%	7.67E-03 ± 11.22%
40	5.77E-03 ± 5.13%	6.92E-03 ± 9.27%	5.67E-03 ± 4.08%	6.12E-03 ± 11.36%
50	4.89E-03 ± 8.08%	5.73E-03 ± 5.07%	4.77E-03 ± 3.65%	5.13E-03 ± 10.24%
60	4.30E-03 ± 7.25%	5.03E-03 ± 4.28%	4.20E-03 ± 5.41%	4.51E-03 ± 10.11%
70	3.87E-03 ± 5.83%	4.51E-03 ± 4.12%	3.79E-03 ± 6.60%	4.06E-03 ± 9.63%
80	3.68E-03 ± 5.04%	4.04E-03 ± 4.23%	3.53E-03 ± 2.39%	3.75E-03 ± 6.93%
90	3.50E-03 ± 5.29%	3.76E-03 ± 3.32%	3.29E-03 ± 2.45%	3.52E-03 ± 6.69%
100	3.40E-03 ± 4.96%	3.60E-03 ± 6.17%	3.14E-03 ± 3.92%	3.38E-03 ± 6.86%

Table 3: Friction coefficient of standard (STD) slippers at different pressures

FNZ slippers				
Pressure [bar]	Test 1	Test 2	Test 3	Mean value
10	1.23E-02 ± 11.31%	1.83E-02 ± 13.51%	1.35E-02 ± 12.40%	1.47E-02 ± 21.54%
20	6.64E-03 ± 12.86%	9.91E-03 ± 13.66%	7.31E-03 ± 10.96%	7.95E-03 ± 21.72%
30	4.81E-03 ± 14.83%	7.44E-03 ± 11.56%	5.45E-03 ± 13.65%	5.90E-03 ± 23.24%
40	3.99E-03 ± 12.86%	5.96E-03 ± 10.91%	4.38E-03 ± 13.88%	4.78E-03 ± 21.88%
50	3.62E-03 ± 11.85%	5.00E-03 ± 9.33%	3.77E-03 ± 10.41%	4.13E-03 ± 18.38%
60	3.27E-03 ± 9.27%	4.36E-03 ± 9.72%	3.43E-03 ± 8.67%	3.69E-03 ± 15.96%
70	3.10E-03 ± 6.89%	4.01E-03 ± 7.22%	3.27E-03 ± 9.79%	3.46E-03 ± 13.95%
80	2.96E-03 ± 8.94%	3.70E-03 ± 6.07%	3.01E-03 ± 6.89%	3.22E-03 ± 12.95%
90	2.86E-03 ± 7.61%	3.46E-03 ± 5.91%	2.91E-03 ± 4.94%	3.08E-03 ± 10.85%
100	2.87E-03 ± 5.46%	3.35E-03 ± 5.93%	2.83E-03 ± 5.19%	3.01E-03 ± 9.60%

Table 4: Friction coefficient of nano-coated (FNZ) slippers at different pressures

The mean friction coefficient for standard and functionalized samples at different working pressures is shown in **table 5**.

Mean friction coefficient			
Pressure [bar]	STD samples	FNZ samples	Percentage gain (%)
10	$2.02\text{E-}02 \pm 11.70\%$	$1.47\text{E-}02 \pm 21.54\%$	27.30
20	$1.08\text{E-}02 \pm 10.62\%$	$7.95\text{E-}03 \pm 21.72\%$	26.41
30	$7.67\text{E-}03 \pm 11.22\%$	$5.90\text{E-}03 \pm 23.24\%$	23.12
40	$6.12\text{E-}03 \pm 11.36\%$	$4.78\text{E-}03 \pm 21.88\%$	21.99
50	$5.13\text{E-}03 \pm 10.24\%$	$4.13\text{E-}03 \pm 18.38\%$	19.50
60	$4.51\text{E-}03 \pm 10.11\%$	$3.69\text{E-}03 \pm 15.96\%$	18.25
70	$4.06\text{E-}03 \pm 9.63\%$	$3.46\text{E-}03 \pm 13.95\%$	14.67
80	$3.75\text{E-}03 \pm 6.93\%$	$3.22\text{E-}03 \pm 12.95\%$	14.10
90	$3.52\text{E-}03 \pm 6.69\%$	$3.08\text{E-}03 \pm 10.85\%$	12.55
100	$3.38\text{E-}03 \pm 6.86\%$	$3.01\text{E-}03 \pm 9.60\%$	10.82

Table 5: Mean friction coefficient of STD and FNZ samples at different pressures

The trend of friction coefficient for STD and FNZ samples at different pressures is shown in **figure 10**. The following figure highlights that the friction coefficient of nano-coated samples is lower than standard ones at different working conditions.

Finally the percentage gain, in terms of friction coefficient, of FNZ samples with respect to STD ones has been calculated (**figure 11**).

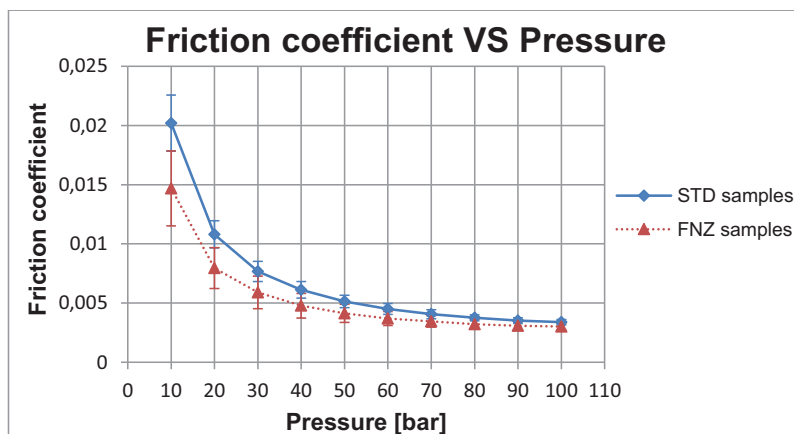


Figure 10: Friction coefficient VS Pressure

The percentage gain of the functionalized samples with respect to standard ones is included between 27% and 10%. The friction coefficient reduction allows to obtain an improvement of the mechanical efficiency of the machine. The results obtained in the following work differ from those obtained in the paper [11]. As regards the paper [11], the test (at variable pressure) has been performed at 700 rpm and at room

temperature. In the following work, the test at variable pressure has been performed at 1000 rpm and an oil temperature equal to 50 °C.

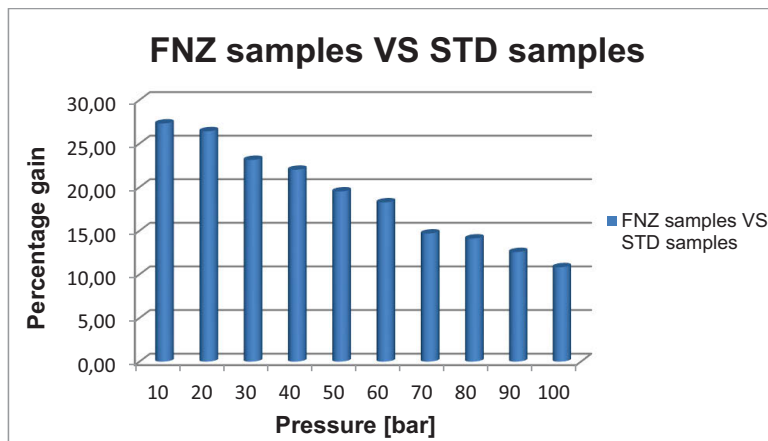


Figure 11: Percentage gain of FNZ samples with respect to STD ones

4.2 Functional test at constant pressure and variable rotational speed

The tests have been performed at constant pressure of 50 bar and at variable rotational speed from 300 to 1800 rpm. Three test have been performed for both standard (3-4) and nano-coated (3-4) slippers under the same working conditions.

The results for standard (**table 6**) and nano-coated (**table 7**) slippers are listed below:

STD samples				
Rotational speed [rpm]	Test 1	Test 2	Test 3	Mean value
300	3.42E-03 ± 4.11%	4.04E-03 ± 6.23%	4.04E-03 ± 5.65%	3.83E-03± 9.27%
600	4.62E-03 ± 0.51%	4.73E-03 ± 0.76%	4.65E-03 ± 0.82%	4.67E-03± 1.26%
900	5.35E-03 ± 0.82%	5.39E-03 ± 0.25%	5.35E-03 ± 0.33%	5.36E-03± 0.41%
1200	6.00E-03 ± 0.76%	5.85E-03 ± 0.92%	5.89E-03 ± 0.55%	5.91E-03± 1.35%
1500	6.66E-03 ± 1.32%	6.31E-03 ± 1.82%	6.39E-03 ± 1.74%	6.45E-03± 2.82%
1800	7.31E-03 ± 2.14%	6.92E-03 ± 1.73%	6.92E-03 ± 1.61%	7.05E-03± 3.15%

Table 6: Friction coefficient of standard (STD) samples at different rotational speed

FNZ samples				
Rotational speed [rpm]	Test 1	Test 2	Test 3	Mean value
300	2.85E-03 ± 5.40%	3.08E-03 ± 3.45%	3.27E-03 ± 2.59%	3.06E-03± 6.91%
600	3.69E-03 ± 3.46%	3.92E-03 ± 2.03%	4.04E-03 ± 2.14%	3.89E-03± 4.54%
900	4.35E-03 ± 1.08%	4.54E-03 ± 1.34%	4.58E-03 ± 2.16%	4.49E-03± 2.76%
1200	4.92E-03 ± 1.36%	5.08E-03 ± 1.67%	5.23E-03 ± 2.15%	5.08E-03± 3.03%
1500	5.39E-03 ± 1.07%	5.62E-03 ± 1.93%	5.73E-03 ± 2.26%	5.58E-03± 3.16%
1800	5.96E-03 ± 2.12%	6.15E-03 ± 2.64%	6.54E-03 ± 3.34%	6.22E-03± 4.72%

Table 7: Friction coefficient of nano-coated (FNZ) samples at different rotational speeds

The mean friction coefficient for standard and functionalized samples at different rotational speeds is shown in **table 8**.

Mean friction coefficient			
Rotational speed [rpm]	STD samples	FNZ samples	Percentage gain (%)
300	3.83E-03± 9.27%	3.06E-03± 6.91%	20.07
600	4.67E-03± 1.26%	3.89E-03± 4.54%	16.76
900	5.36E-03± 0.41%	4.49E-03± 2.76%	16.27
1200	5.91E-03± 1.35%	5.08E-03± 3.03%	14.10
1500	6.45E-03± 2.82%	5.58E-03± 3.16%	13.52
1800	7.05E-03± 3.15%	6.22E-03± 4.72%	11.82

Table 8: Mean friction coefficient of STD and FNZ samples at different rotational speeds

The trend of friction coefficient for STD and FNZ samples at different rotational speeds is shown in **figure 12**. The following figure shows that the friction coefficient of functionalized samples is lower than standard ones at different working conditions. Finally the percentage gain, in terms of friction coefficient, of FNZ samples with respect to STD ones has been calculated (**figure 13**).

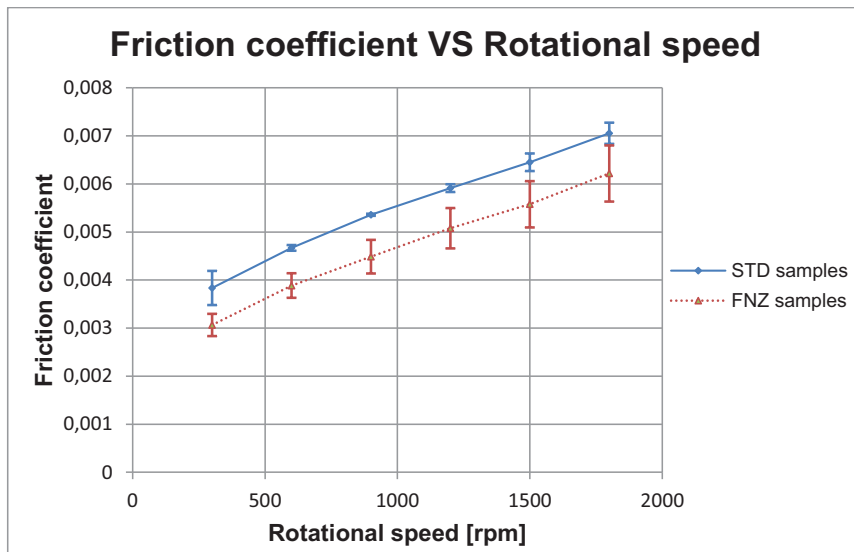


Figure 12: Friction coefficient VS rotational speed

The percentage gain of the functionalized samples with respect to standard ones is included between 20% and 12%. The friction coefficient reduction leads to an improvement of the mechanical efficiency of the machine.

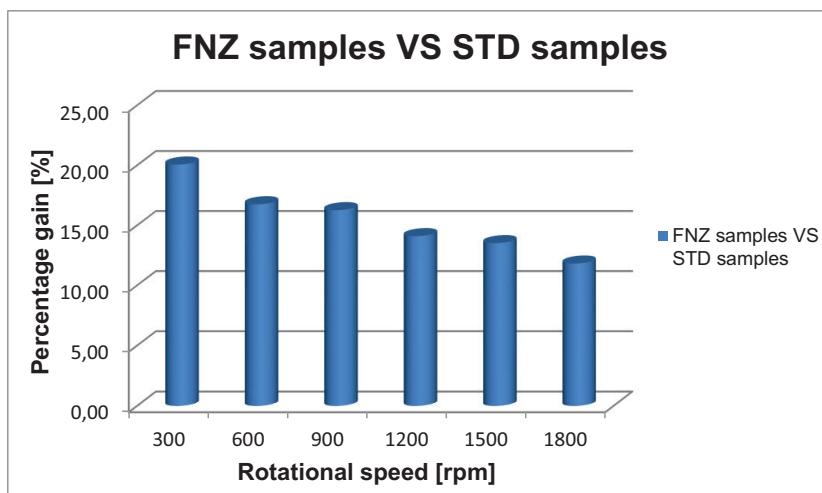


Figure 13: Percentage gain of FNZ samples with respect to STD ones

5 Conclusions

The application of special nano-coating surface treatments has been exploited by a mixed research team with the aim to reduce the friction losses in a axial piston pump. A method for the nano-coating of metallic surface has been developed by ISTE-C.N.R. and applied, in cooperation with IMAMOTER-C.N.R., to the slipper surface commonly used in a hydraulic piston pump. To coat the slippers the dip-coating methodology has been used and a hydraulic test bench, able to reproduce the real hydrostatic lubrication working conditions, has been designed.

The results obtained in the following work compared to those of the paper [11] differ in the operating conditions of the tests. As regards the paper [11] only a test at variable pressure has been performed, whereas in the following work two different tests (test at variable pressure, test at variable rotational speed) have been performed. The rotational speed is equal to 700 rpm in the paper [11], whereas in the following work the rotational speed is 1000 rpm. Oil temperature is not taken into account (tests at room temperature) in the paper [11], whereas in the following work the oil temperature is 50 °C for all tests.

The laboratory studies performed on coated slippers show that:

- the nano-structured coating increases the hydrophobicity and oleophobicity of the functionalized samples
- Water contact angle (WCA) for nano-coated samples is equal to 160°, promoting the super-hydrophobicity
- Oil contact angle for nano-coated samples is equal to 128°, promoting the oleophobicity

The experimental tests performed on the hydraulic test bench show that:

- Nano-coated samples have a friction coefficient lower than standard ones
- The percentage gain, related to the functional test at variable pressure and constant rotational speed, of the nano-coated samples with respect to standard ones is included between 27% and 10%
- The percentage gain, related to the functional test at constant pressure and variable rotational speed, of the nano-coated samples with respect to standard ones is included between 20% and 12%

In conclusion the nano-coated slippers show, in the various operating conditions, a clear friction coefficient reduction with respect to standard slippers. This leads to an improvement of mechanical efficiency and therefore the overall efficiency of the machine increases.

Acknowledgement

The authors express their acknowledge to **HP S.p.A.** (Bondioli & Pavesi Group) for the technical support.

The work has been developed under the project **Surface Nano-structured Coating for Improved Performance of Axial Piston Pumps (SNAPP)**, proposed under the “**Fabbrica del Futuro**” research program, financed by the Italian University and Research Ministry (MIUR) and coordinated by the Italian National Research Council (C.N.R.)

References

- [1] Masashi Miwa, Akira Nakajima, Akira Fujishima, Kazuhito Hashimoto and Toshiya Watanabe. *Effects of the Surface Roughness on Sliding Angles of Water Droplets on Superhydrophobic Surfaces*. Langmuir 2000, 16, 5754-5760.
- [2] Adamson A. W. *Physical Chemistry of Surfaces*. New York: Wiley.
- [3] Israelachvili J. N. *Intermolecular and Surface Forces*. 2nd edn, London: Academic.
- [4] Bhushan B. *Handbook of Micro/Nanotribology*. 2nd edn, Boca Raton, FL: CRC Press.
- [5] Kazama T, Yamaguchi A. *Optimum design of bearing and seal parts for hydraulic equipment*. Wear 1993;161(1–2):161–71.
- [6] Kazama T, Yamaguchi A. *Application of a mixed lubrication model for hydrostatic thrust bearings on hydraulic equipment*. ASME J Tribol 1993;115:686–91.
- [7] Pang Z, Zhai W, Shun J. *The study of hydrostatic lubrication of the slipper in a high-pressure plunger pump*. STLE Tribol Trans 1993; 36(2):316–20.

- [8] Koc E, Hooke CJ, Li KY. *Slipper balance in axial piston pumps and motors*. ASME J Tribol 1992;114(4):766–72.
- [9] Hooke CJ. *The lubrication of slippers in axial piston pumps and motors—the effect of tilting couples*. Proc Inst Mech Eng Part C: J Mech Eng Sci 1989;203(C):343–50.
- [10] Li KY, Hooke CJ. *Note on the lubrication of composite slippers in water-based axial piston pumps and motors*. Wear 1991;147(2):413–37.
- [11] G. Rizzo, G. P. Massarotti, A. Bonanno, R. Paoluzzi, *M. Raimondo,*M. Blosi, *F. Veronesi,*A. Caldarelli, *G. Guarini, *Axial piston pumps slippers with nano-coated surfaces to reduce friction*. International Journal of Fluid Power 2015, 16 (1): 1-10
- [12] Patent 1: RM2011A000104 (deposited in 3 Marzo 2011; PCT procedure is ongoing). Author: M. Raimondo and M. Blosi (ISTEC CNR), F. Bezzi and C. Mingazzini (ENEA UTTMAT Faenza)
- [13] Patent 2: RM2012A000291 (depositato in data 21/06/2012). Author: M. Raimondo and M. Blosi (ISTEC CNR), F. Bezzi and C. Mingazzini (ENEA UTTMAT Faenza)
- [14] M. Raimondo, *Making super-hydrophobic building materials: static and dynamic behavior of nanostructured surface*. at IV ICC4-International Ceramic Conference, Chicago (USA), July 14-19, i 2012 Invited talk
- [15] W. Ma, H. Wu, Y. Higaki, H. Otsuka, A. Takahara, Chem. Commun., 48, 6824-6826 (2012) *sol-gel*.
- [16] Raimondo M, Blosi M, Caldarelli A, Guarini G, Veronesi F. *Wetting behavior and remarkable durability of amphiphobic aluminum alloys in a wide range of environmental conditions*. Chemical Engineering Journal 2014; <http://dx.doi.org/10.1016/j.cej.2014.07.076>

Nomenclature

W	Load capacity	N
p_s	Supply pressure	Pa
p_a	Atmospheric pressure	Pa
R_2	Outer radius	m
R_1	Inner radius	m
T_r	Resistant torque	Nm
L_c	Load cell	kg
g	Gravity acceleration	m/s ²
b_r	Reaction arm	m
F_f	Friction force	N
b_f	Friction arm	m
c_f	Friction coefficient	

Group 6: Industrial Hydraulics

Consistent Automation Solutions for Electrohydraulic Drives in Times of Industry 4.0

Dr.-Ing. Albert Köckemann

Bosch Rexroth, Jahnstraße, 97816 Lohr am Main, E-Mail: albert.koeckemann@boschrexroth.de

Dipl. Ing. Benno Birke

Bosch Rexroth, Jahnstraße, 97816 Lohr am Main, E-Mail benno.birke@boschrexroth.de

Abstract

Electrohydraulic drives are primarily used whenever a low power/weight ratio, a compact build and/or large forces are required for individual applications. These drives are often used together with electric drive technology in machines. However, in terms of automation, unlike electric drives, electrohydraulic drives are still largely connected via analog interfaces and centralized closed control loops today. To compensate for this competitive disadvantage of hydraulic drive technology and, at the same time, significantly enhance its performance and diagnostics capability, a consistent automation solution has been developed that can be configured for both centralized and decentralized solutions. This contribution firstly gives an overview over this complete solution already available and its classification in the automation world. In a second step, the subset of decentralized drive solutions contained therein is presented in more detail and their benefits are explained on the basis of some exemplary applications.

KEYWORDS: Electrohydraulic drives, valves, pumps, Ethernet based bus systems, decentralized axis control, Industry 4.0

1. Initial situation and target

Figure 1 shows both the current situation and a target situation, characterized by the following starting points:

- Actual status of valves/pumps: Today, the majority of valves and control pumps are controlled via analog interfaces (+/-10 Volt, 4...20 mA). For the automation level, suitable interfaces have to be made available.
- Actual status of axis control loops: The control loops are mainly realized centrally in the higher-level control here, control algorithms tailored specifically to hydraulic requirements and an adequate computing capacity have to be available.

- Actual status of real-time-capable bus systems: In the field of automation technology, Ethernet-based bus systems are on the rise. The prevalence of various control manufacturers on individual markets and/or regions, results, unfortunately, in a very heterogeneous situation regarding the bus systems to be supported (at present, the solution presented here supports 6 systems) /1/.

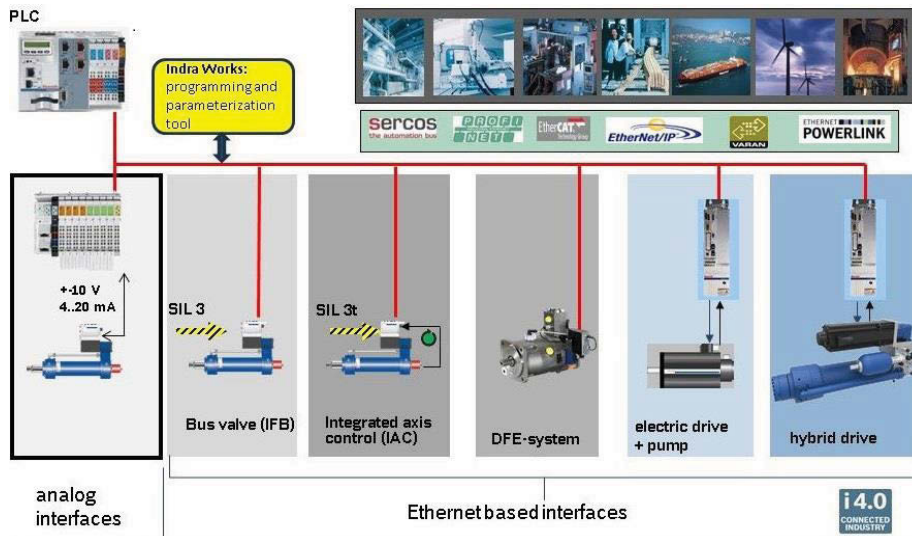


Figure 1: Current and future connectivity of electrohydraulic and hybrid drive technology to automation technology

To achieve the full integration of "classic electrohydraulic drives" on the one hand and also take account of "new hybrid systems" such as the "servo-pump" and the "self-contained axis" on the other, the target situation as shown on the left below has been defined, which is realized today by the newly developed, consistent automation system:

- Valves and control pumps can be controlled directly via the bus system.
- With regard to valves, a distinction must be made between an IFB function (Integrated Field Bus) and an IAC (Integrated Axis Control) function:
 - IFB: Analog interfaces are substituted by an Ethernet-based bus system. The integrated bus functionality allows additional data to be exchanged with the higher-level control for configuring the valve or for transmitting internal state variables. The open and closed-loop control task for the drive remains within the higher-level control (central control structure).

- IAC: In addition, the axis control loops (position, velocity, pressure and/or force control) are realized in a decentralized arrangement. The higher-level control provides command values and status signals in real time.
- The "servo-pump" system (Sytronix) utilizes the automation connections of electric drive technology.
- The same is valid for the hybrid drive, which consists of an electric servo-drive with hydrostatic transmission ("self-contained axis"). The axis control functionality of the hydraulic subsystems, which is required additionally, is implemented as part of the converter firmware /3/.

2. Demands made on the target system

The requirements can be subdivided into the following three areas:

2.1. Functional requirements (obligatory requirements)

- Implementation of all relevant Ethernet-based bus systems customers can use virtually all automation systems relevant on the market (open interfaces).
- Implemented axis controller algorithms are tailored to suit the special requirements of electrohydraulic drives /3/.
- Integrated safety concept also in the field of valve and pump connections, which receive the bus communication on the one hand and implement the required safety standard on the other (examples of this are press safety or the demands made on the closing axis of plastics machines).
- The bus communication is not only used for transmitting command and feedback values, but also for additional information from components and drives in terms of data, a "Condition Monitor (CM) Ready" situation is realized in the control.
- Tools such as the software oscilloscope functions are essential for commissioning.

2.2. Desirable requirements ("usability") and approaches

- One consistent programming and commissioning tool for all drive forms (electric and hydraulic drives),
- Identical bus connections for all drive forms (state machines),
- Identical parameter designations and scaling of machine data for all drive forms,
- Commissioning (in particular of hybrid drives) is simplified by software-supported tools like "wizards" and automatic optimization algorithms.

Due to the PC-supported programming and parameterization tool IndraWorks (IW), which can be used equally for electric and hydraulic drives, these requirements can consistently be met. Consequently, electric and hydraulic drive technology are treated identically. Due to dialogs in IW tailored specifically to the individual devices, special characteristics of drives are taken into account and commissioning is simplified.

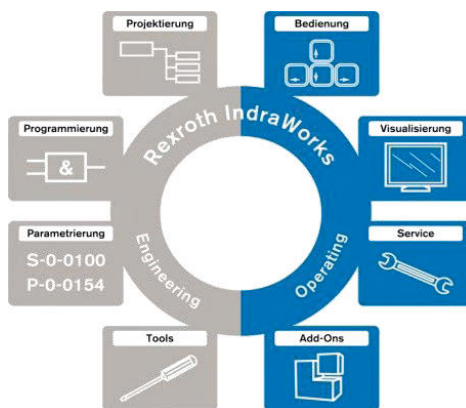


Figure 2: Overview of functions of the IndraWorks tools, which can be used consistently for all drive forms

3. Commercial requirements

- A portfolio of components and drives is required, which is widely scalable with regard to performance and functionality, since customers only pay for what is actually required for the application at hand.
- The extra cost resulting from the digitization of valve and pump electronics has to be justified in the concrete application through added value offered by direct bus integration, reduced commissioning expenditure, lower cabling effort and/or important additional functionalities such as decentralized control and CM functionalities.

4. More detailed description of decentralized drive systems (IAC)

For lack of space only the drive systems in the IAC characteristic (Figure 1) are described exemplarily in the following /4/.

The components available for this can be classified into the following sub-systems:

- In the field of valves, direct and pilot operated proportional and high-response valves of the 4WRPE family are available today in sizes 6, 10, 16, 22, 25, 27, 32.



Figure 3: Valve family with IAC technology (sizes 6, 10, 16 - 32)

- In the field of pumps, control pumps with DFE functionality /2/ of series A10 and A4 in sizes 28, 45, 71, 100, 140, 180, 250 and 355 are available today.



Figure 4: DFE control pump system with IAC functionality

- Digital integrated electronics (OBE=On-Board Electronics) for these valves and pumps are available in the variants IFB and IAC. The functionality of the OBE is described in more detail in the section below.

4.1. Description of the digital OBE

4.1.1. Hardware

The robust IP65 electronics is available in the IFB and IAC characteristics. Both are equipped with interfaces for up to 4 pressure sensors (4 - 20 mA). In the IAC variant, interfaces for position measuring systems (SSI) and incremental interfaces (1 Vpp) are available additionally. For communications, a Multi-Ethernet interface is integrated, which allows one of the following bus systems to be implemented:

- Sercos, EtherCAT, POWERLINK, VARAN, PROFINET, EtherNet/IP.

In other words, every component "speaks six languages". Hardware variances due to different bus systems can thus be avoided. The bus system to be activated is determined by means of software using a corresponding parameter.

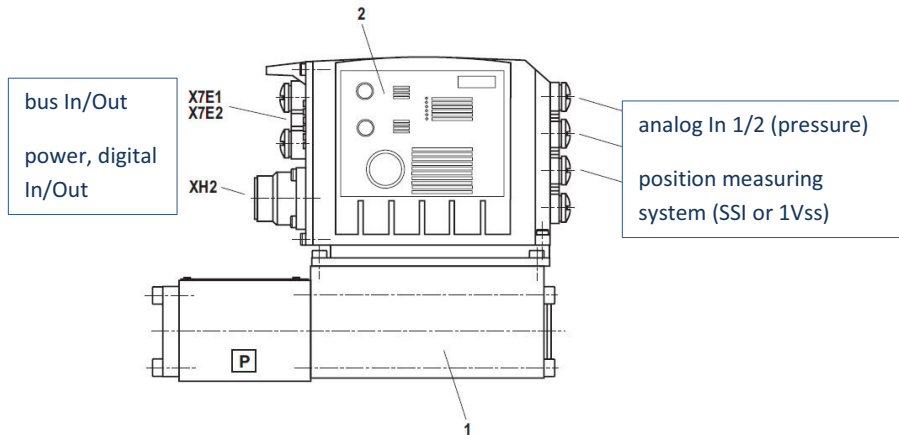


Figure 5: Interfaces of the digital OBE

The functionalities of "Safe Halt", "Safe Direction" and "Central Position Monitoring" are realized independently of the bus system via two certified digital inputs and two associated digital output signals. With regard to the valves, they provide a safe shutdown of the output stages for the solenoid(s). This approach allows a safety functionality to be realized without having to design the entire bus system, master included, as safe system.

4.1.2. Software functionality of the OBE

In the following, some functionalities are described in more detail for the field of valve-controlled drives; for control pumps, comparable functionalities are available - where useful in the technical application:

- **Bus communication:** At present, 6 Ethernet-based bus systems can be realized. The selection of the bus system to be used is made by means of a parameter.
- **Valve controller:** The dynamic behavior of the valve can only be modified by the manufacturer. The valve characteristic (curve) can, however be entered by the customer.
- **Closed-loop flow control:** By means of up to 4 integrated pressure sensors in sandwich plate technology, an electronic "pressure compensator function" (load-independent flow) can be implemented. This may be useful in particular for

applications, in which the use of a position measuring system is out of the question for reasons of expenditure or for technical reasons (e.g. core pull function in the field of plastics machinery).

- **Closed-loop pressure control:** Apart from pure pressure control functions (pressure and differential pressure), alternating controls and force limitation modes can be activated.
- **Position controller:** All of the algorithms required for hydraulic drive technology were implemented in this controller. This includes also processes for state feedback and continuous path control /1/.

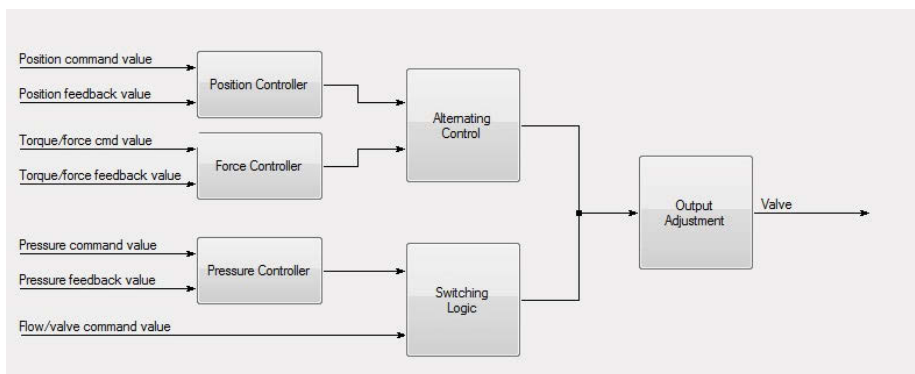


Figure 6: Axis controller structure of the IAC (overview)

Diagnostics and commissioning aids: Apart from analysis tools such as a software oscilloscope and error log, wizards for the pre-calculation of control parameters as well as automatic optimization tools for axis controllers in the continuous path control mode are provided. In future SW versions, functionalities **for Condition Monitoring** will be offered.

- **Monitoring functions:** In addition to monitoring of the valve functionality, the IAC also offers axis monitoring functions (max. velocities, forces, dynamic following errors, etc.).
- **Integrated PLC:** This option will be offered from mid 2016 on and will allow programming of specific functionalities by the customer such as adjustment of the controllers to individual applications, special motion profiles or also application-specific reactions to errors. Here, the customer can flexibly integrate its know-how and protect it accordingly.

5. Application examples for decentralized IAC technology

This drive structure suggests itself particularly for applications, in which:

- the various axes of the machine can be operated independently of one another, or
- the dependencies of axes only have to be taken into account for the generation of command values (such as, for example, with interpolating axes).

A further criterion for the use of IAC can be a large number of axes to be controlled: As a result of the decentralized control approach, the central control is relieved and, in addition, cabling efforts can be drastically reduced.

Application 1: Automation of axes in a sawmill

Examples of axes are shown in Figure 7. A large number of self-contained axes and large physical distances are decisive for the selection of a decentralized drive structure. EtherNet/IP is used as bus system, an AB system as higher-level control.

Compact Single Pass Sawing Line

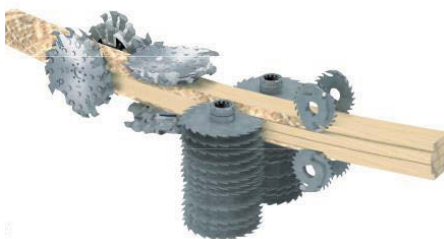


Figure 7: Some axis of the “Sawmill application”

The system, which has been employed in three-shift operation for more than one year under these very harsh operating conditions, documents the robustness and reliability of the selected solution.

Application 2: Axes in the field of rotary indexing machines

For this application (Figure 8) the demands made on the drive axes and the entire automation solution are extremely exacting:

- Up to 48 interpolating electrohydraulic axes plus electric servo-drives,
- The accuracy requirements with regard to continuous path and positioning accuracies are in the order of a few μm ,

- The CNC technology utilized for the axes has to realize up to 28 NC channels.

Here, the IAC technology is operated in conjunction with an MTX control. The bus system used is Sercos.



Figure 8: Application of rotary indexing machines

Thanks to this technology it was possible to increase the productivity of the machine by 20 % compared with the previous solution. At the same time, system costs were reduced by lower cabling and commissioning costs as well as optimized CNC technology. The machines work trouble-free in three-shift operation.

6. Conclusion

The efficiency of electrohydraulic drive technology and not least their full and "easy" integratability into automation solutions are, apart from the drive cost, essential competitive criteria that speak in favor of this drive technology. The concept presented here is characterized by its consistency in terms of automation. The key aspects are

- The integration of open bus interfaces into the hydraulic components,
- The integration of the "hydraulic know-how" into the drive firmware,
- The identical behavior as that of electric servo-drives when it comes to automation,
- One consistent commissioning and diagnostic tool for all drive types, i.e. valve-controlled, pump-controlled and hybrid systems consisting of electric servo-drive with downstream hydrostatic transmission.

Whether central or decentralized axis controls may be the better concept depends on the application at hand. Such concepts make hydraulic drive technology "Industry 4.0"-capable and maintain its competitiveness as physically compact and robust drive technology that generates high speeds and large forces.

7. References

- /1/ Feuser, Alfred: Modern Electrohydraulic Drive Technology for Stationary Machinery in Industrial Automation, ifk 2010, page 29-49
- /2/ Köckemann, Albert: Systemlösungen für die Automation elektrohydraulischer Antriebe ifk (internationales Fluidtechnisches Kolloquium) 4/2004
- /3/ Köckemann, Albert: Dezentrale Steuerungs- und Regelungssysteme für elektrohydraulische Antriebe, ifk (internationales Fluidtechnisches Kolloquium) 2/2000
- /4/ Bosch Rexroth, RD 29391 Ausgabe 2015-07: Regel-Wegeventil, direktgesteuert mit integriertem digitalem Achs-Controller (IAC-Multi-Ethernet)

Adaptive process control for stabilizing the production process in injection moulding machines

Dr.-Ing. Reinhard Schiffers

KraussMaffei Technologies GmbH, Krauss-Maffei-Straße 2, 80997 München, E-Mail: reinhard.schiffers@kraussmaffei.com

Georg P. Holzinger

KraussMaffei Technologies GmbH, Krauss-Maffei-Straße 2, 80997 München, E-Mail: georg.holzinger@kraussmaffei.com

Gernot Huster

KraussMaffei Technologies GmbH, Krauss-Maffei-Straße 2, 80997 München, E-Mail: gernot.huster@kraussmaffei.com

Abstract

Plastic injection moulding machines are a positive example of the possibilities in terms of performance and energy efficiency of modern hydraulic drives technology. In addition to the performance and energy efficiency of the machines, the quality of the plastic mouldings and an easy to use machines control is the focus. To ensure a constant plastics part quality the set process parameters of the injection moulding machines are kept constant by appropriate closed loop control strategies today. Assuming a constant quality of the processed plastic raw material, this strategy is effective. If it comes to a qualitative variation in the processed plastics, which often leads to a change in viscosity of the plastics melt, keeping processing parameters constant will not lead to a constant quality of the moulded parts. The deviations in the plastics viscosity have such a great influence on the moulding process that the relevant process parameters have to be adjusted manually in many cases. Often the stroke of the reciprocating screw system has to be adapted to reach a constant filling volume of the cavity and therefore avoid burr formation or short shots. In this paper an approach for adaptive process control is introduced. This control loop is able to correct the set points of specific machines parameters online within the production cycle and therefore is able to avoid changes in the produced parts quality.

KEYWORDS: plastics injection moulding, injection moulding machine, adaptive control, quality control,

1. Background

Today's injection moulding machines are equipped with very high precision drives. In particular, the translational motion of the reciprocation screws system for injecting the melt into the cavity is controlled precisely with a closed loop control. However, batch variations and start-up effects still have a negative impact on the produced parts quality [1], [2]. Currently the method of choice is to stabilize part quality by keeping the machines set values in the narrowest range. Therefore temperatures, accelerations, velocities etcetera are kept constant over the production time.

There are two types of disturbances to the injection moulding process. Internal effects that result from manufacturing tolerances of the relevant processing technology elements, for example a not consistent closing behaviour of the non-return valve (on top of the injection screw) leads to deviations in displaced melt volume. External effects come to the injection moulding machine with the processed raw material and mainly result in a change in viscosity of the plastics melt. The change in viscosity itself induces more deviations while processing, for example the shear heating while injection is different. The different temperature of the melt in the mould leads to a variation in the molecular structure when cooling down to solid state again. These disturbances affect the process and the quality of the moulded parts (weight, dimensions, surface) in a negative way [3], [4].

Talking about changes in viscosity of the plastics melt the method of choice to correct the negative influence on the plastics part is to adapt the switch-over position from the speed controlled filling phase to the pressure controlled holding-phase. The target is to keep the degree of mould-filling at the position of switch-over constant. The different viscosity comes with different resistance to flow and therefore results in changed amount of displaced melt at identical injection stroke. Today this value is corrected by the machines operator intermittently after checking the parts quality. Thus the effects of changes are only corrected manually and on an incidental base, which may lead to a production of reject parts.

Comparable situations may occur within transient phases in injection moulding processes. In case of a pause due to failure or a planned mould change the thermal equilibrium state which developed over time is changed. The plasticized melt inside the barrel experiences a significantly different energy input since the process is stopped and time proportions are different. The quality (temperature and thus viscosity) of the processed resin is different. When starting the injection moulding process after a production interruption the results are significantly influenced. The task of an adaptive

process control is to correct the processing parameter in a way that the quality of the plastics part is constant. Mainly this is achieved by assuring a volumetrically constant filling of the cavity in each cycle. This is done first by the adaption of the switch-over position and second by adapting the holding pressure level based on the viscosity of the melt, details may be seen in /5/.

2. Plastics injection moulding process

The injection moulding process contains several process steps, where a thermoplastic based material is plasticized and injected into a cavity. The material is pressed into the mould and after cooling down ejected. There are furthermore many special processing technologies in injection moulding that have specific demands towards the process control.

The feedstock is brought into the injection moulding machine with the feed hopper, where the granular material directly flows down to the plastification screw. The material is now plasticised by the energy that is dissipated by the rotation of the screw as well as by the heat conducted from the tempered barrel. While plasticising the screw moves backwards and the plasticized plastic is stored in front of the screw for the next injection cycle. A non-return valve at the tip of the screw prevents the molten plastic from flowing back into the screw flights.

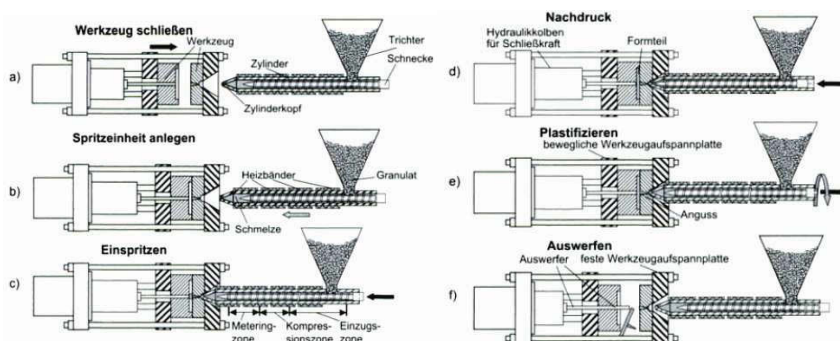


Figure 1: Injection moulding process; a) mould closing; b) moving of injection unit; c) injection phase; d) holding pressure phase; e) plastification phase; f) mould open and ejection; based on /6/

When the mould is closed the injection phase starts, the injection unit with the plastification barrel is moved towards the mould up to contact with the nozzle. Thereafter a speed controlled volumetric filling of the mould and a pressure and time controlled compression (holding-pressure) phase follows. Simultaneously the cooling of the injected plastics material takes place. The holding-pressure phase is mainly needed to compensate the thermal shrinkage of the material. While the formed part cools down the plastification of new material takes place. As the plastic part has reached its solidification temperature the mould can be reopened and the formed part is removed by an ejector system /7/.

3. Function of the adaptive process control concept

The adaptive process control method is introduced with the help of exemplary processing parameters from a standard thermoplastic injection moulding machine. In the first step the viscosity of the plasticized polymer melt is characterized by a defined key indicator in the injection phase. The corresponding process variable is to be measured in a suitable way. For hydro-mechanically driven machines this is done by measuring the driving hydraulic pressure. The pressure is converted to plastics melt pressure with the area ratio between hydraulic cylinder and screw diameter. The position of the screw is measured by an appropriate external position sensor. An injection work equals the displacement of the molten plastic volume flow against a resistance. Similarly to a viscometer, the work is measured during injection phase as an integral of the injection pressure over screw stroke. For integrating over time the result is an injection energy instead of a work (1) /3/.

$$MI = \int_{t(s=MI_{Pos1})}^{t(s=MI_{Pos2})} p(t) dt \quad (1)$$

MI stands for the range of the screw stroke in which the pressure integral is to be calculated (**Figure 2**). This range must be chosen in a way that no dynamic effects (e. g. pressure oscillations) in the displaced melt have a negative impact on the measurement. In order to eliminate effects of a differing closing behaviour of the non-return valve (NRV) the measuring range has to be determined specific for each cycle. The measuring interval position is then shifted based on the deviation in the closing point of the NRV. The evaluation of the pressure gradient at the beginning of the mould filling gives the actual closing position of the NRV and the range of MI is shifted accordingly (**Figure 3**).

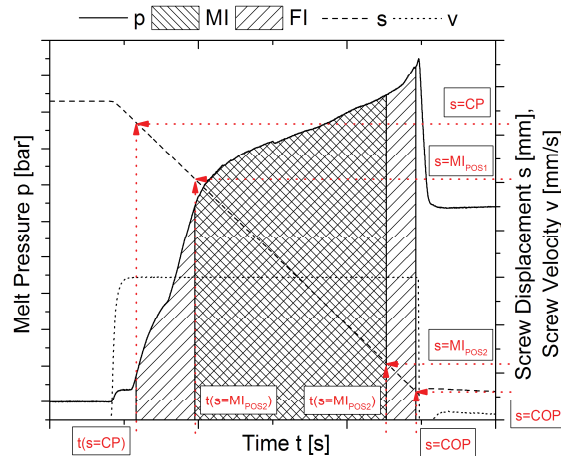


Figure 2: Melt pressure and screw displacement during the injection- and holding phase. The viscosity index (VI) is formed depending on the closing behaviour of the non-return valve. The filling index (FI) describes the volumetric filling of the cavity and is similar to the injection work.

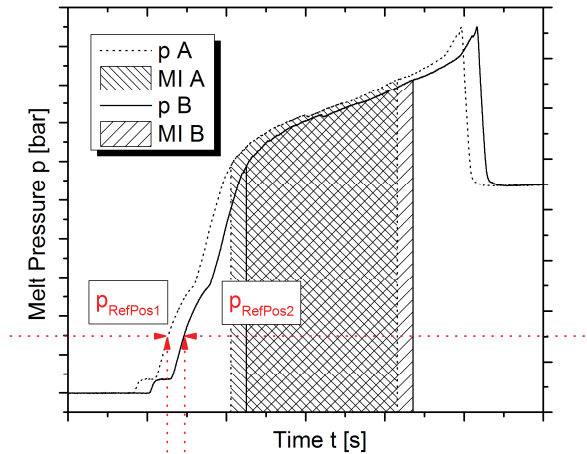


Figure 3: Shift of the measurement interval MI to avoid measurement failures due to unsteady closing of the non-return valve.

Plastic melts are shear viscous and the volume flow rate has a big influence on the resulting viscosity. For this reason, the characteristic flow resistance is furthermore scaled to the mean of the injection speed v_{MI} . For characterizing the quality of the melt, this normalized characteristic parameter may now be used: viscosity index (VI).

This key figure is measured online in the injection phase. An additional scaling may be added with the correction constant K_1 (2).

$$VI = MI * \frac{K_1}{v_{MI}} \quad (2)$$

Also a filling index (FI) is calculated which describes the active cavity filling from the position where the return valve closes $s = CP$ until switch-over $s = COP$ (3) (Figure 2).

$$FI = \int_{t(s=CP)}^{t(s=COP)} p(t) dt \quad (3)$$

During the injection phase the filling index is calculated. The integral starts when the non-return valve is closed (closing position) and ends at the switch-over position.

The approach of an adaptive process control now uses a key ratio for characterizing the process. A moulded part volume equivalent (MPV) is calculated. The filling index is set at a ratio to the viscosity index. This ratio describes the displaced volume of plastic melt at a given individual flow resistance of every single injection moulding cycle (4).

$$MPV = \frac{FI}{VI} \quad (4)$$

Rearranging the equation the value of FI may be determined. With a fixed (reference) value of MPV and a cycle-specific value of VI one can calculate the target value for a constant melt displacement. Hence the injection process is stopped, when the value FI reaches the target value. The reference values are extracted based on a running process inside the quality tolerances. In this manner, the volumetric filling of the cavity may be kept constant (within limitations) independently of viscosity variations induced by the processed resin.

The holding pressure phase starts after switch-over in order to compensate the thermal shrinkage caused by the decrease of the specific volume of the plastic. Therefore a holding pressure is applied to deliver the needed volume. Depending on the used polymer, the cavity geometry and process parameters used the holding pressure has to be chosen.

$$p_{packP} = p_{packL} * (1 + \frac{VI_P - VI_L}{VI_L} * K_2) \quad (5)$$

In general, the higher the holding pressure is applied, and the longer it is applied, the more melted resin is pushed into the cavity. In order to correct the effects of changing

viscosities it is needed to adopt the holding pressure level. This is done in accordance to the above shown variables characterizing the melt (5).

Figure 4 below shows the pressure profile of the injection- and beginning of holding-phase of two polymer melts. A reduction in viscosity of the plastics melt from Example A to B leads to lowered injection pressure. Regarding (4) a lower FI is needed for a correct volumetric filling of the cavity. In that case the switch-over will take part at an earlier state (position). Also the holding pressure level is reduced accordingly to the ratio of VI_p to VI_L in (5).

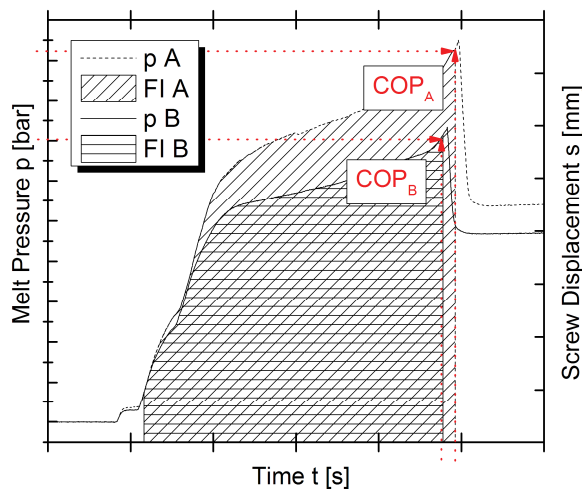


Figure 4: The melt pressure curves for a plastic melt A and B. Hatched shown are the FI's to the corresponding materials. Material B has a lower viscosity than Material A, so that less injection pressure is needed to fill the cavity, therefore, it is switched-over on an earlier screw position from injection- to holding pressure phase.

4. Validation of the adaptive process control concept

In order to evaluate the effectiveness and robustness of the adaptive control concept an extensive field test program was conducted. Representative for the test program two processes will be shown in detail. First reference is a trial using a hydraulically driven injection moulding machine (KraussMaffei KM35-180CX) with a clamping force of 350 kN and an injection screw diameter of 28 mm as shown in **figure 5**.



Figure 5: left: KraussMaffei KM35-180CX injection moulding machine with automation system / right: produced plastic part “crown wheel” made of 11.9 g Nylon (PA66 GF30)

The machine was equipped with the adaptive process control in order to compensate viscosity deviations induced by admixing regrind feedstock. Using regrind feedstock is today commonly applied in injection moulding to reach ecological as well as cost objectives. Due to a thermal degradation a plastic is undergoing when processed the admixing of regrind feedstock will result in a lowered viscosity.

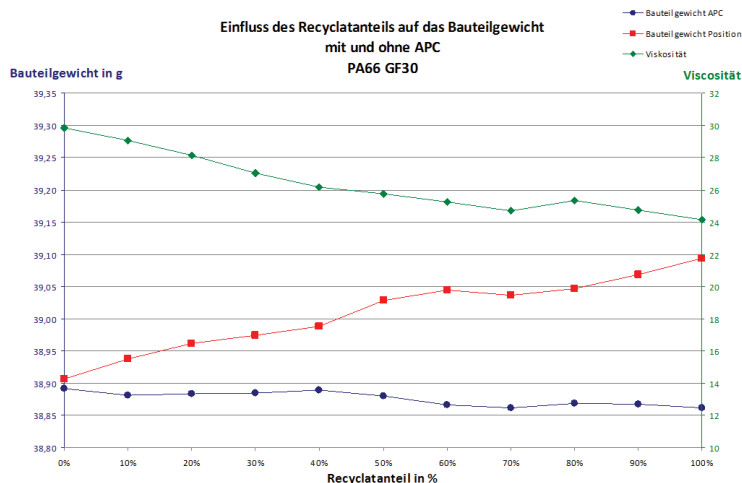


Figure 6: Resulting viscosities for various amounts of admixed regrind feedstock (green), part weight with position based switch-over (red), part weight with adaptive process control (blue)

Figure 6 shows the resulting parts weights as measure for the parts quality and the viscosity of the plastics melt. It can be seen that the amount of regrind admixed has a substantial effect on the plastics melt viscosity (green). Increasing the amount of

regrind from 0 % to 100 % lowers the viscosity by 20 %. When the machine is operated with a constant injection stroke a change in parts weight of 0.187 g (0.480 %) takes place (red). Running the adaptive process control with the reference set to the 0 % regrind the effect is marginal; the deviation in parts weight is reduced to 0.030 g (0.077 %). **Figure 7** shows two screenshots from the machines control with the corresponding pressure curves. One is without adoption of the process; one is showing the pressure curves with automatic adaption of switch-over position and holding pressure level.



Figure 7: Screenshots from machines control, left: resulting difference in pressure curves without adaption of process, right: pressure curves with adaption of switch-over position and holding pressure level.

Second representative process is running in a two component injection moulding machine (KraussMaffei KM500-2000/750CXZ) which is producing a radio cover for the automotive OEM market in back-injection technology. First a transparent PC component for the display is injected.

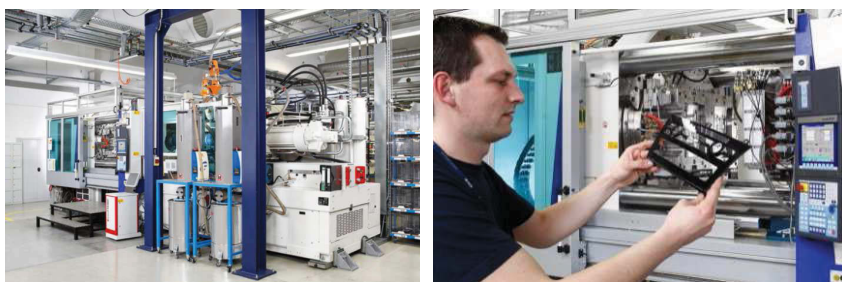


Figure 8: left: KraussMaffei KM500-2000/750CXZ injection moulding machine with peripheral equipment / right: produced plastic part “radio cover” in 2-component back injection moulding process.

Then the mould rotates and black PC-ABS for the case body follows in the same cavity in the second step while the other cavity is already being filled for the next display. This

all takes place on the back of a PC film with scratch-resistant coating and decorated in black that is inserted into the mould. The production cell based on the injection moulding machine and the part produced can be seen in **Figure 8**.

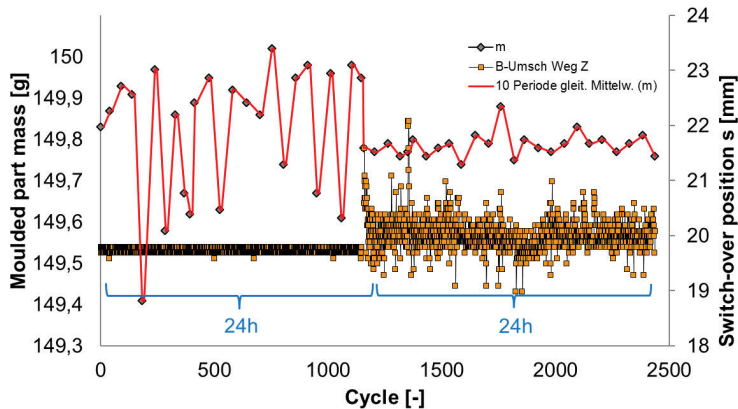


Figure 9: Resulting part weights for 24 h without adaption (left) and 24 h with adaption (right) of the process, the standard deviation of the part weight was reduced from 0.16 g to 0.03 g

In this trial again the part weight was chosen as the representative parameter for the parts quality. In order to compare the robustness of the moulding process with and without the adaptive process control here 48 hours of series production were evaluated. **Figure 9** shows the resulting part weights as well as the switch-over position. The first 24 hours of production the adaptive control was not used e.g. the switch-over position is constant. The resulting standard deviation of the part weight was 0.16 g within the control samples. With the activation of the adaptive process control the standard deviation was brought down to a value of only 0.03 g in the 24 hours of production.

5. Conclusions

Injection moulding machines, which are operated with the introduced adaptive process control, are able to compensate negative effects on part quality like they are caused by viscosity changes in the feedstock. Since the characterization of the actual value of the polymer melt viscosity takes place in the first part of the injection movement an online correction within the same production cycle is possible. This is an important advantage compared to prior approaches and helps to effectively control starting up and restarting injection moulding processes. In case of changing conditions induced by the raw

material the adaptive process control helps to stabilize the produced parts quality by reducing the deviations to a minimum.

6. References

- /1/ S. Kruppa, Adaptive Prozessführung und alternative Einspritzkonzepte beim Spritzgießen von Thermoplasten, Duisburg-Essen, Univ., Dissertation, 2015.
- /2/ R. Schiffers, Verbesserung der Prozessfähigkeit beim Spritzgießen durch Nutzung von Prozessdaten und eine neuartige Schneckenhubführung, Duisburg-Essen, Univ., Dissertation, 2009.
- /3/ S. Kruppa, and G. Holzinger, In Situ Characterization of Polymer Melt and Molded Part Quality, SPE China Plastics Conference Injection Molding, Shanghai, 2013.
- /4/ Schiffers, R. / Kruppa, S. / Moser, S.: The right changeover point for each shot, Hanser Verlag – Kunststoffe International, S. 26-30, 11/2014
- /5/ Patentschrift: Verfahren zur Prozessführung eines Formfüllvorgangs einer Spritzgießmaschine WO2015052072
- /6/ Johannaber, F.; et al.: Kunststoffmaschinenführer 4. Ausgabe, Carl Hanser Verlag, München, 2004
- /7/ Schiffers, R. / Holzinger, G.: Energy efficiency of various hydraulic drives used in injection moulding machines, 8. Internationales Fluidtechnisches Kolloquium (IFK), Dresden 2012

On the Compensation of Dynamic Reaction Forces in Stationary Machinery

Tobias Radermacher, Jan Lübbert, Jürgen Weber

Institut für Fluidtechnik (IFD), Technische Universität Dresden, Helmholtzstrasse 7a,
01069 Dresden, Email: radermacher@ifd.mw.tu-dresden.de, luebbert@ifd.mw.tu-dresden.de,
mailbox@ifd.mw.tu-dresden.de

Abstract

This paper studies a method for active electrohydraulic force compensation in industrial scale high power applications. A valve controlled cylinder moves a mass using the force of inertia to compensate for the reaction forces of an industrial process. Two strategies for force compensation are developed and investigated in a 160 ton clamping unit of an injection moulding machine to significantly reduce the excitation. Results of the different strategies are shown and evaluated. Advantages and drawbacks of the developed electrohydraulic force compensation are discussed.

KEYWORDS: force compensation, clamping unit, injection moulding machine, hydraulic drive train, valve control

1. Introduction

Robustness and the ability to apply high forces dynamically are reasons for the success of hydraulic drive trains in high performance stationary machinery. The stability of a machine is highly affected by the drive train and the acceleration of moving masses; a movement of the whole machine structure needs to be prevented. A conventional solution to reduce excitations is to strengthen the foundation of the machine bed with additional weight or the reduction of acceleration by the operator. Both goes along with shortcomings: A solid foundation may limit space in the machine operation range whilst a reduction of machine acceleration lowers the machine productivity. A promising solution is an active compensation of process forces by a second drive applying counterforces contrarily to the process forces reducing the impact on the machine foundation. Therefore the inertial force of a mass accelerated contrarily to the occuring process forces is used. This work focusses on an electrohydraulic force compensation strategy via a hydraulic cylinder drive. A prototype is developed and applied to the clamping unit of an injection moulding machine, an application with major nonlinearities in the drive train. Chapter 2 gives a short survey

on known force compensation strategies in literature and points out the differences of the novel approach. The novel method of electrohydraulic force compensation is derived in chapter 3 before chapter 4 focusses on the test rig application in detail. Chapter 5 shows measurements of the practical implementation and points out chances and drawbacks of two different compensation strategies. A summary of the achieved results and an outlook for the next working steps is given in chapter 6.

2. Compensation Strategies – State of the Art

The reduction of machine frame excitation is an issue the higher moved masses and acceleration rates are. If neither reaction forces can be tolerated nor a sufficient foundation can be reached (e.g. due to economical, technical or practical reasons) active or passive methods for decoupling or compensation of reaction forces may be an alternative. A scheme of the methods is shown in **Figure 1**.

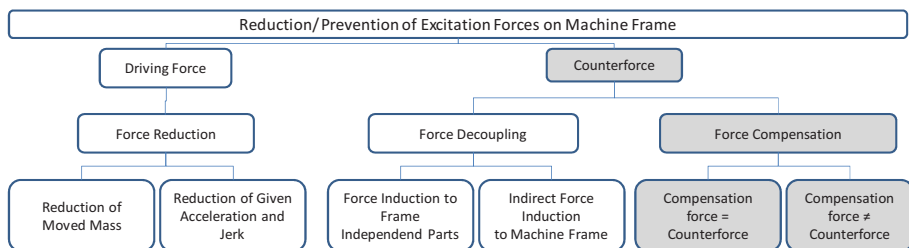


Figure 1: Methods for Reduction of Machine Frame excitation cmp./Gro09/

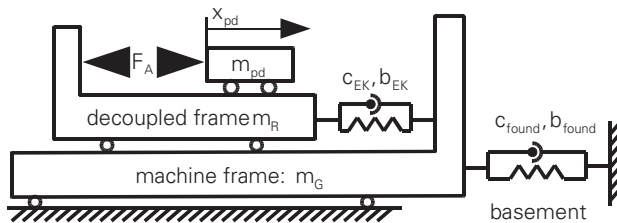
The (mechanical) decoupling of foundation and process using springs, dampers and counter-moving masses is well known, i.e. from cannons. Besides the advantage that no additional energy is needed for the mechanism itself, a drawback of this approach – especially with regard to higher reaction forces is the need to tune spring and damping ratio to a specified (and limited) frequency range. So the full frequency range of the reaction forces generated by the process drive cannot be covered. Another drawback is the displacement of the machine itself with regard to the inertial system. Automatized production processes often rely on proper positioning e.g. for loading and unloading processes in process-chains.

For small applications or if enough construction space is available (passive) force or impulse compensation can be done by mechanical coupling of (counteracting) moved masses (rotational or translational). A well known example for this technique are counterbalance weights in automotive engines.

The use of additional energy to compensate for the reaction forces caused by the process even economically appears to be a promising solution, if productivity can be

significantly improved, and the overall cost per part can be reduced. **Figure 2** shows possibilities for passive and active compensation.

passive compensation via decoupling



active compensation via counteracting force

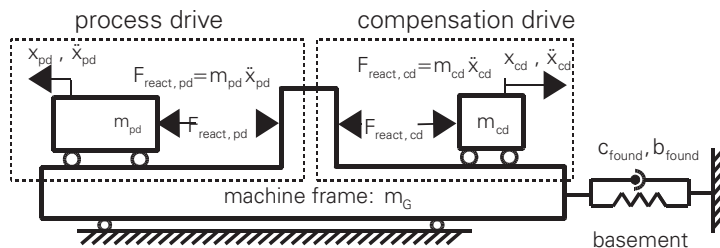


Figure 2: reduction of process-forces to machine frame and basement

Force compensation mechanisms are commonly divided into impulse and force compensation methods. Impulse compensation methods focus on the compensation of process forces in a defined frequency range whereas force compensation is referred to as the compensation of all occurring process forces.

Force compensation with and without mechanical coupling has been investigated and developed since 1984 in numerous different ways /Fli84, Gro14/ and even been applied to a number of machine tools, e.g. /Wan09, NN15/. Ideal compensation is difficult to obtain in practice, and the compensation rate depends on numerous factors. However Großmann's and Müller's experiments show that a real impulse-compensation setting may lead to a reduction of frame-acceleration of about 80% in a setting with given velocity of 0.5 m/s, acceleration of 40 m/s² and jerk of 10000 m/s³ /Gro09b/. In order to reduce cost and machine size a small compensation mechanism is desirable, reducing the reaction forces to the machine basement as good as possible. From this point of view a total compensation of reaction forces is not economic.

However reaction forces to be applied are limited due to the maximal force and the stiffness of the drives and the load of the moved masses, so the drivetrain has to be properly chosen. Linear direct drives feature the potential of high accelerations but as they do not use any transmission maximal force is limited and dynamical stiffness is low in comparison to an electro-mechanic ball screw, which features a high stiffness due to the high transmission ratios. Disadvantages of ball screw drives are the inertia of the rotary parts of the drive train which cannot be used for linear force compensation and the maximum forces that can be dynamically applied. For major scale production machines linear hydraulic drives appear to be a promising solution because of the high forces which may be applied. A drawback is the maximum applicable dynamics due to the comparatively low stiffness. It needs to be investigated in how far this drawback is a major burden for using hydraulic drives for compensation of process forces. Important questions driving this research are:

- To what extent can a small-sized hydraulic mechanism sufficiently compensate for the occurring reaction forces?
- How can the required forces be applied via an electrohydraulic drive train?
- What strategy should be used to achieve this aim?

3. Electrohydraulic Force Compensation in Stationary Machines

A compensation of forces with a second drive of same structure moving contrarily to the process drive extinguishes forces efficiently but may not be applied due to cost and additional space. In these cases a compensation drive with less power will be installed giving rise to the question how much of the excitation should be compensated for. Moreover the benefit of compensation depends on the construction of the drive, the strategy and the process requirements. Repeating processes facilitate more sophisticated strategies with higher calculation effort to be applied.

3.1. Control Strategy

This paper presents two strategies where information about full (elapsed) cycles is used.

Force Peak Compensation (FPC). Assuming the maximum force taking maximum effect on the machine frame, a compensation of force peaks leads to higher possible dynamics. The idea of FPC is described in **Figure 3**.

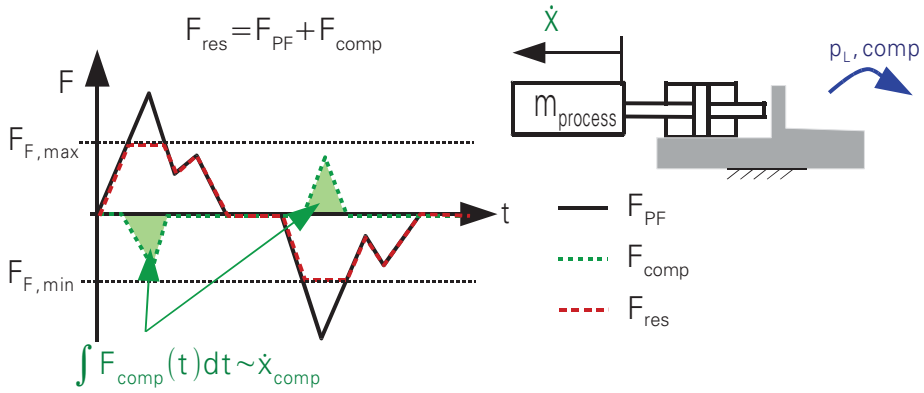


Figure 3: Compensation of force peaks

Occurring force peaks are compensated by a force applied contrarily by the compensation cylinder. Therefore the compensation law:

$$F_{comp} = \begin{cases} -F_{react} + F_{F,max} & \text{for } F_{react} > F_{F,max} \\ 0 & \text{for } F_{min} < F_{react} < F_{F,max} \\ -F_{react} + F_{F,min} & \text{for } F_{react} < F_{F,min} \end{cases} \quad (1)$$

is applied. The compensation thresholds F_{min} , F_{max} can be adjusted depending on the needed compensation effect up to the maximum power of the compensation drive.

Frequency Slope Compensation (FSC). Following the idea that not the biggest amplitude of process forces but specific frequencies have a big impact on the excitation of the structure, compensation action should primarily focus on these frequencies. Therefore the transfer function (TF) or Fourier transformed (F) frequency response from process force F_p to structure velocity \dot{x}_{str} at a point of interest

$$H_{\dot{x},G}(j\omega) = \frac{F\{\dot{x}_{str}(t)\}}{F\{F_p(t)\}} \quad (2)$$

needs to be considered. The TF can be revealed e.g. by step-response experiments or with an impact hammer. The compensation force F_{comp} is derived filtering the reaction force F_{react} with the frequency response $H_{\dot{x},G}(j\omega)$. The compensation force then is calculated in time domain as

$$F_{comp}(t) = -F^{-1} \left\{ F\{F_{react}(t)\} \cdot \frac{H_{\dot{x},G}(j\omega)}{\max\{|H_{\dot{x},G}|\}} \cdot K_g \right\} \quad (3)$$

with scaled $H_{\dot{x},G}$ and a factor $K_g \in [0 \dots 1]$ for compensation adjustment. Forward-backward filtering eliminates phaseshift and reduces compensator action.

3.2. Dimensioning of the Compensation Actuator

Good impact of the compensation drive can be achieved with high and enduring accelerations. Apart from the moved mass determining parameters are system pressure, cylinder size (area, stroke), maximal cylinder velocity and size and dynamics of the valve.

According to Newton's second law a force depends on the mass and its acceleration. In linear hydraulic drive trains (with double rod cylinder) the accelerating force

$$F_L = (p_A - p_B) \cdot A = p_L \cdot A \quad (4)$$

depend on the load pressure p_L and the area A of the piston. The dynamics of the load pressure build-up is characterized by size (Q_{nom}) and dynamics of the valve and the volume (V_0) and stiffness of pipes, cylinder and the oil (K') according to:

$$\dot{p}_L = \frac{K' \cdot (Q_V - A \cdot \dot{x})}{V_0} \quad (5)$$

with the valve flow

$$Q_V = Q_{nom} \cdot \frac{y}{y_0} \cdot \sqrt{\frac{\Delta p}{\Delta p_{nom}}} \quad (6)$$

Figure 4 schematically shows the load pressure build-up in a cylinder drive. In section 1a the limited valve spool velocity prevents faster pressure build-up. Phase 1b is determined by the ratio of chamber volume V_0 and the valve flow Q_0 before in phase 2 cylinder acceleration and chamber volume V increase significantly. In phase 3 acceleration decreases, and the cylinder reaches constant velocity.

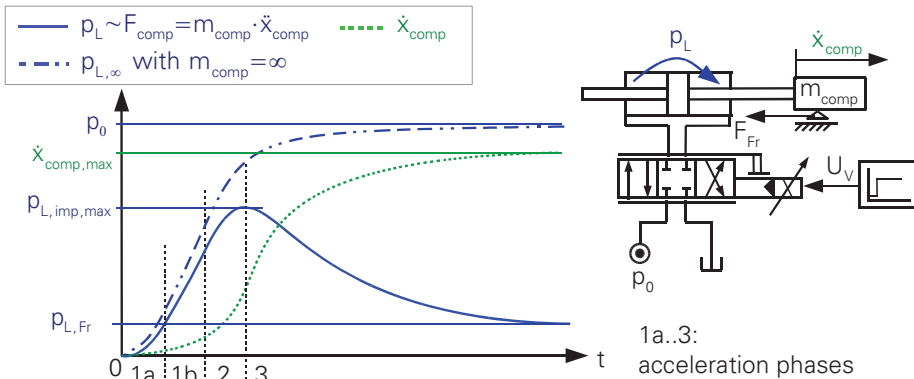


Figure 4: schematic step-response of load pressure and cylinder velocity

With regard to equations (1), (2), (3) a high and long lasting compensation force can be achieved with big mass m , high supply pressure p_0 , small parasite and cylinder volumes and a high flow rate, which plays a major role in the compensation. One tradeoff lies in maximising force amplitude and duration. A shorter cylinder stroke h increases the force amplitude but at the same time limits the duration of the force. A second tradeoff can be found dimensioning the piston area A : Smaller piston areas lead to bigger impulses whereas maximum force requires larger cylinder areas.

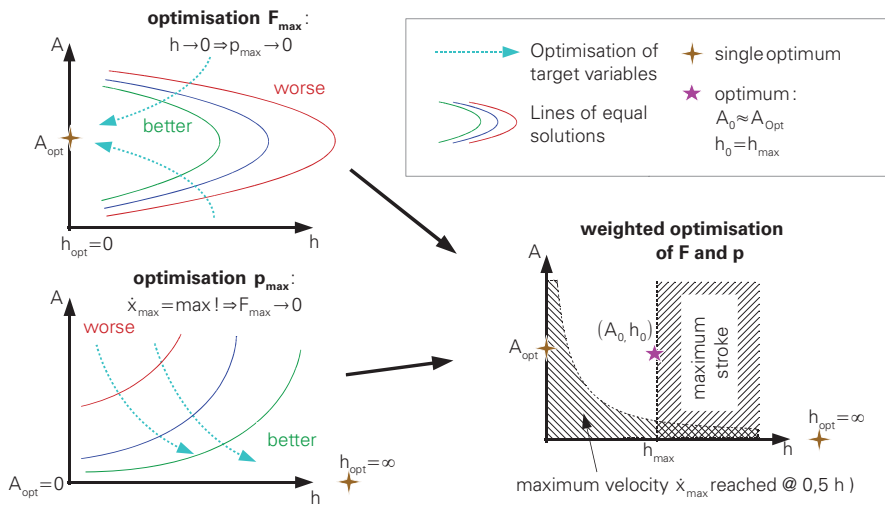


Figure 5: optimisation concerning force amplitude and duration of impulse

Figure 5 shows the optimisation method to determine a best fitting cylinder size with cylinder stroke h as given restriction. Long cylinder strokes allow for long lasting accelerations but the impulse p may be limited by maximum cylinder velocity and the construction space; beyond that some space is needed for the deceleration of the moving mass. For a given valve there is an optimal cylinder area concerning maximal amplitude of force. Too big cylinder areas provoke a slow pressure build up and maximum pressure cannot be reached due to the accelerating cylinder (Figure 4, phase 3).

4. Test Rig

Electrohydraulic force compensation is a reasonable method for high power applications, where linear electric or electromechanic drives are too expensive or do not provide enough force. The test stand is selected to be a 160 ton toggle-lever clamping unit of a high-speed injection moulding machine because it is a popular application where dynamics is restricted by the excitation of the drive train. It consists

of the mechanism as pictured in **Figure 6**, driven by a closed circuit drive with a piston pump and a 22 kW servomotor.

Data processing is done via MATLAB/SIMULINK and a dSpace DS1103 realtime controller board is used for signal acquisition and -output. Different trajectories are tested to illustrate the machine frame excitation.

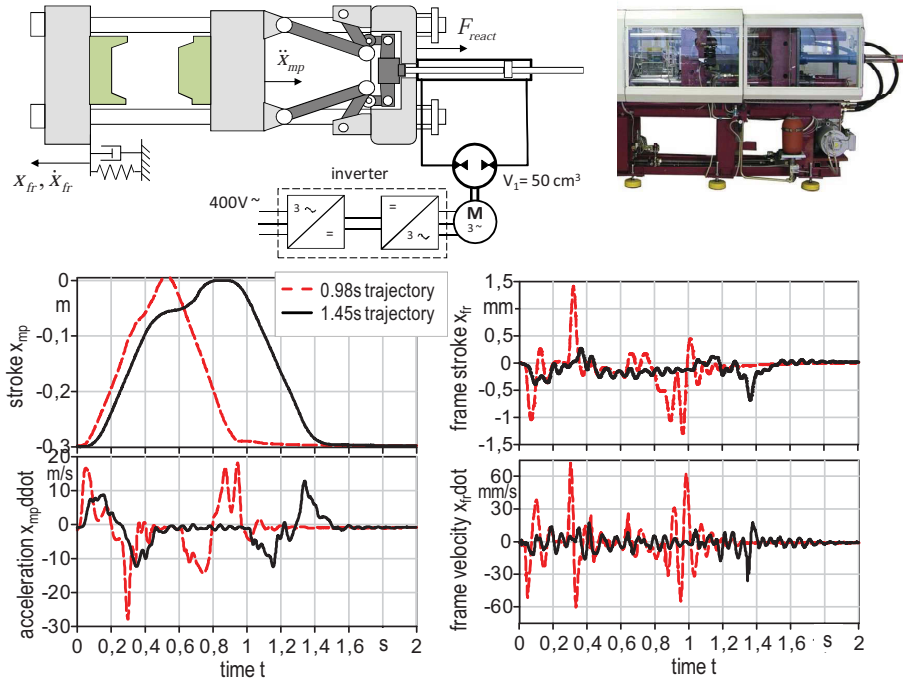


Figure 6: 160 ton toggle lever clamping unit and frame excitation

The shorter the cycle time set by the operator the higher the accelerations of the machines movable platen \ddot{x}_{mp} is. Consequently the machine frame is exposed to higher acceleration rates which lead to an increase of the machine frame excitation x_{fr}, \dot{x}_{fr} , Figure 6. In production the moved mass within the process is, depending on the mould, about 1 ton, and with accelerations of 27 m/s^2 forces of 27 kN excite the machine frame in the given 0.98 s trajectory. Further shortening of the trajectory leads to an excitation that is followed by movement of the whole machine structure what needs to be prevented.

Full compensation can be reached with lower masses and respectively higher accelerations or vice versa. Without exceeding the machine space or too complex constructions the demonstrator machine may be equipped with about 1/10 of the

moving weight (100kg), which has to be mounted in a way that compensation forces may be applied in the right direction.

4.1. Design of the Compensation Drive

The compensation drive has to be mounted symmetrically behind the toggle-lever drive to evenly apply the compensation force. As the driving cylinder of the toggle lever is mounted centrally the compensation force is applied symmetrically by two cylinders. The pressure level of the hydraulic circuit is set to 190 bar. A first attempt for the dimensioning of the compensation drive is a maximum force equal to the reaction force of the machine which leads to a cylinder area of 15 cm^2 . Construction space and optimisation according to Figure 4 and Figure 5 in combination with system simulation turn out to a cylinder length of 200 mm so two 200x40x25 double rod cylinders are used due to the need for a symmetrical construction.

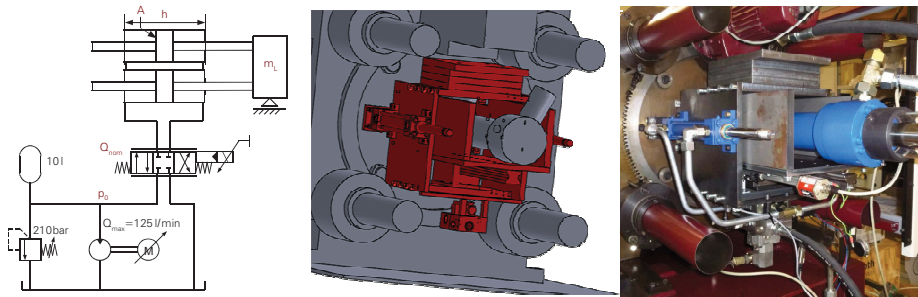


Figure 7: hydraulic circuit and construction of compensation drive

Figure 7 shows the setup: The compensation mass is mounted on a frame which moves together with the cylinder tube; the pistons are linked to the machine via their threads. The valve is a crucial part of the system: For a fast pressure build-up in the cylinder maximum valve dynamics and low pressure losses are necessary, resulting in a valve of maximum size. For the compensation drive a NS10-valve with nominal flow of 75 l/min@70 bar is chosen. The rise time to 100% opening stroke is 7 milliseconds, -3dB-frequency is around 50 Hz. As the eigenfrequency of the machine frame is around 15 Hz there is only a small expected phase-shift due to the valve dynamics. Experiments will show in how far this affects the effectiveness of the algorithm.

Once the compensation drive is installed a response test shows the potential of the compensation drive: The valve is actuated with a 10 V-step signal (valve input is $\pm 10 \text{ V}$). As indication of the excitation frame velocity is depicted in **Figure 8**. With

nearly 15 m/s the compensation drive induces 25% of the impulse of the machine in a 0.98 s trajectory (cmp. Figure 6).

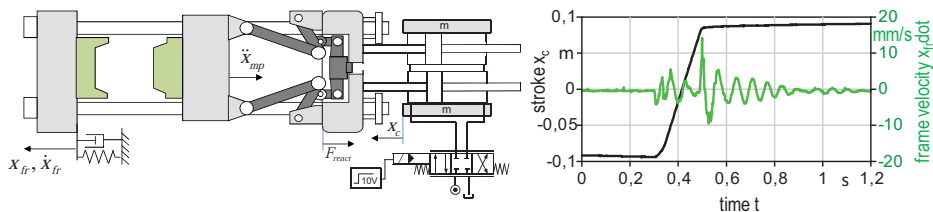


Figure 8: compensation drive and machine frame excitation

The maximum impulse is restricted by maximum cylinder velocity (valve spool opening, seal properties), while maximum acceleration is restricted by pressure built up in the cylinder chambers. Valve spool velocity rate limit plays a crucial role because it limits pressure built up significantly.

5. Test and Results

The different compensation strategies, force peak compensation and frequency slope compensation are applied at the described prototype test rig. Experiments and evaluations are carried out with a controller not accounting for several nonlinearities as the damping of the tie bar screws, the nut bolt play or losses in the hydraulic piping. The transmission of the toggle lever itself is a major nonlinearity but calculations and experiments show that transmission ratio can be taken as constant in the areas where the highest excitations occur. Effectiveness of compensation is measured by means of the reduction of kinetic energy in the machine frame that directly relates to the frame velocity if the moved mass is constant. Moreover the frame stroke is an indication for the energy that needs to be dissipated via the mounting foots of the machine.

Force Peak Compensation (FPC) is applied to the 0.98 s trajectory given in Figure 6. Reaction forces are computed via logged data \ddot{x}_{mp} of the piezo accelerometer at the movable platen and the moved mass' weight.

The algorithm sets a constant compensation level so that the reaction force peak at 0.3 s is considered for compensation in the given trajectory. Results in **Figure 9** show that despite a tracking error due to open loop feedforward and closed loop PID control of the compensation drive, the force peak is reduced by the compensation drive, resulting in an about 0.4 mm reduced frame stroke (about 20..30% considering deviations in repeatability). The maximum frame velocity \dot{x}_{FP} is reduced from 80 to 67 mm/s with FPC.

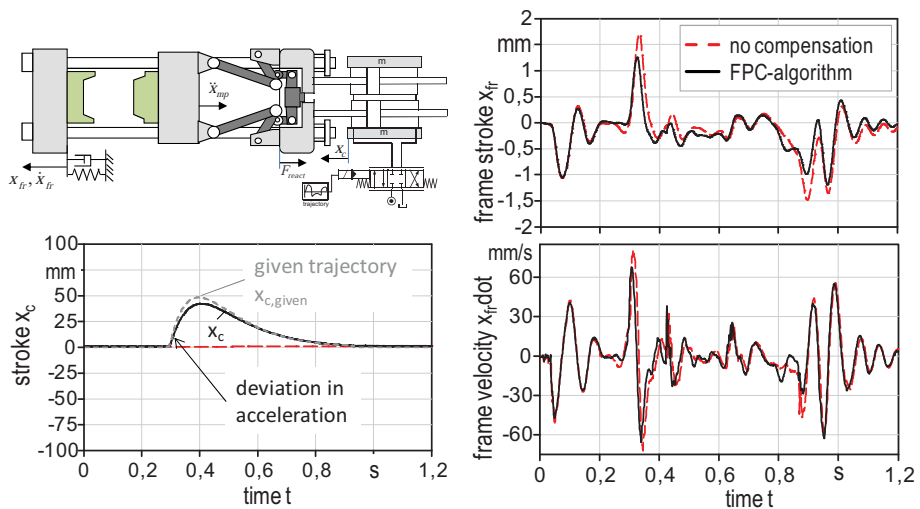


Figure 9: Experimental results of FPC algorithm application

A drawback of the shown implementation of FPC algorithm is that the valve *opening* is used for pressure build up. Line inductivities and reversion of load pressure can lead to higher compensation rates while *closing* the valve. Energy efficiency benefits from small compensation movements by compensating for excitations at decided moments in the trajectory.

For the application of **Frequency Slope Compensation (FSC)** the necessary force is calculated via filtering of the acceleration \ddot{x}_{mp} suppressing the transfer of frequencies near the eigenfrequencies of the machine. **Figure 10** shows the result of the FSC compensation.

It can be seen that the highest excitations are compensated for but also that the algorithm causes some new excitations. FFT-analysis shows that due to the tracking error (Figure 10, lower left) new excitations are caused.

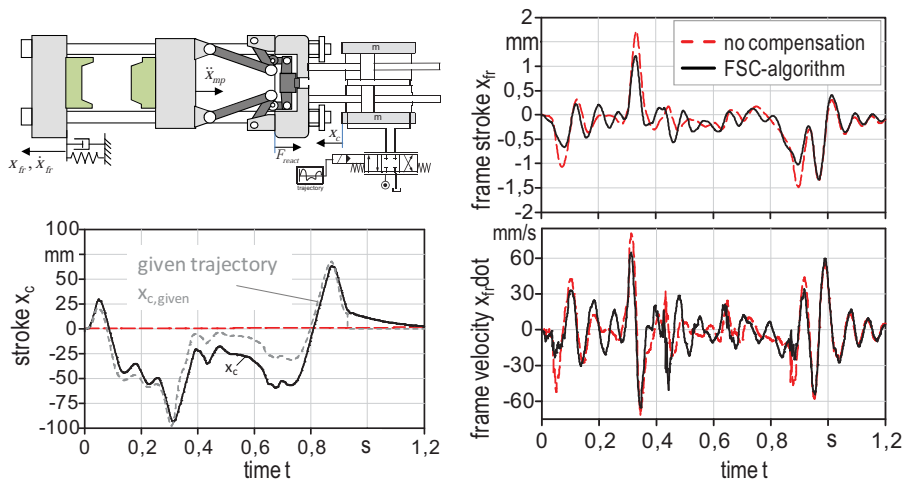


Figure 10: Experimental results of FSC algorithm application

Besides the improvement of the control algorithms there are some factors that physically reduce the effectiveness of the compensation mechanism: the (rate) limitation of valve dynamics and maximum nominal valve flow limit pressure build up as well as pipe inductances.

6. Conclusion and Outlook

Force compensation in machine tools has been applied in practice using linear direct electric drives, gathering higher dynamics, better precision and preventing excitations. This paper investigates a hydraulic linear drive force compensation in theory and practice. A compensator moving 10% of the machines moved mass is developed and applied to the clamping unit of an injection moulding machine prototype with occurring reaction forces up to 40 kN. A valve controlled demonstrator is developed, implemented and tested. Two methods of force compensation are developed and applied in practice: Force Peak Compensation (FPC) algorithm results in a 20% reduction of machine frame movement at a given force peak. Frequency slope compensation (FSC), which is a method pointing towards the reduction of eigenfrequency excitation, results in a similar reduction of force peaks with bigger actuator actions. Both methods show potential concerning the reduction of machine excitation even though not all force peaks can be compensated for. Reasons for these deviations can be found in tracking errors of the compensation drive caused by fluid compressibility and the limited dynamic of force build up in comparison with electro-mechanic drivetrains, which is a challenging issue.

Experimental results show that hydraulic force compensation may be an interesting solution for application in industry if the compensation effect is increased. For judging the effectiveness of the compensation drive and different control strategies with regard to an economic application in high power applications the dynamics of the drive train should be considered in motion planning. Moreover a maximum tracking error for an effective working of the algorithms should not be exceeded. This will be part of future investigations.

7. Literature

- /Mül13/ Müller, J. ; Junker, T. ; Pagel, K. ; Großmann, K. ; Drossel, W.-G.: Impulsentkopplung von Linear-Direktantriebsachsen. In: Werkstatttechnik Online 103 (2013), Nr. 5. <URL: [http://www.werkstatttechnik.de/wt/get_article.php?data\[article_id\]=72935](http://www.werkstatttechnik.de/wt/get_article.php?data[article_id]=72935)> (recalled 2014-07-15)
- /Fli84/ Patent EP0132883A2 (21.7.1983), Philips Patentverwaltung GmbH, Flisikowski, P. (Inv.), "Linearmotor zum raschen Hin- und Herbewegen eines massebehafteten Läuferschlittenbauteils"
- /Gro09/ Großmann, K., Müller, J.: „Impulskompensation an einer linearmotorgetriebenen Maschinenachse“, 14. Dresdner Werkzeugmaschinen-Fachseminar, 2009, p 79-109
- /Gro09b/ Großmann, K., Müller, J.: „Untersuchungsergebnisse zur Wirksamkeit der Impulskompensation von Lineardirektantrieben“, ZWF-Zeitschrift für den wirtschaftlichen Fabrikbetrieb, vol.104 (2009), p761-769
- /Gro14/ Großmann, K., Müller, J., Merx, M., Peukert, Chr.: „Reduktion antriebsverursachter Schwingungen“, ant Journal 4/2014, p.35-42
- /NN15/ N.N.: AZ250 – Nano Machining Center, Sodick Co. Ltd. (Japan); <http://www.sodick.jp/product/tool/nano/index.html> (recalled 2015 Dec 02)
- /Wan09/ Wang, Z.G., Cheng, X., Nakamoto, K., Kobayashi, S., Yamazaki, K.: "Design and development of a precision machine tool using counter motion mechanisms", International Journal of Machine Tools & Manufacture No.50 (2010), pp. 357-365

8. Nomenclature

Symbols

A	Area	m^2	c	spring rate	N/mm
H	transfer function	-	h	length	m
K	scaling factor		m	mass	kg
K	bulk modulus	bar	p	pressure	bar
Q	Flow	l/min	t	time	s
V	volume	m^3	v	velocity	mm/s
b	damping factor	Ns/mm	x	position	mm

Subscripts

0	related	min, max	Minimum, maximum
EK	coupling	mp	Movable platen
F	force	nom	nominal
L	load	p	process
Str	Structure	pd	Process drive
cd	Compensation drive	pf	Process force
$comp$	compensation	$react$	reaction
$found$	foundation	res	resulting

Improvement of hydraulic control quality for deep drawing presses through retrofit

Marcus Helmke

Automation, TRsystems GmbH, Eglisshalde 16, 78647 Trossingen, E-mail: marcus.helmke@trsystems.de

Herbert Majer

Automation, TRsystems GmbH, Eglisshalde 16, 78647 Trossingen, E-mail: herbert.majer@trsystems.de

Andreas Thanassakis

CEO, TR-Electronic, Eglisshalde 6, 78647 Trossingen, E-mail: andreas.thanassakis@tr-electronic.de

Abstract

Retrofits of hydraulic and mechanical deep drawing presses often stop with the exchange of the electrical and the hydraulic parts. But that is only half the job. The use of high definition control electronics, faster CPUs and more dynamic hydraulic actuators, offers the opportunity of redesigning the already existing control concepts of the press. In this paper we present how the performance of the press, i.e. the control quality, can be increased for hydraulic ram and cushion axes. The improvement in control quality is achieved through the use of intelligent closed-loop and open-loop-control algorithms. Therefore, creasing and crack formation can be reduced, since enhancements in control quality have direct influence on the quality of the forming process. Results will be shown for hydraulic drawing cushion control, i.e. pressure control, as well as for hydraulic ram control, i.e. position, velocity and parallelism control. We present findings for hydraulic cushion control of a mechanical press type Arisa S-4-1600-470-230-LDE (link-drive press with 10 hydraulic cushions) and for ram- / cushion-control of hydraulic press type Müller-Weingarten ZE2100 (multi-curve press with 8-point cushion).

KEYWORDS: hydraulic presses, retrofit, model based control

1. Introduction

Installation operators carry out retrofits for their hydraulic or mechanical presses to ensure the machine's availability in the long term. The machine's electrical components are mostly discontinued after 10-15 years. That results in predictive arrangements for the pressing plant's maintenance and production planning staff. The focus of those retrofits is on exchange of the machine's PLC and replacement of electrical components and wiring. If the desired plant has a hydraulic closed loop control system – e.g. drawing cushion – most of the time, the hydraulic control system will be replaced by a stand-alone module (e.g. Rexroth MAC 8). Those stand-alone systems have a large variety of functions and high number of usable parameters, but they can quickly reach their limits, since hydraulic and mechanical presses are special engineered machines and need an equally special engineered solution. The approach presented by TRsystems, describes a solution which refers to the machine's electrical, mechanical and hydraulical properties and thus is a tailored closed loop control. Most of the time, the existing hydraulic/mechanic remains untouched. The greater part of the changes will affect the electrical components only.

2. Mechanical press Arisa S-4-1600-470-230 LDE

2.1. Machine in detail

The Arisa S-4-1600-470-230 LDE (Arisa 1600) is a mechanical transfer press with

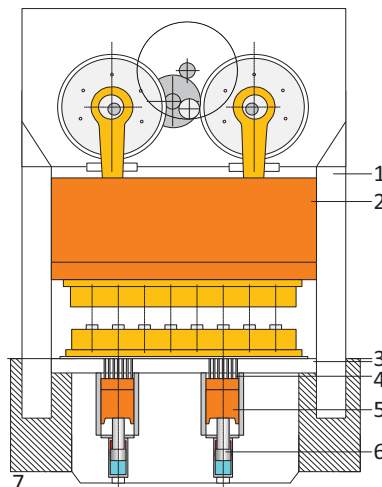


Figure 1: Arisa 1600 – mechanical structure

- (1) sidestand, (2) ram, (3) bolster plate, (4) drawing cushion sleeves,
(5) drawing cushion, (6) positioning and pressure cylinder, (7) basement

Link-Drive engine for the ram and 10 separate hydraulic drawing cushions (see **Figure 1**) /1/. The press' maximal force is at 16.000 kN. The drawing cushions have a 3-chamber-cylinder, which is designed for lifting and pressure functions. The cylinder is controlled by 2 servo valves (Rexroth 4WRTE nominal size 25 and 4WRDE nominal size 10, frequency of 30 Hz) and has a dynamical chamber-shift for pressure control. The machine's 10 drawing cushions make a variety of forming steps possible. Workpieces, produced with this press include structural elements for vehicle constructions and cases for brake boosters. The machine's master control system is a Siemens SIMATIC S7, which controls ram, transfer and blank loader. A Rexroth MX4 system takes care of the drawing cushion's closed loop control.

2.2. Quality of drawing cushion closed loop control before retrofit

Figure 2 shows the quality of first cushion's pressure control before retrofit. The measurements were done with an extern measuring system, connected with the drawing cushion via MINIMESS testpoints. Target pressure for this measurement was 240.0 bar (equals 600.0 kN cushion force), the ram speed was 13 strokes/minute and the drawing depth was set to 150.0 mm.

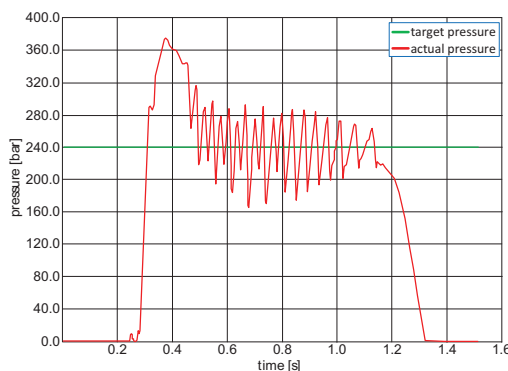


Figure 2: Arisa 1600 – pressure control before retrofit

We were able to verify the trend, recorded in Figure 2, for all possible parameter constellations (see **Table 1** for parameter limitations). The pressure overshoots had a value of 50% or more of the target pressure and were eliminated after additional 30.0 till 50.0 mm drawing depth (depends on ram speed). A residual ripple could be recognized for the whole length of the process, till the ram's bottom dead center. The measurements showed that the ripple had an average value of $\pm 25\%$ of the target pressure and that the controller was not able to eliminate the pressure fluctuations within the given time.

	mimumum	maximum
ram stroke speed	8 1/min	30 1/min
cushion pressure	20.0 bar	240.0 bar
draw depth	20.0 mm	200.0 mm

Table 1: Arisa 1600 - parameter limitations /1/

While the press was working with preselected cushion control, the maximum number of strokes had to be reduced to 15 strokes/minute, although the ram was able to drive with 30 strokes/minute. Working with a ram speed of 16 strokes/minute and more, could result in damaging the cushion's hydraulic, since the rising pressure peaks were able to burst the hose lines between cylinders an servo valves.

2.3. Approach by TRsystems

The existing cushion control was replaced by a Beckhoff industrial PC (IPC), which is able to calculate in real-time. Via Profibus DP/DP, the IPC was connected to the superior machine control. The analogue and digital I/O-modules were connected via EtherCAT (see **Figure 3**).

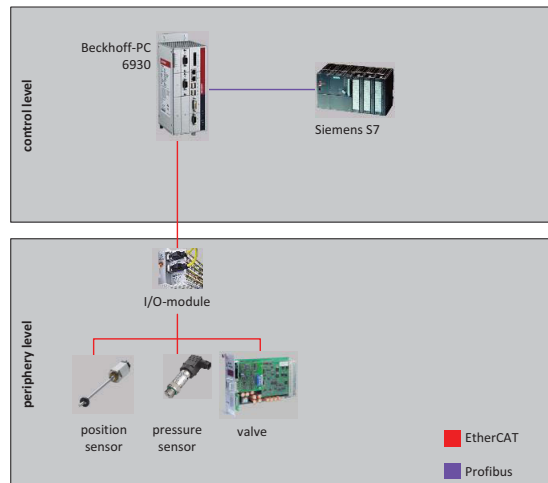


Figure 3: Arisa 1600 – network layout

Our control algorithms are designed in C++ and are executed with the real-time extension TwinCAT. The TwinCAT software is part of the IPC and calculates our control algorithms with a cycle time of 125 μ s /2/. The existing pressure sensors and servo valves remained unchanged. For analogue I/O-modules, we used fast high-resolution modules, which scaled the valve output and input signals (0 – 10 Volt), as

well as the pressure input signals (0 – 400 bar), to 16 bit digital values (before retrofit, inputs and outputs were scaled on 8 bit only) via EtherCAT.

The closed loop pressure control consisted of a PI controller with a model based feed forward control. The feed forward control was designed to reduce the PI controller's part of the control signal and thus to reduce overshoots and residual ripples. We were able to reduce the PI controller signal to 10% and less, as part of the sum signal. Therefore, the feed forward control consisted of a three-dimensional valve characteristic (target pressure over drawing velocity over valve signal). The valve signal was recorded in the three-dimensional characteristic for all possible drawing velocities (8 – 30 strokes/minute) and for all possible pressures (20.0 bar - 240.0 bar) during drawing process. Since implementing the hydraulic characteristics of the whole system, we included disturbances like dead volumes, hidden capacities (hose lines) and current valve attrition.

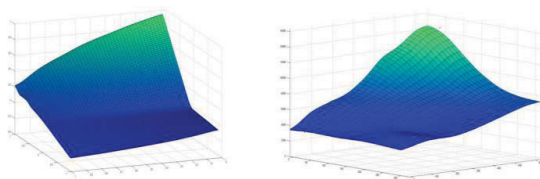


Figure 4: ideal valve characteristic (left) and actual valve characteristic (right)

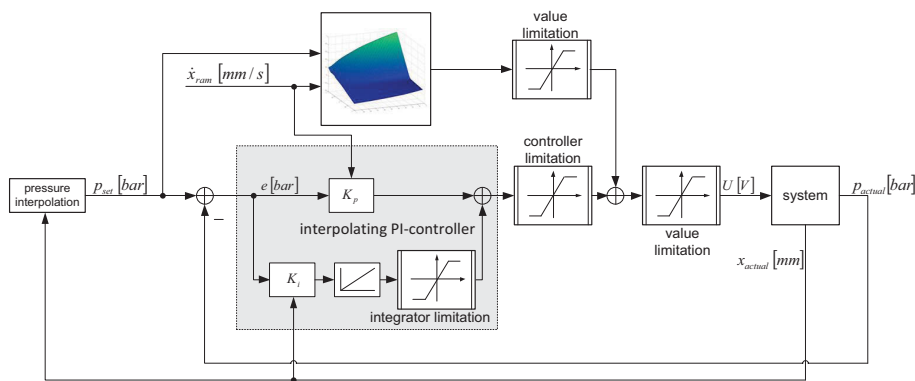


Figure 5: pressure control - calculated control signal

Figure 5 shows, how the feed forward signal is generated. Target pressure and ram velocity are the inputs (x-axis and the y-axis of the characteristic), while the interpolated valve signal is the output (z-axis of the characteristic). The target pressure is parameterized by the machine's operator as desired blank holder force. The ram's velocity (in mm/s) is converted from the actual number of strokes (1/min) by the use of

the ram's kinematics and the current crank angle (via crank angle – position – diagram).

2.4. Quality of drawing cushion closed loop control after retrofit

Figure 6 shows the pressure control for 13 strokes/minute, a drawing depth of 150.0 mm and a set pressure of 240.0 bar. There is nearly no overshoot identifiable and the residual ripple is close to zero percent, only at the end of the process minimal pressure fluctuations can be seen.

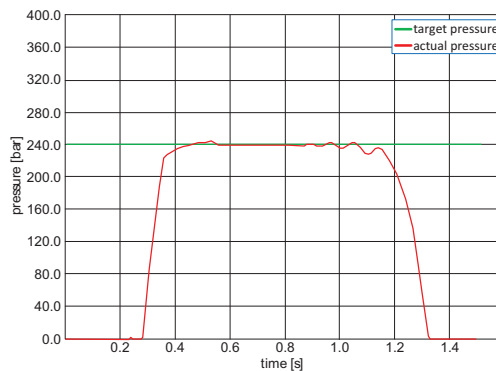


Figure 6: Arisa 1600 – pressure control after retrofit

Since we used modern model based control algorithms and real-time capable hardware (125 μ s cycle time), we were able to make a decisive improvement in control quality. Furthermore, the press was now able to produce with a stroke speed up to 30 stokes per minute with preselected cushion control.

3. Hydraulic tryout press Müller-Weingarten ZE2100.45.2.2

3.1. Machine in detail

The Müller Weingarten ZE2100.45.2.2 (ZE2100) is a hydraulic tryout press consisting of 4 ram cylinders, an 8-point drawing cushion and a 1-point ram cushion. The 4 ram cylinders are supplied by 2 piston accumulators (2 x 325 l at 315 bar oil pressure) and 2 constant pumps (2 x 160kW at 1500 l/min) and are controlled by piston sided Rexroth 2WRCE valves (nominal size 63) /3/. The ram's closed loop control includes position, velocity, parallelism and pressure control. In this paper, we will concentrate on velocity and parallelism control only. Using the MultiCurve-technology, the ram is capable of simulating kinematics of mechanical presses, between 90° crank angle before bottom dead center and bottom dead center. As a result, the drawing speed can reach up to 500.0 mm/s. The blankholder force is provided by an 8-point drawing cushion (8

pressure cylinders) and by a 1-point ram cushion. The ram cushion shall not be considered in detail in this paper. The drawing cushion's pressure is controlled with 8 separate Moog D663 servo valves and the force can reach a maximum of 6000.0 kN, which equals 239.0 bar in each cylinder.

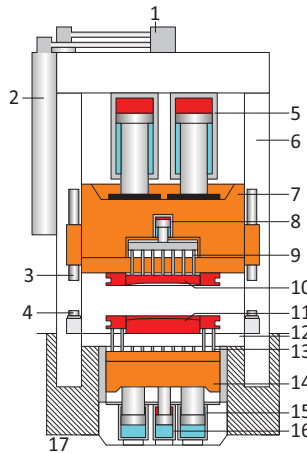


Figure 7: MW ZE 2100 – MultiCurve press

(1) hydraulic block, (2) accumulator, (3) ram adjustment, (4) stamp dampening, (5) ram cylinder, (6) sidestand, (7) ram, (8) ram cushion cylinder, (9) ram cushion sleeves, (10) die top, (11) die bottom, (12) bolster plate, (13) drawing cushion sleeves, (14) drawing cushion, (15) pressure cylinder, (16) positioning cylinder, (17) basement

3.2. Quality of closed loop control before retrofit

Figure 8 shows measurements for drawing cushion pressure control and ram velocity control before retrofit. The measurements were recorded with a special press die, consisting of several force transducers and laser sensors for path measurement.

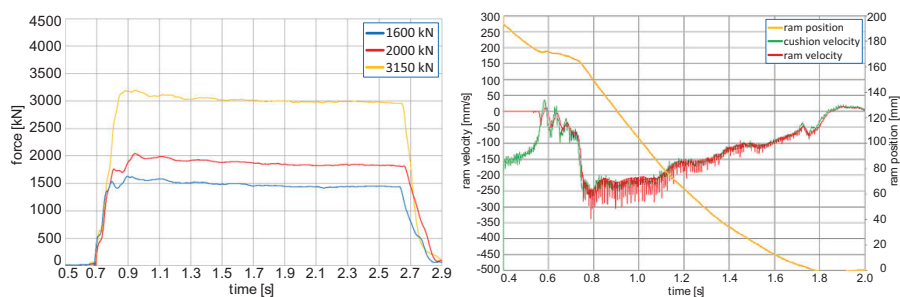


Figure 8: ZE2100 before retrofit – pressure control (left) at 4 strokes/minute and ram velocity control (right) at 8 strokes/minute /4/

The measurements were made for 1600.0 kN, 2000.0 kN and 3150.0 kN cushion target force, while the simulated stroke rate was 4 strokes/minute, which equals about 100.0 mm/s drawing velocity. Figure 8 shows a nearly perfect pressure control quality for those force-velocity-combinations. But increasing the stroke rate, respectively the drawing speed, led to a malfunction of the drawing cushion control. **Figure 9** shows the results for target forces 1250.0 kN, 2000.0 kN and 3150.0 kN at 8, 11 and 14 strokes/minute. It is obvious that with increasing stroke speed, the control quality rapidly decreases and - as a result – the desired forces cannot be kept constant.

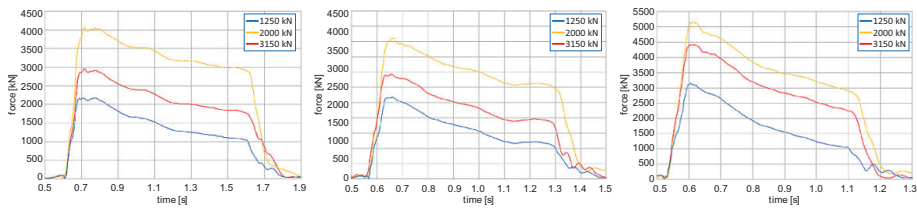


Figure 9: MW ZE2100 – pressure control before retrofit

left: 8 strokes/minute, center: 11 strokes/minute, right: 14 strokes/minute /4/

Taking a closer look at the ram's velocity control (Figure 8), various fluctuations can be detected. The fluctuations before the ram is about to accelerate are not so important, since that is the phase, where the die top is about to touch down on the die bottom. The phase after the acceleration phase should look like the red marked area in **Figure 10**.

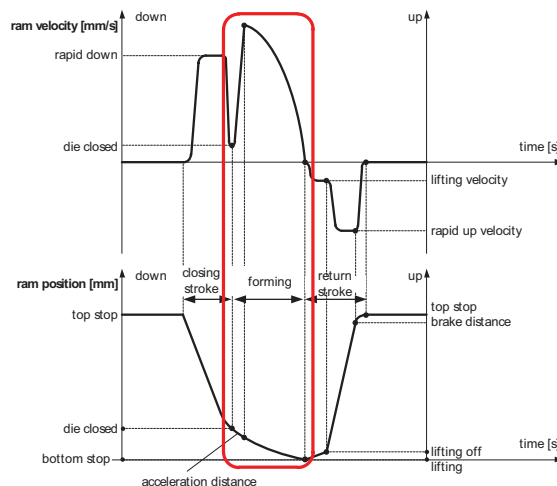


Figure 10: position-velocity-time-diagram for MultiCurve presses

3.3. Approach by TRsystems

We have done a complete electrical retrofit for this machine. That means that PLC, closed loop control, visualization, every I/O-module and all drawing cushion pressure control valves have been exchanged. The existing Moog D663 valves have been replaced by identically constructed but more wear-resistant and more dynamic valves (from 40 Hz frequency to 50 Hz frequency). We used a Beckhoff IPC with the real-time extension TwinCAT for closed loop control and high resolution I/O-modules for analogue inputs and outputs (12 bit modules before retrofit and 16 bit modules after retrofit). The changes in electrical hardware were quite the same as in **chapter 2.3**. Again, the architecture of the drawing cushion's closed loop control consisted of a model based feed forward control and a PI controller. The retrofit also concentrated on optimizing the ram's velocity and parallelism control. This was done by fitting the position feed forward control (for velocity control) and the target value generation (for parallelism control) on the machine's behavior.

3.4. Quality of closed loop control after retrofit

Figure 11 shows the measurements made for drawing cushion pressure control and for ram velocity control after the retrofit. It is obvious that a massive improvement in drawing cushion pressure control could be gained. Furthermore, the ram's velocity signal does now look much more like the velocity curve of a mechanical press (cf. Figure 10).

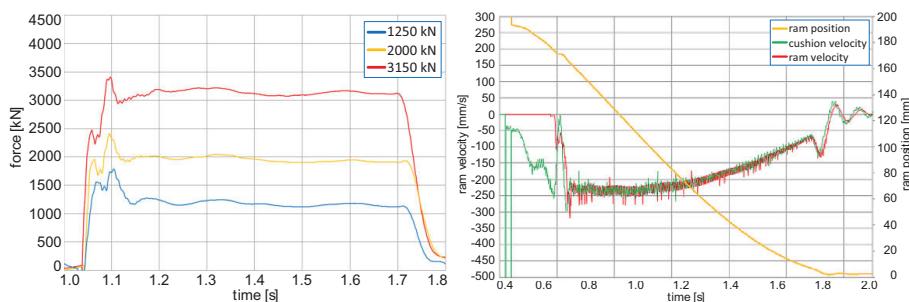


Figure 11: ZE2100 after retrofit – pressure control (left) at 11 strokes/minute and ram velocity control (right) at 8 strokes/minute /5/

Figure 12 shows results for different target forces (1250.0 kN, 2000.0 kN and 3150.0 kN) and different stroke rates (8 strokes/minute, 11 strokes/minute and 14 strokes/minute). Higher drawing speeds are not a problem any longer for the drawing cushion's pressure control. To put it in a nutshell, the controller is able to keep the desired forces nearly constant for the whole length of the process. And that is

achieved, because the PI controller's output signal never reaches a value greater than 10% of the sum signal (feed forward control + PI controller).

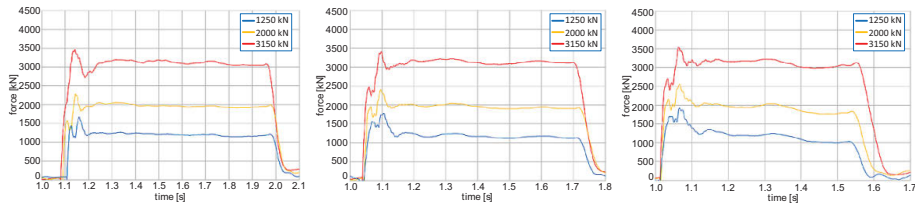


Figure 12: MW ZE2100 – pressure control after retrofit

left: 8 strokes/minute, center: 11 strokes/minute, right: 14 strokes/minute /5/

The last retrofit aspect, mentioned in this paper, is the parallelism control of the ZE2100. The centerpiece of the parallelism control is the calculation of the setpoints. Differences between the 4 position signals (4 cylinders) are converted in responding tilting moments around the x-and y-axis (see **Figure 13**). The tilting moments on the other hand, are converted in resulting cylinder forces at the cylinder center. In the next step, the calculated cylinder forces are sent to the controller as process variables. The reference variable for the controller is a force with 0.0 kN in order to eliminate the tilting moments.

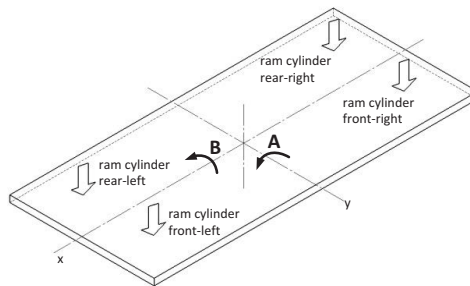


Figure 13: ZE2100 – tilting left/right (A) and front/rear (B) /6/

The ram's tilting control always works together with the velocity and position control. That means the servo valve's sum signal consists of 3 different control outputs. As a consequence of converting the position differences into cylinder forces, an interaction between parallelism control and position/velocity control is prevented. **Figure 14** shows results for ram's parallelism at 8 strokes/minute and with an eccentric drawing cushion force of 2000.0 kN. The measurements were recorded for forming stroke and return stroke, but the parallelism control is active during forming stroke only. During the forming stroke, the tilting around the x-axis has a maximum of 0.1 mm/m and the tilting

around the y-axis is not bigger than 0.2 mm/m. The distances between the left and right cylinders are 3800.0 mm, while the distances between front and rear cylinders are 1700.0 mm. The drawing cushion adapts the ram's tilting movement in all directions very good.

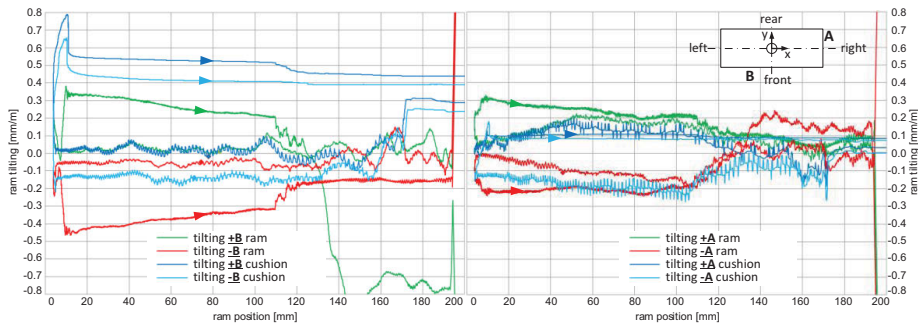


Figure 14: ZE2100 – parallelism control

left: tilting front/rear, right: tilting left/right /5/

In conclusion, the retrofit has led to an enormous enhancement of the quality of the closed loop control. Especially the drawing cushion's pressure control reached a new level of stability. This is due on one hand to the changes in hardware (new servo valves, high resolution modules, real-time control system), and on the other hand, to the model based control algorithms.

4. References

- /1/ Arisa S.A.: S-4-1600-450-230-LDE technical documentation, Logrono, Spain, 2002
- /2/ Beckhoff Automation GmbH.: Press release PR222012 – Beckhoff: ultra-fast performance using standard components, Verl, Germany, April 2012
- /3/ Müller-Weingarten: hydraulic diagram 9098_64 - ZE2100-45.2.2 technical documentation, Esslingen, Germany, August 1998
- /4/ Presswerkverbund Marke Volkswagen: Pressenvermessung Abschlussbericht, Werkzeugbau Wolfsburg, Germany, November 2013
- /5/ Presswerkverbund Marke Volkswagen: Pressenvermessung Abschlussbericht, Werkzeugbau Wolfsburg, Germany, January 2015
- /6/ Majer, Herbert: Vergleich zweier Regelungskonzepte für eine aktive Hydropneumatische Fahrzeugfederung, Stuttgart, Germany, 1989

Potentials of Speed and Displacement Variable Pumps in Hydraulic Applications

Johannes Willkomm

Bosch Rexroth AG, Bgm.-Dr.-Nebel-Str. 2, D-97816 Lohr am Main
E-Mail: johannes.willkomm@boschrexroth.de

Matthias Wahler

Bosch Rexroth AG, Bgm.-Dr.-Nebel-Str. 2, D-97816 Lohr am Main

Professor Dr.-Ing. Jürgen Weber

Institut für Fluidtechnik (IFD), Technische Universität Dresden, Helmholtzstrasse 7a, D-01069 Dresden, E-mail: mailbox@ifd.mw.tu-dresden.de

Abstract

Speed and displacement variable pumps offer a degree of freedom for process control. As a certain operation point can be supplied by different combinations of drive speed and pump displacement intelligent control strategies can address major issues like energy efficiency, process dynamics and noise level in industrial applications. This paper will provide an overview of recent research and development activities to evaluate the named potentials.

KEYWORDS: Energy efficiency, performance, speed variable pump, industrial hydraulics

1. Introduction

Nowadays numerous approaches for controlling hydraulic processes are available for machine manufacturers. In addition to the conventional valve control various displacement controlled concepts have been established due to a rising demand of energy efficient drive systems /1/. Besides variable displacement pumps operated at a constant speed level, falling prices of frequency converters match the awareness of energy efficiency and lead to an increased use of speed variable pump drives in recent years /3, 4, 6/. Combining these two concepts results in a speed and displacement variable pump that can be interpreted as a hydraulic gearbox between the electric drive and the actual process. These so called HydroGear systems allow to leverage the advantages of both control principles while eliminating known drawbacks at the same time /5/. As such, low drive speeds can increase the energy efficiency especially at partial load or

process-related idle time. A variable pump displacement can additionally reduce the motor torque in pressure holding sequences. However, to fully benefit from the degree of freedom efficient control strategies are necessary and will be discussed in the following chapters.

2. Improving Energy Efficiency with HydroGear Systems

The degree of freedom of speed and displacement variable pumps can be used to adjust the operation points of the electric drive and the hydraulic pump to maximize the overall energy efficiency. Depending on the process dynamics there are mainly two different concepts.

2.1. Conventional Energy Optimization

For a given hydraulic system pressure and a demanded volume flow, the drive speed and the pump displacement will be set to minimize the overall losses of the electro hydraulic drive system.

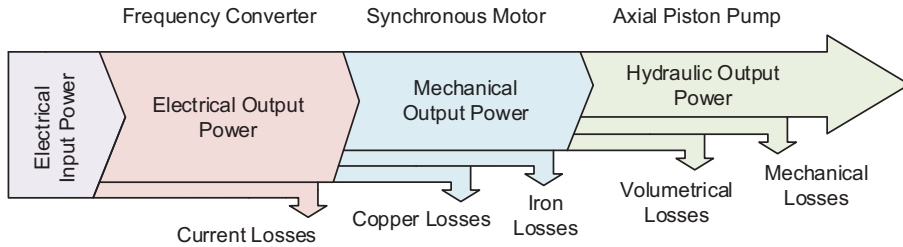


Figure 1: Dominant system losses of HydroGear systems

As shown in **Figure 1** the objective is to minimize the electric input power for a given hydraulic output power. To reduce the complexity of this optimization task only the dominant losses of each component are considered [2, 7]:

Frequency converter:

- Current losses $P_{FC} = K_{FC} \cdot |I|$ (1)

Electric drive:

- Copper losses $P_{Cu} = 3 \cdot R_{Cu} \cdot I^2$ (2)

- Iron losses $P_{Fe} = K_{f,1} \cdot n + K_{f,2} \cdot n^2$ (3)

Hydraulic pump:

- Volumetric losses $P_{Vol} = Q_L \cdot p$, with $Q_L = Q_L(p, Q, n)$ (4)

- Mechanical losses $P_{Mech} = M_R \cdot n$, with $M_R = M_R(p, Q, n)$ (5)

By summarizing all terms the maximization of the energy efficiency can be transformed into a mathematical optimization problem. In [5], therefore, all partial losses are formulated in dependency of the drive speed which takes the role of a decision variable.

$$\min \{P_{tot}\} = \min \{P_{FC} + P_{Cu} + P_{Fe} + P_{Vol} + P_{Mech}\} = \min \{P_{tot}(n)\} \quad (6)$$

The solution of this objective function is the optimum drive speed to serve the given hydraulic operation point. **Figure 2** shows exemplary the optimized speed level n_{opt} as well as the corresponding pump displacement α_{opt} for a selected HydroGear system for varying system pressure and volume flow.

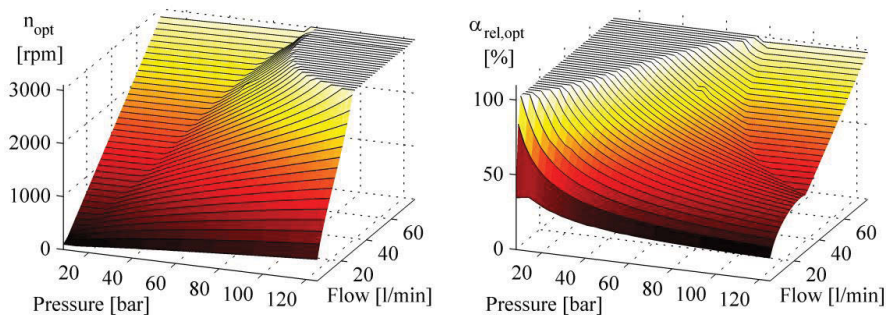


Figure 2: Energy optimized drive speed and pump displacement for the operation range of an exemplary HydroGear system

In terms of process control these maps can be stored inside the controller to track both actuating values. By doing so, in investigated applications energy savings of 20% and more could be achieved in comparison to pure speed variable or pure displacement variable pumps.

2.2. Model Predictive Energy Optimization

In high dynamic process cycles the conventional energy optimization can be improved by considering additional system losses. Fast acceleration sequences of the electric drive lead to high motor torques and finally to increased current losses of the frequency converter as well as increased copper losses in the motor. In addition, due to cost reasons, most frequency converters have no energy recuperation capability. Therefore, the kinetic energy that is saved in the system inertia is lost during deceleration.

$$W_{kin} = \frac{1}{2} J_{tot} \cdot \frac{\pi}{30} \cdot (n_2^2 - n_1^2) \quad (7)$$

On the hydraulic side, the adjustment of the pump displacement requires a certain fluid volume that is taken from the high pressure side of the pump outlet. The resulting energy losses depend on the system pressure and the geometry of the swashplate actuator and can be interpreted as an additional dynamic leakage.

$$W_{Vol,dyn} \sim p \cdot \Delta\alpha \quad (8)$$

To consider the identified dynamic losses in the objective function of equation (6), the optimization of a single operation point has to be replaced by a holistic optimization of an entire process cycle. By means of a time discretization, a model predictive approach is presented in [8] that minimizes the integral of the system losses for recurring processes.

$$\min\{W_{tot}\} = \min\left\{\int_0^{T_{Cyc}} P_{tot}(t) \cdot dt\right\} \xrightarrow{\text{Discretization}} \min\left\{T \cdot \sum_{t=k \cdot T} P_{tot}(n_{k \cdot T})\right\} \quad (9)$$

As the dynamic optimization is based on the information of the time series of pressure $p(t)$ and volume flow $Q(t)$, the underlying hydraulic system can be treated as a black box. The model predictive approach, thus, can be applied to various actuators as hydraulic cylinders, hydraulic motors or any valve controlled subsystem. As a result the machine operator gets the optimum sequence of the drive speed and pump displacement that maximizes the energy efficiency. **Figure 3** shows the introduced concept.

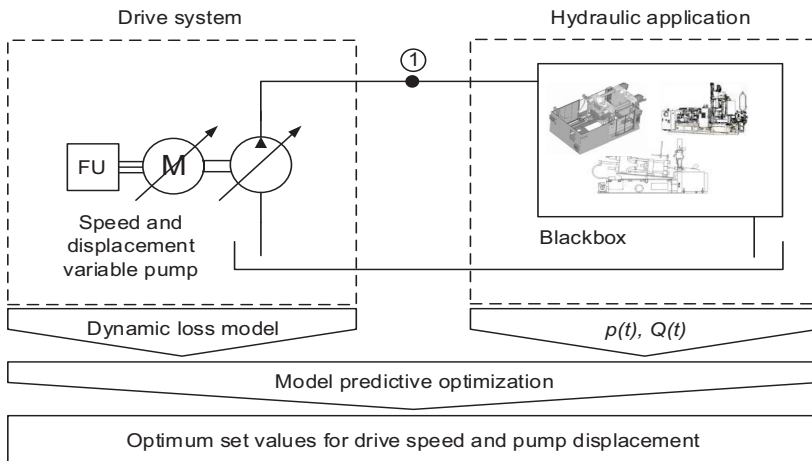


Figure 3: Model predictive energy optimization of HydroGear systems

2.3. Application Example

To evaluate the efficiency of HydroGear systems a stop-and-go movement of a hydraulic cylinder according to **Figure 4** will be discussed in this section.

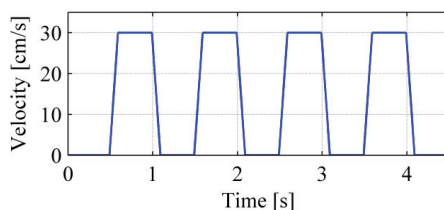


Figure 4: Application Example: Stop-and-go movement of a hydraulic cylinder

To apply the efficiency optimization, the investigated linear movement can be transformed into equivalent sequences of system pressure and volume flow. **Figure 5** shows the resulting sequences of drive speed and pump displacement for both concepts as well as for a pure displacement variable pump operated at a constant speed level as reference system (VDP).

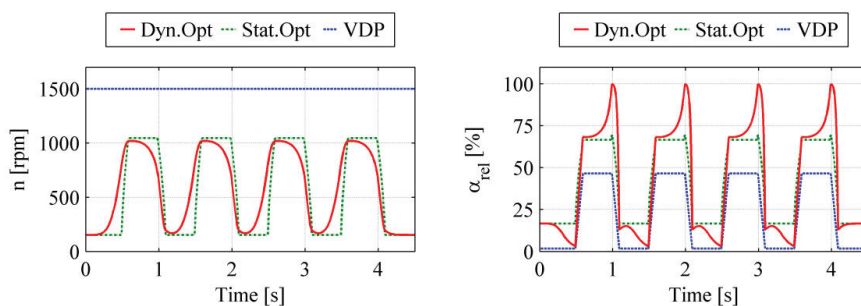


Figure 5: Drive speed and pump displacement for conventional optimization, model predictive optimization and a pure displacement variable pump

The usage of the drive speed as a second actuating variable in HydroGear systems is obvious in the left diagram. Regarding the conventional static optimization, mainly two constant levels for drive speed and pump displacement can be seen that correspond to the stop and the go phases of the movement. Looking at the dynamically optimized sequences, the model predictive approach avoids fast acceleration and deceleration of the electric drive. Instead, the demanded velocity profile of **Figure 4** is ensured by properly adjusting the pump displacement. For example an increase of the pump displacement allows a prior reduction of the drive speed and, thus, a reduction of the overall dynamic losses. **Figure 6** shows a comparison of the energy consumption of

the stop-and-go movement for all three operation concepts that is normalized to the pure displacement variable pump running at constant speed (VDP).

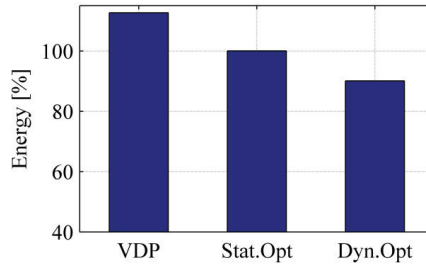


Figure 6: Energy Consumption of the compared control strategies

Both optimization concepts demonstrate the potential energy savings of HydroGear systems. While the conventional static optimization strategy can save 13%, the model predictive approach reaches further 10% energy savings by considering dynamic losses of the actuator systems.

3. Improving Process Dynamics with HydroGear Systems

Besides energy efficiency the degree of freedom of HydroGear systems can be used to maximize the reachable process dynamic. By means of a setpoint jump of the volume flow $Q_1 \rightarrow Q_2$ the potential of using two actuators simultaneously will be shown in the following sections.

3.1. State of the Art

At low volume flows HydroGear systems are usually operated at low drive speed levels due to energy reasons (cmp. **Figure 2**). In the case of a following setpoint jump, however, higher speed levels promises better performance as the effect of a displacement change $d\alpha/dt$ on the volume flow gradient dQ/dt increases proportional to the drive speed level n_0 .

$$Q = n_0 \cdot V_0 \cdot \alpha \rightarrow \frac{dQ}{dt} = n_0 \cdot V_0 \cdot \frac{d\alpha}{dt} \quad (10)$$

Figure 7 illustrates this relation and shows a decreased rising time of the setpoint jump by increasing the drive speed.

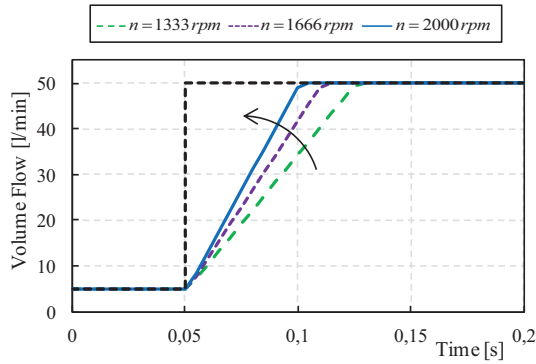


Figure 7: Influence of the speed level on the volume flow gradient of a speed and displacement variable pump

In former publications as well as industrial applications, thus, a prior increase of the drive speed is proposed. In this way, the subsequent setpoint jump can be operated at maximum drive speed while using the maximum dynamic of the displacement actuator at the same time /5/.

3.2. Process Adapted Control

Although the established strategy promises an excellent process dynamic it excludes the acceleration potential of the electric drive to optimize the setpoint jump. In /9/ a process adapted control concept has been proposed that minimizes the rising time by intelligently using the degree of freedom of HydroGear systems. In case of a synchronous use of both actuators equation (10) has to be expanded to:

$$Q = n \cdot V_0 \cdot \alpha \rightarrow \frac{dQ}{dt} = \frac{dn}{dt} \cdot V_0 \cdot \alpha + n \cdot V_0 \cdot \frac{d\alpha}{dt} \quad (11)$$

In combination with the equations of motion of drive speed $n(t)$ and pump displacement $\alpha(t)$ a non-linear equation system can be achieved and transformed into a constrained mathematical optimization problem.

$$n(t) = n_1 + \frac{1}{J_{\text{tot}}} \int_{t_1}^t \left(M_{\text{max}} - \frac{p \cdot \alpha(\tau) \cdot V_0}{2\pi} \right) \cdot d\tau \quad (12)$$

$$\alpha(t) = \alpha_1 + \int_{t_1}^t \dot{\alpha}(\tau) \cdot d\tau \quad (13)$$

The solution of this minimization task is the optimum initial drive speed n_1 to serve the initial volume flow $Q_1 = n_1 \cdot \alpha_1 \cdot V_0$. By accelerating with the maximum available motor

torque M_{\max} and swiveling out the pump's swash plate with the maximum possible gradient $\dot{\alpha}_{\max}$ the final volume flow $Q_2 = n_2 \cdot \alpha_2 \cdot V_0$ will be reached in the shortest possible time. **Figure 8** shows a descriptive explanation of the necessity to calculate the optimum initial drive speed.

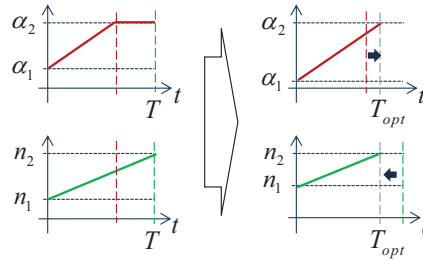


Figure 8: Simultaneous increase of drive speed and pump displacement

While on the left side the final values of drive speed and pump displacement are reached one after the other, an adjustment of n_1 on the right side ensures the simultaneous increase of both actuators and leads finally to the minimum rising time T_{opt} . A detailed derivation can be found in [9].

With respect to the complexity of equations (12, 13) it gets clear that the known strategy of a simple prior increase to the maximum drive speed cannot be the optimum solution. **Figure 9** confirms this conclusion by adding the result of the dynamic maximizing strategy (DMS) on the left side.

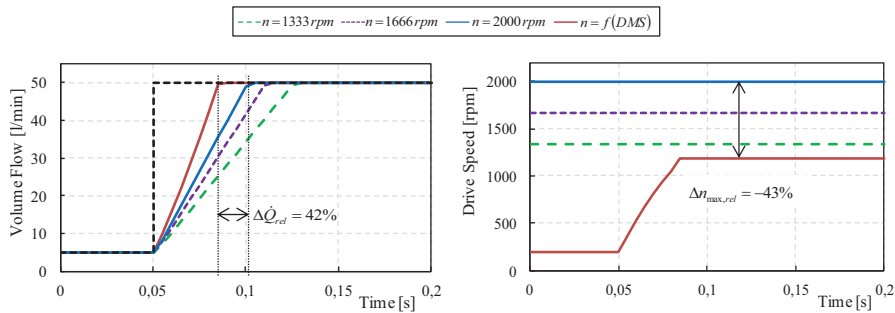


Figure 9: Dynamic maximizing strategy (DMS) of HydroGear systems

The optimized sequence of the drive speed on the right side shows an unexpected result. Instead of the known increase to the maximum drive speed the DMS proposes a decrease to only $n_1 = 200\text{rpm}$ to minimize the rising time in this case. By means of a following acceleration of the electric drive the volume flow gradient can be increased by

over 40%. At the same time the maximum necessary speed level is almost bisected what proves that the pump has not to be operated at critical high drive speeds to realize high volume flow gradients. Besides the optimum process dynamic the DMS, thus, can contribute to a reduction of friction, wear and cavitation in the hydraulic pump, too. As a matter of course the benefit of the DMS depends on the dynamics of both actuators. A high performance synchronous motor will dominate a slow displacement actuator and vice versa. In practice, however, the performances of pump and motor are often in the same range.

4. Improving Noise Level with HydroGear Systems

Ever stricter legal requirements demand the machine manufacturers to reduce the noise level in their production machines. Speed variable pump drives allow to reduce the rotational speed at partial load and pressure holding sequences what leads to a clear reduction of the drive system's noise level. Besides this obvious potential HydroGear systems offer the possibility to avoid defined speed ranges by efficiently choosing the operation point of the electric drive and the hydraulic pump. **Figure 10** shows the original drive speed histogram of a speed controlled process cycle on the left side.

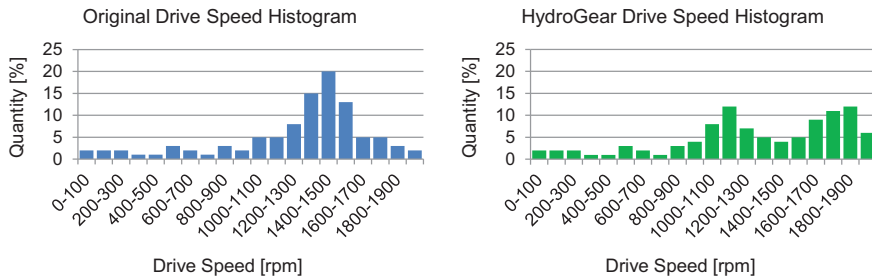


Figure 10: Suppression of critical resonance frequency in a HydroGear system

Assuming a noisy resonance frequency at a speed level of $n = 1500rpm$ the HydroGear system suppresses efficiently the critical interval on the right side without affecting the hydraulic process itself. If necessary it is possible to avoid multiple speed ranges, too. In combination with the model predictive energy optimization of section 2.2, a weighted objective function can be defined that allows the machine operator to adjust the process control to the specific requirements of the application.

$$\min C = \min \left\{ \lambda \cdot \int_0^{T_{Cyc}} f_{losses}(t) \cdot dt + \mu \cdot \int_0^{T_{Cyc}} g_{noise}(t) \cdot dt \right\} \quad (14)$$

The functions $f_{losses}(t)$ and $g_{noise}(t)$ thereby represent appropriate mathematical descriptions of the overall system losses and the noise generation of the electro hydraulic drive system.

5. Serving Power Peaks with HydroGear Systems

Many process cycles have short power peaks that have to be considered for sizing of the drive system. In terms of speed variable pumps this includes the power supply, the frequency converter, the motor and the pump. To avoid oversizing of these components different energy storages can be integrated in the machine concept. Besides hydraulic accumulators and electric capacitors, the use of rotating masses as kinetic energy storage is widespread in industrial applications. **Figure 11** shows a DC coupling of an electro-hydraulic drive unit with a kinetic buffer motor that is used to serve short power peaks.

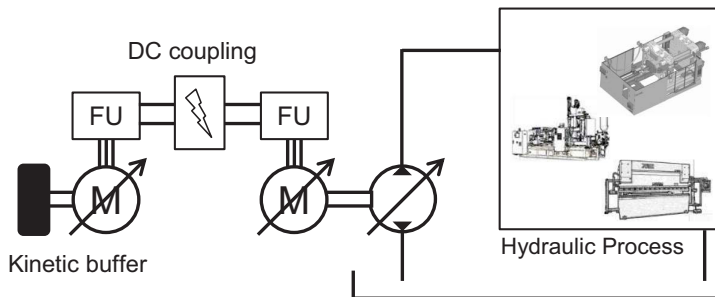


Figure 11: DC coupling of an electro hydraulic drive unit with a kinetic buffer motor

By adding further drive units to the same DC link an efficient power management system can be built to smooth the overall main power. As recuperated energy from a single drive unit can directly be used to load the kinetic buffer or serve another power demanding drive unit, additional hardware as braking resistors or more expensive regenerative frequency converters can be avoided. However, in a DC coupled network the energy exchange depends on the efficiency of all involved energy converters. Therefore, it is desirable to store the energy as close as possible to the drive unit that requires a power peak.

Looking at an electro hydraulic drive system the rotating inertia of motor, pump and coupling is in principle a kinetic energy storage. As the drive speed is directly coupled to the volume flow of the pump, however, loading and unloading the internal kinetic buffer affects the process control. At this point HydroGear systems offer the possibility to compensate the speed variation by means of the variable pump displacement. The degree of freedom allows to decouple the drive speed and the volume flow and finally

to use the internal inertia to serve short power peaks without the need of any additional hardware. **Figure 12** illustrates the concept with a short power peak occurring at $t = 1.5$ s.

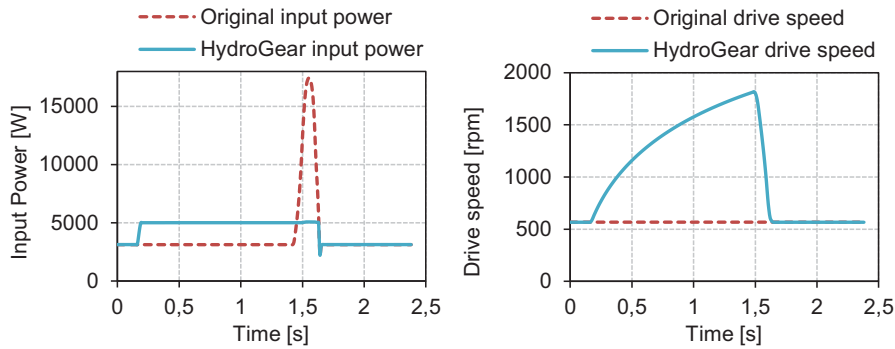


Figure 12: Serving power peaks with HydroGear systems

By means of a prior increase of the drive speed (right) and a simultaneous reduction of the pump displacement, the kinetic buffer can be loaded without affecting the hydraulic process. When the power peak occurs the drive gets strongly decelerated to release the stored kinetic energy. As a result the maximum electrical main power can be noticeably reduced. Instead a small power offset is visible during the loading phase of the kinetic buffer in **Figure 12**. The possible power reduction depends on the given process as the volume flow demand during the power peak defines the minimum possible speed level n_{min} . The storable energy is finally given by equation (15).

$$n_{min} = \frac{Q_{peak}}{V_0} \rightarrow W_{kin} = \frac{1}{2} \cdot J_{tot} \cdot (n_{max}^2 - n_{min}^2) \quad (15)$$

As this energy is mechanically stored in the pump shaft, HydroGear systems allow a potential downsizing of power supply, frequency converter and electric drive.

6. Summary and Outlook

HydroGear systems combine the advantages of frequency controlled and displacement controlled pumps. The two set values offer a degree of freedom for process control that can efficiently be used to increase the performance of electro hydraulic drive systems. By means of a dynamic loss model of the drive system the energy consumption can be reduced by 20% and more comparing to pure speed or pure displacement variable concepts. Considering process dynamics it was shown that a simultaneous use of the two actuators ensures the best possible performance. The volume flow gradient could exemplarily be improved by 40%. Besides energy efficiency and process dynamics, an

improved noise level and a reduction of electrical power peaks are benefits of Hydro-Gear systems. To maximize the impact intelligent control algorithms are necessary. To follow multiple objectives at once, future studies will focus on efficient combinations of the presented concepts.

7. References

- /1/ Helduser, S. Elektrisch-hydraulische Systemtechnik – Entwicklungsschwerpunkte in der Stationärhydraulik. In: *Ölhydraulik & Pneumatik*, No. 1, pp. 16-23, 2006.
- /2/ Manring, N., Johnson, R. Modeling and Designing a Variable-Displacement Open-Loop Pump. In: *Journal of Dynamic Systems, Measurement and Control*, Vol.118, pp. 267-271, 1996.
- /3/ Michel, S., Weber, J. Electrohydraulic Compact-drives for Low Power Applications considering Energy-Efficiency and High Inertial Loads. In: *7th FPNI PhD Symposium on Fluid Power*, Italy, 2012.
- /4/ Michel, S., Weber, J. Energy-efficient electrohydraulic compact drives for low power applications. In: *Bath Symposium on Power Transmission & Motion Control*. Bath, England 2012.
- /5/ Neubert, T. *Untersuchung von drehzahlveränderbaren Pumpen*, PhD Thesis, TU Dresden, Germany, 2002.
- /6/ Radermacher, T., Mäsing, R., Helduser, S. The Drive Counts. In: *Kunststoffe international*, Carl Hanser Verlag, No. 4, pp. 24-28, 2010.
- /7/ Schröder, D. *Verluste und Erwärmung im Antriebssystem – Elektrische Antriebe – Grundlagen*. Springer, Berlin, Germany, 2009.
- /8/ Willkomm, J., Wahler, M., Weber, J. Model Predictive Control of Speed-Variable Variable-Displacement Pumps to Optimize Energy Efficiency. In: *9th International Fluid Power Conference*, Aachen, Germany, 2014.
- /9/ Willkomm, J., Wahler, M., Weber, J. Process-Adapted Control to Maximize Dynamics of Speed- and Displacement-Variable Pumps. In: *Symposium on Fluid Power & Motion Control*. Bath, England, 2014.

8. Nomenclature

α	Swivel Angle	%
I	Motor Current	A
J_{tot}	Inertia of drive system	kgm ²
$K_{f,1/2}$	Drive Constant: Iron Losses – Electric Drive	Ws, Ws ²
K_{FC}	Drive Constant: Current Losses – Frequency Converter	W/A
M_{max}	Maximum Motor Torque	Nm
M_R	Pump Friction Torque	Nm
n	Drive Speed	rpm
p	Pressure	bar
P_{Cu}	Copper Losses in the Synchronous Motor	W
P_{FC}	Current Losses in the Frequency Converter	W
P_{Fe}	Iron Losses in the Synchronous Motor	W
P_{Mech}	Mechanical Losses in the Pump	W
P_{tot}	Overall System Losses	W
P_{Vol}	Volumetric Losses in the Pump	W
Q	Volume Flow	l/min
Q_L	Pump Leakage	l/min
R_{Cu}	Winding Resistance – Electric Drive	Ohm
T_{cyc}	Cycle Time	sec
V_0	Pump Displacement	ccm
W_{kin}	Kinetic Energy	J
W_{tot}	Overall Energy Consumption	J

Condition Monitoring for hydraulic Power Units – user-oriented entry in Industry 4.0

Dipl.-Ing. Martin Laube

Director Engineering and Support Power Units and Manifolds,
Bosch Rexroth AG, Zum Eisengießer 1, 97816 Lohr am Main, E-mail:
martin.laube@boschrexroth.de

Dr.rer.nat. Steffen Haack

Member of the Executive Board and Responsible for Industrial Applications and Sales
Bosch Rexroth AG, Bgm.-Dr.-Nebel-Str. 2, 97816 Lohr am Main, E-mail:
steffen.haack@boschrexroth.de

Abstract

One of Bosch Rexroth's newest developments is the ABPAC power unit, which is both modular and configurable. The modular design of the ABPAC is enhanced by a self-contained Condition Monitoring System (CMS), which can also be used to retrofit existing designs. This dissertation shows how Industry 4.0-Technology provides special advantages for the diverse user profiles. Today, Hydraulic Power Units have either scheduled intervals for preventive maintenance or are repaired in case of component failures. Preventive maintenance concepts, until now, did not fully utilize the entire life expectancy of the components, causing higher maintenance costs and prolonged downtimes. Risk of unscheduled downtime forces the customer to stock an array of spare parts leading to higher inventory costs or in the event a spare is not readily available, the customer may encounter long delivery times and extended downtime. Bearing this in mind, we've conceived the idea of a self-contained intelligent Condition Monitoring System including a predictive maintenance concept, which is explained in the following.

KEYWORDS: Condition Monitoring, Power Unit ABPAC, predictive maintenance

1. Industry 4.0

Acknowledging the fact that Industry 4.0 (i4.0) is a term under ongoing development and with many aspects still being discussed, the following description serves the purpose of broadly defining the new industrial revolution: Industry 4.0, in reference to the fourth Industrial Revolution, is a growing collection of Internet of Things (IoT), which is linked to technologies utilized in an industrial context. This results in the following technological potentials /1/:

- Fusion of the physical world of production with the virtual world of information technology and the internet.
- Humans, machines, objects and systems are connected via information technologies and communicate in an optimized, real time, dynamic, and self-organized way.
- In these intelligent production systems, all branches of the value chain, including supplier to the customer, are connected across the company.
- Within the industrial production environment, individualized customer requests can be addressed in a timely manner with high-quality, higher flexibility, robustness and optimal resource allocation.

2. Opportunities and Challenges – The new modular configurable Power Unit ABPAC

The main task of a Hydraulic Power Unit is to generate a defined amount of hydraulic power. The amount of power is determined by a defined volume/flow, which is then delivered at a certain hydraulic pressure.

These two key parameters are the main selection criteria for a modern hydraulic system. The first step to utilizing the ABPAC configurator is to select the volume/flow and operating pressure required. With this selection, a wide range of recommended pumps and electric motors will be made available. Based on the results from step one, the applicable tank size for the power unit is defined as an output of the configurator. The oil tank is available in four sizes and in three different variations. The tank is designed according to industry standard fluid mechanics and degassing principles. The ABPAC development focused on reducing tank volume without sacrificing hydraulic power.

Furthermore, the configurator allows the user to select from a wide range of accessories and options to adapt the Hydraulic Power Unit precisely to application requirements.

This includes:

- Drip tray
- Pressure filter, return filter
- Air cooler / water cooler
- Accumulator
- Oil heater
- Level switch
- Temperature indicator
- Pressure indicator
- Aluminum profiles (mechanical fixing elements)
- Speed controlled drive units

The full spectrum provided by ABPAC is shown in the following figure (**Figure 1**).

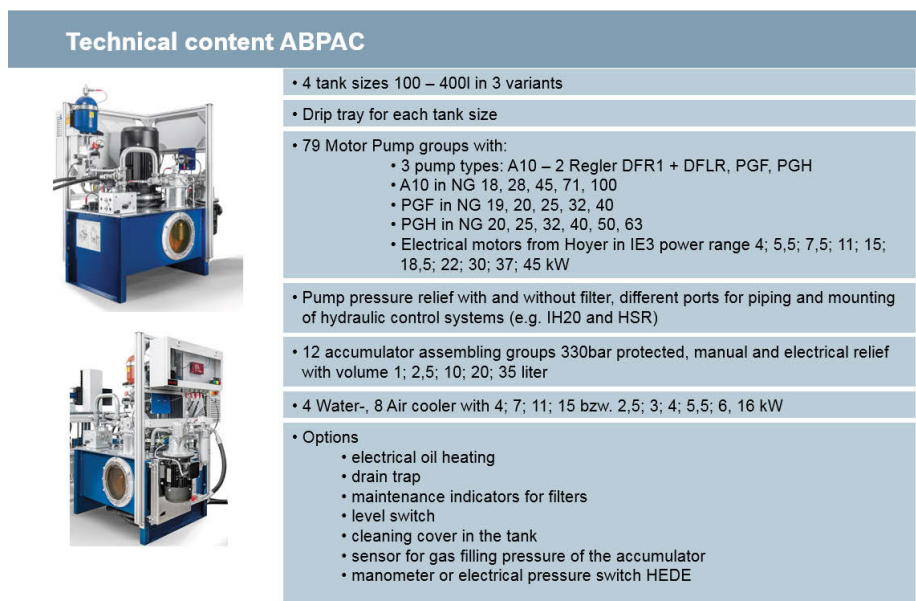


Figure 1: Technical spectrum of ABPAC

At the end of the configuration process, the customer receives the complete product documentation: bill of material, drawings, circuit diagrams and a 3D-model as well as the pricing information for the configured unit.

The greatest advantages of the ABPAC are the reduction of quotation time and design effort, as well as the high level of technical safety in the design process.

The following figure (**Figure 2**) displays three of approx. 20.000 possible ABPAC-configurations and the main parts of a power unit.

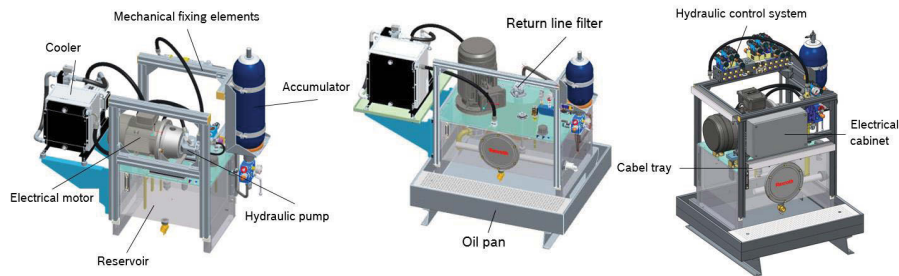


Figure 2: Examples for configured ABPAC

3. Focus on people as key players

Several i4.0 technologies address the following criteria to enhance user experience and shape the digital transformation of organizations:

- Individual address and integration of employees, e.g. by adaption with regard to language, ergonomics and experience
- Flexibility with regard to place and time
- Secure, safe and intuitive human machine interaction
- Contextual information and decision support
- Personalized training and instruction
- Digital and mobile assistance

In summary, the integration of real world and virtual interfaces only provide the technological platform – the crucial step is to provide solutions that convince users and customers that this transition is essential. User-oriented development methods may help to extend the scope from the pure technical performance indicators to a holistic view on user profiles and the experience a product or service generates. The Customer Journey approach is a widely used and proven approach to analyze the touchpoints a customer has with a supplied solution. **Figure 3** provides an impression of a starting template as it is used in Bosch Rexroth innovation studies and product developments to acquire an overview of the different stakeholders within the organization of a customer. The goal is to provide an extended view on the product life cycle with a user centric aspect.

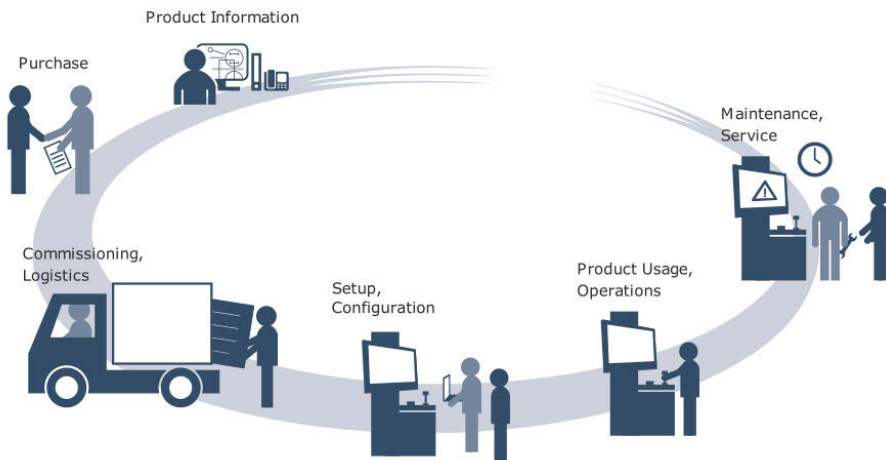


Figure 3: Template for a generic customer journey

4. Condition Monitoring – how it is installed and used in ABPAC

As hardware remains a core component in an industrial context, the intelligent implementation of a cyber-physical systems concept becomes even more important. The authors refer to these kind of products - capable to realize i4.0 use-cases based on modern electronics, communication & software technology - as i4.0 (ready) components.

A pivotal question during a development process of networked products and systems is how to achieve scalability for different customer scenarios.

One exemplary use-case is applying i4.0 technologies in Condition Monitoring of subsystems, such as Hydraulic Power Units (HPU). Of course, the monitoring of several sensor signals and a diagnosis based on known cause-effect relationships would be possible with standard automation technologies. Interest to provide technology that enhances preventive maintenance capability and minimizes the need for unscheduled or demand-oriented maintenance, was the starting point for implementation of an HPU4.0.

4.1. Hardware and software architecture for Condition Monitoring

The basis for all Condition Monitoring Systems are the sensors used in the power unit to monitor the actual values and states. In ABPAC, an array of sensors can be used, i.e. pressure, temperature, fluid level, and oil particle or viscosity sensors, to name a few.

To provide our customers with a retrofit option and the full degree of freedom and control with regards to the machine and process control strategy of the new HPU platform, the ABPAC is equipped with the decentralized i4.0 control unit IndraControl FM. As an i4.0 component, this control features the Open Core Interface (OCI) and the possibility to setup a local web socket server such as the WebConnector. As shown in **Figure 4**, this enables the user to combine proven PLC routines with web technologies such as HTML5.

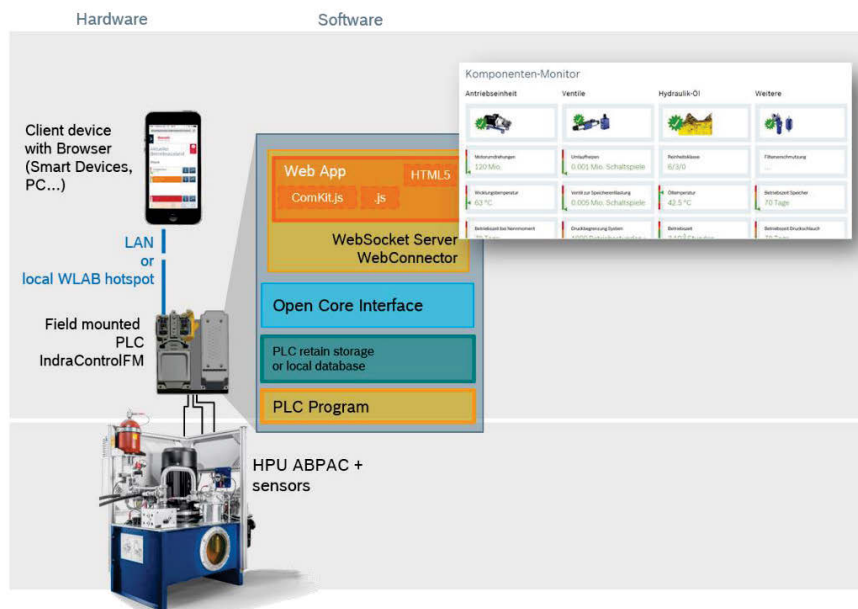


Figure 4: Hardware and software architecture of the ABPAC Condition Monitor

The realized web application generates a platform independent, use-case tailored solution for the technician on site: The HPU behaves as a local hotspot and the authorized technician can access the current and historic condition data of the HPU via a standard web browser without installing additional software. Additionally, the customer benefits from incorporated Bosch Rexroth expertise concerning the cause-effect relationships between certain measured values and component wear mechanisms.

4.2. Challenges of predictive maintenance in hydraulic power units

For maintenance personnel it is always a balancing act (see **Figure 5**): Do they replace components or fluid too often with prevention in mind, generating unnecessary costs as the components could still be functional or do they respond only in the event of a

machine failure, risking an unscheduled production stop with devastating costs. The cost for replacement components may only amount to a few Euros, but the cost of emergency repairs and the loss of production can quickly amount to a higher sum.

The new ABPAC from Rexroth with the decentralized condition monitoring functions, provides advanced notification of hydraulic system issues before they result in costly machine downtime. Components and hydraulic oil are changed only when necessary, which results in lower maintenance costs and increased productivity.

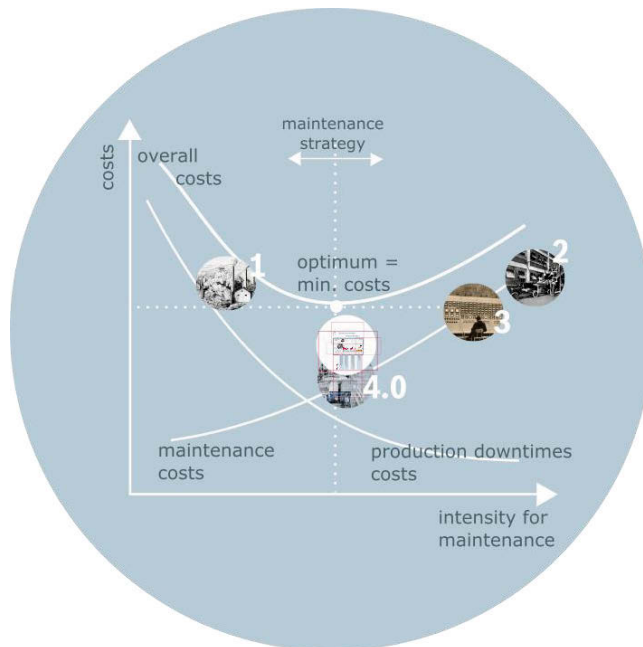


Figure 5: cost comparison of different maintenance strategies

4.3. Prediction models used in ABPAC for predictive maintenance

With the new power unit series ABPAC, Rexroth consistently relies on decentralized condition monitoring functions and predictive maintenance strategies. To implement this approach, extensive knowledge of hydraulics and a high understanding of the cause-effect relationships is required. This applies in particular for complex hydraulic systems such as Hydraulic Power Units and numerous components and technologies that must work symbiotically together.

Applying statements about the wear and tear conditions, realistic life models of all components and the entire system must be defined. Here, Rexroth leverages decades of experience in hydraulics in a wide variety of applications and environments.

Based on this, maintenance and product specialists have developed life models for components, subsystems and the hydraulic fluid, which are validated through experiments and displayed in the software.

In addition, Rexroth has integrated a cabinet-free electronic unit, containing an intelligent evaluation logic software for the new power unit series ABPAC. The data is recorded locally via a sensor node and continuously monitors the operating conditions and wear relevant criteria, comparing the measured values with the stored lifetime models. The focus lies on the hydraulic oil, the valves and the drive unit. Furthermore, the system also detects the filter contamination or the duration of use of pressure hoses and other components.

Sensors monitor continuously the output, suction, reservoir pressure, temperature, level, particles and other contamination of the hydraulic oil. Based on this information the evaluation logic observes the oil condition and makes predictions about the remaining service life. The Condition Monitoring System also counts the cycles of the valves and compares them with the nominal lifetime. According to this information, it is then possible for the maintenance personnel to schedule any necessary changes. With the help of drive data, the electronic system can calculate for example, the volumetric efficiency with the comparison of rotational speed and pressure over the period of operation, this indicator shows the wear of the pump.

The simplest way to display the above mentioned generated information, in a user friendly form is with the traffic light system, used in the ABPAC now (**Figure 6**). This logic shows the current state of the hydraulic oil and the components in a green, yellow or red light system. At a glance, the operator can see whether an action is needed or not. In addition, the logic calculates the remaining expected lifetime. To assess the underlying absolute values it is possible for the maintenance personnel to look at a trend analysis over a given operating time.



Figure 6: Traffic light logic (at present only in German)

4.4. Output systems (Odin, CM on side,...) for condition monitoring use-cases

Today, Bosch Rexroth service customers have the opportunity to combine the Condition Monitoring System and their installed control and observation system with the cloud-based, predictive analytics service ODIN (Online Diagnostics Network). It combines comprehensive deterministic algorithms with Big Data analytics.

Accordingly, **Figure 7** illustrates the resulting toolbox of vertical networks that ensures a use-case tailored implementation.

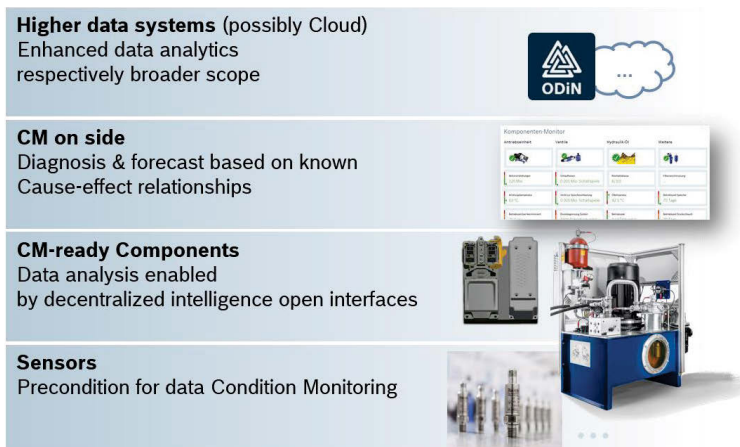


Figure 7: Applied toolbox of vertical networks for a condition monitoring

5. Conclusion

The authors have discussed i4.0 and the use of i4.0 technologies, using the example of the new ABPAC from Bosch Rexroth. Having elaborated on the understanding and definition of i4.0 and the incorporation of i4.0 and configuration of the ABPAC. The main focus deals with the topic, Condition Monitoring, and how it is advantageously used in the ABPAC. The authors exposed the dilemma in which users concerned with maintenance are able to use predictive maintenance to their advantage. To realize a predictive maintenance concept, it was necessary that the ABPAC use a comprehensive sensor-package in which data is collected from all relevant systems (efficiency level, pressure, filling level, temperature and solid contamination). Additionally, the Condition Monitoring System of ABPAC uses a decentralized sensor node with integrated SPS for the internal analysis and the comparison of the current state with prediction models. This allows for a trend forecast to be generated, which can then be displayed on smart devices or via the Data-Mining-System (ODiN) making predictive maintenance a reality for maintenance personnel. In conclusion, by applying i4.0 technologies, demand-oriented maintenance strategies become economically feasible by providing improved machine availability without extensive additional investments or implementation efforts.

6. References

- /1/ Kothe, J, Kübert T, Mikelsons, L 2015. 5th ICAFT SFU "Accuracy in Forming Technology", November 10-11, 2015, Chemnitz, Germany.

Group 7: Hydraulic Components

Electrohydraulic servovalves – past, present, and future

Professor Andrew Plummer

Centre for Power Transmission and Motion Control, Department of Mechanical Engineering,
University of Bath, BA2 7AY, UK. E-mail: A.R.Plummer@bath.ac.uk

Abstract

In 2016 it is 70 years since the first patent for a two-stage servovalve was filed, and 60 years since the double nozzle-flapper two-stage valve patent was granted. This paper reviews the many alternative servovalve designs that were investigated at that time, focusing on two-stage valves. The development of single-stage valves – otherwise known as direct drive or proportional valves – for industrial rather than aerospace application is also briefly reviewed. Ongoing research into alternative valve technology is then discussed, particularly focussing on piezoelectric actuation and the opportunities afforded by additive manufacturing.

KEYWORDS: Servovalve, Direct drive valve, Nozzle-flapper, Piezoelectric

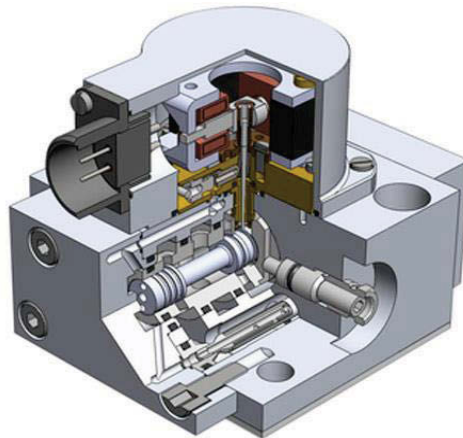
1. Introduction

The servovalve is the key component enabling the creation of closed loop electrohydraulic motion control systems (or 'servomechanisms', the traditional term now largely fallen out of use). 'Servovalve' has come to mean a valve whose main spool is positioned in proportion to the electrical input to the valve, where the spool movement is achieved through internal hydraulic actuation. The spool movement changes the size of metering orifices, thus enabling the valve to control flow; however this flow is dependent on the pressure difference across the orifice unless some form of pressure compensation is used. The most common servovalve design is the two-stage nozzle-flapper valve with mechanical feedback (**Figure 1**). The key parts are:

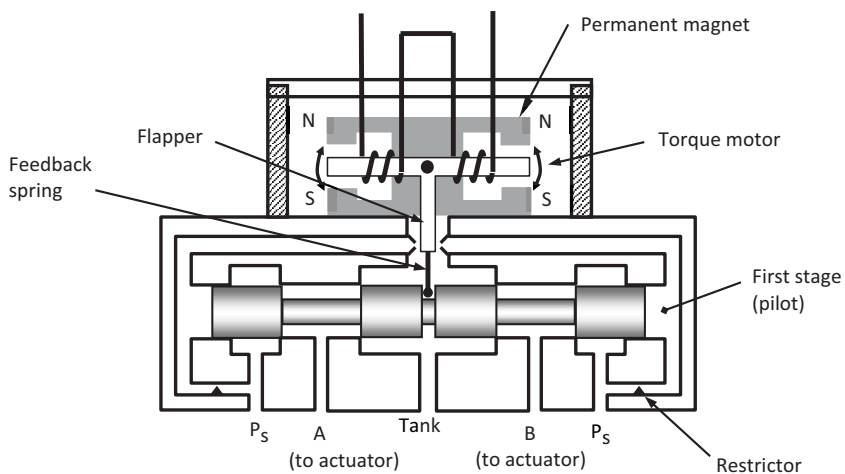
- An electromagnetic torque motor acting as the electrical to mechanical transducer, supported on a flexure tube which gives a friction-free pivot as well isolating the torque motor from the hydraulic fluid (**Figure 2a**).
- A flapper, driven by the torque motor, differentially restricts the flow from a pair of nozzles (**Figure 2b**); the flapper stroke is ~0.1mm. A single nozzle can be used (**Figure 2c**) for modulating pressure on just one end of the spool, but the

unbalanced flow force on the flapper places greater demands on the torque motor.

- The first stage hydraulic circuit forms an H-bridge, where the pair of nozzles are the variable restrictors, generating a pressure difference across the spool when the flapper is off-centre (**Figure 2d**).
- The feedback spring allows the spool to move (stroke $\sim 1\text{mm}$) until the restoring force on the flapper is in equilibrium with the electromagnetic torque, so the flapper recentralises.



(a) Typical design (courtesy Moog)



(b) Schematic

Figure 1: A two stage nozzle-flapper servovalve

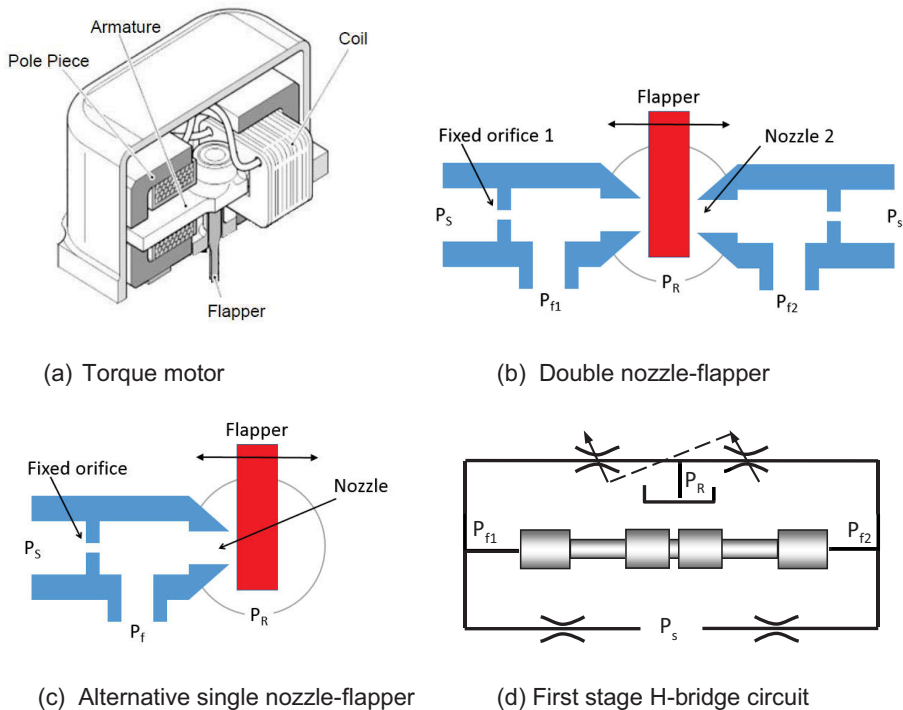


Figure 2: Nozzle-flapper first stage components

The servovalve is a power amplifier as well as an electrical to hydraulic transducer. The electrical input power has an order of magnitude of 0.1W, amplified in the first stage to at least 10W of hydraulic power, and then converted by the main spool to controlling around 10kW of hydraulic output power. So the valve power amplification factor is 10^5 . In a three-stage valve, the original spool flow moves a larger spool, with electrical position feedback, giving a further power amplification factor of about 100, and a similar factor again for a four-stage valve.

2. Historical development

Embryonic electrohydraulic servovalves were developed for military applications in the Second World War, such as for automatic fire control (gun aiming) [1,2]. Such servovalves typically consisted of a solenoid driven spool with spring return. These were able to modulate flow, but with poor accuracy and a slow response. Tinsley Industrial Instruments Ltd. (London) patented the first two-stage servovalve [3] (**Figure 3**). A solenoid (34) moved a sprung first stage spool (47), which drove a rotary main stage (51), whose position was fed back to the first stage by a cam (54), with feedback spring (59) converting position into force.

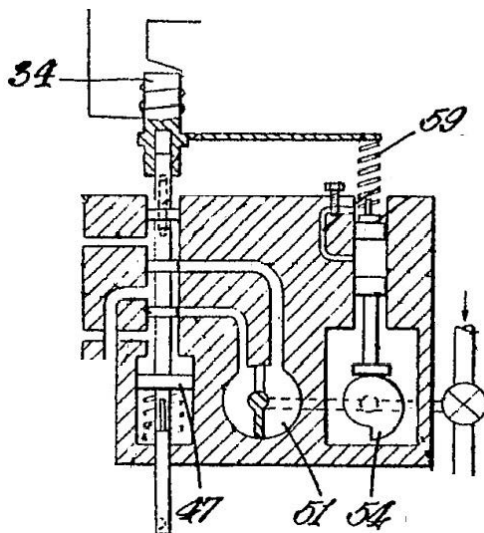


Figure 3: Tinsley 1946 two-stage servovalve, consisting of: solenoid (34); first stage spool (47); main stage (51); feedback cam (54); feedback spring (59)

Servovalve development progressed at a tremendous rate through the 1950's, largely driven by the needs of the aerospace industry (particularly missiles). The technical status and available products at that time are well documented in a series of reports commissioned by the US Air Force /4,5/. In 1955 servovalves were manufactured (or at least prototyped) in the US by Bell, Bendix, Bertea, Cadillac Gage, Drayer Hanson, GE, Hughes, Hydraulic Controls, MIT, Midwestern Geophysical Labs, Honeywell, Moog, North American Aviation, Peacock, Pegasus, Raytheon, Sanders, Sperry, Standard Controls and Westinghouse /4/. It was recognised that single-stage valves with direct electromagnetic actuation of the main metering spool were limited to low flows, due to the small force available from the electromagnetic actuator for overcoming friction, inertial and flow forces. Increasing the size of the electromagnetic actuator to increase force reduces dynamic response due to larger mass and higher coil inductance.

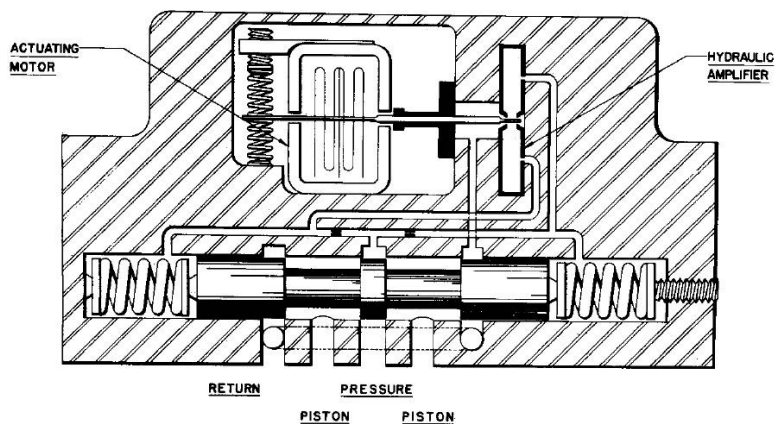
Two stage valves mostly used a nozzle-flapper or a small spool for the first stage, although the jet-pipe first stage was known, but considered to be slower and was confined to industrial rather than aerospace use. The nozzle-flapper, either single or double, had become well established in pneumatic control systems from about 1920 manufactured for example by Foxboro /2/. The second (main) stage spool was sometimes spring-centred, or if unrestrained it was recognised that internal feedback was required to make the main spool position proportional to the electrical input signal. Thus within an actuator position control system the valve acts (to a first approximation)

as an integrator – which is desirable – rather than a double integrator – which often leads to instability /1/. Main spool position feedback was either mechanical, via a feedback spring loading the electromagnetic actuator (force feedback) or via translation of the first stage housing (position feedback), or electrical using a main spool position transducer. Hydraulic feedback, comparing load pressure to first stage pressure, was used for pressure control applications.

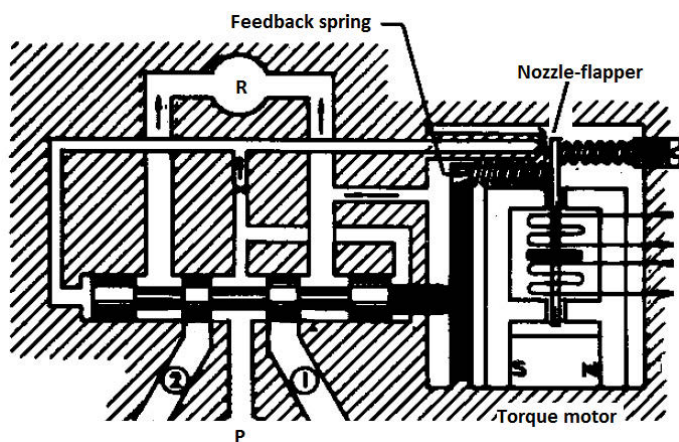
Of 21 designs, the two-stage flow control valves are listed in Table 1, ordered in terms of first stage design and then by main stage feedback. Some are illustrated in **Figures 4 and 5**. In addition to these, integrated valves and cylinders from Hughes and Honeywell, and a plate valve from MIT are described in /4/.

Manufacturer / Type	Electromagnetic driver	First stage	Main stage spool feedback
Bell	torque motor	double nozzle-flapper	no feedback (spring-centred spool)
Moog (Fig. 4a)	torque motor	double nozzle-flapper	no feedback (spring-centred spool)
Cadillac Gage FC-2 (Fig. 4b)	torque motor	single nozzle-flapper	mechanical force feedback
Pegasus (Fig. 4c)	solenoid with spring return	single nozzle-flapper	mechanical position feedback (moving nozzle)
North American	torque motor (PWM)	first stage spool (oscillating)	no feedback (spring-centred spool)
Drayer-Hanson, later made by Lear. (Fig. 5a)	torque motor	first stage spool	mechanical force feedback
Cadillac Gage CG (Fig. 5b)	torque motor (long stroke)	first stage spool	mechanical position feedback (via concentric spools)
Raytheon	antagonistic solenoid pair	first stage spool	mechanical position feedback (via moving bush)
Sanders (Fig. 5c)	torque motor	first stage spool	mechanical position feedback (via moving bush)
Hydraulic Controls	torque motor	first stage spool	electrical position feedback
Bertea	voice coil	first stage spool	electrical position feedback

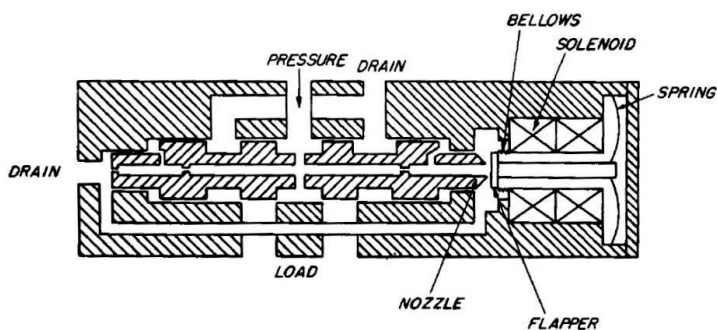
Table 1: Valve designs in 1955 /4/



(a) Moog series 2000 (dry torque motor)

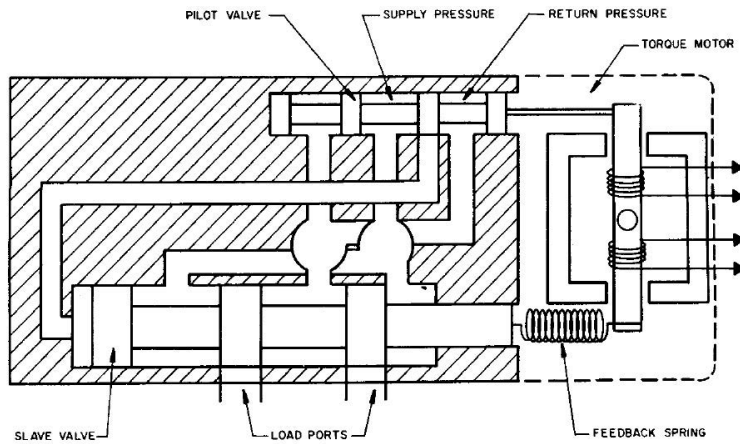


(b) Cadillac Gage FC-2

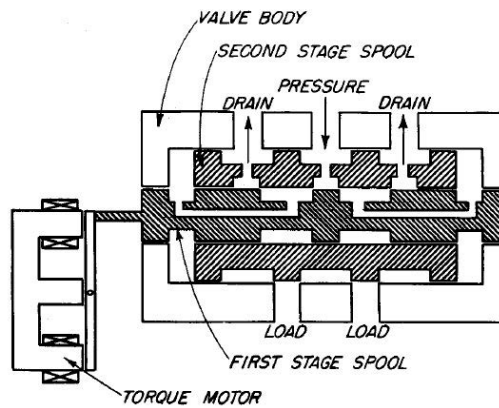


(c) Pegasus 120-B

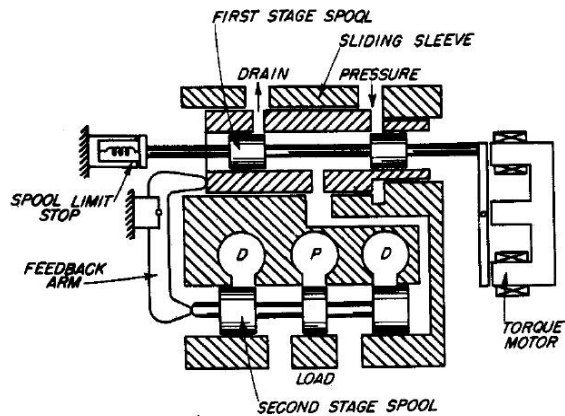
Figure 4: Nozzle-flapper valve designs from 1955 /4/



(a) Lear (previously Drayer-Hanson) /5/



(b) Cadillac Gage CG



(c) Sanders

Figure 5: Valve designs with spool first stage from 1955 /4/

The Hydraulic Controls valve was originally designed at MIT and is described in detail in the seminal book edited by Blackburn, Reethof and Shearer /1/; the book was based on lecture courses given by MIT staff to industrial engineers in the 1950's. This valve showed that electrical spool position feedback could be used very effectively, and popularised the use of torque motors /6/.

The Cadillac Gage FC-2 valve (Figure 4b) is noteworthy as a precursor to the 2-stage valve design that would soon become the *de facto* standard: it combines a torque motor with a nozzle-flapper first stage (albeit in single nozzle form) and mechanical force feedback from the main spool using a feedback spring. This design is also described in a patent filed in 1953 /7/.

The Moog valve (Figure 4a) was originally designed by W.C. (Bill) Moog at the Cornell Aeronautical Laboratory for aircraft and missile control applications /1/. Moog introduced a number of significant practical improvements. Supporting the torque motor on a flexure provided a lightweight frictionless pivot which much reduced valve threshold (input deadband), described in a patent filed in 1950 /8/. When this was granted in 1953, Moog filed another patent, highlighting the deficiencies of this single nozzle design, and proposing the double nozzle-flapper to eliminate sensitivity to supply pressure /9/.

A common fault was due to magnetic particles carried in the oil accumulating in torque motors, but that was solved for the first time in the Series 2000 by isolating the torque motor from the oil /5/. Bell Aerospace file a patent for a similar design the same year /10/.

By 1957, a further 17 new valve designs were available and had also been assessed for the US Air Force /5/, including those manufactured by Boeing, Lear, Dalmo Victor, Robertshaw Fulton, Hydraulic Research, Hagan and National Water. Double nozzle-flapper two-stage valves were starting to dominate. It was noted that nozzle-flapper arrangements were cheaper to manufacture than spool first stages, and all spool first-stages required dither to tackle friction and sometimes overlap.

The following designs had some novel features:

- Sanders SA17D – voice coil / double nozzle-flapper (the flapper actually being a sliding baffle) / mechanical force feedback: all components axially aligned
- Cadillac Gage FC200 – torque motor (dry) / double nozzle-flapper / hydraulic feedback (spool restricts first-stage 'fixed' orifices when it moves)

- Pegasus Model 20 – voice coil or solenoid / double nozzle-double flapper / mechanical position feedback achieved by attaching nozzles to the ends of the spool; effectively a bi-directionally symmetrical version of Figure 4c.
- Hagan – voice coil / first stage spool, spinning to reduce friction / no feedback

Common technical problems reported are null-shift (thought to be mostly due to torque motor magnet temperature sensitivity), nozzle and flapper erosion, torque motor non-linearity if designed to use very small currents, and high frequency instability (squeal). Only Moog and Cadillac Gage are producing commercially available valves in large quantity by this time, although Bendix has many valves under test with end users /5/.

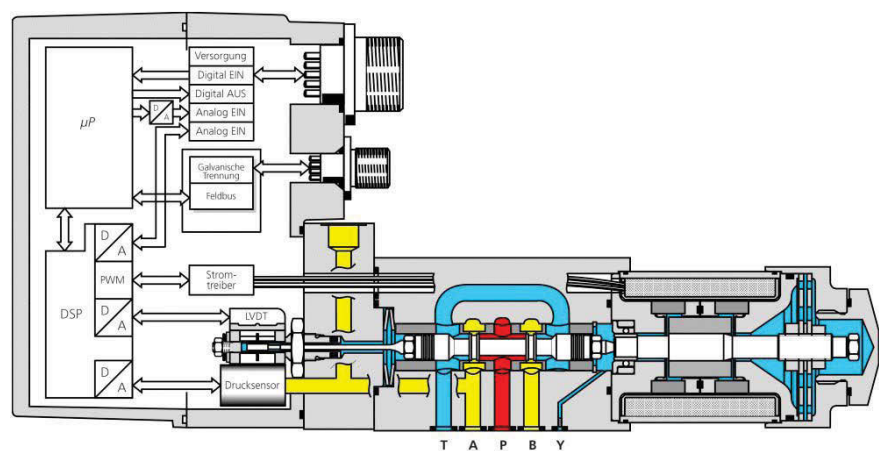
3. Industrial valves

By the end of the 1950's, the two-stage mechanical force feedback servovalve had become established for military and aircraft applications /11/ These included aircraft and missile flight control, radar drives and missile launchers, and also servohydraulic thrust vectoring was starting to be used for space rockets during launch.

Potential industrial application for servohydraulics was also recognised at this time, including for numerical control of machine tools and injection moulding machines, gas and steam turbine controls, steel rolling mills, and precise motion control in the simulation and test industry. Some industrial valves were designed by modifying aerospace valves, for example the '73' series was the first industrial valve from Moog in 1963 /12/. Industrial valves needed to be cheap and low maintenance and began to include:

- Larger bodies for easier machining
- Separate first stage for easier adjustment and repair
- Standardised port patterns
- Better in-built filtering to handle the lower industrial filtration standards

Electrical rather than mechanical spool position feedback allows for higher loop gains improving dynamic response, and also correction for errors due to hysteresis or temperature effects. The inherent safety and compactness of mechanical feedback valves are attractive to aerospace, but industrial valves began to adopt electrical feedback in the 1970's. A landmark was the Bosch plate type servovalve introduced in 1973, with a jet-pipe first stage, a hall-effect position feedback transducer and most importantly on-board electronics to close the loop /12/.



Source: MOOG

Figure 6. Force motor directly driven valve with integrated electronics /13/

	Direct Drive Valve (DDV)			Two-stage Servovalve	
Valve type	Open loop Proportional Valve	Position controlled Proportional Valve	Force motor DDV	Hydraulic pilot, mechanical feedback (MFB)	Hydraulic pilot, electrical feedback(EFB)
Spool actuation	Proportional solenoid, open-loop	Proportional solenoid, closed-loop	Linear force motor (voice coil)	Hydraulic, mechanical feedback	Hydraulic, electrical feedback
Actuation force	<50N	~50N	~200N	~500N	~500N
Static accuracy:					
Hysteresis	5% +	2%	0.2%	2%	0.2%
Dynamic response:					
Step response (100%)	100ms	50ms	15ms	10ms	3ms
90deg phase lag frequency	5Hz	10Hz	50Hz	100Hz	200Hz
Cost	very low	low	medium	high	very high
Size	large	very large	very large	small	medium

Table 2: Example values for typical 4-way valve rated at 40 L/min with 70bar pressure drop (equivalent to 15 L/min at 10 bar valve pressure drop).

Rexroth, Bosch, Vickers and others developed single-stage valves directly positioning the spring-centred spool with a pair of proportional solenoids in open loop, similar to single-stage designs in the early 1950's which had been rejected for aerospace use. Improved accuracy and speed of response was achieved using electrical position feedback for closed loop control. Linear electrical force motors, or voice coil actuators, provide improved linearity compared to proportional solenoids, and limited force output was overcome by replacing Alnico magnets with rare earth magnets in the 1980's. Direct drive valves of this type were developed by Moog (**Figure 6**), and latterly Parker, with dynamic response capabilities similar to two-stage valves.

Table 2 indicates typical valve performance, including valve spool actuation forces. A high valve spool actuation force is required not only to overcome flow forces and accelerate the spool, but also to drive through small contaminant particles which would otherwise jam the valve (chip shear).

4. Novel valve designs

Alternative valve designs have been explored over many years for increasing the dynamic response, reducing leakage, improving manufacturability or providing other advantages over conventional servovalves (either single or two-stage). Most investigations have involved new ways of actuating the spool, often using active materials.

4.1. Piezoelectric valve actuation

Piezoelectric ceramics deform very rapidly when an electric field is applied but maximum strains are small, in the region of 0.15%. Thus actuation using a stack (**Figure 7a**) realistically requires motion amplification, even for first stage actuation (e.g. flapper movement of around 0.1mm). Rectangular bending actuators (**Figure 7b**) can provide sufficient displacement but fairly small forces. Newly available ring bender actuators (**Figure 7c**) provide sufficient displacement for first stage actuation, and reasonable force levels (~10N – 100N) /14/. Such benders are available with ceramic layers as thin as 20µm, in which case electrode voltages of around 50V provide sufficient field strength. However piezoelectric materials suffer from hysteresis (typically 20%), creep, and stack actuator length is temperature dependent /15/. As the actuator behaves like a capacitor, speed of response is generally constrained by the amplifier current limit.

In the 1955 valve survey /4/, only electromagnetic actuation is shown for the electrical to mechanical conversion, but it states that “piezoelectric crystals have been used on certain experimental models to obtain improved response. However, they have not been

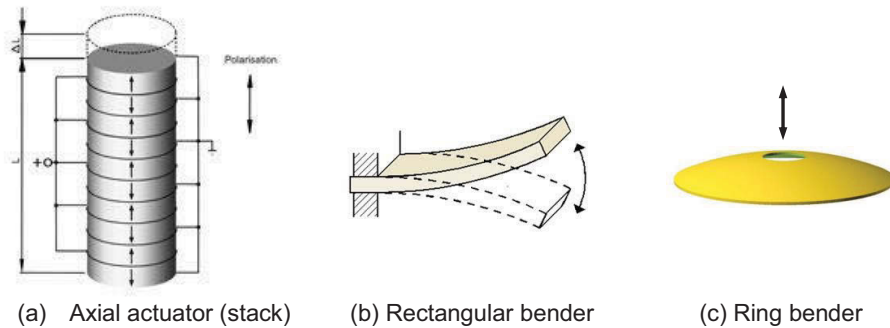
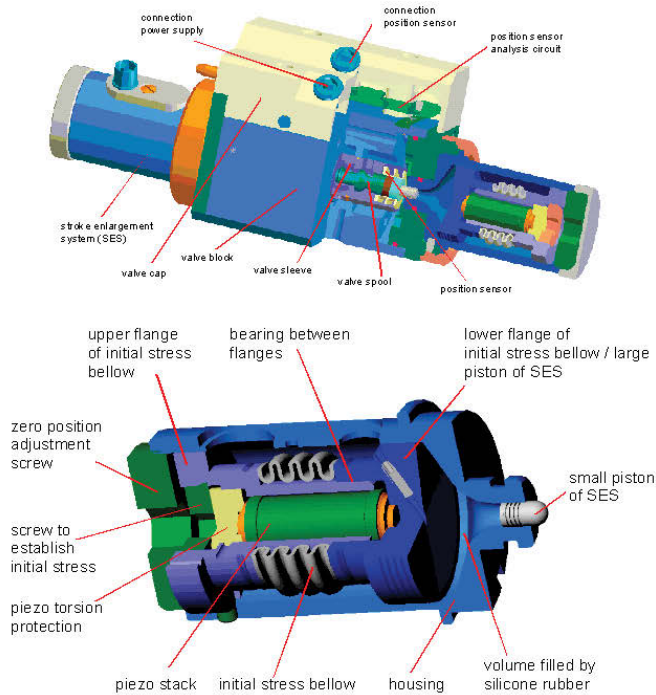


Figure 7. Piezoelectric actuation

accepted to date because of high susceptibility to vibration, temperature changes, and electrical noise and because of the difficulty in obtaining sufficiently large displacements from the crystals". A patent for a piezoelectric valve was filed in 1955, covering both a piezo-actuated flapper for a double nozzle-flapper valve, and also delivering fluid using an oscillating piezo-disc i.e. a piezo-pump /16/.

Moving the spool with a stack requires some motion amplification. In a valve described in /17/ this is done with a hydrostatic transformer filled with silicone rubber and a 40:1 piston area ratio. A -90° bandwidth frequency of 270Hz is achieved, and using two opposing actuators at either end of the spool reduces temperature sensitivity (**Figure 8**). Mechanical amplification using a lever is reported in /18/ (**Figure 9**).

Replacing the torque motor in a two-stage valve with a piezoelectric actuator is reported in a number of studies. In /19/ the authors present a servovalve where a flextensional actuator (a stack in a flexing frame providing motion amplification) moves a flapper in a mechanical feedback valve (**Figure 10**). An aerospace servovalve, again with a feedback wire, is presented in /20/. This uses a rectangular piezoelectric bender to move a deflector jet, arguing that the smaller flow forces experienced in a deflector jet (or jet pipe) first stage are more suited to bender use (**Figure 11**). In comparison with a torque motor, it is suggested that a piezoelectric bender may prove easier to manufacture and commission, and give more repeatable performance. In a recent valve prototype, a ring bended is used as the first stage actuator /21,22/. This time the first stage is a miniature spool with some overlap used to minimize first stage leakage flow. Electrical spool position feedback is used (**Figure 12**).



Source: IFAS

Figure 8: Spool actuation with hydrostatically amplified piezoelectric stack motion /17/

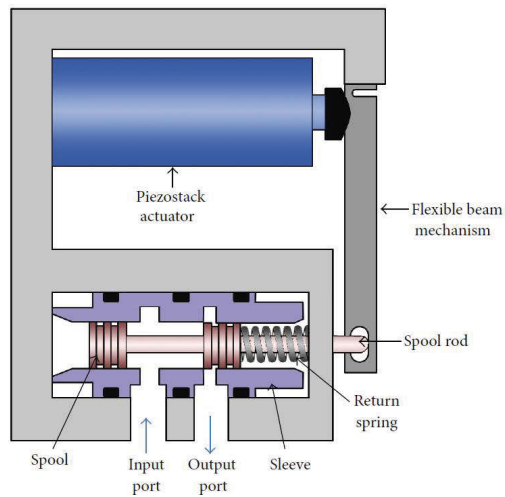


Figure 9: Spool actuation with mechanically amplified piezoelectric stack motion /18/

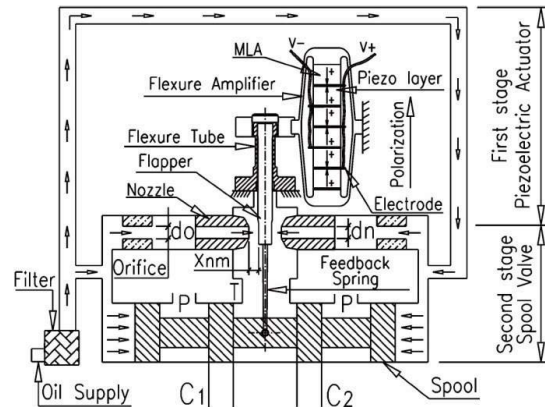


Figure 10: Piezo-stack with flextensional amplification for two-stage valve /19/

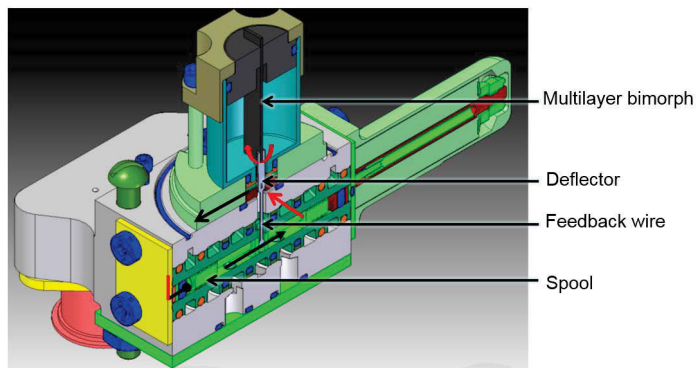


Figure 11: Piezo rectangular bender deflector jet two-stage MFB valve /20/

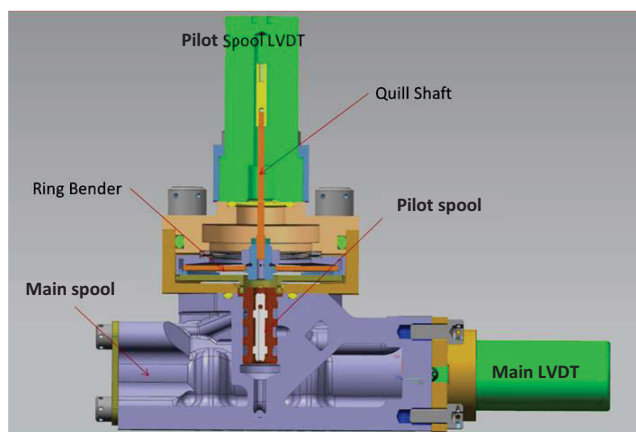


Figure 12: Piezo ring bender actuated pilot spool in two-stage EFB valve /22/

Another piezo-stack actuated first stage concept is described in /23/. As shown in **Figure 13**, all four orifices in the first stage H-bridge are modulated using automotive fuel injectors with $40\mu\text{m}$ stroke, and a -90° bandwidth of over 1kHz is achieved.

Figure 14 shows a novel concept for increasing the frequency response of a direct-drive valve. The spool bushing sleeve is moved $\pm 20\mu\text{m}$ using a stack, complementing the conventional $\pm 1\text{mm}$ spool movement driven by a linear force motor. Thus fine flow control can be achieved at much higher frequency than the 60Hz bandwidth of the conventional valve /23/

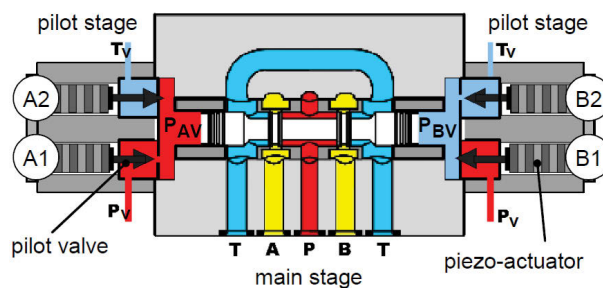


Figure 13: Independent piezo control for first stage H-bridge orifices /23/

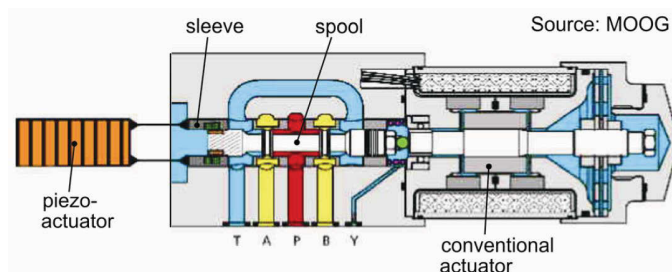


Figure 14: Dual-actuated valve, combining high frequency and long stroke actuators /23/

4.2. Some other novel designs

Magnetostriction is another material phenomenon which can be used to create a 'smart' actuator. Magnetostrictive spool valve actuation has also been experimented with for many years; recent attempts are reported in /24,25/. The challenges are quite similar to piezoelectric actuation, including limited displacement, hysteresis, and temperature sensitivity.

Alternatives to a spool valve main stage have also been explored. Individual main stage orifice control gives the opportunity for more energy efficient use of hydraulic power. Individual control is achieved through applying electric fields to restrict flow of an Electro-Rheological (ER) fluid in /26/. Another application of a functional fluid is reported in /27/. This time a magnetic fluid is used to improve the performance of a torque motor by increasing its damping; the magnetic fluid fills the air gaps and increases its viscosity in the magnetic field.

4.3 The additive manufacturing advantage

Additive manufacturing (AM) gives a radical new way to manufacture hydraulic components. AM can be used to reduce the weight of a valve body, and importantly give very much greater design freedom because many manufacturing constraints are removed. For the piezvalve of Figure 12, powder bed fusion via laser melting has been adopted to manufacture the body from titanium alloy /21,22/. The research included detailed investigation of resulting fatigue life and other material characteristics. **Figure 15** shows the final valve, and **Figure 16** details the AM valve body. **Figure 17** is an example CT scan showing internal galleries in the body.

5. Conclusions

Many of the basic design ideas in single or two-stage servovalve design had been conceived by the mid-1950's: 60 years ago. The two-stage mechanical feedback servovalve became established through the 1960's for aerospace and then high performance industrial applications. The single stage valve, with proportional solenoid or linear force motor direct spool valve, became established in the 1970's and 80's as a lower cost solution for industrial applications, increasingly with electrical spool position feedback and integrated electronics.

The torque motor driven two-stage valve has been remarkably successful and longlived. Nevertheless, manual assembly and adjustment of torque motors has always proved necessary, which is one motivation for investigating alternative technology, principally harnessing active materials. Also, in a few applications, the potential for faster dynamics that piezoelectric or some other active materials promise is attractive, but this is very much the minority of cases. Despite 60 years of research into alternatives, the torque motor has survived, although the gradual improvements in piezoelectric actuator technology, including drive electronics and hysteresis compensation methods, may eventually provide a viable competitor.

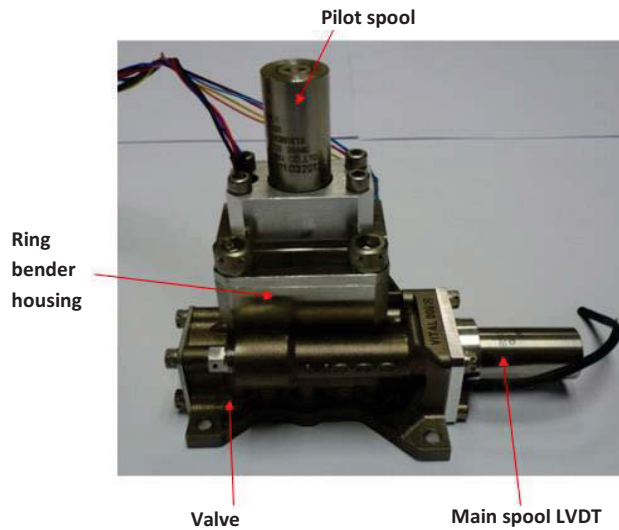


Figure 15. Prototype AM piezovalve /22,23/

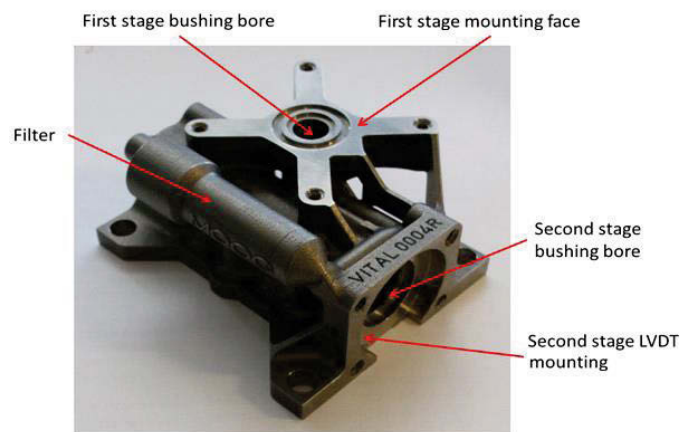


Figure 16: Detail of AM valve body

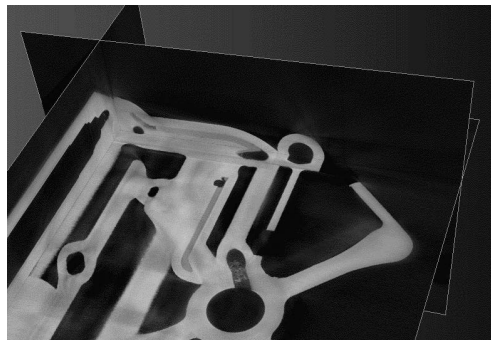


Figure 17: Three-axis view of CT scan of AM valve body

Additive manufacturing, particularly where manufacturing volumes are not too large (such as in aerospace), removes many manufacturing constraints in valve bodies and other hydraulic components. This will enable a paradigm shift in design ideas which can be physically realised, and the full potential of this manufacturing technology has not yet been recognised.

A further continuing trend is increased valve intelligence. Integrating self-tuning functions, condition monitoring, and increased communication capability is a trend in industrial valves which will also be adopted in aerospace valves in time.

It should be noted, however, that a shift away from valve-controlled hydraulic systems is occurring. Electrohydrostatic actuation (servopump controlled actuators), or pump-displacement controlled machines are much more energy efficient. Nevertheless the power density and dynamic response of such systems are well below that of traditional valve controlled systems, so the technology trajectory is by no means certain.

6. References

- /1/ Blackburn, J., Reethof, G., Shearer, J., Fluid Power Control, MIT Press, 1960
- /2/ Bennett, S., A history of control engineering. Peter Peregrinus, 1993.
- /3/ Gall, D, Steghart, F (Tinsley Industrial Instruments Ltd) Improvements in or relating to Servo Systems. Patent GB620688. Filed May 1946, granted March 1949.
- /4/ Boyar. R. E., Johnson, B. A., and Schmid, L., Hydraulic Servo Control Valves Part 1, WADC Technical Report 55-29, Wright-Patterson Air Force Base, Ohio, 1955.
- /5/ Johnson, B. A., Hydraulic Servo Control Valves Part 3, WADC Technical Report 55-29, Wright-Patterson Air Force Base, Ohio, 1957.
- /6/ Maskrey, R., Thayer, H., A brief history of electrohydraulic servomechanisms. ASME Journal of Dynamic Systems Measurement and Control, June 1978
- /7/ Carson, T. H. Flow control servo valve. Patent US2934765. Filed Sept 1953, granted April 1960 (assigned to Ex-Cell-O Corp, owner of Cadillac Gage)
- /8/ Moog, W.C. Electrohydraulic servo mechanism. Patent US2625136. Filed April 1950, granted Jan 1953.

- /9/ Moog, W.C. Electrohydraulic servo valve. Patent US2767689. Filed May 1953, granted Oct 1956.
- /10/ Wolpin, M.P., Smith B., Kistler, W.P. (Bell Aerospace Corp) Flapper valves. Patent US2934765. Filed May 1955, granted Oct 1965.
- /11/ Thayer, W.J., Transfer functions for Moog Servovalves. Moog Technical Bulletin 103, 1958.
- /12/ Jones, J.C. Developments in design of electrohydraulic control valves from their initial concept to present day design and applications. Workshop on Proportional and Servovalves, Melbourne, Australia, 1997.
- /13/ Moog Control Ltd Developments in servovalve technology. Industrial application note, 1999.
- /14/ Bertin, M.J.F., Plummer, A. R., Bowen, C. R., and Johnston, D. N. An investigation of piezoelectric ring benders and their potential for actuating servovalves. In: Bath/ASME Symposium on Power Transmission and Motion Control FPMC2014, Bath, September 2014.
- /15/ D.A. Hall, Review of nonlinearity in piezoelectric ceramics, J. Mater. Sci. 36, 2001, 4575–4601.
- /16/ Johnson, R., Stahl, R., Walters, G. (Textron Inc) Non-magnetic electro-hydraulic transfer valve. Patent US2928409. Filed Jan 1955, granted Mar 1960.
- /17/ Murrenhoff, H., Trends in valve development. O + P (Ölhydraulik und Pneumatik) 46, 2003, Nr. 4
- /18/ J. Jeon, C. Han, Y.-M. Han and S.-B. Choi, "A New Type of Direct-Drive valve System Driven by a Piezostack Actuator and Sliding Spool," Smart Materials and Structures, 2014.
- /19/ S. Karunanidhi, M. Singaperumal, Mathematical modelling and experimental characterization of a high dynamic servo valve integrated with piezoelectric actuator, Proc. Inst. Mech. Eng. Part J. Syst. Control Eng. 224, 2010, 419–435.
- /20/ Sangiah, D., Plummer, A. R., Bowen, C. and Guerrier, P., A novel piezohydraulic aerospace servovalve. Part I : Design and modelling. Proceedings of the Institution of Mechanical Engineers, Part I: Journal of Systems and Control Engineering, 227 (4), 2014, pp. 371-389.

- /21/ Persson, L.J., Plummer, A.R., Bowen, C. ,Brooks, I. Design and Modelling of a Novel Servovalve Actuated by a Piezoelectric Ring Bender. Proc ASME/Bath Symposium on Fluid Power and Motion Control, Chicago, October 2015.
- /22/ Persson, L.J., Plummer, A.R., Bowen, C. ,Brooks, I. A lightweight, low leakage piezoelectric servovalve. Recent Advances in Aerospace Actuation Components and Systems 2016 (R3ASC'16), Toulouse, March 2016.
- /23/ Reichert, M. Murrenhoff, H., New Concepts and Design of High Response Hydraulic Valves Using Piezo-Technology. Power Transmission and Motion Control Symposium, Bath, September 2006.
- /24/ Z. Yang, Z. He, D. Li, G. Xue, X. Cui, Hydraulic amplifier design and its application to direct drive valve based on magnetostrictive actuator, Sens. Actuators Phys. 216 (2014) 52–63.
- /25/ S. Karunanidhi, M. Singaperumal, Design, analysis and simulation of magnetostrictive actuator and its application to high dynamic servo valve, Sens. Actuators Phys. 157 (2010) 185–197./24/
- /26/ Fees, Gerald: Study of the static and dynamic properties of a highly dynamic ER servo drive. O+P“ Ölhydraulik und Pneumatik” 45 (2001) Nr. 1.
- /27/ Li, S., Song, Y., Dynamic response of a hydraulic servo-valve torque motor with magnetic fluids. Mechatronics 17 (2007) 442–447

A new energy saving load adaptive counterbalance valve

Dr.-Ing. Bernd Zähe

Sunhydraulik GmbH, Brüsseler Allee 2, 41812 Erkelenz, E-mail BerndZ@sunhydraulik.de

Professor Dr.-Ing. Peter Anders

Hochschule Furtwangen, Fakultät ITE Tuttlingen, Kronenstraße 16, 78532 Tuttlingen, E-mail an@hs-furtwangen.de

M.Sc Simon Ströbel

X-DOT ENGINEERING, Blumenstrasse 36, 72355 Schömburg, E-mail info@xdot-engineering.de

Abstract

The paper shows standard circuits with load reactive and non load reactive counterbalance valves. A Matlab simulation based on a linear model for the circuit with load reactive counterbalance valves shows what parameters have a significant influence on the stability of the system. The most important parameters of the counterbalance valve that influence the stability are pilot gain and relief gain. The factors describe how pilot pressure and load pressure affect the flow across the counterbalance valve. A new counterbalance valve (patent pending) has the pilot gain and relief gain required for stability only in operating ranges that require the parameters for stability. When the load is not moving or the counterbalance valve is not required for positive (non overrunning) loads, the new valve has a higher pilot ratio, which means that the valve opens further at lower inlet pressures. The new counterbalance valves saves about 30% power compared with a standard counterbalance valve that has the same parameters for stability when it is lowering an overrunning load. The standard counterbalance can be replaced with the new load adaptive valve in the same cavity. The paper shows test results and the design of the valve.

KEYWORDS: Counterbalance, load holding, energy efficiency, stability, simulation

1. Load reactive versus non load reactive counterbalance valves

Counterbalance valves are often used in the return line of cylinders or motors to prevent uncontrolled overrunning of the load and to ensure a leak free positioning of the actuator when the directional valve is in a center position. **Figure 1** shows the two basic circuits.

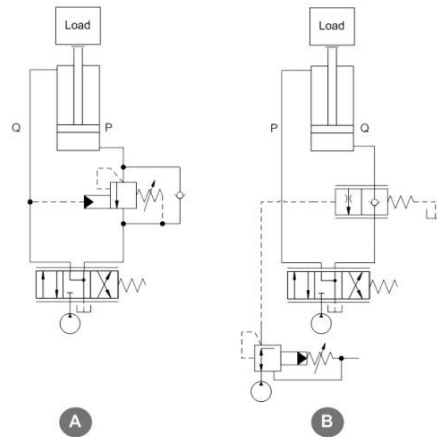


Figure 1: Circuits with two types of counterbalance valves

Circuit A uses a directional or proportional valve to control the flow to the cylinder or motor. The counterbalance can be seen as a relief valve that preloads and limits the pressure in the return line. Circuit B uses a pressure reducing valve (not shown) to control the pressure on the inlet side, or the directional valve connects p to a low pressure source. The non-load reactive counterbalance valve in the return line functions as a flow control valve piloted from an additional pressure control valve. That circuit is more stable than circuit A since the counterbalance valve sees a constant pilot pressure that doesn't change with the speed of the cylinder, but the circuit is also more expensive and the counterbalance valve has no built in relief function. The counterbalance valve in this paper is a load reactive counterbalance valve, typically used in circuit A.

Figure 2 shows a typical circuit with a load reactive counterbalance valve in the return line. The stability of the circuit can be calculated based on two equations that describe the pressure build up in both sides of the cylinder (1) and a third equation that describes the force balance of the cylinder piston with attached mass (2).

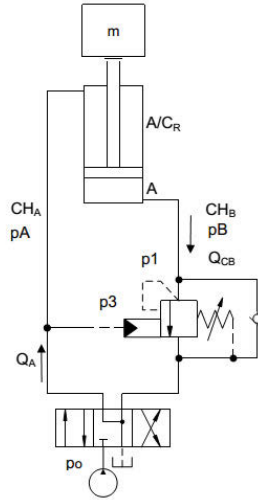


Figure 2: Typical circuit with a load reactive counterbalance valve

$$\dot{p} = \frac{1}{C_H} (\text{in flow} - \text{out flow}) \quad (1)$$

$$m \ddot{x} = p_A * A / C_R - p_B * A \quad (2)$$

2. Linear model and calculation of stability (Hurwitz criterion)

The parameter in the linear model that varies more than all others with the operating point is the change in flow per pressure drop across the directional valve. The flow across the directional control valve or proportional valve:

$$Q_{AOP} = \alpha_D * D^2 * \sqrt{\frac{2 * (p_0 - p_A)}{\rho}} \quad (3)$$

can be linearized. G_{DCV} describes the change in flow per change in pressure differential

$$G_{DCV} = \frac{dQ}{d(p_0 - p_A)} = \frac{\alpha_D * D^2}{\sqrt{2 * \rho} * \sqrt{p_0 - p_A}} \quad (4)$$

The flow across the directional valve is

$$Q_A = Q_{AOP} + G_{DCV} * (p_0 - p_A) \quad (5)$$

with Q_{AOP} the flow in the operating point calculated from the nonlinear orifice equation (3). The flow across the counterbalance valve is a function of pilot pressure (in the circuit

p_3 on port 3 of the counterbalance valve which is identical with the inlet pressure p_A while p_1 , the pressure on port 1, is identical with p_B .

$$Q_{CB} = G_{pilot} * p_A + G_{relief} * p_B \quad (6)$$

The equations can be combined to describe the system in a matrix form

$$\begin{pmatrix} \dot{p}_A \\ \dot{p}_B \\ \ddot{x} \end{pmatrix} = \begin{pmatrix} -\frac{G_{DCV}}{C_{HA}} & 0 & -\frac{A}{C_{HA} * C_{HB}} \\ -\frac{G_{pilot}}{C_{HB}} & -\frac{G_{relief}}{C_{HB}} & \frac{A}{C_{HB}} \\ \frac{A}{CR * m} & -\frac{A}{m} & 0 \end{pmatrix} * \begin{pmatrix} p_A \\ p_B \\ \dot{x} \end{pmatrix} \quad (7)$$

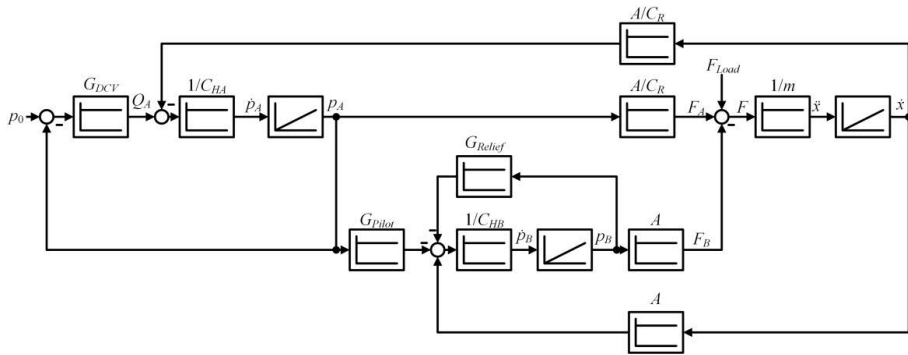


Figure 3: Block Diagram of the 3rd order model

Figure 3 shows the block diagram of the model. The corresponding 3rd order differential equation describes a stable system if the coefficients of the characteristic equation met the Hurwitz or Routh criterion (see /1/). That leads to:

$$\frac{C_{HA}}{C_{HB}} + \frac{G_{DCV}}{G_{relief}} \frac{C_{HB}}{C_{HA} * CR^2} + \frac{m^2}{A^2} \left(\frac{G_{DCV} * G_{relief}}{C_{HB}} + \frac{G_{DCV}^2}{C_{HA}} \right) > \frac{G_{pilot}}{G_{relief} * CR} \quad (8)$$

and

$$\frac{G_{DCV}}{C_{HA}} + \frac{G_{relief}}{C_{HB}} > 0 \quad (9)$$

and

$$G_{DCV} * CR^2 + G_{pilot} * CR + G_{relief} > 0 \quad (10)$$

Equation (10) describes the 3rd Hurwitz criterion under the assumption that $\frac{G_{pilot}}{G_{relief} * CR}$

is positive. Equation (8) shows:

1. Two parameters of the counterbalance valve affect the stability: G_{pilot} which is the change in flow per pilot pressure change and G_{relief} the change in flow per load pressure change. The pilot gain G_{pilot} needs to be low for stability, which means that valves with a low pilot ratio and a low nominal flow (restrictive) valves improve the stability. The pilot ratio of counterbalance valves is the ratio of the effective area for pilot pressure divided by the effective area for load pressure. A pilot ratio of 3 means that a pilot pressure 10 bar reduces the setting by 30 bar. In equation (8) the ratio of pilot gain and relief gain is identical with the pilot ratio:

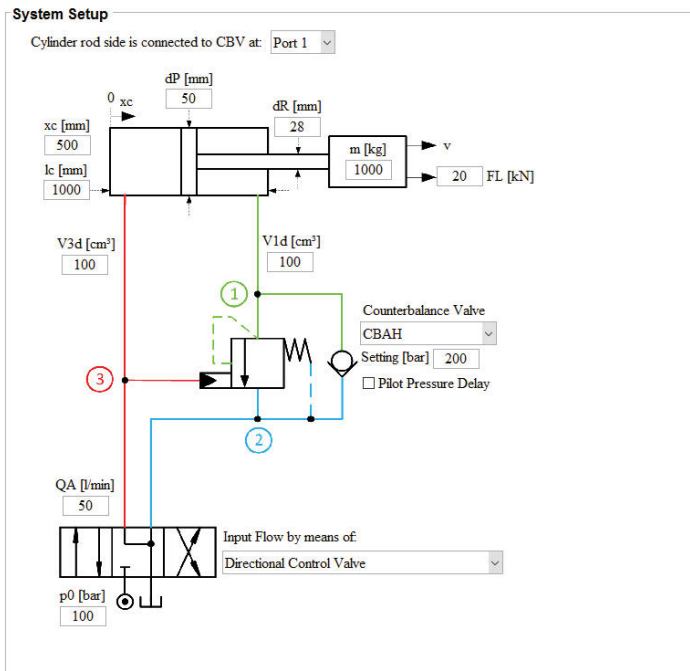
$$\frac{G_{pilot}}{G_{relief}} = \frac{dQ/dp_3}{dQ/dp_1} = \frac{dp_1}{dp_3} = PR \quad (11)$$

2. The directional valve should have a high flow gain G_{DCV} which means that the damping is better if flow changes when the pressure differential changes. The flow does not change if the directional control valve is a pressure compensated flow control valve.

Equations 10 and 11 show that negative numbers for one of G_{pilot} , G_{relief} or G_{DCV} need to be compensated by positive gains of the others. Simulations show that in some cases stability is possible with negative numbers for the flow gain of the directional control valve G_{DCV} , but in general positive numbers helps to improve stability.

3. Simulation based on a linear model

The Matlab based simulation program is based on parameters that describe a linearized model. The user enters the following parameters: supply pressure, meter in flow, cylinder dimensions, attached mass, capacitance in A and B, he selects the counterbalance valve from a list (see **Figure 4**). The valve is described by pilot gain and relief gain. The most nonlinear element in the circuit is the directional control valve that functions like an orifice on the meter in side. The user can define the flow and the supply pressure, the program will calculate the orifice size and linearize it in the operating point (see eq. 3,4,5,6).



Static Operating Point

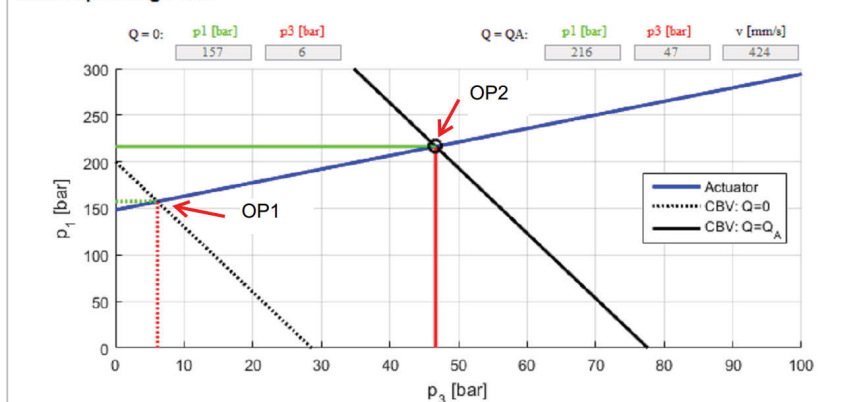


Figure 4: Menu for entering parameters of the complete circuit and diagram with effective setting p_1 vs pilot pressure at two different flows

The program calculates the pressures p_1 and p_3 on both sides of the cylinder. Figure 4 shows an example for the static operating point. The blue line shows combinations of pressures p_1 and p_3 that are in equilibrium with the given external force on the cylinder. The dotted line shows the performance curve of the counterbalance valve for very low flow (crack pressure \rightarrow OP1). The example shows a counterbalance valve with a setting

of 250 bar which is above the load induced pressure of the load of 200 bar. Increasing pilot pressure reduces the effective setting of the counterbalance valve. The gradient is the pilot ratio of the counterbalance valve. The black line parallel to the dotted line shows the performance of the counterbalance valve at a higher flow (50 l/min → 02).

An advantage of the linearized model is that results are available within fractions of a second. After entering 10 parameters the user sees the static operating point (required inlet pressure to move the cylinder with the required speed) and the system dynamic.

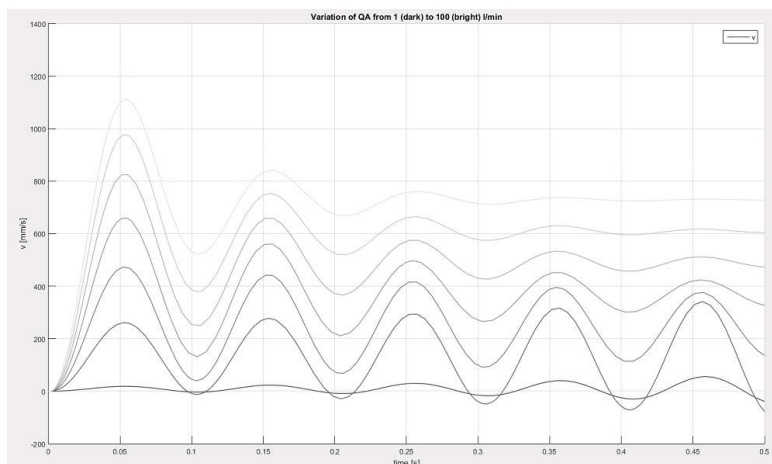


Figure 5: Parameter variation. Flow 1-100 l/min in 8 steps.

Figure 5 shows a parameter variation in that the flow changes from 1 to 100 l/min for a given supply pressure. The damping changes because the directional valve sees a lower pressure differential at higher flow (the supply pressure remains constant, but the inlet pressure is higher for higher flows) and (more important) because the valve is opened further for higher flow. Equation 4 shows that the flow gain G_{DCV} is higher at higher flows because the valve is further opened, the effective diameter D is larger, so the directional valve contributes more to damping than at low flows (compare with stability criterion eq.8).

4. New loadadaptive counterbalance valve

The calculation and the simulation shows that pilot gain and pilot ratio influence the stability. Since stability is required the application limits the maximum pilot gain and the maximum pilot ratio. Therefore a customer can't use a counterbalance valve with higher pilot ratio or pilot gain without affecting the stability that moves with a negative load. A load is negative if it pushes in the direction of the movement.

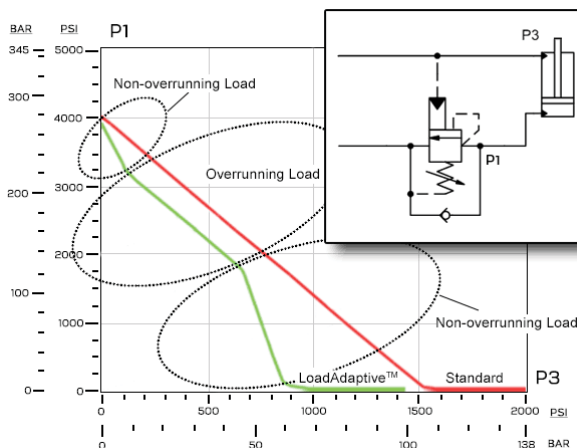


Figure 6: Performance curve of a standard (red) and a loadadaptive (green) counterbalance valve. Setting vs pilot pressure

But the load isn't always negative and it isn't always moving. **Figure 6** shows the performance curve of a standard counterbalance valve (red). Increasing pilot pressure reduces the setting of the valve. The curve is measured at a constant flow. There are three different operating areas. The valve controls the movement of a negative load in only one of them. For very low pilot pressures the counterbalance valve is not open yet. Initially it has a setting about 30% above the highest expected induced load pressure. So the setting can be reduced rapidly with high pilot ratio by about 20% without causing instability since the actuator is not moving yet. When the pilot pressure further increases the load will eventually move. At that stage a low pilot ratio (a flat gradient) is required for stability. Very high pilot pressures are not required on actuators with negative load since the load helps to open the counterbalance. Combinations of high pilot pressure and low 'load pressure' occur when the actuator sees positive loads. In that operating range the counterbalance valve causes unnecessary pressure losses. A counterbalance valve to control a negative load is not needed since there is no negative load. The new load adaptive counterbalance valve fully opens at pressures about 30% below the pilot pressure that is required to fully open the equivalent standard counterbalance.

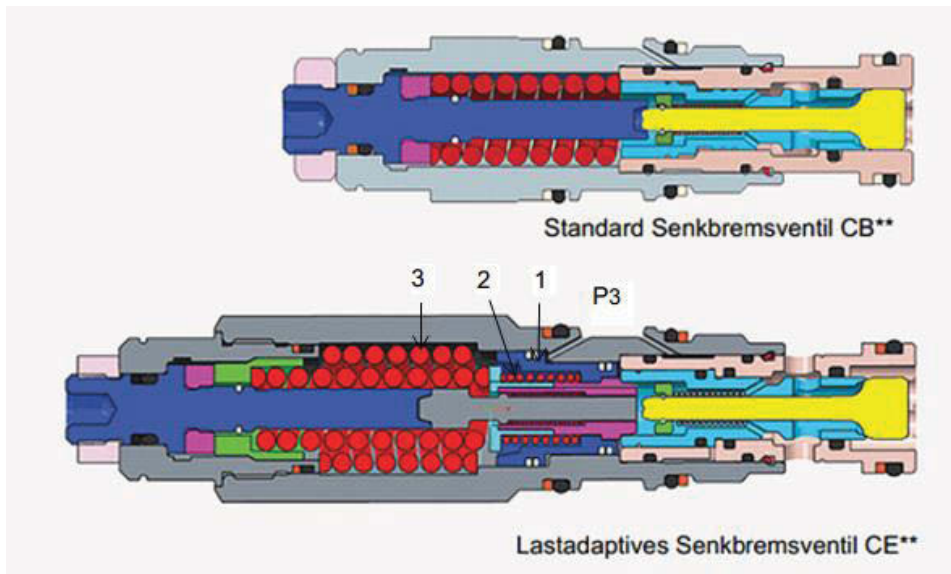


Figure 7: Standard counterbalance and new load adaptive version (below)

Figure 7 shows the cross section of a standard counterbalance and the new load adaptive version. An additional sleeve (1) is active to reduce the setting of the valve by about 20%. The setting is not further reduced because the inner spring (2) limits the maximum force between the sleeve and the adjust spring (inner spring). The sleeve will stop on the preloaded outer spring (3) when pilot pressure further increases. So it doesn't affect the performance of the valve. The same main stage elements are active to control negative loads as in the standard 'base' model. Eventually higher pilot pressure times an effective area will exceed the preload of the outer spring (3) and the sleeve (1) will help to fully open the counterbalance valve. So the additional sleeve is active-inactive-active with increasing pilot pressure resulting in an effective pilot ratio (gradient in the p_1 - p_3 diagram) that is steep-flat-steep.

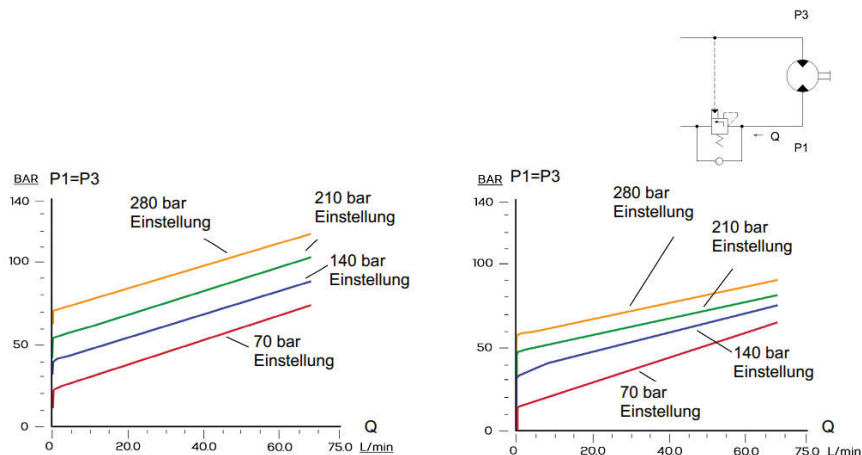


Figure 8: Pilot pressure vs flow to drive a winch without external load. Left: with standard counterbalance. Right: with load adaptive counterbalance

Figure 8 shows the performance the required inlet pressures to drive a motor that sees no outer force. A counterbalance valve with pilot ratio 3:1 avoids cavitation on p3 and would stop overrunning load. The curves show the inlet pressure vs flow for different settings of a standard counterbalance valve (left) and a load adaptive counterbalance (right). The savings are about 30%. The stability of the circuit is expected to be the same for negative loads when stability is critical.

5. Circuits with changing effective pilot ratio to save energy

Circuits with standard counterbalance valves in parallel to improve stability and/or efficiency are common. The purpose is to control negative loads at low speed with a 'stable' low capacity counterbalance valve and to open a second valve for high speed when the circuit is more stable (see above, parameter study). Other circuits use throttles in the pilot line to influence the performance of the counterbalance valve. **Figure 9** shows an example. The circuit uses a needle valve (N) and a pressure compensated flow control valve (F) in the pilot line of the counterbalance. At low pressure differential $p_3 - p_2$ the compensator in flow control valve is not saturated yet and both the needle valve and the flow control function as orifices. As a result the pressure between both valves is a fraction of p_3 , so the effective pilot ratio of the counterbalance is reduced. At higher inlet pressures (positive load on the cylinder) the pilot flow increases until the flow control valve limits the pilot flow. At higher pilot pressures the pressure drop across the needle valve will remain constant and will no longer be reduced to a fraction of the inlet pressure.

The diagram on the left hand side shows the resulting performance curve for different flows. The performance is similar to the performance of load adaptive valve.

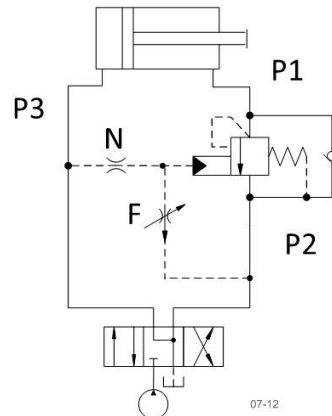
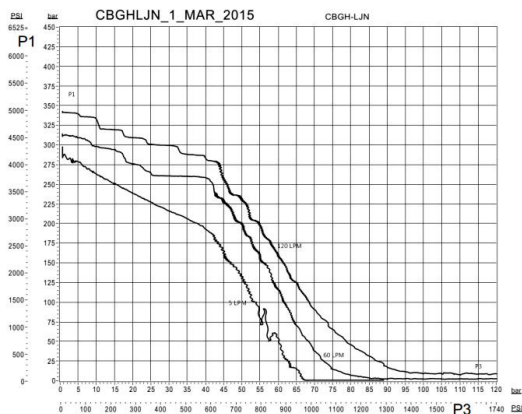


Figure 9: Standard counterbalance and new load adaptive version (below)

6. Summary

The paper describes which parameters affect the stability of a circuit with a counterbalance valve that is used to control negative loads. A Matlab based simulation program shows static and dynamic performance. The results of parameter variations on the dynamic performance can be shown in curves for pressure or velocity vs time or as poles in the Laplace-plane. Pilot gain and pilot ratio of the counterbalance valve influence the stability. A low pilot ratio is often required to achieve stability but reduces the efficiency of the circuit. A new load adaptive counterbalance valve has the low pilot ratio only when it is required for stability. That is when the actuator moves a negative load. The valve has a higher pilot ratio when the load is not moving or when a positive load requires no counterbalance valve. The valve saves on average 30% power compared with a standard counterbalance valve.

7. References

/1/ Otto Föllinger: 'Regelungstechnik', 5.Auflage, Heidelberg 1985

/2/ Peter Chapple: 'Principles of Hydraulic Systems Design, Second Edition', Momentum Press, New York 2015

8. Nomenclature

A	Cylinder Area
C_{HA}, C_{HB}	Capacitance A/B
CR	Cylinder Ratio
D	Effective Orifice Diameter
F	External Force on Cylinder
G_{DCV}	Gain of Directional Control Valve, Change in Flow per Change in pressure Differential ($p_O - p_A$)
G_{Pilot}	Pilot Gain of Counterbalance Valve, Change in Flow per Change in Pilot Pressure p_A
G_{Relief}	Relief Gain of Counterbalance Valve, Change in Flow per Change in Load Pressure p_B, p_1
m	Mass of Cylinder incl. attached Load
p_0, p_A, p_B	Supply Pressure, Pressure in A, B
p_1, p_3	Pressures on Port 1 (load), Port 3 (pilot) of the Counterbalance Valve
PR	Pilot Ratio of the Counterbalance Valve (Change in effective setting per change in pilot pressure)

Development of an Electronically Controlled Self-Teaching Lift Valve Family

Dr.-Ing. Eneko Goenechea

Bucher Hydraulics AG, Industriestrasse 15, 6345 Neuheim, Switzerland,
E-mail: eneko.goenechea@bucherhydraulics.com

Abstract

Other than mobile hydraulics and high voltage switchgears, Bucher Hydraulics is also involved in the less-known area of hydraulic lifts. In fact, Bucher Hydraulics did invent the electronically controlled lift valve in the 1970s. Since then, Bucher Hydraulics developed a wide line of products for hydraulic elevators, such as valves and power units. In 2012, this valve family included various sizes, pressure ranges, systems with constant motor speeds, inverter-driven motors, energy-efficient solutions with hydraulic counterweight, as well as customized solutions. As the common principle, all these solutions apply an electronic closed-loop control that uses a volumetric flow sensor and a proportional actuator. Since 2012, Bucher Hydraulics is substituting this valve family with a new generation, the iValve. Every iValve uses several self-teaching algorithms to adapt to its environment. Their on-board and cabinet electronics control solenoid currents and measure flow, pressure, and temperature. These features enable the iValve to self-monitor, to adapt to operating parameters, and to analyze and log information about itself and the attached system. This report on a highly specialized product is meant to provide inspiring insights.

KEYWORDS: iValve, lift control valve, closed-loop control, electronic control, self-teaching, remote analysis

1. Function of a Hydraulic Lift

The hydraulic system of a lift is simple. The hydraulic solution is mostly chosen due to its

- Robustness, long life respectively low cost of ownership
- High power density regarding the whole building

In 95% of the cases, an oil-immersed asynchronous machine drives a screw pump with constant frequency. The lift control valve connects tank, pump, and cylinder. The cylinder pushes the load upwards either directly or indirectly via a pack of ropes. For the downwards drive, the weight of the load drives the system. In few cases, a counterweight might be present but it will never fully compensate the weight of the empty cabin. The valve block realizes most functions and features of the power unit, such as the control of all upwards and downwards speeds, manual and electric emergency lowering, a hand pump, ball valve, pressure gauge, pressure switches, a redundant emergency brake, and others.

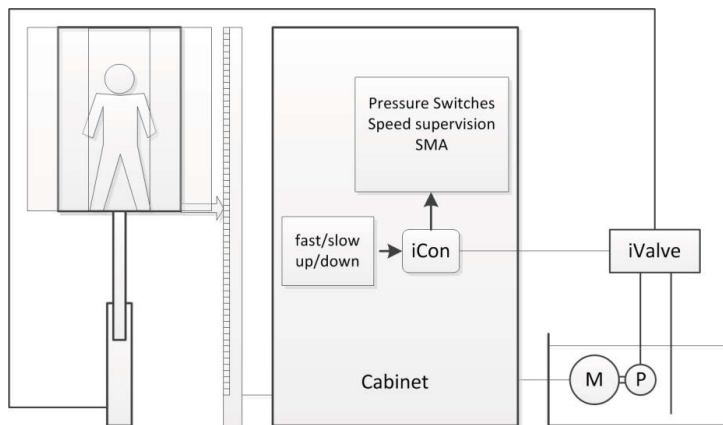


Figure 1: Hydraulic Lift Control

The master of the lift system is the cabinet, not the valve (see Figure 1). The valve in fact has no information concerning any redundant breaks, the position of the cabin or the doors, or the status of the motor. The valve receives four principal signals from the cabinet: slow up, fast up, slow down and fast down. From these signals, it calculates all transitions and dependencies. To travel upwards, the cabinet starts the motor and then signals “fast up” to the valve. Therefore, the valve’s bypass from pump to tank is normally open (see Figure 2). Receiving “fast up”, the valve will quickly close the bypass up to the point that the circulating pressure reaches the load pressure of the cylinder. After that, it

will continue to slowly close the bypass carefully controlling the acceleration curve for the cabin until it reaches final travel speed. When the cabin reaches a certain position in the shaft the cabinet will switch from “fast up” to “slow up”, causing the valve to decelerate to slow speed, which is approximately 10% of travel speed. The lift then travels slow speed until the cabin reaches the stop position. During the slow speed phase, the power unit bypasses approx. 90% of the volumetric flow at full load pressure. Hence, energy efficiency and oil temperature require keeping the slow speed travel short. At the stop position, the cabinet signals “stop” by taking away the signal “slow up” and the valve does an open-loop controlled soft-stop, as parameterized (3-20 mm).

Mechanically regulated lift valve

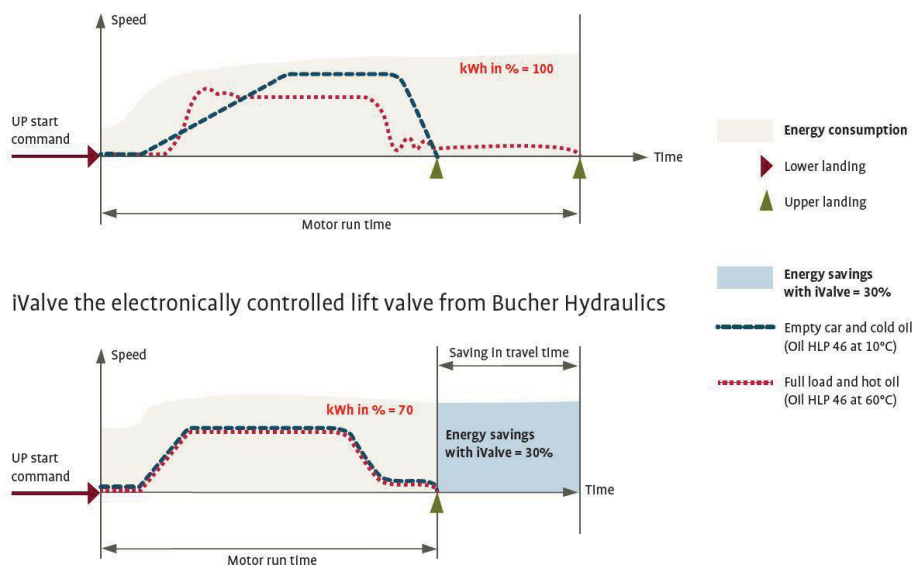


Figure 2: The Upwards Driving Curve

Travelling downwards works similar, except, the load pressure is the driving force. The oil is throttled directly from the cylinder to the tank.

2. The Environment of a Hydraulic Lift Valve

The population of lift installations is very heterogeneous. There are plunger, tele and pulling cylinders, single or tandem, direct or indirect, loads from a few hundred kilos up to several tons, travel speeds from 0.15 m/s up to 1 m/s. Units that run all day at up to 60°C and those standing in a shaft at about 0°C. Most installations run on HLP, some use biodegradable oil instead. The smallest installations use pumps with 20 l/min. The

upper end is open. The pressure range is limited to 67 bar dynamic due to the cylinders and hoses you can afford including the demanded safety margins.

Also, customers are heterogeneous. While one prefers perfect ride comfort, the other prefers a significant jerk at the start and the end of the ride to signalize motion. A well designed and carefully built lift has a dynamic pressure rise of about 3 bar driving upwards. Nevertheless, more than 20 bar may occasionally occur. The worst enemy of driving comfort is the stick-slip of the cylinder and the mechanic structure. The pressure loss due to stick-slip should be less than 2 bar and can be more than 8 bar in a typical installation with 18-28 bar static load of the empty cabin.

The industrial challenge is to fulfill all (sometimes opposing) demands with the least quantity of variances and different parts. The iValve i250 (Figure 3) ranges from 20 l/min to 250 l/min - the i500 from 150 l/min to 500 l/min. Power units up to 4000 l/min can be equipped with the MultiValveSystem (MVS), an electronic option that parallelizes up to eight i500 valves in a master/slave system.



Figure 3: iValve i250

Lift companies try to save money by reducing the installation time and, at the same time, the expertise necessary to set up the system. The above-named demands thus ought to be fulfilled without further adjustments.

A wide range of working parameters should be covered by one design and no physical adjustments, meaning that the control elements will be oversized for each single working point. This means in turn that the amplification of the elements of the control loop in the single working point will be extraordinarily high.

The ratio between the proportional signal at the pilot solenoid and the control result of the valve for example may reach 1:1.7 million. This defines the demands on design and manufacturing.

Nevertheless, craftsmen not hydraulic experts install hydraulic lifts, mostly during the construction of a building. Therefore the hydraulic power units of hydraulic lifts face an unmatched level of contamination with e.g. builder's dust. These contaminations have to be taken into account during the design phase of these piloted proportional valves.

3. Hydraulic Lift Control Valve Solutions

The demands named above often require custom-made solutions in the design phase of the lift control valve family, of which I would like to name a few below.

3.1. Pilot

A single piloted slide controls the main up- and downward-flow. Upwards, the orifice of the bypass controls the speed. The piloting pressure is taken from the pump pressure. Downwards, the speed is throttled and piloted directly from the load pressure. The dynamic pressures of the system behave inversely in up or down direction. For stability reasons and driving comfort, the pilots must follow precise rules. Therefore, the pilot of the iValve, which is situated on top of the proportional solenoid, in facts consists of two separated pilots with distinct ways of working. The up- or down pilot is chosen by a specialized start sequence.

In order to cope with the extraordinary contamination level in lift hydraulics, the valve was tested and optimized in contamination tests (see Figure 4). Today, the valve withstands a direct contamination induced through the screw pump of 2 ml test dust (KSL14027<500 μm + 20 % Fe<100 μm) in up and down travel suffering only small control errors. This test dose is limited by the capacity of the pump to withstand the contamination.

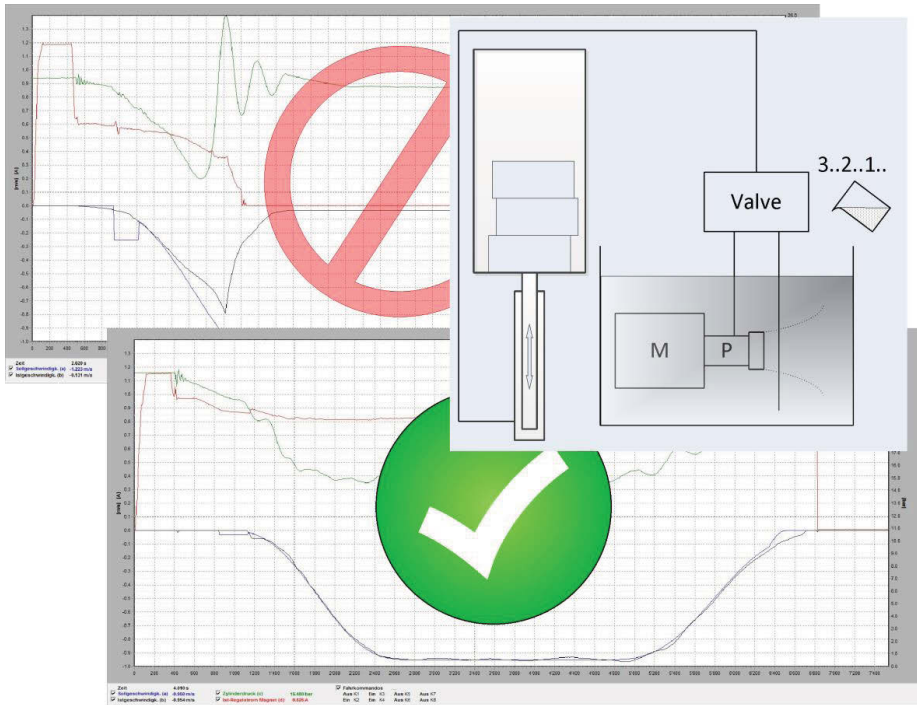


Figure 4: Contamination Test

3.2. Flow Sensing Check Valve

The proven pressure plate principle for the volumetric flow sensor is now integrated into the necessary check valve. The leakage-free check valve, on which the lift rests in standstill, not only unlocks to go downward but is poled inversely by its pilot for the up or downwards ride. So it measures the volumetric flow in both directions.

The sensor of the i250 measures (1.3 times 250 l/min =) 325 l/min during the test of the pipe rupture valve. The same sensor installed in a 20 l/min installation must control a leveling speed of 2 l/min. The viscosity ranges from 12 cSt to 500 cSt and the pressure loss – the biggest allies in favor of turbulence and viscosity independence – directly costs energy and limits possible lift designs. It must stay beyond 2 bar at 250 l/min.

Please find a detailed description of the sensor in patent /1/.

3.3. Electronics

The volumetric flow sensor joins a cluster of sensors and feedbacks, which are available to augment the perspective of the software domain. The volumetric flow goes hand in hand with the pressure, temperature and currents to the solenoids. In addition, the valve registers the command signals that it receives from the cabinet and the driving curve that it generates from the command history.

The main board situated in the cabinet called iCon (see Figure 5) and the embedded valve electronic situated in the iBox both communicate via serial interface. Combining all information, the valve can achieve knowledge on its own condition as well as the condition of the connected system.

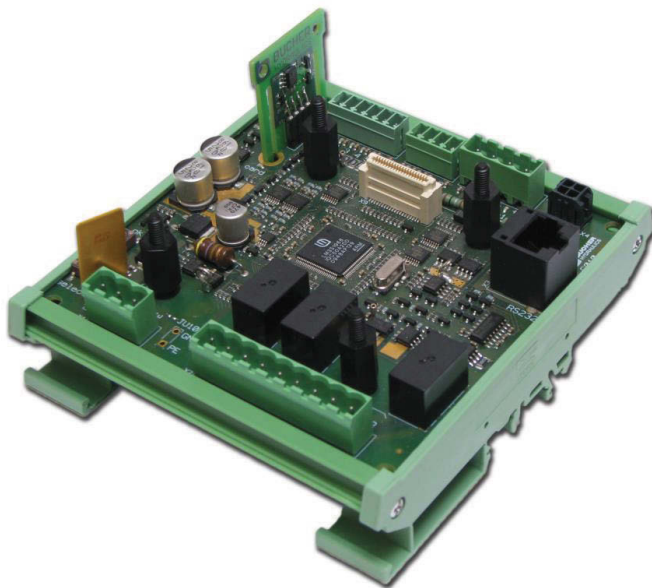


Figure 5: iCon

3.3.1. Self-Teaching Algorithms

In the first place, the sensor array is used to realize self-teaching algorithms, which aim at the main target of this development: Reducing the need to adjust the valve during installation. Today, several self-teaching algorithms optimize different aspects of the riding curve. There is for example T1, which optimizes the starting time by learning the optimal current to energize when the valve gets the first command to ride upwards or downwards after standstill. Another self-teaching algorithm - T3 - optimizes the

deceleration curve of the ride in order to achieve 0.3 sec of slow speed travel time at the end of a ride at any load and any temperature upwards or downwards.

3.3.2. Self-Monitoring

Secondly, the wide range of information is used to realize features of self-diagnosis. One self-monitoring domain is the detection of safety relevant errors in the valve. During every ride the valve monitors the compliance with several requirements and sends a fail-safe signal to the cabinet – the Self Monitoring Acknowledge (SMA) – Signal. This monitoring function and signal is part of the requirements defined by the appropriate Norm DIN EN81-2 /2/.

Another self-monitoring domain is widely known as condition monitoring. The feature registers changes in the behavior of the valve and traces them back to the aging of the oil, clogging of a filter, or others. The aim is to foresee these effects before they become fatal to make service visits more projectable. In order to realize the advantages of condition monitoring by warning the service technician in advance and while still in his office, a connection must be integrated into the cabinet, because the cabinet connects to the outside. Bucher Hydraulics offers an optional electronic card - the iAccess card - for the connection via DCP0 bus protocol.

3.3.3. Diagnosis and Analysis

Thirdly, the gathered information can be used to realize a lot of character traits or errors in the connected system.

The ride quality, energy efficiency and many characteristics of a hydraulic lift not only depend on the possibilities of the lift control valve but also are often limited by properties of the system. This is obvious in a system with extraordinary friction or stick slip. Nevertheless, a scratching counterweight or irregular rails can also lead to persistent problems. A chattering relay, poor timing between commands and a motor contactor, bad wiring – countless possible electronic and software errors can lead to time-consuming issues difficult to solve. In those cases, the technician can count on an informative array of LEDs or a hand terminal, or he can directly watch the driving curves on a laptop using the software iWin. In cases when the effect occurs only once every one hundred rides, the technician can leave behind a logging device and later send it to Bucher Hydraulics for analysis.

4. Examples

Observe below the vast variety of effects and errors you can isolate and identify even though they might origin in the most different domains of the whole hydraulic and mechanic system using just four signals.

The capacity to log driving curves over a long time is particularly helpful because the slightest circuit-, timing-, or assembly-fault, in case it leads to a sporadic error, can cause time consuming search activities and often leads to the need to exchange entire parts of the system.

4.1. Motor Starts too Late at Up Travel

The customer claims that there is a significant jerk sometimes when the lift is starting to ride upwards.

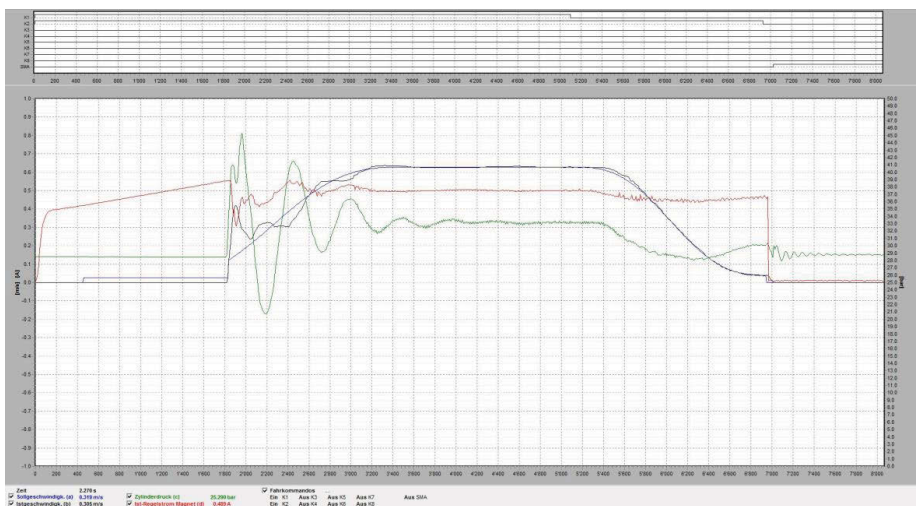


Figure 6: Motor Started Approximately 2 Seconds too Late

The explanation: The logging device was installed to monitor the installation for several weeks. The analysis of the measurements showed that once in a while this cabinet produces a delay between the commands to the valve and the motor contactor. When the command to the valve comes prior to the motor the lift jerks.

4.2. Localizing the Source of a Disturbance – Shaft

In the early introduction of the valve, a customer claimed that he could falsely activate the safety signal (SMA) by jumping in the lift while riding downwards. Bucher Hydraulics thereupon integrated the PSQ-analysis into the evaluation algorithm as in Figure 7. This algorithm localizes the source of a disturbance in the hydraulic lift system.

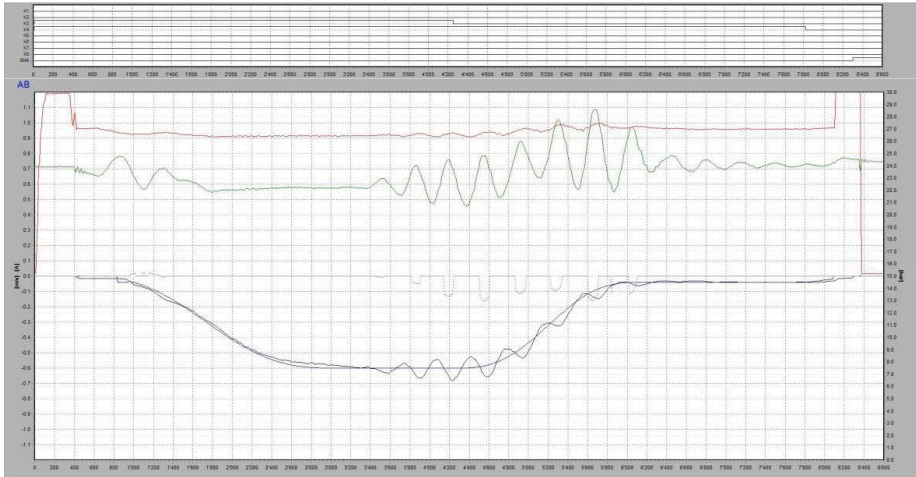


Figure 7: PSQ for Jumping People in the Cabin

The algorithm calculates the phase between the pressure disturbance and the volumetric flow disturbance. Thus it can reliably distinguish between a disturbance originating in the shaft – a changing or moving load, rail errors, or cylinder errors – or in the valve.

4.3. Localizing the Source of a Disturbance – Valve

To show the success of the PSQ-analysis Figure 8 is a curve with a damaged solenoid ram in the proportional pilot. During the long ride the solenoid sticks and the current falls until the solenoid breaks free. In the following wave the PSQ clearly signalizes a positive result localizing the origin in the valve.

In a real lift this valve will deny to send the SMA signal. Thus the lift control will block the lift operation.

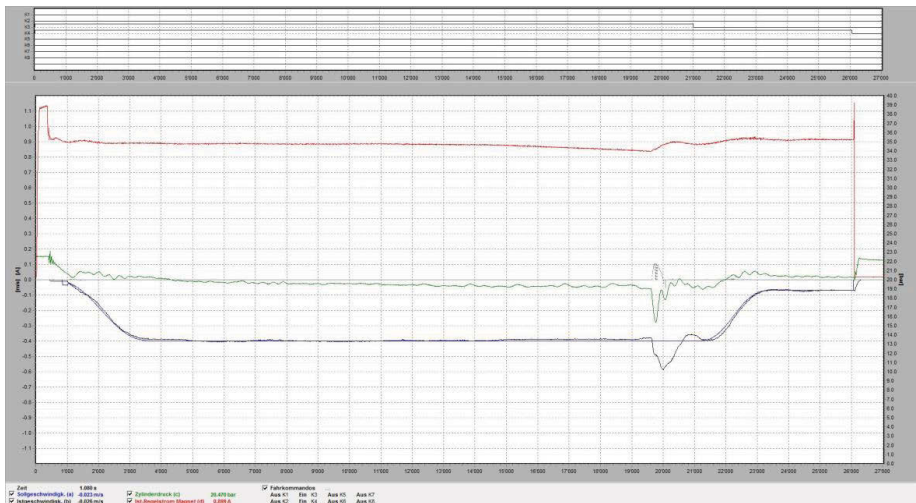


Figure 8: PSQ for a Damaged Solenoid Ram

4.4. Pressure Relief Valve Badly Adjusted

The customer claims that at full load the lift does not achieve full speed upwards.

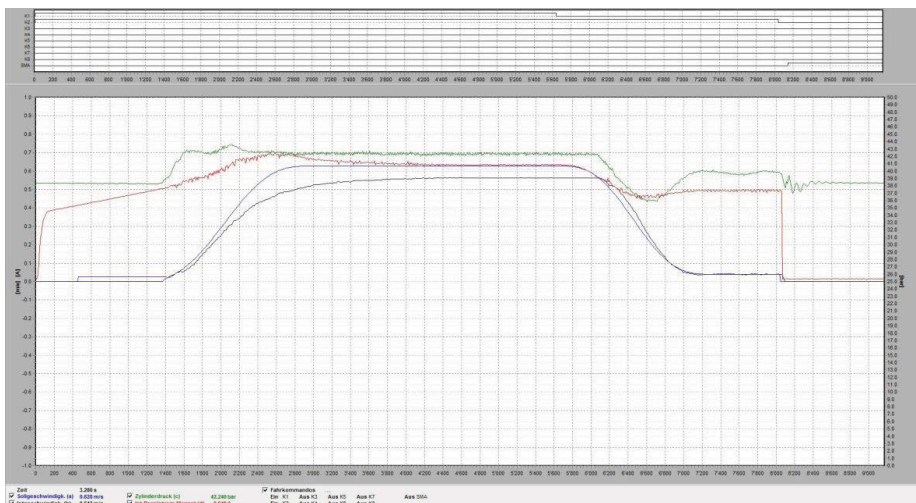


Figure 9: Dynamic Pressure is Limited

Explanation: The pressure relief valve is set to a value, that the customer quoted in his order. While often the cabin ends up being lighter, it sometimes end up being heavier. In this case the pressure will be cut off when it reaches the set value. In a typical lift installation this happens in the second half of the acceleration. So the lift accelerates smoothly to a value below the desired speed as seen in Figure 9.

4.5. Desired Speed Higher than Pump Can Provide

The case shown above must not be confused with the case where a desired speed is parameterized which is higher than the pump can provide.



Figure 10: Volumetric Flow is Limited

In this case, not the dynamic pressure but the volumetric flow is limited. The cabin accelerates to the speed that the pump can provide. Reaching this value, the speed suddenly stays constant. The pressure at acceleration is significantly higher at full speed. Hydraulic/mechanical interactions also lead to increased pressure changes at deceleration. Overall, an expert can easily distinguish between these two cases using such curves.

4.6. Mechanical Stop in the Shaft

The customer claims that sometimes the lift does not achieve the lower stop and/or sometimes it starts with a significant jerk from the lower stop upwards. Driving curves of the lift are do not show any special behaviour. The logging device is installed.

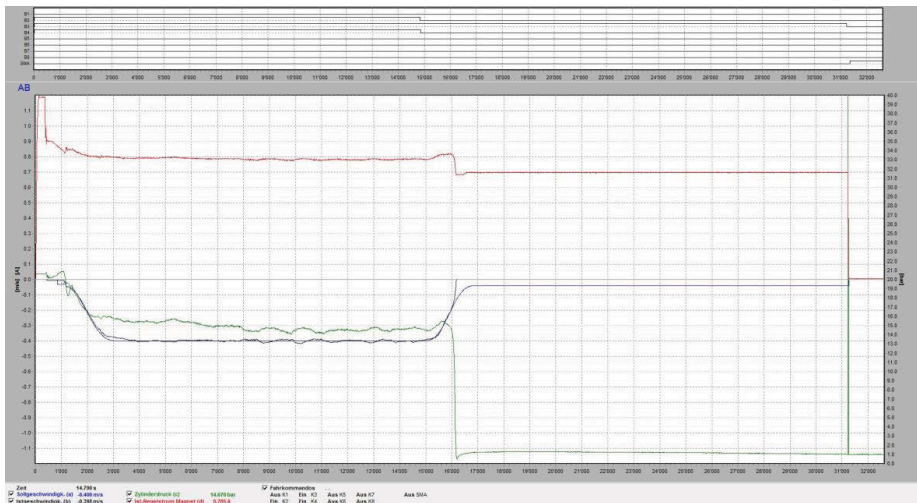


Figure 11: Mechanical Failure in the Shaft

Explanation: As Figure 11 shows, in the last centimeter of the downward ride the pressure can break down. Clearly, some mechanical obstacle carries the entire load. Later, the customer confirmed that the cylinder fastening loosened from time to time.

5. Summary

The iValve is a family of electronically controlled lift valves. Every iValve is equipped with an array of sensors and algorithms to receive and achieve various information. This information enables the software of the valve to do extensive analysis concerning the valve as well as the attached system. Some of these algorithms are called iTeach. They help the valve to adopt to its environment. Besides, every accessible information is helpful to provide and enhance remote customer support.

6. References

- /1/ Goenechea et al., WO 2011/003210 A1, 2011, Neuheim, Switzerland
- /2/ Normenausschuss Maschinenbau (NAM) im DIN, DIN EN 81-2:2010-08, 2010 Berlin, Germany

Development of an innovative diaphragm accumulator design and assembly process

Dipl.-Ing. Thorsten Hillesheim

Freudenberg Sealing Technologies GmbH & Co. KG, Sinzigerstr. 47, D-53424 Remagen,
E-mail: thorsten.hillesheim@fst.com

Abstract

Freudenberg Sealing Technologies has developed a new concept for the manufacture of diaphragm accumulators. Its advantages are a reduced need for components, fewer process steps, shorter assembly times, a higher level of product cleanliness, and an expansion of the product portfolio into additional fields of application. These diaphragm accumulators also weigh significantly less. This is opening up new opportunities for applications in the automotive and industrial fields. The assembly concept is based on a hermetically sealed pressure chamber in which the joining of the two housing halves with the help electromagnetic pulse technology (EMPT) as well as the filling of the gas side with nitrogen takes place in a single operation. In this way, downstream filling to generate the initial gas charge is no longer necessary.

KEYWORDS: Accumulator technology, diaphragm accumulator, multilayer diaphragm, electromagnetic welding, innovative assembly process

1. Introduction

Among other purposes, nitrogen-filled diaphragm accumulators are used as pressure and volume compensators, pulsation dampers and energy storage units. They consist of a gas and a liquid sphere, separated by a diaphragm. Some typical applications as energy storage involve its use in the hydraulic circuits of automatic transmissions and control oil supply system units. If the pressure rises in the oil circuit, the diaphragm accumulator absorbs the liquid. In the process, the gas is compressed and the pressure rises. If the pressure in the hydraulic system falls again, the gas expands and forces the stored liquid back into the oil circuit.

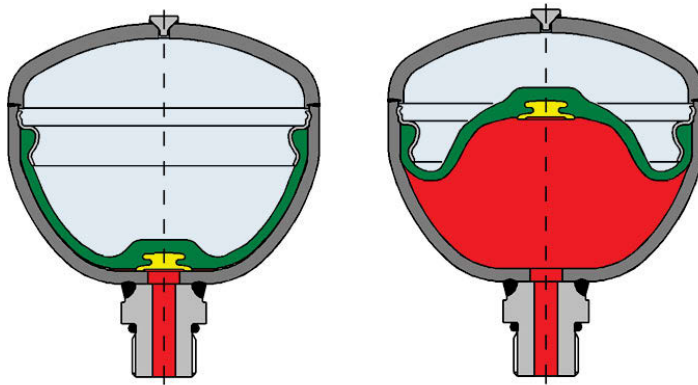


Figure 1: Principle of the diaphragm accumulator in the discharged and charged state /1/

A diaphragm accumulator is thus the ideal solution to cover peak needs, which for example occur when a gear is activated in automatic transmissions. It allows oil pumps and propulsive electric motors to be designed for average energy consumption, making them smaller and thus considerably more economical. That in turn makes a substantial contribution to lower fuel use and the reduction of CO₂ emissions.

2. Motivation for the new design and assembly concept

The technology of the diaphragm accumulator has more than proven itself in the automotive and industrial fields. But disadvantages run counter to the above-mentioned advantages. They largely relate to the way diaphragm accumulators have been manufactured to this point. The pressure hull usually consists of two deep-drawn housing halves that are usually welded, that is, joined by the substance-to-substance jointing process. The two connections on the pressure hull for the liquid and the gas are also welded on. A defined filling of the accumulator with nitrogen takes place after assembly to adjust its specific initial gas charge. Other required processes involve corrosion protection by painting.

The disadvantages of the current process include its numerous production steps and the multitude of required parts. This makes diaphragm accumulators considerably "overdeveloped" for standard applications, especially those with low system pressures. This results in costs that are higher than necessary, especially when volumes are increasing. A further negative factor is the product's high weight due to the materials used to this point, such as steel, and the components that are required. In addition, this

limits a potential expansion of the product line into new fields in the automotive and industrial areas.

This was motivation enough for Freudenberg Sealing Technologies to develop a new concept for the production of diaphragm accumulators. It employs a hermetically sealed pressure chamber in which both the joining of the two aluminum housing halves with the help of electromagnetic pulse technology (EMPT), and the filling of the gas side with nitrogen occurs in a single step. A downstream stage in the process is therefore no longer necessary to generate the initial gas charge.

The advantages of the new production technology are fewer process steps, a reduced need for components, shorter assembly times with higher process quality, and a higher level of product cleanliness. There are also new opportunities for further applications in the automotive and industrial areas. If you compare the new assembly concept with the previous production of diaphragm accumulators in detail, the situation becomes even clearer: the elimination of three welding processes, no gas filling unit, no additional clamping ring for the diaphragm attachment, the elimination of a downstream filling process, and no painting.

3. Electromagnetic pulse technology

Freudenberg Sealing Technologies decision to utilize electromagnetic pulse technology for the assembly of diaphragm accumulators is based on the high stability of the process and the quality of substance-to-substance jointing process, aside from reducing the number of process steps. The process also produces higher component cleanliness.

Electromagnetic pulse technology is based on the contact-less forming of electrically conductive materials by using powerful magnetic fields. One of the best-known applications is the forming of tubes. It can be used to compress or expand them. But joining and cutting are possible as well. Furthermore, there is the possibility of processing non-rotationally symmetrical cross-sections. The equipment for electromagnetic forming consists of a pulse generator, a coil and a field shaper. Pulsed currents up to 1,000 kA are necessary to achieve the magnetic pressures required for the forming of metallic materials.

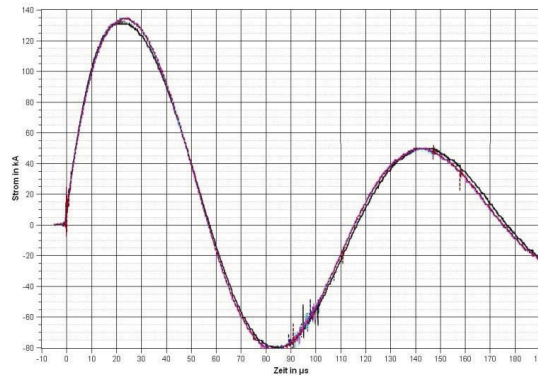


Figure 2: Current flow curve for joining process

They are produced by a pulse generator that mainly consists of a capacitor and coil, that is, an oscillating circuit. The coil, which has conductor cross-sections ranging from 10 to several hundred square millimeters, is constructed of one or several windings with a high-strength, conductive material.

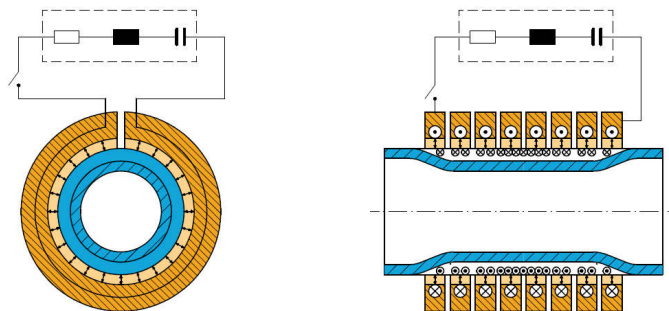


Figure 3: Principle of electromagnetic pulse forming [2/

The technology is physically based on the fact that two parallel, current-carrying conductors repel each other if the current flows oppose one another. If an electrically conductive workpiece with a closed cross-section (tube) is located inside a coil, an electric current in a contrary direction to the coil current is induced as a result of the penetrating magnetic field. In this way, every current-bearing volume element of the tube exerts an inward-directed force that is perpendicular to the longitudinal axis. If it is greater than the flow limit of the material, the plastic reforming begins and the diameter of the tube is reduced. This occurs within 10 to 200 microseconds, depending on the

energy and the material. The resulting force represents a "magnetic pressure" that acts upon the surface of the material. The force can reach a magnitude of several hundred megapascals. With this magnetic pressure, the field strength on the outer edge of the tube wall decreases geometrically and is thus a relevant factor. To put it another way, the smaller the distance to the coil, the greater the field strength on the edge of the tube.

A field shaper is frequently used to increase the magnetic pressure. It is a cylindrical, longitudinally slit body consisting of a conductive material and fills the space between the coil and the workpiece as optimally as possible. Its main task is to concentrate the magnetic field on the area to be transformed. This is achieved with a special geometry that influences the current density and thus changes the field strength between the field shaper and the workpiece. A positive ancillary effect of the field shaper is the equipment's increased flexibility. The reason: At little expense, the user can use an existing coil to process other tube diameters or material geometries by using field shapers of various sizes. The magnetic pressure can also be improved with highly conductive materials and a high frequency.

4. The use of EMP technology for diaphragm accumulators

The arrangement described here with an exterior coil is not merely used to compress a workpiece but also to join two workpieces. Thus homogeneous and disparate materials can be bonded to one another. The joining is possible with form-fitting, friction-locking or welding methods, depending on the requirements and the conductivity of the two materials. In the case of welding joining, thanks to powerful magnetic pressures, the atoms of the two joining pieces approach one another to the point that an exchange of electrons results, producing an extremely stable, gas-tight welding. This is precisely what Freudenberg Sealing Technologies employs in the production of its new diaphragm accumulators. The upper and lower shells of the diaphragm accumulator's pressure chamber are joined using a welding process. The process takes place within a hermetically sealed pressure chamber where the magnetic coil is located.

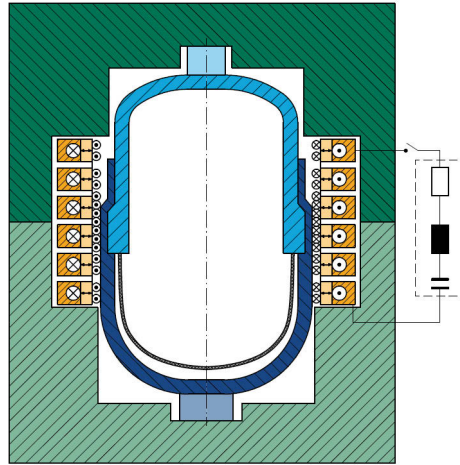


Figure 4: Pressure chamber with integrated magnetic coil

The elimination of process steps is a key advantage of electromagnetic pulse forming technology for the production of diaphragm accumulators: The joining process and the filling of the accumulator take place in a single process step. The number of individual components is also reduced.

5. Simulation

FEM simulations are carried out in advance to facilitate the design of the diaphragm accumulator. That is because there are many parameters affecting the efforts to achieve optimal performance in welding of the upper and lower shells. They primarily involve the geometry and the material of the two housing halves, current flow, component speed, and the arrangement of the field shaper and coil.

One of the main goals is to determine the optimal joint geometry based on wall thickness, material and resilience in light of the maximum working pressure that can be applied. This also includes simulations to determine the shell geometries that the joining permits without deformation and the stability that is achieved after forming at high interior pressures.

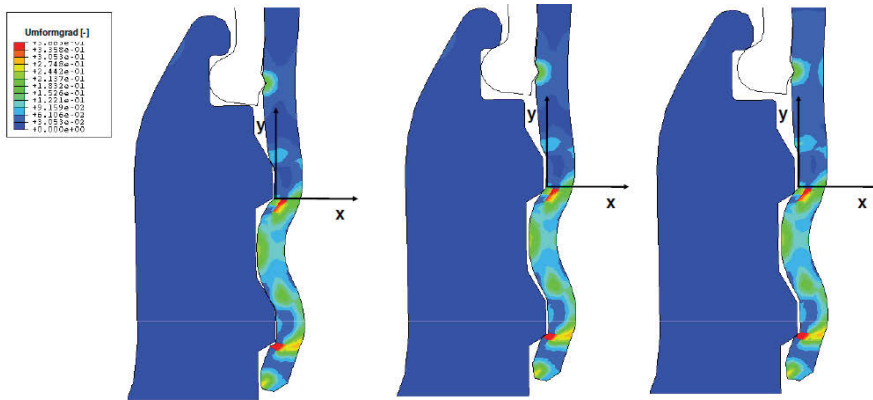


Figure 5: FEM simulation joining area

Furthermore, there was an investigation into the respective speeds of the components accelerated with the EMPT process to draw conclusions about the weld quality for different process parameters. Here the influence of the current flow on the magnetic pressure and thus the strength of the bond played a major role.

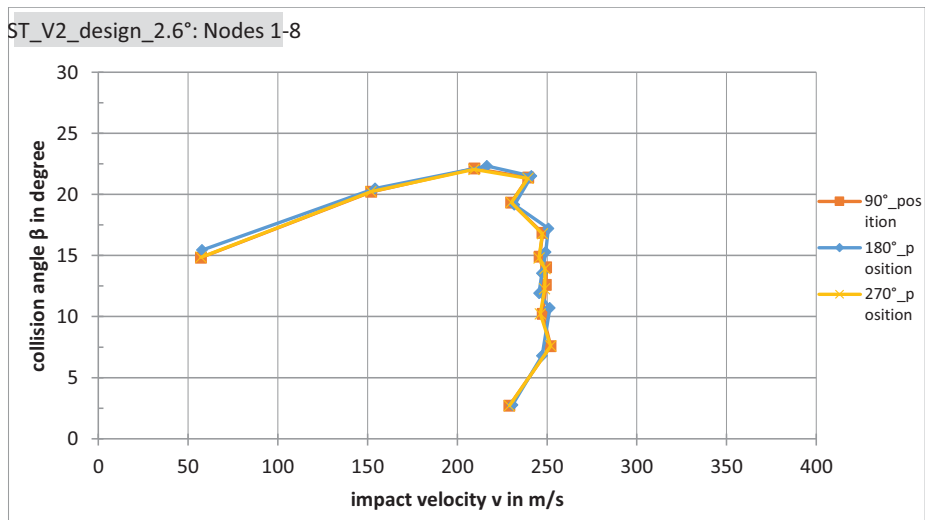


Figure 6: Simulated impact velocity vs. collision angle

Another important point involves the rolling behavior of the outer shell and the inner shell during the forming process. It not only shows how the joint is proceeding. It also demonstrates that a high forming speed produces a pressure wave in front of the contact point or joining point, removing dirt and separated particles from the area. This

reduces the number of defects and also contributes to an extremely stable joining process.

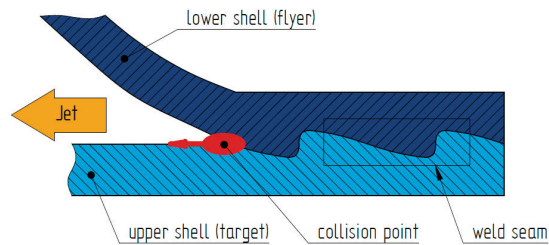


Figure 7: Functioning electromagnetic pulse welding /2/

6. Validation

The goal of validation is to determine or verify the optimal mix of process parameters, wall thicknesses and geometries. Test series were run on all the versions using a statistical DOE, or design of experiments.

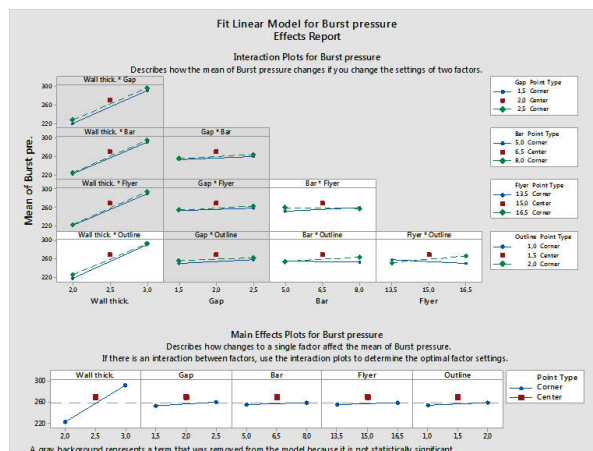


Figure 8: Example main effects diagram statistical design of experiments

In the first test series, the quality of the welding process was investigated with peel tests and micrographs of the joining points.



Figure 9: Peel test joining point

If these results were satisfactory, the respective static bursting pressures of the individual prototype configurations were determined. If a combination made it through this test series with positive results, the dynamic behavior of the prototype under interior pressure was tested.

After a likewise positive result, the diaphragm accumulator configurations were checked for their functional behavior in a life test. In this test series, the electromagnetic pulse forming allowed very good replicability thanks to its controllability.



Figure 10: Micrograph joining point

The mechanical tests of the diaphragm accumulator mainly include pressure testing; for example, the measurement of the deformation under a pressure load without filling gas. In this case, the diaphragm accumulator is charged with a rising pressure (1 bar/s) using a hydraulic fluid (the EOL test is the basis). The measurement focuses on the expansion of the accumulator's height and diameter until bursting pressure is achieved. A cyclical pressure load at 5 Hz is applied to test dynamic strength. The test result is

based on the number of cycles until failure. More than 2 million cycles were achieved. The operation of the burst test is similar to the test for deformation, except that the rise in pressure is 3 bar/s. It takes place both after the dynamic strength test and with "new" diaphragm accumulators. The values measured for the burst pressure are correspond to the requirements and the simulation.



Figure 11: Example - failure image in static burst test

The functional tests take into account the tests of pressure losses in the initial charging at various pressures and temperatures as well as the measurement of any potential leakage due to permeation during the test timeframe. The testing involves a diaphragm with a specific material combination as well as a multilayer diaphragm with an interior plastic sheet to improve its gas permeation behavior. The findings show that the gas permeation is in the calculated range and that the diaphragm's new attachment methods on the lower housing half have no impact on the system's lifespan.

To additionally test load capacity at varying temperatures, the diaphragm accumulator is constantly exposed to changing temperatures at varying pressure profiles. The measured parameters are the pressure of the initial gas charging and the number of cycles until failure. For the testing of the static seal and the permeability of the diaphragm, the diaphragm accumulator is charged with a differential pressure at a differential temperature of 80°C. In each case, a new pressure measurement is taken after 100 hours.

To investigate the effect of corrosion on the joining point, a test is carried out in a salt spray chamber in accordance with ISO 9227 (previously 50021 SS) over a time period of at least 240 hours with subsequent test series on the static and dynamic strength of the joining point. The new diaphragm accumulators also survived this without damage.

7. Applications

The uses of diaphragm accumulators are diverse. There are a number of areas of application in the automotive field alone. For example, they include energy storage in double-clutch and automatic transmissions.



Figure 12: Dual clutch transmission as example of an application /3/

The typical applications in the chassis include active roll stabilization, energy storage in hydropneumatic suspensions, pulsation damping, and hydraulic systems for chassis damping. Hydraulic accumulators are also used in brake systems. The applications range from pulsation damping to energy storage in hybrid vehicles.

Another example of an application would be as energy storage in hydraulic control oil supply systems. This involves valve combinations that reduce volume flow and system pressure in medium- and high-pressure equipment and thus pilot control devices.



Figure 13: Prototype diaphragm accumulator

Among other things, the diaphragm accumulator enables greater switching capacity and, when required, emergency switching in the event of a shut-down or defective main supply circuit.

8. Summary

The new design and assembly concept for diaphragm accumulators is essentially a response to the previous disadvantages, such as the numerous process steps and the multitude of required parts. Especially with rising volumes and applications with low system pressures, this leads to higher costs than are necessary. Another concern is the high weight of the material, which is steel. The new assembly concept, which entails the joining of the two housing halves as well as the filling of the gas side with nitrogen in a single step, significantly reduces the number of process steps and required components. The low weight also opens up new fields of application.

9. References

- /1/ Freudenberg Sealing Technologies GmbH & Co. KG instruction materials
- /2/ Weddelling, C., 2015. Electromagnetic Form-Fit Joining. Dr.-Ing. Dissertation, TU Dortmund, Shaker Verlag Aachen, ISBN 978-3-8440-3405-9
- /3/ www.fiat500usa.com/2010/05/inside-fiats-dual-dry-clutch.html

Potential and application fields of lightweight hydraulic components in multi-material design

Dr.-Ing. Andreas Ulbricht

CG Rail GmbH (Chinesisch-Deutsches Forschungs- und Entwicklungszentrum für Bahn- und Verkehrstechnik Dresden GmbH), Freiburger Straße 33, D-01067 Dresden, E-mail: info@cgrail.de

Prof. Dr.-Ing. habil. Maik Gude; Dipl.-Ing. Daniel Barfuß; Dipl.-Ing. Michael Birke; Dipl.-Ing. Andree Schwaar; Dr.-Ing. Andrzej Czulak

Institute of Lightweight Engineering and Polymer Technology (ILK), TU Dresden, Holbeinstraße 3, D-01307 Dresden, E-Mail: maik.gude@tu-dresden.de

Abstract

Hydraulic systems are used in many fields of applications for different functions like energy storage in hybrid systems. Generally the mass of hydraulic systems plays a key role especially for mobile hydraulics (construction machines, trucks, cars) and hydraulic aircraft systems. The main product properties like energy efficiency or payload can be improved by reducing the mass. In this connection carbon fiber reinforced plastics (CFRP) with their superior specific strength and stiffness open up new chances to acquire new lightweight potentials compared to metallic components.

However, complex quality control and failure identification slow down the substitution of metals by fiber-reinforced plastics (FRP). But the lower manufacturing temperatures of FRP compared to metals allow the integration of sensors within FRP-components. These sensors then can be advantageously used for many functions like quality control during the manufacturing process or structural health monitoring (SHM) for failure detection during their life cycle.

Thus, lightweight hydraulic components made of composite materials as well as sensor integration in composite components are a main fields of research and development at the Institute of Lightweight Engineering and Polymer Technology (ILK) of the TU Dresden as well as at the Leichtbau-Zentrum Sachsen GmbH (LZS).

KEYWORDS: Lightweight design, Lightweight hydraulic components, Carbon fibre reinforced plastic (CFRP), Composite, Multi material design, Sensor integration, Optic fibre sensors, structural health monitoring

1. Introduction

The increasing pressure for the development of energy-efficient systems requires the realization of economic lightweight structures. Therefore fiber reinforced plastics (FRP) are more and more used for highly stressed structures which are currently made of metals. The development of hydraulic components made of FRP is a particular challenge due to the very high mechanical loads and partial extreme environmental conditions like highly varying temperatures. Here, the outstanding mechanical properties of carbon fiber reinforced plastics (CFRP) can be advantageously utilized for cylindrical components with a well-defined state of stress like hydraulic actuators or accumulators.

Furthermore the application of FRP for hydraulic components offers new opportunities to integrate sensors or other elements into the composite structure to realize different functionalities like structure health monitoring (SHM) or heating. These sensors are integrated inside the FRP-structure during the primary manufacturing process. So these sensors can be already used for measuring of processing parameters to control the quality and to adapt the process parameters if required. Thus, new possibilities of interoperability and real-time monitoring regarding the so called "Internet of Things" (IoT) – one of the keywords of Industry 4.0 – can be realized.

The development and technological realization of lightweight hydraulic components in multi material design like lightweight bladder accumulators, hydraulic lightweight actuators or manifolds as well as the integration of sensors into composite structures are main activities at the Institute of Lightweight Engineering and Polymer Technology (ILK) at the TU Dresden /1,2,3,4,5/.

2. Lightweight hydraulic components in multi-material-design

Following the development of lightweight hydraulic components are addressed in two examples, first a bladder accumulator in multi-material design and second a metallic lightweight manifold block. The bladder accumulator Type IV pressure vessel (bladder accumulator) and the hydraulic manifold block were designed for 315 bar operating and 1260 bar burst pressure /6/. Afterwards both components were manufactured and fully tested to reach the baseline for further industrialization (components are shown in **Figure 4**). Results showed that considerable potential in mass reduction are given compared to the given state of the art design (**Table 1**).

	Reference [kg]	ILK [kg]	Reduction [%]	Dimension
Manifold block	13,75	2,44	-82	15x13x10 cm
Bladder accumulator	28	11,84	-57	10 liter

Table 1: Achieved mass reduction of lightweight hydraulic components

2.1. Lightweight bladder accumulator

A comprehensive development specification for lightweight bladder accumulators was developed within an iterative chain of design, production, inspection and testing (**Figure 1**). The baseline is a design tool based on VASILIEV shown in /1/. Within this analytical tool the resulting dome architecture for an isotenoid deformation behavior is determined and the contour directly exported for 3D-CAD modelling. The laminate layup is then first determined by the vessel formula to aim the one to two ratio of axial to circumferential fibers and detailed with the help of finite element analysis (FEA).

Considering the manufacturing restrictions of the winding process, the laminate layup is adapted the way to reduce fiber accumulation at the boss sections by increasing the fiber angle in the cylindrical section. Mainly geodesic winding is chosen to avoid fiber slippage during the laminate build up. As the fiber deposition is mandatory for the resulting mechanical behaviour the manufactured vessel is inspected by computer tomographic (CT) scanning to identify the real laminate layup. By FEA and manufacturing iterations combined with CT inspection the winding architecture is optimized to the isotenoid deformation behavior to optimize the material effort and the incorporated lightweight potential.

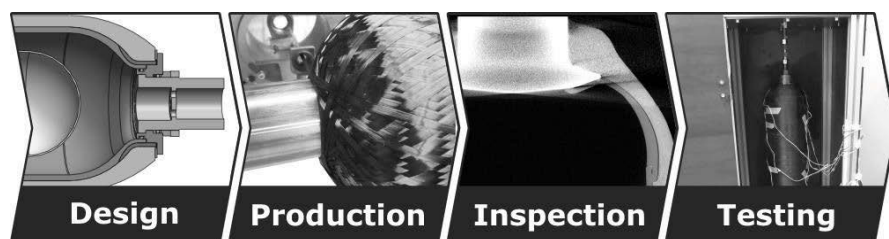


Figure 1: Development chain for lightweight bladder accumulators

The final design has been thoroughly tested. Static testing up to 710 bar was conducted without reaching a fatal bursting of the accumulator. Additionally a more important dynamic test cycle was performed. With a minimum working pressure of 100 bar and a maximum of 315 bar, the structure withstood 100,000 periodic load cycles without any sign of degradation (**Figure 2**).

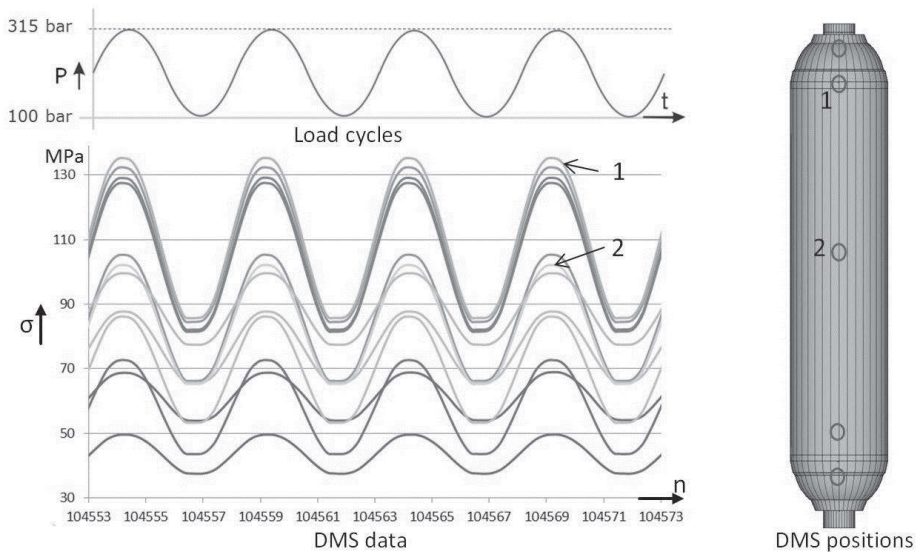


Figure 2: Test cycle of the bladder accumulator

2.2. Lightweight manifold block

Compared to the above shown design specification a point design (**Figure 3**) of a metallic lightweight manifold block is performed to prove general feasibility of near-net-shape manufacturing of manifold blocks in an aluminum casting design. To maintain the operating pressure and the sealing concept of the reference steel manifold block the pressure loads and tightening torques had to be sustained. Therefore an iterative design cycle of CAD design and FEA was performed. The manifold block is designed to a high and low cycle fatigue approach to reach the necessary fatigue strength for up to one million load cycles. Due to the use of the aluminum casting alloy AlSi7Mg0.3 and its reduced strength the threads' length as well as the wall thicknesses were redesigned. Additional casting requirements for wall thickness changes had to be addressed and to avoid blowholes, etc. form-filling simulations were performed showing a good casting behavior for the aluminum casting material utilizing it for near-net-shape manufacturing.



Figure 3: Development chain of a casted lightweight manifold block

The casting design of the manifold block was also verified through static and dynamic testing. For simplification all cavities had been loaded simultaneously with the same pressure level. In a first static test with 500 bar no critical stresses could be identified. Similar to the bladder accumulator test program a load cycle between 0 and 315 bar was chosen, as the manifold is either fully or non-pressurized during operation. The manifold block showed no damages after 100,000 load cycles.

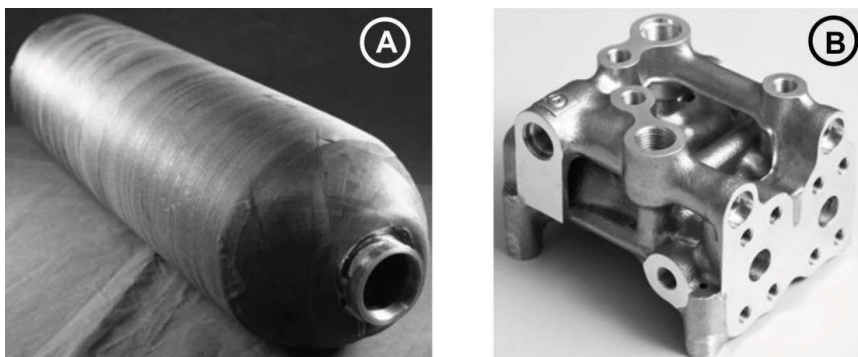


Figure 4: Lightweight hydraulic bladder (A) and aluminium casted manifold block (B)

3. Application fields for integrated sensors in FRP-lightweight structures

Lightweight hydraulic components made of fiber reinforced plastics (FRP) can be equipped with a smart integrated system for quality control during fabrication, for monitoring the component state – keyword industry 4.0 – and for structural health monitoring to estimate life time and to determine damages. Interesting parameters are temperature, pressure, position of the piston and the strain within the structure. A basic design for a smart integrated system is shown in **Figure 5**.

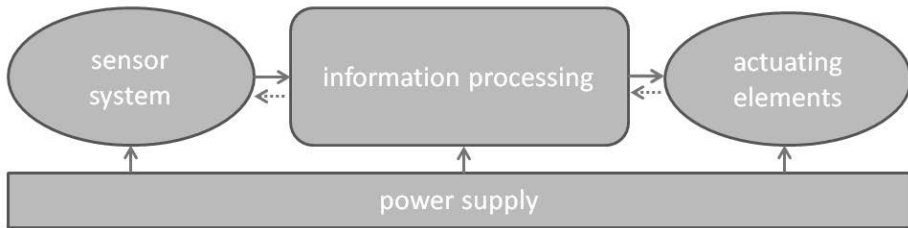


Figure 5: Principle of a monitoring system capable of being integrated

One or more sensor elements convert physical properties into electrical signals. Usually a conditioning unit is required. A processing unit computes the signals based on an adapted algorithm and deduce actions, for instance control an actuating element. For all these components a power supply is required.

The monitoring system can be usually realized in two different ways – either by external analysis or by fully integrated monitoring system. In the first way the power supply and the information process unit are external. An external analysis system has usually significant more performance but larger dimensions which cannot be integrated. Furthermore a more expensive analysis system can be used for many components.

The second application is the fully integrated monitoring and control system. With such an integrated system an online analysis by specific parameters of the whole structure can be provided. The integrated information processing unit can control integrated actuating elements, save data for a later evaluation or send a signal to an external system. For such a fully integrated system the costs relative to the component costs and the long-term stability are more important.

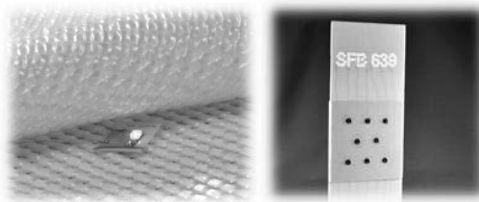


Figure 6: Example: LED before and after integration

For lightweight hydraulic components specific sensors and actuating elements are of interest:

- The position of the piston is determined by a strain. This strain can be detected by integrated strain gauge sensors or optical glass fiber sensors (figure 8).



Figure 7: Sensor node ready for integration

- The temperature can be measured with integrated sensors (NTC, PTC, Thermocouple, Platinum-sensor). These information can prevent temperature hotspots or give an indication of the viscosity of the oil.

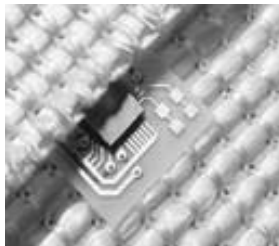


Figure 8: Temperature sensor in an ASIC-environment, ready for integration

- The dynamic pressure can be measured with integrated piezo ceramics. The deformation of the piezo ceramic by pressure will be converted into a voltage representing the dynamic pressure.

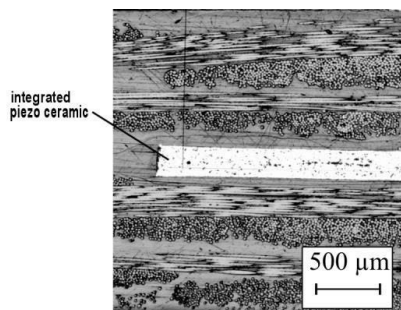


Figure 9: Integrated piezo ceramic

- With an above-mentioned integrated electronical control system enhanced with an integrated heating system composed of a copper wire or a carbon fiber an active temperature control for better performance of the oil can be integrated into lightweight hydraulic components made of composite material

4. High pressure vessels made of CFRP with integrated fiber-optic Rayleigh sensors

One application example for SHM in combination with hydraulics is the integration of high-resolution fiber-optic sensors (FOS) in high-pressure vessels. In terms of automation FOS are integrated in the composite structure during a braiding process (**Figure 10**). For that purpose a braiding wheel was supplemented with an appliance for automatic sensor application, which was used to manufacture preforms of high-pressure vessels with FOS-networks integrated between the fiber layers.

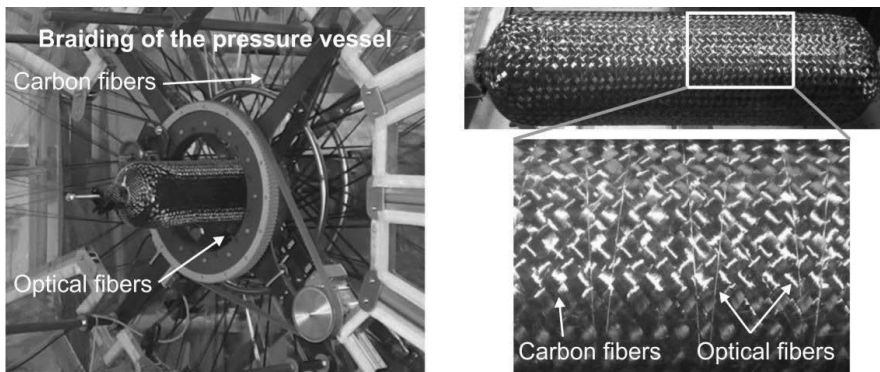


Figure 10: FOS integration during the braiding process /7/

The sensor network was then used in quasi-static pressure tests to monitor the load level until failure (**Figure 11**). Results showed reliable real-time tracking of the failure behavior /7/.

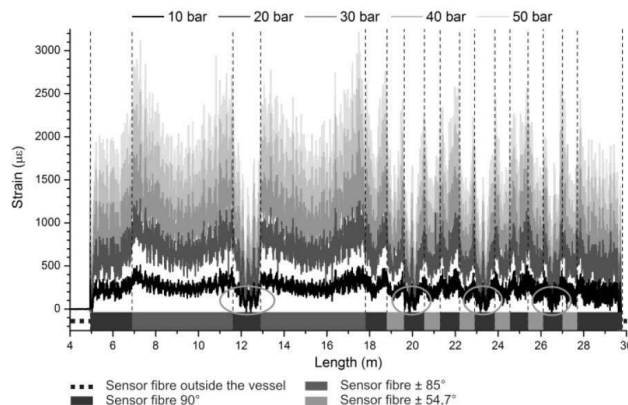


Figure 11: Stress state monitoring during quasi-static pressure test /7/

5. Summary

The successful realization and test of an innovative lightweight bladder accumulator made of CFRP and a casted lightweight aluminum manifold – both components with a mass reduction of more than 50 % compared to the metallic reference structure – show the enormous lightweight potential for hydraulic components. Furthermore lightweight hydraulic components made of FRP can be equipped with integrated sensor networks and other functional elements for (A) structural health monitoring (online and offline), (B) measurement and optimization of process parameters during manufacturing (Industry 4.0) and (C) other functions like heating or measuring the position of the piston. A CFRP-pressure vessel has been exemplarily equipped with a high resolution optic-fiber sensor systems, which was integrated during the braiding process of the CFRP-pressure vessel. This cost-efficient solution provides the possibility to measure the temperature during the curing process and to monitor the deformation (strain) during operation.

6. References

- /1/ Helms, O.: *Konstruktion und technologische Umsetzung von hochbeanspruchten Lasteinleitungssystemen für neuartige Leichtbaustrukturen in Faserverbundbauweise*. Dissertation, Technische Universität Dresden, 2006.
- /2/ Ulbricht, A.: *Zur Gestaltung und Dimensionierung von zylindrischen Leichtbaustrukturen in Faserkunststoffverbund-Metall-Mischbauweise*. Dissertation, Technische Universität Dresden, September 2011.
- /3/ Ulbricht, A.; Hufenbach, W.: *Multi-Material-Design gefragt – Leichtbau-Hydraulikkomponenten für mobile Anwendungen*. fluid 03/2014, page 56-58, 2014.
- /4/ Hufenbach, W.; Böhm, R.; Thieme, M.; Tyczynski, T.: *Damage monitoring in pressure vessels and pipelines based on wireless sensor networks*. Procedia Engineering 10 (2011), page 340 – 345, 2011.
- /5/ Hufenbach, W.; Adam, F.; Fischer, W.-J.; Kunadt, A.; Weck, D.: *Mechanical behaviour of textile-reinforced thermoplastics with integrated sensor network components*. Materials & Design, Volume 32, Issue 10 (2011), pages 4931-4935, 2011.

- /6/ Hufenbach, W.; Ulbricht, A. et al.: *Lightweight hydraulic components in novel multi-material-design for mobile applications*. 2014. 9th International Fluid Power Conference, Aachen, March 24-26, 2014.
- /7/ Hufenbach, W.; Gude, M.; Czulak, A.; Kretschmann, M.: *Development and implementation of an automatic integration system for fibre optic sensors in the braiding process – with objective of online monitoring of composite structures*. Published in SPIE Proceedings Vol. 9061: Sensors and Smart Structures Technologies for Civil, Mechanical, and Aerospace Systems 2014.

CFD Simulation and Measurement of Flow Forces Acting on a Spool Valve

Ing. Patrik Bordovsky

RWTH Aachen University, Institute for Fluid Power Drives and Controls (IFAS), Aachen, Germany, E-Mail: Patrik.Bordovsky@ifas.rwth-aachen.de

Dr.-Ing. Katharina Schmitz

Walter Hunger International GmbH, Würzburg, Germany, E-Mail: K.Schmitz@hunger-international.de

Professor Dr.-Ing. Hubertus Murrenhoff

RWTH Aachen University, Institute for Fluid Power Drives and Controls (IFAS), Aachen, Germany

Abstract

Directional control valves are widely used in hydraulic systems to control the flow direction and the flow rate. In order to design an actuator for such a valve a preliminary analysis of forces acting on the spool is necessary. The dominant axial force is the so called steady flow force, which is analysed within this study. For this purpose a 2/2-way spool valve with a sharp control edge was manufactured and investigated. CFD simulations were carried out to visualize the fluid flow inside the valve. The measured and simulated axial forces and pressure drops across the test valve are compared and show good qualitative correlation. However, the simulated values of axial forces are in average by 32 % lower compared with the measured ones. Therefore, the components of the axial force were scrutinized revealing a dominance of the pressure force acting on ring areas in the spool chamber. Although CFD simulations are preferably used to save resources, the results of this study emphasise the importance of the experiments.

KEYWORDS: CFD simulation, Flow force, Spool valve, Validation

1. Introduction

One of the challenges when designing actuators for directional spool valves is the estimation of flow forces acting on spools. Especially when developing proportional or servo-valves the flow forces play an important role as they have a significant impact on dynamic performance and linearity of the valves. It is generally desired to reduce the flow forces both to improve the static and dynamic behavior of the valves and to reduce

the required power consumption of the actuators. For this purpose much research has been conducted already.

The first experimental and theoretical studies focused mainly on predicting and describing the flow forces acting on spool valves with sharp control edges. In the last decades, CFD (Computational Fluid Dynamics) simulations were performed in order to analyse and/or reduce the flow forces. For example, Lisowski /1/ validated a three dimensional CFD simulation of a directional control valve and proposed a solution for reducing flow forces. Yaun /2/ investigated the flow forces experimentally and using CFD simulations and provided recommendations for CFD simulations. Concerning the turbulence, different models were proposed by Schuster /3/ in favour of the k- ϵ model and by Tanaka /4/ in favour of the SST model.

Within this paper the simulated and measured steady flow force acting on a test valve spool are compared to each other. First, the relevant theory is described. Second, the test valve and the test rig are introduced. The third part is dedicated to the setting of CFD simulations and the simulation and experiment results are shown and discussed in the last part of this paper.

2. Flow Forces

In order to stroke a spool valve, an actuator must exert the force F_a (Figure 1).

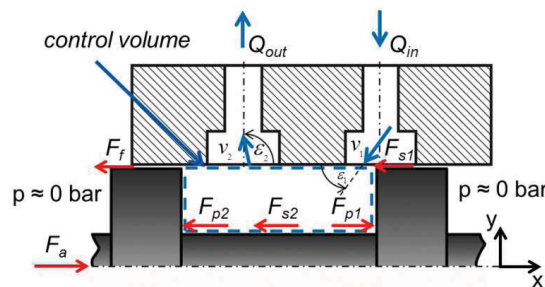


Figure 1: Forces acting on a spool

Assuming only axial forces, the spool movement can be described using the equation of motion (1).

$$m\ddot{x} = \sum F = F_a + F_{p1} - F_{p2} - F_f - F_{s1} - F_{s2} \quad (1)$$

The friction force F_f is a result of dry and skin friction in the gap between the spool and sleeve. The shear forces F_{s1} and F_{s2} are axial components of a drag, which is caused by fluid motion across the surface of the spool. Applying Bernoulli's law, the pressure forces F_{p1} and F_{p2} acting on both ring areas of spool can be summed up.

The sum of forces F_{s2} , F_{p1} and F_{p2} equals the so called flow force. It results from fluid flowing through the valve orifices and in the valve chamber. The analytical description of flow forces can be derived using the law of conservation of momentum /5/, which says that the rate of change of momentum of a system equals the sum of all forces acting on the system.

All forces apart from flow forces and the radial clearance between the spool and the sleeve are usually neglected. Assuming an incompressible fluid and control volume defined by the geometric boundaries of the valve chamber (Figure 1), the flow force F_{fl} is described by equation (2).

$$\rho L \frac{\partial Q}{\partial t} - \rho Q v_1 \cos \varepsilon_1 - \rho Q v_2 \cos \varepsilon_2 = -F_{fl} \quad (2)$$

The first term of equation (2) describes the unsteady flow force and is not considered in this study. The steady flow force $F_{fl,s}$ is composed of the second and the third term of equation (2). The second term describes the inflow momentum and the third term the outflow momentum, which is usually being neglected. This leads to a common definition of the steady flow force (3).

$$F_{fl,s} = \rho Q v_1 \cos \varepsilon_1 \quad (3)$$

However, different formulas describing the inflow velocity v_1 have been derived as published in /6/. Combining equation (3) with the orifice equation (4)

$$Q = \alpha_D \pi dx \sqrt{\frac{2\Delta p}{\rho}} \quad (4)$$

and equation (5) describing the definition of the inflow velocity /5/,

$$v_1 = \frac{Q}{\sin \varepsilon_1 \pi dx} \quad (5)$$

the steady flow force $F_{fl,s}$ can be expressed by equation (6) /5/.

$$F_{fl,s} = 2 \alpha_D^2 \pi dx \Delta p \frac{\cos \varepsilon_1}{\sin \varepsilon_1} \quad (6)$$

3. Experimental Setup

For the purpose of investigating steady flow forces a 2/2-way proportional test spool valve was manufactured at the Institute for Fluid Power Drives and Controls (IFAS) of RWTH Aachen University.

3.1. Test Valve

Figure 2 shows cross sections of the test valve, which is composed of a valve block, sleeve, spool and two lids. The test valve has two main ports P and T and two leakage ports L. Both the spool and the sleeve are removable. Hence, it is possible to replace them and investigate the influence of different shapes of control edges on flow forces.

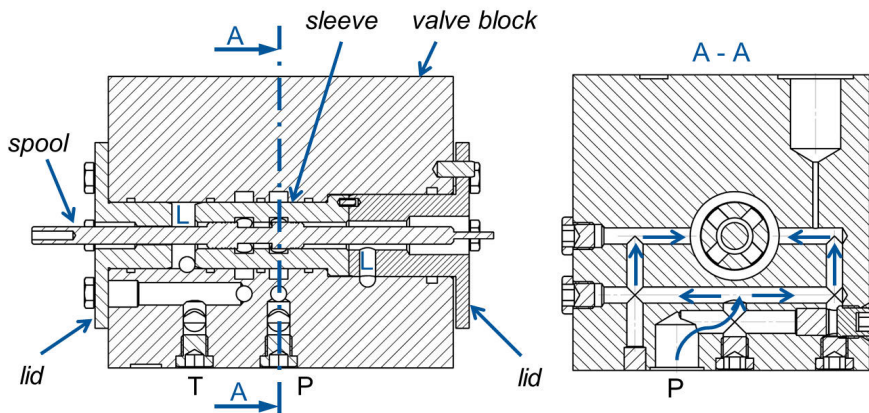


Figure 2: Longitudinal (left) and lateral (right) cross section of the test valve

On the left hand-side of the spool, a connection to the load cell is provided, whereas a displacement sensor is connected to the right-hand side of the spool. In order to simplify CFD simulations, symmetrical in- and outflow ports to, resp. from the spool were designed (see Figure 2).

A preliminary survey of directional proportional valves from different manufacturers was carried out to match the dimensions of the test valve with dimensions of common valves. It was found out, that the ratio between the shank and the spool diameter is about 0.6. The diameter of the ports in the sleeve usually equals the shank diameter. Relevant dimensions of the valve are presented in Table 1. The nominal flow rate of the test valve is approximately 109 l/min, at the pressure drop of 35 bar and maximum stroke of 1 mm. The nominal flow rate was measured with the hydraulic oil HLP46 at 60 °C.

Dimension	Value	Unit
Shank diameter	6	mm
Spool diameter	10	mm
Chamber length	20	mm
Radial clearance	8	μm

Table 1: Dimensions of the test valve

In order to eliminate friction forces, circumferential grooves were manufactured on the spool as illustrated in **Figure 3**.



Figure 3: Test valve spool

3.2. Measurement

IFAS features a test rig designated for measurements of characteristics of industrial valves. For the purpose of measurement of flow forces the test rig was modified (**Figure 4**).

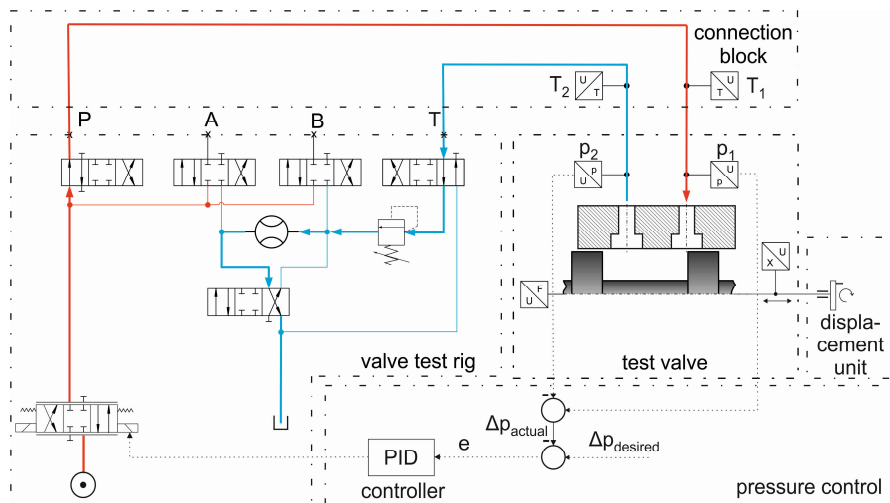


Figure 4: Circuit diagram of the test rig

The hydraulic power unit supplies the circuit with constant pressure. The switching valves are used to control the fluid flow from the hydraulic power unit through the test valve to a tank. The pressure relief valve was used to keep the pressure p_2 at 100 bar in order to avoid cavitation. The test valve is mounted on the connection block using the interface for industrial valves of the nominal size 16. The servo-valve controls the

pressure drop over the test valve. The stroke of the test valve is set manually with the displacement unit. The main part of the test rig is shown in **Figure 5**.

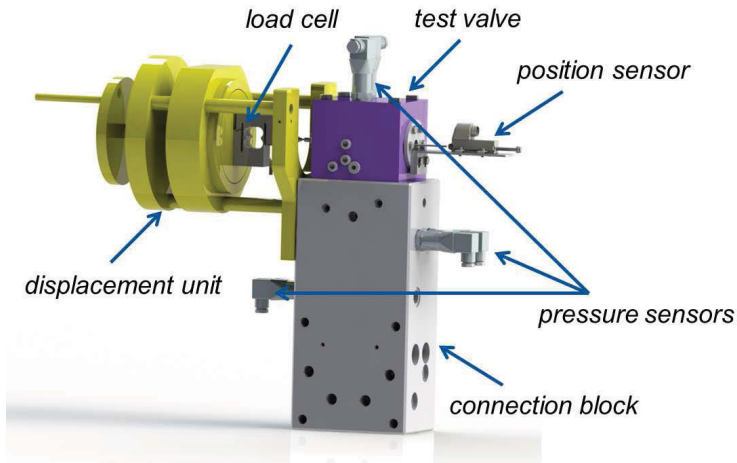


Figure 5: Main part of the test rig

3.2.1. Measurement of Flow Forces

The oil temperature of 40 °C in the tank was controlled and the oil temperature in the test valve reached between 55 and 60 °C depending on the actual operating point.

Since only the steady flow force $F_{fl,s}$ was investigated, measurements in discrete operation points were carried out. However, it is not possible to measure directly the steady flow force. Instead, the axial force F_{ax} (7) was measured, considering that the friction force F_f acts against the direction of the steady flow force.

$$F_{ax} = F_{fl,s} + F_{s1} - F_f \quad (7)$$

The axial forces were measured at 10 different valve strokes beginning with 0.1 mm and ending at 1 mm. At each stroke, the pressure drop was set and controlled by the servo-valve.

3.2.2. Measurement of Friction Forces

The friction force cannot be measured separately during the fluid flow. Hence, the friction force was measured when the port T (Figure 4) was closed. So the spool chamber was pressurized and the spool was moved as slowly as possible. As shown in **Figure 6**, the friction forces are almost negligibly dependent on the spool stroke and on the chamber pressure.

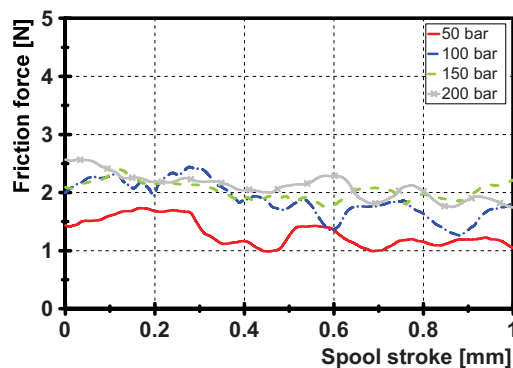


Figure 6: Friction forces at different pressure levels

4. CFD Simulation

The CFD simulations were carried out using ANSYS CFX 16.0 within ANSYS Workbench assuming symmetrical three dimensional steady incompressible isothermal viscous fluid flow. In addition, both the radial clearance and the friction between the spool and the sleeve were neglected.

4.1. Flow Domain

The full flow domain is shown in **Figure 7**. Thanks to the symmetry of the flow domain only a quarter model was used for the simulations. Hence two sym-metry planes were defined. All walls were considered as hydraulically smooth.

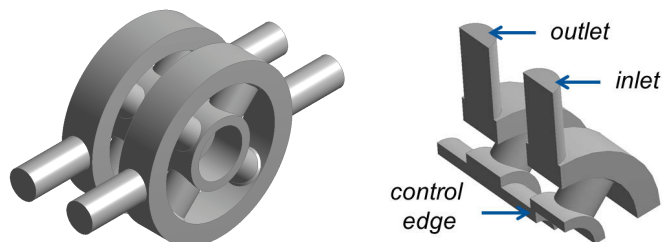


Figure 7: Full (left) and quarter (right) model of the fluid domain

4.2. Mesh

The meshes were created in ANSYS Meshing. The fluid domain was meshed with tetrahedral and prism elements with the average mesh count about 1,2e6 nodes (3,5e6 elements). The boundary layers were resolved with 10 prism layers as shown in **Figure 8**. The height of the first prism layer was set to 5 μm . In order to achieve high quality meshes, local sizing functions were used. So the mesh metric “Skewness” was below 0.8 and the mesh metric “Orthogonal Quality” was above 0.2 meaning a good mesh quality according to [7].

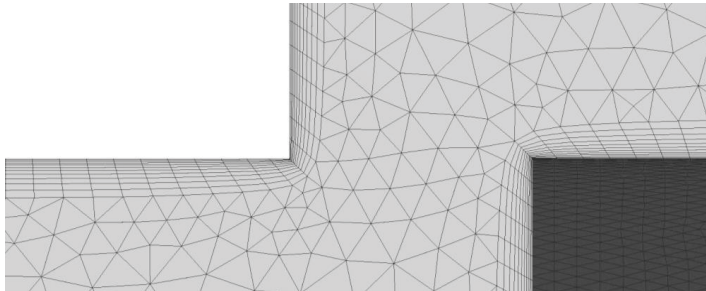


Figure 8: Detailed view on the mesh in the region of the sharp control edge

4.3. Simulation Parameters

The parameters of CFD were set according to recommendations described in [7] to achieve as accurate results as possible. Furthermore, a sensitivity study of different parameter sets has been carried out including different boundary conditions, turbulence models and their parameters, timescale control, advection scheme etc. Especially the choice of the turbulence model and the near wall treatment can have a significant impact on the accuracy of simulation results.

Based on the sensitivity study, the RNG $k\text{-}\epsilon$ model and the scalable wall function were chosen. At the inlet, the mean flow velocity calculated from the measurement data was defined. The reference pressure was set to 100 bar, so the average static pressure of 0 bar was set at the outlet. The RMS (root mean square) residuals of $1\text{e-}5$ were used as the convergence criteria. Additionally, the axial force acting on the spool and the inlet pressure were defined as target variables. Other parameters which are not discussed in this paper were left as default. All simulations were performed considering the hydraulic oil HLP46 with constant density of 856 kg/m^3 and constant kinematic viscosity of $24\text{ mm}^2/\text{s}$.

5. Results

The results of the simulations and a comparison with the measurements are presented in this chapter. Figures 9 – 12 depict the results of the CFD simulation carried out for the pool stroke of 1 mm at pressure drop of 50 bar.

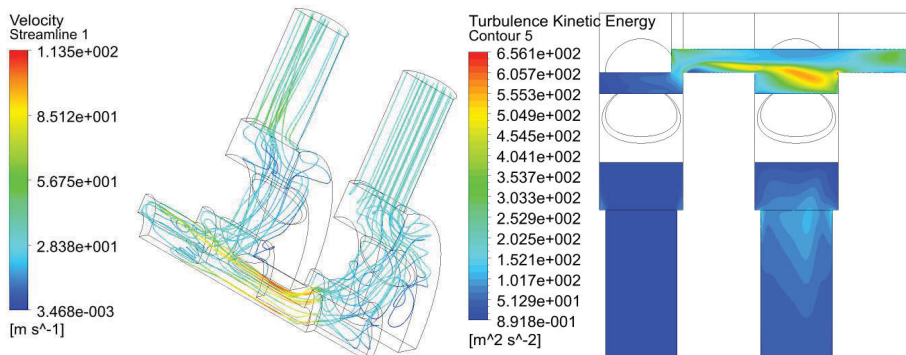


Figure 9: Streamlines (left) and turbulent kinetic energy (right) across the flow domain

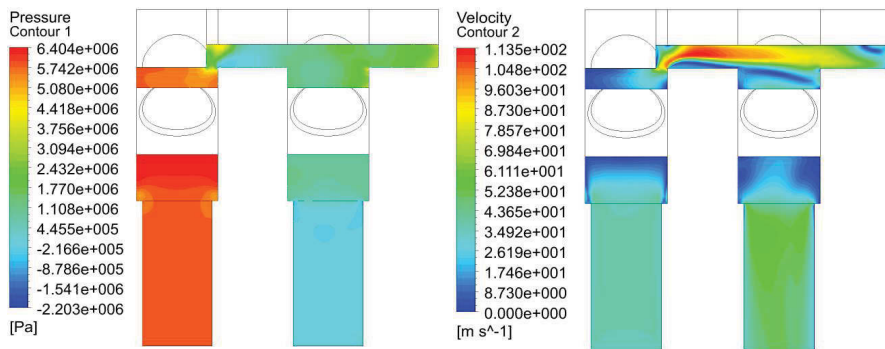


Figure 10: Static pressure (left) and velocity (right) across the symmetry plane

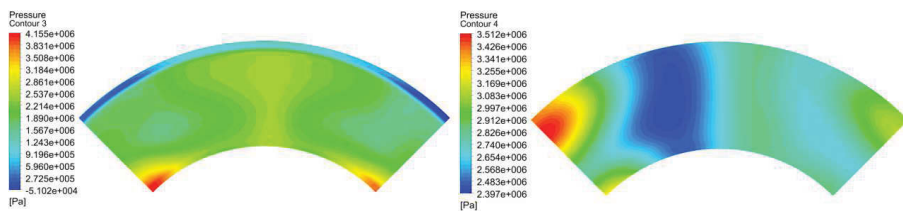


Figure 11: Static pressure on the ring area near the control edge (left) and on the opposite land ring area (right)

Figure 9 demonstrates the turbulent character of the flow with strong curvatures and flow separations. The static pressure and the velocity across the symmetry plane are depicted in **Figure 10**. The pressure distribution on the ring area opposite the control edge is unsymmetrical as shown in **Figure 11**. Further-more, two recirculation zones in the spool chamber are visible in **Figure 12**.

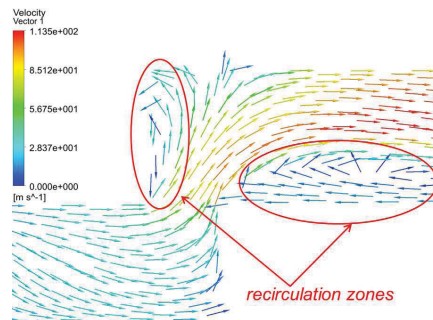


Figure 12: Velocity vectors in the vicinity of the control edge

The overview of the components of the simulated axial force is depicted in **Figure 13**.

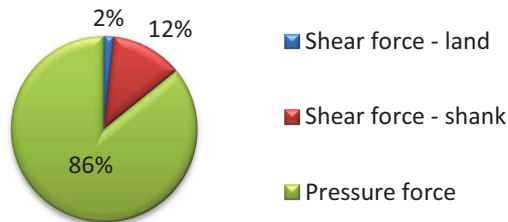


Figure 13: Simulated components of axial force

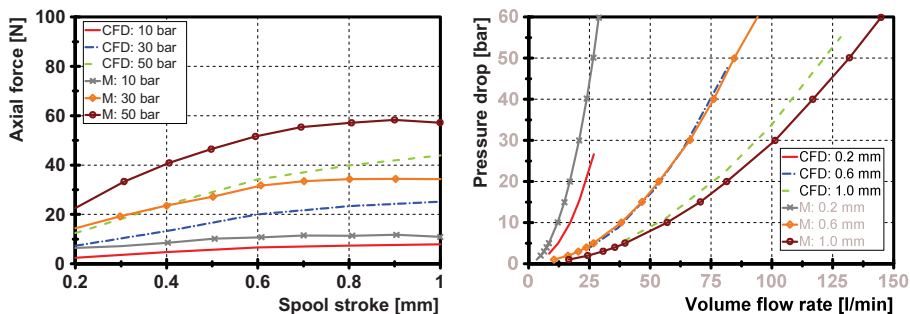


Figure 14: Measured and simulated axial forces (left) and pressure drops (right)

Since the mean flow velocity defined in the simulation was obtained from the measurement data, the measured and the simulated axial forces and inlet pressures are compared to each other (see **Figure 14**).

6. Discussion and Conclusions

The measured and simulated axial forces and pressure drops coincide qualitatively. However, the simulated values of axial forces are in average by 32 % lower compared with the measured ones. This highlights the importance of experiments, as the CFD simulations can be error prone. Since a very good reproducibility of the measurements has been achieved it is assumed, that the accuracy of the measurements is very high. Only the measured friction forces are likely affected by poor sensor accuracy in the lower measurement range. Moreover, it was assumed that the measured friction force corresponds to the friction force, which acts on the spool, while the fluid is flowing. Although all recommendations /7/ for increasing the accuracy of CFD simulations were fulfilled, the simulation results are inaccurate. It was observed for one particular case, that the pressure force entails 86 % of the simulated axial force. So the potential source of uncertainty is the pressure distribution in the spool chamber and especially on the ring areas of the spool.

Further investigations including transient simulations will be undertaken to increase the accuracy of the CFD simulations and to optimize existing formulas for the estimation of flow forces.

7. References

- /1/ Lisowski, E. "Three dimensional CFD analysis and experimental test of flow force acting on the spool of solenoid operated directional control valve", *Energy Conversion and Management*. 2013.
- /2/ Yuan, Q. "Flow Forces Investigation through Computational Fluid Dynamics and Experimental Study", *Proceedings of the 9th International Fluid Power Conference*. Aachen. Germany. 2014.
- /3/ Schuster, G. *CFD-gestützte Maßnahme zur Reduktion von Strömungskraft und Kavitation am Beispiel eines hydraulischen Schaltventils*. PhD thesis. Shaker Verlag, Aachen. 2005.
- /4/ Tanaka, K. "Steady and Unsteady Flow Force acting on a Spool Valve". *Conference Proceedings of Power Transmission and Motion Control*. Bath. United Kingdom. 2012.
- /5/ Murrenhoff, H. *Grundlagen der Fluidtechnik - Teil 1: Hydraulik*. Shaker Verlag, Aachen. 2012.

- /6/ Schrank, K. "Beschreibung der Strömungskraft in Längsschieber-ventilen mittels Impulserhaltung", *O+P Journal*. 2013.
- /7/ ANSYS Documentation (Version 16.0).

8. Nomenclature

d	Spool diameter	m
F_a/F_f	Actuator/Friction force	N
F_{ax}	Axial force acting on the spool	N
$F_{fl}(F_{fls})$	(Steady) Flow force	N
F_{s1}/F_{s2}	Shear force on the spool land/shank	N
F_{p1}/F_{p2}	Pressure forces acting on ring areas	N
L	Length of the spool chamber	m
Δp	Pressure drop across the valve	Pa
Q_{in}/Q_{out}	Inflow/Outflow volume flow rate	m ³ /s
v_1/v_2	Inflow/Outflow fluid velocity	m/s
m	Mass	kg
x	Spool stroke	m
α_D	Discharge coefficient	-
$\varepsilon_1/\varepsilon_2$	Inflow/Outflow fluid jet angle	°
ρ	Fluid density	kg/m ³

DRESDNER VEREIN ZUR FÖRDERUNG DER FLUIDTECHNIK e.V.

DVF

Duties and goals of the association

The support of scientific research and development in education and application of research results in the fluid power domain. The association is purely non-profit and serves the public good. This includes:

- Lectures and presentations on conventions and conferences
- Scientific knowledge transfer with other universities and industry domestic and abroad
- Publication of research results
- Supply and distribution of educational material, dissertations and publications of the Institute of Fluid Power, TU Dresden
- Support of educational and cultural events in the fluid power area
- Preparation and organization of scientific fluid power conferences such as the International Fluid Power Colloquium (IFK)
- Organization and execution of fluid power conferences in the Dresden area.

Management:

Dr.-Ing. Thomas Neubert (Chairmen), Hydrive Engineering GmbH

Prof. Dr.-Ing. Jürgen Weber (Vice-Chairmen), Institut für Fluidtechnik, TU Dresden

Dr.-Ing. Hilmar Jähne (Director), Hydrive Engineering GmbH

Dr.-Ing. Norman Bügener (Treasurer), Dowaldwerke GmbH

Contact:

Dresdner Verein zur Förderung der Fluidtechnik e.V.

c/o Institut für Fluidtechnik

Technische Universität Dresden

01062 Dresden

Tel.: 0351/463-33559

Fax: 0351/463-32136

E-Mail: dvf@ifd.mw.tu-dresden.de

DRESDNER VEREIN ZUR FÖRDERUNG DER FLUIDTECHNIK e.V.

DVF

Aufgaben und Ziele des Vereins

Förderung der wissenschaftlichen Forschung und Entwicklung, der Aus- und Weiterbildung sowie der Anwendung von Forschungsergebnissen auf dem Gebiet der Fluidtechnik. Der Verein verfolgt ausschließlich gemeinnützige Zwecke. Diese Aufgabe schließt ein:

- Vorträge und Referate auf Zusammenkünften und Tagungen
- Wissenschaftlicher Gedankenaustausch mit anderen Hochschulen und Industrievertretern im In- und Ausland
- Veröffentlichung von Forschungsergebnissen
- Bereitstellung und Vertrieb von Lehrmaterialien, Dissertationen und Publikationen des Instituts für Fluidtechnik
- Unterstützung von Bildungs- und Weiterbildungsmaßnahmen auf dem Gebiet der Fluidtechnik
- Vorbereitung und Organisation von wissenschaftlichen Tagungen, wie das Internationale Fluidtechnische Kolloquium
- Organisation und Durchführung der Dresdner Fluidtechnischen Kolloquien

Vorstand:

Dr.-Ing. Thomas Neubert (Vorsitzender), Hydrive Engineering GmbH

Prof. Dr.-Ing. Jürgen Weber (Stellvertreter), Institut für Fluidtechnik, TU Dresden

Dr.-Ing. Hilmar Jähne (Geschäftsführer), Hydrive Engineering GmbH

Dr.-Ing. Norman Bügener (Schatzmeister), Dowaldwerke GmbH

Kontakt:

Dresdner Verein zur Förderung der Fluidtechnik e.V.

c/o Institut für Fluidtechnik

Technische Universität Dresden

01062 Dresden

Tel.: 0351/463-33559

Fax: 0351/463-32136

E-Mail: dvf@ifd.mw.tu-dresden.de

